RUSSIAN ACADEMY OF SCIENCES
National Geophysical Committee

RUSSIAN NATIONAL REPORT

Meteorology and Atmospheric Sciences

2019–2022

for the XXVIII General Assembly
of the International Union of Geodesy and Geophysics
(Berlin, Germany, July 11–20, 2023)

МАКС ПРЕСС

МОСКВА – 2023

УДК 55
ББК 26.2
Н35

https://elibrary.ru/uvaqrb

Editors:
I.I. Mokhov (MASS Chairman)
A.A. Krivolutsky (MASS Scientific Secretary)

Russian National Report: Meteorology and Atmospheric Sciences: 2019–2022: for the XXXVIII General Assembly of the International Union of Geodesy and Geophysics (Berlin, Germany, July 11–20, 2023) / Ed.: I.I. Mokhov, A.A. Krivolutsky. – Moscow: MAKS Press, 2023. – 440 p.
ISBN 978-5-317-07017-5
https://doi.org/10.29003/m3460.978-5-317-07017-5

This report of the Meteorology and Atmospheric Sciences Section (MASS) of the Russian National Geophysical Committee presents information about results of atmospheric, meteorological and climate research in Russia in 2019-2022. It is based on reports of 10 National Commissions.

Key words: Russian National Report, Meteorology and Atmospheric Sciences: 2019-2022, atmospheric chemistry, atmospheric electricity, atmospheric radiation, climate, clouds and precipitation, dynamical meteorology, middle atmosphere, ozone, planetary atmospheres, polar meteorology.

Н35 **Национальный отчет России по метеорологии и атмосферным наукам в 2019–2022 гг. :** XXXVIII Генеральная Ассамблея Международного союза геодезии и геофизики (Берлин, Германия, 11–20 июля 2023 г.) / Ред.: И.И. Мохов, А.А. Криволуцкий. – Москва : МАКС Пресс, 2023. – 440 с.
ISBN 978-5-317-07017-5
https://doi.org/10.29003/m3460.978-5-317-07017-5

В данном отчете Секции метеорологии и атмосферных наук российского Национального геофизического комитета представлена информация о результатах атмосферных, метеорологических и климатических исследований в России в 2019–2022 гг. на основе отчетов 10 национальных комиссий.

Ключевые слова: Российский национальный отчет, метеорология и атмосферные науки: 2019–2022 гг., атмосферная радиация, атмосферное электричество, динамическая метеорология, климат, облака и осадки, озон, планетные атмосферы, полярная метеорология, средняя атмосфера, химия атмосферы.

УДК 55
ББК 26.2

Отчет Секции метеорологии и атмосферных наук будет размещен на сайте Национального геофизического комитета РАН:
ngc.gcras.ru

ISBN 978-5-317-07017-5

Contents

Preface

The Section of Meteorology and Atmospheric Sciences (MASS) of the National Geophysical Committee prepares a report on the main results of Russian atmospheric research for the General Assembly of the International Union of Geodesy and Geophysics (IUGG) every four years. The IUGG includes the International Association of Meteorology and Atmospheric Sciences (IAMAS) and seven International Associations: Cryospheric Sciences (IACS), Geodesy (IAG), Geomagnetism and Aeronomy (IAGA), Hydrological Sciences (IAHS), Physical Sciences of the Oceans (IAPSO), Seismology and Physics of the Earth's Interior (IASPEI), and Volcanology and Chemistry of the Earth's Interior (IAVCEI). This MASS report was prepared for the 28th IUGG General Assembly (Berlin, Germany, July 11–20, 2023).

The MASS report includes the results on ten areas of research. Like in the IAMAS, ten national commissions are responsible for these areas:

- Commission on Atmospheric Chemistry (Chairman I.K. Larin, Talrose Institute for Energy Problems of Chemical Physics, Russian Academy of Sciences),
- Commission on Atmospheric Electricity (Chairman V.N. Stasenko, Institute of Applied Geophysics, Roshydromet),
- Commission on Atmospheric Ozone (Chairman B.D. Belan, V.E. Zuev Institute of Atmospheric Optics, Russian Academy of Sciences, Siberian Branch),
- Commission on Atmospheric Radiation (Chairman Yu.M. Timofeyev, St. Petersburg State University),
- Commission on Climate (Chairman I.I. Mokhov, A.M. Obukhov Institute of Atmospheric Physics, Russian Academy of Sciences, Moscow State University),
- Commission on Clouds and Precipitation (Chairman N.A. Bezrukova, Central Aerological Observatory, Roshydromet),
- Commission on Dynamic Meteorology (Chairman I.A. Repina, A.M. Obukhov Institute of Atmospheric Physics, Russian Academy of Sciences),
- Commission on Middle Atmosphere (Chairman A.A. Krivolutsky, Central Aerological Observatory, Roshydromet),
- Commission on Planetary Atmospheres (Chairman O.I. Korablev, Space Research Institute, Russian Academy of Sciences),
- Commission on Polar Meteorology (Chairman A.V. Klepikov, Arctic and Antarctic Research Institute, Roshydromet).

MASS reports are published in English; they are available on the website of the National Geophysical Committee (http://ngc.gcras.ru/).

Along with the National Reports, quite detailed reviews prepared within the framework of ten National Commissions in the main areas of atmospheric, meteorological and climate research in recent years are usually published in the leading Russian scientific journal "*Izvestiya. Atmospheric and Oceanic Physics*" [1–45].

References

1. *Russian National Report: Meteorology and Atmospheric Sciences: 2015–2019*, Ed. by I.I. Mokhov and A.A. Krivolutsky. MAKS Press, Moscow, 2019, 330 pp.
2. Mokhov I.I. Russian studies of atmospheric sciences and meteorology in 2015–2018. *Izv., Atmos. Ocean. Phys.,* 2016, **55** (6), 503–504.
3. Kurgansky M.V., Krupchatnikov V.N. Dynamic meteorology research in Russia, 2015–2018. *Izv., Atmos. Ocean. Phys.,* 2019, **55** (6), 505–536.
4. Krivolutsky A.A., Repnev A.I., Tuniyants T.I., Mironova I.A., Gruzdev A.N. Results of Russian studies of the middle atmosphere in 2015–2018. *Izv., Atmos. Ocean. Phys*., 2019, **55** (6), 537–551.
5. Larin I.K. Russian investigations in atmospheric chemistry for 2015–2018. Izv., Atmos. Ocean. Phys., 2019, **55** (6), 552–561.
6. Mareev E.A., Shatalina M.V., Dement'eva S.O., Evtushenko A.A., Svechnikova E.K., Slyunyaev N.N., Stasenko V.N. Russian studies of atmospheric electricity in 2015–2018. *Izv., Atmos. Ocean. Phys*., 2019, **55** (6), 562–572.
7. Timofeev Yu.M., Shul'gina E.M. Russian investigations in the field of atmospheric radiation in 2015–2018. *Izv., Atmos. Ocean. Phys*., 2020, **56** (1), 1–15.
8. Korablev O.I. Studies of planetary atmospheres in Russia (2015–2018). *Izv., Atmos. Ocean. Phys*., 2020, **56** (2), 130–140.
9. Elansky N.F. Russian studies of atmospheric ozone and its precursors in 2015–2018. *Izv., Atmos. Ocean. Phys*., 2020, **56** (2), 141–155.
10. Mokhov I.I. Russian climate research in 2015–2018. *Izv., Atmos. Ocean. Phys.*, 2020, **56** (4), 325–343.
11. Bezrukova N.A., Chernokulsky A.V. Russian studies of clouds and precipitation in 2015–2018. *Izv., Atmos. Ocean. Phys*., 2020, **56** (4), 344–363.
12. Klepikov A.V., Danilov A.I. Results of Russian studies of polar meteorology in 2015– 2018. *Izv., Atmos. Ocean. Phys*., 2021, **57** (3), 233–246.
13. Mokhov I.I Russian studies of atmospheric sciences and meteorology in 2011–2014. *Izv., Atmos. Ocean. Phys*., 2016, **52** (2), 116.
14. Kurgansky M.V., Krupchatnikov V.N. Research in dynamic meteorology in Russia in 2011–2014. *Izv., Atmos. Ocean. Phys*., 2016, **52** (2), 117–131.
15. Elansky N.F. Russian studies of atmospheric ozone in 2011–2014. *Izv., Atmos. Ocean. Phys*., 2016, **52** (2), 132–146.
16. Larin I.K. Russian investigations in atmospheric chemistry for 2011–2014. *Izv., Atmos. Ocean. Phys.*, 2016, **52** (2), 147–153.
17. Mareev E.A., Stasenko V.N., Bulatov A.A., Dement'eva S.O., Evtushenko A.A., Il'in N.V., Kuterin F.A., Slyunyaev N.N., Shatalina M.V. Russian studies of atmospheric electricity in 2011–2014. *Izv., Atmos. Ocean. Phys*., 2016, **52** (2), 154–164.
18. Timofeev Yu.M., Shul'gina E.M. Russian investigations in the field of atmospheric radiation in 2011–2014. *Izv., Atmos. Ocean. Phys.*, 2016, **52** (6), 467–482.

19. Korablev O.I. Studies of planetary atmospheres in Russia (2011–2014). *Izv., Atmos. Ocean. Phys*., 2016, **52** (6), 483–496.
20. Krivolutsky A.A., Kukoleva A.A. Results of Russian investigations into the middle atmosphere (2011– 2014). *Izv., Atmos. Ocean. Phys*., 2016, **52** (6), 497–511.
21. Bezrukova N.A., Chernokulsky A.V. Russian studies on clouds and precipitation in 2011–2014. *Izv., Atmos. Ocean. Phys*, 2016, **52** (6), 512–523.
22. Mokhov I.I. Russian climate studies in 2011–2014. *Izv., Atmos. Ocean. Phys*., 2017, **53** (5), 550–563.
23. Lagun V.E., Klepikov A.V., Danilov A.I. Polar meteorology: Results of Russian research in 2011–2014. Izv., Atmos. Ocean. Phys., 2017, **53** (5), 564–577.
24. *Russian National Report: Meteorology and Atmospheric Sciences: 2011–2014*, Ed. by I.I. Mokhov and A.A. Krivolutsky, MAKS Press, Moscow, 2015, 270 pp.
25. Mokhov I.I. Russian studies of atmospheric sciences and meteorology in 2007–2010. *Izv., Atmos. Ocean. Phys*., 2012, **48** (3), 254.
26. Lykosov V.N., Krupchatnikov V.N. Some directions in the development of dynamic meteorology in Russia in 2007–2010. Izv., Atmos. Ocean. Phys., 2012, **48** (3), 255–271.
27. Larin I.K. Russian investigations in atmospheric chemistry for 2007–2010. *Izv., Atmos. Ocean. Phys*., 2012, **48** (3), 272–280.
28. Elansky N.F. Russian studies of atmospheric ozone in 2007–2011. *Izv., Atmos. Ocean. Phys*., 2012, **48** (3), 281–298.
29. Krivolutsky A.A., Repnev A.I. Results of Russian studies of the middle atmosphere, 2007–2010. *Izv., Atmos. Ocean. Phys*., 2012, **48** (3), 299–308.
30. Korablev O.I., Zasova L.V., Fedorova A.A., Titov D.V., Ignatiev N.I., Rodin A.V., Shematovich V.I., Belyaev D.A., Khatuntsev I.V., Izakov M.N., Shakun A.V., Burlakov A.V., Mayorov B.S. Studies of the planetary atmospheres in Russia (2007–2010). *Izv., Atmos. Ocean. Phys.*, 2012, **48** (3), 309–331.
31. Mokhov I.I. Results of Russian climate studies in 2007–2010. *Izv., Atmos. Ocean. Phys*., 2013, **49** (1), 1–15.
32. Timofeev Yu.M., Shul'gina E.M. Russian investigations in the field of atmospheric radiation in 2007– 2010. *Izv., Atmos. Ocean. Phys*., 2013, **49** (1), 16–32.
33. *Russian National Report: Meteorology and Atmospheric Sciences: 2007–2010*, Ed. by I.I. Mokhov and A.A. Krivolutsky, MAKS Press, Moscow, 2011, 213 pp.
34. Mokhov I.I. Russian studies in meteorology and atmospheric sciences from 2003 to 2006. *Izv., Atmos. Ocean. Phys*., 2009, **45** (2), 153.
35. Lykosov V.N., Krupchatnikov V.N. Some aspects in the development of dynamic meteorology in Russia in 2003–2006. *Izv., Atmos. Ocean. Phys*., 2009, **45** (2), 154–168.
36. Mokhov I.I. Russian climate studies in 2003–2006. *Izv., Atmos. Ocean. Phys*., 2009, **45** (2), 169–181.
37. Timofeev Yu.M., Shul'gina E.M. Russian studies of atmospheric radiation in 2003–2006. *Izv., Atmos. Ocean. Phys*., 2009, **45** (2), 182–198.
38. Larin I.K. Russian investigations in atmospheric chemistry for 2003–2006. *Izv., Atmos. Ocean. Phys.*, 2009, **45** (2), 199–206.
39. Elansky N.F. Russian studies of the atmospheric ozone in 2003–2006. *Izv., Atmos. Ocean. Phys*., 2009, **45** (2), 207–220.
40. Danilov A.I., Lagun V.E. Polar meteorology: The results of Russian research in 2003–2006. *Izv., Atmos. Ocean. Phys*., 2009, **45** (4), 517–527.

41. Krivolutsky A.A. Russian studies of the middle atmosphere in 2003–2006. *Izv., Atmos. Ocean. Phys*., 2009, **45** (4), 528–540.
42. Mareev E.A., Stasenko V.N. Russian studies in the field of atmospheric electricity in 2003–2007. Atmos. Ocean. Phys., 2009, **45** (5), 663–674.
43. *Russian National Report: Meteorology and Atmospheric Sciences: 2003–2006*, Ed. by I.I. Mokhov and A.A. Krivolutsky, MAKS Press, Moscow, 2007, 179 pp.
44. Mokhov I.I. Climate studies in Russia in 1999–2002. *Izv., Atmos. Ocean. Phys*., 2004, **40** (2), 127–133.
45. *Russian National Report: Meteorology and Atmospheric Sciences: 1999–2002*, Ed. by I.I. Mokhov and A.A. Krivolutsky, MAKS Press, Moscow, 2003, 136 pp.

Igor I. Mokhov
MASS Chairman

Atmospheric Chemistry

I.K. Larin
V.L. Talrose Institute of Energy Problems
of Chemical Physics RAS
e-mail: iklarin@narod.ru

A brief overview of the work of Russian scientists in the field of atmospheric chemistry in 2019–2022 is presented, including work on the chemistry of the troposphere, the chemistry of the ozone layer, work on the study of heterophase processes, as well as work on the chemical aspects of climate and its change. The review was prepared in the Commission on Atmospheric Chemistry of the Section of Meteorology and Atmospheric Sciences of the National Geophysical Committee.

Keywords: chemical processes, heterophase processes, troposphere, stratosphere, climate.

First of all, it should be noted that in 2019 the work "Russian research in the field of atmospheric chemistry in 2015–2018" was published [1].

Chemistry of the troposphere

One of the main areas of research in this area is the study of elementary chemical reactions of atmospheric significance, data on which are then used in mathematical models of the atmosphere. In this connection, we should mention the work [2], in which the rate constants of the reaction of chlorine atoms with CH_3Br in the temperature range 273–355 K. were measured using the resonance fluorescence method to register active chemical reagents in a flow reactor. It is shown that the measured rate constants increase when the reaction is carried out at a lower temperature, which is typical for heterogeneous reactions. It is assumed that the interaction of the atom with CF_3Br occurs on the surface of the reactor. Along with the resonant fluorescence method, mass spectral technique is used to study chemical reactions. In [3], using this technique, the rate constant of the reaction of benzene with atomic fluorine was determined by the method of competing reactions. The studies were carried out in a low-pressure flow reactor with mass spectrometric analysis of reagents and reaction products. The reactions of fluorine atoms with cyclohexane, trifluoroacetic and trichloroacetic acids were used as competing reactions. The ratios of the rate constants of benzene and these competing reactions with atomic fluorine are determined for the first time. Based on the experimental data obtained and the reaction rate constants known from the literature, the value of the reaction rate constant of fluorine atoms with ben-

zene is calculated. In another work [4], the mass spectra of negative ions of aqueous solutions of completely neutralized monochloroacetic acid molecules were obtained by the mass spectrographic method of electrospray of electrolyte solutions in vacuum. In [5] this technique was used to study the properties of toxic substances. The paper describes the results of a mass spectrometric study of chemical substances – chloroacetic acids (monochloroacetic, dichloroacetic, trichloroacetic acids) and pyridine with the use of an inlet of the studied substances in the form of a modulated molecular beam. The advantage of molecular beam injection is to minimize the formation of foreign substances during the analysis, since the method eliminates the collision of molecules of the studied substance with the heated walls of the ion source, on which pyrolysis reactions and other reactions of the formation of new substances can occur.

In addition to laboratory measurements, chemical reactions are studied in a model and theoretical way. Thus, in [6], a method was proposed for calculating the exact kinetic autonomous invariants of multistage linear chemical reactions occurring in a gradient-free reactor through any number of elementary stages involving an arbitrary number of reagents within the framework of the law of acting masses. For dynamic models of linear reactions, it is always possible to find general and particular analytical solutions that are expressed explicitly in terms of initial conditions. The idea of the method is based on the choice of such initial conditions that make it possible to express nonequilibrium concentrations of reagents through constant kinetic parameters (constants of stage velocities and flow rates). In a similar paper [7], the features of the course of chemical reactions in multicomponent systems are considered. It is indicated, in particular, that with an increase in the number of components involved in such reactions, the structural diversity of the products formed increases sharply, which becomes almost limitless. In another computational work [8], the transition states, oscillation frequencies and reaction paths of $CO + N_2O \rightleftarrows CO_2 + N_2$ were calculated using quantum mechanics methods. Both the forward and reverse transition of the oxygen atom and the process going through the formation of several intermediate complexes are considered. In the framework of the theory of the transition state, the rate constants of the forward and reverse reactions are calculated. In [9], experimental data on the reactions of separation of hydrogen atoms from hydrocarbons, halogenalkanes and oxygen-containing compounds by oxygen atoms (50 reactions) were analyzed within the framework of the model of intersecting parabolas. The influence of five factors on the activation energy of these reactions has been established: the enthalpy of the reaction, triplet repulsion, electronegativity of the atoms of the reaction center, dipole-dipole interaction of the reaction center with polar groups, π-electrons of neighboring aromatic rings. Important information about chemical processes occurring in polluted

urban air can be obtained from data on the chemical composition and acidity of urban precipitation. As an example, we can cite the work [10], which analyzes the composition of precipitation collected during 2014–2016 on the territory of the Meteorological Station of Moscow State University, including their isotopic composition. It was shown that the distribution of the isotopic composition of precipitation in Moscow, observed during 2014–2016, has a sinusoidal appearance and correlates well with changes in the temperature of the surface air layer. In the seasonal course of the average monthly values of ^{18}O in precipitation, their natural increase is observed from January to May – July. During the 3-year period under review, the most isotopically light precipitation fell in January, the most isotopically heavy – in the summer months. In a similar work [11], the chemical composition of precipitation in Moscow is analyzed already in the period from 1982 to 2017. The whole series of observations can be divided into three periods, which are characterized by the acidity of precipitation, changes in mineralization and the predominance of certain ions. In 1982–1998, the most polluted atmospheric with high acidity were observed; in 1999–2004, acid precipitation was almost completely absent, and mineralization decreased. The last period of 2005–2017 differs from the previous one by an increase in the frequency of acid precipitation, while the mineralization has practically not changed, despite a noticeable increase in chlorides in recent years. Finally, the paper [12] examines the influence of natural and anthropogenic factors on the state of the Moscow air environment. Based on long-term observations of the Meteorological Observatory of the Faculty of Geography of Lomonosov Moscow State University, the authors conducted a joint analysis of time series of atmospheric aerosol turbidity, acidity and chemical composition of precipitation. The presence of several periods of purification and air pollution of the city was shown. These periods are determined by both natural processes (forest fires) and anthropogenic factors. Catastrophic air and precipitation pollution occurs during forest fires.

In connection with the relevance of environmental protection and safe energy issues, we will point to the work [13], which examines the current state of the prospects for the development of hydrogen energy. A significant number of works in the field of tropospheric chemistry have been devoted to the monitoring of pollutants, including products of forest fires, aerosols, as well as small components of the troposphere, such as ozone, carbon monoxide and dioxide, nitrogen dioxide, etc. [14–55].

Heterophase processes

Heterophase processes are of great importance for understanding ozonospheric chemistry. Recall that these processes played a decisive role in the depletion of the ozone layer at the end of the 20th century and in the for-

mation of the Arctic and Antarctic ozone holes. In recent years, new important results have been obtained in this area. At the same time, considerable attention was paid to the processes occurring in the Young layer (lower and middle stratosphere). Thus, in [56], the results of 3D modeling of the spatio-temporal structure of the distribution of gas impurities and particles of the Young layer in the atmosphere in the winter of 2002 are presented, the calculated and mass concentrations, as well as the variability of the content of water, sulfuric and nitric acids in the particles are given. Similar problems were solved in [57]. Sulfate particles of the Young layer affect the properties of the environment. In [58], the authors explain how this effect changes the atmospheric lifetime of odd oxygen. Another paper, [59], explains the effect of sulfate particles on the rate of ozone depletion in the lower stratosphere. The dramatic decrease in the rate of ozone depletion found in calculations at altitudes less than 16 km in comparison with the rate of ozone depletion calculated with the participation of gas chemical reactions indicates the inhibitory role of aerosol particles. The reason is the capture of N_2O_5 molecules from the air by aerosol particles. Their rapid runoff entails a sharp decrease in the concentrations of NO_x family components in the air, as well as, although less pronounced, a decrease in the concentrations of components of the HO_x and O_x families involved in ozone depletion.

A new numerical model of atmospheric transport and transformation of gaseous and aerosol impurities is described in [60], taking into account the processes of photochemistry, nucleation involving neutral molecules and ions, as well as condensation/evaporation and coagulation. The results obtained in relation to the northern hemisphere and winter time indicate the significant role of the ion nucleation process in the formation of atmospheric aerosol. At the same time, along with the level of air ionization, the key factors determining the dynamics of ion nucleation are also temperature and relative humidity. The work [61] analyzes samples from a well, 70 m deep, drilled at the Vostok station (Central Antarctica), which cover the Late Holocene epoch (the last 2000 years). The climatic conditions (air temperature and snow accumulation rate) in the vicinity of the Vostok station have been reconstructed. The results obtained are compared with published paleoclimatic reconstructions. In [62], the author explains how mechanical action can lead to heterogeneous reactions in powder systems. However, for this it is necessary that the reaction be exothermic, i.e. it goes with the release of heat. The work [63] chronologically describes the history of tropospheric aerosol research at the V.E. Zuev Institute of Atmospheric Optics SB RAS. In order to take into account heterophase reactions in atmospheric chemistry, it is necessary to know the rate constants of heterogeneous reactions. Such data are obtained using special laboratory kinetic installations in which the chemical reaction takes place not in the gas phase, but on the walls of the reactor. As

an example, we can cite the work [64], in which the reaction of dimethyl sulfide with IO radicals was studied. The temperature dependence of this heterogeneous reaction was determined. In [65], using the same technique as in [64], the heterogeneous reaction of hydrogen sulfide with IO radicals was studied.

Among the works on heterophase topics, works in which aerosol data of a local nature are analyzed are of particular interest. An example of such work is the work [66], which presents data on the seasonal variability of aerosol composition in various regions of Belgium in 2001–2003. In [67], aerosol data obtained on the Northern Earth are discussed. It was shown that the average values of most aerosol characteristics measured in April – June 2018 are slightly lower than in the Arctic settlement. Barentsburg (arch.Svalbard), and several times less than in the south of Western Siberia in the same period. In [68], the authors analyze the formation of sulfates in carbonate particles using atmospheric monitoring data in Irkutsk. The authors managed to show that the main source of sulfates in carbonate particles in the atmosphere of Irkutsk is SO_2 captured from the air. Their accumulation in the composition of particles is caused by heterophase reactions and is accompanied by the substitution of bicarbonates (HCO_3^-) for sulfate anions.

In addition to the above, heterophase chemistry deals with the study of reactions of active chemical components with and coatings of different chemical composition. Thus, in [69, 70], the capture of NO3 radicals by a coating of methane soot was studied. On the basis of chromatographic and mass spectrometric analyzes of the composition of the initial methane soot and solid products of its reaction with the oxidizing gas-phase reagent NO3, it was found that one of the main products of this heterogeneous reaction are phthalic acid derivatives, compounds of the paraffin group, and acetophene derivatives.Certain information about heterophase processes occurring in the atmosphere can be obtained by studying the chemical composition and other characteristics of precipitation falling on the Earth's surface in the form of rain or snow. The relevant data are discussed in [71, 72]. In conclusion of this section, we will point to the work [73], which discusses the hypothesis proposed earlier (Zuev et al., 2014) about the possibility of the formation of black carbon nanoparticles in the eruptive column of a volcanic eruption. Other issues of heterophase chemistry are discussed in [74–77].

Chemistry of the ozone layer

In this area, a number of new results have been obtained in the last four years, both in the field of the theory of the ozone layer and in the field of observations of its recovery after depletion at the end of the last century under the influence of anthropogenic factors. Thus, in [78], according to the data of the domestic network of filter ozonometers M-124 and the results of satellite

monitoring, the variability of total ozone in the Arctic in the winter season of 2015/16 was investigated and the development of the first ozone mini-hole in the entire history of observations was established at the end of January 2016. In [79], an overview of the work carried out in the Laboratory of Chemistry and Atmospheric Dynamics of the Central Aerological Observatory on the creation and use of global numerical models of the atmosphere is presented. The created models allow for a wide range of numerical studies, including both temperature and circulation experiments. Among the model works, we will name the work [80], in which, according to the results of five 50-year calculations with the 5th version of the joint climate model of the INM RAS, it was shown that the winter seasons with the El Niño phenomenon are characterized by a higher temperature of the Arctic stratosphere compared to the seasons with La Niña. In [81], the response of the Arctic stratosphere to the El Nino climatic phenomenon was considered, taking into account its Eastern and Central Pacific types for the period 1950–2005. based on regression and composite analysis using calculations of six joint climate models of the CMIP5 project and reanalysis data. In [82], estimates of the chemical destruction of ozone in the winter-spring seasons for the Arctic stratosphere are given on the basis of long-term observations of the vertical distribution of ozone. The features and possible causes of an unusually strong and stable stratospheric polar vortex in the Arctic in the winter season of 2019/20, which led to a record destruction of the ozone layer in recent years, and the dynamic processes associated with this polar vortex are analyzed. These data are supplemented by data from [83], which reports that in the winter-spring of 2019–2020, the most significant ozone anomaly in the Arctic in the entire history of observations was observed. It was caused by an unusually strong and prolonged polar vortex, which caused unprecedented chemical destruction of ozone. The analysis of Aura OMI/MLS data showed that the total ozone content steadily decreased and amounted to 230 DU on March 18 at the Alert point, 222 DU on March 18 in Eureka, 229 DU on March 20 in Tula and 226 DU on March 18 in Resolute. The minimum temperature was 9–10% below normal from December to April in the stratosphere over Tomsk and the Arctic. The paper [84] discusses the question of how quasi-two-year oscillations of the zonal wind in the equatorial stratosphere can affect the interannual changes in the power of the ozone hole in Antarctica. Other information about ozone in Antarctica and the South Seas is contained in [85–87]. The influence of space weather on the properties of the atmosphere is discussed in [88]. It is shown, in particular, that high-energy solar protons have a powerful effect on photochemical processes in the polar regions and, accordingly, on atmospheric circulation and planetary cloud cover. Variations of solar UV radiation simulate the rate of descent of zonal winds in the equatorial stratosphere during a quasi-two-year oscillation and thus control the

total duration of the cycle and, accordingly, variations in the total ozone content in Antarctica. In [89], the effect of various factors on the total ozone content and erythemic UV radiation on the territory of Northern Eurasia for the period from 1979 to 2059 was analyzed using the chemical and climatic model of the INM–RSHU (CCM INM–RSHU). Among the model developments, we will mention the work [90] on the creation of a spectrum of distant ultraviolet radiation from the Sun in the wavelength region responsible for the dissociation of molecular oxygen. In the work [91] describing rocket means of sounding the atmosphere, it was shown that in the altitude range from 25 to 75 km, the temperature and wind speed trends over the Volgograd atmospheric rocket sounding station in 1969–1995 are nonlinear and nonmonotonic at most altitudes. An increase in the values of the range of trend variations of the analyzed parameters was found in the observed period with altitude: temperature – up to 15–19 K in the lower and middle mesosphere, the zonal component of wind speed – up to 15 m/s in the stratopause, the meridional component – up to 10 m/s in the lower mesosphere.

Along with the modeling work, considerable attention has been paid in recent years to observations of ozone content and its variability. As an example, we can cite the work [92], in which, according to satellite data on the total ozone content (TOC) for 1979–2015, the seasonal and long-term variability of the number of positive and negative TOC anomalies for the Earth as a whole, the Northern Hemisphere, Russia and the latitudinal belt to which it belongs was studied. It was found that the long-term variability of the TOC significantly exceeds the seasonal one and is due to the slowest of the tidal fluctuations with a period of 18.6 years. In [93], observations of ozone over Nizhny Novgorod in the winter of 2017–2018 are reported. In [94], the results of ground-based microwave profiles of stratospheric ozone over Moscow in the cold half-years 2014–2015 and 2015–2016 were presented, and the causes of the observed ozone changes in the upper stratosphere were considered. In winter 2014–2015 there was an increased activity of planetary waves, large temperature drops at the beginning of winter and low temperatures from January to March. The polar vortex was shallow and long–lived, in February – March the cold air of the vortex was over Moscow. This led to a strong negative correlation of the measured ozone content with temperature. The highest ozone content at the level of 2 mbar was observed in mid-March. On the contrary, in November – December 2015 with less activity of planetary waves, an intense polar vortex arose, which was completely destroyed by the major final warming in early March 2016. The paper [95] presents the theory of chain processes of the ozonosphere, on the basis of which the lifetime of odd oxygen and the rate of ozone destruction in catalytic cycles are calculated [96–99]. We will finish the section with [100], which discusses the effects of a nuclear explosion on ozone.

Chemical aspects of climate change

The works in this area were related to climate, climate change forecasting, greenhouse gases and related issues. Although the question of the anthropogenic causes of changes in the modern climate is beyond doubt for most climatologists, the question of what happens earlier is an increase in greenhouse gases or an increase in near–surface temperature? This issue has already been discussed (see the 4th section in [1]). Its discussion was continued in [101]. In this work, in numerical experiments with the climate model of the IFA RAS and the conceptual climate model of the climate with a carbon cycle, the phase shift between changes in surface temperature and CO_2 content under external influence in the form of time-in-phase external emissions of carbon dioxide and methane into the atmosphere was investigated. It is found that with a sufficiently large time scale of external influence, changes in CO_2 lag behind the corresponding temperature changes. It should be added to this that (as the authors write) the phase shift between changes in global near-surface temperature and CO_2 content in the atmosphere generally does not characterize cause-and-effect relationships in the Earth system. The issues of climate theory are covered in [102]. Its author – the co–chairman of the Scientific Council of the Russian Academy of Sciences on the Problems of the Earth's Climate, Academician of the Russian Academy of Sciences I.I. Mokhov – analyzes in detail the trends of observed temperature variations, their global and regional features. The paper notes that the increase in global surface temperature is accompanied by a rapid increase in the number of natural disasters, primarily due to hydrological and meteorological anomalies. It is argued that the climatic anomalies of recent years indicate not only an increase in the risk of extreme regional events, but also new processes and phenomena that characterize the achievement of a certain critical level of climate change. According to the results of the analysis of modern climate changes using model estimates taking into account natural and anthropogenic factors, as a result of rapid warming in recent decades, the earth's climate system has reached a regime comparable to the Holocene optimum regime. In [103], the mechanism of natural climate fluctuations in the Arctic with a period of about 60 years was investigated according to a 1200-year preindustrial experiment with the INM-CM5 climate model. It is shown that a quarter of the period preceding the Arctic warming, there is a more intense than usual influx of Atlantic water into the Arctic Ocean, near the coast and the shelf boundary, salinity and density are less than usual. As a result of Atlantic water advection after Arctic warming, the water near the coast and the shelf boundary becomes saltier and heavier, which leads to a weakening of the Atlantic water flow and a change in the oscillation phase. The conclusions are confirmed by the calculation of the generation of temperature, salinity and flow anomalies

for various terms, as well as by the assessment of the contribution of various terms to the change in the phase of oscillations. In [104], the contribution of carbon dioxide and methane emissions from Russia to global climate change was analyzed. It has been shown that taking into account changes in climatic conditions can greatly affect the impact of emissions of various greenhouse gases on the climate system, especially over long time horizons. When making decisions, it should be taken into account that, depending on the planning horizon, the role of natural greenhouse gas flows into the atmosphere from terrestrial ecosystems may change. Currently, in the Russian regions, terrestrial ecosystems, absorbing CO_2 from the atmosphere, contribute to slowing the growth of global temperature, and emitting CH4 into the atmosphere accelerate warming. At the same time, the overall effect of natural flows of these greenhouse gases from Russian regions in modern conditions contributes to slowing warming. The role of this warming-slowing effect increases in the first half of the XXI century, and after reaching the maximum (depending on the scenario of anthropogenic emissions) decreases by the end of the century under all considered scenarios of anthropogenic impacts due to the increase in natural emissions of CH_4 and a decrease in CO_2 uptake by terrestrial ecosystems. In [105] the influence of anthropogenic and natural factors on the climate of the hemisphere was considered. Based on three- component autoregressive models and data from the 19th century. It is estimated in the formation of temperature at different time horizons of the Atlantic multidecade oscillation, the El Nino/Southern oscillation, the Pacific inter-decade oscillation and the Antarctic oscillation. A significant contribution to the temperature trends of the key modes of climatic variability at relatively short intervals lasting within two to three decades is noted – comparable to the contribution of greenhouse gases and even exceeding it. Estimates characterizing the features of polar, middle and tropical latitudes in the Southern (UP) and Northern (SP) hemispheres are compared. According to the estimates obtained at time intervals of half a century or more, the dominant contribution to the formation of temperature trends in different latitudinal zones and for the Earth as a whole is associated with the radiation effect of greenhouse gases in the atmosphere. In [106], the issue of the stability of permafrost methanhydrates was considered. The results of numerical simulation of the thermal regime of the permafrost of Western Siberia (Yamal Peninsula) and the stability zone of methane hydrates over the past 10 thousand years were obtained. Thermobaric conditions of stability and dissociation of continental methane hydrates are obtained. It is shown that relic methane hydrates can currently exist in the permafrost strata of Yamal at depths up to 150 m, which could “survive” the warming in the Holocene and persist at subzero temperatures in the permafrost. In [107], estimates of changes in the frequency of transitions between different phases of processes over the past seven decades

(1950–2019) were obtained. The strongest interannual variations of global near-surface temperature are associated with positive (El Niño phase) and negative (La Niña phase) surface temperature anomalies in the equatorial latitudes of the Pacific Ocean. Significant differences in trends for El Niño and La Niña phenomena of different types characterized by surface temperature anomalies in the equatorial latitudes of the eastern (Niño3) and central (Niño4) regions of the Pacific Ocean have been revealed.In [108], quantitative estimates were obtained of the relationship between intra- and interannual variations in the area of snow cover in the Northern Hemisphere, including in Eurasia and North America, with changes in near-surface temperature based on satellite data and reanalysis data for the period 1979–2020. In [109], quantitative estimates of the contribution of anthropogenic impacts characterized by changes in the radiation effects of greenhouse gases in the atmosphere and key modes of natural climatic variability to the trends of near-surface temperature of different latitudinal zones of the Northern (SP) and Southern hemisphere (UP) at different time horizons were obtained using observational data. The results of the analysis indicate a significant role of changes in the radiation effects of greenhouse gases in the atmosphere in the formation of the trend of global near-surface temperature, which increases with an increase in the time horizon. At the same time, significant differences were noted for the latitudinal zones of the UP and SP associated with the influence of different modes of natural climatic variability. In [110, the influence of methane emissions from cryolithzones in Russia on the global climate was considered. Statistical relationships of their intensity with air temperature, precipitation, the thickness of the seasonally shallow layer and the temperature of permafrost soils have been established. Using the CMIP5 ensemble climate scenario, a forecast of changes in methane emissions in the cryolithozone for the middle of the XXI century was obtained. Using the INM-CM48 model of the Earth system, it is shown that the projected increase in methane emissions by 20 Tg/year will lead to an increase in the average annual global temperature by no more than 0.05 °C. The uncertainty of the estimates obtained is analyzed and an alternative conceptual model of rapid threshold changes in methane emissions is considered. In [111], based on numerical calculations with a global climate model, global and regional climate changes in the Holocene were estimated. According to the results obtained, the current average annual global near–surface temperature in recent decades has exceeded the corresponding values for the previous 10 thousand l., including during the so-called “Holocene optimum” (otherwise, the average Holocene, about 6 thousand l.n.). Global and regional climate changes and changes in the characteristics of the carbon cycle in the last century, according to model calculations (taking into account anthropogenic impacts), differ significantly from changes in previous centuries and millennia, when

natural impacts on the climate system played a key role. The paper [112] evaluates the features of modern rapid climate changes in the Arctic and their consequences based on the results obtained in recent years. In [113], estimates of changes in the frequency of atmospheric blockages were obtained based on CMIP5 ensemble calculations using modern climate models of general circulation using various criteria for detecting atmospheric blockings and different RCP scenarios of anthropogenic impacts for the XXI century. [114] presents the results of climate change modeling in 2015–2100 using the INM-CM5 climate model of the Russian Academy of Sciences. It is shown that in summer it is on the territory of Russia that the temperature of the hottest month can grow faster than the seasonal average temperature. The change in the area of sea ice in the Arctic is considered and it is shown that, according to modeling data, under no scenario does the Arctic Ocean completely free from ice in the 21st century. Are the data presented in [115] analysis of variations in the flux of total solar radiation in the 17–24 cycles of solar activity and their relationship with global climate warming. The influence of galactic cosmic rays and volcanic activity on the climate is considered. It is shown that the Earth's temperature in cycles 17–20 experienced variations in accordance with the course of solar activity without an observed trend: the temperature increased with the increase in solar activity and decreased in solar minima. Global warming began in 1976 in the 21st cycle of solar activity. Taking into account the observed trend in the 21–24 cycles of solar activity, changes in the global temperature of the Earth, as well as in the 17–20 cycles, were associated with cyclic variations in the flux of total solar radiation. Galactic cosmic rays, changing the transparency of the atmosphere against the background of decreases in the flow of total solar radiation, additionally contributed to an increase in temperature minima. Strong volcanic eruptions were accompanied by 1–2 annual temperature drops that did not disrupt the cyclical process of climate change on Earth. In the absence of trends in cosmophysical factors affecting the climate, the process of gradual increase in the average annual temperature of the Earth in the 21–24 cycles of solar activity is explained by an anthropogenic factor. In [116], the change in the equilibrium sensitivity of the INM-CM4-8 climate model to the quadrupling of CO_2 concentration with changes in cloud parameterization in this model is considered. It is shown that the regulation of accounting for various mechanisms of cloud formation and dissipation can lead to a change in the equilibrium sensitivity of the model in the range from 3.6 to 8.1 degrees, which more than half covers the range of variation of this value for modern climate models.

The climate changes mentioned above change not only the environment, but also living conditions. These issues are discussed in [117–120]. In [121], the influence of global warming on the rate of destruction of stratospheric

ozone in catalytic cycles is considered. Other climatic issues are considered in the works [122–132].

References

1. Larin I.K., *Izv.*, *Atmos. and Oceanic Phys*. **55**. 552-561. (2019).
2. Larin I.K., Spasskii A.I., Trofimova E.M., *Russ. J. Phys. Chem. B* . **13**. 256–261. (2019).
3. Vasiliev E.S., Volkov N.D., Karpov G.V., Morozov I.I., Nigmatullin G.V., Umanskii S.Y., Butkovskaya N.I., Saygina E.A., Savilov S.V., *Russ. J. Phys. Chem. B* . **15**. 789–794. (2021).
4. Vasiliev E.S., Karpov G.V., Volkov N.D., Morozov I.I., Savilov S.V., *Russ. J. Phys. Chem. B* . **15**. 228–232. (2021).
5. Vasiliev E.S., Volkov N.D., Karpov G.V., Morozov I.I., Chemical safety science. 3. 78–88. (2019). (in Russian).
6. Fedotov V.K., Kol'tzov N.I., Kinetics and Catalysis. 60. 776–782. (2019.)
7. Nenajdenko V.G., *Russian Chemical Reviews*. 89. 1274–1336. (2020).
8. Krupnov A.A., Pogosbekian M.Y., Kinetics and Catalysis. 60. 164–174. (2019).
9. Denisov E.T., T.G. Denisova, Kinetics and Catalysis 60. 1–7. (2019).
10. Vasil'chuk Yu.K., Budantseva N.A., Vasil'chuk J.Yu., Eremina I.D., Bludushkina L.B., *Vestnik Moskovskogo universiteta. Seriya 5, Geografiya*. 2. 35–43. (2021).(In Russian).
11. Eremina I.D., *Vestnik Moskovskogo universiteta. Seriya 5.Geografiya* 3. 3–10. (2019). (In Russian).
12. . Gorbarenko E.V., Eremina I.D. *Vestnik Moskovskogo universiteta. Seriya 5. Geografiya*. . 90-103 (2022). (In Russian).
13. Filippov S.P., Yaroslavtsev A.B., *Russian Chemical Reviews*. 90. 627-643. (2021).
14. Larin I.K., Belyakova T.I., Messineva N.A., Spasskii A.I., Trofimova E.M., *Russ. J. Phys. Chem. B* . **15**. 795–800. (2021).
15. Larin I.K., Belyakova T.I., Messineva N.A., Spasskii A.I., Trofimova E.M., *Russ. J. Phys. Chem. B* . **14**, 893–898. **(**2020).
16. Chistiakova N.F., Zhuravleva N.N., Andreev O.V., Martyushova A.I., Meteorology i Gydrology. 5. 76–85. (2021).(In Russian).
17. Ionov D.V., Poberovskii A.V., *Russ. Meteorol. Hydrol.* 45. 720–726. (2020).
18. Gruzdev A.N., *Izv.*, *Atmos. and Oceanic Phys*. **55**. 65–72. (2019).
19. Elansky N.F., Golitsyn G.S., Belikov I.B., Skorokhod A.I., Crutzen P.J., Brenninkmeijer C.A.M., *Izv.*, *Atmos. and Oceanic Phys*. **57**. 72–90. (2021).
20. Gruzdev A.N., Elokhov A.S., *Izv.*, *Atmos. and Oceanic Phys*. **57**. 91–103. (2021).
21. Rakitin V.S., Elansky N.F., Skorokhod A.I., Dzhola A.V.. Rakitina A.V., Shilkin A.V., Kirillova N.S., Kazakov A.V., *Izv.*, *Atmos. and Oceanic Phys*. **57**. 116–125. (2021).
22. Bazhenov O.E., Enikov A.V., Sysoev S.M., *Atmos Ocean Opt* . **32**. 686–700. (2019).
23. Elansky N.F., Shilkin A.V., Ponomarev N.A., Zakharova P.V., Kachko M.D., Poliakov T.L., *Izv.*, *Atmos. and Oceanic Phys*. **58**. 80–94. (2022).
24. Ageev B.G., Sapozhnikova V.A., Gruzdev A.N., Golovatskaya E.A., Dukarev E.A., Savchuk D.A., *Atmos Ocean Opt* . **32**. 275–283. (2019).

25. Chesnokova T.Y., A.V. Chentsov, Y.V. Voronina, M.V. Makarova V.I. Zakharov, N.V. Rokotyan, B.Langerock, *Atmos Ocean Opt* . **32.** 378–386. (2019).
26. Gorbarenko E.V., *Russ. Meteorol. Hydrol.* 45. 478–487. (2020).
27. Golubkov G.V., V.L. Bychkov, V.O. Gotovtsev, S.O. Adamson, Yu.A. Djakov, I.D. Rodionov, M.G. Golubkov, *Rus. J. Physical Chemistry B*. **14**. 351–354. (2020).
28. Ivanova A.P., *Russ. Meteorol. Hydrol.* 44. 756–763. (2019).
29. Golovushkin N.A., I.N. Kuznetsova, I.B. Konovalov, M.I. Nahaev, *Atmos Ocean Opt* **33**. P. 267–273. *(*2020)
30. Ageev B.G., Yu.N. Ponomarev, *Atmos Ocean Opt* . **33.** 321–323. (2020).
31. Belan B.D., G.A. Ivlev, T.K. Sklyadneva, *Atmos Ocean Opt* . **33**. 638–644. (2020).
32. Shatalina V.V., N.V. Il'in, E.A. Mareev, Meteorology i Gydrology. № 6. 107–112. (2021). (in Rusian).
33. Shatalina V.V., V.V. Klimenko, E.A. Mareev, *Doklady earth sciences*. **499**. 595–598. (2021).
34. Dementyeva S.O. N.V. Ilin, M.V. Shatalina, E.A. Mareev, *Izv.*, *Atmos. and Oceanic Phys*. **56**. 123–129. (2020).
35. Shatalina V.V., E.A. Mareev, V.V. Klimenko, F.A. Kuterin, K.A. Nikoll, *Radiophysics and quantum electronics*. **62**. 183–191. (2019).
36. Gorchakov G.I., O.I. Datsenko, A.V. Karpov, S.F. R.A. Gushin, I,A. Gorchakova, S.F.Mirsaitov, T.Ya. Ponomareva, *Atmos Ocean Opt* . **34**. 438–442. (2021).
37. Gorchakov G.I., A.V. Karpov, R.A. Gushin, O.I. Datsenko, *Izv.*, *Atmos. and Oceanic Phys*. **57**. 486-494. (2021).
38. Karpov A.V., G.I, Gorchakov, R.A. Gushin, O.I. Datsenko, *Izv.*, *Atmos. and Oceanic Phys*. **57.** 495–503. (2021).
39. Morozov I.I., E.S.Vasiliev, N.D. Volkov *et al. Russ. J. Phys. Chem. B* **16**. 877–882. (2022).
40. Chengxun Y., L. Zhijian, V.L. Bychkov. *et al. Russ. J. Phys. Chem. B* **16**. 955–964. (2022).
41. Miroshnichenko E.A., T.S. Kon'kova, Y.N. Matyushin *et al. Russ. J. Phys. Chem. B* . **16**. 1015–1018. (2022).
42. Zakharov V.V., I.N. Zyuzin, B.L. Korsunskiy *et al. Russ. J. Phys. Chem. B* . **16**. 1038–1043. (2022).
43. Kalashnik M.V. *Izv.*, *Atmos. and Oceanic Phys*. **58**. 529**–**535. (2022).
44. Nerobelov G.M., O. Al-Subari, Y.M. Timofeyev *et al. Izv.*, *Atmos. and Oceanic Phys*. **58**. 494–499. (2022).
45. Ashabokov B.A., L.M. Fedchenko, V.A. Shapovalov et al., *Izv.*, *Atmos. and Oceanic Phys*. **58**. 569–577. (2022).
46. Skorokhod A.I., V.S. Rakitin, N.S. Kirillova *Russ. Meteorol.Hydrol.* **47**. 183–190. (2022).
47. Filei A.A., A.I.Andreev, M.O. Kuchma *et al. Russ. Meteorol. Hydrol.* **47**. 272–280. (2022).
48. Panov D.Y., E.Y.Sakharova. *Russ. Meteorol.Hydrol.* **47.** 473–478.(2022).
49. Malkarova A.M., Meteorology i Gydrology. 7. 5–10. (2022) (in Russian).
50. Kovalev N.A., O.V. Netyagin, I.V. Sazhin *Russ. Meteorol. Hydrol.* **47**. 530–534. (2022).
51. Kuryatnikova N.A., N.S. Malygina, E.Y. Mitrofanova, *Atmos Ocean Opt* **35**. 146–150 (2022).

52. Shikhov A.N., A.V.Chernokulsky, A.A.Sprygin *et al. Atmos Ocean Opt* **35**. 793–801.(2022).
53. Dembelov M.G., Y.B. Bashkuev, *Atmos Ocean Opt* **35**. 359–365. (2022).
54. Golovko V.V., G.A. Zueva, T.I. Kiseleva *Atmos Ocean Opt* **35**. 673–679.(2022).
55. Andreev V.V., M.Y.Arshinov, B.D.Belan *et al. Atmos Ocean Opt*. 35. 741–757. (2022).
56. Aloyan A.E., V.O. Arutyunyan, A.N. Yermakov, *Russ. Meteorol. Hydrol.* 44. 311–316. (2019).
57. Aloyan A.E., A.N. Yermakov, V.O. Arutyunyan, *Russ. J. Phys. Chem. B* **13**. 214–218 (2019).
58. Larin I.K., A.E. Aloyan, A.N. Yermakov, *Russ. J. Phys. Chem. B* **15**. 357–361 (2021).
59. Larin I.K., A.E. Aloyan, A.N. Yermakov, *Russ. J. Phys. Chem. B* **15.** 577–581 **(**2021).
60. Aloyan A.E., V.O. Arutyunyan, A.N. Yermakov, *Izv.*, *Atmos. and Oceanic Phys*. **57**. 104–109 **(**2021).
61. Veres A.I., A.A.V.Ya. Ekaikin, Lipenkov, A.V. Turkev, T.V. Khodger, *Arctic and Antarctic research*. **66**. 482–500 (2020). (in Russian).
62. Rogachev A.S., *Russian Chemical Review*. **88**. 875–900 (2019).
63. Panchenko M.V., M.V. Kabanov, Yu.A. Pzhalagov *et.al*., *Atmos Ocean Opt* . **32**. 703–716 (2019). (in Russian).
64. Larin I.K., T.I. Belyakova, N.A. Messineva, A.I. Spaskii, E.M. Trofimova, Kinetics and Catalysis.62. 245–254. (2021).
65. Larin I.K., A.I. Spaskii, E.M. Trofimova, *Russ. J. Phys. Chem. B* **14**. 781–786 (2020).
66. Yermakov A.N., A.E. Aloyan, V.O. Arutyunyan, *Russ. Meteorol. Hydrol.* 45. 185–192 (2020).
67. Sakerin S.M., L.P. Golobokova, D.M. Kabanov, et al., *Atmos Ocean Opt* .**32.** 511–520 (2019). (in Russian).
68. Yermakov A.N., A.E. Aloyan, V.O. Arutyunyan, *Izv.*, *Atmos. and Oceanic Phys*. **55**. 271 (2019).
69. Zelenov V.V., E.V. Aparina, V.I. Kozlovskiy, I.V. Sulimenkov, D.A. Kardansky, A.E. Nosyrev, *Russ. J. Phys. Chem. B* **13**. 219–224 (2019).
70. Zelenov V.V., E.V. Aparina, *Russ. J. Phys. Chem. B* **15**. 919–927. (2021).
71. Vlasov D.V., I.D. Eremina "Modern trends and prospects for the development of hydrometeorology in Russia." Materials of the III All-Russian Scientific and Practical Conference. Moscow. Irkutsk. 880 (2020). (in Rus).
72. Zavgorodnyaya Yu.A., O.B. Popovicheva, V.O. Kobelev, D.P. Starodymova, V.P. Shevchenko, N.S. Kasimov, *Arctic and Antarctic research*. **67**. 261 (2021). (in Rus).
73. Beresnev S.A., M.S. Vasilieva, *Atmos Ocean Opt* .**33**. 531–538. (2020).
74. Kozlov S.N., B.E. Zhestkov *Russ. J. Phys. Chem. B* . **16**. 1030–1037. (2022).
75. Shilin A.G., A.S.Shilina, Y.V. Andreev *et al. Russ. Meteorol.Hydrol.* **47**. 542–547. (2022).
76. Gubanova D.P., O.G. Chkhetiani, T.M. Kuderina *et al. Atmos Ocean Opt* **35**. 680–690. (2022).
77. Babushkin P.A., G.G. Matvienko, V.K. Oshlakov, *Atmos Ocean Opt* . **35**. 485–489. (2022).

78. Nikiforova M.P., P.N. Vargin, A.M. Zvyagintzev, *Russ. Meteorol. Hydrol.* 44. 23–32 (2019).
79. Krivolutsky A.A., T.Y. V'yushkova, L.A. Cherepanova, M.V. Banin, A.I. Repnev, A.A. Kukoleva, *Russ. Meteorol. Hydrol.* 46. 596–605 (2021).
80. Vargin P.N., M.A. Kolennikova, S.V. Kostrykin, E.M. Volodin, *Russ. Meteorol. Hydrol.* 46. 1–9. (2021).
81. Kolennikova M.A., P.N. Vargin, D.Yu. Gushina, *Russ. Meteorol. Hydrol.* 46. 351–364. (2021).
82. Tsvetkova N.D., P.N. Vargin, A.N. Lukyanov, B.M. Kiryushov, V.A. Yushkov, V.U. Khattatov, *Russ. Meteorol. Hydrol.* 46. 606–615. (2021).
83. Bazhenov O.E., *Optika Atmosfery i Okeana*. **35**. 390–396 (2021). (in Rus).
84. Gabis I.P., *Russ. Meteorol. Hydrol.* 46. 287–294. (2021).
85. Vargin P.N., M.P. Nikiforova, A.M. Zvyagintzev, *Russ. Meteorol. Hydrol.* 45. 63–73. (2020).
86. Sibir E.E., V.F. Radionov, E.N. Rusina, *Russ. Meteorol. Hydrol.* 45. 161–168. (2020).
87. Smyshlyaev S.P., P.F. Blakitnaya, M.A. Motsakov, *Russ. Meteorol. Hydrol.* 45. 153–160. (2020).
88. Troshichev O.A., I.P. Gabis, A.A. Krivolutsky, *Arctic and Antarctic Research*. **67**. 177–207. (2021). (in Rus).
89. Pastukhova A.S., N.E. Chubarova, Y.Y. Zhdanova, V.Ya. Galin, S.P. Smyshlyaev, *Izv.*, *Atmos. and Oceanic Phys*. **55**. 242–250. (2019).
90. Nusinov A.A., T.V. Kazachevskaya, V.V. Katyushina, *Geomagnetism and aeronomy*. 59. 265–271. (2019).
91. Kuminov A.A., V.A. Yushkov, Y.N. Gvozdev, O.V. Shtyrkov, A.D. Lykov, N.V. Belugin, *Russ. Meteorol. Hydrol.* 46. 571–578. (2021).
92. Dvoretskaya I.V., G.M. Kruchenitskii, K.A. Statnikov, *Russ. Meteorol. Hydrol.* 45. 398–402. (2020).
93. Belikovich M.V., V.G. Ryskin, M. Yu. Kulikov, A.A.Krasil'nikov, A.A. Shvetsov, A.M. Feygin, Radiophysics and Quantum Electronics.63. 191-206 (2020).
94. Kropotkina E.P., S.B. Rosanov, A.N. Lukin, A.N.Ignat'ev, *Geomagnetism and aeronomy*. **59**. 212–220. (2019).
95. Larin I.K., *Russ. J. Phys. Chem. B* . **13**. 867–873. (2019).
96. Larin I.K., *Russ. J. Phys. Chem. B* . **38**. 65–71. (2019). (in Rus).
97. Larin I.K., *Russ. J. Phys. Chem. B* . **39**. 85–92. (2020). (in Rus).
98. Larin I.K., *Izv.*, *Atmos. and Oceanic Phys*. **58**. 150–157. (2022).
99. Larin I.K., *Izv.*, *Atmos. and Oceanic Phys*. **56**. 165–172. (2020).
100. V.B.Kashkin, R.V. Odintzov, T.V. Rubleva, *Optika Atmosfery i Okeana*. **35**. 212–216. (2022). (inRus).
101. Muryshev K.E., A.V. Eliseev, S.N., Denisov, I.I. Mokhov, Arzhanov M.M., A.V. Timazhev, *Izv.*, *Atmos. and Oceanic Phys*. **55**. 235–241. (2019).
102. Mokhov I.I. Climate change: causes, risks, consequences, problems of adaptation and regulation, Collection of abstracts of the All-Union Conference. Moscow, November 26, 2019. 180 p.
103. Volodin E.M. CITES '2019. International Youth School and Conference on Computing and Information Technologies for Environmental Sciences. 2019. P. 39–41 (in Rus).
104. Denisov S.N., A.V. Eliseev, I.I. Mokhov, Doklady earth sciences. 488. 1066–1071. (2019).

105. Mokhov I.I., D.A. Smirnov, *Izv.*, *Atmos. and Oceanic Phys*. **58**. 131–139. (2022).
106. Arzhanov M.M., V.V. Malakhova, I.I. Mokhov, M R. Parfenova, CITES '2019. International Youth School and Conference on Computing and Information Technologies for Environmental Sciences. 012019 (2019)
107. Mokhov I.I ., *Izv.*, *Atmos. and Oceanic Phys*. **58**. 2. (2022).
108. Mokhov I.I., M.P. Parfenova, *Russ. Meteorol. Hydrol.* . 47. 98–106. (2022).
109. Mokhov I.I., D.A. Smirnov, Doklady earth sciences. 503. 114–118. (2022).
110. Anisimov O.A., A.S. Zimov, E.M. Volodin, S.A. Lavrov, *Russ. Meteorol. Hydrol.* 45. 377–385. (2020).
111. Mokhov I.I., A.V. Eliseev, V.V. Guryanov, Doklady earth sciences. 490. 23–27 (2020).
112. Mokhov I.I., *Arctic and Antarctic research* **66**. 446–462. (2020). (in Rus).
113. Mokhov I.I., A.V.Timazhev, *Russ. Meteorol. Hydrol.* 44. 369–377. (2019).
114. Volodin E.M., A.S. Gritzun, *Izv.*, *Atmos. and Oceanic Phys*. **56**. 218–228. (2020).
115. Biktash L.Z., *Geomagnetism and aeronomy*. **59**. 368–373. (2019).
116. Volodin E.M., *Izv.*, *Atmos. and Oceanic Phys*. **57**. 127 (2021).
117. Klueva M.V., Y.L. Shkol'nik, Yu.L. Rudakova, T.V. Pavlova, V.M. Kattsov, Meteorology i Gydrology.№ 6.47–60. (2020). (inRus).
118. Torzhkov I.O., E.A. Kushner, A.V. Konstantinov, T.S. Koroleva, S.V. Efimov, Y.L. Shkolnik, Meteorology i Gydrology. 44. 180–186. (2019). (in Rus).
119. Golitzen G.S., A.A. Vasiliev, Meteorology i Gydrology. 9-12. (2019). (in Rus).
120. Ginzburg A.S., S.A. Dokukin, *Izv.*, *Atmos. and Oceanic Phys*. **57**. 47–59. (2021).
121. Larin I.K., *Russ. J. Phys. Chem. B* . **39**. 344–350. (2020). (in Rus).
122. Ginzburg A.S., G.A. Alexandrov, A.V. Chernokulsky, *Izv.*, *Atmos. and Oceanic Phys*. **58**. 536–544. (2022).
123. Mokhov I.I., A.V. Timazhev, *Izv.*, *Atmos. and Oceanic Phys*. **58**. 545–552. (2022)
124. Kulikova I.A., E.N. Kruglova, V.M. Khan, *Russ. Meteorol. Hydrol.* **47**. 1–13.(2022).
125. Ryzhakova N.K., N.S. Rogova, E.A. Pokrovskaya *et al. Izv.*, *Atmos. and Oceanic Phys*. **58**. 553–559. (2022).
126. Lysenko S.A., V.F. Loginov, P.O. Zaiko *Russ. Meteorol.Hydrol.* **47**. 41–49. (2022).
127. Volodin E.M. *Russ. Meteorol.Hydrol.* **47**. 327–333. (2022).
128. Porfiriev B.N., A.Yu. Kolpakov, D.O. Eliseev, et al., Meteorology i Gydrology. 5. 96–106. (2022) (in Rus).
129. Semenov S.M. , *Russ. Meteorol.Hydrol.* **47**. 725–734. (2022).
130. Sirin A.A., M.A. Medvedeva, V.Y. Itkin *et al. Russ. Meteorol. Hydrol.* **47.** 748–757. (2022).
131. Zinchenko A.V., V.I. Privalov, V.M. Ivakhov *et al. Russ. Meteorol.Hydrol.* **47**. 767–780.
132. Denisov S.N., A.V. Eliseev, I.I. Mokhov *Russ. Meteorol. Hydrol.* **47**. 735–747. (2022).

Atmospheric Electricity

E.A. Mareev[1], *V.N. Stasenko*[2], *M.V. Shatalina*[1]
[1] Institute of Applied Physics RAS
[2] Institute of Applied Geophysics

Introduction

This work presents an overview of Russian studies on the atmospheric electricity in 2019–2022. In recent years, many areas of fair-weather electricity physics, the processes in the clouds and the formation of their electrical structure, the relationship of thunderstorm activity and other dangerous weather phenomena are developing. Experimental studies on atmospheric electricity in Russian scientific centers supply a lot of data and make a significant contribution to the improvement of theoretical and numerical models of various electrical processes in the atmosphere. Research into the physics of lightning, both experimental and theoretical, brings new understanding to the physics of the development of lightning leader discharges. Investigations of high-energy processes, such as X-ray and gamma outbreaks during thunderstorms, continue to develop. Much attention is paid to observations of thunderstorm events with the help of lightning direction finding systems, as well as to the analysis of data from global systems. In more detail the main results in each of the areas are given in the relevant sections of this article.

Fair weather electricity

In 2019–2022 the study of fair-weather electricity in different regions of Russia continued, in particular, much attention is paid to the diurnal and seasonal variations of the electric field. Various effects influencing the behavior of the atmospheric electric field of fair weather are experimentally investigated in urban and rural conditions.

It is known that long-term ground-based observations of variations in atmospheric electricity parameters are an important experimental basis for modern research. Variations in the electric field in the surface layer of the atmosphere during the day are due to both global and local factors. The paper [1] presents the results of the analysis of the relationship between the duirnal variation of solar wind characteristics (solar wind speed, ion concentration) and the electric field strength of the surface atmosphere. To measure diurnal variations in the electric field strength of the atmosphere in this work, a hardware-software complex was used to measure and transmit to the central server the values of the electric field strength of the atmosphere at the Cheget peak. Monitoring in high-mountainous regions is characterized by the fact

that the anthropogenic component in the formation of the electric field of the atmosphere is practically excluded. In [2, 3] the data of long-term observations of the elements of atmospheric electricity in the Elbrus region are presented. The global representativeness of the electric field measurement data has been established. Observation points in the high-mountain zone are recommended for monitoring the electric field of the atmosphere at the global and regional levels. It is shown [3] that the local variations are caused by electric field disturbances caused by the space charge near the earth's surface due to the electrode effect and the influence of turbulent mixing. Analytical solutions of the equation for the total electric current in the region of the electrode effect are obtained and investigated.

In order to separate global and local effects of atmospheric electricity, analyzes of fair-weather electric field data were performed in Nizhny Novgorod [4] and Tomsk [5]. It is shown that diurnal variations in the electric field potential gradient are characterized by continental-type oscillations with a double maximum and minimum. Diurnal variations in the fair-weather atmospheric electric field for different seasons and weekdays (working days and weekends) in urban conditions were studied. The highest values of the field amplitude are reached in the winter period. The field-intensity maximum in the first half of the day is characteristic of the urban environment and shows that local effects associated with the presence of aerosol particles in the air significantly contribute to the formation of diurnal variation, especially in summer [4]. Estimates of the relationship between the daily and seasonal variability of the potential gradient in Tomsk and the variability of some geophysical quantities are obtained. It is shown that the share of the contribution of various predictors to the variability of the potential gradient, as well as the direction of their correlation changes during the day [5, 6].

Much attention is paid to the effect of atmospheric aerosols on the electric field of the atmosphere measured on the earth's surface. In [7] the influence of emissions from open pit mining is investigated. It has been demonstrated that intense dust formation and the associated electrification of aerosol particles of different sizes lead to the accumulation of an excess space charge in the surface layer of the atmosphere, which contributes to the formation of increased values of the electric field near the earth's surface. The average value of the electric field strength was 600–700 V/m, which exceeds by an order of magnitude the results of measurements carried out at such heights by other researchers in undisturbed weather conditions.

In recent years, theoretical studies of the atmospheric electric field in the surface layer have become more active. A mathematical model of the mechanism of generation of diurnal variations of the electric field in a turbulent surface layer is constructed. The dependence of the phase shift of the oscillations of the surface electric field relative to the variations of the total current

in the atmosphere on the degree of turbulent mixing has been studied [8]. An electrodynamic model of a nonstationary turbulent-convective prism layer is developed in the electrode effect approximation. It has been demonstrated that in an aerosol-free atmosphere, the time to establish a steady state in the electrode layer is approximately 5 minutes, for the classical layer (the characteristic height is about 4–5 m), and in a turbulent one, approximately 15 minutes. (height about 10 m). In the case of strong turbulent mixing, the scale of distribution of electrical quantities increases to hundreds of meters. [9]

In the papers [10–12] consider a quasi-stationary approximation for turbulent electrical processes in the atmospheric boundary layer. The results of theoretical modeling are compared with various natural data on the measurement of the electric field and current. In [10] a three-dimensional model is used to study the space-time statistical features of variations in the atmospheric electric field and space charge. The model is a combination of large-eddy simulation supplemented with a subgrid kinematic model for scalar and the three-dimensional Poisson equation for the electric potential. It is shown that the cross-correlation of electric field at spatially separated points located on one straight line near the earth's surface decreases with increasing distance with a characteristic scale of a few tens meters and has a dependence on the angle between this line and the direction of the wind. Mean large-scale horizontal electric field defined through the position and amplitude of the potential extrema at the same height depends on height non-monotonically having a maximum value of about 5 V/m. Scaling exponents of structure functions for electric field variations are found to be significantly larger than those for space charge variations.

Turbulent electrical processes in the atmospheric boundary layer and their detection by a horizontal passive annular antenna acting as a collector of atmospheric electric current are studied in electrostatic and quasi-stationary approximations [11, 12]. On the basis of eddy-resolving modeling, variations of electrical variables are calculated, spatial correlation functions and spectral density of fluctuations of the atmospheric current density components are estimated, as well as the response of the current in the collector to local turbulent perturbations of the conduction current density and the instantaneous change in the global potential difference between the ionosphere and the earth's surface. Based on the simulation results, an estimate was obtained of the ratio of the density of the total vertical atmospheric electric current and the conduction current density at the antenna installation height, which can be used to extrapolate the results of ground-based measurements beyond the atmospheric boundary layer [11]. Relationships for a horizontal ring passive antenna used as a collector for long-term observatory observations of atmospheric electric current density are studied analytically and numerically. In the electrostatic approximation, the spatial distributions of the potential and the

electric field are determined depending on the geometric characteristics of the antenna located in a uniform atmospheric electric field, and the parameters of the motion of atmospheric ions in its vicinity are calculated. The dependence of the deposition time of atmospheric ions with a given mobility onto the collector is established as a function of the impact parameter and the initial height determined by this parameter. The results of direct observations of the atmospheric electric current density by the collector are compared with the results of synchronous observations of the atmospheric electric field strength and electrical conductivity in the surface layer [12].

In [13] method for non-contact monitoring of geological inhomogeneities and zones of geodynamic processes from the earth's surface by analyzing the results of measuring the electric field in the surface layer is proposed. Such geological inhomogeneities are characterized by excessive discharge of soil radon into the atmosphere, which is the main cause of air ionization in the surface layer, which leads to a reverse electrode effect, which is revealed in the analysis of electric field data.

Anomalies of the electric field potential gradient have been observed in the near-ground air before earthquakes in different regions of the world. Such anomalies are likely caused by radon air ionization. The impact of surface electric field as earthquakes precursor was estimated according to continuous observations of the electric field in Kamchatka in 1997–2002 [14].

Global electric circuit

The concept of a global electrical circuit (GEC) became a fundamental idea atmospheric electricity researches, since it integrates all electrical processes occurring in the atmosphere into a single concept. In recent years, interest in the study of GEC has gradually increased. Much attention is currently being paid to the numerical simulation of the GEC and its relationship with other global processes.

The papers [15–17] investigate certain aspects of numerical models of the GEC and its elements. In [15] the consistent inclusion of sources of the global electrical circuit of ionospheric and magnetospheric nature into its distributed numerical models is discussed. It is shown that the most natural approach to such an inclusion is to introduce into the boundary conditions at the outer boundary of the model atmosphere the corresponding perturbation of the potential specified up to an unknown constant. The work [16] is devoted to effects on vertical charge distribution and storage of extensive layer clouds in the GEC. Calculations and measurements show the upper cloud boundary charge is usually positive, the cloud interior positive and the lower cloud boundary negative, with the upper charge density larger, but of the same magnitude ($\sim nCm^{-2}$) as cloud base. Globally, the total positive charge stored

by layer clouds is approximately 10^5 C, which, combined with the positive charge in the atmospheric column above the cloud up to the ionosphere, balances the total negative surface charge of the fair-weather regions. The description of global electric circuit (GEC) generators in continuous numerical models is analysed and discussed [17]. As in modern three-dimensional GEC models the formal generalisation of voltage-source thunderstorms turns out to be difficult to implement, two alternative approaches involving the replacement of voltage-source generators with equivalent current-source generators are developed.

A review of works on the influence of electric generators is considered. acting at ionospheric and magnetospheric heights on electric fields in the surface layer. Based on the solution of theoretical problems, estimates of these fields are given, both for stationary and non-stationary cases, the signal transmitted down to the earth's surface depends on the frequency. The most effective ionospheric electric fields penetrate into the surface in the case of low frequencies (quasi-stationary case). At the same time, high-frequency fields penetrate into the surface layer with an efficiency of 1% of the value of quasi-stationary fields [18]

The papers [19–23] are devoted to study of the variations of the GEC and their connections to climate and geophysical parameters. The diurnal variation of the GEC is simulated using the Weather Research and Forecasting model by estimating contributions of grid columns to the ionospheric potential (IP) [19]. The model daily variation of IP demonstrates stable seasonal trends. The chosen parametrization of IP and modelling approach make it possible to obtain a good agreement with the experimentally observed values. Contributions of different land and ocean regions to the diurnal variation of the global electric circuit are investigated in [20] and [21]. The model predicts that contributions from land regions have maxima at about 14:00–18:00 local time (LT), whereas contributions from oceans have maxima at about 2:00–6:00 LT, and different ocean regions show nearly the same relative diurnal variation. It is remarkable that contributions from ocean regions with many islands (Maritime Continent and Middle America) have maxima at both 14:00–18:00 and 2:00–6:00 LT.

Considering that the El Ni˜no – Southern Oscillation (ENSO) can be quantitatively characterized by sea surface temperatures (SSTs) in the Ni˜no 3.4 region, this allowed us to identify and study in detail the effect of ENSO on regional contributions to the GEC [21]. The simulations have shown that contributions to the GEC from the land and oceanic parts of the Earth's surface respond oppositely to the ENSO cycle. The oceanic contribution is positively correlated with the Ni˜no 3.4 SST, largely owing to increases in convection over the Pacific Ocean. In contrast to the oceans, the land contribution shows a negative correlation with ENSO due to decreases in

convection over the Maritime Continent and South America. The observed correlations are statistically significant and are clearly seen on the decadal timescale; at the same time contributions to the IP for individual years do not always clearly reflect the corresponding Ni˜no 3.4 SST anomalies. Further analysis shows that anomalies in the Niño 3.4 sea surface temperature, which characterize the ENSO phase, and anomalies in the relative IP are positively correlated at 9:00–15:00 UTC and negatively correlated at 18:00–23:00 UTC. Electric field measurements at Vostok station in Antarctica reveal that the ENSO has a statistically significant effect on the global electric circuit, as earlier predicted by simulations. Analysis of 10 October-February periods during 2006–2016 indicates that the shape of the diurnal variation of the surface electric field is significantly different for El Niño and La Niña years, with an especially pronounced deviation during the super El Niño of 2015/16. Simulations with the Weather Research and Forecasting model imply that the observed patterns are the result of changes in the global distribution of electrified clouds over the Pacific Ocean, Maritime Continent, and South America during ENSO events [23].

Also, in recent years, experimental work has been carried out to study individual elements of the GEC. In [24] a tethered balloon equipped with an instrumented platform was used to examine the altitude distribution of principal quantities of the lowest atmospheric region of the GEC, radon volumetric activity, and aerosol particles concentration. Altitude soundings covered approximately 0.5 km of the lowest atmosphere and were accompanied by simultaneous ground-based measurements. This method of spaced observations allowed us to analyze the spatial and temporal changes in electrical quantities of the atmospheric boundary layer (ABL) more deeply than was possible before. Estimates show the significant contribution of the ABL to the GEC, which must be taken into account when considering it. The development of an atmospheric electricity-monitoring network stimulates research into the relationship between the GEC and environmental conditions is presented in [25].

Electric processes in clouds

Theoretical and experimental studies of electrical processes in clouds are an important part of atmospheric electricity research. The study of electrical processes in clouds covers a wide range of tasks, including theoretical and experimental studies of the emergence and evolution of convective systems, modeling and forecasting the development of thunderclouds, searching for correlations between recorded meteorological data and observed lightning activity, and the influence of cloud microphysics on observed electrical parameters.

The prediction of thunderstorm events using numerical mesoscale models is one of the most important practical applications for modeling electrical processes in clouds. A description of a regional system for short-term forecasting of dangerous convective phenomena based on the WRF-ARW model is presented in [26]. A method for predicting dangerous convective phenomena based on the analysis of the calculated spatial and temporal distributions of the radar reflectivity of the phenomenon and their comparison with characteristic parameters is proposed. The method was verified using the data of the World Wide Lightning Location Network (WWLLN) lightning direction finding network and field measurements of the quasi-static electric field.

Several works are devoted to numerical model of a convective cloud in various regions. In [27] a three-dimensional model of a convective cloud considering electrical processes is presented. A new important aspects of the electric charge mechanism and field formation in clouds were investigated. The calculations of electric fields generated by point and spatially extended charge sources, taking into account jumps in electrical conductivity at the "plane-parallel cloud–free atmosphere" boundary both in the stationary and non-stationary cases are investigated in [28]. Asymptotic formulas are obtained that make it possible to calculate the electric field strengths in the free atmosphere as a function of the distance to the source.

Simultaneous measurements of the brightness temperature and short-period electric field fluctuations were carried out to reveal possible connections between the electrification rate and turbulence intensity in clouds. Detailed statistical characteristics of brightness temperature fluctuations and short-period electric field fluctuations are obtained for the first time for the indicated types of events. It is shown that measured spectral densities of the atmosphere brightness temperature and electric field fluctuations correspond well enough in the considered frequency range to the results of presented theoretical consideration [29]. Microwave diagnostics of discharges arising in an artificial cloud of charged water droplets, which simulates the environment of thunderclouds, has been developed and created. The attenuation of probing microwave radiation with a wavelength of 8 mm passing through an artificial electrified cloud was measured with a time resolution of 10 ns. With the help of the created microwave diagnostics, the temporal characteristics of intracloud discharges were studied [30]. In [31] some processes of atmospheric electricity associated with water microdroplets in the atmosphere are analyzed. It is shown that microdroplets acquire a charge in the process of growth, and the loss of charge by microdroplets, which occurs at the lower boundary of the cumulus cloud, leads to the development of a breakdown in the form of lightning and is accompanied by a rapid (within minutes) aggregation of cumulus cloud microdroplets into raindrops.

Based on the MRL-5 and LS8000 data on the development of 100 clouds, a layout of a physical-statistical empirical model for the development of lightning activity in convective clouds was developed. The model can be used to verify numerical models and develop new methods for forecasting and diagnosing hazardous weather phenomena associated with convective clouds [32]. The development of a supercell cloud that existed for more than 20 hours on August 19, 2015 was studied. An analysis of the Doppler and polarimetric characteristics made it possible to identify a region of strong convergence characteristic of a tornado [33, 34]. [33] The evolution of a convective cloud in the North-West of Russia (St. Petersburg) has been calculated. The spatio-temporal distribution of the main characteristics of the cloud, precipitation and associated hazardous weather phenomena depending on the specified parameter is obtained. The results of model calculations for the case of high initial heat fluxes are in satisfactory agreement with the data of field measurements [35].

Data on the dynamics of the electric field strength and space charge of strong thunderstorms in different regions of the world are investigated. The data were obtained from the results of modeling using a numerical three-dimensional non-stationary model of a convective cloud developed at the MGO A. I. Voeikova. The multilayer charge structure of the cloud with thin layers of "shielding" charges is reproduced, the corresponding structure of the electric field strength for each of the stages of electrization is presented. [36] A comparison of thundercloud characteristics in different regions of the world was conducted. The clouds studied developed in India, China and in two regions of Russia. The statistical characteristics of the clouds were tabulated from radar scans and correlated with lightning observations. Thunderclouds in India differ significantly from those observed in other regions. The relationships among lightning strike frequency, supercooled cloud volume, and precipitation intensity were analyzed. In most cases, high correlation was observed between lightning strike frequency and supercooled volume [37, 38].

Physics of lightning

Research into the physics of lightning in Russia, both experimental and theoretical, brings new understanding to the physics of the development of lightning leader discharges. A computational model of high-current pulsed arc discharge in air is proposed in [39]. This is, in general, a 2D model which takes into account the gas dynamics of the discharge channel, real air thermodynamics in a wide range of pressures and temperatures, the electrodynamics of the discharge including the pinch effect, and radiation. The 1D version of the model is tested and verified on several numerical and experimental works reported recently. It is concluded that low and moderate current discharges are satisfactorily described with the model. The model was then

applied to simulate the electric discharge in air for the currents 1–250 kA and characteristic rise times in 13–25 μs, and the results of the calculations were compared with experimental ones. It was concluded that most characteristics of the discharge are predicted well.

In a series of papers [40–45] a numerical model for the development of a lightning discharge has been developed. The morphology and electrical parameters of the calculated discharge tree of the incipient model lightning leader agree with the modern data on the lightning-discharge development. A numerical model with physical timing and grid spacing of 3 m is applied to studying the progression (including stepping and branching) of negative lightning stepped leader. The asymmetry between positive and negative streamers is taken into account via using polarity-dependent initiation and propagation field thresholds. The stepped nature of negative leader is confirmed to be caused by this asymmetry[40]. A small-scale transport model of the electric-discharge tree formation and analyze its implementation for a characteristic case of the thundercloud conditions. The following innovative features of the model can be emphasized: no connection to the spatial grid, high spatiotemporal resolution, and allowance for the asymmetry of the development of the positive and negative streamers and the time evolution of the discharge-channel parameters. The criterion of the streamer-to-leader transition, which is used in this work, is formulated in terms of the channel temperature and is based on the well-known mechanism of ionization-overheating instability, which is universal for the spark discharge [41,42]. The noise-induced kinetic transition in two-component environment where the interacting components have contrasting lifetimes and diffusion coefficients is considered. The considered system is studied by the tools of directed percolation [43]. It is shown that the dielectric strength of air falls noticeably compared to its conventional value. The results of the study can be important to solve the problems of initiation and propagation of lightning discharges, blue starters, and blue jets [44].

In [46–49] the process of formation of downward lightning and the orientation of the channel of the downward leader, which are necessary for solving applied problems in the field of lightning protection, are considered in detail. It is shown that it is necessary to take into account the mechanism of the formation of a bipolar leader in the electric field of a thundercloud, in which the thunderstorm cell cannot be considered as a conducting charged electrode. An algorithm is proposed for calculating the height of the lightning orientation, the charge per unit length of its channel, and the contraction radius, based on the value of the current of the main stage. A structure of field studies of lightning is proposed, which makes it possible to accumulate the required statistics of its currents for a foreseeable period at real material costs. The necessity of studying the mechanism of competing development of coun-

ter discharges from ground electrodes is proved, and their method is proposed. The specificity of the development of a counter-discharge from a grounded electrode in the field of a negative stepped lightning leader has been established. It is shown that high voltage control pulses are effective only when acting directly on the counter leader. Analytical expressions are obtained for estimating the conditions for starting a counter-discharge directly in the streamer form, bypassing the stage of a non-stationary ultracorona, and also for determining the amplitude of the control pulse capable of exciting ascending lightning from an electrode of a given height in an atmosphere free from the ultracorona charge. It has been experimentally proven that the consequences of the impact of such impulses are a delay in the formation of a counter leader, but not its stimulation. The reason for the decrease in the efficiency of lightning rods of early streamer initiation compared to traditional ones of the same height has been established.

In 2019–2022, studies of the formation of a lightning leader discharge initiation were continued and developed. In the streamer coronas of the negative leaders of long laboratory sparks, localized plasma formations called "space leaders" were observed. In [50], the mechanism of formation of local plasma formations, collectively referred to as "hot spots", capable of initiating a volume leader, was discussed. The formation of a positive streamer in the vicinity of charged needle-like ice hydrometeors in an external electric field simulating the field of a thundercloud is analyzed. The results of numerical simulation of a streamer discharge are presented, taking into account the dielectric polarization and ice conductivity. The charge values required for this are within the range of values measured in precipitation [51]. A simplified and obvious electro technique model of the electric field enhancement in front of the propagating gas-discharge plasma channel is presented. A theory, developed some time ago by Yakovlenko, is criticized proving that a displacement of the electric field due to the plasma polarization behind the flat channel front is sufficient for the field enhancement ahead of the front. Arguing with this opinion, it is shown, in terms of the developed electro technique model, that for a significant field enhancement, as is known long ago, the cross-sectional area of the channel should be much less than that of the gas-discharge gap. The polarization self-acceleration of electrons is discussed [52]. The streamer zone of positive leader during the breakthrough phase of long sparks was experimentally investigated with two methods: is the analysis of streamer-zone images obtained with a high-speed framing camera with image enhancement and the microwave probing, which was applied to long sparks for the first time. Both methods are based on the assumption of constancy of electric field and similarity of all streamers inside the streamer zone. The overall results of this study are generally consistent with this assumption [53].

In the work [54], which is aimed at revealing the genesis of unusual plasma formations (UPFs) in artificial clouds of charged water droplets, the two UPFs were presented that occurred inside the initial corona streamer burst of positive polarity emitted from the grounded plane, prior to the formation (or in the absence) of associated hot leader channel. Occurrence of UPFs may be a necessary component of the lightning initiation process. UPFs can occur inside the initial corona streamer burst, before the development (or in the absence) of hot leader channel. UPFs contain hot channel segments that are formed, possibly via the thermal-ionizational instability, on a time scale of 1 μs or less and occur in the vicinity of cloud boundary, where the electric field is highest, as this boundary is penetrated by the streamer burst.

High altitude discharges

Transient luminous events (TLEs) such as sprites, blue jets and elves have been studied intensively during the last three decades, and much is now known of their properties. The study of these high-altitude discharges by Russian scientists continues quite actively. Satellite observations, laboratory and numerical simulations are being carried out. The global distribution of sprites based on the new parameterization and WWLLN is studied in [55]. It is shown that on average, 870 nighttime sprites per twenty-four hours can be initiated globally, 41.4% of them over land and 58.6% over ocean. The annual dynamics of the number of sprites over land and ocean is investigated, revealing the maximum number of events in August and the minimum in January and February.

In [56] the various types of TLEs, including recently discovered dancing sprites, gnomes, ultraviolet atmospheric flashes and other effects, are reviewed. The sprite initiation, visible evolution, streamer structure, and their relationship with intra-cloud process are discussed. A few analytical results are discussed, which have been recently derived from simple physical models of the TLEs phenomena. Authors focus their attention on the properties of ultraviolet flashes in the mesosphere, which have been observed onboard Russian microsatellites “Universitetsky-Tanyana” and “Vernov.” Such a kind of optical flash is referred to as a transient atmospheric event, which differs from the TLEs in optical energy, duration and other parameters.

Laboratory research of high-altitude discharges is a rather complex and non-trivial task. The most important factor determining the dynamics and structure of high-altitude discharges is the presence of a significant difference in atmospheric pressure along their length. At the Institute of Applied Physics RAS (Nizhny Novgorod), the “Sprite” experimental setup was created. It makes possible to form an extended neutral gas concentration gradient and ignite a large-scale electric discharge in it. The paper [57] presents the results

of laboratory experiments simulating some properties of high-altitude discharges, primarily sprites and giant jets. The similarity of laboratory and full-scale discharges is shown, physical problems and possible ways to solve them by methods of limited laboratory modeling are indicated.

The influence of the electrode material (aluminum and stainless steel) during the formation of mini-jets on the color of a repetitively pulsed diffuse discharge in air, nitrogen, and argon has been studied. It is shown that the color of the discharge plasma in the mini-jet region corresponds to the color of high-altitude atmospheric discharges (red sprites and blue jets) and differs from the color of diffuse discharges in air and nitrogen at the same pressure [58].

High-energy phenomena in the Earth's atmosphere

The study of high-energy phenomena in the Earth's atmosphere is a young and rapidly developing branch of atmospheric physics, closely related to the study of high-altitude discharges. The phenomena of the occurrence of energetic elementary particle fluxes in thunderclouds are divided into two classes, the relationship and interrelationship of which remains a debatable issue: gamma-ray flashes of terrestrial origin (terrestrial gamma-ray flashes, TGF) and ground-level thunderstorm increases in the flux of energetic particles (thunderstorm ground enhancements, TGE). Relativistic runaway electron avalanches (RREA) occurring in thunderstorm large-scale electric fields are one of the sources of atmospheric gamma radiation. Relativistic feedback is the generation of RREAs by positrons or backscattered gamma rays of the previously produced RREAs. In strong electric fields, relativistic feedback can make RREAs self-sustainable that hypothetically can cause a terrestrial gamma-ray flash (TGF). The work [59] introduces a kinetic approach to study the positron relativistic feedback, which is predominant for the directly observed conditions within thunderstorms. The criterion for self-sustaining production of RREAs by the positron feedback in thunderstorms is derived. It is shown that the derived conditions of self-sustainable RREA development are not achieved for the parameters of electric field observed in real thunderclouds.

The study of high-energy atmospheric phenomena requires an analysis of data on the distribution of cloud particles and the electrical structure formed by them. In [60] information on meteorological conditions for energetic emission from thunderclouds, obtained from satellite observations in the infrared and optical ranges, was compared. By comparing the data obtained in observations with the results of simulations using a microphysical parameterization for WRF, a technique is developed for estimating charge distribution parameters [61].

Authors report the observation results of the hard radiation flashes which accompanied the lightning discharges above the mountains of Northern Tien Shan [62]. Time series of the counting rate intensity, numerical estimations of absolute flux, and energy distribution of accelerated electrons and of (20−2000) keV gamma rays were obtained at the height of 3700 m a. s. l., immediately within thunderclouds, and in closest vicinity ($\lesssim$100 m) to discharge region. Two different kinds of radiation emission events are presented here: a relatively prolonged rise of gamma ray intensity with minute-scale duration (the thunderstorm ground enhancement, TGE) which has preceded a negative field variation, and a short sub-millisecond radiation burst, which accompanied a close lightning discharge in thundercloud. It was revealed also an indication to positron generation in thunderclouds at the time of gamma ray emission, as well as modulation of the neutron counting rate in Tien Shan neutron monitor which was operating at a (1.5–2) km order distance from the region of lightning development.

A review of modern observations of the enhancement of the neutron flux in thunderclouds and during thunderstorms, which is associated with photonuclear reactions due to bremsstrahlung of high-energy runaway electron avalanches that can develop in a thunderstorm electric field, is performed in [63]. The difficulty of selecting thunderstorm neutrons is noted, due to the fact that the detectors are in a mixed field of various radiations, including not only neutrons, but also high-energy primary electrons and their bremsstrahlung. Particular attention is paid to the discovery in a thundercloud and on the Earth's surface during a thunderstorm of an annihilation line of a positron and an electron with a photon energy of 0.511 MeV, which is a reliable evidence of the generation of neutrons in a thunderstorm atmosphere and the photonuclear origin of thunderstorm neutrons. The consequences of this discovery are discussed.

Integrated methods for thunderstorm investigation

Actual data on the influence of dangerous weather phenomena (showers, thunderstorms, etc.), large-scale atmospheric circulations, and the effects of the solar-terrestrial relationship on daily and seasonal variations in the atmospheric electric field in the regions are still not enough to organize a reliable storm warning. In recent years, systems for collecting and analyzing data of instrumental continuous monitoring of lightning activity have been developing in Russia. Thunderstorm activity monitoring helps to solve many problems: protection of infrastructure facilities, warning of hazardous phenomena associated with intense precipitation, the study of the conditions for the occurrence of thunderstorms and the degree of their impact on human activity, as well as the impact of thunderstorm activity on the formation of near-Earth space.

The papers [64,65] discuss variations in the surface electric field and other geophysical parameters during winter thunderstorms in Kamchatka. Results of an investigation of the peculiarities of a spectrum of the electromagnetic signals induced nearby discharges between an artificial thunderstorm cell and a ground have presented in [66]. It was experimentally found that the impulse current parameters and an intensity, form, spectral characteristics of the induced electromagnetic signals depend on a variant of a discharge formation from an artificial thunderstorm cell (upward discharge, downward discharge, or counterpart discharge). Role of the powerful streamer discharges during the main stage formation in the appearance of the ultrahigh frequency range of the induced electromagnetic signals has considered. The possibility of applying the results obtained for improving the operation of lightning direction finding systems (LDFS) is being considered.

The results of the work aimed at creating a multi-position experimental network for monitoring thunderstorm activity are presented [67]. Calculations of zones of equal accuracy for variants of implementation of goniometric and difference-range methods for determining coordinates are given. Passive radio engineering monitoring means of storm activity in VLF range are considered in the work [68]. The comparative analysis of characteristics of modern Russian and foreign lightning location systems which have a broad practical application is carried out. Possibilities of improvement of precision and probabilistic characteristics of VLF methods and techniques for location of various types of lightning high current components are estimated.

A large number of works are devoted to the analysis of data from local and global LDFS. A comparison of the characteristics of multi-point LDFS showed that LDFS with base distances up to 400 km ensure the efficiency of registering lightning flashes by more than 90%, and individual lightning discharges from 50 to 90% [69]. It is demonstrated that LDFS with small bases have higher accuracy and probabilistic characteristics compared to large bases. The use of a difference-range LDFS with efficient, easy-to-select installation location and reliable sensors, similar to the indicators in the structure of the Russian Federal Service for Hydrometeorology and Environmental Monitoring (Roshydromet) in the European part of Russian and the Urals, the use of domestic developments of both hardware and software, will allow solving the problems of storm warning with accuracy and probabilistic characteristics of detection of thunderstorms at the level of foreign analogues [69].

The article [70] presents the results of using the LS8000 LDFS to determine the parameters of cloud-to-ground lightning discharges of positive and negative polarity in the territory of the North Caucasus, limited by 47° N, most of which belongs to mountainous regions. For this territory, the average values of the current amplitude in the cloud-to-ground lightning channels of positive and negative polarity were obtained, depending on the orography and

the height of the area above sea level. It is shown that the peak values of the current decrease with increasing terrain height. The duration of the rise of the lightning discharge current to the peak value, obtained using the LS8000 LDFS, is considered.

The instrumental continuous monitoring of lightning activity in Yakutia has been carried by the LDFS since the 2000s. The longest thunderstorm seasons are often observed in the southern part of Yakutia [71]. There was a slight increase in the duration of the thunderstorm season until 2015 in the central part of Yakutia. The interannual variations in the total number of lightning strokes showed periodic fluctuations (with a period of about three years) over the whole area of investigation. The periods of high lightning activity shifted within a season from year to year, as revealed by the monthly stroke number variation. The ratio of cloud-to-ground (CG) lightning strokes and the ratio of negative CG strokes was slightly decreasing by 2015 in the central part of Yakutia. Estimates of the variability of the parameters of the analytical expression for the latitude-longitude distribution of the lightning discharge density on a ten-year scale are obtained [72].

The comparative analysis of field data on weather radar reflectivity and lightning activity for the convective season of 2016 (May 16 – September 18) is performed. The accuracy of the thunderstorm detection algorithm implemented in the DMRL-C radars is evaluated. A new algorithm based on the sum of positive values of reflectivity is proposed. In terms of accuracy and reliability, the algorithm per forms better than more complex models. The algorithm can be used for thunder storm detection from field or model data on the reflectivity of the convective system [73].

The comparison of spatial and temporal variability of lightning activity associated with wildfires in several natural geographical zones of Western Siberia from 2016–2021 is performed in [74]. The study was based on the WWLLN data and The Fire Information for Resource Management System (FIRMS) for the warm (April – October) season. It was revealed that areas of hotspots and lightning activity most often coincide in the southwestern part of the territory (near Khanty-Mansiysk and Tyumen), in the mountain regions (Kuznetsk Alatau, Altai), and in the northern part of Kazakhstan. The revealed lightning–fire association allows to understand this process in the region that will be useful in the prediction of the potential fire danger in different natural zones. The density of lightning discharges over the territory of Western Siberia, according to WWLLN data, is characterized by spatial inhomogeneity with five main centers identified. Lightning activity for the period from 2016-2020 in the south of Western Siberia, it was observed from May to September with a maximum of discharges in July (38.3%) and a minimum in September (2.5%). A statistically significant relationship has been obtained between fields with critical values of the instability index K-index

and centers of high density of lightning discharges. [74, 75] Based on WWLLN data for 2007–2009 global maps of thunderstorm activity were built [76]. The key features of the spatial distribution and seasonal trends obtained by ground-based and satellite methods are in satisfactory agreement.

The characteristics of dangerous meteorological phenomena in Nizhny Novgorod are obtained on the basis of field observations of the electric field. As a result of the analysis of experimental data on the reception and registration of a quasi-stationary electric field, together with meteorological radar data, statistics of thunderstorm events were obtained and their classification was carried out. Field observation data are compared with the results of numerical calculations based on the WRF model [77]. The results of observations of radio emission from thunderclouds in a wide frequency range with a high temporal resolution carried out in the Upper Volga region near Nizhny Novgorod are compared with the data from worldwide and regional lightning location networks [78].

In [79] the characteristics of thunderstorm cells were studied by the method of cluster analysis. The data of the Vereya-MR lightning detection networks, accumulated over the period from 2012 to 2018, were taken as the basis. The behavior of thunderstorms in the entire territory of the Russian Federation and in the Baikal natural territory is compared. It has been determined that the power of thunderstorms over the Baikal region is less. Based on the results of this work, the locations of new points of a new LDFS are proposed and additional methods of cluster analysis are considered.

Conclusions

In 2019–2022 in the Russian Federation, a wide range of experimental and theoretical studies of atmospheric electrical power under various conditions has been carried out. Studies of the global electric circuit and its connection with other geophysical processes have been carried out. Comprehensive studies of the development of lightning discharges in the atmosphere have been carried out. In a number of regions of Russia, studies of the climatology of atmospheric electrical phenomena, regional meteorological features of thunderstorms, and improvement of methods for modeling and forecasting thunderstorm phenomena are being successfully continued.

Over the past 4 years, conferences devoted to the problems of atmospheric electricity have been successfully held: VII International Conference on Lightning Protection (St. Petersburg, 2022), Fourth and Fifth All-Russian Conference “Global Electric Circuit” (Borok, Yaroslavl region, 2019 and 2021), VIII Open All-Russian Conference on Atmospheric Electricity (September 23–27, Nalchik 2019). Russian scientists took an active part in the XVII International Conference on Atmospheric Electricity (ICAE2022, Tel

Aviv, Israel, June 2022), which is held every 4 years and is the main international forum on atmospheric electricity, as well as in the 27th General Assembly International Union of Geodesy and Geophysics "IUGG 2019", which was held in Montreal, Canada, from July 8 to 18, 2019.

References

1. Adzhiev A.H., Kupovykh G.V., Kerefova Z.M., Cherkesov A.A. The influence of solar wind on dynamics of the electric field in the atmospheric surface layer. Izvestiya SFedU. Engineering sciences. 2019. № 5. P. 114–122. (in Russian).
2. Adzhiev A.Kh., Kerefova Z.M., Klovo A.G., Kudrinskaya T.V., Kupovykh G.V., Timoshenko D.V., Cherkesov A.A. Analysis of the data of long-term atmospheric-electrical observations on the territory of the North Caucasus region. Trudy Voyenno-kosmicheskoy akademii imeni A.F. Mozhayskogo. 2020. № S674. P. 75–79. (in Russian).
3. Adzhiev A.K., Klovo A.G., Kudrinskaya T.V., Kupovykh G.V., Timoshenko D.V. Diurnal variations of the electric field in the atmospheric boundary layer. Izvestiya, Atmospheric and Oceanic Physics. 2021. T. 57. № 4. C. 397-405.
4. Shatalina M.V., Mareev E.A., Klimenko V.V., Kuterin F.A. & K.A. Nicoll Experimental Study of Diurnal and Seasonal Variations in the Atmospheric Electric Field. Radiophysics and Quantum Electronics. 2019. Vol. 62, № 3. P. 183–191.
5. Nagorskiy P.M., Pustovalov K.N., Smirnov S.V. Daily and seasonal variations of the undisturbed electric field and their relationship with the variability of geophysical quantities in the south of Western Siberia. Trudy Voyenno-kosmicheskoy akademii imeni A.F.Mozhayskogo. 2022. № S685. P. 213–222. (in Russian).
6. Pustovalov K.; Nagorskiy P.; Oglezneva M.; Smirnov S. The Electric Field of the Undisturbed Atmosphere in the South of Western Siberia: A Case Study on Tomsk. Atmosphere 2022, 13, P. 614.
7. Zekoreev R. Kh. Investigation of the state of the electric field of the atmosphere in the area of open pit mining. Science. Innovations. Technologies 2022. № 3. P. 139–158.
8. Zainetdinov B.G., Klovo A.G., Kudrinskaya T.V., Kupovykh G.V., Timoshenko D.V., Formation of diurnal variations of the atmospheric electric field near the earth's surface under various meteorological conditions. Trudy Voyenno-kosmicheskoy akademii imeni A.F.Mozhayskogo. 2020. № S674. P. 176–180. (in Russian).
9. Svidelsky S.S., Litvinova V.S., Kupovykh G.V., Klovo A.G., Formation of the atmospheric electrode layer structure. Izvestiya SFedU. Engineering sciences. 2020. № 5. P. 130–141.
10. Anisimov S.V., Galichenko S.V., Prokhorchuk A.A., Klimanova E.V., Statistics of variations in atmospheric electrical parameters based on a three-dimensional model and field observations. Atmos Res. 2021. Vol. 259. P. 105660.
11. Anisimov S.V., Galichenko S.V., Prokhorchuk A.A., Aphinogenov K.V., Measurement of the atmospheric electric-current density by a horizontal ring passive antenna in the surface layer: electrostatic approximation. Radiophysics and Quantum Electronics. 2022. Vol. 65, № 10. P. 801–819.

12. Anisimov S.V., Galichenko S.V., Prokhorchuk A.A., Aphinogenov K.V., Klimanova E.V., Measurement of the density of atmospheric electric current by a passive horizontal ring antenna in the surface layer: quasi-stationary approximation. Radiophysics and Quantum Electronics. 2022. Vol. 65, № 11. P. 893–913.
13. Shuleikin V.N., Schukin G.G. Use of elements of surface atmospheric electricity in problems of applied geophysics. Trudy Voyenno-kosmicheskoy akademii imeni A.F.Mozhayskogo. 2022. № S685. P. 236–244. (in Russian).
14. Smirnov S. Negative Anomalies of the Earth's Electric Field as Earthquake Precursors. Geosciences. 2019. Vol. 10, № 1. P. 10.
15. Kuterin F.A., Slyunyaev N.N., Implementation of ionospheric generators in the numerical model of the global electric circuit, Geomagnetism and Aeronomy. 2020. T. 60. № 6. C. 768–780.
16. R. Giles Harrison, Keri A. Nicoll, Evgeny Mareev, Nikolay Slyunyaev and Michael J. Rycroft Extensive layer clouds in the global electric circuit: their effects on vertical charge distribution and storage. Proceedings of the Royal Society A: Mathematical, Physical and Engineering Sciences. 2020. Vol. 476, № 2238. P. 20190758.
17. Slyunyaev N.N., Kalinin A. V., Mareev E.A. Thunderstorm generators operating as voltage sources in global electric circuit models. J Atmos Sol Terr Phys. 2019. Vol. 183. P. 99–109.
18. Morozov V.N. Influence of electric field generators operating in the upper layers of the atmosphere on the electricity of the surface layer. Proceedings of the Main Geophysical Observatory. A.I. Voeikova. 2022. № 605. P. 58–91.
19. Ilin N. V., Shatalina M. V., Slyunyaev N.N. Simulation of seasonal dynamics of the global electric circuit diurnal variation. Известия Российской академии наук. Физика атмосферы и океана. 2019. Vol. 55, № 5. P. 76–84.
20. Ilin N. V., Slyunyaev N.N., Mareev E.A. Toward a Realistic Representation of Global Electric Circuit Generators in Models of Atmospheric Dynamics. Journal of Geophysical Research: Atmospheres. 2020. Vol. 125, № 6.
21. Slyunyaev N.N., Ilin N. V., Mareev E.A., Price C.G., The global electric circuit land–ocean response to the El Niño – Southern Oscillation. Atmos Res. 2021. Vol. 260. P. 105626.
22. Slyunyaev N.N., Ilin N. V., Mareev E.A. Modeling Contributions of Continents and Oceans to the Diurnal Variation of the Global Electric Circuit. Geophys Res Lett. 2019. Vol. 46, № 10. P. 2019GL083166.
23. Slyunyaev N.N., Frank-Kamenetsky A. V., Ilin N. V., Sarafanov F. G., Shatalina M.V., Mareev E.A., Price C.G., Electric Field Measurements in the Antarctic Reveal Patterns Related to the El Niño – Southern Oscillation. Geophys Res Lett. 2021. Vol. 48, № 21.
24. Anisimov S.V., S.V. Galichenko, K.V. Aphinogenov, E.V. Klimanova, A.A. Prokhorchuk, A.S. Kozmina, A.V. Guriev, Mid-latitude atmospheric boundary layer electricity: A study by using a tethered balloon platform. Atmos Res. 2021. Vol. 250. P. 105355.
25. Anisimov S.V., S.V. Galichenko, K.V. Aphinogenov, E.V. Klimanova, A.S. Kozmina, Small air ion statistics near the earth's surface. Atmos Res. 2022. Vol. 267. P. 105913.
26. Dementyeva S.O., Ilin N.V., Shatalina M.V., Mareev E.A., Forecast of convective events and its verification against atmospheric electricity observations, Izvestiya, Atmospheric and Oceanic Physics. 2020. T. 56. № 2. C. 123–129.

27. Lesev V.N., Shapovalov V.A., Ashabokov B.A., Shapovalov A.V., Korotkov P.K., 3D model of a convective cloud: the interaction of microphysical and electrical processes. JP Journal of Heat and Mass Transfer. 2021. Vol. 23, № 1. P. 1–18.
28. Morozov V.N. Interaction of Cloud Charge Structures with the Surrounding Conductive Atmosphere with Inhomogeneous Electrical Conductivity. Proceedings of the Main Geophysical Observatory. A.I. Voeikova. 2019. № 592. P. 23–79. (in Russian).
29. Klimenko V.V., Lubyako L.V., Mareev E.A., Shatalina M.V., Ground-based measurements of microwave brightness temperature and electric field fluctuations for clouds with a different level of electrical activity. Atmos Res. 2022. Vol. 266. P. 105937.
30. Bogatov N. A., Syssoev V.S., Sukharevsky D. I., Naumova M. Yu., Microwave diagnostics of electrical discharges in an artificial cloud of charged water drops, Technical Physics. 2022, № 3. P. 294–299.
31. Smirnov, B.M., Son, E.E. Electric Processes in Atmospheric Air. High Temp. 2022. Vol. 60, № 4. P. 589–624.
32. Mikhaylovskiy Yu.P., Popov V.B., Sin'kevich A.A., Abshayev A.M., Abshayev M.T., Adzhiev A.Kh., Gekkieva Zh.M., Zanyukov V.V., Physical and statistical empirical model of development of lightning activity of convective clouds. Proceedings of the Main Geophysical Observatory. A.I. Voeikova. 2019. № 595. P. 83–105. (in Russian).
33. Abshaev M.T., Abshaev A.M., Mikhaylovskiy Yu. P., Sinkevich A.A., Popov V.B., Adzhiev A.H. Investigation of the peculiarities of the development of electrification and hail formation processes in a supercell cloud by radiophysical means. Proceedings of the Main Geophysical Observatory. A.I. Voeikova. 2020. № 596. P. 96–130. (in Russian).
34. Abshaev, M.T., Abshaev, A.M., Sinkevich, A.A. et al. Features of Development of a Supercell Convective Cloud at the Stage of Maximum Lightning Activity (August 19, 2015, the North Caucasus). Russ. Meteorol. Hydrol. 2022. Vol. 47. P. 315–325.
35. Veremey N.E., Dovgalyuk Yu.A., Toropova M.L., Sinkevich A.A., Mikhailovsky Yu.P., Kashleva L.V., Zainetdinov B.G., Kurov A.B. Influence of thermal inhomogeneities the underlying surface on the formation and development of convective clouds and associated hazardous weather phenomena. Proceedings of the Main Geophysical Observatory. A.I. Voeikova. 2022. № 606. P. 32–49. (in Russian).
36. Mikhailovskii Yu.P.,Toropova M.L.,Veremei N.E., Dovgalyuk Yu.A., Sin'kevich A.A.,Yang J.Lu J. Dynamics of cumulonimbus electrical structures. Radiophysics and Quantum Electronics. 2021. Vol. 64, № 5. P. 309–320.
37. Sin'kevich A., Boe B. , Pawar S. et al. Investigation of Thundercloud Features in Different Regions. Remote Sens. 2021. Vol. 13, № 16. P. 3216.
38. Sin'kevich A.A., Mikhailovskii Yu.P., Toropova M.L. et al. Thunderstorm with waterspout structure and lightning frequency dependence from its characteristics. Optika Atmosfery i Okeana. 2020. V. 33. No. 09. P. 705–709. (in Russian).
39. Bocharov A.N., Mareev E.A., Popov N.A. Numerical simulation of high-current pulsed arc discharge in air. J Phys D Appl Phys. 2022. Vol. 55, № 11. P. 115204.

40. Syssoev A.A., D. I. Iudin, A. A. Bulatov, V. A. Rakov. Numerical Simulation of Stepping and Branching Processes in Negative Lightning Leaders. Journal of Geophysical Research: Atmospheres. 2020. Vol. 125, № 7.
41. Bulatov A.A., Iudin D.I., Sysoev A.A. Self-Organizing Transport Model of a Spark Discharge in a Thunderstorm Cloud. Radiophysics and Quantum Electronics. 2020. Vol. 63, № 2. P. 124–141.
42. Syssoev A.A., Iudin D.I. On a possible mechanism of space stem formation at the negative corona streamer burst periphery. Atmos Res. 2021. Vol. 259. P. 105685.
43. Iudin D.I., Iudin F.D., Syssoev A.A. et al. Noise-induced kinetic transition in two-component environment. J Comput Appl Math. 2021. Vol. 388. P. 113268.
44. Syssoev A.A., Iudin D.I., Iudin F.D. et al. On the Problem of Critical Electric Field of Atmospheric Air. Atmosphere. 2021. Vol. 12, № 8. P. 1046.
45. Syssoev A.A., Iudin D.I., Iudin F.D. et al. Relay charge transport in thunderclouds and its role in lightning initiation. Sci Rep. 2022. Vol. 12, № 1. P. 7090.
46. Bazelyan, E.M., Aleksandrov, N.L. Electric Field in a Positive Streamer in Long Air Gaps. Plasma Phys. Rep.. 2022. Vol. 48. P. 789–797.
47. Bazelyan, E.M. The Problem of Control Actions on the Lightning Discharge. Plasma Phys. Rep. 2021. Vol. 47. P. 279–288.
48. Bazelyan, E.M., Popov, N.A. Stepwise Development of a Positive Long Spark in the Air. Plasma Phys. Rep. 2020. Vol. 46. P. 293–305.
49. Bazelyan, E.M. Mechanism of Orientation and Parameters of Lightning in Context of Lightning Protection. Plasma Phys. Rep. 2019. Vol. 45. P. 252–263.
50. Kutsyk, I.M., Babich, L.P. Heating of a Local Region of a Branching Streamer as a Starting Point of a Space Leader and a Negative-Leader Step. Plasma Phys. Rep. 2021. Vol. 47, № 3. P. 251–256.
51. Babich L.P., Bochkov E.I. Role of Charged Ice Hydrometeors in Lightning Initiation. Proceedings of RFNC-VNIIEF. 2019. № 24–1. P. 198–207.
52. Babich L.P. Electrotechnique Interpretation of the Electric Field Amplification in Front of the Plasma Channel. IEEE Transactions on Plasma Science. 2020. Vol. 48, № 12. P. 4089–4092.
53. Bogatov N.A., Kostinskiy A. Yu, Syssoev V. S. et al. Experimental Investigation of the Streamer Zone of Long-Spark Positive Leader Using High-Speed Photography and Microwave Probing. Journal of Geophysical Research: Atmospheres. 2020. Vol. 125, № 11.
54. Kostinskiy A.Yu., Bogatov N.A., Syssoev V. S. et al. Unusual Plasma Formations Produced by Positive Streamers Entering the Cloud of Negatively Charged Water Droplets. Journal of Geophysical Research: Atmospheres. 2022. Vol. 127, № 21.
55. Evtushenko A., Ilin N., Svechnikova E. Parameterization and global distribution of sprites based on the WWLLN data. Atmos Res. 2022. Vol. 276. P. 106272.
56. Surkov V. V., Hayakawa M. Progress in the Study of Transient Luminous and Atmospheric Events: A Review. Surv Geophys. 2020. Vol. 41, № 5. P. 1101–1142.
57. Evtushenko A.A., Gushchin M.E., Korobkov S.V., Strikovskiy A.V., Mareev E.A. Simulation of high-altitude discharges in a large plasma facility. Geomagnetism and Aeronomy. 2020. Vol. 60, № 3. P. 345–354.
58. Tarasenko V.F., E.Kh. Baksht, A.G. Burachenko, N.P. Vinogradov. Modeling the color of high-altitude atmospheric discharges using a repetitively pulsed dis-

charge in air, nitrogen and argon. Optika Atmosfery i Okeana. 2022. Vol. 35, № 4. P. 279–283. (in Russian).
59. Stadnichuk E., Svechnikova E. The criterion for self-sustaining production of relativistic runaway electron avalanches by the positron feedback in thunderstorms. Atmos Res. 2022. Vol. 277. P. 106329.
60. Svechnikova E. K., Ilin N. V., Mareev E. A. .Meteorological Characteristics of Energetic Atmospheric Phenomena. Particles and Nuclei, Letters. 2020. Vol. 17, № 6(231). P. 791–802. (in Russian).
61. Svechnikova E.K., Ilin N. V., Mareev E. A., Chilingarian A. Characteristic Features of the Clouds Producing Thunderstorm Ground Enhancements. Journal of Geophysical Research: Atmospheres. 2021. Vol. 126, e2019JD030895.
62. Shepetov A., Antonova V., Kalikulov O. et al. The prolonged gamma ray enhancement and the short radiation burst events observed in thunderstorms at Tien Shan. Atmos Res. 2021. Vol. 248. P. 105266.
63. Babich L.P. Thunderous neutrons. Uspekhi Fizicheskih Nauk. 2019. Vol. 189, № 10.
64. Smirnov S.E., Mikhailov Y.M., Mikhailova G.A., Kapustina O.V. Features of winter thunderstorms in Kamchatka, Geomagnetism and Aeronomy. 2019. T. 59. № 6. C. 696–703.
65. Mikhailov Y.M., Mikhailova G.A., Kapustina O.V., Smirnov S.E. Tropical cyclones and possible winter thunderstorms on Kamchatka. Geomagnetism and Aeronomy. 2020. T. 60. № 5. C. 619–635.
66. Temnikov A., Belova O., Chernensky L. et al. Peculiarities of spectrum of electromagnetic signals induced by discharges from artificial thunderstorm cell. J Electrostat. 2022. Vol. 115. P. 103660.
67. Gotyur I. A., Korovin E. A., Chernyshev S. V. Experimental network of sensors for monitoring thunderstorm activity. Trudy Voyenno-kosmicheskoy akademii imeni A.F.Mozhayskogo. 2022. № S685. P. 66–74. (in Russian)
68. Kononov I.I., Korovin E.A., Shchukin G.G., Yusupov I.E. Current state and prospects of development of passive radio engineering monitoring of storm activity. IOP Conf Ser Mater Sci Eng. 2019. Vol. 698, № 4. P. 044046.
69. Snegurov A.V., Snegurov V.S. Comparison of characteristics of multipoint lightning direction finding systems.Proceedings of the Main Geophysical Observatory. A.I. Voeikova. 2019. № 595. P. 22–62. (in Russian).
70. Adjiev A.H., Kerefova Z.M., Kuzmin V.A. Definition of lightning parameters with the use of thunderstorm registry LS 8000. Hydrometeorology and ecology. Proceedings of the Russian state hydrometeorological university. 2021. № 64. P. 531–543.
71. Tarabukina L., Kozlov V. Seasonal Variability of Lightning Activity in Yakutia in 2009–2019. Atmosphere. 2020. Vol. 11, № 9. P. 918.
72. Tarabukina L.D., Kozlov V.I., Innokentiev D.E. Analysis of 11-years dynamics in spatial distribution of lightning density in North Asia. Vestnik KRAUNTS. Physical and mathematical sciences. 2021. № 1. P. 159–173. (in Russian).
73. Ilin N. V., Kuterin F.A. Accuracy of Thunderstorm Detection Based on DMRL-C Weather Radar Data. Russian Meteorology and Hydrology. 2020. Vol. 45, № 9. P. 669–675.
74. Nechepurenko O.E., Gorbatenko V.P., Pustovalov K.N., Gromova A.V. Lightning activity over western Siberia. Geospheric research.2022. № 4. P. 123–134. (in Russian).

75. haryutkina, E.; Pustovalov, K.; Moraru, E.; Nechepurenko, O. Analysis of Spatio-Temporal Variability of Lightning Activity and Wildfires in Western Siberia during 2016–2021. Atmosphere. 2022. Vol. 13, № 5. P. 669.
76. Denisenko V.V., Lyakhov A.N. Comparison of ground-based and satellite data on spatiotemporal distribution of lightning discharges under solar minimum. Solar-Terrestrial Physics. 2021. T. 7. № 4. C. 104–112.
77. Shatalina M.V., Ilyin N.V., Mareev E.A. Characteristics of Hydrometeorological Hazards in Nizhny Novgorod According to In-situ Observations of Electric Field. Russian Meteorology and Hydrology. 2021. № 6. P. 107–111.
78. Karashtin A.N., Shlyugaev Y.V., Karashtina O.S. Cloud-to-ground lightning discharge indicator in the radio frequency emission of thunderclouds as observed in the Upper Volga region of Russia. Atmos Res. 2021. Vol. 256. P. 105559.
79. Tkachev I.D., Vasilyev R.V., Belousova E.P., Cluster analysis of lightning discharges: based on Vereya-MR network data, Solnechno-zemnaya fizika. 2021. Vol. 7. Iss. 4. P. 91–98.

Climate

I.I. Mokhov
A.M. Obukhov Institute of Atmospheric Physics RAS
Lomonosov Moscow State University
mokhov@ifaran.ru

Introduction

This review presents results of Russian studies of climate and its changes (published in 2019–2022). A previous similar review was published in [1, 2] (see also [3]). Roshydromet publishes annual reports on climate features in the territory of the Russian Federation [4–8], in 2022 the Third Assessment Report on climate change and its consequences in the territory of the Russian Federation was published [9]. Information on climate research is regularly published in the Climate Change Bulletin.

The problem of climate change is one of the key global problems. Modern climate changes with an increase in global surface air temperature are accompanied by a rapid increase in regional natural anomalies. The most significant contribution is associated with hydrological and meteorological extreme events. The last decades are characterized by significant global and regional climatic changes, especially in high latitudes [1, 2, 4–8]. The maximum warming in the last half century in the Arctic latitudes has reached values of about 5°C – five times more than for the Earth as a whole. The greatest rate of temperature changes in the Arctic latitudes is the so-called Arctic amplification.

In Russia, as a northern country, the current increase in average surface air temperature by 0.5°C per decade is more than twice the rate of global warming. Both intra-annual and inter-annual temperature variations in Russia as a whole are also much larger than global variations. In this regard, the problem of climate change and related environmental changes in the Russian regions is of particular importance, including socio-economic and political, taking into account that Russia has signed and ratified the Paris Agreement – an international agreement under the UN Framework Convention on Climate Change.

References

1. Russian National Report: Meteorology and Atmospheric Sciences (2015–2018). Ed. by I.I. Mokhov, A.A. Krivolutsky. Moscow, MAKS Press, 2019, 332 pp.
2. Mokhov I.I. Russian climate research in 2015-2018. Izv., Atmos. Oceanic Phys., 2020, **56** (4), 325–343.

3. Mokhov I.I. Russian atmospheric and meteorological research in 2015–2018. Izv., Atmos. Oceanic Phys., 2019, **55** (6), 503–504.
4. Report on climate features in the territory of the Russian Federation for 2018. Moscow: Roshydromet. 2019. 79 pp. (In Russian).
5. Report on climate features in the territory of the Russian Federation for 2019. Moscow: Roshydromet. 2020. 97 pp. (In Russian).
6. Report on climate features in the territory of the Russian Federation for 2020. Moscow: Roshydromet. 2021. 104 pp. (In Russian).
7. Report on climate features in the territory of the Russian Federation for 2021. Moscow: Roshydromet. 2022. 104 pp. (In Russian).
8. Report on climate features in the territory of the Russian Federation for 2022. Moscow: Roshydromet. 2023. 108 pp. (In Russian).
9. Third assessment report on climate change and its consequences on the territory of the Russian Federation. General summary. St. Petersburg: Science-intensive technologies. 2022. 676 pp. (In Russian).

Climate and its changes from observations, reanalyses and paleoreconstructions

Within the framework of climate studies based on observational data in comparison with reanalysis data and paleoreconstructions, many significant results have been obtained in recent years, including those noted in [1–121]. Significant modern global and regional climate changes, especially in high latitudes, were noted.

A wide range of research results on climate anomalies and changes at the regional and global levels obtained in recent years is presented in the Third Assessment Report on Climate Change and its Consequences on the Territory of the Russian Federation, published in 2022 [112].

According to the data of Roshydromet (https://www.meteorf.gov.ru/), the linear trend of general warming in Russia, which has been significantly manifested since the mid-1970s, explains more than 50% of the interannual variance of the annual-mean surface air temperature [93–97]. For the last half century, a general warming has been noted in all Russian regions and for all seasons. The maximum rate of warming in the Arctic regions reaches and exceeds 1 K per decade. The whole amount of precipitation per year for Russia as a whole has significantly increased over the past half century at a rate of about 2% per decade. Precipitation increases in all seasons, but most significantly in spring. In a significant part of Russia, there is a tendency for a decrease in the duration of snow cover and, at the same time, with a general increase in the maximum depth of snow cover during the winter. Warming in the Arctic is accompanied by a reduction in the area of sea ice in the Arctic Ocean, and this is even more noticeable along the Northern Sea Route.

Measurements (since 1990) of the thickness of the seasonally thawed layer, which is an indicator of the state of permafrost, within the framework of

the CALM International Monitoring Program (CircumPolar Active-Layer Monitoring) indicate a general steady trend of increasing the depth of permafrost thawing in the 21st century. For the last decades, there has been a tendency to increase the duration of the growing season (with temperatures above 5°C) at an average rate for Russia of about 4 days per decade, while the spring transition through 5°C occurs earlier by about 2 days every decade. Against the background of warming in Russia, there is a general decrease in the surface wind speed in all seasons. The noted climatic changes are manifested against the background of a regular increase in the concentration of CO_2 in the atmosphere, including measurements at the Russian Arctic stations Teriberka and Tiksi, the annual mean concentration of CO_2 exceeded 420 ppm. After 2020, with a minimum annual increase in CO_2 concentration of about 2 ppm, the annual increase exceeded 3 ppm.

To diagnose the mechanisms of formation of climatic changes with an assessment of the role of natural and anthropogenic factors, studies of temperature changes at different levels in the atmosphere are essential. According to Roshydromet, with a general warming in recent decades of the tropospheric layer of 850-300 hPa in the Northern Hemisphere at a rate of about 0.2 K per decade, the lower stratosphere (100-50 hPa layer) cooled at a rate of about twice as much – about -0.4 K per decade. At the same time, in tropical latitudes, the rate of cooling of the lower stratosphere is about 3.5 times greater than the rate of heating of the tropospheric layer above the boundary layer [93–97]. In [33] the results of the data analysis for the temperature at the mesopause level for the period 2000-2018 are presented. According to the estimates obtained, the temperature at the mesopause level decreased statistically significantly in summer seasons at a rate of -2.5K per decade; in winter seasons, the changes were estimated to be statistically insignificant.

Under the rapid warming in recent decades, the most noticeable changes are manifested in the frequency and intensity of extreme weather and climate events, in particular in the Russian regions [13, 14, 51, 64, 79, 80, 93–98]. According to Roshydromet, the number of dangerous meteorological phenomena in Russia has more than doubled since the end of the 20th century. The average growth rate of their number in the last quarter of a century was about two dozen events per year. The number of extreme events in summer exceeds 40% of their total number in the whole year [64]. In the formation of extreme weather and climate phenomena, a special contribution is associated with the hydrological cycle. Including with warming, the likelihood of extreme precipitation increases due to an increase in the moisture capacity of the atmosphere. Among the most frequent phenomena in the Russian regions are extreme precipitation, especially during the summer months, as well as strong winds.

In [27], quantitative estimates of long-term changes in various types of precipitation, including convective precipitation, in the regions of Northern Eurasia over the past half century are presented. The main analysis is carried out for 326 stations with more complete data. An increase in the total amount of precipitation over the analyzed period was noted with a relatively strong increase in convective precipitation and a decrease in precipitation from stratus clouds. The main changes in the total amount of precipitation, their intensity and the amount of heavy precipitation occur in the summer seasons. It is significant that the contribution of strong convective showers to the total amount of precipitation increases statistically significantly for extended regions of Northern Eurasia. Precipitation associated with stratus clouds generally decreases for most regions of Northern Eurasia in all seasons except winter.

In [30], an analysis was made of changes in the frequency and intensity of dangerous convective phenomena, including heavy showers, thunderstorms, hail, squalls, tornadoes) in Russian regions during warm seasons using various data. Quantitative estimates of the frequency of thunderstorms, cumulonimbus clouds, hail, strong winds, and extreme showers are obtained based on observational data at Russian meteorological stations for the period 1966–2020. Quantitative estimates of the frequency and intensity of tornado and squall events that caused windblows (1986–2021), the height of the upper boundary of deep convection clouds (for 2002–2021) were made using satellite data. Based on the ERA5 reanalysis data, estimates of the frequency of occurrence of conditions typical for the development of moderate and intense hazardous convective phenomena were obtained. The results obtained indicate a general intensification of convective processes and phenomena in most regions of Russia.

The strongest regional weather and climate anomalies are associated with blocking of zonal transport in the mid-latitude troposphere, and their predictability is not only of fundamental but also applied importance [13, 14, 22, 51, 54, 64, 66, 79, 80]. The problem of predictability of atmospheric blockings in the Northern Hemisphere on intraseasonal timescales is considered in [51] using the operational version of the semi-Lagrangian atmosphere model for long-range forecasting (SL-AV), as well as the coupled atmosphere–ocean model and the reanalysis. In [15], the features of the variability of anticyclonic activity, including blocking activity, in the atmosphere of the middle latitudes of the Northern Hemisphere since the middle of the 20th century in different seasons are considered. A significant relationship between the characteristics of anticyclonic activity and the leading modes of climatic variability was noted.

In [13], the results of the analysis of climatic variability, in particular, temperature extremes, in the Russian regions are presented by the daily mean data on the surface air temperature at 367 stations for 1960–2016. It is noted

that since the 1980s the number of days with extremely high summer temperatures in the European part of Russia is monotonously growing, with strong peaks in some years, and in the Asian part since the early 2000s growth has stalled. The number of negative temperature anomalies decreases. Changes in the winter seasons are generally consistent with the general warming trend, with oscillations in the Asian part corresponding to the leading atmospheric circulation modes, including the North Atlantic Oscillation and the Scandinavian mode. The statistics of extremeness indices in opposite phases of modes revealed a strong response in winter, which makes it possible to qualitatively explain the features of long-term variations.

To understand the features of modern climate change, paleoclimatic studies are of special importance [17, 18, 37, 53, 85, 86]. In [86], in particular, a review of applications of the method for constructing optimal empirical models for climatic systems, including paleoclimatic systems, is presented. This method, which includes the construction of reduced models of the system under study in the form of random dynamic systems, in combination with Bayesian optimization of the model structure, makes it possible to reconstruct statistically detected patterns, including for paleoclimatic changes, in particular in the Pleistocene with glacial cycles, as well as for El Niño events – Southern Oscillation on scales of the order of a year and for the tropical Pacific climate on centennial scales. The climatic anomalies of recent years testify not only to an increase in the risk of extreme events, but also to new processes and phenomena that characterize the achievement of a certain critical level of climate change. Based on the results of the analysis of modern climate changes using, along with observational data and paleoreconstructions, model estimates taking into account natural and anthropogenic factors, it can be concluded that during the warming of the last decades, the Earth's climate system entered a regime comparable to the Holocene optimum regime [64].

References

1. Abida A. et al. Regional climates. BAMS, 2020, **101** (8), S321-S420.
2. Abram N. et al. Summary for Policymakers. In: IPCC Special Report on the Ocean and Cryosphere in a Changing Climate. H.-O. Pörtner et al. (eds.). Cambridge Univ. Press, Cambridge / New York, NY, 2019, 3–35.
3. Akperov M.G. et al. Lapse rate peculiarities in the Arctic from reanalysis data and model simulations. Russ. Meteorol. Hydrol., 2019, **44** (2), 97–102.
4. Alekseev G.V. et al. Influence of sea surface temperature in the tropics on the Antarctic sea ice under global warming. Ice and Snow, 2019, **59** (2), 213–221. (In Russian).
5. Aleshina M.A., Semenov V.A., Chernokulsky A.V. A link between surface air temperature and extreme precipitation over Russia from station and reanalysis data. Environ. Res. Lett., 2021, **16,** 105004**DOI** 10.1088/1748-9326/ac1cba

6. Allan R.P. et al. Advances in understanding large-scale responses of the water cycle to climate change. Ann. N.Y. Acad. Sci., 2020, **1472** (1), 49–75.
7. Allan R.P. et al. Summary for Policymakers. In: Climate Change 2021: The Physical Science Basis. Contribution of Working Group I to the Sixth Assessment Report of the Intergovernmental Panel on Climate Change. Masson-Delmotte V. et al. (eds.). Cambridge Univ. Press, Cambridge / New York, NY, 2021, 3−32.
8. Anisimov O.A. et al. Methane emission in the Russian permafrost zone and evaluation of its impact on global climate. Russ. Meteorol. Hydrol., 2020, **45** (5), 377–385.
9. Anisimov O., Zimov S. Thawing permafrost and methane emission in Siberia: Synthesis of observations, reanalysis, and predictive modeling. Ambio, 2021, **50**, 2050–2059.
10. Babina E.D., Semenov V.A. Intramonthly variability of daily surface air temperature in Russia in 1970–2015. Russ. Meteorol. Hydrol., 2019, **44** (8), 513–522.
11. Bagatinsky V.A., Diansky N.A. Variability of the North Atlantic thermohaline circulation in different phases of the Atlantic Multidecadal Oscillation from ocean ojective analyses and reanalyses. Izv., Atmos. Oceanic Phys., 2021, **57** (2), 208–219.
12. Bagatinsky V.A., Diansky N.A. Contributions of temperature and salinity climatic changes to the formation of North Atlantic thermohaline circulation trends in 1951–2017. Moscow Univ. Phys. Bull., 2022, **77** (3), 564–580.
13. Bardin M.Yu., Platova T.V. Long-period variations in extreme temperature statistics in Russia as linked to the changes in large-scale atmospheric circulation and global warming. Russ. Meteorol. Hydrol., 2019, **44** (12), 791–801.
14. Bardin M.Yu., Platova T.V. Cold waves over the European part of Russia: Structure, circulation conditions and changes in seasonal statistics. Fund. Appl. Climatol., 2022, **8** (3), 5–30. (In Russian).
15. Bardin M.Yu. et al. Variability of anticyclonic activity in the Northern extratropics. Fund. Appl. Climatol., 2019, **3** (3), 32–54. (In Russian).
16. Bardin M.Yu. et al. Modern surface climate change as inferred from routine climate monitoring data. Russ. Meteorol. Hydrol., 2020, **45** (5), 317–329.
17. Bezverkhny V.A. The 100 000 – year periodicity in glacial cycles and oscillations of world ocean level. Izv., Atmos. Oceanic Phys., 2019, **55** (4), 334–340.
18. Bezverkhny V.A. On the 100 000 – year rhythmicity in geodynamics and the paleoclimate. Izv., Phys. Solid Earth, 2019, **55** (3), 488–495.
19. Biskaborn B.K. et al. Permafrost is warming at a global scale. Nat. Comm., 2019, **10**, 264, https://doi.org/10.1038/s41467-018-08240-4
20. Bokuchava D.D., Semenov V.A. The role of natural fluctuations and factors of external forcing in the Early 20th Century Warming in Northern Hemisphere. Ice and Snow, 2022, **62** (3), 455–474. (In Russian).
21. Bondur V.G. et al. Spatiotemporal analysis of multi-year wildfires and emissions of trace gases and aerosols in Russia based on satellite data. Izv., Atmos. Oceanic Phys., 2020, **56** (12), 1457–1469.
22. Bondur V.G. et al. Satellite monitoring of Siberian wildfires and their effects: Features of 2019 anomalies and trends of 20-year changes. Doklady Earth Sci., 2020, **492** (1), 370–375.
23. Bondur V.G. et al. Satellite monitoring of the variability of wildfire areas and emissions of harmful gas components into the the atmosphere for various re-

gions of Russia over a 20-year period. Doklady Earth Sci., 2021, **500** 2), 890–894.
24. Borzenkova I.I., Ershova A.A., Zhiltsova E.L., Shapovalova K.O. Arctic sea ice in the light of current and past climate changes. Ice and Snow, 2021, **61** (4), 533-546. (In Russian).
25. Canadell J.G. et al. Global carbon and other biogeochemical cycles and feedbacks. In: Climate Change 2021: The Physical Science Basis. Contribution of Working Group I to the Sixth Assessment Report of the Intergovernmental Panel on Climate Change. Masson-Delmotte V. et al. (eds.). Cambridge Univ. Press, Cambridge / New York, NY, 2021, 673–816.
26. Chen J. et al. Sustainability challenges for the social-environmental systems across the Asian drylands belt. Environ. Res. Lett., 2022, **17** (2), 023001, http://dx.doi.org/10.1088/1748-9326/ac472f
27. Chernokulsky A., Kozlov F., Zolina O. et al. Observed changes in convective and stratiform precipitation in Northern Eurasia over the last five decades. Environ. Res. Lett., 2019, **14**, 045001, https://doi.org/10.1088/1748-9326/aafb82
28. Chernokulsky A. et al. Tornadoes in Northern Eurasia: from the Middle Age to the Information Era. Mon. Wea. Rev., 2020, DOI 10.1175/MWR-D-19-0251.1.
29. Chernokulsky A.V. et al. Tornadoes in the Russian regions. Russ. Meteorol. Hydrol., 2021, **46** (2), 69–82.
30. Chernokulsky A.V. et al. Atmospheric severe convective events in Russia: Changes observed from different data. Russ. Meteorol. Hydrol., 2022, **47** (5), 343–354.
31. Chilingarov A.N. et al. To the initiative of holding the Fifth International Polar Year. Hydrometeorol. Ecol., 2022, 66, 104–109. (In Russian)
32. Climate of the Arctic: Processes and Changes. I.I. Mokhov and V.A. Semenov (eds.). Moscow, Fizmatkniga, 2022, 360 pp.
33. Dalin P., Perminov V., Pertsev N., Romejko V. Updated long-term trends in mesopause temperature, airglow emissions, and noctilucent clouds. J. Geophys. Res.: Atmos., 2020, **125**, e2019JD030814, https://doi.org/10.1029/2019JD030814
34. Datsenko N.M. et al. Comparative analysis of spectra of the 2000-year reconstructions of average surface air temperature in the Northern Hemisphere. Russ. Meteorol. Hydrol., 2021, **46** (10) 651–657.
35. Diansky N.A., Bagatinsky V.A. Thermohaline structure of waters in the North Atlantic in different phases of the Atlantic Multidecadal Oscillation. Izv., Atmos. Oceanic Phys., 2019, **55** (6), 628–639.
36. Douville H. et al. Water cycle changes. In: Climate Change 2021: The Physical Science Basis. Contribution of Working Group I to the Sixth Assessment Report of the Intergovernmental Panel on Climate Change. Masson-Delmotte V. et al. (eds.). Cambridge Univ. Press, Cambridge / New York, NY, 2021, 1055–1210.
37. Ekaykin A.A., Lipenkov V.Y., Tchikhatchev K.B. Preservation of the climatic signal in the old ice layers at Dome B area (Antarctica). Ice and Snow, 2021, **61** (1), 5–13. (In Russian)
38. Gavrilov A., Seleznev A., Mukhin D. et al. Linear dynamical modes as new variables for data-driven ENSO forecast. Cli. Dyn., 2019, **52** (3–4), 2199–2216.
39. Georgiadi A.G., Groisman P.Y. Long-term changes of water flow, water temperature and heat flux of two largest arctic rivers of European Russia, Northern

Dvina and Pechora. Environ. Res. Lett., 2022, **17** (8), 085002, http://dx.doi.org/10.1088/1748-9326/ac82c1
40. Gochakov A.V. et al. Long-term variability of Rossby wave breaking in the subtropical jet stream area. Russ. Meteorol. Hydrol., 2022, **47** (2), 79–88.
41. Grigorieva V., Gulev S.K. Wave climate in Subarctic seas from voluntary observing ships. Russ. J. Earth Sci. 2020, **20** (6), ES6015.
42. Gruzdev A.N., Bezverkhny V.A. Analysis of solar cycle-like signal in the North Atlantic Oscillation index. J. Atmos. Solar-Terr. Phys., 2019, **187**, 53–62.
43. Gulev S.K. et al. Changing State of the Climate System. In: Climate Change 2021: The Physical Science Basis. Contribution of Working Group I to the Sixth Assessment Report of the Intergovernmental Panel on Climate Change. Masson-Delmotte V. et al. (eds.). Cambridge Univ. Press, Cambridge / New York, NY, 2021, 287–422.
44. Gushchina D.Yu. et al. Effects of the Pacific Decadal Oscillation on the characteristics of two types of El Niño under possible climate change. Russ. Meteorol. Hydrol., 2022, **45** (10), 683–693.
45. Gushchina D., Kolennikova M., Dewitte B., Yeh S.W. On the relationship between ENSO diversity and the ENSO atmospheric teleconnection to high-latitudes. Intern. J. Climatol., 2022, **42** (2), 1303–1325.
46. Hock R. et al. High Mountain Areas / In: IPCC Special Report on the Ocean and Cryosphere in a Changing Climate. H.-O. Pörtner et al. (eds.). Cambridge Univ. Press, Cambridge / New York, NY, 2019, 131–202, https://doi.org/10.1017/9781009157964.004
47. Izhitskiy A.S. *et al* The world's largest heliothermal lake newly formed in the Aral Sea basin. Environ. Res. Lett., 2021, **16,** 115009.
48. Jakovlev A.R., Smyshlyaev S.P. Impact of the Southern Oscillation on Arctic stratospheric dynamics and ozone layer. Izv., Atmos. Oceanic Phys., 2019, **55** (1), 86–98.
49. Jia G. et al. Land–climate interactions. In: Climate Change and Land: an IPCC special report on climate change, desertification, land degradation, sustainable land management, food security, and greenhouse gas fluxes in terrestrial ecosystems. P.R. Shukla et al. (eds.), 2019, 131–247, https://doi.org/10.1017/9781009157988.004
50. Kislov A.V., Morozova P.A. Level variations in the Caspian Sea under different climate conditions by the data of simulation under CMIP6 project. Water Resources, 2021, 48 (6), 844–853.
51. Kulikova I.A. et al. Evaluation of practical predictability of blocking anticyclones using modern hydrodynamic models. Russ. Meteorol. Hydrol., 2022, **47** (1), 1–13.
52. Lappapainen H.K. et al. Overview: Recent advances in the understanding of the Northern Eurasian environments and of the urban air quality in China – A pan-Eurasian experiment (PEEX) programme perspective. Atmos. Chem. Phys., 2022, **22** (7), 4413–4469.
53. Loskutov E., Vdovin V., Klinshov V. et al. Applying interval stability concept to empirical model of Middle Pleistocene transition. Chaos, 2022, **32** (2), 021103.
54. Lupo A.R. et al. Changes in global blocking character during recent decades. Atmosphere, 2019, **10** (2), 92, https://doi.org/10.3390/atmos10020092

55. Makarov A.S. et al. Ice conditions of the Russian Arctic Sea in connection with the occurring climate changes and peculiarities of the ice cover evolution in 2021. Oceanology, 2022, **62** (6), 735–745.
56. Matveeva T.A., Semenov V.A., Astafyeva E.S. Arctic sea ice coverage and its relation to the surface air temperature in the Northern Hemisphere. Ice and Snow, 2020, **60** (1), 134–148. (In Russian).
57. Meleshko V.P. et al. The Arctic climate warming and extremely cold winters in North Eurasia during 1979–2017. Russ. Meteorol. Hydrol., 2019, **44** (4), 223–230.
58. Meredith M. et al. Polar Regions. In: IPCC Special Report on the Ocean and Cryosphere in a Changing Climate. H.-O. Pörtner et al. (eds.). Cambridge Univ. Press, Cambridge / New York, NY, 2019, 203–320, https://doi.org/10.1017/9781009157964.005.
59. Methane and Climate Change: Scientific Problems and Technological Aspects. V.G. Bondur et al. (eds.), Noscow, RAS, 2022, 388 pp. (In Russian).
60. Mokhov I.I. Russian climate research in 2015-2018. Izv., Atmos. Oceanic Phys., 2020, **56** (4), 325–343.
61. Mokhov I.I. Features of modern climate changes in the Arctic and their consequences. Arctic and Antarctic Research, 2020, **66** (4), 446–462. (In Russian).
62. Mokhov I.I. Anomalous winters in regions of Northern Eurasia in different phases of the El Nino phenomena. Doklady Earth Sci., 2020, **493** (2), 649–653.
63. Mokhov I.I. Extreme atmospheric and hydrological phenomena in Russian regions: Relationship with the Pacific Decadal Oscillation. Doklady Earth Sci., 2021, **500** (2), 861–865.
64. Mokhov I.I. Climate change: Causes, risks, consequences, and problems of adaptation and regulation. Herald Russ. Acad. Sci., 2022, **92** (1), 1–11.
65. Mokhov I.I. Changes in the frequency of phase transitions of different types of El Nino phenomena in recent decades. Izv,, Atmos. Oceanic Phys., 2022, 58 (1), 1–6.
66. Mokhov I.I., Bondur V.G., Sitnov S.A., Voronova O.S. Satellite monitoring of wildfires and emissions into the atmosphere of combustion products in Russia: Relation to atmospheric blockings. Doklady Earth Sci., 2020, **495** (2), 921–924.
67. Mokhov I.I., Makarova M.E., Poroshenko A.G. Tropical cyclones and their transformation into extratropical: Estimates of the half-century trends. Doklady Earth Sci., 2020, **493** (1), 552–557.
68. Mokhov I.I., Medvedev N.N. The amplitude–frequency features of different El Nino types and their changes in recent decades. Moscow Univ. Phys. Bull., 2022, **77** (3), 542–548.
69. Mokhov I.I., Parfenova M.R. Variability features of Antarctic and Arctic sea ice in recent decades under global and regional climate change. Voprosy Geografii (Questions of Geography), 2020, **150**, 304–319. (In Russian).
70. Mokhov I.I., Parfenova M.R. Relationship of the extent of Antarctic and Arctic sea ice with temperature changes, 1979–2020. Doklady Earth Sci., 2021, **496** (1), 66–71.
71. Mokhov I.I., Parfenova M.R. Changes in the snow cover extent in Eurasia from satellite data in relation to hemispheric and regional temperature changes. Doklady Earth Sci., 2021, **501** (1), 963–968.

72. Mokhov I.I., Parfenova M.R. The relationship between snow cover and sea ice extent and temperature changes in the Northern Hemisphere based on data for recent decades. Izv., Atmos. Oceanic Phys., 2022, **58** (4), 353–363.
73. Mokhov I.I., Parfenova M.R. Relationships between satellite-derived snow cover extent in the Northern Hemisphere and surface air temperature. Russ. Meteorol. Hydrol., 2022, **47** (2), 98–106.
74. Mokhov I.I., Poroshenko A.G. Action as an integral characteristic of atmospheric (climatic) structures: Estimates for tropical cyclones. Izv., Atmos. Oceanic Phys., 2020, **56** (6), 539–544.
75. Mokhov I.I., Poroshenko A.G. Statistical and model estimates of the relationship between the size and lifetime of Polar Lows. Moscow Univ. Phys. Bull., 2021, **76** (6), 477–481.
76. Mokhov I.I., Poroshenko A.G. Statistical and model estimates of the relationship between the intensity and duration of tropical cyclones. Russ. Meteorol. Hydrol., 2021, **46** (5), 302-306.
77. Mokhov I.I., Smirnov D.A. Empirical estimates of the contribution of greenhouse gases and natural climatic variability to surface air temperature trends for various latitudes. Doklady Earth Sci., 2022, **503** (1), 114–118.
78. Mokhov I.I., Smirnov D.A. Estimating contributions of natural climate variability modes and greenhouse gases to surface temperature trends in the Southern Hemisphere from observations. Izv., Atmos. Oceanic Phys., 2022, **58** (2), 131–139.
79. Mokhov I.I., Timazhev A.V. Frequency of summer atmospheric blockings in the Northern Hemisphere in different phases of El Nino and Pacific Decadal and Atlantic Multidecadal Oscillations. Izv., Atmos. Oceanic Phys., 2022, **58** (3), 199–207.
80. Mokhov I.I., Timazhev A.V. Integral index of atmospheric blocking activity in the Northern Hemisphere in recent decades. Izv., Atmos. Oceanic Phys., 2022, **58** (6), 545–552.
81. Mokhov I.I., Chernokulsky A.V., Osipov A.M. Atmospheric centers of action in the Northern and Southern Hemispheres: Features and variability. Russ. Meteorol. Hydrol., 2020, **45** (11), 749–761.
82. Mokhov I.I., Yushkov V.P., Timazhev A.V., Babanov B.A. Squalls with a hurricane wind in Moscow. Moscow Univ. Phys. Bull., 2020, **75** (6), 712–716.
83. Mokhov I.I., Smirnov D.A. Contributions to surface air temperature trends estimated from climate time series: Medium-term causalities. Chaos, 2022, **32**, 063128, https://doi.org/10.1063/5.0088042
84. Mokhov I.I., Timazhev A.V. Seasonal hydrometeorological extremes in the Northern Eurasian regions depending on ENSO phase transitions. Atmosphere, 2022, **13** (2), 249, https://doi.org/10.3390/atmos13020249
85. Mukhin D., Gavrilov A., Loskutov E. et al. Bayesian data analysis for revealing causes of the middle Pleistocene transition. Sci. Rep., 2019, **9** (1), 7328, https://www.nature.com/articles/s41598-019-43867-3.
86. Mukhin D.N., Seleznev A.F., Gavrilov A.S., Feigin A M. Optimal data-driven models of forced dynamical systems: general approach and examples from climate. Izv. VUZ. Appl. Nonlin. Dyn., 2021, **29** (4), 571–602. (In Russian).
87. Nerushev A.F. et al. Statistical model of the time variability of the characteristics of high-altitude jet currents in the Northern Hemisphere based on satellite measurements. Izv., Atmos. Oceanic Phys. 2021, **57** (4), 354–364.

88. Overland J., Wang M., Dunlea E. et al. The urgency of Arctic change. Polar Sci., 2019, **21**, 6-13. Polonsky A.B. The ocean's role in climate change. Cambridge Scholars Publ., Newcastle upon Tyne. 2019. 276 pp.
89. Polonsky A.B. The IOD-ENSO interaction: The role of the Indian Ocean current's system. Atmosphere, 2021, **12** (12), 1662, https://doi.org/10.3390/atmos12121662.
90. Perevedentsev Yu.P. et al. Climate change on the territory of Russia in the late 20th – early 21st centuries. Russ. Meteorol. Hydrol., 2021, **46** (10), 658–666.
91. Polonsky A.B., Serebrennikov A.N. Intensification of eastern boundary upwelling systems in the Atlantic and Pacific Oceans. Russ. Meteorol. Hydrol., 2020, **45** (5), 422–429.
92. Polonsky A.B., Sukhonos P.A. Influence of the North Atlantic Oscillation on the heat budget of the mixed layer in the North Atlantic. Russ. Meteorol. Hydrol., 2020, **45** (9), 623–629.
93. Report on climate features in the territory of the Russian Federation for 2018. Moscow: Roshydromet. 2019. 79 pp. (In Russian).
94. Report on climate features in the territory of the Russian Federation for 2019. Moscow: Roshydromet. 2020. 97 pp. (In Russian).
95. Report on climate features in the territory of the Russian Federation for 2020. Moscow: Roshydromet. 2021. 104 pp. (In Russian).
96. Report on climate features in the territory of the Russian Federation for 2021. Moscow: Roshydromet. 2022. 104 pp. (In Russian).
97. Report on climate features in the territory of the Russian Federation for 2022. Moscow: Roshydromet. 2023. 108 pp. (In Russian).
98. Russian National Report: Meteorology and Atmospheric Sciences (2015–2018). Ed. by I.I. Mokhov, A.A. Krivolutsky. Moscow, MAKS Press, 2019, 332 pp.
99. Semenov V.A. Modern Arctic climate research: Progress, change of concepts, and urgent problems. Izv., Atmos. Oceanic Phys., 2021, **57** (1), 18–28.
100. Semenov V.A., Matveeva T.A. Arctic sea ice in the first half of the 20th century: Temperature-based spatiotemporal reconstruction. Izv., Atmos. Oceanic Phys., 2020, **56** (5), 534–538.
101. Semenov S.M. et al. Statistical model for assessing the formation of climate-related hazards based on climate monitoring data. Russ. Meteorol. Hydrol., 2020, **45** (5), 339–344.
102. Serykh I.V., Sonechkin D.M. Nonchaotic and globally synchronized short-term climatic variations and their origin. Theor. Appl. Climatol., 2019, **137**, 2639–2656.
103. Shakhova N., Semiletov I., Chuvilin E. Understanding the permafrost-hydrate system and associated methane releases in the East Siberian Arctic shelf. Geosci., 2019, **9** (6), 251.
104. Schepaschenko D. et al. Russian forest sequesters substantially more carbon than previously reported. Sci. Rep., 2021, **11** (1).
105. Slyunyaev N.N., Ilin N.V., Mareev E.A., Price C.G. The global electric circuit land-ocean response to the El Nino – Southern Oscillation. Atmos. Res., 2021, **260**, 105626.
106. Slyunyaev N.N., Ilin N.V., Mareev E.A., Price C.G. A new link between El Nino – Southern Oscillation and atmospheric electricity. Environ. Res. Lett., 2021, 16 (4), 044025.

107. Smith P. et al. Interlinkages between desertification, land degradation, food security and greenhouse gas fluxes: Synergies, trade-offs and integrated response options. In: Climate Change and Land: an IPCC special report on climate change, desertification, land degradation, sustainable land management, food security, and greenhouse gas fluxes in terrestrial ecosystems P.R. Shukla et al. (eds.), 2019, 551–672, https://doi.org/10.1017/9781009157988.008.
108. Sonechkin D.M., Vakulenko N.V., Volodin E.M. Sun-induced synchronizations of the interannual to interdecadal hemispheric mean (land and sea) temperature variations. J. Atmos. Solar-Terr. Phys., 2020, 105450.
109. Steidinger B.S. et al. Climatic controls of decomposition drive the global biogeography of forest-tree symbioses. Nature, 2019, **569** (7756), 404–408.
110. Sukhonos P.A., Diansky N.A. Connections between the long-period variability modes of both temperature and depth of the upper mixed layer of the North Atlantic and the climate variability indices. Izv., Atmos. Oceanic Phys., 2020, **56** (3), 300–311.
111. Surkova G., Krylov A. Extremely strong winds and weather patterns over arctic seas. Geography, Environment, Sustainability, 2019, **12** (3), 34–42.
112. Third Assessment Report on Climate Change and Its Consequences on the Territory of the Russian Federation. St. Petersburg, Naukoemkie Technologii, 2022, 676 pp. (In Russian).
113. Vakulenko N.V. Changes in general atmospheric circulation in the Northern Hemisphere in 1998–2018. Russ. Meteorol. Hydrol., 2020, **45** (10), 677–682.
114. Vanderkelen I. et al. Global heat uptake by inland waters. Geophys. Res. Lett., 2020, **47** (12), e2020GL087867, https://doi.org/10.1029/2020GL087867.
115. Vargin P.N. et al. Study of the variability of spring breakup dates and Arctic stratospheric polar vortex parameters from simulation and reanalysis data. Izv., Atmos. Oceanic Phys., 2020, **56** (5), 458–469.
116. Vasiliev A.A. et al. Permafrost degradation: Results of the long-term geocryological monitoring in the western sector of Russian Arctic. Earth's Cryosphere, **XXIV** (2), 14–26.
117. Vyruchalkina T.Yu. et al. Evolution of the Caspian Sea level under the influence climatic changes of the wind field. Trudy GOIN, 2019, 220, 135–147. (In Russian).
118. Vyruchalkina T.Yu. et al. Effect of long-term variations in wind regime over Caspian Sea region on the evolution of its level in 1948–2017. Water Resources, 2020, 47 (2), 348–357.
119. Zherebtsov G.A., Kovalenko V.A., Molodykh S.I., Kirichenko K.E. Solar variability manifestations in weather and climate characteristics. J. Atmos. Solar-Terr. Phys., 2019, **182**, 217–222.
120. Zuev V.V., Savelieva E.S. Dynamics of Stratospheric Polar Vortices. Novosibirsk, Geo, 2020, 115 pp. (In Russian)ю
121. Zveryaev I.I., Arkhipkin A.V. Leading modes of interannual soil moisture variability in European Russia and their relation to regional climate during the summer season. Cli. Dyn., 2019, **53**, 3007–3022.

Climate theory and climate system modelling

Various areas of climate theory and problems of modeling the climate system are considered in [1–112]. Climate and Earth system models of varying degrees of complexity (from the simplest conceptual models to the most complex and detailed global and regional models) are used. New parameterizations, algorithms and model components are being developed for the modification of climate models and models of the Earth system as a whole. Increasingly, Earth system models are being developed that include the interaction of the climate system with the natural carbon cycle and other natural cycles.

Different numerical experiments were carried out with the climate general circulation model and the Earth system model at the INM RAS, including within the framework of the CMIP6 international climate model comparison project [109] (see also [104–108]). The results of the performed model calculations are used, among other things, in the reports of the Intergovernmental Panel on Climate Change (IPCC).

The development of models of the Earth system implies, in particular, a more detailed account of the upper layers of the atmosphere, including the ionosphere. In [26], a joint model of the global dynamics of the Earth's thermosphere and ionosphere (for altitudes of 90–500 km) is presented. The model is based on a three-dimensional model of the general circulation of the thermosphere and a dynamic model of the F layer of the ionosphere, which takes into account plasma-chemical processes, ambipolar diffusion, and advective transport of ions due to the neutral wind. The proposed model is generally capable of reproducing the main characteristics of the upper atmosphere. The sensitivity of the thermospheric characteristics to the ionospheric parameters and the sensitivity of the distribution of the electron density field in the ionospheric F layer to the thermospheric parameters were studied for a given diurnal cycle.

In [43], the results of a study of the ionospheric potential using the chemical climate model SOCOL (Solar Climate Ozone Links) are presented. In the considered case, the parameterization of the electric potential difference between the Earth's surface and the lower boundary of the ionosphere was used depending on the thunderstorm and electrified properties of clouds. The results obtained contribute to the understanding of the features of the change in the ionospheric potential in the daily and annual variations. A comparison is made with the corresponding studies using the INMCM4 climate model with a similar parameterization of the ionospheric potential.

In [67], the results of an assessment of the regional impact of accounting for the atmospheric cycle of sulfur dioxide on the terrestrial carbon cycle are presented on the basis of numerical experiments with a climate model of intermediate complexity (IAP RAS CM).

A number of interesting results have been obtained in the field of model studies of the mechanisms of climatic variability, including the study of the features of the manifestation and mechanisms of formation of quasi-cyclic climatic modes and their influence on global processes [23, 39, 51, 81, 104, 105]. In particular, the climatic processes associated with the Atlantic multidecadal oscillation, quasi-biennial cyclicity, and El Niño phenomena are studied.

Review [98] considers the issues of modeling changes in the regimes of tropical cyclones, the Hadley circulation, and jet streams in the atmosphere under global warming. It is concluded that in the 21st century, the greatest expansion of the latitudinal range of manifestation of tropical cyclones over the past 3 million years is likely. The trends in the penetration of tropical cyclones into extratropical latitudes are also estimated.

A number of climate studies have been carried out using conceptual models [4–7, 15, 21, 66, 70, 71, 75, 76, 80, 85, 90–95]. In [15], particularly, the features of climatic variability in the North Atlantic are studied using a simple stochastic model that uses a random forcing to simulate heat transfer between the atmosphere and the ocean and the influence of the Atlantic meridional circulation on the ocean surface temperature. In particular, the results show that the relationship between the indices of the Atlantic meridional circulation and the Atlantic Multidecadal Oscillation depends on oceanic feedbacks and the intensity of dissipation.

In [66], using the energy-balance climate model, the analytical conditions for the formation of the so-called Arctic (polar) amplification were obtained depending on various types of radiation impacts on the Earth's climate system, including solar and volcanic activity and anthropogenic changes in the carbon dioxide content in the atmosphere, and taking into account various climate feedbacks. The conditions for the formation of the Arctic amplification were obtained also under the simultaneous action of various factors, in particular, with a simultaneous change in the solar constant and the CO_2 content in the atmosphere.

For the development of modeling studies of paleoclimatic processes, relevant projects organized within the framework of international CMIP programs, in particular PMIP (Paleoclimate Modeling Intercomparison Project), are of significant importance. In order to assess the ability of climate models to adequately reproduce paleoclimatic changes, appropriate paleoreconstructions are needed. In [58], using model simulations, estimates were made of the uncertainty of paleoclimatic conditions in the Pleistocene. In particular, the uncertainty of the reaction of the thermal state of underwater deposits was estimated – this is essential in determining the stability of methane hydrate deposits in connection with climate change. The conclusion is supported that the characteristic time of the total inertia of permafrost and methane hydrate

deposits is not less than several thousand years. In accordance with this, the release of methane into the atmosphere in the Arctic latitudes can be explained by multi-millennial climatic changes, and not by the warming of recent decades.

In [8], the role of northern peatlands in the Earth's carbon cycle, which have been a natural sink of carbon since the last glacial maximum, was estimated. According to [8], northern peatlands, together with the oceans, should potentially play an important role in reducing the concentration of carbon dioxide in the atmosphere over the next 5 millennia.

In [67], global and regional climate changes in the Holocene were estimated using numerical simulations with a global climate model. According to the obtained model results, the current annual-mean global surface air temperature in recent decades has exceeded the corresponding values for the previous 10 thousand years, including during the period of the so-called Holocene optimum (Middle Holocene), about 6 thousand years ago. Modern temperature conditions for individual regions, in particular in Europe, may not yet reach the level of maximum warming in the middle Holocene. According to model simulations, global and regional climate changes and changes in the characteristics of the carbon cycle in the last century (taking into account anthropogenic forcings) differ significantly from changes in previous centuries and millennia, when natural forcings on the climate system played a key role.

The fundamental development of climate modeling over long time intervals, including modeling of glacial cycles in the Pleistocene, is associated with taking into account the dynamics of ice sheets and their interaction with other subsystems of the Earth's climate system. In [82], a review was made of the construction and development of glaciological models, which should be included in climate models and Earth system models.

In [22], using global chemical-climatic modeling, it was found that the geomagnetic field minima about 42 thousand years ago, in combination with solar minima, caused significant changes in the concentration and circulation of atmospheric ozone and synchronous global climate shifts with serious environmental changes that led to mass extinction.

Estimates of methane emissions into the atmosphere are of great importance in connection with the possible decomposition of methane hydrates, including on the Arctic shelf of Russia, under warming and thawing of permafrost [10, 11, 13, 56, 57, 59, 61, 64, 86]. At present, these estimates, in particular for the seas of the Eastern Arctic, differ by orders of magnitude [56, 57, 59, 61, 64, 86]. It should be noted that the emission of methane into the atmosphere, noted from observations on the Arctic shelf, can be associated with the adaptation of the thermal regime of shelf bottom sediments (with a characteristic time of about 10^4 years) to the warming regime at the Holo-

cene optimum. According to model estimates, additional global warming, taking into account the interaction with the natural methane cycle (due to the corresponding positive feedback with climate), is relatively small against the background of expected temperature changes in the 21st century with scenarios of anthropogenic forcings [64]. In [11], using the INM-CM48 terrestrial system model, no significant positive relationship was found between the methane emission on the shelf and the global surface air temperature, and it was concluded that observed features the methane emission on the shelf is mainly due to geological factors.

Various international programs, initiatives and projects with Russian participation, including CMIP6, CORDEX (ArcCORDEX), ISIMIP, NEFI (NEESPI), PEEX, PMIP and others, contribute to the development of various areas of modeling the climate system and the Earth system as a whole.

References

1. Abram N. et al. Summary for Policymakers. In: IPCC Special Report on the Ocean and Cryosphere in a Changing Climate. H.-O. Pörtner et al. (eds.). Cambridge Univ. Press, Cambridge / New York, NY, 2019, 3–35.
2. Akperov M.G. et al. Lapse rate peculiarities in the Arctic from reanalysis data and model simulations. Russ. Meteorol. Hydrol., 2019, **44** (2), 97–102.
3. Akperov M. et al. Impact of Atlantic water inflow on winter cyclone activity in the Barents Sea: insights from coupled regional climate model simulations. Environ. Res. Lett., 2020, **15**, 024009.
4. Alexandrov D.V., Bashkirtseva I.A., Ryashko L.B. Anomalous climate dynamics induced by multiplicative and additive noises. Phys. Rev. E., 2020, **102** (1), 012217.
5. Alexandrov D.V., Bashkirtseva I.A., Ryashko L.B. Variability in the noise-induced modes of climate dynamics. Phys. Lett. A., 2020, **384** (19), 126411, https://doi.org/10.1016/j.physleta.2020.126411.
6. Alexandrov D.V., Bashkirtseva I.A., Ryashko L.B. How random noise induces large-amplitude oscillations in an El Niño model. Physica D: Nonlin. Phenom., 2022, **440**, 133468.
7. Alexandrov D.V., Bashkirtseva I.A., Crucifix M., Ryashko L.B. Nonlinear climate dynamics: From deterministic behaviour to stochastic excitability and chaos. Phys. Rep., 2021, **902**, 1–60.
8. Alexandrov G.A., Brovkin V.A., Kleinen T., Yu Z. The capacity Of Northern peatlands for long-term carbon sequestration. Biogeosci., 2020, 17 (1), 47–54.
9. Allan R.P. et al. Summary for Policymakers / In: Climate Change 2021: The Physical Science Basis. Contribution of Working Group I to the Sixth Assessment Report of the Intergovernmental Panel on Climate Change. Masson-Delmotte V. et al. (eds.). Cambridge Univ. Press, Cambridge / New York, NY, 2021, 3−32.
10. Anisimov O.A. et al. Methane emission in the Russian permafrost zone and evaluation of its impact on global climate. Russ. Meteorol. Hydrol., 2020, **45** (5), 377–385.

11. Anisimov O.A., Volodin E.M. Climate effect of methane emission on the East Siberian Arctic shelf. Russ. Meteorol. Hydrol., 2022, **47** (10), 46–58.
12. Anisimov O., Zimov S. Thawing permafrost and methane emission in Siberia: Synthesis of observations, reanalysis, and predictive modeling. Ambio, 2021, **50**, 2050–2059.
13. Arzhanov M.M. et al. Modeling thermal regime and evolution of the methane hydrates stability zone of the Yamal Peninsula permafrost. Permafrost Periglac. Proc., 2020, 31 (4), 487–496.
14. Bagatinsky V.A., Diansky N.A. Contributions of temperature and salinity climatic changes to the formation of North Atlantic thermohaline circulation trends in 1951-2017. Moscow Univ. Phys. Bull., 2022, **77** (3), 564–580.
15. Bekryaev R.V. Interrelationships of the North Atlantic multidecadal climate variability characteristics. Russ. J. Earth Sci., 2019, **19** (3), doi:10.2205/2018ES000653.
16. Brierley C.M. et al. Large-scale features and evaluation of the PMIP4-CMIP6 midHolocene simulations. Clim. Past, **16** (5), 1847–1872.
17. Brodowsky C. et al. Modeling the sulfate aerosol evolution after recent moderate volcanic activity, 2008–2012. J. Geophys. Res.: Atmos., 2021, **126**, e2021JD035472, https://doi.org/10.1029/2021JD035472.
18. Canadell J.G. et al. Global carbon and other biogeochemical cycles and feedbacks. In: Climate Change 2021: The Physical Science Basis. Contribution of Working Group I to the Sixth Assessment Report of the Intergovernmental Panel on Climate Change. Masson-Delmotte V. et al. (eds.). Cambridge Univ. Press, Cambridge / New York, NY, 2021, 673–816.
19. Chilingarov A.N. et al. To the initiative of holding the Fifth International Polar Year. Hydrometeorol. Ecol., 2022, 66, 104–109. (In Russian)
20. Climate of the Arctic: Processes and Changes. I.I. Mokhov and V.A. Semenov (eds.). Moscow, Fizmatkniga, 2022, 360 pp.
21. Colman R., Soldatenko S. Understanding the links between climate feedbacks, variability and change using a two-layer energy balance model. Cli. Dyn., 2020, **54** (7–8), 3441–3459.
22. Cooper A. et al. A global environmental crisis 42,000 years ago. Science, 2021, **371**, 811–818.
23. Diansky N.A., Bagatinsky V.A. Thermohaline structure of waters in the North Atlantic in different phases of the Atlantic Multidecadal Oscillation. Izv., Atmos. Oceanic Phys., 2019, **55** (6), 628–639.
24. Diansky N.A. et al. Predictive estimates of climate changes in the Arctic based on the combined scenario. Russ. Arctic, 2019, 4. 24-33. (In Russian)
25. Douville H. et al. Water cycle changes / In: Climate Change 2021: The Physical Science Basis. Contribution of Working Group I to the Sixth Assessment Report of the Intergovernmental Panel on Climate Change. Masson-Delmotte V. et al. (eds.). Cambridge Univ. Press, Cambridge / New York, NY, 2021, 1055-1210.
26. Dymnikov V.P. et al. Coupled Earth's termosphere-ionosphere global dynamics model. Izv., Atmos. Oceanic Phys., 2020, **56** (3), 241-252.
27. Eliseev A.V. et al. A correlation between lightning flash frequencies and the statistical characteristics of convective activity in the atmosphere. Doklady Earth Sciences, 2019, **485** (1), 273–278.
28. Eliseev A.V. et al. Impact of sulfur dioxide on the terrestrial carbon cycle. Izv., Atmos. Oceanic Phys., 2019, **55** (1), 38–49.

29. Fadeev R.Y. et al. Climate version of the SL-AV global atmospheric model: Development and preliminary results. Russ. Meteorol. Hydrol., 2019, **44** (1), 13–22.
30. Frolov A.V. Dynamic-stochastic modeling of the paleo-Caspian Sea long-term level variations (14-4 thousand years BC). Water Resources, 2021, **48** (6), 854–863.
31. Frolov I.E. et al. Ice balance modeling in the Arctic Ocean in 1979–2019. Ice and Snow, 2022, **62** (1), 113-124. (In Russian).
32. Galin V.Ya., Dymnikov V.P. Dynamic-stochastic parameterization of cloudiness in the general circulation model of the atmosphere. Izv., Atmos. Oceanic Phys., 2019, **55** (5), 381–385.
33. Ginzburg A.S., Demchenko P.F. Anthropogenic meso-meteorological feedbacks: A review of a recent research. Izv., Atmos. Oceanic Phys., 2019, **55** (6), 573–590.
34. Golubenko K., Usoskin I., Mironova I., Karagodin A., Rozanov E. Natural sources of ionization and their impact on atmospheric electricity. Geophys. Res. Lett., 2020, 47 (12), e2020GL088619.
35. Grant L. et al. Attribution of global lake systems change to anthropogenic forcing. Nature Geosci., 2021, **14** (11), 849–854.
36. Gulev S.K. et al. Changing State of the Climate System. In: Climate Change 2021: The Physical Science Basis. Contribution of Working Group I to the Sixth Assessment Report of the Intergovernmental Panel on Climate Change. Masson-Delmotte V. et al. (eds.). Cambridge Univ. Press, Cambridge / New York, NY, 2021, 287–422.
37. Hock R. et al. High Mountain Areas / In: IPCC Special Report on the Ocean and Cryosphere in a Changing Climate. H.-O. Pörtner et al. (eds.). Cambridge Univ. Press, Cambridge / New York, NY, 2019, 131–202.
38. Ilin N.V., Slyunyaev N.N., Mareev E.A. Toward a realistic representation of global electric circuit generators in models of atmospheric dynamics. J. Geophys. Res.: Atmos., 2020, **125** (6), e2019JD032130.
39. Jakovlev A.R., Smyshlyaev S.P. Impact of the Southern Oscillation on Arctic stratospheric dynamics and ozone layer. Izv., Atmos. Oceanic Phys., 2019, **55** (1), 86–98.
40. Jia G. et al. Land–climate interactions. In: Climate Change and Land: an IPCC special report on climate change, desertification, land degradation, sustainable land management, food security, and greenhouse gas fluxes in terrestrial ecosystems. P.R. Shukla et al. (eds.), 2019, 131–247.
41. Kageyama M. et al. A multi-model CMIP6-PMIP4 study of Arctic sea ice at 127 ka: Sea ice data compilation and model differences. Clim. Past, 2021, **17** (1), 37–62.
42. Kageyama M. et al The PMIP4 Last Glacial Maximum experiments: Preliminary results and comparison with the PMIP3 simulations. Clim. Past, **17** (3), 1065–1089.
43. Karagodin A., Mironova I., Golubenko K. et al. The representation of ionospheric potential in the global chemistry-climate model SOCOL. The Sci. Total Environ., 2019, **697**, 134172.
44. Karagodin-Doyennel A., Rozanov E., Sukhodolov T. Iodine chemistry in the chemistry-climate model SOCOL-AERV2-I. Geosci. Mod. Dev., 2021, **14** (10), 6623–6645.

45. Kislov A.V., Morozova P.A. Level variations in the Caspian Sea under different climate conditions by the data of simulation under CMIP6 project. Water Resources, 2021, 48 (6), 844–853.
46. Klimenko V.V. et al. Global EAGLE model as a tool for studying the Influence of the atmosphere on the electric field in the equatorial ionosphere. Russ. J. Phys. Chem. B, 2019, **13**, 720–726.
47. Korneva I.A. et al. Applying the energy- and water balance model for incorporation of the cryospheric component into a climate model. Part III. Modeling mass balance on the surface of the Antarctic ice sheet. Russ. Meteorol. Hydrol., 2019, **44** (2), 87–96.
48. Krivolutsky A.A. et al. Numerical global models of the ionosphere, ozonosphere, temperature regime, and circulation for altitudes of 0–130 km: Results and prospects. Russ. Meteorol. Hydrol., 2021, **46** (9), 59–69.
49. Kulikova I.A. et al. Evaluation of practical predictability of blocking anticyclones using modern hydrodynamic models. Russ. Meteorol. Hydrol., 2022, **47** (1), 1–13.
50. Kulyamin D.V., Ostanin P.A. Modelling of equatorial ionospheric anomaly in INM RAS coupled thermosphere–ionosphere model. Russ. J. Numer. An. Math. Modell., 2020, **35** (1), 1–9.
51. Kuznetsova D.A., Bashmachnikov I.L. On the mechanisms of variability of the Atlantic Meridional Overturning Circulation (AMOC). Oceanol., 2021, **61**, 803–814.
52. Larin I.K. On the influence of global warming on the ozone layer and UVB radiation. Izv., Atmos. Oceanic Phys., 2021, **57** (1), 110–115.
53. Loskutov E., Vdovin V., Klinshov V. et al. Applying interval stability concept to empirical model of Middle Pleistocene transition. Chaos, 2022, **32** (2), 021103.
54. Lunt D.J., Bragg F., Steinig S. et al. DEEPMIP: Model intercomparison of Early Eocene Climatic Optimum (EECO) large-scale climate features and comparison with proxy data. Clim. Past, 2021, **17** (1), 203–227.
55. MacDougall A.H., Frölicher T.L., Jones C.D. et al. Is there warming in the pipeline? A multi-model analysis of the zeroemission commitment from CO_2. Biogeosci., 2020, **17**, 2987–3016.
56. Malakhova V.V. The response of the Arctic Ocean gas hydrate associated with subsea permafrost to natural and anthropogenic climate changes. IOP Conf. Ser.: Earth Environ. Sci., 2020, **606**, 012035.
57. Malakhova V.V., Eliseev A.V. Salt diffusion effect on the submarine permafrost state and distribution as well as on the stability zone of methane hydrates on the Laptev Sea shelf. Ice and Snow. 2020, **60** (4), 533–546. (In Russian).
58. Malakhova V.V., Eliseev A.V. Uncertainty in temperature and sea level datasets for the Pleistocene glacial cycles: Implications for thermal state of the subsea sediments. Glob. Planet. Change, 2020, **192**, 103249.
59. Malakhova V., Golubeva E. Model study of the effects of climate change on the methane emissions on the Arctic shelves. Atmosphere, 2022, **13** (2), 274, https://doi.org/10.3390/atmos13020274.
60. Meredith M. et al. Polar Regions / In: IPCC Special Report on the Ocean and Cryosphere in a Changing Climate. H.-O. Pörtner et al. (eds.). Cambridge Univ. Press, Cambridge / New York, NY, 2019, 203–320.
61. Methane and Climate Change: Scientific Problems and Technological Aspects. V.G. Bondur et al. (eds.), Noscow, RAS, 2022, 388 pp. (In Russian).

62. Mokhov I.I. Russian climate research in 2015–2018. Izv., Atmos. Oceanic Phys., 2020, **56** (4), 325–343.
63. Mokhov I.I. Features of modern climate changes in the Arctic and their consequences. Arctic and Antarctic Research, 2020, **66** (4), 446–462. (In Russian)
64. Mokhov I.I. Climate change: Causes, risks, consequences, and problems of adaptation and regulation. Herald Russ. Acad. Sci., 2022, **92** (1), 1–11.
65. Mokhov I.I. Geophysical thermodynamics: Features of atmospheric temperature stratification in the annual cycle. Moscow Univ. Phys. Bull., 2022, **77** (3), 549–554.
66. Mokhov I.I. Analytical conditions for the formation of Arctic Amplification in the Earth's climate system. Doklady Earth Sci., 2022, **505** (1), 496–500.
67. Mokhov I.I., Eliseev A.V., Guryanov V.V. Model estimates of global and regional climate changes in the Holocene. Doklady Earth Sci., 2020, **490** (1), 23–27.
68. Mokhov I.I., Malakhova V.V., Arzhanov M.M. Model estimates of intra- and intersentennial degradation of permafrost on the Yamal Peninsula under warming. Doklady Earth Sci., 2022, **506** (2), 782–789.
69. Mokhov I.I., Pogarsky F.A. Variations in the characteristics of sea waves in the Arctic basin caused by climate changes in the 21st century based on model simulations. Doklady Earth Sci., 2022, **496** (2), 164–167.
70. Mokhov I.I., Poroshenko A.G. Statistical and model estimates of the relationship between the size and lifetime of Polar Lows. Moscow Univ. Phys. Bull., 2021, **76** (6), 477–481.
71. Mokhov I.I., Poroshenko A.G. Statistical and model estimates of the relationship between the intensity and duration of tropical cyclones. Russ. Meteorol. Hydrol., 2021, **46** (5), 302–306.
72. Mokhov I.I., Timazhev A.V. Vertical temperature stratification of the atmosphere depending on the length of the annual insolation cycle from simulations with the coupled general circulation model. Doklady Earth Sci., 2020, **494** (2), 795–798.
73. Molodykh S.I., Zherebtsov G.A., Karakhanyan A.A. Estimation of solar activity impact on the outgoing infrared-radiation flux. Geomagn. Aeron., 2020, **60** (2), 205–211.
74. Morozova P.A. et al. Water budget of the Caspian Sea in the Last Glacial Maximum by data of experiments with mathematical models. Water Resources, 2021, 48 (6), 823–830.
75. Muryshev K.E. et al. Phase shift between changes in global temperature and atmospheric CO2 content under external emissions of greenhouse gases into the atmosphere. Izv., Atmos. Oceanic Phys., 2019, **55** (3), 235–241.
76. Muryshev K.E. et al. Influence of nonlinear processes on the time lag between changes in the global temperature and the carbon dioxide content in the atmosphere. Doklady Earth Sci., 2021, **501** (1), 949–954.
77. Osipov A.M., Gushchina D.Yu. Mechanism of generating two types of El Nino under modern climatic conditions. Moscow Univ. Geogr. Bull., 2021, 1, 128–135. (In Russian).
78. Otto-Bliesner B.L. et al. Large-scale features of Last Interglacial climate: Results from evaluating the lig127k simulations for the Coupled Model Intercomparison Project (CMIP6)-Paleoclimate Modeling Intercomparison Project (PMIP4). Cli. Past, 2021, **17** (1), 63–94.

79. Pastukhova A.S. et al. Numerical simulation of variations in ozone content, erythemal ultraviolet radiation, and ultraviolet resources over Northern Eurasia in the 21st century. Izv., Atmos. Oceanic Phys., 2019, **55** (3), 242–250.
80. Petrov D.A. Properties of the frequency spectra of the sea surface and land surface air temperature anomalies in a simple stochastic climate model with fluctuating parameters. Izv., Atmos. Oceanic Phys., 2019, **55** (4), 324–333.
81. Polonsky A.B. The Ocean's Role in Climate Change. Cambridge Scholars Publ., Newcastle upon Tyne. 2019. 276 pp.
82. Postnikova T.N., Rybak O.O. Global glaciological models: a new stage in the development of methods for predicting glacier evolution. Part 2. Formulation of experiments and practical applications. Ice and Snow, 2022, **62** (2), 287–304. (In Russian)
83. Rubinstein K.G. et al. Regional model of atmospheric dynamics for the system of numerical modelling of the Arctic climate. Hydrometeorol. Res. Forecast., 2019, 3 (373), 60–72. (In Russian)
84. Russian National Report: Meteorology and Atmospheric Sciences (2015–2018). Ed. by I.I. Mokhov, A.A. Krivolutsky. Moscow, MAKS Press, 2019, 332 pp.
85. Ryashko L., Alexandrov D.V, Bashkirtseva I. Analysis of stochastic generation and shifts of phantom attractors in a climate–vegetation dynamical model. Mathematics, 2021, **9**, 1329.
86. Shakhova N., Semiletov I., Chuvilin E. Understanding the permafrost–hydrate system and associated methane releases in the East Siberian Arctic shelf. Geosci., 2019, **9**, 251.
87. Shestakova A.A., Volodin E.M. Tropospheric vertical structure simulation with the INMCM climate model. Russ. Meteorol. Hydrol., 2019, **44** (2), 103–111.
88. Smith P. et al. Interlinkages between desertification, land degradation, food security and greenhouse gas fluxes: Synergies, trade-offs and integrated response options. In: Climate Change and Land: an IPCC special report on climate change, desertification, land degradation, sustainable land management, food security, and greenhouse gas fluxes in terrestrial ecosystems. P.R. Shukla et al. (eds.), 2019, 551–672.
89. Smyshlyaev S., Galin V., Blakitnaya P., Jakovlev A. Numerical modelling of the natural and manmade factors influencing past and current changes in polar, midlatitude and tropical ozone. Atmosphere, 2020, **11**, 76.
90. Soldatenko S.A. Estimated impacts of climate change on eddy meridional moisture transport in the atmosphere. Appl. Sci., 2019, **9** (23), 4992.
91. Soldatenko S.A. Estimating the effect of radiative effect uncertainties on climate response to changes in the concentration of stratospheric aerosols. Atmosphere, 2020, **11** (6), 654.
92. Soldatenko S.A. Effects of global warming on the poleward heat transport by non-stationary large-scale atmospheric eddies, and feedbacks affecting the formation of the Arctic climate. J. Marine Sci. Engin., 2021, 9 (8), 867.
93. Soldatenko S.A., Colman R. Climate variability from annual to multi-decadal timescales in a two-layer stochastic energy balance model: Analytic solutions and amplications for general circulation models. Tellus A, 2019, **71** (1), 1–15.
94. Soldatenko S.A., Yusupov R.M. Estimating the influence of thermal inertia and feedbacks in the atmosphere-ocean system on the variability of the global surface air temperature. Izv., Atmos. Oceanic Phys., 2019, **55** (6), 591–601.

95. Soldatenko S.A., Yusupov R.M. Model for estimating the transient response of the global mean surface temperature to changes in the concentrations of atmospheric aerosols and radiatively-active gases. Atmos. Ocean. Optics, 2019, 32 (4), 309–316. (In Russian).
96. Sonechkin D.M., Vakulenko N.V., Volodin E.M. Sun-induced synchronizations of the interannual to interdecadal hemispheric mean (land and sea) temperature variations. J. Atmos. Solar-Terr. Phys., 2020, 105450.
97. Stepanenko V.M. et al. An overview of parameterizations of heat transfer over moss-covered surfaces in the Earth system models. Izv., Atmos. Oceanic Phys., 2020, **56** (2), 101–111.
98. Studholme J., Fedorov A.V., Gulev S.K., Emanuel K., Hodges K. Poleward expansion of tropical cyclone latitudes in warming climates. Nature Geosci., 2021, https://doi.org/10.1038/s41561-021-00859-1.
99. Sukhodolov T. et al. Atmosphere–ocean–aerosol–chemistry–climate model SOCOLv4.0: description and evaluation. Geosci. Model Dev., 2021, **14**, 5525–5560.
100. Sukhonos P.A., Diansky N.A. Connections between the long-period variability modes of both temperature and depth of the upper mixed layer of the North Atlantic and the climate variability indices. Izv., Atmos. Oceanic Phys., 2020, **56** (3), 300–311.
101. Third Assessment Report on Climate Change and Its Consequences on the Territory of the Russian Federation. St. Petersburg, Naukoemkie Technologii, 2022, 676 pp. (In Russian).
102. Vanderkelen I. et al. Global heat uptake by inland waters. Geophys. Res. Lett., 2020, **47** (12), e2020GL087867, https://doi.org/10.1029/2020GL087867.
103. Vargin P.N. et al. Study of the variability of spring breakup dates and Arctic stratospheric polar vortex parameters from simulation and reanalysis data. Izv., Atmos. Oceanic Phys., 2020, **56** (5), 458–469.
104. Volodin E.M. Estimation of the contribution of different mechanisms of the phase evolution of quasi-biennial oscillation using the results of climate simulation. Izv., Atmos. Oceanic Phys., 2019, **55** (1), 32–37.
105. Volodin E.M. On the mechanism of Arctic climate oscillation with a period of about 15 years according to data of the INM RAS climate model. Izv., Atmos. Oceanic Phys., 2020, **56** (2), 112–122.
106. Volodin E.M. Equilibrium sensitivity of a climate model to an increase in the atmospheric CO_2 concentration using different methods to account for cloudiness. Izv., Atmos. Oceanic Phys., 2021, **57** (2), 127–132.
107. Volodin E.M. Relationship between natural climate variability and equilibrium sensitivity in the climate model of the Institute of Numerical Mathematics of the Russian Academy of Sciences to increasing CO_2. Izv., Atmos. Oceanic Phys., 2021, **57** (5), 447–450.
108. Volodin E. The mechanisms of cloudiness evolution responsible for equilibrium climate sensitivity in climate model INM-CM4-8. Geophys. Res. Lett., 2021, **48** (24), e2021GL096204.
109. Volodin E.M., Gritsun A.S. Simulation of possible future climate changes in the 21st century in the INM-CM5 climate model. Izv., Atmos. Ocean Phys., 2020, **56** (3), 218–228.

110. Vyruchalkina T.Yu. et al. Evolution of the Caspian Sea level under the influence climatic changes of the wind field. Trudy GOIN, 2019, 220, 135–147. (In Russian)
111. Winkler A.J., Myneni R.B., Brovkin V., Alexandrov G.A. Earth system models underestimate carbon fixation by plants in the high latitudes. Nature Comm., 2019, **10** (1), 885.
112. Xu L.Y. et al. The effect of super volcanic eruptions on ozone depletion in a chemistry–climate model. Adv. Atmos. Sci., 2019, **36**, 823–836.

Global and regional climate change simulations with assessment of natural and anthropogenic contribution

In [1–53], the results of modeling global and regional climate changes, in particular in the Russian regions, are presented, with an assessment of the role of natural and anthropogenic factors at different time horizons.

The results of comprehensive studies of climate change in Russian regions are given in [51] (see also [25, 26]). According to [51], global warming in the 21st century will be accompanied by the formation of an increasingly warm and humid climate in most Russian regions. An increase in winter temperature and an increase in precipitation in the colder regions is accompanied by an increase in spring snow stock with a complication of the flood situation in the catchment areas of the largest rivers during the snowmelt period. In the southern Russian regions, an increase in aridity is expected with an increase in the influence of extremely high temperatures and extreme precipitation in the summer seasons. Significant environmental and socio-economic consequences are associated with the degradation of permafrost and the reduction in the extent of sea ice in the Arctic. In general, according to simulations with CMIP6 models with scenarios of the SSP family, estimates of expected climate changes in the Russian regions in the 21st century are in qualitative agreement with the estimates obtained earlier with the SRES and RCP scenarios. This indicates a fairly high degree of sustainability of climate change assessments for Russian regions.

In [53], the results of climate change modeling in 2015–2100 are presented using the global climate model INM-CM5 under various scenarios of anthropogenic forcings (SSP1-2.6, SSP2-4.5, SSP3-7.0 and SSP5-8.5). Among other things, it was noted that the complete absence of sea ice in the Arctic Ocean in the 21st century is not achieved under any of the analyzed scenarios. This is because this climate model is characterized by a relatively slow rate of global warming compared to other models in the CMIP6 ensemble. By the end of the 21st century, a weakening of the intensity of the Hadley circulation in both hemispheres is manifested with expansion towards the poles. A change in the Ferrel cell is also noted. Against the background of the

warming of the troposphere and the cooling of the stratosphere, the features of the change in westerly winds in the middle latitudes are manifested.

In [5], estimates of changes in precipitation characteristics in Russian regions were obtained based on simulations with the ensemble of climate models CMIP6 under the scenario of anthropogenic forcings SSP585 for the 21st century. For most Russian regions, a general increase in the total amount of precipitation and the frequency of extreme precipitation in winter seasons was obtained. For summer seasons, there is a slight decrease in the total amount of precipitation and their frequency in the south of the European part of Russia.

Comprehensive studies of key processes and changes in the Arctic climate system carried out in [13]. Estimates of possible regional changes in the temperature regime and sea ice, including those along the Northern Sea Route, changes in wind-wave and cyclonic activity, and changes in permafrost are presented. Estimates of the impact of climate change on the regimes of methane hydrates, in particular, subaqueous deposits of methane hydrates, are given. The results of comprehensive studies of changes in the methane cycle, including the regimes of methane hydrates in the Arctic regions, under climate change are presented in [32].

In [2], for the first time, quantitative estimates of changes in wind energy resources in the Arctic were obtained using a regional climate model under different scenarios of anthropogenic forcings (RCP4.5 and RCP8.5) for the 21st century. A noticeable increase in the 21st century in the power of wind energy potential, proportional to the cube of wind speed, over the Barents, Kara and Chukchi seas and coastal regions in winter has been revealed. In summer, a general increase in the power of the wind energy potential over the Arctic Ocean is manifested. Changes are more significant under the scenario with higher anthropogenic forcing (RCP8.5).

In [41], the analysis of the changes in the duration of navigation period along the Northern Sea Route was carried out based on simulations with climate models of the CMIP5 ensemble under the RCP 8.5 scenario in the 21st century using Bayesian averaging methods with the selection of various parts of the Northern Sea Route. It was found that the differences in the quality of reproduction by models of the duration of the navigation period and its changes in the western part of the Northern Sea Route are greater than in the eastern part.

In [40], estimates of changes in the frequency of atmospheric blockings in the Northern Hemisphere with different criteria for their detection were obtained using numerical simulations with climate general circulation models of the CMIP5 ensemble under various RCP scenarios of anthropogenic forcings for the 21st century. The quality of reproduction of atmospheric blocking characteristics by different climate models was assessed by comparing merid-

ional seasonal distributions of atmospheric blocking frequency with reanalysis data. According to the results obtained, it is necessary to select ensembles of models that better reproduce modern atmospheric blocking regimes and their variations. When selecting the best models, in particular, the risk of an increase in the frequency of atmospheric blockings under warming is revealed, which was not revealed from simulations with an ensemble of all analyzed models.

In [19], a review of publications with estimates of changes in the runoff of Russian rivers under climate change in the 21st century, carried out in recent years, is made. It is noted that the use of regional hydrological models helps to reduce the uncertainty of possible future changes in the water regime of rivers. In [29], the changes in the runoff of the Amur and Selenga rivers were analyzed according to simulations with the ensemble of climate models CMIP6 under different SSP scenarios in the 21st century using the Bayesian approach. The large intermodel differences noted for both watersheds are associated with estimates of both long-term average runoff and interannual variability. The runoff in the Amur basin shows a positive trend in the 21st century under all analyzed scenarios of anthropogenic forcing. For the Selenga River runoff, trends in the 21st century have not been identified under all the scenarios of anthropogenic forcings used. Significant interdecadal variations in the interannual runoff variability were noted.

In [15], model estimates of the contribution of anthropogenic and natural emissions of greenhouse gases from the territory of different countries to global climate change in the 21st century were obtained under various scenarios of anthropogenic forcings. Quantitative estimates are made of the impact of taking into account changes in regional climatic conditions on the intensity of greenhouse gas exchange between the atmosphere and natural ecosystems at different time horizons in comparison with anthropogenic emissions. In particular, for Russia, China, Canada and the USA in the second half of the 21st century, the absorption of CO_2 by natural ecosystems decreases under all analyzed scenarios of anthropogenic forcing with the weakening of the corresponding climate stabilizing effect. At the same time, the emission of methane into the atmosphere by bog ecosystems in the analyzed regions increases significantly in the 21st century according to model estimates. As a consequence, the net effect of natural fluxes of greenhouse gases into the atmosphere for individual regions can accelerate warming.

References

1. Abram N. et al. Summary for Policymakers. In: IPCC Special Report on the Ocean and Cryosphere in a Changing Climate. H.-O. Pörtner et al. (eds.). Cambridge Univ. Press, Cambridge / New York, NY, 2019, 3–35.

2. Akperov M.G. et al. Wind energy potential in the Arctic and Subarctic regions and its projected change in the 21st century based on regional climate model simulations. Russ. Meteorol. Hydrol., 2022, **47** (6), 428–436.
3. Akperov M. et al. Future projections of cyclone activity in the Arctic for the 21st century from regional climate models (Arctic-CORDEX). Glob. Planet. Change, 2019, **182**, 103005.
4. Akperov M., Zhang W., Miller P.A. et al. Responses of Arctic cyclones to biogeophysical feedbacks under future warming scenarios in a regional Earth system model. Enveron. Res. Lett., 2021, **16**, 064076. https://doi.org/10.1088/1748-9326/ac0566.
5. Aleshina M.A., Semenov V.A. Changes in precipitation characteristics over Russia in XX–XXI centuries from CMIP6 models ensemble. Fund. Appl. Climatol., 2022, 8 (4), 424–440. (In Russian).
6. Alexandrov G.A., Ginzburg V.A., Romanovskaya A.A., Insarov G.E. CMIP6 model projections leave no room for permafrost to persist in Western Siberia under the SSP5-8.5 scenario. Cli. Change, 2021, **169**, (3–4), DOI:10.1007/s10584-021-03292-w.
7. Allan R.P. et al. Summary for Policymakers. In: Climate Change 2021: The Physical Science Basis. Contribution of Working Group I to the Sixth Assessment Report of the Intergovernmental Panel on Climate Change. Masson-Delmotte V. et al. (eds.). Cambridge Univ. Press, Cambridge / New York, NY, 2021, 3−32, doi:10.1017/9781009157896.001.
8. Anisimov O., Zimov S. Thawing permafrost and methane emission in Siberia: Synthesis of observations, reanalysis, and predictive modeling. Ambio, 2021, **50**, 2050–2059.
9. Arzhanov M.M. et al. Modeling thermal regime and evolution of the methane hydrates stability zone of the Yamal Peninsula permafrost. Permafrost Periglac. Proc., 2020, **31** (4), 487–496.
10. Brown J.R. et al. Comparison of past and future simulations of ENSO in CMIP5/PMIP3 and CMIP6/PMIP4 models. Clim. Past, 2020, **16** (5), 1777–1805.
11. Canadell J.G. et al. Global carbon and other biogeochemical cycles and feedbacks. In: Climate Change 2021: The Physical Science Basis. Contribution of Working Group I to the Sixth Assessment Report of the Intergovernmental Panel on Climate Change. Masson-Delmotte V. et al. (eds.). Cambridge Univ. Press, Cambridge / New York, NY, 2021, 673–816.
12. Caretta M.A. et al. Water. In: Climate Change 2022: Impacts, Adaptation and Vulnerability. Contribution of Working Group II to the Sixth Assessment Report of the Intergovernmental Panel on Climate Change. H.-O. Pörtner et al. (eds.). Cambridge Univ. Press, Cambridge / New York, NY, 2022, 551–712.
13. Climate of the Arctic: Processes and Changes. I.I. Mokhov and V.A. Semenov (eds.). Moscow, Fizmatkniga, 2022, 360 pp.
14. Denisov S.N. et al. Contribution of natural and anthropogenic emissions of CO2 and CH4 to the atmosphere from the territory of Russia to global climate changes in the twenty-first century. Doklady Earth Sci., 2019, **488** (1), 1066–1071.
15. Denisov S.N. et al. Model estimates for contribution of natural and anthropogenic CO_2 and CH_4 emissions into the atmosphere from the territory of Russia, China, Canada, and the USA to global climate change in the 21st century. Russ. Meteorol. Hydrol., **47** (10), 735–747.

16. Diansky N.A. et al. Predictive estimates of climate changes in the Arctic based on the combined scenario. Russ. Arctic, 2019, 4. 24–33. (In Russian)
17. Douville H. et al. Water cycle changes. In: Climate Change 2021: The Physical Science Basis. Contribution of Working Group I to the Sixth Assessment Report of the Intergovernmental Panel on Climate Change. Masson-Delmotte V. et al. (eds.). Cambridge Univ. Press, Cambridge / New York, NY, 2021, 1055–1210.
18. Eliseev A.V., Vasilieva A.V. Natural fires: Observational data and modelling. Fund. Appl. Climatol., 2020, 3, 73–119.
19. Gelfan A.N. et al. Runoff of Russian rivers under current and forecasted climate changes: A review. 2. Climate change impact on the water regime of Russian rivers in the XXI century. Water Resources, 2022, **49** (3), 351–365.
20. Golub M. et al. A framework for ensemble modelling of climate change impacts on lakes worldwide: the ISIMIP Lake Sector. Geosci. Model Dev., 2022, **15**, 4597–4623.
21. Grant L. et al. Attribution of global lake systems change to anthropogenic forcing. Nature Geosci., 2021, 14 (11), 849–854.
22. Gulev S.K. et al. Changing State of the Climate System. In Climate Change 2021: The Physical Science Basis. Contribution of Working Group I to the Sixth Assessment Report of the Intergovernmental Panel on Climate Change. Masson-Delmotte V. et al. (eds.). Cambridge Univ. Press, Cambridge / New York, NY, 2021, 287–422.
23. Hock R. et al. High Mountain Areas. In: IPCC Special Report on the Ocean and Cryosphere in a Changing Climate. H.-O. Pörtner et al. (eds.). Cambridge Univ. Press, Cambridge / New York, NY. 2019. P. 131–202.
24. Jia G. et al. Land–climate interactions. In: Climate Change and Land: an IPCC special report on climate change, desertification, land degradation, sustainable land management, food security, and greenhouse gas fluxes in terrestrial ecosystems. P.R. Shukla et al. (eds.), 2019, 131–247.
25. Kattsov V.M., Shkolnik I.M., Pavlova V.N. et al. Development of a technique for regional climate probabilistic projections over the territory of Russia aimed at building scenarios of climate impacts on economy sectors. P. 2: Climate impact projections. Tr. MGO, 2019, **593**, 6–52. (In Russian)
26. Kattsov V.M. et al. Climate change projections over the territory of Russia through the XXI century based on ensembles of CMIP6 models. Proc. MGO, 2022, **604**, 5–54. (In Russian)
27. Khlebnikova E.I. et al. Changes in indicators of temperature extremes in the 21st century: Ensemble projections for the territory of Russia. Russ. Meteorol. Hydrol., 2019, **44** (3), 159–168.
28. Khlebnikova E.I. et al. Changes in precipitation regime over the territory of Russia: Data of regional climate modelling and observations. Russ. Meteorol. Hydrol., 2019, **44** (7), 431–439.
29. Lipavsky A.S. et al. Bayesian projections of the Amur and Selenga River runoff changes in the 21st century based on CMIP6 model ensemble simulations. Russ. Meteorol. Hydrol., 2022, **47** (5), 370–384.
30. Martynova Yu.V. et al. Variation of Northern hemispheric wintertime storm tracks under future climate change in INM-CV5 simulations. Izv., Atmos. Oceanic Phys., 2022, **58** (3), 208–218.

31. Meredith M. et al. Polar Regions. In: IPCC Special Report on the Ocean and Cryosphere in a Changing Climate. H.-O. Pörtner et al. (eds.). Cambridge Univ. Press, Cambridge / New York, NY, 2019, 203–320.
32. Methane and Climate Change: Scientific Problems and Technological Aspects. V.G. Bondur et al. (eds.), Noscow, RAS, 2022, 388 pp. (In Russian)
33. Mirvis V.M. et al. Anomalous winter and summer weather patterns over Russia in the 21st century as simulated by CMIP6 models. Russ. Meteorol. Hydrol., 2022, **47** (6), 334–342.
34. Mokhov I.I. Russian climate research in 2015-2018. Izv., Atmos. Oceanic Phys., 2020, **56** (4), 325–343.
35. Mokhov I.I. Features of modern climate changes in the Arctic and their consequences. Arctic and Antarctic Research, 2020, **66** (4), 446–462. (In Russian)
36. Mokhov I.I. Climate change: Causes, risks, consequences, and problems of adaptation and regulation. Herald Russ. Acad. Sci., 2022, **92** (1), 1–11.
37. Mokhov I.I., Malakhova V.V., Arzhanov M.M. Model estimates of intra- and intersentennial degradation of permafrost on the Yamal Peninsula under warming. Doklady Earth Sci., 2022, **506** (2), 782–789.
38. Mokhov I.I. et al. Atmospheric centers of action in the Northern Hemisphere: Current features and expected changes in the 21st century based on simulations with the CMIP5 and CMIP6 ensembles of climate models. Doklady Earth Sci., 2022, **507** (2), 1132–1139.
39. Mokhov I.I., Pogarsky F.A. Variations in the characteristics of sea waves in the Arctic basin caused by climate changes in the 21st century based on model simulations. Doklady Earth Sci., 2022, **496** (2), 164–167.
40. Mokhov I.I., Timazhev A.V. Atmospheric blocking and changes in its frequency in the 21st century simulated with the ensemble of climate models. Russ. Meteorol. Hydrol., 2019, **44** (6), 369–377.
41. Parfenova M.R. et al. Changes in the duration of the navigation period in Arctic seas along the Northern Sea Route in the twenty first century: Bayesian estimates based on calculations with the ensemble of climate models. Doklady Earth Sci., 2022, **507** (1), 952–958.
42. Pavlova V., Shkolnik I., Pikaleva A. et al. Future changes in spring wheat yield in the European Russia as inferred from a large ensemble of high-resolution climate projections. Environ. Res. Lett., 2019, **14**, 034010, DOI: 10.1088/1748-9326/aaf8be.
43. Pikaleva A.A. et al. High-resolution ensemble climate projections of water deficit in arid regions by the mid-21st century. Russ. Meteorol. Hydrol., 2020, 45 (12), 844–850.
44. Polonsky A.B. The ocean's role in climate change. Cambridge Scholars Publishing, Newcastle upon Tyne. 2019. 276 pp.
45. Russian National Report: Meteorology and Atmospheric Sciences (2015–2018). Ed. by I.I. Mokhov, A.A. Krivolutsky. Moscow, MAKS Press, 2019, 332 pp.
46. Santolaria-Otin M., Zolina O. Evaluation of snow cover and snow water equivalent in the continental Arctic in CMIP5 models. Cli. Dyn., 2020, **55**, 2993–3016.
47. Shkolnik I.M. et al. Modeling evolution of drought conditions in the 21st century to substantiate measures for adaption of Russian agriculture to climate impacts. Russ. Meteorol. Hydrol., 2022, **47** (5), 394–404.
48. Smith P. et al. Interlinkages between desertification, land degradation, food security and greenhouse gas fluxes: Synergies, trade-offs and integrated response op-

tions. In: Climate Change and Land: an IPCC special report on climate change, desertification, land degradation, sustainable land management, food security, and greenhouse gas fluxes in terrestrial ecosystems P.R. Shukla et al. J (eds.). 2019, 551–672.
49. Smyshlyaev S., Galin V., Blakitnaya P., Jakovlev A. Numerical modelling of the natural and manmade factors influencing past and current changes in polar, mid-latitude and tropical ozone. Atmosphere, 2020, **11**, 76.
50. Tebaldi C. et al. Climate model projections from the Scenario Model Intercomparison Project (ScenarioMIP) of CMIP6. Earth System Dyn., 2021, **12** (1), 253–293.
51. Third Assessment Report on Climate Change and Its Consequences on the Territory of the Russian Federation. St. Petersburg, Naukoemkie Technologii, 2022, 676 pp. (In Russian)
52. Volodin E.M. Possible climate change in Russia in the 21st century based on the INM-CM5-0 climate model. Russ. Meteorol. Hydrol., 2022, **47** (5), 327–333.
53. Volodin E.M., Gritsun A.S. Simulation of possible future climate changes in the 21st century in the INM-CM5 climate model. Izv., Atmos. Ocean Phys., 2020, **56** (3), 218–228.

Climate change impacts and problems of adaptation and mitigation

The problems associated with the consequences of climate change, including the problems of adaptation and mitigation, are analyzed in [1–111]. In connection with the rapid modern climate change in the regions of Russia, in particular in the Arctic latitudes, not only issues related to the adaptation of the Russian socio-economic system to the negative effects of climate change and hydrometeorological safety are relevant, but also the issues of timely consideration of new opportunities. It is necessary, for example, to strategically assess under warming the potential for reducing the frost period and lengthening the growing season in the regions of Russia, the prospects for the Northern Sea Route, etc.

Various problems related to the consequences of climate change in the Russian regions, including the problems of adaptation and regulation, are analyzed in [108]. It was noted that in order to assess the consequences of climate change based on the results of modeling, spatiotemporal refinement of predictive climate estimates is required, as well as massive numerical simulations for a more reliable statistical description of the expected changes (see also [40]). As part of assessing the impact of climate change on the natural environment, the features of natural land systems, the carbon balance of soils, and marine natural systems are considered. Among the impacts of climate change on the population, the problems of the demographic situation and migration, labor resources and employment, the impact of weather and climate extremes on public health, and the epidemiological situation are highlighted. The problems of the impact of climate change on various sectors of

the Russian economy are also considered, including the mining industry, agriculture, water management, forestry, energy, transport, construction and housing and communal services, infrastructure in the permafrost zone, maritime activities, tourism and recreation.

The problems of adaptation in the Russian Arctic regions sensitive to climate change are analyzed in [25]. Among other things, the issues of preventing disturbances in the surface covers in regions with permafrost, minimizing anthropogenic pollution, maintaining and increasing the surface albedo in winter seasons are discussed. It is noted that the analysis of all indicators in the system for monitoring the effectiveness of adaptation and predictive assessments contribute to the adoption of relevant management decisions on the advisability of correcting the applied adaptation decisions.

Problems related to the impact of climate change on public health are analyzed in [32, 33, 85–88]. The review [86] presents the main materials of international organizations on the problem of assessing the impact of climate risks on the health of the urban population and action programs for adapting the health care system and other management structures. The results of Russian studies on assessing the impact of heat and cold waves on the mortality rates of the population of megalopolises and large cities located in various climatic zones – Arctic, subarctic and southern regions, including those in conditions of0 continental and monsoon climate, are systematized. It is noted that heat waves in cities with a temperate continental climate lead to a more significant increase in mortality from all causes than cold waves, compared with cities in other climatic zones. Cold waves are generally associated with much greater public health risks in northern cities than in southern ones. Quantitative estimates of threshold temperature conditions are proposed, upon reaching which it is necessary to carry out appropriate preventive measures.

In [19], the results of many years of research in connection with the problems of adaptation to climate change in the Russian economy are presented. In particular, methodological issues of using climate data in socio-economic assessments are discussed, modern processes are analyzed with predictive estimates of changes expected in the 21st century. The corresponding assessments of the impact of climate change on the economy and social sphere in Russia, including the development of key industries, are presented. The problems of the climate risk reduction strategy for the sustainable development of Russia are analyzed, including the main directions and measures for reducing net greenhouse gas emissions and adapting the population and the economy to the consequences of climate change.

In [11, 12], the problem of decarbonization of global industry, which dominates in direct and indirect emissions of greenhouse gases into the atmosphere, is analyzed. It is noted that the growth of emissions from industry

has slowed down in the last decade, and the solution to the problem of decarbonization requires a dynamic reduction in the emission of greenhouse gases into the atmosphere in the next 30-50 years with a significant modernization of the global industry with the large-scale use of new technologies.

The possibility of an energy transition from the dominant fossil hydrocarbons to the predominant use of renewable energy sources (when their part in the total energy balance exceeds 40%) is assessed in [3] (see also [4]). According to the estimates obtained, such a transition could take place in the 2060s, provided that the relative contribution of nuclear energy almost triples. It is noted that only with the joint use of renewable energy sources and nuclear power plants, it is possible to sufficiently replace hydrocarbons to achieve the goals of climate security without harming the economy.

In connection with the need to fulfill the terms of the Paris Agreement (2015) of the UN Framework Convention on Climate Change, an adequate quantitative assessment of all sources of greenhouse gas emissions into the atmosphere and their sinks is necessary, including an adequate accounting of the carbon balance of forests, terrestrial and aquatic ecosystems. Terrestrial ecosystems in Russian regions, by absorbing CO_2 from the atmosphere, contribute to slowing down the growth of global surface temperature, and by emitting CH_4 into the atmosphere, they accelerate warming. The overall effect of the natural flows of these greenhouse gases from the Russian regions under current conditions contributes to slowing down warming. According to the model estimates obtained in [21], the role of this slowing down warming effect in the first half of the 21st century grows, and after reaching a maximum (depending on the scenario of anthropogenic emissions) by the end of the century, it decreases under various analyzed scenarios of anthropogenic forcings due to the growth of natural emissions. CH_4 and a decrease in CO_2 uptake by terrestrial ecosystems (see also [22, 66]).

Potential new risks and opportunities need to be taken into account. When making decisions, it should be taken into account that, depending on the planning horizon, the role of natural emissions of greenhouse gases into the atmosphere from terrestrial ecosystems, including the stabilizing effect due to the absorption of CO_2 emissions by forests, may change. Quantitative assessments are needed at different time horizons of the role of key sources and sinks of greenhouse gases associated with various natural ecosystems – from steppe to tundra, as well as swamps, lakes, etc. [7, 9, 21, 22, 28, 31, 44, 49, 50, 56, 57, 66, 90, 91, 95, 108–111].

In [73, 75] the problems of formation of the international legal system associated with the system of control over emissions of greenhouse gases into the atmosphere as the causes of global warming of anthropogenic origin are noted. The development of international activities to control anthropogenic climate change from the time of signing in 1992 of the UN Framework Con-

vention on Climate Change to the adoption of the Paris Agreement on Climate Change in 2015 is discussed. The process of adoption of the Kyoto Protocol to the UN Framework Convention, international activities on the formation of a market for trading in greenhouse gas emissions and amendments to the Kyoto Protocol adopted in 2012 extending the Protocol until 2020 are analyzed. The main provisions of the Paris Climate Agreement and related to its ratification problems of legal regulation of control over anthropogenic emissions of greenhouse gases and aerosols at the international and national levels are considered.

As for Russia, under the continuation of global warming, along with taking into account new opportunities, including the prospects for using the Northern Sea Route, an increase in the growing season, etc., it is necessary to solve the problems of adaptation and regulation. in connection with the negative consequences of permafrost thawing, increased risk of floods, abnormal heat and droughts, forest fires, etc. [66].

In connection with ongoing and expected climate changes, in order to effectively solve the problems of adaptation to them and their possible regulation, a fundamental revision of the system of criteria for assessing new risks, negative consequences and potential benefits is required. A strategic approach is needed (not only for one or two decades), as well as the development of a common system of mutually agreed regional assessments of the predictability of seasonal climatic anomalies in interannual and interdecadal variability.

References

1. Abram N. et al. Summary for Policymakers. / In: IPCC Special Report on the Ocean and Cryosphere in a Changing Climate. H.-O. Pörtner et al. (eds.). Cambridge Univ. Press, Cambridge / New York, NY, 2019, 3–35.
2. Adler C. et al. Mountains. In: Climate Change 2022: Impacts, Adaptation and Vulnerability. Contribution of Working Group II to the Sixth Assessment Report of the Intergovernmental Panel on Climate Change. H.-O. Portner et al. (eds.). Cambridge Univ. Press, Cambridge / New York, NY, 2022, 2273–2318.
3. Akaev A.A., Davydova O.I. The Paris Agreement on climate is coming into force: Will the great energy transition take place? Herald Russ. Acad. Sci., 2020, **90** (5), 588–599.
4. Akaev A.A., Davydova O.I. A Mathematical description of selected energy transition scenarios in the 21st century, intended to realize the main goals of the Paris Climate Agreement. Energies, 2021, **14**, 2558, https://doi.org/10.3390/en14092558.
5. Akperov M.G. et al. Wind energy potential in the Arctic and Subarctic regions and its projected change in the 21st century based on regional climate model simulations. Russ. Meteorol. Hydrol., 2022, **47** (6), 428–436.
6. Aleksandrovkii A., Klimenko V., Fedotova E. et al. Estimation of hydropower plants energy characteristics change under the influence of climate factors. Adv. Engineer. Res., 2020, **191**, 7–13.

7. Alexandrov G.A., Brovkin V.A., Kleinen T., Yu Z. The capacity of northern peatlands for long-term carbon sequestration. Biogeosci., 2020, **17** (1), 47–54.
8. Allan R.P. et al. Summary for Policymakers. In: Climate Change 2021: The Physical Science Basis. Contribution of Working Group I to the Sixth Assessment Report of the Intergovernmental Panel on Climate Change. Masson-Delmotte V. et al. (eds.). Cambridge Univ. Press, Cambridge / New York, NY, 2021, 3−32.
9. Anisimov O., Zimov S. Thawing permafrost and methane emission in Siberia: Synthesis of observations, reanalysis, and predictive modeling. Ambio, 2021, **50**, 2050–2059.
10. Babiker M. et al. Cross-sectoral perspectives. In: IPCC, 2022: Climate Change 2022: Mitigation of Climate Change. Contribution of Working Group III to the Sixth Assessment Report of the Intergovernmental Panel on Climate Change. P.R. Shukla et al. (eds.). Cambridge Univ. Press, Cambridge / New York, NY, 2022, 1245–1354.
11. Bashmakov I.A. Russian low carbon development strategy. Voprosy economiki, 2020, 7, 51–74. (In Russian).
12. Bashmakov I.A. The scale of action required to decarbonize global industry. Fund. Appl. Climatol., 2022, **8** (2), 151–174. (In Russian)
13. Bashmakov I.A. et al. Industry. In: IPCC, 2022: Climate Change 2022: Mitigation of Climate Change. Contribution of Working Group III to the Sixth Assessment Report of the Intergovernmental Panel on Climate Change. P.R. Shukla et al. (eds.). Cambridge Univ. Press, Cambridge / New York, NY, 2022, 1161–1244.
14. Bednar-Friedl B. et al. Europe. In: Climate Change 2022: Impacts, Adaptation and Vulnerability. Contribution of Working Group II to the Sixth Assessment Report of the Intergovernmental Panel on Climate Change. H.-O. Portner et al. (eds.). Cambridge Univ. Press, Cambridge / New York, NY, 2022, 1817–1927.
15. Cabeza L.F. et al. Buildings. In: IPCC, 2022: Climate Change 2022: Mitigation of Climate Change. Contribution of Working Group III to the Sixth Assessment Report of the Intergovernmental Panel on Climate Change. P.R. Shukla et al. (eds.). Cambridge Univ. Press, Cambridge / New York, NY, 2022, 953–1048.
16. Callaghan T.V. et al. Improving dialogue among researchers? Local and indigenous peoples and decision-makers to address issues of climate change in the north. Ambio, 2020, **49** (6), 1161–1178.
17. Canadell J.G. et al. Global carbon and other biogeochemical cycles and feedbacks. In: Climate Change 2021: The Physical Science Basis. Contribution of Working Group I to the Sixth Assessment Report of the Intergovernmental Panel on Climate Change. Masson-Delmotte V. et al. (eds.). Cambridge Univ. Press, Cambridge / New York, NY, 2021, 673–816.
18. Caretta M.A. et al. Water. In: Climate Change 2022: Impacts, Adaptation and Vulnerability. Contribution of Working Group II to the Sixth Assessment Report of the Intergovernmental Panel on Climate Change. H.-O. Pörtner et al. (eds.). Cambridge Univ. Press, Cambridge / New York, NY, 2022, 551–712.
19. Climate Change and the Russian Economy: Trends, Scenarios, Forecasts. B.N. Porfiriev, V.I Danilov-Danilyan (eds.). Moscow, “Sci. Consultant”, 2022, 100 pp.
20. Danilov-Danilyan V.I. et al. The problem of climate change: The field of convergence and interaction between natural sciences and the sociohumanities. Herald Russ. Acad. Sci., 2020, **90** (5), 577–587.

21. Denisov S.N. et al. Contribution of natural and anthropogenic emissions of CO2 and CH4 to the atmosphere from the territory of Russia to global climate changes in the twenty-first century. Doklady Earth Sci., 2019, **488** (1), 1066–1071.
22. Denisov S.N. et al. Model estimates for contribution of natural and anthropogenic CO_2 and CH_4 emissions into the atmosphere from the territory of Russia, China, Canada, and the USA to global climate change in the 21st century. Russ. Meteorol. Hydrol., 2022, **47** (10), 735–747.
23. Dhakal S. et al. Emissions trends and drivers supplementary material. In: IPCC, 2022: Climate Change 2022: Mitigation of Climate Change. Contribution of Working Group III to the Sixth Assessment Report of the Intergovernmental Panel on Climate Change. P.R. Shukla et al. (eds.). Cambridge University Press, Cambridge / New York, NY, 2020, 215–294.
24. Douville H. et al. Water cycle changes. In: Climate Change 2021: The Physical Science Basis. Contribution of Working Group I to the Sixth Assessment Report of the Intergovernmental Panel on Climate Change. Masson-Delmotte V. et al. (eds.). Cambridge Univ. Press, Cambridge / New York, NY, 2021, 1055–1210.
25. Edel'geriev R.S.Kh., Romanovskaya A.A. New Approaches to the Adaptation to Climate Change: The Arctic Zone of Russia. Russ. Meteorol. Hydrol., 2020, **45** (5), 305–316.
26. Edel'geriev R.S.Kh. et al. Global Climate and Soil Cover in Russia: Manifestations of Drought, Prevention Measures, Control, Elimination of Consequences and Adaptation Measures (Agriculture and Forestry). Nat. Rep., V. 3. Moscow, MBA Publ. House, 2021, 700 pp. (In Russian).
27. Faleev M.I. et al. Global climate change as a factor of natural and anthropogenic challenges activation to the population and the environment. Civil Sec.Technol., 2022, **19** (2), 4–10. (In Russian).
28. Geraskina A.P. et al. Wildfires as a factor of loss of biodiversity and forest ecosystem functions. Forest Sci. Iss., 2022, **5** (1), 1–70.
29. Ginzburg A.S. et al. Climatic criteria of the need for preventive adaptation. Izv., Atmos. Oceanic Phys., 2022, **58** (6), 536–544.
30. Ginzburg V.A. et al. Conditions for stabilization of average global surface temperature at the levels of +2°C and +1.5°C by the geoengineering method based on stratospheric aerosols. Russ. Meteorol. Hydrol., 2020, **45** (5), 345–352.
31. Global Climate and Soil Cover in Russia: Desertification and Land Degradation, Institutional, Infrastructural, Technological Adaptation Measures (Agriculture and Forestry). Nat. Rep., V. 2. R.S.-H. Edelgerieva et al. (eds.). Moscow, MBA Publ. House, 2019, 476 pp.
32. Grigorieva E.A., Revich B.A. Health risks to the Russian population from weather extremes in the beginning of the XXI century. Part 2. Floods, Typhoons, Ice Rain, Droughts. Iss. Risk Analysis, 2021, 18 (3), 10–31. (In Russian).
33. Grigorieva E.A., Revich B.A. Health risks to the Russian population from temperature extremes at the beginning of the XXI century. Atmosphere, 2021, **12** (10), 1331.
34. Gulev S.K. et al. Changing State of the Climate System. In: Climate Change 2021: The Physical Science Basis. Contribution of Working Group I to the Sixth Assessment Report of the Intergovernmental Panel on Climate Change. Masson-Delmotte V. et al. (eds.). Cambridge Univ. Press, Cambridge / New York, NY, 2021, 287–422.

35. Gurlev I.V. et al. Analysis of the state and development of the transport system of the Northern Sea Route. Arctic: Ecol. Econ. 2022, **12** (2), 258–270.
36. Hock R. et al. High Mountain Areas. In: IPCC Special Report on the Ocean and Cryosphere in a Changing Climate. H.-O. Pörtner et al. (eds.). Cambridge Univ. Press, Cambridge / New York, NY, 2019, 131–202.
37. Insarov G.E. et al. Concept of risk and visualization of its changes in the reports of the Intergovernmental Panel on Climate Change. Fund. Appl. Climatol., 2020, 2, 6–34. (In Russian).
38. Ivanov A.L. et al. Land Use in Russia in the Context of Global Climate Change and Unprecedented Socio-economic Challenges: The State of Soil (Zonal) Cover, Trends, Degradation, Accounting Methodology, Forecasts. M.: "IBA Publishing House", 2022, 100 pp. (In Russian).
39. Jia G. et al. Land–climate interactions. In: Climate Change and Land: an IPCC special report on climate change, desertification, land degradation, sustainable land management, food security, and greenhouse gas fluxes in terrestrial ecosystems. P.R. Shukla et al. (eds.), 2019, 131–247.
40. Kattsov V.M. et al. Probabilistic regional climate projecting as a basis for the development of adaptation programs for the economy of the Russian Federation. Russ. Meteorol. Hydrol., 2020, **45** (5), 330–338.
41. Kattsov V.M. et al. Development of a technique for regional climate probabilistic projections over the territory of Russia aimed at building scenarios of climate impacts on economy sectors. Part 2: Climate impact projections. Proc. MGO, 2019, **593**, 6–52. (In Russian).
42. Kattsov V.M., Shkolnik I.M., Pavlova V.N. et al. Development of a technique for regional climate probabilistic projections over the territory of Russia aimed at building scenarios of climate impacts on economy sectors. P. 2: Climate impact projections // Tr. MGO. 2019. No. 593. P. 6–52. (In Russian)
43. Kislov A.V., Surkova G.V. The impact of global warming on Russia's climate resources. Economics. Taxes. Law, 2021, **14** (4), 6–14. (In Russian)
44. Climate of the Arctic: Processes and Changes. I.I. Mokhov and V.A. Semenov (eds.). Moscow, Fizmatkniga, 2022, 360 pp.
45. Klimenko V.V. et al. Heat waves: A new danger for the Russian power system. Doklady Phys., 2020, **65** (9), 349–354.
46. Klimenko V.V. et al. Energy, demography, and climate: Is there an alternative to abandoning fossil fuels? Doklady Phys., 2022, **67**, 433–438.
47. Klimenko V.V. et al. From Rio to Paris via Kyoto: How the efforts to protect the global climate affect the world energy development. Therm. Engin., 2019, **66**, 769–778.
48. Klimenko V.V. et al. Climatic extremes: A new challenge for Russian power systems. Therm. Engin., 2021, **68**, 171–184.
49. Klimenko V.V. et al. Dynamics of biotic carbon fluxes under different scenarios of forest area changes. Izv., Atmos.Oceanic Phys., 2020, **56** (4), 405–413.
50. Klimenko V.V. et al. An impact of atmospheric and climate changes on the energy potential of Russian forest resources. Doklady Phys., 2019, **64**, 401–407.
51. Klimenko V.V. et al. Russian hydropower under the global climate change. Doklady Phys., 2019, **64**, 39–43.
52. Klyueva M.V. et al. Summer tourism in the context of future climate change in Russia: Projections based on the large ensemble of high-resolution conditional forecasts. Russ. Meteorol. Hydrol., 2020, 6, 47–59. (In Russian).

53. Kostianaia E.A., Kostianoy A.G. Regional climate change impact on coastal tourism: A case study for the Black Sea coast of Russia. Hydrol., 2021, **8** (3), 133; https://doi.org/10.3390/hydrology8030133
54. Larin I.K. On the influence of global warming on the ozone layer and UVB Radiation. Izv., Atmos. Oceanic Phys., 2021, **57** (1), 110–115.
55. Lipka O.N. et al. Applied aspects of adaptation to climate change in Russia. Fund. Appl. Climatol., 2020, **1**, 65–90. (In Russian).
56. Lukina N.V. Global challenges and forest ecosystems. Herald Russ. Acad. Sci., 2020, 90 (6), 303–307.
57. Lukina N. et al. Linking forest vegetation and soil carbon stock in northwestern Russia. Forests., 2020, **11** (9), 979.
58. Makosko A.A. et al. Transport complex of Russia. In: Strategic Planning for the Sustainable Functioning of the Economic Complex of the Russian Federation. V.G. Bondur, A.A. Makosko, B.M. Nakonechny (eds.). Moscow, RAS, 2021, 77–124.
59. Makosko A.A., Matesheva A.V. Assessment of the long-range pollution trends of the atmosphere in the Arctic zone of Russia in 1980–2050 considering climate change scenarios. Arctic: Ecol. Econ., 2020, 1, 45–52. (In Russian).
60. Makosko A.A., Matesheva A.V. On the assessment of environmental risks from air pollution in the Arctic zone under a changing climate in the XXI century. Arctic: Ecol. Econ., 2022, **12** (1), 34–45. (In Russian).
61. Melnikov V.P. et al. Adaptation of Arctic and Subarctic infrastructure to changes in the temperature of frozen soils. Earth's Cryosphere, 2021, **XXV** (6).
62. Meredith M. et al. Polar Regions. In: IPCC Special Report on the Ocean and Cryosphere in a Changing Climate. H.-O. Pörtner et al. (eds.). Cambridge Univ. Press, Cambridge / New York, NY, 2019, 203–320.
63. Methane and Climate Change: Scientific Problems and Technological Aspects. V. G. Bondur et al. (eds.), Noscow, RAS, 2022, 388 pp. (In Russian).
64. Mokhov I.I. Russian climate research in 2015–2018. Izv., Atmos. Oceanic Phys., 2020, **56** (4), 325–343.
65. Mokhov I.I. Features of modern climate changes in the Arctic and their consequences. Arctic and Antarctic Research, 2020, **66** (4), 446–462. (In Russian)
66. Mokhov I.I. Climate change: Causes, risks, consequences, and problems of adaptation and regulation. Herald Russ. Acad. Sci., 2022, **92** (1), 1–11.
67. Oganesyan V.V., Sterin A.M. Estimation of potential finantial damage from severe and adverse weather events in the Russian Federation in 1987–2017. Russ. Meteorol. Hydrol., 2019, 12, 97–108. (In Russian).
68. Parfenova M.R. et al. Changes in the duration of the navigation period in Arctic seas along the Northern Sea Route in the twenty first century: Bayesian estimates based on calculations with the ensemble of climate models. Doklady Earth Sci., 2022, **507** (1), 952–958.
69. Pastukhova A.S. et al. Numerical Simulation of Variations in Ozone Content, Erythemal Ultraviolet Radiation, and Ultraviolet Resources over Northern Eurasia in the 21st Century. Izv., Atmos. Oceanic Phys., 2019, **55**, 242–250.
70. Pathak M. et al. Technical Summary. In: Climate Change 2022: Mitigation of Climate Change. Contribution of Working Group III to the Sixth Assessment Report of the Intergovernmental Panel on Climate Change. P.R. Shukla et al. (eds.). Cambridge Univ. Press, Cambridge / New York, NY, 2022, doi: 10.1017/9781009157926.002.

71. Pavlova V., Karachenkova A., Shkolnik I. et al. Future changes in spring wheat yield in the European Russia as inferred from a large ensemble of high-resolution climate projections. Environ. Res. Lett., 2019, 14 (3), 034010.
72. Pavlova V.N. et al. Assessment of climate favorability for the grain cultivation based on the frequency of severe droughts. Russ. Meteorol. Hydrol., 2021, **45** (12), 864–869.
73. Pekarnikova M.E., Polonsky A.B. Anthropogenic climate change and international-juridical activity on climate mitigation. Part 2. Implementation of climate legal acts at the present stage and their prospects. Gosudarstvo i Pravo, 2021, 5, 118–124. (In Russian).
74. Pekarnikova M.E., Polonsky A.B. Analysis of the realism of achieving the main goal of the Paris Agreement under the existing system of legal regulation and control of anthropogenic emissions of greenhouse gases. Fund. Appl. Climatol., 2022, **8** (2), 190–208. (In Russian).
75. Polonsky A.B., Pekarnikova M.E. Anthropogenic climate change and international-juridical activity on climate mitigation. Part 1. From the UN Framework Convention to the Paris Agreement. Gosudarstvo i Pravo, 2021, 4, 104–113. (In Russian).
76. Porfiriev B.N. Economic dimension of the climate challenge to Russia's sustainable development. Herald Russ. Acad. Sci., 2019, **89** (2), 134–139.
77. Porfiriev B.N. et al. Economic assessment of permafrost degradation effects on road infrastructure Sustainability under climate change in the Russian Arctic. Herald Russ. Acad. Sci., 2019, **89**, 567–576.
78. Porfiriev B.N. et al. Economic assessment of permafrost degradation effects on the housing sector in the Russian Arctic. Herald Russ. Acad. Sci., 2021, **91** (1), 17–25.
79. Porfiriev B.N. et al. Economic assessment of the consequences of permafrost degradation for healthcare facilities in the Russian Arctic. Herald Russ. Acad. Sci., 2021, **91** (12), 1125–1136. (In Russian).
80. Porfiriev B.N. The low-carbon development paradigm and climate change risk reduction strategy for the economy. Studies Russ. Econ. Develop., 2019, 2, 111–118.
81. Porfiriev B.N. Effective action strategy to cope with climate change and its impact on Russia's economy. Studies Russ. Econ. Develop., 2019, 3, 235–244.
82. Porfiriev B.N. Decarbonization vs. adaptation of the economy to climate change within the sustainable development strategy. Problemy prognozirovaniya, 2022, 4, 45–54. (In Russian).
83. Porfiriev B.N. et al. Opportunities and risks of the climate policy in Russia. Voprosy Ekonomiki, 2022, 1, 72–89. (In Russian)
84. Pustovalov K.N. et al. Variations in resources of solar and wind energy in the Russian sector of the Arctic. Atmos. Oceanic Optics, 2019, 2020, **33** (3), 282–288.
85. Revich B.A. New and old health risks in a changing climate. Iss. Risk Analysis, 2021, **18** (2), 8–11. (In Russian).
86. Revich B.A., Grigorieva E.A. Health risks to the Russian population from weather extremes in the beginning of the XXI century. Part 1. Heat and cold waves. Iss. Risk Analysis, 2021, 18 (2), 12–33. (In Russian)
87. Revich B.A. et al. Climate Change and Public Health: Assessments, Indicators, Predictions. Moscow, IEF RAS, 2019, 196 pp.

88. Revich B.A., Eliseev D.O., Shaposhnikov D.A. Risks for public health and social infrastructure in Russian Arctic under climate change and permafrost degradation. Atmosphere, 2022, **13** (4), 532.
89. Romanovskaya A.A., Federici S. How much greenhouse gas can each global inhabitant emit while attaining the Paris Agreement temperature limit goal? The equity dilemma in sharing the global climate budget to 2100. Carb. Manag., 2019, **10** (4), 361–377.
90. Romanovskaya A.A., Korotkov V.N., Polumieva P.D. et al. Greenhouse gas fluxes and mitigation potential for managed lands in the Russian Federation. Mitigat. Adapt. Strateg. Glob. Change, 2020, **25** (4), 661–687.
91. Russian National Report: Meteorology and Atmospheric Sciences (2015–2018). Ed. by I.I. Mokhov, A.A. Krivolutsky. Moscow, MAKS Press, 2019, 332 pp.
92. Shirov A.A., Kolpakov A.Yu. Russian economy and mechanisms of global climate regulation. J. New Econ. Assoc., 2016, 4, 87–110.
93. Shkolnik I.M., Pigoltsina G.B., Efimov S.V. Agriculture in the arid regions of Eurasia and global warming: RCM ensemble projections for the middle of the 21st century. Russ. Meteorol. Hydrol., 2019, **44** (8), 540–547.
94. Shaw R. et al. Asia. In: Climate Change 2022: Impacts, Adaptation and Vulnerability. Contribution of Working Group II to the Sixth Assessment Report of the Intergovernmental Panel on Climate Change. H.-O. Pörtner et al. (eds.). Cambridge Univ. Press, Cambridge / New York, NY, 2022, 1457–1579.
95. Schepaschenko D. et al. Russian forest sequesters substantially more carbon than previously reported. Sci. Rep., 2021, **11** (1), 252
96. Skea J. et al. Summary for Policymakers. In: Climate Change 2022: Mitigation of Climate Change. Contribution of Working Group III to the Sixth Assessment Report of the Intergovernmental Panel on Climate Change, P.R. Shukla et al. (eds.). Cambridge Univ. Press, Cambridge / New York, NY, 2022, doi: 10.1017/9781009157926.001.
97. Smith P. et al. Interlinkages between desertification, land degradation, food security and greenhouse gas fluxes: Synergies, trade-offs and integrated response options. In: Climate Change and Land: an IPCC special report on climate change, desertification, land degradation, sustainable land management, food security, and greenhouse gas fluxes in terrestrial ecosystems, P.R. Shukla et al. (eds.). 2019, 551–672.
98. Smyshlyaev S., Galin V., Blakitnaya P., Jakovlev A. Numerical modelling of the natural and manmade factors influencing past and current changes in polar, midlatitude and tropical ozone. Atmosphere, 2020, **11**, 76.
99. Soldatenko S.A. Estimating the effect of radiative effect uncertainties on climate response to changes in the concentration of stratospheric aerosols. Atmosphere, 2020, **11** (6), 654. 259
100. Soldatenko S.A., Bogomolov A., Ronzhin A. Mathematical modelling of climate change and variability in the context of outdoor ergonomics. Matematics, 2021, **9** (22), 2920.
101. Soldatenko S.A., Yusupov R.M. Optimal control for the process of using artificial sulfate aerosols for mitigating global warming. Atmos. Oceanic Optics, 2019, 32 (1), 55–63.
102. Soldatenko S.A., Yusupov R.M. Optimal control perspective on weather and climate modification. Matematics, 2021, **9** (4), 1–16.

103. Soldatenko S.A., Yusupov R.M. Model for estimating the transient response of the global mean surface temperature to changes in the concentrations of atmospheric aerosols and radiatively active gases. Atmos. Oceanic Optics, 2019, **32** (5), 578–585.
104. Soldatenko S.A et al. Cybernetic approach to problem of interaction between nature and human society in context of unprecedented climate change. SPIIRAS Proc., 2020, 19 (1), 5–42. (In Russian).
105. Soldatenko, S.; Yusupov, R.; Colman, R. Cybernetic approach to problem of interaction between nature and human society in the context of unprecedented climate change. SPIIRAS Proc., 2020, **19**, 5–42.
106. Steidinger B.S. et al. Climatic controls of decomposition drive the global biogeography of forest-tree symbioses. Nature, 2019, **569** (7756), 404–408.
107. Streletsky D.A., Suter L.J., Shiklomanov N.I. et al. Assessment of climate change impacts on buildings, structures and infrastructure in the Russian regions on permafrost. Environ. Res. Lett., 2019, **14** (2), 025003.
108. Third Assessment Report on Climate Change and Its Consequences on the Territory of the Russian Federation. St. Petersburg, Naukoemkie Technologii, 2022, 676 pp. (In Russian).
109. Torzhkov I.O., Konstantinov A.V., Koroleva T.S. et al. Assessment of future climate change impacts on forestry in Russia. Russ. Meteorol. Hydrol., 2019, **44** (3), 180–186.
110. Vaganov E.A. et al. Assessment of the contribution of Russian forests to climate change mitigation. Econ. Reg., 2021, **17** (4), 1096–1109. (In Russian).
111. Winkler A.J., Myneni R.B., Brovkin V., Alexandrov G.A. Earth system models underestimate carbon fixation by plants in the high latitudes. Nature Comm., 2019, **10** (1), 885.

Conclusion

Modern climate change already dictates new requirements for timely and more detailed and versatile consideration of regional environmental and socio-economic consequences with the formation of appropriate systems of adaptation and possible regulation. It is necessary to develop a common system of mutually agreed upon regional assessments of the risk and predictability of anomalous climatic regimes and their variability, taking into account natural and anthropogenic forcings at different time horizons. Quantitative assessments of the components of the carbon balance of the Earth's system are becoming increasingly important, including more detailed regional assessments of the role of Russian forests and other natural ecosystems within the framework of the carbon polygones system.

In Russia, in 2019, the National Action Plan for the first stage of adaptation to climate change until 2022 was adopted. After that, the National Action Plan for the second stage of adaptation to climate change until 2025 was adopted (http://static.government.ru/media /files/). The goal is to prevent negative impact of climate change on the sectors of the economy and the quality of life and to take into account in advance the new opportunities that

open up at the federal, sectoral and regional levels. There should be organizational, legal, scientific, methodological and information support for the necessary adaptation measures. The development of a system for adequate and timely consideration of new risks and opportunities associated with climate change should include the corresponding development of climate monitoring, in particular satellite monitoring, and modeling of climate change and its consequences under various scenarios of natural and anthropogenic forcings. This should be facilitated by the Federal Scientific and Technical Program in the field of environmental development of the Russian Federation and climate change for 2021-2030 (http://static.government.ru/media/files/).

Particular attention should be paid to climate change and its consequences in the polar latitudes, which have not only regional but also global significance rapidly increasing in recent years. The Strategy for the Development of the Arctic Zone of the Russian Federation and ensuring national security for the period up to 2035 (http://www.kremlin.ru/acts/bank/45972/) notes the features of the Arctic zone that determine special approaches to its socio-economic development and ensuring national security in the Arctic, taking into account the extreme natural and climatic conditions, the high sensitivity of ecological systems and the growth of conflict potential. Strong and rapid climatic changes in the Arctic latitudes contribute to the emergence of both new economic opportunities and risks for economic activity and the environment, in particular for navigation along the Northern Sea Route and the use of natural resources on the shelf.

Clouds and Precipitation

Bezrukova N.A.[1]
Chernokulsky A.V.[2]
[1] Central Aerological Observatory bezrukova@cao-rhms.ru
[2] A.M. Obukhov Institute of Atmospheric Physics RAS
a.chernokulsky@ifaran.ru

Introduction

Clouds and precipitation play a fundamental role in the global hydrological cycle and influence the radiation balance of the planet [1]. Precipitation forecasting and weather modification are of important practical importance, including for agriculture [2]. Extreme precipitation, related flash floods, and dangerous convective phenomena are associated with significant economic and social damage, in particular 800 such events with substantial damage were recorded in Russia in 2019–2021 [3].

Despite the significant fundamental and applied importance, many unresolved problems still exist in the field of cloud and precipitation research. In particular, clouds and their response to external forcing are the major source of substantial difference among global climate models in climate sensitivity estimates, including increased sensitivity in the recent CMIP6 models [IPCC, 2021]. The accuracy of cloud processes simulations depends on the scale, which is substantially smaller than the resolution of up-to-date numerical models.

In 2019–2022, the topic of clouds and precipitation has been the focus of a number of Russian studies presented in this chapter, including studies of general cloud and precipitation climatology, studies of convective processes and phenomena, cloud microphysics, observational and modeling issues, issues of weather modification.

General problems of cloud and precipitation climatology

Investigations of various aspects of cloud climatologies are presented in [4–27]. In [4], the area-perimeter fractal parameter for clouds being close to 4/3 is explained from the point of view of random walk of a fluid particle in the 6D phase-space of speeds and coordinates.

Papers [5, 6, 8–11] are devoted to the investigation of cloud change peculiarities in the Arctic and sub-Arctic regions. In the study [5], for the first-time cloud cover is analyzed since 1936 based on verified sets of data from 86 Russian weather stations. Total cloud cover in the Russian Arctic is reported to increase in warmer periods, with the largest increase observed for

convective clouds, especially over the Chukchi Sea. Statistically confirmed is the transition of stratified cloud forms to convective ones. The connection of cloud cover characteristics with different modes of climatic variability is analyzed. The strongest correlations were found for the Atlantic circulation indexes and sea ice concentration in all the regions of the Eurasian Arctic, with the correlations for the Pacific circulation indexes being less significant.

Paper [11–13] presents new knowledge about the vertical macrostructure of cloud layers at 0–10 km in different latitudes of the globe and over the Russian regions, based on radar sounding data on the vertical profiles of temperature and humidity for the 1964–2018 period. Long-term estimates of the occurrence of cloud layers were obtained, with the account of monthly, seasonal and annual cloud amount. The geographical distribution of seasonal and annual means, as well as root-mean-square deviations was obtained for the number of cloud layers, and the amplitude of their regional changes is determined. In particular, it was pointed out that in high latitudes of both hemispheres and mid latitudes of the Northern hemisphere the occurrence of cloud layers increased from the lower to the upper layer, while in low latitudes it was maximal for the middle layers and minimal for the upper ones. In mid latitudes of the Southern hemisphere cloud layer occurrence was, on the contrary, minimal for the middle layes and maximal for the upper ones. The peculiarities of space and time fractioning on cloud and cloud-free layers were specified. At maximum, 20 cloud layers were recorded.

Papers [15–23] analyze the statistical characteristics of clouds over the Russian territory. In [15], based on the 1967–2019 ground observations, cloud amount was found to increase in all seasons over most of Russia. The occurrence of episodes with lower cloud cover was also revealed in [23] based on data for the airfield observations.

Study [16] shows and increase of the convective cloud amount, based on the 1967–2020 ground observations, and an increase in the height of deep convection clouds over the northern Eurasia (with the trend of 280 m per decade) that revealed for the 2000–2020 years based on the MODIS satellite data. In papers [18–21] statistical models of the textural features and physical parameters of different cloud types are constructed for the northern and southern parts of Western Siberia, based on satellite MODIS data. Cloud cover classifications with 16 types for summer and 12 types for winter are presented. The most frequent types of cloud transformations are established and reasons for such transformations are defined.

In paper [24, 25], clouds are considered as the manifestation of wave disturbances. Study [24] presents the results of studying the variability of the characteristics of internal gravity waves and their cloud manifestations, based on satellite HIMAWARI-8 data. Similar episodes of observing signatures of internal gravitational waves are found. The paper discusses processes occur-

ring in the system ‘atmosphere – underlying surface’ and their influence on the creating of more favorable conditions for the generation and propagation of the wave processes considered. In [25], author analyze the photos of clouds observed over the mountains of the southern Crimea on March 24, 2011. Based on the results of photography from different sides and altitude levels, as well as theoretical and experimental studies of similar situations, the assumption that clouds existed in the ridges of the waves arising when the airflow flows around the mountains is tested. The wave nature of the registered clouds is revealed.

An interactive WMO atlas of clouds [26] was translated into Russian in 2020, and a school textbook on clouds [27] was published for the first time in many years, which increases public awareness of the processes in clouds and precipitation and their role in the weather and climate.

Papers [28–60] are devoted to investigations of climatological aspects of precipitation different types including extreme ones based on different data. The causes of precipitation formation and changes are analyzed, [41–55], the statistical characteristics of precipitation are investigated [54–60].

Long-term changes in precipitation characteristics, both observed and expected, are discussed in [30–36]. Particularly, paper [30] analyzes tendencies in changes of characteristics (the number of cases, duration and weight) for all the types of glaze-rime deposits over the Russian territory, based on 1984-2019 data from 1338 weather stations. It is found that the east of the European part of Russia and the north of Weser Siberia demonstrates an increase in the number of cases of the occurrence, duration and weight of glaze. On the Arctic coast and south of the European part of Russia, the number of cases, duration and weight of crystalline rime tend to decrease. At the same time, these characteristics are found to increase on the European territory, in Western Siberia, Amur region, and some regions of Chukotka. A statistically significant tendency of the number of cases, duration and weight of wet snow deposit to increase is observed over the major part of Russia.

Based on 1966-2016 observation data from the Russian weather stations, characteristics of different precipitation types, including convective, large-scale and drizzle precipitation, are estimated in [34]. For the aforementioned 50-year period, a decrease of large-scale precipitation and an increase of convective precipitation is revealed. A statistically significant increase of the contribution of heavy showers (95 percentiles) to the total precipitation is highlighted (1-2%/decade up to 5%/decade for some stations). The largest share of heavy shower rains in total precipitation is recorded in the Russian Far East. This is basically due to positive changes in the intensity of convective precipitation, with a linear trend over 1 mm/day/decade, which implies a 13,8% increase per 1°C temperature growth. Enhanced extreme precipitation is also recorded in some East Europe regions [35] and in permafrost regions

of Siberia [36]. An increased frequency of days with extreme precipitation over the Russian territory was also recorded based on the data of ERA5 reanalysis, with the total number of rainy days decreased [31].

In paper [31–33], expected changes in precipitation characteristics are estimated for the XXI century, based on the results of modeling using global climatic models from the CMIP6 project [31] and the regional model of the Main Geophysical Observatory [32, 33]. As it follows from model calculations, during winter periods of the nearest future decades, relative total precipitation and extreme precipitation frequency over most of Russia will continue to increase. During the summers, however, a slight decrease of seasonal precipitation totals and the number of days with precipitation will be observed over the south of the European territory of Russia [31]. Using of large ensemble that based on the regional climatic high-resolution model permits one to reveal the peculiarities of changes in extreme precipitation regime, which should be considered in adapting to climate changes on a regional scale [33].

Papers [37–40] consider the estimates of snow cover climatology in extratropical latitudes of the Northern hemisphere. Study [38] estimates relation of annual and interannual snow cover variations in Eurasia with changes in the surface air temperature in the Northern hemisphere, based on 1979–2020 satellite and reanalysis data. Seasonal features of the relation between snow cover and temperature regime, particularly, during the formation of snow cover in autumn, as well as their changes over the last decades are pointed out. For the period of 2005–2019, an increase, by an absolute value, of snow cover area sensitivity to changes in surface air temperature over Eurasia is found, with their negative correlation for the last four decades being, on the whole, statistically insignificant.

Paper [39] analyzes changes in snow cover area and water equivalent of snow over the continental regions of the Arctic, based on multiple sets of observation data and CMIP5 model ensemble for the period of 1979–2005. The CMIP5 models are found to considerably underestimate the area of winter snow cover, but better correlate with autumn observations. On the whole, the annual cycle of snow cover area is adequately reproduced by a CMIP5 model ensemble. On the contrary, the annual cycle of the water equivalent is considerably shifted, especially over North America, where, according to some models, snow is still preserved even in summer, which differs from observations. Most CMIP5 models suggest the reduction in time of snow cover and water equivalent of snow. These tendencies are, however, much weaker (and less statistically significant) than observed ones.

Papers [41–55] discuss the conditions of precipitation formation and the cause of its long-term variability. The quantitative input to precipitation increase of such factors as the global or local air temperature increase [46, 47,

49], ocean surface temperature [41, 53], sea ice condition [42], climatic variability modes [48], circulation features [44, 45, 50, 51, 54, 55], urban local effects [43] or orographic effects [52] is discussed.

Study [47] verifies a hypothesis of an exponential increase of precipitation intensity with rising temperature in accordance with Clausius-Clapeyron equation (7% per 1 °C) for Russian regions based on 1966-2017 observation data and 1979–2020 ERA5 reanalysis data for total precipitation and both large-scale and convective precipitation. An overall increase of extreme precipitation of all types is found for winter in accordance with Clausius-Clapeyron rate. For the Russian Far East region, the extreme character of large-scale precipitation increases with rising air temperature with nearly twice Clausius-Clapeyron rate. However, in summer, a peaked structure of the 'precipitation-temperature' scaling is observed, especially for convective precipitation in southern regions. Extreme precipitation reaches its peak values within a temperature range between 15 °C and 20 °C. At higher air temperatures precipitation intensity starts to diminish as the temperature continues to rise, which is linked to the important role of atmospheric moisture.

In paper [52], the role of an orographic and a lake effect in extreme precipitation formation over the southern coast of the Caspian Sea is analyzed. The quantitative contribution of these effects is estimated with idealized experiments using the WRF-ARW model. The experiments demonstrate that the lake effect only occurs in the presence of orography, and the total contribution of the warm Caspian Sea and orography to precipitation increase in the south of the sea being, on the average, about 50%. In [43], the influence of the city of St. Petersburg on the wind and precipitation fields is estimated based on data from 15 stations of Leningrad Region for the 1994–2018 period. An increase of precipitation and a decrease of surface wind speed outside the city over downwind regions, as well as a wind speed decrease within the city area are revealed.

In [54, 55], extreme precipitation in the European sector of the Arctic is investigated. Extreme precipitation events are classified in terms of a certain probability distribution, i.e., Pareto law. The events deviating from this base distribution are represented by the largest diurnal precipitation totals. The assumption is made that for such events the correspondence with probability is lost, i.e. any anomalies can occur, but not exceeding some limiting values typical for the given type of climate. Thus, for the whole set of extremes, it is possible to introduce a specific law of distribution of random values describing anomalies not exceeding a particular limit, while the presence of this limit can be revealed only when approaching it. Synoptic objects are determined, which major precipitation anomalies belong to. In summer, these are cyclones and baric troughs with high water vapor content (above ~25 kg/m^2) and mesoscale systems within fronts, which are characterized by strong wind

shear [54]. Extreme precipitation in a cold period is due to the advection of moist air mass from the Atlantic. The transport proceeds in the circulation system of intensive cyclones of the polar front. Sometimes mesoscale convective systems are found within atmospheric fronts, thus contributing to precipitation formation. The influence of polar lows on the formation of a large amount of precipitation has not been revealed [55].

Together with [54, 55], the problems of the statistical determination of precipitation are investigated in [56–60]. The problems of the analysis of convective precipitation datasets including several events a year are considered in [56]. Recommendations for converting the statistics of data sets including several events a year to that for a single event a year are developed. Mathematical models for statistical determination of maximal diurnal and total precipitation during a wet period are proposed in [59]. The proposed models are based on a generalized negative binomial distribution of wet period duration, which is a mixed Poisson distribution. The distribution shows significant correspondence with the observed data on wet period duration. Asymptotic approximations for the distributions of maximal diurnal and total precipitation during a wtr period are proposed, and precision limits for the proposed approximations are presented. Several tests are proposed to estimate anomalous extreme diurnal precipitation, total precipitation, and precipitation intensity [60].

An approach to the estimation of statistical characteristics of precipitation totals for short time periods is considered in [58]. Based on the results of processing pluviographic data for Moscow region, a conclusion is made about substantial changes of the temporal structure of convective precipitation. The temporal structure of convective events is investigated in more detail in [57], based on the analysis of 80-year pluviographic observations in the valley of the Tobol River. It is pointed out that for 75% of observed convective precipitation events over 50% of precipitation amount occur during the first third of the precipitation period. Only 5% of precipitation rains are characterized by uniform intensity. Satisfactory modeling of shower characteristics with lognormal distribution is presented.

Convective clouds, convective processes and phenomena

One of the most hazardous weather phenomena leading to social and economy consequences are associated with convective processes in the atmosphere (heavy shower rains and thunderstorms, hail, squalls, and tornados). Therefore, during 2019–2022, a number of publications were devoted to investigation of convective clouds and hazardous convective phenomena, including analysis of their characteristics [61–97], analysis of electric processes in clouds [98–112], investigation of typical conditions and peculiari-

ties of the formation and development of convective clouds and dangerous convective phenomena [113–124], and diagnosis of some most outstanding events (case studies) [125–142].

Papers [61–97] are devoted to investigations of deep convective clouds (and mesoscale convective systems), which resulted in formation of extreme wind phenomena, such as squalls and tornados. Several studies describe convective cloud characteristics and phenomena typical of separate regions; the estimates obtained are based on different types of data (aircraft, satellite and radar observations, as well as lightning detection systems) for regions of North Caucasus [64, 65, 67, 75, 76], south of the Far East [61, 90], middle Volga [83], Perm' Territory [86], central [84] and northwest of the European part of Russia [77, 92], south of Western Siberia [85, 88, 89, 95, 96], Yakutia [72], and tropical regions [78, 79, 94, 97].

Studies [68, 81, 87] compare convective cloud characteristics and phenomena over different regions, including northwest of the European part of Russia, North Caucasus, central India and eastern China. The characteristics of cumulus clouds at an early stage of their transformation to thunderclouds are analyzed. The altitude of the cloud top was the only cloud characteristic that enhanced when a cloud is turning into a thundercloud, in any region. Maximal reflectivity increased when a cloud turned into a thundercloud in the Russian regions, but changed insignificantly over India. An important difference between the Indian clouds and continental clouds over Russia and China is a lower content of large ice particles in Indian clouds (during a post-monsoon period) that largely determine cloud reflectivity above a zero isotherm.

Some other regional regularities have been revealed. In particular, paper [64] estimates the relation between the number of days with thunderstorms and thunderstorm duration in the North Caucasus in 2008-2019. The duration of thunderstorms is established to have increased by 3.89 hour per day with growing number of days with thunderstorms. Typical distributions of basic radar parameters of single-cell hail clouds (including time of hail formation, the height of the appearance of the first radio echo and its excess over the zero isotherm, the height of hail generation and it excess over the zero isotherm, lifetime of single-cell hail clouds as well as their speed and travel distance) for the regions of North Caucasus are presented in [65].

In [73], the relation between the parameters of hail formation area (height, speed and travel direction) in the phase of the first radio echo detection and in the phase of hail generation and growth is investigated based on MRL-5 radar data for the North Caucasus in 2011–2020. The most probable velocities and directions of the area against the leading flow are revealed, and the time between the phase of the first radio echo detection and the phase of hail generation and growth is estimated.

In [92], authors compare the parameters of thunderstorm and lightning-free clouds, and presents statistical data on their differences. A regression analysis of the dependence of lightning frequency on radar characteristics of clouds is fulfilled using neural networks. A mathematical expression is obtained to calculate lightning frequency, using data on the maximal value of cloud differential reflectivity and the volume of supercooled cloud portion with reflectivity of ≥35 dBZ.

The published regional investigations can be employed to estimate the occurrence of hazardous phenomena (in particular, with the purpose of adapting to climate change). Among them is the work presented in [84] devoted to the creation of a cartographic database on hazardous convection phenomena for the Central Federal District of the Russian Federation. The database contains information about the phenomena (more than two thousand events over 2001-2020, including heavy shower rains and hail, squalls and tornados), their damaging consequences (based on satellite observations) and generation conditions (based on CFS and ERA-5 reanalysis).

Paper [85] estimates the time variability of mesoscale convective complexes (MCC) over the south of Western Siberia for 2010-2019. During the observation period, 279 MCC cases are recorded, and two centers with the maximal MCC occurrence were distinguished. In estimating MCC characteristics, the areas of air-mass MCCs are found to be less than the areas of frontal ones, with their cloud tops being higher. The MCC area and intensity of thunderstorm activity are also estimated in [88].

Note that lightning in Siberia is a major source of forest fires. Study [96] uses lightning detection data on lightning activity and satellite data on fires and shows that 30% of forest fires are formed due to lightning in the north of Western Siberia. The similar figures are found for Yakutia, where lightning activity is observed to increase over the last years [72].

A summarizing study of changes in the occurrence and intensity of hazardous convective weather phenomena, including heavy showers, thunderstorms, hail, squalls and tornados, in various Russian regions during warm seasons based on different independent information sources, is presented in [16]. The frequency of thunderstorms, hail, and strong wind, contribution of extreme showers into total precipitation, as well as the amount of cumulonimbus clouds are estimated based on the 1966–2022 data from the Russian meteorological stations. The frequency and intensity of tornado and squall events that caused windthrow in 1986–2021 as well as the height of deep convection cloud tops in 2002–2021 arere estimated based on satellite data. ERA5 reanalysis data is used to analyze the frequency of conditions characteristic of the development of moderate and intensive hazardous convective events in 1979-2020. The results indicate the general intensification of such events in most regions of Russia, with the exclusion of some southern regions

on the European territory of Russia. The occurrence of moderate phenomena tends to decrease, while for the strongest ones tends to increase.

In work series [70, 71, 82, 95], a characteristic values of tornado numbers over the territory of northern Eurasia is established. The number of tornados from the data of observational stations and available statistics, on the whole, is shown to be substantially underestimated. For the period beginning from the 10th century up to 2020, over 3000 tornadoes are revealed based on eye-witness evidences (of tornado itself or the damage they caused) and present-day satellite observations on windthrow. It is shown that both single tornadoes and tornado outbreaks (multiple tornadoes that formed within a system of meso- or synoptic scale) are characteristic of the Russian territory. During the 2009-2018 period, more than 100 tornados are recorded in Russia every year, with 15 ones with wind speed over 50 m/s and one tornado with wind speed over 70 m/s. In some years, these values may be much larger, i.e., 342, 52 and 3, respectively. On average, tornadoes in Russia occur on 41 days a year, and up to 68 days in some years. The frequency of tornados of different intensity and probability of their passage through a specific point are estimated. This data can be useful in the evaluation of potential hazard due to tornado.

Convective clouds are an important part of the global electric circuit. Studies [98–112] is devoted to studying electric processes in convective clouds and electric structure of such clouds. In particular, studies [102, 103, 105, 106] analyze changes in the characteristics of atmospheric electricity in the course of convective cloud development. Specifically, in paper [102] the relation between convective cloud structure and lightning frequency is evaluated. The frequency of electric discharges is established to correlate well with the volumes of supercooled, high-reflectivity cloud portions. The frequency of electric discharges increases approximately 20 minutes after the volumes of supercooled cloud portions with reflectivity values exceeding 35–55 dBZ become maximal. Precipitation flux reaches its maximum prior to the time when lightning frequency reaches maximal values. In [105, 106] a set of variations of meteorological and electric parameters of the surface atmosphere during heavy shower precipitation (with intensity over 5 mm/h) is investigated. It is pointed out that frontal showers cause larger changes in the negative electric conductivity than showers connected with air-mass convective clouds. A considerable increase in negative electric conductivity (of more than twice that under normal conditions) is observed in frontal showers with drop size of 4 mm.

In [99, 104] it is demonstrated, based on model data, that with the account of the process of heterogeneous freezing of cloud drops more intensive cloud electrification and charge separation occurs, with the frequency of lightning discharges increasing by a factor of 2 or 3. The strongest mechanisms of the electrification of cloud elements are connected with the interaction between

cloud particles and precipitation (hailstone – ice crystal, melting hailstone – cloud drop, raindrop – cloud drop). Herein, electric processes themselves can play a significant role in the evolution of clouds and related hazardous weather phenomena. Thus, coronal discharges are found to favor water drop freezing at lower temperatures, thus leading to quicker crystallizing of convective clouds [98]. It is stated that the character and the rate of coronal discharge influence the formation and development of hazardous phenomena connected with convective clouds (showers, hail, and thunderstorms) largely depend on the share of a supercooled liquid cloud portion in the total cloud volume. If this share is large enough, hail intensity and thunderstorm activity increase by tens of percent. Otherwise, the input of coronal discharges to cloud crystallizing is insignificant, only leading to a time shift of the phenomena maximums: both thunder and hail start and halt earlier.

Enhancement of an energy particle flux below thunderstorm clouds is known to be due to the generation and acceleration of secondary cosmic rays in the electric field of a convective cloud. In [108, 111], a new method of evaluating the electric structure of a cloud producing a flux of energetic particles is proposed. The method uses ground measurements of the strength of an electric field and an energetic particle flux under a cloud. To evaluate the state of the atmosphere WRF model data is employed. The method is used to investigate clouds producing downward energetic particle fluxes observed at Aragatz research station. A typical charge distribution in a cloud is determined: a double-layer structure with a 0.5–5 nC/m^3 charge density is in the lower layer and –0.2…–3 nC/m^3 is in the upper one. The lower layer (positively charged) forms in the area where graupels prevail, while the upper layer (negatively charged) forms in the area where snow particles prevail. Full electric charges of active areas producing a particle flux are within 1–20 C and –1…–30 C, respectively. The vertical distance between the two areas is about 1–2 km, which appears to be sufficient for a flux of energetic particles to form.

Investigation of the conditions favorable to form well-developed convective clouds leading to the occurrence of hazardous weather phenomena (large hail, heavy showers, squalls and tornado) are still of great interest to scientists, e.g., for improving forecasting of such events. In these investigations, both a classical synoptic analysis and analysis of dynamic and thermodynamic characteristics of the atmosphere are employed [113–124]. In particular, prognostic and diagnostic skills of convective instability indexes are estimated. In [113], it was demonstrated that a maximal convective speed and surface pressure Laplacian are the best predictors in forecasting squalls. In particular, surface pressure Laplacian makes it possible to distinguish squall-free areas. Besides, the speed of the horizontal transport in the middle troposphere is shown to influence an increase of maximal squall wind speed by about 4-

4.5 m/s, although its contribution is approximately 4 times as low as that of the vertical convective speeds and 2–2.5 times as low as that of surface pressure Laplacian. In paper [120] it is established that a considerable temperature contrast at the front (on average, 9.6°C/500 km) as well as the presence of a jet stream in the lower and middle troposphere, oriented along the frontal zone, are important factors in the formation of heavy squalls and tornado. In most cases, for squalls and tornados formation, a combination of an air mass with high water content (on average, about 400 mm), moderate or strong convective instability (CAPE > 1000 J/kg), and strong wind shear is required. Specifically, for squall generation, water content and convective instability of the atmosphere are more important, while for tornado generation, wind shear in the lower layer is a key factor. A similar conclusion about a more important role of wind shear and helicity in tornado generation and a more important role of thermodynamic instability in squall generation is made in [86].

In paper [114], a 2D mathematical model of moist air convection in sub-cloud and cloud layers is proposed. Based on the model, the influence of surface atmospheric parameters on convection development in sub-cloud and cloud layers is estimated, and a criterion of convection development in a sub-cloud area is derived. It is established that convection development in a cloud layer depends on absolute values of dew-point depression in the surface layer and, to a larger extent, on the vertical gradients of the mass share of water vapor. It is shown that explosive growth of convection occurs with certain critical values of the vertical gradient of the mass share of water vapor.

Studies of the role of various factors in the intensification of convective phenomena continue. In particular, in [123] it is demonstrated that as a result of convective cells' merging, microphysical and dynamic processes are intensified, which largely favors large hail growth and hail phase duration increase. In [121], based on model simulations, the influence of underlying surface's thermal inhomogeneity on the formation and development of convective clouds and hazardous convective phenomena is quantified. It is found that with an increase of a heat flux from the surface all cloud characteristics are first enhanced abruptly. But increasing it further leads to much smaller changes in values of cloud characteristics, which practically goes to saturation. This is associated with the fact that thermal disturbance only plays a role in the rise of thermal up to convectively unstable atmospheric layers. Further on, the main factor determining the evolution of the cloud is the release of heat during phase transitions.

Studies of some especially outstanding convective storms (supercell clouds or mesoscale systems/clusters) connected with hazardous convective phenomena also continue [125–142]. Such case studies include diagnosis of conditions leading to convective storm formation and subsequent hazardous phenomena, such as heavy showers and floods [133, 137], large hail [125,

130, 132], waterspouts and land tornados [127–129, 131, 135, 136, 141] as well as long-lived squalls [126, 141, 142]), analysis of their development, and discussion of modeling and forecast potentials. For some events, extreme values of a number of characteristics were pointed out. For example, for one of the supercells the speed of its motion of up to 85 k/h is reported [130]. Significant instability conditions were stated for most events investigated.

In [131], authors are investigated the characteristics of the cumulonimbus cloud with a waterspout observed over the Gulf of Finland on August12, 2018. The characteristics were evaluated by the data of Doppler polarization weather radar, radiometer, and lightning direction finder. A whirling motion descent in the cloud is shown to precede the waterspout occurrence (which shows its nature to be similar to tornado). Based on radar cloud characteristics during the waterspout occurrence, a conclusion is made that "column Zdr" and the area in the lower cloud portion with Doppler speed values differing in direction and large values of speed spectrum width are adequate identifiers for waterspout detection. However, the use of this peculiarity does not seem to be practical for the detection of any tornado. For example, the radar cloud characteristics obtained during a series of waterspouts over the Black Sea on July 16, 2019 [136] testify to the fact that the cloud with a waterspout that reached the coast and traveled a long distance over land did not differ by its radar characteristics from the clouds without tornados that were observed on that day in the vicinity of the coast.

In paper [127], algorithms of hydrometeor classification and determination of updrafts by DMRL-C radar data on polarization characteristics are first applied to the cumulonimbus cloud with a waterspout over Ladoga Lake. Using these algorithms, the appearance of large ice particles at the beginning of thunderstorm activity in the cloud was detected, and an extended updraft connected with the waterspout is recorded.

It was for the first time on the territory of Russia that the so-called "derecho" events, i.e. long-lived convective storms with a considerable destruction length (over 400 km, in accordance with the classical definition) and hurricane wind speed, are registered. Two similar events are detected based on the data on damage and analysis of satellite data on windthrow [142]. These events occurred on June 27 and 29, 2010 against the background of record heat and caused unprecedented damage to forests. It is found that the total area of windthrow areas accounts for 1250 km^2. The length of the damaged area exceeds 500 km for one storm and 600 km for the other. The formation of the mesoscale convective systems was triggered by fast-moving waves that formed at the polar front under conditions of significant temperature gradients over the western periphery of long-lived blocking anticyclones on days of their termination. Both events developed under conditions of moderate and strong convective instability and extremely large wind shear

due to the presence of a strong jet stream in the middle atmosphere. Mesoscale simulation using the WRF model indicated significant underestimation of the windfall effect. An important role of blocking anticyclones in the formation of long-lived convective clouds is also discussed in [141] in connection with the event of May 15, 2021. This event also developed over the western periphery of the blocking but at the time of its maximal development, and not at the time of its termination (as with the 2010 events).

Cloud microphysics

Microphysical cloud properties are investigated on the ground in field and stationary laboratory conditions as well as in the atmosphere on board the Russian aircraft weather laboratory Yak-42D of Roshydromet. The aircraft is equipped with diverse measurement instrumentation and hardware-and-software systems enabling measurements of navigation flight parameters and recording size spectrum characteristics and images of cloud particles within the range of 25–6000 μm, cloud water content as well as thermodynamic characteristics of the atmosphere, simultaneously with visual observations [143, 144].

On board the aircraft are mounted instruments [145] enabling analysis of aerosol pollution and radiation fluxes of the atmosphere. During nearly a decade of flights, unique experimental data was obtained on the structure and properties of various cloud forms in different seasons and synoptic situations on meso- and microscales. The collected measurements composed a base of the results of cloud atmosphere aircraft sounding. Special software available to users was created for the extraction from this base and primary analysis of archived data. A program was developed to calculate the realizations of wind speed and temperature component pulsations, turbulence parameters (dispersions, root-mean-square deviations, and turbulence energy), and microphysical parameters, using data obtained by the aircraft laboratory. Specifically, the software developed was employed to process and analyze the thermodynamic system's data from 16 flights under the program of the 2019–2021 State Assignment "Geomonitoring" and to systematize data on the thermodynamic structure of cloudy atmosphere in 2022. The aircraft measurement system makes it possible to investigate wind speed structure with high space resolution and to determine vertical and horizontal wind shear. Particularly, according to the data of two research flights, maximal values of the horizontal and vertical shear of wind speed components were measured above the boundary layer and were 0.2 (m/s)/km and 1.2 (m/s)/100 m, respectively [146, 147].

Aircraft experimental studies are primarily carried out in cloud zones of atmospheric fronts. In particular, the structure of wind shear and turbulence

characteristics in a warm front cloud system were analyzed based on the 17.12.2019 data collected by the aircraft lab Yak-42D "Roshydromet" over Moscow region. Based on 21.01.2021 aircraft data it was done to investigate the cloud system of stratified Ns-AsCs-Ci of a warm front with pronounced temperature contrasts, east-south-east of Moscow [148]. Up to a 7800 m level, the flight was performed inside a cloud system; the forms of crystals were observed to vary depending on flight height and cloud type. The presence of liquid water was observed in clouds of all types, including high-level Ci clouds. Distributions of cloud particle characteristics and values of their volume-modal radii, depending on height and cloud type, were obtained and cloud water content was calculated. Zones of liquid water in high Ci clouds were detected at air temperature of -48°C.

An experimental aspect of investigations is represented by the results of the field aircraft investigations of the interrelation of microphysical characteristics and turbulence in supercooled clouds [149]. Within zones with both supercooled drops and ice crystals, anisotropy of the turbulent pulsations of airflow speeds was observed: the energy of the vertical pulsations was sometimes more than twice as high as that of the horizontal ones. The speeds of updrafts were over 4.5 m/s, which favored the assent of drops and growth of liquid phase in the presence of ice crystals. Due to the revealed mechanism of supercooled drop accretion in clouds with mixed phase composition, in regions with increased turbulence intensity at low temperatures, aircraft icing seems highly likely to occur.

Paper [8] is devoted to measurements of cloud water content: various sensor designs and algorithms to calculate the portion of small droplets and total water content are presented. The research flights provided data on capture ratios for various sensors in mixed-phase and droplet clouds. Despite the restrictions in measurements of water content in small-droplet spectrum portion, the data from [150] aroused interest in researchers.

New experimental data give impetus to modeling cloud processes: a block to determine the initial concentration of cloud drops for numerical models of convective clouds with parameterized microphysics was developed and activation of condensation nuclei was calculated. Test numerical experiments with a 3D model of convective clouds using the above block demonstrated its efficiency at an initial stage of convective cloud formation even under conditions of increased stratification instability [151]. Recommendations for utilization of the block of calculating microphysical processes were developed. The presently available models of convective clouds were analyzed in terms of their practicability when routinely utilized in weather modification operations. The technical characteristics of the models were found to preclude such a use.

Based on measurements of cloud drop concentrations (2–48 μm), cloud ice crystals (12.5–1562.5 μm), and ice crystal precipitation particles

(50–6250 μm), in the archive collected in the course of operational and research flights of the aircraft lab, an approximation of the distribution function for cloud drops and ice crystals was obtained for constructing numerical models of clouds and precipitation as well as the results of their intended modification [151, 152]. The opinion is confirmed about the existence of a large range of crystal shape indicator variations compared to the range of the variation of a similar parameter for cloud droplet distribution, which corresponds to the situation in the natural environment. A comprehensive analysis of the aircraft data on cloud characteristics permits one to determine the rate of cloud suitability for their modification by seeding agents and, therefore, to determine the efficiency of intended precipitation redistribution. Simultaneously, radar parameters of modified clouds are estimated. Preliminary estimates obtained testify to the effectiveness of cloud modification by agents.

Along with aircraft measurements, cloud microphysical parameters are also investigated on the basis of other observations and experiments, including laboratory ones [153–158]. In [154, 157] microphysical properties of water microdroplet are investigated in a specifically designed laboratory wind tunnel. In the experiment [154], droplet clusters are kept in a freely levitated state within an upward-oriented flow of water vapor to analyze the condensational growth of spherical water microdroplets. It if found that in the presence of an electrostatic field of $1.5 \cdot 105\ \mathrm{V\ m^{-1}}$, droplet growth is accelerated by factors 1.5 to 2.0 as compared to conditions without any external electric field. Presumably water molecules in the ambient air are accelerated through the presence of the electric field. A kinetic model to predict the acceleration of condensational growth confirms this hypothesis to be feasible. The droplets themselves are polarized so that the deposition of steam molecules is facilitated in the electric field. In [157], the path oscillations of single, spherical water droplets levitated in a wind tunnel is studied for better comprehending the mechanical motion of small raindrops. This scientific paper fills an experimental gap in the studies of the path oscillations of single, liquid spheres of microscopic sizes at low Bond numbers <1 and relatively low Reynolds numbers $\sim 10^2$. Authors found that the studied oscillations elongate the paths, reduce the terminal velocity of the smallest droplets, and make the rain droplet fall in a non-uniform motion even after reaching terminal velocity. In [153], microphysical characteristics of contrails are evaluated with the use of the unique high-altitude polarization lidar. It is shown that the condensation trail appearing in the atmosphere behind the plane 30–40 min after the emission of fuel combustion products from the engines consists of small chaotically oriented ice particles, mostly of the column shape.

The interaction of cloud environment and aerosol is studied, including the hygroscopic and condensation properties of aerosols, which determine their role as cloud condensation nuclei (CCN) [159–168].

Analysis of the relation between the aircraft measurements of aerosol concentration and the ground measurements [159] shows the initial height of occurrence of background aerosol particle concentration to be, on average, 2000-3000 m during the warm season, depending on the position of elevated temperature inversion, and 800–100 m during the cold season (November-March) due to the absence of strong turbulent flows. Ground and aircraft experimental data on the structure and variability of surface and tropospheric aerosol was obtained, including the data on CCN. The data on the concentrations, size spectra and samples of cloud particles in different cloud types and precipitation, obtained in 2020–2022 flights, were systematized. Diurnal variation of the concentration of submicron aerosol particles in various synoptic situations was investigated. Based on the CCN data acquired with the CCN-200 instrument and the data on the fine structure of micron and submicron aerosol, the relation between CCN concentration and different aerosol fractions was analyzed. The influence of ground sources of pollution (large settlements, industrial projects, etc.) on aerosol amount in the lower troposphere was investigated. CCN characteristics in Moscow region were explored [158]. The paper presents the results of 2017–2020 measurements of the CCN concentration and supersaturation spectrum in the surface layer of Moscow environs. CCN mean monthly concentrations and the parameters of their supersaturation distribution were evaluated for different months. The prevailing CCN size and their distribution by fractions of atmospheric aerosol particles of different sizes were estimated.

The role of subpollen particles (released from pollen grains) can act as CCN and ice nuclei, which is investigated in [160, 165]. In particular, authors investigate and characterize the hygroscopic growth and CCN activation of birch, pine, and rapeseed subpollen particles. Secondary particles are obtained by the aqueous extraction of biological material from pollen grains and the subsequent solidification of atomized liquid droplets. The parameters of cloud activation are determined in the size range of 20–270 nm and subsaturated and supersaturated conditions. Authors found that the hygroscopic parameter varies in the range from 0.12 to 0.13 for supersaturated conditions (water-vapor supersaturations of 0.1–1.1%). All investigated subpollen particles samples exhibited a sharp increase of water uptake above ∼95 % RH, suggesting a liquid–liquid phase separation. In general, the results of measurements have shown that the condensation activity of subpollen particles is comparable with the condensation activity of secondary organic aerosols and depends weakly on the type of primary pollen.

In [167], the evolution of a convective thunderstorm cloud and precipitation on August 11, 2017 (near Beijing, China), against a background of high atmospheric aerosol pollution is simulated. Different microphysical parameters of droplets and ice particles that depend on atmospheric aerosol pollution

are varied. It is found that the effect of aerosol pollution both on the raindrop size spectrum and on the transition of cloud droplets to raindrops does not influence significantly dynamic, microphysical and electrical properties of the cloud. At the same time, the change in the ice particle spectrum towards the size decrease that happens under the influence of increased aerosol pollution, has a significant impact on the evolution of the cloud and precipitation. The amount of precipitation decreases both within the cloud and on the underlying surface.

The impact of the COVID-19 lockdown 2020 in Moscow on CCN reduction and further influence on cloud characteristics is analyzed in [168]. MODIS observations is used to retrieve number concentration of cloud droplets at cloud lower boundary during spring 2018–2020 for the Moscow region. For similar synoptic situations of the northern clear air advection, number concentration of cloud droplets is found to be within the limits of 200–300 cm^{-3}. During the lockdown period, with similar northern advection conditions, authors find the reduction of this concentration on 40–50 cm^{-3} (or 14–16%), with the increase in droplet effective radius by 8 ± 1% and cloud optical thickness reduction by 5 ± 2%.

Optical characteristics of cloud medium are discussed in [169–185]. A number of important results in the field of cloud particle optics have been obtained. In particular, a solution to the problem of light scattering on spherical particles adapted for the interpretation of lidar signals has been obtained [173]. The solution was obtained for typical wavelengths used in lidar remote sensing problems for water and ice. A unique database of radar-to-lidar signal ratios for typical ice crystal shapes and wide crystal size distributions was constructed based on joint lidar and radar remote sensing of cirrus clouds [181]. It is shown that the lidar-radar ratio is most sensitive to crystal size, while the depolarization ratio is most sensitive to crystal shape. For the first time, the light backscattering matrices for icy atmospheric hexagonal particles are calculated for the case of chaotic spatial orientation within the framework of the physical optics approximation for single scattering [183, 185], A data bank of light backscattering matrices on atmospheric ice crystals of 10-100 μm size was created for the interpretation of lidar remote sensing data, spectral and linear depolarization ratios are obtained [180], light backscattering matrices for irregular shaped particles are calculated [184].

In [169] mathematical models are developed and calculations of short optical impulses transfer from sub-cloud lightning through cloud layer into space are carried out. Its optical and geometric thicknesses in the vertical direction are chosen as the main variables of the cloud layer. It is shown that the presence of a cloud layer leads to the formation of a secondary source at the upper boundary of the cloud and to a significant distortion of the temporal shape of the initial pulse.

The chemical composition of precipitation (both liquid and solid), and snow cover is studied in [186–], including analyzing the isotopic composition [186, 194, 196, 200, 211, 213], acidity [188, 201, 202, 211], the content of aerosols of different origin [187, 190, 191, 199, 208, 210, 212, 218], the content of heavy metals and other toxic elements [187, 195, 197, 198, 201–206, 209, 212, 216, 217], and aromatic hydrocarbons [189, 192, 193, 207, 214, 215]. Chemical composition studies are conducted for different regions of Russia, including Moscow region [192, 198, 201, 202, 211, 213], north of European part [187, 195, 200, 203, 206, 207, 217], Baltic region [188, 190, 204, 218], Barentsburg (Svalbard) [196], Ural [186, 205], north of West Siberia [194], south of West Siberia [208, 210, 214, 215], south of East Siberia [191, 193, 209, 212, 216], Transbaikal region [197, 199]. The studies allow specifying for a number of large Russian cities the distribution and level of deposition of pollutants from the atmosphere, including depending on the location and intensity of pollution local sources and transboundary transport.

The wet deposition and washout rates of soluble forms of potentially toxic elements in rains for the first time are estimated for the Moscow metropolitan area [201, 202]. It is found that during continuous rains, the wet deposition of potentially toxic elements decreases sharply on the second and subsequent days due to the active below-cloud washout of aerosols during the initial precipitation events. It is shown that the length of the dry period and aerosol content before the onset of rain determines the amount of solid particles in rainwater, which leads to an increase in rainwater pH, and strongly affects wet deposition and washout rates of potentially toxic elements of mainly anthropogenic origin. It is also shown that the intensity of precipitation contributes to an increase in the wet deposition and washout rates of a number of elements [201]. The authors also show the increased solubility in rainwater of metals and metalloids with decreasing pH and longer periods of precipitation and decreased solubility with increasing intensity of precipitation, duration of the preceding dry period and solids content in rainwater [202]. For a number of metals and metalloids, a 20–50% increase in solubility is observed in acid rain compared to non-acid rain.

In [209, 216], the distribution of fluorine, sodium, and lithium in the snow cover in the areas close to the Siberian aluminum smelters is studied based on long-term field studies. The results show that changes in the concentrations of fluorine, sodium, and lithium in the snow cover near various plants have the same dispersion patterns, which can be described by an exponential dependence on the distance to the source. It is suggested that deposition of aerosols from industrial aluminium production can be achieved at a minimum distance from the plants or within the plant area through particle enlargement by various technological methods in aluminium production or by changing the atmospheric scattering capacity [209]. Involvement of meteorological

data made it possible to determine the influence on the fluorine concentration in the snow cover of such associated factors as: distance from the emission source, amount of atmospheric precipitation, air temperature and duration of thaws during the period starting from formation of a stable snow cover to the date of sampling [216].

The possibility of contamination of the snow cover surface with polycyclic aromatic hydrocarbons (PAHs) by precipitation of small PAH crystals from the atmosphere as part of cryohydrates during frost formation is discussed in [189]. The authors suggest that process begins in the atmosphere when finely dispersed PAH crystals interact with cloud supercooled droplets. Due to the presence of temperature inversion over the snow cover and its drying effect on the near-snow layer of air, a stable mass transport of water vapor down to the snow cover is formed, which can initiate the flow of fine cryohydrates from the PAHs. The paper [189] presents the results of observations of changes in the concentration of individual PAHs in the upper 18 mm layer of snow at accumulation of the surface hoarfrost during a long period between snowfalls. Some micromorphological features of different forms of skeletal rime microcrystals involved in the above process are shown. Since the conditions for formation of surface hoarfrost occur more frequently than for snowfalls, hoarfrost may be an informative object for testing hydrocarbon pollution of snow cover during the intervals between snowfalls.

Development of methods for observing clouds and precipitation

Investigations aiming to improve the accuracy of observing cloud and precipitation characteristics, to validate the global and regional models, creating of long-term and homogeneous data series on cloud and precipitation characteristics, and to develop methods of reconstructing the characteristics of clouds and precipitation from remote sounding data.

Papers [145, 146, 219–221] present and discuss various data on balloon and aircraft observations of cloud characteristics. Study [145] describes the aircraft data acquisition system mounted on board the new-generation aircraft lab of thYak-42D “Roshydromet” designed to explore the atmosphere and underlying surface (see chapter 3 for details). Paper [221] describes a new platform to measure the profiles of temperature, water vapor, and aerosol with a 1-meter resolution in the tropical tropopause layer. The platform presents a descending system of measurement instruments under a drifting balloon. The system comprises verified sensors of water vapor, temperature, pressure, and cloud and aerosol particles. Feasibility of utilizing this platform in future missions to study cloud characteristics in the tropics at the tropopause level is demonstrated.

Regular ground-based and upper-air observational data [222–224] that may be valuable in analyzing space-and-time peculiarities of cloud and precipitation characteristics (see also section 1) and can be used for the validation of network products, such as satellite data and reanalysis systems [225–230]. The error in the reconstruction of precipitation field, using ERA5 reanalysis data, as compared with the data from stations, is estimated in [227]. It is shown that reanalysis overestimates precipitation amount by 14% or more in summer and by up to 37% in spring, and herewith, erroneously identifies from 30% (in winter and autumn) and 40% (in winter and summer) of days as those without precipitation. A random error is on average by one third less than daily precipitation total variability, while the share of days with precipitation, revealed by the ERA5, is 84–89% and, on average, is less in summer than in the other seasons. On the whole, ERA5 provides lower accuracy for regions and seasons that have few days with precipitation and small precipitation amount. A technology to remove errors in ERA5 reanalysis, considering observation data, is suggested, and a corrected database for southern Siberia is presented in [226]. Other ground-based observations of precipitation, using different instruments (including precipitation collectors, optical rain gauges, etc.), are discussed in [231–236].

Due to the objective difficulties in making contact measurements, remote sounding data on hydrometeors, obtained by satellite or ground-based instruments, is used. Among the sources of remote ground-based data used to estimate cloud and precipitation characteristics, weather radar is most widely employed [237–253].

The input of different hydrometeors to the total radar reflectivity is estimated in [239]. It is shown that in solving the dissipation theory inverse problems, the input of rain drops to reflectivity at a 10 cm wavelength can be neglected, while at a 3.2 cm wavelength this input must be taken into account. Herewith, the contribution of cloud droplets and crystals at both wavelengths can be neglected. The influence of the form of drops, and their deformation as well, on their scattering properties and radar reflectivity is evaluated in [241, 250]. Analysis shows that the form of drops does not noticeably influence radar reflectivity in the absence of electric fields, and vice versa, it does affect radar reflectivity considerably in the presence of an electric field. Therefore, in calculating precipitation intensity by radar reflectivity, the corresponding correction must be introduced.

A technique to determine wind shear based on weather radar data by the reconstruction of wind profile, using estimates of the reflection spectrum width, is suggested in [238]. A new algorithm of identifying thunderstorms, based on the sum of positive radar reflectivity vales, and exceeding by justification and reliability more sophisticated models, is presented in [244].

In paper [245], the author proposes a method of evaluating maximum possible daily shower precipitation (as exemplified by the region of Middle Ural), based on the joint use of ground, upper-air, satellite, and radar data. Maximum possible precipitation is determined based on total cloud system moisture content described in terms of cloud systems' stationarity or time dynamics; herewith, different methods of moisture content are separately considered: those based on the characteristics of vertical temperature distribution in the troposphere, on convection speed, and on the height of top cloud boundary. This technique can be useful in solving applied problems.

Along with weather radar techniques, methods of the reconstruction of cloud characteristics using data from other ground-based observations, such as cloud camera [254], infrared [255], lidar [256, 257] and microwave remote sensing [258–266], those based on lightning detection systems [267–270], or the joint use of different types of observation [245, 271], are being developed.

In paper [254], authors suggest a scheme to evaluate the characteristics of algorithms of cloud characteristic retrieval from optical images obtained by ground-based cloud cameras. Several new algorithms based on deep learning method, designed for cloud finding by wide-angle sky cameras, are also presented. It is shown that algorithms based on convolutional neural networks deliver a superior quality compared to all previously published approaches. A considerable drop in the ability to generalize the training data in the case of a strong covariate shift between the training and test subsets of imagery, which may occur in the case of regional subsampling, is revealed.

Microwave radiometry potentials for experimental studies of cloud water content, in particular, in periods of the occurrence of hazardous weather phenomena connected with the development of convective clouds and thunderstorm processes, are discussed in [264]. In paper [263], feasibility of investigating the variability of water content in different cloud types with spatial resolution over 200 m and 10 s time resolution, based on spectral microwave radiometric measurements in the region of 18.0–27.2 GHz water vapor absorption line, is demonstrated. Time series of the spectra of brightness temperature values can serve as the basis for real-time analysis of the time variability of cloud water content. Multi-frequency microwave radiometric measurements may also be used in periods of heavy rain formation [261]. Radiometric measurements in an angular scanning regime allow the retrieval of the spatial gradient of cloud water content, e.g., at the "land-sea" boundary [259]. In particular, cloud water gradient values for summer and winter, averaged over 7-year measurements, demonstrate the presence of a positive gradient (with higher values over land and lower over sea) during both summer and winter, which qualitatively agrees with the available satellite data. It is shown in [266] that microwave measurements and measurements of atmos-

pheric electric field made simultaneously can be used to reveal possible relations between electrification rate and turbulence intensity in clouds.

In [268], using two statistical methods, the radii of a circular area of sampling of the WWLLN lightning detection network data are estimated; with such radii the best agreement with the number of days with thunderstorms by the data of regular weather observations is obtained. These radii are shown to be within the range from 12 to 36 km, with a 23 km mean value. In the daytime, the radii are less than at night, being, on average, 21 and 26 km, respectively. It is shown that increasing (diminishing) the radius of WWLLN data sampling results in a larger (smaller) mean annual number of days with lightning by ~1day relative to weather forecast.

Peculiarities of satellite observations of cloud characteristics are discussed in [272–297]. In particular, methods are being developed to reconstruct the characteristics of clouds and precipitation based on passive remote sensing [272, 273, 275, 276, 278–289, 291, 292, 295, 297], including Russian satellites «Meteor-M No 2», «Electro-L» and «Arktika-M» [272, 273, 275, 276, 279, 284, 286, 295], based on active remote sensing [290, 294], based on observations of the Earth's gravitational field [274] and data from global navigation satellite systems [277, 296]. Artificial neural network methods are actively used to process satellite information [272, 281, 285–289, 294]. For example, using a deep neural network, it was proposed to detect overshooting tops above a cumulonimbus anvil to identify cumulonimbus cloud centers [281]. The detection probability of vertices is 50-70%, the false detection rate is 45–55%. Automated detection of deep convection clouds is also discussed in [285]. In [277, 296] the principal possibility of monitoring of convective processes using satellite navigation system receivers is discussed.

Several methods and algorithms for reconstruction of different characteristics of clouds and precipitation are presented. Thus, in [274] a technique for estimating the annual spatial distribution of solid atmospheric precipitation is presented based on data from GRACE (Gravity Recovery and Climate Experiment) project in coordinate grid cells with a 1° latitude and longitude step. The method allows to calculate the water equivalent in the land, including the water reserves in the snow cover. Based on the identified patterns in the study area and spatial detailing, it is possible to construct annual raster maps of solid atmospheric precipitation distribution with spatial resolution up to 90 m.

A number of techniques have been developed for the MSU-MR radiometer onboard the Russian hydrometeorological satellite Meteor-M No. 2 (and Meteor-M No 2-2). In [275] an algorithm for determining the optical thickness and effective radius of cloud particles is presented for this instrument, which is based on the physical principles of using cloud spectral brightness coefficients at 0.64 and 1.68 μm wavelengths. An algorithm for determining

the phase state of clouds (droplet, crystalline, and mixed) by spectral brightness coefficients at wavelengths of 1.6 and 3.7 μm and brightness temperatures at wavelengths of 11 and 12 μm is presented in [276]. Based on a comparison with other methods, it is noted that the largest discrepancies are observed for thin semi-transparent clouds due to additional radiation coming from the underlying surface, and also for mixed clouds due to the specifics of the algorithm. In [284], a technique for reconstructing the height of cloud tops, based on measurements of the cloud's emission in a split window of atmospheric transparency window at wavelengths of 11 and 12 μm, is presented. The results of comparison of the reconstructed estimates of the height of the cloud tops from MSU-MR data and from CALIOP satellite lidar data show a relatively good agreement.

Based on the use of data from different radiometers (installed on satellites NOAA, Meteor-M No 2, Meteosat) the technology for diagnosing cloud cover parameters, daily, monthly and annual precipitation totals, dangerous weather phenomena is developed and introduced into operational practice at the Federal organization "SRC Planet" [279, 280, 289]. The technology is based on original author's methods of automated threshold pixel-by-pixel interpretation and classification of satellite information by indirect features. The distinctive feature is the high efficiency (the interpretation results enter the database in less than 0.5 min) and periodicity (15 min), as well as the possibility of a complex analysis of the synoptic situation over a large area. The technology is tested and implemented in operational work.

In [282, 288] the approach to classification of clouds by different types based on satellite data, including at night, is further developed. A unified classification of recognizable cloud types is given. A statistical model of image texture of different cloud types and its physical parameters based on two-parameter distributions is proposed. The description of the algorithm of atmospheric fronts detection and determination of their types by satellite data is presented, the results of its testing for the territory of Western Siberia are given.

In [294] an algorithm for reconstructing the height of the lower boundary of clouds based on passive observations from space, based on the application of an adapted self-organizing Kohonen map, is proposed. At the stage of neural network training authors use MODIS passive remote sensing data and CALIOP lidar observations, while during the image clustering they use only MODIS images and thematic products of their processing. The key attributes of clustering are defined, one of which is the geometric thickness of clouds. The limitations of the developed algorithm and promising directions of its refinement involving additional information are given. In general, it is shown that the results of lower cloud boundary height reconstruction from MODIS data agree well with CALIOP measurements over the region under study for low-level and high-level optically thin clouds with optical thickness less than 15.

Modelling of clouds and precipitation

Issues related to the reliability of reproducing the processes of formation, growth and dissipation of clouds, formation of precipitation (of different forms) in numerical modeling remain a topical scientific challenge. This is important both for weather forecasting, including forecasting precipitation-related hazards, and for climate prediction, given that cloud response to external forcing is still the main cause of uncertainty in assessing climate sensitivity to such forcings. Various issues of cloud processes modeling in global and regional climate models are considered in [298–307], studies [308, 309] are devoted to the modeling of precipitation.

In [306] the effect of cloud parameterization changes on the equilibrium climate sensitivity in the climate model of Institute of Numerical Mathematics Russian Academy of Sciences (INM-CM4-8, the model with the lowest sensitivity among all CMIP6 ensemble models) is studied. It is shown that reasonable changes in cloud parameterization can lead to changes in sensitivity in the model in the range from 1.8 to 4.1 K, which is more than half the interval for the ensemble of CMIP6 models. Three main mechanisms are responsible for the increased sensitivity: an increase in cloud dissipation in a warmer climate due to an increased water vapor deficit in the cloudless part of the cell, a weakening of cloud formation processes in the boundary layer in a warmer climate, and a rapid cloud response to an increase in CO_2 concentration due to changes in stratification. For the quadrupling of CO_2 concentration, changes in the cloud parameterization can lead to changes in the equilibrium sensitivity of the INM-CM4-8 model in the range from 3.6 to 8.1 K [303]. Also, the parameterization of the cloud-aerosol interaction has been updated in the INM-CM model [307], in which the sulfate aerosol concentration is taken into account. It is shown that accounting for sulfate aerosol allows us to correctly reproduce changes in cloud transmission from 1980 to 2005 compared to observational data. The mean global radiative forcing due to indirect aerosol impact accounts for 0.13 W/m^2 for 2005 relative to 1850 according to the model simulations.

In [298] authors formulate a method for dynamic-stochastic parameterization of the nonconvective cloudiness score in the general atmospheric circulation model based on general assumptions about the distribution of moisture fields within the integration cell. A comparison with CALIPSO observational data shows the reasonableness of using this parameterization.

In [308], a model of the orographic component of precipitation is proposed that based on an algorithm for calculating the condensation rate of water vapor in the air forced up along a mountain slope. The model takes into account the attenuation of the vertical component of wind velocity initiated by the orography, depending on stratification, as well as the fraction of mois-

ture falling as precipitation from the total water mass. Data from ERA5 reanalysis (temperature, humidity characteristics, wind speed components) is used as initial data. It is shown that the proposed algorithm satisfactorily reproduces synoptic precipitation variability, its seasonal course and climatic variability, as well as the spatial distribution across the slopes of Elbrus. The proposed model can be used to calculate annual accumulation on mountain glaciers and in global climate models as a parameterization of orographic precipitation.

In [299–302; 305] the results of modeling of convective processes in clouds are presented. In particular, [305] presents a three-dimensional numerical model of a convective cloud taking into account electrical processes using detailed microphysical equations with several tens of classes of droplets and crystals. In particular, the model accounts for 61 droplet size categories and 75 crystal size categories. The model has been used to determine the spatial distribution and quantitative values of volumetric electric charges and field strengths in and around the cloud at successive points in time during evolution. The model has been used to quantify the influence of electrical processes on precipitation formation. The three-dimensional model of a convective cloud developed at the Main Geophysical Observatory also continues to be developed, using which estimates of various characteristics of convective clouds have been obtained (see Section 2 for details).

In [299] a modification of the Price-Rind scheme for calculating the lightning frequency was developed, which can be used in models with large time and space steps. At such time and space steps, the degree exponent in the dependence of flash frequency on convective cloud top height is 2 times smaller over land and a quarter smaller over the ocean than in the original version of the Price-Rind scheme. The modified version of the scheme is implemented in the climate mode lof Institute of Atmospheric Physics Russian Academy of Sciences. The results of calculations of lightning activity characteristics with the modified scheme agree better with satellite data for lightning frequency than with the original version. It is shown that with global warming (cooling) lightning frequency increases (decreases) according to model calculations in all seasons. Sensitivity of lightning frequency to changes in the near-surface atmospheric temperature at the global level is obtained equal to 10%/K.

One of the main goals of cloud and precipitation modeling is to improve the quality forecast and shorten its lead-time. Considerable attention is paid to the development of methods for forecast of dangerous convective phenomena based on global and regional experience. Various aspects of forecasting cloud characteristics using different models and methods are discussed in [310–313]. Studies [314–331] are devoted to forecasting precipitation, including extreme precipitation, both using models (COSMO-Ru2, SL-AV,

WRF) for short- and medium-term forecasting [322–331] and satellite and weather radar data for nowcasting [314–321]. In addition to the forecast of heavy precipitation, the forecast of other dangerous convective phenomena is considered in [332–345]. Researchers are also interested in the forecast of fog [346] and ice phenomena [347, 348], as well as issues of assessing the quality of the forecast [349, 350].

The prediction of cloud characteristics is important for the aviation functioning. In [312] a review of works devoted to the influence of icing on the operation of air transport is presented. The problems of ground icing, which leads to the deterioration of airport flight-strips and complicates pre-flight aerodrome operations, are discussed. The causes of aircraft icing in flight, methods of icing observation, approaches to icing forecasting in clouds and precipitation are considered. Methods for predicting icing of aircraft engines in areas of high concentration of ice crystals are analyzed. In [347, 348], it was proposed to use a thermal balance model with WRF-ARW model predictions as input data for icing phenomena and maximum icing thickness forecasts. In [311], the possibility of using a semiempirical method for predicting total cloudiness in the practice of meteorological support for aviation, based on information about the dew point depression, is discussed. The method of fog prediction based on the convolutional neural network model based on the meteorological and aerological observation data for the previous 12 h was proposed in [346]. It is shown that the described method makes it possible to predict the occurrence and dissipation of fog, including at aerodromes, with an advance of 3 to 12 h.

In [314] a review of studies devoted to the history of development and the current state of thunderstorm nowcasting technologies is presented. The role of information about thunderstorms obtained from various sources (satellites, radars, lightning detection systems, ground-based microwave radiometers), and the value of the output of numerical weather prediction models for lightning nowcasting are shown. The features of thunderstorm nowcasting systems used by the world weather services are discussed. In [317], the situations with thunderstorms at Moscow airfields are analyzed using the Vnukovo DMRL-C hazard map, information from lightning detection system installed at airfields and the output of the COSMO-Ru02 model for the territory of the Central Federal District with high temporal resolution. The consistency of the information on thunderstorms provided by different sources of information and the possibility of thunderstorm nowcasting and very short forecasting (2 h in advance) are discussed. A series of papers [316, 319–321] discuss the results of tests of the operational precipitation nowcasting system of the Hydrometeorological Center of Russia in different periods of the year based on radar data on the European territory of Russia. Peculiarities of winter precipitation nowcasting under conditions of its weaker intensity com-

pared to summer precipitation are evaluated. The problems of object-oriented verification of precipitation area forecasts using extreme value theory methods are discussed.

Object-oriented quality assessment of precipitation forecasting is carried out also in [349] for COSMO-Ru2 model and in [323, 340, 350] for WRF model. Thus, it is shown in [323] on the example of heavy precipitation reproduction in Perm region based on WRF model that local zones of intensive precipitation are simulated reasonably well during convective permission modeling, and their maximum intensity is close to actual values. When modeling using any convection parameterization (except for the Cain-Fritsch scheme), the area of precipitation zones is significantly overestimated, while the maximum intensity is underestimated, which leads to a reduction in the number of false alarms when forecasting heavy showers. In [315] the results of assimilation of lightning observations in the WRF model are presented. It is found that the mean absolute errors for all quantities due to consideration of lightning are reduced. The work of the used procedure is demonstrated on the example of comparing the maps of accumulated daily precipitation for seven forecasts with and without taking into account the lightning detection data. It is shown that the configuration of prognostic precipitation fields and their intensities are noticeably closer to the reference ones both in the regions where thunderstorms were observed and in the regions without them. This is especially pronounced for precipitation of low intensity (0–7 mm). The lightning detection data are also successfully used to verify the model forecast of convective phenomena [338]. The joint use of model data, as well as satellite and radar data (although without assimilating these data into the model) to calculate the maximum velocity of convective fluxes in clouds is considered in [332, 336]. It is shown that diagnostic calculations of maximum convective velocity on the basis of satellite and radar information allow specifying the short-term forecast of dangerous convective weather phenomena, especially the place and time of their occurrence. The proposed approach is used in the methods of forecasting dangerous convective weather phenomena in the summer period of the year, implemented in the operational practice of the Hydrometeorological Center of Russia.

The ensemble approach for forecasting heavy precipitation and thunderstorm activity has recently been developed. The advantages and features of this approach are evaluated in [328, 345]. Thus, in [328] an ensemble multimodel technique is proposed for forecasting heavy summer precipitation in Perm Krai with 15 and 27 h advance using global hydrodynamic models GFS, GEM and ICON. It is shown that averaging over the ensemble of global models leads to a sharp reduction in the number of false alarms. A scheme for combining global models has been developed, which consists in filtering forecasts of heavy rainfall by GEM model and using average values by GFS,

GEM and ICON models in the remaining points. The application of the scheme makes it possible to improve the reliability of short-term forecasts of heavy summer frontal rainfall in Perm Krai compared to any of the models separately. In [345], the results of ensemble forecasting of thunderstorm cloud development using a convective cloud model are presented. It is shown that the introduction of perturbations into the initial data leads to the development of clouds with different characteristics, with changes noted both for the maximum values during cloud development and in the dynamics of cell development itself during the transition to the thunderstorm stage. The greatest variability is noted for the microphysical parameters of precipitation and vertical velocities in the cloud.

Possibilities and shortcomings of forecasting dangerous convective phenomena, including precipitation, squalls, hail, and tornadoes based on certain predictors (instability indices) are discussed in [324, 331, 334, 335, 339, 341, 343, 344]. In a series of papers [339, 341, 343, 344] it is proposed to use the output fields of the GFS NCEP model with different lead-time and statistical analysis methods for predicting hail and determining its maximum size. In [335], the issue of simulating atmospheric stratification using the WRF numerical weather forecast model is considered. The errors of reproducing the stratification at different vertical levels (both at the ground and for the middle and upper troposphere) and under different weather conditions (thunderstorm and "good weather" cumulonimbus clouds) are considered. It is shown that there are errors in the surface values of temperature and dew point temperature, as well as errors in the assessment of humidity of the lower and middle troposphere, which can lead to errors in the convection forecasting. In [334] a methodology for automated short-term forecasting of waterspout hazards based on the composite instability index (based on the COSMO-Ru2 model output fields) and further recognition of waterspout hazardous areas in real time using radar and satellite observations is proposed. The fundamental possibility of issuing warnings about waterspout occurrence in automatic mode is substantiated. The success of using the technique is also discussed in [136].

Intended weather modification. Methods, seeding agents, and technical aids

The history and analysis of the development of work connected with intended modification (IM) of hydro-meteorological processes, carried out at the Hydrometeorological Service of Russia, are described in 2022 reviews [351, 352, 375]. The authors of paper [352] reviewed over 100 major projects on cloud dissipation and redistribution of precipitation over a target area during political, cultural, and sporting festivities. Depending on synoptic situation, one of the four modification techniques are employed: dissipation of

stratiform clouds; initiation of early precipitation on the windward side of the target area by seeding clouds to form a "shadow" of precipitation, intensive seeding (overseeding) of precipitation-generating clouds overrunning the target area to diminish precipitation generation efficiency, as well as the destruction of thick cumulonimbus clouds by a dynamic technique [352]. In 2022, a representative forum of scientists involved with cloud and precipitation physics, cloud climatology, cloud and precipitation formation processes, including their intended modification, was held in Stavropol (IV International Conference "Problems of atmospheric physics, climatology and monitoring of the environment", 23–25 May 2022) hosted by the High-Mountain Geophysical Institute). The conference marked a jubilee of the project on hail protection in this country, initiated in 1967 [351, 375]. The issues of the journal "Russian Meteorology and Hydrology", Nos. 7 and 8, 2022, were solely dedicated to problems of intended modification of hydrometeorological processes.

By now, notable practical progress has been made in atmospheric precipitation redistribution. At present, the Central Aerological Observatory that pioneered this research direction in the USSR in 1948, beginning with the work of I. I. Gaivaronsky et al., possesses an advanced technology, the most effective in the world practice, capable of intended precipitation enhancement over large territories in the interests of agriculture, energetics, road and public utilities maintenance, firefighting, etc. An important aspect of planning precipitation enhancement operations is the problem to determine periods of maximal development and lifetime of clouds suitable for a certain type of modification. Climatic data on instability conditions are analyzed, such as vertical profiles of temperature and humidity, cloud water content, the presence of condensation nuclei, and other microphysical cloud characteristics.

With adequate selection of modification time period, in the presence of clouds with water content sufficient for additional precipitation fall, the problem would be solved successfully using a certain technique. The detection of clouds with sufficient water content to moisten cereals in the southern and Volga regions of Russia is discussed in papers [353, 354] where periods most effective for precipitation enhancement operations are determined. Taking into account the conditions of winter wheat vegetation, it was established that the duration of the period with cloud cover suitable for precipitation enhancement operations would not be more than 11–15 days, while an expected surplus of moisture in the form of precipitation would vary between 10 and 27 mm in spring and summer, and between 6 and 25 mm in winter. Based on the aircraft sounding over Moscow [355, 356], the estimates of the suitability of supercooled wavy, stratiform and convective clouds suitable for precipitation enhancement operations in the central region of the European part of Russia are presented. The data obtained can be used in planning, preparation and implementation of the modification of such cloud types. The effective-

ness of convective cloud modification with ice-generating agents in enhancing precipitation is considered in [357, 358], using a 3D numerical model of a convective cloud. Conditions necessary for producing maximal possible surplus precipitation with relatively low agent consumption are determined, using clouds characteristic of two different regions of Russia as an example. To this end, sufficiently large areas with supercooled liquid-water cloud zones must be present, where artificial crystallization nuclei introduced would provide necessary conditions for transformation of cloud drops to ice particles.

A solution of the problem of monitoring and short-term forecast of the availability of clouds suitable for obtaining surplus precipitation by seeding hygroscopic agents , which arises at the start of operations, is suggested in paper [358]. A method of remote estimation of cloud water content by spectral microwave radiometric measurements within the range of water vapor absorption line of 18.0–27.2 GHz is suggested in [263]. Here, investigation of the variability of water content in different cloud types with space resolution over 200 m and 10 s time resolution is shown to be possible. Paper [359] investigates the influence of crystallizing seeding of thunderstorm characteristics of 40 clouds with hail and hail-hazardous clouds, following the Russian rocket technology of anti-hail protection. For each seeded cloud, a reference cloud that had not been seeded was selected. To this end, the parameter DV35 (radio echo from a cloud with reflectivity over 35 dBZ above zero isotherm) was used. Rocket seeding of hail and hail-hazardous clouds with a crystallizing agent is shown to result in statistically significant changes in cloud characteristics. Cloud seeding provides an increase of the frequency of internal cloud discharges by a factor of 4.4, an increase of the frequency of "cloud-earth" negative discharges by a factor of 3.7, with nearly complete elimination of "cloud-earth" positive discharges. Such considerable changes of electric characteristics in seeded hail and hail-hazardous clouds seem to evidence that their thunderstorm activity can be controlled. Paper [372] also confirms that electric activity in clouds increases after seeding.

Seeding agents are being also upgraded in [361–368]. The presence in the atmosphere of electric field and charge on agent particles can influence specific output of ice-forming nuclei during cloud modification operations [369]. Therefore, investigation of the influence of electric field strength upon specific charges on agent particles that are formed at pyrotechnic substance sublimation seems to be of practical importance in determining seeding agent dosage. Paper [370] presents the results of studying changes in the ice-forming properties of natural and man-made aerosols containing aluminosilicates, when acted upon by iodine. Natural and man-made contaminating iodine vapors, as well as those invariably formed through cloud modification by pyrotechnic substances and other means, can enhance the ice-forming activity of natural aerosols, of those, in particular, that contain aluminosilicates.

Changes in the electric state of convective clouds acted upon by crystallizing agent AgJ seeded from aircraft are investigated in paper [371, 372] The electric state was determined by lightning discharge frequency which was calculated from radar characteristics of target clouds, using regression equations previously constructed in Russia and abroad. Analysis reveals increased electric activity in clouds, following their seeding, which can be manifested by increased lightning frequency.

Aerosol generators are increasingly often employed in the world practice in intended precipitation redistribution and hail protection operations. Paper [373] presents theoretical and experimental estimates of the propagation of agents from ground aerosol generators over the boundary atmospheric layer: AgJ concentration values become higher than background ones up to 1200 m at a 3–9 km distance from the generator. An experiment to enhance precipitation over the Crimean territory demonstrated that as clouds were passing over the aerosol generators, the height of the top cloud boundary, maximal reflectivity and precipitation intensity were increasing, which testify to a positive cloud modification effect. The use of aerosol generators can be an addition to an aircraft seeding technique, especially in nighttime cloud modification operations and operations carried out over mountainous terrain.

The use of the experimental technology to prevent fires and higher fire-hazard class confirmed its high effectiveness [374]: the number of fires over the territory of Yakutia in 1922 diminished by a factor of 2.8 as compared with 2021, the total area affected by fires decreased by a factor of 17, the number of days with fire hazard class 5 in 2022 was 4.08 times as low as in 2021 and 2.3 times as low as the mean long-term number for the period from 2017 to 2021, over most target area during the period of aircraft operations fire hazard class was between 1 and 2. Since 1968, the domestic FSBI "Avialesoohrana" (Aircraft Forest Protection) has fulfilled operations to extinguish forest fires and diminish fire hazard with deliberately induced precipitation, using the methods and techniques of intended precipitation enhancement developed by research institutes of Roshydromet. The efficiency of the operations conducted in the absence of Doppler weather radar network with the sparse network of weather stations over most of Siberia and the Far East is analyzed. Reasonably high effectiveness of the utilized technique is demonstrated: the actual precipitation total was 1.4–1.5 times as large as the expected precipitation amount averaged over the data of prognostic models [375].

Information about hail fighting in the USSR and, briefly, about the history of hail fighting development in the Russian Federation is presented in [376, 377]. This includes the basics of the currently employed automated rocket technology of hail prevention, the characteristics the present-day anti-hail system in the North Caucasus and the estimates of its physical efficiency,

major problems and recommendations for its further upgrading. Scientific discussions of hail fighting methods and effects associated with the investigation of hail formation and hail fighting mechanisms are reported to proceed [377, 378]. Here, technical problems to be solved in using agent generators are considered, and statistical characteristics of the hail fighting effect are analyzed.

The economy efficiency of the 2016–2020 anti-hail operations is analyzed in paper [377]. A comparative analysis of the characteristics of total summer precipitation on hail-protected and the adjoining territories for a 60-year period demonstrated a tendency of this parameter to decrease in May – August [378]. In the center of hail-protected territories precipitation amount is recorded to increase by 7–9% as compared with background values from weather stations. Verification by Fisher criterion confirmed the change in the characteristics of total summer precipitation, as recorded at Korneshty weather station (hail-protected territory), to be at a 0.05 significance level. In September, the first month after anti-hail operations, weather stations in the region of intended weather modification register total precipitation increase by over 30%. This fact is explained as a consequence of cloud seeding with agents based on silver iodide. In [379] is suggested a combined technique (an agent plus an artificially induced lightning) to act on hail-thunderstorm cloud, aimed at preventing hail formation and fall. Physical justification of the technique is provided, and the results of a preliminary field experiment to act on hail-thunderstorm cloud by anti-hail rockets "Alazan'-6" with conductive surface are presented. It is pointed out how the suggested technique can be employed in practice to protect various objects on the ground from lightning and hail: rocket launching systems, nuclear power stations, valuable forests, gardens, plantations, etc. In conventional generators used in weather modification operations [380], under certain conditions, a secondary ignition of combustion products is possible, with practically complete burnout of active substances and considerable, by several orders, decrease of the ice-forming activity of produced aerosol. Feasibility of a considerable reduction of this deficiency through alteration of both physical and chemical properties of ice-forming aerosol is discussed.

Paper [381] draws the attention of specialists to the fact that any actions on clouds lead to changes of all related processes. Electric processes are closely connected with cloud microphysics and dynamics and largely influence the dynamics of air flows and precipitation formation, including hail. A review of physical hypotheses as well as laboratory and field experiments in studying the feasibility of acting on electric processes in clouds is presented. It is shown that the most theoretically grounded and experimentally confirmed are operations using ice-forming agents that permit modification of the number and size of ice particles which, in their turn, determine the inten-

sity of cloud electrifying processes. A concept of the deployment of mobile stations of modifying hail processes is proposed, aiming at revealing deficiencies due to fixed station locations [382]. The concept is based on the analysis of the 2010–2019 annual reports of Stavropol Paramilitary Service. Methods and programs of optimizing the order of radar observations during anti-hail operations based on automated convective cell identification and control of the parameters of all convective cells are developed in [383]. Paper [384] simulates hailstone size in seeded clouds. Cloud composition and evolution at different times under natural conditions are investigated through numerical experiments. Cloud seeding is simulated, using the functions of artificial crystal sources.

The results of snow avalanche fighting operations fulfilled by different organizations on the territory of the former USSR [385] and long-term experimental studies carried out under high-mountain conditions made it possible to develop a technology of preventive avalanche based on avalanche hazard prediction, diagnosis of snow condition, and dynamic action on snow stability. The opinions concerning this problem, expressed in various scientific publications, are debatable. Paper [386] analyzes a 90-year experience in preventive avalanche operations in the Khibiny mountains and the use of similar techniques in other regions of Russia and abroad, which are based on disturbing snow cover stability by explosions.

The authors believe that despite the long experience acquired, the scientific basis of the above techniques is not sound enough, and methodology of their utilization is not currently available. Insufficient knowledge of the mechanisms of snow avalanche, a great spatial variability of snow properties and snow stability in an avalanche center are the major factors preventing the solution of the above problems, Paper [387] is devoted to a 70-year history of avalanche investigations on Sakhalin Island, basic stages of anti-avalanche activity, and establishing specialized organizations involved with diminishing snow avalanche hazards.

Avalanche hazard investigations use modeling as well. A description of a 3D model of avalanche motion is given in paper [388] with preliminary results of modeling avalanche motion as applied to a real relief of an avalanche-hazardous area on the territory of a mountain ski resort in Elbrus region.

Investigations of fog formation and dissipation processes are continued, and statistical data is collected on the occurrence and intensity of fogs, especially in regions with key transport nodes, major technical structures, near aerodromes [389] and highways [390, 391]. Technologies to dissipate warm fogs with hygroscopic agents and automated systems to dissipate supercooled fogs with cooling agents are being developed. Paper [392] is devoted to the investigation of ion wind capability to initiate motion in a motionless warm

fog contained in a closed volume. The work was aimed at experimental testing of the practicability of coronal discharge in warm fog modification. The experiment was fulfilled, using a specialized laboratory setup constructed at the Institute of Applied Geophysics. The efficiency of the equipment in the investigation of the influence of a coronal discharge on warm fog was clearly demonstrated.

During the period considered, research works devoted to the feasibility of comprehensive positive influence on arid terrain, with a final goal of enhancing or producing precipitation by geoengineering methods, were published. The application of the regional WRF model in [393] demonstrated that underlying surface characteristics and thus the coastal circulation can be changed by geoengineering methods such as reforestation. Changes in temperature, humidity and impulse exchange between the earth surface and the atmosphere lead to changes in breeze intensity, cloud cover, and, finally, precipitation amount. Earth surface albedo decrease to 0.2 over coastal plains increases air temperature (by 1–2 K), temperature difference between sea and land surfaces, the strength of breezes, the coefficients of water vapor mixing in the boundary layer above 3 km (approximately by 0.5 g/kg), the vertical mixing in the planetary boundary layer. By the author's estimates, 1.5 Gt of surplus rain water is also produced; this is equivalent to the annual consumption by five million people. So, the exemplified geoengineering method along with the advanced techniques of fresh water accumulation and underground storage provide an effective solution of the problem of water deficit in arid coastal regions.

Paper [394] put forward the idea, presented physical grounds, and demonstrated the feasibility of stimulating atmospheric convection in dramatically arid regions, aimed at producing artificial convective clouds and precipitation. A review of the previous work with meteodrones [395] and the numerical experiments fulfilled [394] are indicative of the following: a jet with the initial speed of 300 m/s, temperature of 300°C, and flow volume of 240 m^3/s, without additional energizing, can reach a condensation level under certain natural conditions – the absence of an inversion layer, temperature vertical gradient > 8 °C/km and humidity >85%. The results of the numerical experiments can be used in developing criteria to choose days with conditions favorable for such field experiments. "The method and device for creating artificial clouds and precipitation" was patented. Papers [396, 397] present the results of mathematical model development and numerical modeling of the ascent of a vertically directed jet fed by the heat of water vapor condensation on hygroscopic two-layer $NaCl/TiO_2$ nanoaerosol (capable of absorbing water vapor amount largely exceeding its mass) injected into the jet at the start of the operation. The estimate of the feasibility of producing artificial convective clouds, depending on the jet parameters, condensation heat, and verti-

cal profiles of wind speed in sub-cloud layer <6m/s, temperature gradient >7,5°C/km and air humidity > 65% is confirmed.

References

1. IPCC, 2021: Climate Change 2021: The Physical Science Basis. Contribution of Working Group I to the Sixth Assessment Report of the Intergovernmental Panel on Climate Change [Masson-Delmotte, V., P. Zhai, A. Pirani, S.L. Connors, C. Péan, S. Berger, N. Caud, Y. Chen, L. Goldfarb, M.I. Gomis, M. Huang, K. Leitzell, E. Lonnoy, J.B.R. Matthews, T.K. Maycock, T. Waterfield, O. Yelekçi, R. Yu, and B. Zhou (eds.)]. Cambridge University Press, Cambridge, United Kingdom and New York, NY, USA, 2391 pp. doi:10.1017/9781009157896.
2. The third assessment report on climate changes and their consequences over Russia / V.M. Kattsov ed.; Roshydromet – Saint Petersburg, 2022, 676 pp. .
3. Shamin S.I., Sanina A.T. Major trends in hydrometeorological hazards that did damage on the territory of the Russian Federation // Transactions of RIHMI-WDC, 2021, vol. 188, P.154–166 (in Russian).
4. Golitsyn, G.S., Chkhetiani, O.G. & Vazaeva, N.V. Clouds and Turbulence Theory: Peculiar Self-Similarity, 4/3 Fractal Exponent and Invariants. Izv. Atmos. Ocean. Phys. 58, 645–648 (2022). https://doi.org/10.1134/S0001433822060081.
5. Chernokulsky A., Esau I. Cloud cover and cloud types in the Eurasian Arctic in 1936–2012 // International Journal of Climatology, 2019, V.39, issue 15, P.5771–5790, doi: 10.1002/joc.6187.
6. Aleksandrova, M. Cloudiness over the oceans at subarctic latitudes as a visible part of atmospheric moisture transport / M. Aleksandrova // Russian Journal of Earth Sciences. – 2021. – Vol. 21, No. 1. – P. ES1004. – DOI 10.2205/2020ES 000738.
7. Pokrovsky, O. M. Cloud changes in the period of global warming: the results of the international satellite project // Issledovanie Zemli is kosmosa (Exploring Earth from space). – 2019. – № 1. – P. 3–13. (in Russian).
8. Zotova E., A. Schmitt, B. Ivanov, P. Svyaschennikov Seasonal and annual variability of Svalbard cloud cover // Russian Arctic. 2022. № 18. P. 30–43.
9. Sviashchennikov, P., Drugorub, A. (2022). Long-term trends in total cloud cover in the Arctic based on surface observations in 1985–2020. Bulletin of Geography. Physical Geography Series, (22), 33–43. https://doi.org/10.12775/bgeo-2022-0003.
10. Belikov, Y.E., Dyshlevsky, S.V. & Repin, A.Y. Effect of Thin High Clouds and Aerosol Layers on the Heating and Dissipation of Low-level Clouds in the Arctic. Russ. Meteorol. Hydrol. 46, 245–255 (2021). https://doi.org/10.3103/S10683 73921040051.
11. Chernykh I.V., Aldukhov O. A. Annual cycle of continuous cloud layer parameters over the Arctic against the background of their global estimates from long-term radiosonde data // Transactions of RIHMI-WDC – 2019. – № 185. – P. 115–135 (in Russian).
12. Chernykh I.V., Aldukhov O. A. Frequency of reconstructed cloud layers over different latitudinal zones of the globe from upper air data for 1964–2018 // Transactions of RIHMI-WDC. – 2019. – № 184. – P. 102–117 (in Russian).

13. Chernykh I.V., Aldukhov O. A. Long-term spatial and temporal variations in the number of cloud layers from radiosonde profiles for Russian stations // Transactions of RIHMI-WDC. – 2020. – № 187. – P. 34–60 (in Russian).
14. Chernykh, I.V., Aldukhov, O.A. Long-term Estimates of the Number of Cloud Layers from Radiosonde Data for 1964–2017 in Different Latitudinal Zones. Russ. Meteorol. Hydrol. 45, 227–238 (2020). https://doi.org/10.3103/S1068373920040020.
15. Dementieva T.V., Korshunova N.N. Empirical-statistical analysis of the amount of total and low-level cloudiness in Russia // Transactions of RIHMI-WDC. – 2020. – № 187. – P. 197–204. (in Russian).
16. Chernokulsky A.V., Eliseev A.V., Kozlov F.A., Korshunova N.N., Kurgansky M.V., Mokhov, I.I., Semenov V.A., Shvets' N.V., Shikhov A.N., Yarinich Y.I. Atmospheric Severe Convective Events in Russia: Changes Observed from Different Data // Russian Meteorology and Hydrology, 2022, vol. 47, no. 5, pp. 343–354, doi: 10.3103/S106837392205003X.
17. Shikhovtsev, A.Y.; Kovadlo, P.G.; Khaikin, V.B.; Kiselev, A.V. Precipitable Water Vapor and Fractional Clear Sky Statistics within the Big Telescope Alt-Azimuthal Region. Remote Sens. 2022, 14, 6221. https://doi.org/10.3390/rs14246221.
18. Skorokhodov A.V., Astafurov V.G. Short-term variability of single-layer cloud field structure over western Siberia from MODIS and VIIRS satellite data // // Issledovanie Zemli is kosmosa (Exploring Earth from space) – 2022. – V. 202, № 6. – P. 3–12. (in Russian).
19. Astafurov V.G., Skorokhodov A.V., Kur'yanovich K.V., Mitrofanenko, Ya. K. Parameters of various cloud types over the natural zones of western Siberia according to MODIS satellite data // Atmospheric and oceanic optics. – 2020. – V. 33, № 4. – P. 266–271. – DOI 10.15372/AOO20200404 (in Russian).
20. Skorokhodov, A.V. Variability of Cloud Parameters from Satellite Data. // Russ. Meteorol. Hydrol. 44, 452–458 (2019). https://doi.org/10.3103/S1068373919070033.
21. Astafurov, V.G., Skorokhodov, A.V. & Kur'yanovich, K.V. Summer Statistical Models of Cloud Parameters over Western Siberia According to MODIS Data. // Russ. Meteorol. Hydrol. 46, 735–746 (2021). https://doi.org/10.3103/S1068373921110029.
22. Shakina N.P., Skriptunova E.N. Regime of low clouds and ceiling forecasting at the aerodromes in Asian Russia // Hydrometeorological research and forecasting. – 2019. – № 2(372). – P. 59–75. (in Russian).
23. Ivanova A.R., Skriptunova E.N. Change of episodes with low ceiling and low visibility at aerodromes in the Russian Federation for 2001–2010 // Hydrometeorological research and forecasting. – 2022. – № 2(384). – P. 53–68. – DOI 10.37162/2618-9631-2022-2-53-68. (in Russian).
24. Skorokhodov, A.V. Research into the Variability of Characteristics of Cloud Manifestations of Internal Gravity Waves during Their Lifetime Based on Himawari-8 Satellite Data. Izv. Atmos. Ocean. Phys. 56, 156–164 (2020). https://doi.org/10.1134/S0001433820020115.
25. Kozhevnikov, V.N. Clouds as Manifestation of Wave Disturbance above Mountain Ridges. Izv. Atmos. Ocean. Phys. 58, 121–130 (2022). https://doi.org/10.1134/S0001433822020062.

26. WMO Cloud atlas: https://cloudatlas.wmo.int/ru/home.html (access date: 01.04.2023).
27. Rybakova Zh.V. Clouds and their transformations (textbook) / Kuzhevskaya ed. Tomsk: TSU publishing, 2020, 234 pp. ISBN 978-5-94621-880-1 (in Russian).
28. Brusova, N. E., Kuznetsova I.N., Nakhaev M.I. Precipitation regime features in the Moscow region in 2008-2017 // Hydrometeorological research and forecasting. – 2019. – № 1(371). – P. 127–142. (in Russian).
29. Arzhanova M.N., Korshunova N.N. Monitoring of gaze and rime coating characteristics over the Russian territory in the cold season of 2017/18 // Transactions of MGO. – 2020. – № 597. – P. 90–103. (in Russian).
30. Arzhanova M.N., Korshunova N.N. Estimating long-term changes of glaze-ice and rime deposition characteristics over the Russian territory // Transactions of RIHMI-WDC. – 2021. – № 188. – P. 18–29. (in Russian).
31. Aleshina M.A., Semenov V.A. Changes in precipitation characteristics over Russia in XX-XXI centuries from CMIP6 models ensemble // Fundamental and applied climatology. – 2022. – V. 8, № 4. – P. 424–440. – DOI 10.21513/2410-8758-2022-4-424-440. (in Russian).
32. Khlebnikova, E.I., Rudakova, Y.L. & Shkolnik, I.M. Changes in Precipitation Regime over the Territory of Russia: Data of Regional Climate Modeling and Observations. Russ. Meteorol. Hydrol. 44, 431–439 (2019). https://doi.org/10.3103/S106837391907001X.
33. Khlebnikova, E.I., Shkolnik, I.M. & Rudakova, Y.L. Projected Changes in Rare Precipitation Extremes: Results of Regional Climate Modeling for the Territory of Russia. Russ. Meteorol. Hydrol. 47, 355–362 (2022). https://doi.org/10.3103/S1068373922050041.
34. Chernokulsky A.V., Kozlov F.A., Zolina O.G., Bulygina O.N., Mokhov I.I., Semenov V.A. Observed changes in convective and stratiform precipitation in Northern Eurasia over the last five decades // Environmental Research Letters, 2019, V.4, No.4, P. 045001. DOI: 10.1088/1748-9326/aafb82.
35. Vyshkvarkova, E.; Sukhonos, O. Compound Extremes of Air Temperature and Precipitation in Eastern Europe. Climate 2022, 10, 133. https://doi.org/10.3390/cli10090133.
36. Wang, P., Huang, Q., Tang, Q., Chen, X., Yu, J., Pozdniakov, S. P., & Wang, T. (2021). Increasing annual and extreme precipitation in permafrost-dominated Siberia during 1959–2018, 603, 126865. https://doi.org/10.1016/j.jhydrol.2021.126865.
37. Mokhov, I. I. Relationships between Satellite-derived Snow Cover Extent in the Northern Hemisphere and Surface Air Temperature / I. I. Mokhov, M. R. Parfenova // Russian Meteorology and Hydrology. – 2022. – Vol. 47, No. 2. – P. 98–106. – DOI 10.3103/S1068373922020030.
38. Mokhov, I. I. Changes in the Snow Cover Extent in Eurasia from Satellite Data in Relation to Hemispheric and Regional Temperature Changes / I. I. Mokhov, M. R. Parfenova // Doklady Earth Sciences. – 2021. – Vol. 501, No. 1. – P. 963–968. – DOI 10.1134/S1028334X21110106.
39. Essery, R., Kim, H., Wang, L., Bartlett, P., Boone, A., Brutel-Vuilmet, C., Burke, E., Cuntz, M., Decharme, B., Dutra, E., Fang, X., Gusev, Y., Hagemann, S., Haverd, V., Kontu, A., Krinner, G., Lafaysse, M., Lejeune, Y., Marke, T., Marks, D., Marty, C., Menard, C. B., Nasonova, O., Nitta, T., Pomeroy, J., Schädler, G., Semenov, V., Smirnova, T., Swenson, S., Turkov, D., Wever, N.,

and Yuan, H.: Snow cover duration trends observed at sites and predicted by multiple models, The Cryosphere, 14, 4687–4698, https://doi.org/10.5194/tc-14-4687-2020, 2020.
40. Santolaria-Otín, M., Zolina, O. Evaluation of snow cover and snow water equivalent in the continental Arctic in CMIP5 models. Clim Dyn 55, 2993–3016 (2020). https://doi.org/10.1007/s00382-020-05434-9.
41. Aleshina M.A., Semenov V.A., Chernokulsky A.V. Study of the role of global and regional factors in changing the extremes of summer precipitation on the Black Sea coast of the Caucasus with the use of results of experiments with the climate model // Fundamental and applied climatology. – 2019. – V. 3. – P. 59–75. – DOI 10.21513/2410-8758-2019-3-59-75 (in Russian).
42. Liu, Y, Zhu, Y, Wang, H, et al. Role of autumn Arctic Sea ice in the subsequent summer precipitation variability over East Asia. Int J Climatol. 2020; 40: 706–722. https://doi.org/10.1002/joc.6232.
43. Ladokhina E.M., Rubinshtein K.G. Study of the impact of the megalopolis of St. Petersburg on wind and precipitation for validation of numerical weather forecast Atmospheric and Oceanic Optics. – 2021. – V. 34, № 1(384). – P. 36–45. (in Russian).
44. Antokhina, O. Y. Atmospheric Precipitation Within the Selenga River Basin and Large-Scale Atmospheric Circulation Over Eurasia in July / O. Y. Antokhina // Geography and Natural resources. – 2019. – Vol. 40, No. 4. – P. 373–383. – DOI 10.1134/S1875372819040097.
45. Evstigneev, V.P.; Naumova, V.A.; Voronin, D.Y.; Kuznetsov, P.N.; Korsakova, S.P. Severe Precipitation Phenomena in Crimea in Relation to Atmospheric Circulation. Atmosphere 2022, 13, 1712. https://doi.org/10.3390/atmos13101712.
46. Allan, R.P., Barlow, M., Byrne, M.P., Cherchi, A., Douville, H., Fowler, H.J., Gan, T.Y., Pendergrass, A.G., Rosenfeld, D., Swann, A.L.S., Wilcox, L.J. and Zolina, O. (2020), Advances in understanding large-scale responses of the water cycle to climate change. Ann. N.Y. Acad. Sci., 1472: 49-75. https://doi.org/10.1111/nyas.14337.
47. Aleshina M.A., Semenov V.A., Chernokulsky A.V. A link between surface air temperature and extreme precipitation over Russia from station and reanalysis data // Environmental Research Letters, 2021, V. 16, P. 105004. DOI: 10.1088/1748-9326/ac1cba.
48. Basharin D., Stankūnavičius G. European precipitation response to Indian ocean dipole events // Atmospheric Research, V. 273, 2022, P. 106142, https://doi.org/10.1016/j.atmosres.2022.106142.
49. Hosseini-Moghari S-M., Sun S., Tang Q., Groisman P.Ya. Scaling of precipitation extremes with temperature in China's mainland: Evaluation of satellite precipitation data // Journal of Hydrology, Vol. 606, 2022, P.127391, https://doi.org/10.1016/j.jhydrol.2021.127391.
50. Leonov I.I. Formation conditions of hazardous hard rime accretion in the polar Urals // Hydrometeorological research and forecasting. – 2022. – № 4(386). – С. 20–35. – DOI 10.37162/2618-9631-2022-4-20-35 (in Russina).
51. Leonov I.I., Sokolikhina N.N. Formation conditions of an ice storm in Vladivostok in November 2020// Hydrometeorological research and forecasting. – 2021. – № 4(382). – P. 69–83. – DOI 10.37162/2618-9631-2021-4-69-83. (in Russian).

52. Shestakova, A.A., Toropov, P.A. Orographic and lake effect on extreme precipitation on the Iranian coast of the Caspian Sea: a case study. Meteorol Atmos Phys 133, 69–84 (2021). https://doi.org/10.1007/s00703-020-00735-4.
53. Gavrikov, A.V., Zolina, O.G., Razorenova, O.A. et al. Extreme Precipitation in June 2021 over the Black Sea in the Context of Long-Term Climate Change. Oceanology 62, 303–309 (2022). https://doi.org/10.1134/S0001437022030055.
54. Kislov, A.V., Antipina, U.I. & Korneva, I.A. Extreme Precipitation in the European Arctic in Summer: Statistics and Synoptic Models. Russ. Meteorol. Hydrol. 46, 434–443 (2021). https://doi.org/10.3103/S1068373921070025.
55. Kislov, A.; Matveeva, T.; Antipina, U. Precipitation Extremes and Their Synoptic Models in the Northwest European Sector of the Arctic during the Cold Season. Atmosphere 2022, 13, 1116. https://doi.org/10.3390/atmos13071116.
56. Klimenko, D.E., Cherepanova, E.S. & Kuz'minykh, A.Y. Evaluating Parameters of the Distributions of Extreme Storms with Several Events per Year Taken into Account. Water Resour 46, 630–637 (2019). https://doi.org/10.1134/S0097807819040110.
57. Klimenko D.E., Cherepanova E.S., Kuznetsova T.V. Assessment and mapping of parameters of flood-forming rainstorms within the Tobol river // Geography and Natural resources. – 2019. – № 3. – P. 165–172. – DOI 10.21782/GIPR0206-1619-2019-3(165-172) (in Russian).
58. Bolgov, M.V., Trubetskova, M.D. & Kharlamov, M.A. Estimation of Statistical Characteristics of Rainfall in the Moscow Region . Russ. Meteorol. Hydrol. 45, 508–514 (2020). https://doi.org/10.3103/S1068373920070067.
59. Korolev, V.; Gorshenin, A. Probability Models and Statistical Tests for Extreme Precipitation Based on Generalized Negative Binomial Distributions. Mathematics 2020, 8, 604. https://doi.org/10.3390/math8040604.
60. Korolev, V.; Gorshenin, A.; Belyaev, K. Statistical Tests for Extreme Precipitation Volumes. Mathematics 2019, 7, 648. https://doi.org/10.3390/math7070648.
61. Permyakov, M.S., Potalova, E.Y. & Kleshcheva, T.I. Thunderstorm Activity in the Primorsky Krai. Russ. Meteorol. Hydrol. 44, 818–824 (2019). https://doi.org/10.3103/S1068373919120045.
62. Fil' A.Yu., Krokhin V.V., Bokhan V.D., Veryatin V.Yu. Some methods of convective activity analysis in the Northwest Pacific // Hydrometeorological research and forecasting. – 2019. – № 1(371). – P. 48-59. (in Russian).
63. Shikhov A.N., Chernokulsky A.V., Sprygin A.A., Azhigov I.O. Identification of mesoscale convective cloud systems with tornadoes using satellite data // Current issues of remote sensing of the Earth from space. – 2019. – V. 16, № 1. – P. 223–236. – DOI 10.21046/2070-7401-2019-16-1-223-236. (in Russian).
64. Adzhiev A.Kh., Kupovykh G.V., Gyatov R.A., Kerefova Z.M. Relationship between the number of days with thunderstorms and the duration of thunderstorms according to visual and instrumental observations // Notes in Higher education. North-Caucasian region. Natural sciences. – 2020. – № 3(207). – P. 30–36. – DOI 10.18522/1026-2237-2020-3-30-36. (in Russian).
65. Appaeva Zh.Yu. Results of statistical studies of the main characteristics of thunderstorm clouds based on radar observations // Transactions of MGO. – 2020. – № 598. – P. 188–196. (in Russian).
66. Ashabokov B.A. et al. Modeling of reducing risk of direct impact (hailstones) in agriculture // Ecology, Economics, Informatics. – 2020. – V. 1, № 5. – P. 21–26. – DOI 10.23885/2500-395X-2020-1-5-21-26. (in Russian).

67. Zharashuev M.V. The cyclical nature of hail activity in the North Caucasus // Transactions of MGO. – 2020. – № 598. – P. 197–203 (in Russian).
68. Sin'kevich, A.A., Popov, V.B., Abshaev, A.M. et al. Radar Characteristics of Convective Clouds during Transition to the Cumulonimbus Stage in Different Regions of the World. Atmos Ocean Opt 34, 134–139 (2021). https://doi.org/10.1134/S1024856021020081.
69. Sprygin A.A. Parameters of long-lived severe convective structures in the European part of Russia and neighboring territories and the possibility to unify their forecast // Hydrometeorological research and forecasting. – 2020. – № 1(375). – P. 21–47. – DOI 10.37162/2618-9631-2020-1-21-47. (in Russian).
70. Chernokulsky A., Kurgansky M., Mokhov I., Shikhov A., Azhigov I. Selezneva E., Zakharchenko D., Antonescu B., Kühne T. Tornadoes in Northern Eurasia: from the Middle Age to the Information Era // Monthly Weather Review, 2020, Vol. 148, No 8, P.3081–3110, DOI: 10.1175/MWR-D-19-0251.1.
71. Shikhov, A.N., Chernokulsky, A.V., Azhigov, I.O., and Semakina, A.V.: A satellite-derived database for stand-replacing windthrow events in boreal forests of European Russia in 1986–2017, Earth Syst. Sci. Data, 12, 3489–3513, https://doi.org/10.5194/essd-12-3489-2020, 2020.
72. Tarabukina, L.; Kozlov, V. Seasonal Variability of Lightning Activity in Yakutia in 2009–2019. Atmosphere 2020, 11, 918. https://doi.org/10.3390/atmos11090918.
73. Alita S.L., Appaeva Zh. Yu. On the spatial evolution of the hail formation area in single-cell hail clouds // Transactions of MGO. – 2021. – № 601. – P. 116–124. (in Russian).
74. Alekseeva A.A., Bukharov V.M., Losev V.M. Diagnosis of severe squalls based on the data of dmrl-c doppler weather radars and numerical modeling // Hydrometeorological research and forecasting. – 2021. – № 3(381). – P. 6–23. – DOI 10.37162/2618-9631-2021-3-6-23. (in Russian).
75. Zharashuev M.V. Comparison of statistical data on thunderstorm and hail activity in the North Caucasus // Transactions of MGO. – 2021. – № 603. – P. 145–154. (in Russian).
76. Zharashuev M.V. Statistical analysis of lightning activity in the North Caucasus // Russian Meteorology and Hydrology. – 2021. – № 6. – P. 112–115. – DOI 10.52002/0130-2906-2021-6-112-115. (in Russian).
77. Mikhaylushkin, S. Yu. et al. P. Ю. Mesoscale features of the distribution of radar characteristics of cumulonimbus clouds and their relationship with surface meteorological values // Transactions of MGO. – 2021. – № 603. – P. 130–144. (in Russian).
78. Petrov, V.V. Microphysical and Thermodynamic Characteristics of Tropical Convective Clouds (According to Experiments in Cuba). Russ. Meteorol. Hydrol. 46, 616–623 (2021). https://doi.org/10.3103/S1068373921090077.
79. Sin'kevich, A.A., Toropova, M.L., Mikhailovskii, Y.P. et al. Features of the Relationship between Electrical and Radar Parameters of Thunderclouds in India (Field Studies). Russ. Meteorol. Hydrol. 46, 410–415 (2021). https://doi.org/10.3103/S106837392106008X.
80. Sosnin E.A., Kuznetsov V.R., Panarin V.A. Energy release in a thundercloud, which is necessary for the transient middle atmosphere light phenomena formation // Atmospheric and Oceanic Optics – 2021. – V. 34, № 8(391). – P. 617-620. – DOI 10.15372/AOO20210807. (in Russian).

81. Toropova M.L. Parameters of convective clouds during the transition to the thunderstorm stage according to the data of three-dimensional numerical simulation // Transactions of MGO. – 2021. – № 602. – P. 23–41. (in Russian).
82. Chernokulsky A.V., M. V. Kurgansky, I. I. Mokhov, A. N. Shikhov, I. O. Azhigov, E. V. Selezneva, D. I. Zakharchenko, B. Antonescu, and T. Kuhne Tornadoes in the Russian Regions // Russian Meteorology and Hydrology, 2021, V.46, No 2, P. 69–82, DOI: 10.3103/S1068373921020023.
83. Shatalina, M.V., Il'in N.V., Mareev E.A. M. B. Characteristics of hydrometeorological hazards in Nizhny Novgorod according to in-situ observations of electric field // Russian Meteorology and Hydrology. – 2021. – № 6. – P. 107–111. – DOI 10.52002/0130-2906-2021-6-107-111. (in Russian).
84. Shikhov A.N. et al. Development of a GIS database and web service "Hazardous convective weather events on the territory of central federal district" // InterCarto. InterGIS. – 2021. – V. 27, № 3. – P. 120–135. – DOI 10.35595/2414-9179-2021-3-27-120-135. (in Russian).
85. Kuzhevskaya, I.V. The spatio-temporal distribution of mesoscale convective complexes over the Southeastern Western Siberia / I.V. Kuzhevskaya, V.A. Zhukova, T.S. Koshikova [et al.] // Geosphere Research. – 2021. – No. 3. – P. 115–124. – DOI 10.17223/25421379/20/9. .
86. Shikhov, A.; Chernokulsky, A.; Kalinin, N.; Bykov, A.; Pischalnikova, E. Climatology and Formation Environments of Severe Convective Windstorms and Tornadoes in the Perm Region (Russia) in 1984–2020. Atmosphere 2021, 12, 1407. https://doi.org/10.3390/atmos12111407.
87. Sin'kevich, A.; Boe, B.; Pawar, S.; Yang, J.; Abshaev, A.; Dovgaluk, Y.; Gekkieva, J.; Gopalakrishnan, V.; Kurov, A.; Mikhailovskii, Y.; Toropova, M.; Veremei, N. Investigation of Thundercloud Features in Different Regions. Remote Sens. 2021, 13, 3216. https://doi.org/10.3390/rs13163216.
88. Nagorskiy, P.M., Zhukov, D.F., Kartavykh, M.S. et al. Properties and Structure of Mesoscale Convective Systems over Western Siberia According to Remote Observations. Russ. Meteorol. Hydrol. 47, 938–945 (2022). https://doi.org/10.3103/S1068373922120056.
89. Nechepurenko O.E., Gorbatenko V.P., Pustovalov K.N., Gromova K.N. Lightning activity over Western Siberia // Geospheric Research. – 2022. – № 4. – P. 123–134. – DOI 10.17223/25421379/25/8. (in Russian).
90. Permyakov, M.S., Kleshcheva, T.I., Potalova, E.Y. et al. Regional Features of Lightning Activity in the South of the Russian Far East. Russ. Meteorol. Hydrol. 47, 629–636 (2022). https://doi.org/10.3103/S106837392208009X.
91. Plyusnin, S.D., Garaba, I.A. & Popova, V.P. Propagation of Convective Storms. Russ. Meteorol. Hydrol. 47, 507–515 (2022). https://doi.org/10.3103/S1068373922070032.
92. Sin'kevch A.A. et al. A study of thunderstorm characteristics in northwest Russia using neural networks// Atmospheric and Oceanic Optics. – 2022. – V. 35, № 12(407). – P. 1008–1014. – DOI 10.15372/AOO20221207 (in Russian).
93. Sozaeva L. T., Kagermazov A.Kh., Zhaboeva M.M. Statistical models for estimating the maximum size hail // Transactions of MGO. – 2022. – № 605. – P. 149–163. (in Russian).

94. Toropova, M.L., Sin'kevich, A.A., Pawar, S. et al. Characteristics of Thunderstorms during the Monsoon and Post-monsoon Seasons in India. Russ. Meteorol. Hydrol. 47, 620–628 (2022). https://doi.org/10.3103/S1068373922080088.
95. Shikhov A.N., Chernokulsky A.V. Azhigov I.O. Spatial and Temporal Distribution of Windthrows in the Forest Zone of Western Siberia in 2001–2020 // Cosmic Research, 2022, Vol. 60, Suppl. 1, pp. S91–S103. DOI: 10.1134/S001095252270010.
96. Kharyutkina, E.; Pustovalov, K.; Moraru, E.; Nechepurenko, O. Analysis of Spatio-Temporal Variability of Lightning Activity and Wildfires in Western Siberia during 2016–2021. Atmosphere 2022, 13, 669. https://doi.org/10.3390/atmos13050669.
97. Khaykin, S.M., Moyer, E., Krämer, M., Clouser, B., Bucci, S., Legras, B., Lykov, A., Afchine, A., Cairo, F., Formanyuk, I., Mitev, V., Matthey, R., Rolf, C., Singer, C. E., Spelten, N., Volkov, V., Yushkov, V., and Stroh, F.: Persistence of moist plumes from overshooting convection in the Asian monsoon anticyclone, Atmos. Chem. Phys., 22, 3169–3189, https://doi.org/10.5194/acp-22-3169-2022, 2022.
98. Dovgalyuk Yu. A., Veremey N.E., Toropova M.L., Sinkevich A.A., Mikhailovsky Yu. P. Numerical simulation of impact of electrical processes on the formation of dangerous phenomena associated with convective clouds // Transactions of MGO. – 2019. – № 595. – P. 63–82. (in Russian).
99. Dovgalyuk Yu. A., Veremei N.E., Sinkevich A.A., Mikhailovsky Yu. P., Toropova M.L. Investigation of the electrical structure of cb with hail using three-dimensional numerical simulation (based on the case, observed in the Northwest of Russia) // Transactions of MGO. – 2019б. – № 592. – P. 7-22. (in Russian).
100. Zharashuev M.V. Statistical analysis of the lightning discharges frequency (cloud – cloud type) in the North Caucasus republics and the Stavropol territory // Transactions of MGO. – 2019. – № 595. – P. 145–152. (in Russian).
101. Morozov V.N. The interaction of cloud charge structures with the surrounding conducting atmosphere with non-uniform electrical conductivity // Transactions of MGO. – 2019. – № 592. – P. 23–79. (in Russian).
102. Sin'kevich, A.A., Mikhailovskii, Y.P., Matrosov, S.Y. et al. Relationships between the Structure of Convective Clouds and Lightning Frequency Derived from Radiophysical Measurements. Russ. Meteorol. Hydrol. 44, 394–403 (2019). https://doi.org/10.3103/S1068373919060049.
103. Abshaev A.M. et al. Development of convective cloud electrification from empirical and numerical models // Transactions of Mozhaiskiy academy. – 2020. – № S674. – P. 68–74. (in Russian).
104. Dovgalyuk, Y.A., Veremei, N.E., Sin'kevich, A.A. et al. Numerical Simulation of Evolution and Electric Structure of the Cumulonimbus Cloud in Northwestern Russia. Russ. Meteorol. Hydrol. 45, 239–244 (2020). https://doi.org/10.3103/S1068373920040032.
105. Kal'chikin V.V. et al. Atmospheric-electric and meteorological spectrum dynamics of the surface layer during heavy precipitation // Transactions of Mozhaiskiy academy . – 2020. – № S674. – P. 188–194. (in Russian).
106. Kalchikhin, V.; Kobzev, A.; Nagorskiy, P.; Oglezneva, M.; Pustovalov, K.; Smirnov, S.; Filatov, D. Connected Variations of Meteorological and Electrical Quantities of Surface Atmosphere under the Influence of Heavy Rain. Atmosphere 2020, 11, 1195. https://doi.org/10.3390/atmos11111195.

107. Kuzmin V.A. Investigation of the intensity of the electric field of the atmosphere during thunderstorms // Transactions of MGO. – 2021. – № 601. – P. 104–115. (in Russian).
108. Svechnikova, E.K. Discharge Distribution in a Cloud Assessed from the Energetic Particle Flux Measured under the Cloud / E.K. Svechnikova, N.V. Ilin, E.A. Mareev // Doklady Earth Sciences. – 2021. – Vol. 496, No. 2. – P. 171–175. – DOI 10.1134/S1028334X21020197.
109. Mikhailovsky Y. P. Dynamics of the Electrical Structure of Cumulonimbus Clouds / Y. P. Mikhailovsky, M. L. Toropova, N. E. Veremey [et al.] // Radiophysics And Quantum Electronics. – 2021. – Vol. 64, No. 5. – P. 309–320. – DOI 10.1007/s11141-022-10133-y.
110. Karashtin A.N., Shlyugaev Yu.V.,b, Karashtina O.S. Cloud-to-ground lightning discharge indicator in the radio frequency emission of thunderclouds as observed in the Upper Volga region of Russia // Atmospheric Research, 2021, V. 256, P.105559, https://doi.org/10.1016/j.atmosres.2021.105559.
111. Svechnikova, E. K., Ilin, N. V., Mareev, E. A., & Chilingarian, A. A. (2021). Characteristic features of the clouds producing thunderstorm ground enhancements. Journal of Geophysical Research: Atmospheres, 126, e2019JD030895. https://doi.org/10.1029/2019JD030895.
112. Shepetov A., Antonova V., Kalikulov O. et al. The prolonged gamma ray enhancement and the short radiation burst events observed in thunderstorms at Tien Shan // Atmospheric Research, 2021, V. 248, P. 105266, https://doi.org/10.1016/j.atmosres.2020.105266.
113. Alekseeva A.A. Specific features of the conditions of occurrence of active convection accompanied by severe squalls // Hydrometeorological research and forecasting. – 2019. – № 2(372). – P. 41–58. (in Russian).
114. Abshaev, M.T.; Zakinyan, R.G.; Abshaev, A.M.; Al-Owaidi, Q.S.K.; Kulgina, L.M.; Zakinyan, A.R.; Wehbe, Y.; Yousef, L.; Farrah, S.; Al Mandous, A. Influence of Atmosphere Near-Surface Layer Properties on Development of Cloud Convection. Atmosphere 2019, 10, 131. https://doi.org/10.3390/atmos10030131.
115. Kuznetsov A.D. et al. On the impact of aircrafts traffic on the development of cumulonimbus clouds // Transactions of MGO. – 2020. – № 599. – P. 162–175. (in Russian).
116. Sivkov B.A. and Kalinin N.A. Peculiarities of the thermodynamic state of the atmosphere under heavy precipitation in the Perm region // Hydrometeorological research and forecasting. – 2020. – № 1(375). – P. 83–95. – DOI 10.37162/2618-9631-2020-1-83-95 (in Russian).
117. Zolotukhina O.I. Thermodynamic conditions of formation of dangerous convective phenomena in the area of Vostochny cosmodrome// Transactions of Mozhaiskiy academy. – 2020. – № S674. – P. 181–187 (in Russian).
118. Kulikov, M.Y.; Belikovich, M.V.; Skalyga, N.K.; Shatalina, M.V.; Dementyeva, S.O.; Ryskin, V.G.; Shvetsov, A.A.; Krasil'nikov, A.A.; Serov, E.A.; Feigin, A.M. Skills of Thunderstorm Prediction by Convective Indices over a Metropolitan Area: Comparison of Microwave and Radiosonde Data. Remote Sens. 2020, 12, 604. https://doi.org/10.3390/rs12040604.
119. Alekseeva A.A. and Peskov B.E. Physical and synoptic predictors and their optimal values leading to the formation of heavy rainfall // Hydrometeorological research and forecasting. – 2021. – № 3(381). – P. 24–43. – DOI 10.37162/2618-9631-2021-3-24-43. (in Russian).

120. Kalinin, N.A., Shikhov, A.N., Chernokulsky, A.V. et al. Environments of Formation of Severe Squalls and Tornadoes Causing Large-scale Windthrows in the Forest Zone of European Russia and the Ural. Russ. Meteorol. Hydrol. 46, 83–93 (2021). https://doi.org/10.3103/S1068373921020035.
121. Veremei N.E. et al. Influence of thermal inhomogeneities of the underlying surface on the formation and development of convective clouds and dangerous weather phenomena associated with them // Transactions of MGO. – 2022. – № 606. – P. 32-49. (in Russian).
122. Ashabokov, B.A., Fedchenko, L.M., Shapovalov, V.A. et al. Numerical Modeling of the Influence of the Atmospheric Wind Field Structure on the Macro- and Microstructure Characteristics of Convective Clouds. Izv. Atmos. Ocean. Phys. 58, 569–577 (2022). https://doi.org/10.1134/S0001433822060032.
123. Makitov, V.S., Inuhin, V.S., Kushchev, S.A. et al. Hail Cloud Formation as a Result of the Merging of Convective Cells. Izv. Atmos. Ocean. Phys. 58, 384–390 (2022). https://doi.org/10.1134/S0001433822040090.
124. Shikhov A.N., Chernokulsky A.V. Sprygin A.A., Yarinich Yu.I. Estimation of Convective Atmospheric Instability during Squalls, Tornadoes, and Large Hail Events from Satellite Observations and ERA5 Reanalysis Data // Atmospheric and Oceanic Optics, 2022, Vol. 35, No. 6, pp. 793–801. DOI: 10.1134/S1024856022060227.
125. Barekova M.V. et al. Radar studies of an intense hailstorm process developing over the central North Caucasus 07.06.2012 // Reports of the Adyghe Academy of Sciences. – 2019. – V. 19, № 2. – P. 64-78. (in Russian).
126. Kulichkov, S.N., Chunchuzov, I.P., Popov, O.E. et al. Internal Gravity and Infrasound Waves during the Hurricane of May 29, 2017, in Moscow. Izv. Atmos. Ocean. Phys. 55, 167–177 (2019). https://doi.org/10.1134/S0001433819020105.
127. Sin'kevich, A.A., Popov, V.B., Mikhailovskii, Y.P. et al. Characteristics of Cumulonimbus with Waterspout over Ladoga Lake from Remote Measurements. Atmos Ocean Opt 33, 387–392 (2020). https://doi.org/10.1134/S1024856020040156.
128. Sin'kevich, A.A., Mikhailovskiy, Y.P., Toropova, M.L. et al. Thunderstorm with Waterspout Structure and the Dependence Lightning Frequency on its Characteristics. Atmos Ocean Opt 33, 645–649 (2020). https://doi.org/10.1134/S1024856020060226.
129. Romanskii, S.O., Verbitskaya, E.M. & Sulyandziga, P.B. A Numerical Study of Intense Convection That Caused the Tornado in Blagoveshchensk on July 31, 2011. Russ. Meteorol. Hydrol. 45, 403–410 (2020). https://doi.org/10.3103/S1068373920060035.
130. Abshaev M.T. et al. Investigation of the peculiarities of the development of electrification and hail formation processes in a supercell cloud by radiophysical means // Transactions of MGO. – 2020. – № 596. – P. 96–130. (in Russian).
131. Popov, V.B., Sin'kevich, A.A., Yang, J. et al. Characteristics and Structure of the Cumulonimbus Cloud with Waterspout over the Gulf of Finland. Russ. Meteorol. Hydrol. 45, 607–614 (2020). https://doi.org/10.3103/S1068373920090010.
132. Bukharov M.V., Bukharov V.M. Analysis of the rapidly growing mesoscale system of deep convection on satellite maps of the diagnosis // Hydrometeorological research and forecasting. – 2020. – № 2(376). – P. 23–38. – DOI 10.37162/2618-9631-2020-2-23-38. (in Russian).

133. Osipova O.P. Synoptic conditions of catastrophic floods in Irkutsk region in 2019 // Geography and Natural Resources. – 2020. – № 4(163). – P. 56-65. – DOI 10.21782/GIPR0206-1619-2020-4(56-65). (in Russian).
134. Shikhov A.N. et al. Tornadoes in the environments of weak convective instability: analysis of two cases in the eastern part of the European Russia / Current issues of remote sensing of the Earth from space. – 2020. – V. 17, № 5. – P. 255–268. – DOI 10.21046/2070-7401-2020-17-5-255-268. (in Russian).
135. Chernokulsky, A.; Shikhov, A.; Bykov, A.; Azhigov, I. Satellite-Based Study and Numerical Forecasting of Two Tornado Outbreaks in the Ural Region in June 2017. Atmosphere 2020, 11, 1146. https://doi.org/10.3390/atmos11111146.
136. Kalmykova O.V., Fedorova V.V., Fadeev R.O. Analysis of occurrence conditions of the waterspouts outbreak over the Black Sea on July 16, 2019 and forecast skill assessment // Hydrometeorological research and forecasting. – 2021. – № 1(379). – P. 112–129. – DOI 10.37162/2618-9631-2021-1-112-129. (in Russian).
137. Motovilov Yu.G., Gelfan A.N., Polyanin V.O. Catastrophic floods in the Angara river basin in 2019: modeling the conditionsof formation and water regime of rivers // Izvestiya, geography series. – 2021. – V. 85, № 2. – P. 302–316. – DOI 10.31857/S2587556621020102. (in Russian).
138. Alekseeva A.A., Bukharov V.M., Losev V.M The convective storm in the moscow region on june 28, 2021 // Hydrometeorological research and forecasting. – 2022. – № 1(383). – P. 22-42. – DOI 10.37162/2618-9631-2022-1-22-42. (in Russian).
139. Sprygin A.A., Vyazilov A.E. A case study of the mesoscale convective system over central regions of European Russia on August 7, 2021 // Hydrometeorological research and forecasting. – 2022. – № 2(384). – P. 69–91. – DOI 10.37162/2618-9631-2022-2-69-91. (in Russian).
140. Abshaev, M.T., Abshaev, A.M., Sinkevich, A.A. et al. Features of Development of a Supercell Convective Cloud at the Stage of Maximum Lightning Activity (August 19, 2015, the North Caucasus). Russ. Meteorol. Hydrol. 47, 315–325 (2022). https://doi.org/10.3103/S1068373922040070.
141. Chernokulsky A.V., Shikhov A.N., Azhigov I.O., Eroshkina N.A., Korenev D.P., Bykov A.V., Kalinin N.A., Kurgansky M.V., Pavlyukov Yu.B., Sprygin A.A., Yarinich Yu.I. Squalls and Tornadoes over the European Territory of Russia on May 15, 2021: Diagnosis and Modeling // Russian Meteorology and Hydrology, 2022, vol. 47, no. 11, pp. 859–873, doi: 10.3103/S1068373922110073.
142. Chernokulsky A., Shikhov A., Bykov A., Kalinin N., Kurgansky M., Sherstyukov B., Yarinich Yu. Diagnosis and modelling of two destructive derecho events in European Russia in the summer of 2010 // Atmospheric Research, 2022, Vol. 267, P. 105928 DOI: 10.1016/j.atmosres.2021.105928.
143. Strunin M.A. Investigation of methods of the thermodynamic condition of atmosphere using aircraft-observatory. Roshydromet. Central Aerological Observatory. Monograph. Moscow. 2020. 212 p. OOO “Chance” ISBN 978-5-6042605-9-3 (in Russian).
144. Strunin M.A Estimation of accuracy of temperature and wind measurements in the AMDAR system using the Yak-42D “Roshydromet” research aircraft data. Russian Meteorology and Hydrology. 2020. Vol. 45. No.8, P. 587–598. DOI: 10.3103/S1068373920080105.

145. Volkov V.V., Kolokutin G.E., Strunin M.A., Bazanin N.V. The onboard data-acquisition system on research aircraft for studying atmospheric process. Instruments and Experimental Techniques. 2019. No. 3. P. 104–110. DOI: 10.1134/S0032816219020332.
146. Volkov V.V., Strunin A.M., Strunin M.A. Determination Of Wind Shear And Turbulence Intensity According To Yak42-D “Roshydromet” Research Aircraft Data. Russian Meteorology and Hydrology. 2021. T. 46. № 9. P. 640-649. DOI: 10.3103/S1068373921090107.
147. Strunin A.M., M.A. Strunin. Spectral characteristics of turbulence and turbulent fluxes in convective clouds of a tropical region based on aircraft observations. International Conference on Clouds and Precipita-tion 2021, 2–6 August 2021, Pune, India.
148. Volkov V.V., Kirin D.V., Petrov V.V., Strunin A.M. Study of the microphysical characteristics of winter clouds of a warm front from the aircraft laboratory Yak-42D "Roshydromet". Proceedings of In-ternational Scientific Conference "Problems of Atmospheric Physics, Climatology and Environmental Monitoring" NCFU, Nalchik, 08-10 of Sept. 2021 г. pp. 68–73. (in Russian).
149. Petrov V.V., N.V. Bazanin, D.V. Kirin, V.V. Volkov, A.M. Strunin. Relationship Between Microphysi-cal Characteristics and Turbulence in Winter Clouds. Physics of the Atmosphere, Climatology and Envi-ronmental Monitoring. Modern Problems of Atmospheric Physics. 2022, pp. 269–275. https://doi.org/10.1007/978-3-031-19012-4_26.
150. Volkov V.V., Petrov V.V., Krutikov N.O. Measurement of Cloud Water Content from a Research Aircraft. Physics of the Atmosphere, Climatology and Environmental Monitoring. Modern Problems of Atmospheric Physics. 2022, pp. 339–346. .
151. Vladimirov S.A., Pastushkov R.S. Calculation of activation of condensation nuclei for numerical models of convective clouds and active influences on them. Proceedings of International Scientific Confer-ence "Problems of Atmospheric Physics, Climatology and Environmental Monitoring" NCFU, Nalchik, 08–10 of Sept. 2021 (in Russian).
152. Vladimirov S.A., Kirin D.V., Krutikov N.O., Pastushkov R.S. Approximation of the distribu-tion functions of cloud drops and ice crystals according to measurements of the microphysical complex of the Yak-42D "Roshydromet" laboratory aircraft for the construction of numerical models of clouds and pre-cipitation and active influences on them. Proceedings of International Scientific Conference "Problems of Atmospheric Physics, Climatology and Environmental Monitoring" NCFU, Nalchik, 08–12 of Sept. 2021 (in Russian) .
153. Samokhvalov, I.V., Bryukhanov, I.D., Shishko, V.A. et al. Estimation of Microphysi-cal Characteristics of Contrails by Polarization Lidar Data: Theory and Experiment. Atmos Ocean Opt 32, 400–409 (2019). https://doi.org/10.1134/S1024856019040122.
154. Gabyshev D.N., Fedorets A.A., Aktaev N.E., Klemm O., Andreev S.N. Acceleration of the condensational growth of water droplets in an external electric field // Journal of Aerosol Science, V. 135, P.103–112, 2019, https://doi.org/10.1016/j.jaerosci.2019.06.002.
155. Krämer, M., Rolf, C., Spelten, N., Afchine, A., Fahey, D., Jensen, E., Khaykin, S., Kuhn, T., Lawson, P., Lykov, A., Pan, L. L., Riese, M., Rollins, A., Stroh, F., Thornberry, T., Wolf, V., Woods, S., Spichtinger, P., Quaas, J., and

Sourdeval, O.: A microphysics guide to cirrus – Part 2: Climatologies of clouds and humidity from observations, Atmos. Chem. Phys., 20, 12569–12608, https://doi.org/10.5194/acp-20-12569-2020, 2020.
156. Yakovleva, V.; Zelinskiy, A.; Parovik, R.; Yakovlev, G.; Kobzev, A. Model for Recon-struction of γ-Background during Liquid Atmospheric Precipitation. Mathematics 2021, 9, 1636. https://doi.org/10.3390/math9141636.
157. Gabyshev, D.N.; Szakáll, M.; Shcherbakov, D.V.; Fedorets, A.A.; Dyachkov, S.M. Os-cillatory Signatures in the Raindrop Motion Relative to the Air Medium with Terminal Veloci-ty. Atmosphere 2022, 13, 1137. https://doi.org/10.3390/atmos13071137.
158. Karagodin, A.; Rozanov, E.; Mironova, I. On the Possibility of Modeling the IMF By-Weather Coupling through GEC-Related Effects on Cloud Droplet Coalescence Rate. Atmos-phere 2022, 13, 881. https://doi.org/10.3390/atmos13060881.
159. Stulov E.A., Sosnikova E.V., Kirin D.V., Monakhova N.A., Pozdeev V.N. Study of the charac-teristics of cloud condensation nuclei in the Moscow Region. Proceedings of International Scientific Con-ference "Problems of Atmospheric Physics, Climatology and Environmental Monitoring" NCFU, Nalchik, 08–10 of Sept. 2021 pp. 63–68. (in Russian).
160. Mikhailov E. F., O. A. Ivanova, E. Y. Nebosko [et al.] Subpollen Particles as Atmos-pheric Cloud Condensation Nuclei // Izvestiya, Atmospheric and Oceanic Physics. – 2019. – Vol. 55, No. 4. – P. 357–364. – DOI 10.1134/S000143381904008X.
161. Pripachkin D. A., Budyka A. K. Influence of Aerosol Particle Parameters on Their Scavenging from the Atmosphere by Raindrops // Izvestiya, Atmospheric and Oceanic Phys-ics. – 2020. – Vol. 56, No. 2. – P. 173–178. – DOI 10.1134/S0001433820020103.
162. Mikhailov, E. F. and Vlasenko, S. S.: High-humidity tandem differential mobility ana-lyzer for accurate determination of aerosol hygroscopic growth, microstructure, and activity coefficients over a wide range of relative humidity, Atmos. Meas. Tech., 13, 2035–2056, https://doi.org/10.5194/amt-13-2035-2020, 2020.
163. Pol'kin, V.V., Panchenko, M.V. & Terpugova, S.A. Condensation Activity of Differ-ent-Size Particles of Atmospheric Aerosol Using Photoelectric Counter Measurements. Atmos Ocean Opt 35, 133–141 (2022). https://doi.org/10.1134/S1024856022020075.
164. Ansmann, A., Ohneiser, K., Mamouri, R.-E., Knopf, D. A., Veselovskii, I., Baars, H., Engelmann, R., Foth, A., Jimenez, C., Seifert, P., and Barja, B.: Tropospheric and stratospher-ic wildfire smoke profiling with lidar: mass, surface area, CCN, and INP retrieval, Atmos. Chem. Phys., 21, 9779–9807, https://doi.org/10.5194/acp-21-9779-2021, 2021.
165. Mikhailov, E.F., Pöhlker, M.L., Reinmuth-Selzle, K., Vlasenko, S.S., Krüger, O.O., Fröhlich-Nowoisky, J., Pöhlker, C., Ivanova, O.A., Kiselev, A.A., Kremper, L. A., and Pöschl, U.: Water uptake of subpollen aerosol particles: hygroscopic growth, cloud conden-sation nuclei activation, and liquid–liquid phase separation, Atmos. Chem. Phys., 21, 6999–7022, https://doi.org/10.5194/acp-21-6999-2021, 2021.
166. Morozov V.N. Influence of clouds and aerosol particles on the distribution of electri-cal conductivity atmosphere // Transactions of MGO, V. 606, P. 7¬8–93, 2022. (in Russian).

167. Dovgalyuk Y. A., Veremei N. E., Sinkevich A. A. et al. Effects of High Aerosol Air Pollution on the Evolution of Convective Clouds during a Thunderstorm in China According to Three-dimensional Numerical Simulations // Russian Meteorology and Hydrology. – 2022. – Vol. 47, No. 3. – P. 197–206. – DOI 10.3103/S1068373922030050. .
168. Shuvalova, J.; Chubarova, N.; Shatunova, M. Impact of Cloud Condensation Nuclei Reduction on Cloud Characteristics and Solar Radiation during COVID-19 Lockdown 2020 in Moscow. Atmosphere 2022, 13, 1710. https://doi.org/10.3390/atmos13101710.
169. Busygin, V.P., Krasnokutskaya, L.D. & Kuzmina, I.Y. Transfer of Lightning Optical Radiation into Space through the Cloud Layer. Izv. Atmos. Ocean. Phys. 55, 453–461 (2019). https://doi.org/10.1134/S0001433819050049.
170. Timofeev, D.N., Konoshonkin, A.V., Kustova, N.V. et al. Estimation of the Absorption Effect on Light Scattering by Atmospheric Ice Crystals for Wavelengths Typical for Problems of Laser Sounding of the Atmosphere. Atmos Ocean Opt 32, 564–568 (2019). https://doi.org/10.1134/S1024856019050178.
171. Shishko, V.A., Bryukhanov, I.D., Nie, E.V. et al. Algorithm for Interpreting Light Backscattering Matrices of Cirrus Clouds for the Retrieval of Their Microphysical Parameters. Atmos Ocean Opt 32, 393–399 (2019). https://doi.org/10.1134/S1024856019040134.
172. Okamoto H., Sato K., Borovoi A., Ishimoto H., Masuda K., Konoshonkin A., and Kustova N., "Interpretation of lidar ratio and depolarization ratio of ice clouds using space-borne high-spectral-resolution polarization lidar," Opt. Express 27, 36587-36600 (2019) https://doi.org/10.1364/OE.27.036587.
173. Shishko V., Konoshonkin A., Kustova N., Timofeev D., and Borovoi A., "Coherent and incoherent backscattering by a single large particle of irregular shape," Opt. Express 27, 32984-32993 (2019) https://doi.org/10.1364/OE.27.032984.
174. Artyushina A.V., Zhuravleva T.B., Nasrtdinov I.M. The influence of 3D Cloud Effects on Solar Intensity in the Earth Limb Sensing Scheme: Results of Numerical Experiments // Transactions of Mozhaiskiy academy. – 2020. – № S674. – P. 87–91. (in Russian).
175. Okamoto H., Sato K., Borovoi A., Ishimoto H., Masuda K., Konoshonkin A., and Kustova N., "Wavelength dependence of ice cloud backscatter properties for space-borne po-larization lidar applications," Opt. Express 28, 29178-29191 (2020) https://doi.org/10.1364/OE.400510.
176. Shishko V.A., Konoshonkin A.V., Kustova N.V., and Timofeev D.N. "Light scattering by spherical particles for data interpretation of mobile lidars," Optical Engineering 59(8), 083103 (14 August 2020). https://doi.org/10.1117/1.OE.59.8.083103.
177. Sterlyadkin, V.V. Some Aspects of the Scattering of Light and Microwaves on Non-Spherical Raindrops. Atmosphere 2020, 11, 531. https://doi.org/10.3390/atmos11050531.
178. Veselovskii, I., Hu, Q., Goloub, P., Podvin, T., Korenskiy, M., Pujol, O., Dubovik, O., and Lopatin, A.: Combined use of Mie–Raman and fluorescence lidar observations for im-proving aerosol characterization: feasibility experiment, Atmos. Meas. Tech., 13, 6691–6701, https://doi.org/10.5194/amt-13-6691-2020, 2020.

179. Korshunov, V.A. Multiple Scattering in Cirrus Clouds and Taking It into Account When Interpreting Lidar Measurements in the Stratosphere. Atmos Ocean Opt 35, 151–157 (2022). https://doi.org/10.1134/S1024856022020051.
180. Tkachev I.V., Timofeev D.N., Kustova N.V., Konoshkin A.V. Databank of Mueller matrices on atmospheric ice crystals of 10-100 mm for interpretation of ground-based and space-borne lidar data // Atmospheric and Oceanic Optics. – 2021. – V. 34, № 3(386). – P. 199–206. – DOI 10.15372/AOO20210306. (in Russian).
181. Wang Z., Shishko V., Kustova N., Konoshonkin A., Timofeev D., Xie C., Liu D., and Borovoi A., "Radar-lidar ratio for ice crystals of cirrus clouds," Opt. Express 29, 4464-4474 (2021) https://doi.org/10.1364/OE.410942.
182. Galileiskii V.P. Experimental study of the reflection of light radiation from crystalline particles in the lower troposphere // Atmospheric and Oceanic Optics. – 2022. – V. 35, № 11(406). – P. 918–922. – DOI 10.15372/AOO20221107. (in Russian).
183. Timofeev, D.N., Konoshonkin, A.V., Kustova, N.V. et al. Light Backscattering Proper-ties of Distorted Hexagonal Atmospheric Ice Particles within the Physical Optics Approxima-tion. Atmos Ocean Opt 35, 158–163 (2022). https://doi.org/10.1134/S1024856022020130.
184. Kustova, N.; Konoshonkin, A.; Shishko, V.; Timofeev, D.; Borovoi, A.; Wang, Z. Co-herent Backscattering by Large Ice Crystals of Irregular Shapes in Cirrus Clouds. Atmosphere 2022, 13, 1279. https://doi.org/10.3390/atmos13081279.
185. Kustova, N.; Konoshonkin, A.; Shishko, V.; Timofeev, D.; Tkachev, I.; Wang, Z.; Bo-rovoi, A. Depolarization Ratio for Randomly Oriented Ice Crystals of Cirrus Clouds. Atmos-phere 2022, 13, 1551. https://doi.org/10.3390/atmos13101551.
186. Kazantseva A. S., O. I. Kadebskaya, Y. V. Dublyanskii, V. N. Kataev The Results of Precipitation Isotope Composition Monitoring in the Northern and Middle Urals // Russian Meteorology and Hydrology. – 2020. – Vol. 45, No. 3. – P. 201–206. – DOI 10.3103/S1068373920030085. .
187. Mityaev M.V., Gerasimova M.V., Ryzhik I.V., Ishkulova T.G. Insoluble fractions of aerosols and heavy metals in fresh snow in the north-west of the Kola peninsula in 2018 // Ice and Snow (Led i Sneg), V.59, No 3, 2019, P. 307–318, DOI: 10.15356/2076-6734-2019-3-386 (in Russian).
188. Semenets E.S., Pavlova M.T. Acidity of the atmospheric precipitation in the northwest of Russia // Transactions of MGO, V. 593, 2019, P. 99–115 (in Russian).
189. Tentyukov M.P., Gabov D.N., Simonenkov D.V., Yazikov E.G. Pollution of the snow surface with polycyclic aromatic hydrocarbons during the formation of frost // Ice and Snow (Led i Sneg), V. 59, No 4, 2019, P. 483–493, DOI: 10.15356/2076-6734-2019-4-405 (in Russian).
190. Chechko V. A., Topchaya V. Y. Distribution and Composition of Aerosol Particles in Rainfall over the Coast of the Kaliningrad Oblast // Russian Meteorology and Hydrology. – 2019. – Vol. 44, No. 5. – P. 331-337. – DOI 10.3103/S10683 73919050042. .
191. Efimova N.V., Drozd V.A., Golokhvast K.S., Elfimova T.A., Motorov V.R. Study of the particle size composition of atmospheric suspension of the administrative and industrial center of Eastern Siberia. Gigiena i Sanitaria (Hygiene and

Sanitation, Russian journal) 2019; 98 (10): 1043-1048. DOI: http://dx.doi.org/10.18821/0016-9900-2019-98-10-1043-1048 (In Russian).
192. Khaustov A., Redina, M. (2021) Polycyclic Aromatic Hydrocarbons in the Snow Cover of Moscow (Case Study of the RUDN University Campus), Polycyclic Aromatic Com-pounds, 41:5, 1030–1041, DOI: 10.1080/10406638.2019.1645707.
193. Zhurba O.M., Alekseyenko A.N., Shayakhmetov S.F., Merinov A.V. Study of polycy-clic aromatic and petroleum hydrocarbons in a snow cover in an urbanized territory. // Gi-giena i Sanitaria (Hygiene and Sanitation, Russian journal) 2019; 98 (10): 1037–1042. DOI: http://dx.doi.org/10.18821/0016-9900-2019-98-10-1037-1042 (In Russian).
194. Malygina N.S., Eyrikh A.N., Agbalyan E.V., Papina T.S. Isotopic composition and source regions of winter precipitation in the Nadym lowland // Ice and Snow (Led i Sneg), V. 60, No 1, 2020, P. 96–108, DOI: 10.31857/S2076673420010026 (in Russian).
195. Vasilevich M.I., Vasilevich R.S. Influence of atmospheric circulation on layer-wise dy-namics of chemical properties of snow cover // Russian Meteorology and Hydrology. – 2020. –No. 11. – P. 74–83 (in Russian).
196. Skakun A.A. et al. Stable isotopic composition of atmospheric precipitation and natu-ral waters in the vicinity of Barentsburg (Svalbard) // Ice and Snow (Led i Sneg), V. 60, No 3, 2020, P. 379–394, DOI: 10.31857/S2076673420030046 (in Russian).
197. Epova E.S., Soloduhina M.A., Eremin O.V., Mihaylova L.A., Alekseeva O.G., Burla-ka L.M. Lapa S.E. Monitoring of arsenic, lead, cadmium, zinc, and copper in the environ-mental components of the Sherlovaya Gora village (Eastern Transbaikalia). Gigiena i Sani-taria (Hygiene and Sanitation, Russian journal) 2020; 99 (2): 210–216. DOI: http://dx.doi.org/10.33029/0016-9900-2020-99-2-210-216 (In Russian).
198. Vlasov, D.; Vasil'chuk, J.; Kosheleva, N.; Kasimov, N. Dissolved and Suspended Forms of Metals and Metalloids in Snow Cover of Megacity: Partitioning and Deposition Rates in Western Moscow. Atmosphere 2020, 11, 907. https://doi.org/10.3390/atmos11090907.
199. Ukraintsev A.V., Plyusnin A.M., Zaikovskii V.I. Morphology and chemical composi-tion of dispersed particles in the snow cover of burnt forest areas in Western Transbaikalia (Russia) // Applied Geochemistry, Vol. 122, 2020, P. 104723, https://doi.org/10.1016/j.apgeochem.2020.104723.
200. Borodulina G.S., Tokarev I.V., Levichev M.A. Isotopic composition (δ18O, δ2H) of the snow cover in Karelia // Ice and Snow (Led i Sneg), V. 61, No 4, 2021, P. 521–532, DOI: 10.31857/S2076673421040105 (in Russian).
201. Vlasov D. V., Eremina I. D., Shinkareva G. L., Chubarova N.E., Kasimov N.S. Daily variations in wet deposition and washout rates of potentially toxic elements in Moscow dur-ing spring season // Geography, Environment, Sustainability. – 2021. – Vol. 14, No. 1. – P. 219–233. – DOI 10.24057/2071-9388-2020-162.
202. Vlasov D. V., Kasimov N.S., Eremina I. D., Shinkareva G. L., Chubarova N.E. Parti-tioning and solubilities of metals and metalloids in spring rains in Moscow megacity // At-mospheric Pollution Research, 2021, Vol. 12, No 1, P. 255–271, https://doi.org/10.1016/j.apr.2020.09.012.
203. Kotova, E.I. and Topchaya, V.Yu. "Chemical and algological composition of the snow cover at the mouth of the Onega River (White Sea basin)" Pure and Ap-

plied Chemistry, vol. 94, no. 3, 2022, pp. 291–295. https://doi.org/10.1515/pac-2021-0309.
204. Topchaya, V.Yu. and Kotova, E.I. "Composition of rainfall in the coastal zone of the Kaliningrad region of the Russian Federation (based on data from 2019)" Pure and Applied Chemistry, vol. 94, no. 3, 2022, pp. 285–290. https://doi.org/10.1515/pac-2021-0302.
205. Krupnova, T.G.; Rakova, O.V.; Struchkova, G.P.; Tikhonova, S.A.; Kapitonova, T.A.; Gavrilkina, S.V.; Bulanova, A.V.; Yakimova, O.N. Insights into Particle-Bound Metal(loid)s in Winter Snow Cover: Geochemical Monitoring of the Korkinsky Coal Mine Area, South Ural Region, Russia. Sustainability 2021, 13, 4596. https://doi.org/10.3390/su13094596.
206. Opekunov, A.Y., Opekunova, M.G., Kukushkin, S.Y. et al. Mineralogical–Geochemical Characteristics of the Snow Cover in Areas with Mining and Ore-Processing Fa-cilities. Geochem. Int. 59, 711–724 (2021). https://doi.org/10.1134/S0016702921060070.
207. Kozhevnikov, A.Y., Falev, D.I., Sypalov, S.A. et al. Polycyclic aromatic hydrocarbons in the snow cover of the northern city agglomeration. Sci Rep 11, 19074 (2021). https://doi.org/10.1038/s41598-021-98386-x.
208. Volodina D.A., Talovskaya A.V., Devyatova A.Yu., Edelev A.V. and Yazikov E.G. "Elemental composition of dust aerosols near cement plants based on the study of samples of the solid phase of the snow cover" Pure and Applied Chemistry, vol. 94, no. 3, 2022, pp. 269-274. https://doi.org/10.1515/pac-2021-0315.
209. Ianchenko N.I., Talovskaya A.V. and Zanin A.A. "Comparative assessment of fluo-rine, sodium, and lithium distributions in snow cover in Siberia" Pure and Applied Chemistry, vol. 94, no. 3, 2022, pp. 261–267. https://doi.org/10.1515/pac-2021-0319.
210. Kuryatnikova, N.A., Malygina, N.S. & Mitrofanova, E.Y. Atmospheric Input and Di-versity of Bioaerosols in Winter Precipitation in the South of Western Siberia. Atmos Ocean Opt 35, 146–150 (2022). https://doi.org/10.1134/S1024856022020063.
211. Vasil'chuk Yu. K., Budantseva N.A., Vasil'chuk J.Yu. Eremina I.D., Bludushkina L.B. Variations of the δ18O values and water-soluble salts in precipitation in Moscow during 2014 to 2016 // Bulletin of Moscow State University (Vestnik Moskovskogo Universiteta), 2021, No 2., P. 35–43 (in Russian).
212. Lisetskaya L.G., Shayakhmetov S.F. Assessment of the level of pollution of the snow cover with chemical compounds and elements in the territory of the Shelekhov district in Eastern Siberia // Gigiena i Sanitaria (Hygiene and Sanitation, Russian journal) 2022; 101 (12): 1443–1449. DOI: http://dx.doi.org/10.47470/0016-9900-2022-101-12-1443-1449 (In Russian).
213. Vasil'chuk, Y., Chizhova, J., Budantseva, N. et al. Stable isotope composition of pre-cipitation events revealed modern climate variability. Theor Appl Climatol 147, 1649–1661 (2022). https://doi.org/10.1007/s00704-021-03900-w.
214. Noskova T.V., Lovtskaya O.V., Panina M.S., Podchufarova D.P. and Papina T.S. "Or-ganic carbon in atmospheric precipitation in the urbanized territory of the South of Western Siberia, Russia" Pure and Applied Chemistry, vol. 94, no. 3, 2022, pp. 309–315. https://doi.org/10.1515/pac-2021-0321.
215. Moskovchenko, D.; Pozhitkov, R.; Lodygin, E.; Toptygina, M. Polycyclic Aromatic Hydrocarbons in the Snow Cover in the City of Tyumen (Western Siberia, Russia). Toxics 2022, 10, 743. https://doi.org/10.3390/toxics10120743.

216. Ianchenko, N.I. "Features of the fluoride behavior in the snow cover under the action of technological and weather conditions" Pure and Applied Chemistry, vol. 94, no. 9, 2022, pp. 1071-1077. https://doi.org/10.1515/pac-2021-0901.
217. Yakovlev, E., Druzhinina, A., Zykova, E., Zykov, S., & Ivanchenko, N. (2022). As-sessment of Heavy Metal Pollution of the Snow Cover of the Severodvinsk Industrial District (NW Russia). Pollution, 8(4), 1274–1293. doi: 10.22059/poll.2022.341500.1438.
218. Topchaya V.Yu., Chechko V.A. Study of insoluble atmospheric material of the snow cover of the coastal zone of the southeastern Baltic Sea // Regional Studies in Marine Science, 2022, Vol. 52, P. 102399, https://doi.org/10.1016/j.rsma.2022.102399.
219. Ehrlich, A., Wendisch, M., Lüpkes, C., Buschmann, M., Bozem, H., Chechin, D., Clemen, H.-C., Dupuy, R., Eppers, O., Hartmann, J., Herber, A., Jäkel, E., Järvinen, E., Jourdan, O., Kästner, U., Kliesch, L.-L., Köllner, F., Mech, M., Mertes, S., Neuber, R., Ruiz-Donoso, E., Schnaiter, M., Schneider, J., Stapf, J., and Zanatta, M.: A comprehensive in situ and remote sensing data set from the Arctic CLoud Observations Using airborne measurements during polar Day (ACLOUD) campaign, Earth Syst. Sci. Data, 11, 1853–1881, https://doi.org/10.5194/essd-11-1853-2019, 2019.
220. Wendisch, M., and Coauthors, 2019: The Arctic Cloud Puzzle: Using ACLOUD/PASCAL Multiplatform Observations to Unravel the Role of Clouds and Aerosol Particles in Arctic Amplification. Bull. Amer. Meteor. Soc., 100, 841–871, https://doi.org/10.1175/BAMS-D-18-0072.1.
221. Kalnajs, L. E., Davis, S. M., Goetz, J. D., Deshler, T., Khaykin, S., St. Clair, A., Hertzog, A., Bordereau, J., and Lykov, A.: A reel-down instrument system for profile measurements of water vapor, temperature, clouds, and aerosol beneath constant-altitude scientific balloons, Atmos. Meas. Tech., 14, 2635–2648, https://doi.org/10.5194/amt-14-2635-2021, 2021.
222. Shvets N.V., Razuvaev N.V., Katina S.P. Specialized data array of the number of days with precipitation ≥1 mm // Transactions of RIHMI-WDC. – 2019. – № 185. – P. 67-76. (in Russian).
223. Chernykh I.V., Aldukhov O.A. Description of the database "Reporting data on cloud layer boundaries reconstructed from radiosonde observations of temperature and humidity at 58 stations on the territory of the Russian Federation and neighboring regions"// Transactions of RIHMI-WDC. – 2020. – № 186. – P. 21–34. (in Russian).
224. Shvets N.V. Precipitation intensity: measurement methods, observation databases, use of precipitation intensity data in climate research and applications // Transactions of RIHMI-WDC. – 2020. – № 186. – P. 69–89. (in Russian).
225. Lockhoff, M., O. Zolina, C. Simmer, and J. Schulz, 2019: Representation of Precipitation Characteristics and Extremes in Regional Reanalyses and Satellite- and Gauge-Based Estimates over Western and Central Europe. J. Hydrometeor., 20, 1123–1145, https://doi.org/10.1175/JHM-D-18-0200.1.
226. Voropay, N., A. Ryazanova, E. Dyukarev, 2021: High-resolution bias-corrected precipitation data over South Siberia, Russia // Atmospheric Research, Vol. 254, P. 105528, https://doi.org/10.1016/j.atmosres.2021.105528.
227. Grigorev V. Yu. Frolova N.L., Kireeva M.B., Stepanenko V.M. Spatial and temporal variability of ERA5 precipitation accuracy over Russia // Izvestiya, geog-

raphy series. – 2022. – V. 86, № 3. – P. 435-446. – DOI 10.31857/S25875566 22030062. (in Russian).
228. Podlesnyi S.V., Devyatova E.V., Saunkin A.V., Vasilyev R.V. Comparing methods to estimate cloud cover over the Baikal natural territory in December 2020 // Solar-Terrestrial Physics. – 2022. – V. 8, № 4. – P. 102–109. – DOI 10.12737/szf-84202210. (in Russian).
229. Sinitsyn, A.V., Gulev, S.K. Comparison of Field and Satellite Data on the Total Cloudiness for the Atlantic Ocean in the Period 2004–2014. Oceanology 62, 1–7 (2022). https://doi.org/10.1134/S0001437022010131.
230. Kharyutkina, E.; Loginov, S.; Martynova, Y.; Sudakov, I. Time Series Analysis of Atmospheric Precipitation Characteristics in Western Siberia for 1979–2018 across Different Datasets. Atmosphere 2022, 13, 189. https://doi.org/10.3390/atmos13020189.
231. Arshinov M. Yu., Belan B.D., Davydov D.K., Kozlov A.V., Tolmachev G.N. Automatic precipitation collectors // Russian Meteorology and Hydrology. – 2019. – № 7. – P. 118–123. (in Russian).
232. Zharashuev M. Precipitation measurement with increased catchment area // Russian Engineer. – 2019. – № 3(64). – P. 45–48. (in Russian).
233. Kalchikhin, V.V., Kobzev, A.A. Estimation of parameters of dangerous weather phenomena associated with atmospheric precipitates using the optical rain gauge // Atmospheric and Oceanic Optics. – 2019. – V. 32, № 10. – P. 867–869. – DOI 10.15372/AOO20191011. (in Russian).
234. Ekaykin, A.A., N.A. Teben'kova, V.Y. Lipenkov [et al.] Underestimation of Snow Accumulation Rate in Central Antarctica (Vostok Station) Derived from Stake Measurements // Russian Meteorology and Hydrology. – 2020. – Vol. 45, No. 2. – P. 132–140. – DOI 10.3103/S1068373920020090. .
235. Kalchikhin, V.V., Kobzev, A.A., Tikhomirov, A.A. et al. Optimization of Calibration Procedure for an Optoelectronic Precipitation Gage. Atmos Ocean Opt 34, 726–729 (2021). https://doi.org/10.1134/S1024856021060142.
236. Kalchikhin, V.V., Kobzev, A.A., Tikhomirov, A.A. et al. Element-by-Element Calibration of an Optoelectronic Precipitation Gage. Atmos Ocean Opt 35, 77–80 (2022). https://doi.org/10.1134/S1024856022010080.
237. Voskanyan K.L. et al. Comparison of the efficiency of detection of meteorological objects by two doppler radars in the territory of the Leningrad region // Transactions of MGO. – 2019. – № 592. – P. 80–97. (https://elibrary.ru/item.asp?id=37793446) (in Russian).
238. Denisenkov, D.A., Zhukov, V.Y. & Shchukin, G.G. Wind Shear Detection from Weather Radar Data. Russ. Meteorol. Hydrol. 44, 782–789 (2019). https://doi.org/10.3103/S1068373919110086.
239. Kagermazov A.H., Sozaeva L.T. Estimation of the contribution of different hydrometeors to the total radar reflectivity in hail clouds // Transactions of MGO. – 2019. – № 594. – P. 107–119. (in Russian).
240. Klimenko, D.E. Studying the Areal Rainfall Reduction in the Urals Based on Radar Data. Russ. Meteorol. Hydrol. 44, 484–493 (2019). https://doi.org/10.3103/S1068373919070070.
241. Sozaeva L.T., Makitov V.S. Influence the deformation of the drops growing in the electromagnetic field on their scattering properties // Science. Innovation. Technology. – 2019. – № 3. – P. 95–106. – DOI 10.37495/2308-4758-2019-3-115-130. (in Russian).

242. Alekseeva A.A., Bukharov V.M., Vasil'ev E.V., Losev V.M. Diagnosis of squalls in snowstorms based on DMRL-C doppler weather radar data // Hydrometeorological research and forecasting. – 2020. – № 3(377). – P. 6–18. – DOI 10.37162/2618-9631-2020-3-6-18. (in Russian).
243. Dovgalyuk, Y.A., Veremei, N.E., Sin'kevich, A.A. et al. Investigation of Electrification Mechanisms and Relationship between the Electrical Discharge Frequency and Radar Characteristics of the Thunderstorm in China. Russ. Meteorol. Hydrol. 45, 712–719 (2020). https://doi.org/10.3103/S1068373920100052.
244. Ilin, N.V., Kuterin, F.A. Accuracy of Thunderstorm Detection Based on DMRL-C Weather Radar Data. Russ. Meteorol. Hydrol. 45, 669–675 (2020). https://doi.org/10.3103/S1068373920090083.
245. Klimenko, D.Y. Estimating the Probable Maximum Precipitation by Physical Methods Using Satellite and Radiolocation Observation Data: Case Study of the Middle Urals. Water Resour 47, 641–650 (2020). https://doi.org/10.1134/S0097807820040065.
246. Kostarev S.V., Vetrov A.L., Sivkov B.A., Pomortseva A.A. Radar characteristics of cloud systems during heavy rain events // Geographical bulletin. – 2020. – № 3(54). – P. 113–124. – DOI 10.17072/2079-7877-2020-3-113-124. (in Russian).
247. Sozaeva L.T., Zhaboeva M.M. Backscatter of radar radiation by cloud and rain drops // Transactions of MGO. – 2020. – № 599. – P. 140–150. (in Russian).
248. Sin'kevich, A.A., Toropova, M.L., Mikhailovskii, Y.P. et al. Features of the Relationship between Electrical and Radar Parameters of Thunderclouds in India (Field Studies). Russ. Meteorol. Hydrol. 46, 410–415 (2021). https://doi.org/10.3103/S106837392106008X.
249. Sozaeva L.T. Backscatter of radio waves by spheroidal rain drops // Reports of the High School. Radiophysics. – 2021. – V. 64, № 8–9. – P. 732–737. – DOI 10.52452/00213462_2021_64_08_732. (in Russian).
250. Sozaeva L.T., Zhaboeva M.M. Evaluation of the effect of drop deformation of precipitation intencity with help of radar method // Transactions of MGO. – 2021. – № 602. – P. 104–115. (in Russian).
251. Zharashuev M.V. Optimization of the radar network of the Russian Federation // Transactions of MGO. – 2022. – № 606. – P. 145–151 (in Russian).
252. Sozaeva L.T. On the possibility of using a spheroidal particle model to calculate the scattering characteristics of radio waves from elongated cloud crystals // Transactions of MGO. – 2022. – № 606. – P. 133–144. (in Russian).
253. Shapovalov, A.V., Shapovalov, V.A., Stasenko, V.N. et al. Application of Radar, Lightning Location, and Numerical Simulation Data to Study the Relationship between Total Lightning Activity and Severe Weather Events. Russ. Meteorol. Hydrol. 47, 613–619 (2022). https://doi.org/10.3103/S1068373922080076.
254. Krinitskiy, M.; Aleksandrova, M.; Verezemskaya, P.; Gulev, S.; Sinitsyn, A.; Kovaleva, N.; Gavrikov, A. On the Generalization Ability of Data-Driven Models in the Problem of Total Cloud Cover Retrieval. Remote Sens. 2021, 13, 326. https://doi.org/10.3390/rs13020326.
255. Sorokin, A.G., Dobrynin, V.A. Method of studying infrasound waves from thunderstorms // Solar-Terrestrial Physics. – 2022. – Vol. 8, No. 1. – P. 62–68. – DOI 10.12737/stp-81202208.
256. Korshunov V.A., Zubachev D.S. Characteristics of cirrus clouds from lidar measurements at Obninsk // Transactions of MGO. – 2021. – № 602. – P. 68–78. (in Russian).

257. Makhotina, I.A., Chechin, D.G. & Makshtas, A.P. Cloud Radiative Forcing over Sea Ice in the Arctic during the Polar Night According to North Pole-37, -39, and -40 Drifting Stations. Izv. Atmos. Ocean. Phys. 57, 451–460 (2021). https://doi.org/10.1134/S0001433821050091.
258. Biryukov, E.Y., Kostsov, V.S. The Use of Linear Regression Relations Derived from Model and Experimental Data for Retrieval of the Water Content of Clouds from Ground-Based Microwave Measurements. Atmos Ocean Opt 32, 569–577 (2019). https://doi.org/10.1134/S1024856019050051.
259. Biryukov, E.Y., Kostsov, V.S. Application of the Regression Algorithm to the Problem of Studying Horizontal Inhomogeneity of the Cloud Liquid Water Path by Ground-Based Microwave Measurements in the Angular Scanning Mode. Atmos Ocean Opt 33, 602–609 (2020). https://doi.org/10.1134/S10248 5602006007X.
260. Karavaev D.M., Shchukin G.G. Study on variations in water vapor and cloud liquid using microwave radiometry // Atmospheric and Oceanic Optics. – 2019. – V. 32, № 11. – P. 930–935. – DOI 10.15372/AOO20191109 (in Russian).
261. Rostokin I.N., Fedoseeva E.V., Shchukin G.G. Multifrequency microwave radiometric studies of radiothermal radiation of convective clouds under conditions of formation and development of dangerous atmospheric meteorological events // Transactions of Mozhaiskiy academy. – 2019. – № 670. – P. 140–145. (in Russian).
262. Bykov V.Yu., Il'in G.N., Karavaev D.M., Shchukin G.G. Microwave radiometric measurements of vapor and liquid droplet moisture content in the troposphere // Transactions of Mozhaiskiy academy. – 2020. – № S674. – P. 128–132. (in Russian).
263. Akvilonova, A.B., Egorov, D.P., Kutuza, B.G. et al. Studying Characteristics of the Cloudy Atmosphere Based on Measuring Its Downwelling Microwave Radiation Spectra in the 18.0–27.2 GHz Water Vapor Resonant Absorption Band. Russ. Meteorol. Hydrol. 47, 953–961 (2022). https://doi.org/10.3103/S1068 37392212007X.
264. Karavaev, D.M., Lebedev, A.B., Shchukin, G.G. et al. Prospects for Application of Ground-based Microwave Radiometry for Analysis of Atmospheric Fronts and Early Prediction of Severe Weather Events. Russ. Meteorol. Hydrol. 47, 946–952 (2022). https://doi.org/10.3103/S1068373922120068.
265. Karavaev D.M., Lebedev, A.B., Moiseeva, N.O., Shchukin, G.G. The use of ground-based microwave radiometers to diagnose the mesostructure of atmospheric fronts // Transactions of Mozhaiskiy academy. – 2022. – № S685. – P. 141–146. (in Russian).
266. Klimenko, V.V., L.V. Lubyako, E.A. Mareev , M.V. Shatalina (2022) Ground-based measurements of microwave brightness temperature and electric field fluctuations for clouds with a different level of electrical activity // Atmospheric Research, vol. 266, P. 105937, https://doi.org/10.1016/j.atmosres.2021.105937.
267. Adzhiev A.Kh. et al. Hardware and software package for monitoring electrical and thunderstorm atmospheric phenomena // Radio Engineering and Telecommunications Systems. – 2019. – № 4(36). – P. 5–11. (in Russian).
268. Kleshcheva, T.I., Potalova, E.Y. & Permyakov, M.S. Comparison of World Wide Lightning Location Network (WWLLN) Data and Standard Observations at Weather Stations in the Southern Russian Far East. Russ. Meteorol. Hydrol. 46, 403–409 (2021). https://doi.org/10.3103/S1068373921060078.

269. Zharashuev M.V. A method for automated statistical analysis of cloud-to-ground discharges in the North Caucasus // Russian Meteorology and Hydrology. – 2022. – № 4. – P. 111–116. – DOI 10.52002/0130-2906-2022-4-111-116. (in Russian).
270. Kurov A.B. et al. Investigation of lightning detection network blitzortung operation features // Transactions of MGO. – 2022. – № 606. – P. 50-62. (in Russian).
271. Spivak, A. A. A Complex Prognostic Feature of Dangerous Atmospheric Events / A. A. Spivak, Y. S. Rybnov, S. A. Riabova // Doklady Earth Sciences. – 2022. – Vol. 504, No. 1. – P. 291–295. – DOI 10.1134/S1028334X22050154.
272. Andreev, A.I., Shamilova, Y.A. & Kholodov, E.I. Using Convolutional Neural Networks for Cloud Detection from Meteor-M No. 2 MSU-MR Data. Russ. Meteorol. Hydrol. 44, 459–466 (2019). https://doi.org/10.3103/S10683 73919070045.
273. Asmus, V.V., Ioffe, G.M., Kramareva, L.S. et al. Satellite Monitoring of Natural Hazards on the Territory of Russia. Russ. Meteorol. Hydrol. 44, 719–728 (2019). https://doi.org/10.3103/S1068373919110013.
274. Danilova, I.V., Onuchin, A.A. The Estimation of Solid Precipitation Distribution in the Taiga Zone of the Yenisei River Basin Using Satellite Data. Russ. Meteorol. Hydrol. 44, 71–77 (2019). https://doi.org/10.3103/S1068373919010084.
275. Filei A.A. Retrieval of the cloud optical depth and particle effective radii from MSU-MR daytime measurements // Atmospheric and Oceanic Optics. – 2019. – V. 32, № 8. – P. 650–656. – DOI 10.15372/AOO20190807. (in Russian).
276. Filei A.A. Determination of cloud phase using MSU-MR measurements on-board Meteor-M N 2 // Atmospheric and Oceanic Optics. – 2019. – V. 32, № 5. – P. 376–380. – DOI 10.15372/AOO20190506. (in Russian).
277. Khutorova O.G., Blizorukov A.S., Dementiev V.V., Khutorov V.E. Mesoscale tropospheric structure sensing during weather front passage // Current issues of remote sensing of the Earth from space. – 2019. – V. 16, № 6. – P. 254–262. – DOI 10.21046/2070-7401-2019-16-6-254-262. (in Russian).
278. Kostsov, V. S., Kniffka, A., Stengel, M., and Ionov, D. V.: Cross-comparison of cloud liquid water path derived from observations by two space-borne and one ground-based instrument in northern Europe, Atmos. Meas. Tech., 12, 5927–5946, https://doi.org/10.5194/amt-12-5927-2019, 2019.
279. Volkova E.V., Kukharskii A.V., Muzylev E.L., Startseva Z.P. Determination of precipitation amounts from satellite data for part of the European territory of Russia // Transactions of Mozhaiskiy academy. – 2020. – № S674. – P. 139–145. (in Russian).
280. Volkova E.V., Kukharskii A.V. The automated technology for retrieving cloud cover properties, precipitation and weather hazards based on SEVIRI/Meteosat (MSG) data for the European part of Russia // Hydrometeorological research and forecasting. – 2020. – № 4(378). – P. 43–62. – DOI 10.37162/2618-9631-2020-4-43-62. (in Russian).
281. Gotyur I.A., Meshkov A.N., Rud' M.Yu., Yaremenko I.A. A method of searching for cumulonimbus clouds from hydrometeorological satellites using artificial neural network technology // Transactions of Mozhaiskiy academy. – 2020. – № S674. – P. 146–151. (in Russian).
282. Skorokhodov A.V. Nighttime cloud classification by VIIRS satellite data // Current issues of remote sensing of the Earth from space. – 2020. – V. 17, № 3. – P. 240–251. – DOI 10.21046/2070-7401-2020-17-3-240-251. (in Russian).

283. Tarasov A.V. Estimation of the accuracy of cloud masking algorithms using Sentinel-2 and Planetscope data // Current issues of remote sensing of the Earth from space. – 2020. – V. 17, № 7. – P. 26-40. – DOI 10.21046/2070-7401-2020-17-7-26-38. (in Russian).
284. Filei A.A. Retrieval of the cloud top height from using Meteor-M No. 2-2 MSU-MR measurements // Atmospheric and Oceanic Optics. – 2020. – V. 33, № 12(383). – P. 918–925. – DOI 10.15372/AOO20201203. (in Russian).
285. Shishov A.E., Gorlach I.A. An algorithm for the detection and tracking of deep convection using satellite data and integer programming // Hydrometeorological research and forecasting. – 2020. – № 2(376). – P. 39–59. – DOI 10.37162/2618-9631-2020-2-39-59. (in Russian).
286. Bloshchinskiy V. D., Kuchma M. O., Andreev A. I., and Sorokin A. A. "Snow and cloud detection using a convolutional neural network and low-resolution data from the Electro-L No. 2 Satellite," Journal of Applied Remote Sensing 14(3), 034506 (15 July 2020). https://doi.org/10.1117/1.JRS.14.034506.
287. Andreev, A.I., Shamilova, Y.A. Cloud Detection from the Himawari-8 Satellite Data Using a Convolutional Neural Network. Izv. Atmos. Ocean. Phys. 57, 1162–1170 (2021). https://doi.org/10.1134/S0001433821090401.
288. Astafurov, V.G., Skorokhodov, A.V. Using the Results of Cloud Classification Based on Satellite Data for Solving Climatological and Meteorological Problems. Russ. Meteorol. Hydrol. 46, 839–848 (2021). https://doi.org/10.3103/S1068373921120050.
289. Volkova, E.V., Andreev, A.I. & Kostornaya, A.A. Cloud Cover and Precipitation Monitoring Based on Data from Polar Orbiting and Geostationary Satellites. Russ. Meteorol. Hydrol. 46, 830–838 (2021). https://doi.org/10.3103/S1068373921120049.
290. Skorokhodov A.V., Konoshonkin A.V. Comparison of satellite active and passive observations of specularly reflecting layers in the high-level clouds // Current issues of remote sensing of the Earth from space. – 2021. – V. 18, № 3. – P. 279–287. – DOI 10.21046/2070-7401-2021-18-3-279-287. (in Russian).
291. Shakina, N.P., Gorlach, I.A. & Skriptunova, E.N. Significance of Satellite Data on Convective Clouds for Flight Accident Analysis and Prevention. Russ. Meteorol. Hydrol. 46, 866–871 (2021). https://doi.org/10.3103/S1068373921120086.
292. Savorskiy V.P. Correction of cloud water estimates from satellite monitoring data // Current issues of remote sensing of the Earth from space. – 2022. – V. 19, № 1. – P. 78–86. – DOI 10.21046/2070-7401-2022-19-1-78-86. (in Russian).
293. Skorokhodov A.V., Konoshonkin A.V. Statistical analysis for parameters of specularly reflective layers in high-level clouds over Western Siberia based on MODIS data // Atmospheric and Oceanic Optics. – 2022. – V. 35, № 9(404). – P. 711–716. – DOI 10.15372/AOO20220903. (in Russian).
294. Skorokhodov A.V., Kuryanovich K.V. Using CALIOP data to estimate the cloud base height in MODIS images // Current issues of remote sensing of the Earth from space. – 2022. – V. 19, № 2. – P. 43–56. – DOI 10.21046/2070-7401-2022-19-2-43-56. (in Russian).
295. Frolova E.A., Nesterov E.S., Salagina A.A. Using Arktika-M No. 1 satellite MSU-GS data for monitoring and analyzing mesoscale cyclones in the Arctic region // Current issues of remote sensing of the Earth from space. – 2022. – V. 19, № 4. – P. 293–305. – DOI 10.21046/2070-7401-2022-19-4-293-305. (in Russian).

296. Khutorova O.G., Maslova M.V., Khutorov V.E. Monitoring of convective processes with satellite navigation system receivers // Atmospheric and Oceanic Optics. – 2022. – V. 35, № 6(401). – P. 505–509. – DOI 10.15372/AOO20220612. (in Russian).
297. Tarasenkov, M.V.; Engel, M.V.; Zonov, M.N.; Belov, V.V. Assessing the Cloud Adjacency Effect on Retrieval of the Ground Surface Reflectance from MODIS Satellite Data for the Baikal Region. Atmosphere 2022, 13, 2054. https://doi.org/10.3390/atmos13122054.
298. Galin V.Y., V.P. Dymnikov. Dynamic–Stochastic Parametrization of Cloudiness in the General Circulation Model of the Atmosphere // Izvestiya, Atmospheric and Oceanic Physics. – 2019. – Vol. 55, No. 5. – P. 381–385. – DOI 10.1134/S0001433819050062.
299. Eliseev A. V., A. N. Ploskov, I. I. Mokhov, A. V. Chernokulsky A Correlation between Lightning Flash Frequencies and the Statistical Characteristics of Convective Activity in the Atmosphere // Doklady Earth Sciences. – 2019. – Vol. 485, No. 1. – P. 273–278. – DOI 10.1134/S1028334X19030048. .
300. Mikhailovskii, Yu.P., Popov V.B., Sin'kevich A.A. et al. Physical and statistical empirical model of lightning activity development in convective clouds // Transactions on MGO. – 2019. – № 595. – P. 83–105. (in Russian).
301. Ashabokov, B. A. Total Approximation Method for an Equation Describing Droplet Breakup and Freezing in Convective Clouds / B.A. Ashabokov, A.K. Khibiev, M.K. Shkhanukov-Lafishev // Computational Mathematics and Mathematical Physics. – 2020. – Vol. 60, No. 9. – P. 1518–1527. – DOI 10.1134/S0965542520090055.
302. Ashabokov B.A., Khibiev A.Kh., Shkhanukov-Lafishev M.Kh. A locally one-dimensional scheme for a general parabolic equation describing microphysical processes in convective clouds // Reports of the Adyghe Academy of Sciences. – 2021. – V. 21, № 4. – P. 45–55. – DOI 10.47928/1726-9946-2021-21-4-45-55 (in Russian).
303. Volodin, E. M. Equilibrium Sensitivity of a Climate Model to an Increase in the Atmospheric CO_2 Concentration Using Different Methods to Account for Cloudiness / E. M. Volodin // Izvestiya, Atmospheric and Oceanic Physics. – 2021. – Vol. 57, No. 2. – P. 127–132. – DOI 10.1134/S0001433821020122.
304. Pressman, D.Y. Approximation of Equations for a Model of the Cloud Atmosphere. Russ. Meteorol. Hydrol. 46, 723–734 (2021). https://doi.org/10.3103/S1068373921110017.
305. Lesev V.N., V.A. Shapovalov, B.A. Ashabokov, A.V. Shapovalov and P.K. Korotkov, 3D model of a convective cloud: the interaction of microphysical and electrical processes, JP Journal of Heat and Mass Transfer 23(1) (2021), 1–18. DOI: 10.17654/HM023010001.
306. Volodin, E. (2021). The mechanisms of cloudiness evolution responsible for equilibrium climate sensitivity in climate model INM-CM4-8. Geophysical Research Letters, 48, e2021GL096204. https://doi.org/10.1029/2021GL096204.
307. Poliukhov, A.A., Chubarova, N.Y. & Volodin, E.M. Impact of Inclusion of the Indirect Effects of Sulfate Aerosol on Radiation and Cloudiness in the INMCM Model. Izv. Atmos. Ocean. Phys. 58, 486–493 (2022). https://doi.org/10.1134/S0001433822050097.
308. Toropov P.A., Shestakova A.A., Yarynich J.I., Kutuzov S.S. Simulation of orographic precipitation's component on the Mount Elbrus example // Ice and Snow (Led i Sneg) – 2022. – V. 62, № 4. – P. 485–503. – DOI 10.31857/S2076673422040146. (in Russian).

309. Piskunov, V.N., Gainullin, K.G., Petrov, A.M. et al. Simulation of the Kinetics of Precipitation Formation in a Mixed-Phased Cloud. Izv. Atmos. Ocean. Phys. 58, 376–383 (2022). https://doi.org/10.1134/S0001433822040120.
310. Shatunova, M.V., Khlestova, Y.O. & Chubarova, N.E. Forecast of Microphysical and Optical Characteristics of Large-Scale Cloud Cover and Its Radiative Effect Using the COSMO Mesoscale Weather Prediction Model. Atmos Ocean Opt 33, 154–160 (2020). https://doi.org/10.1134/S1024856020020098.
311. Alekhin S.G. Semi-empirical method for short-term prediction of total clouds // Transactions of Mozhaiskiy academy. – 2020. – № 672. – P. 148–157. (in Russian).
312. Ivanova, A.R. Icing Effects on Air Transport Operation: State-of-the-art and Prediction Problems. Russ. Meteorol. Hydrol. 46, 461–473 (2021). https://doi.org/10.3103/S1068373921070050.
313. Alekhin S.G., Ivanov R.D., Shemelov V.A. Method of constructing prognostic equations for determining the height of the lower cloud boundary based on semiempirical dependencies // Transactions of Mozhaiskiy academy. – 2022. – № 684. – P. 62–68. (https://www.elibrary.ru/item.asp?id=50188215) (in Russian).
314. Ivanova, A.R. International Practices of Thunderstorm Nowcasting. Russ. Meteorol. Hydrol. 44, 756–763 (2019). https://doi.org/10.3103/S1068373919110050.
315. Rubinstein, K.G., Gubenko, I.M., Ignatov, R.Y. et al. Experiments on Lightning Detection Network Data Assimilation. Atmos Ocean Opt 33, 219–228 (2020). https://doi.org/10.1134/S1024856020020086.
316. Muravev A.V., Kiktev D.B., Smirnov A.V., Zaichenko M.Yu. Operational precipitation nowcasting system based on radar data and comparative pointwise verification results for the warm and cold seasons // Hydrometeorological research and forecasting. – 2019. – № 2(372). – P. 12–40. (in Russian).
317. Ivanova A.R., Denisenko I.A. Feasibility of the thunderstorm nowcasting at Moscow aerodromes using radar and lightning detector information // Hydrometeorological research and forecasting. – 2020. – № 1(375). – P. 142–161. – DOI 10.37162/2618-9631-2020-1-142-161. (in Russian).
318. Andreev, A. I., N. I. Pererva, M. O. Kuchma Development of precipitation nowcasting method using geostationary satellite data // Current problems in remote sensing of the Earth from space. – 2020. – Vol. 17, No. 6. – P. 18–22. – DOI 10.21046/2070-7401-2020-17-6-18-22.
319. Muravev A.V., Bundel A.Yu., Kiktev D.B., Smirnov A.V. Verification of radar precipitation nowcasting of significant areas using the generalized pareto distribution. Part 1: elements of theory and methods for estimating parameters // Hydrometeorological research and forecasting. – 2022. – № 3(385). – P. 6–41. – DOI 10.37162/2618-9631-2022-3-6-41. (in Russian).
320. Muravev A.V., Bundel A.Yu., Kiktev D.B., Smirnov A.V. Verification of radar precipitation nowcasting of significant areas using generalized pareto distribution. Part 2: application to forecasts in warm and cold periods of 2017-2018 // Hydrometeorological research and forecasting. – 2022. – № 3(385). – P. 42–77. – DOI 10.37162/2618-9631-2022-3-42-77. (in Russian).
321. Muravev A.V., Bundel A.Yu., Kiktev D.B., Smirnov A.V. Expertise in spatial verification of radar precipitation nowcasting: identification and statistics of objects, situations and conditional samples // Hydrometeorological research and forecasting. – 2022. – № 2(384). – P. 6–52. – DOI 10.37162/2618-9631-2022-2-6-52. (in Russian).

322. Kagermazov A. Kh., Sozaeva L.T., Zharashuev M.V. Forecast of flood-forming precipitation in the North Caucasus using the global atmosphere model // Russian Meteorology and Hydrology. – 2019. – № 6. – P. 80–86. (in Russian).
323. Kalinin N.A., Shikhov A.N., Bykov A.V., Tarasov A.V. Analysis of numerical forecasts of heavy precipitation with the WRF model using various convection schemes (a case study for the Perm Krai) // Hydrometeorological research and forecasting. – 2019. – № 3(373). – P. 43–59. (in Russian).
324. Kalinin N.A. Heavy precipitation formation conditions and forecasting with the atmospheric instability indices in the territory of Ural Prikamye // Geographical Bulletin. – 2019. – № 4(51). – P. 96–112. – DOI 10.17072/2079-7877-2019-4-96-112. (in Russian).
325. Tishchenko, V.A., Khan, V.M., Kruglova, E.N. et al. Monthly and Seasonal Prediction of Precipitation and Air Temperature in the Amur River Basin. Russ. Meteorol. Hydrol. 44, 169–179 (2019). https://doi.org/10.3103/S10683 73919030026.
326. Shestakova A.A., Toropov P.A. Simulation of extreme winter precipitation on the southern coast of the Caspian Sea // Bulletin of Moscow State University. Series 5: Geography. – 2019. – № 6. – P. 51–59. (in Russian).
327. Travova S.V., Tolstykh M.A., Shashkin V.V. Verification of heavy precipitation forecasts of the SL-AV20 global operational atmosphere model // Hydrometeorological research and forecasting. – 2020. – № 1(375). – P. 96–112. – DOI 10.37162/2618-9631-2020-1-96-112. (https://www.elibrary.ru/item.asp?id=42 771316) (in Russian).
328. Vetrov, A.L., Kostarev, S.V. Applicability of Multimodel Ensemble Prediction of Heavy Precipitation for the Perm Region: A Case Study for the Summer of 2019. Russ. Meteorol. Hydrol. 46, 444–453 (2021). https://doi.org/ 10.3103/S1068373921070037.
329. Sviyzov E.M., Vetrov A.L. Numerical modeling of heavy summer rainfalls with different grid spacing of the regular grid step // Geographical Bulletin. – 2021. – № 4(59). – P. 73-83. – DOI 10.17072/2079-7877-2021-4-73-83. (in Russian).
330. Mishra, A.K., Kumar P., Dubey, A.K., Javed, A., Saharwabi, M.S., Sein, D.V., Martynov, S.D., Jacob, D. (2021) Impact of horizontal resolution on monsoon precipitation for CORDEX-South Asia: A regional earth system model assessment // Atmospheric Research, Vol. 259, P. 105681, https://doi.org/10.1016/ j.atmosres.2021.105681 .
331. Kalinin N.A., Sivkov B.A. Numerical forecast of summer precipitation of different intensity using the WRF model and atmospheric instability indices // Geographical Bulletin. – 2022. – № 3(62). – P. 92–108. – DOI 10.17072/2079-7877-2022-3-92-108. (in Russian).
332. Alekseeva A.A., Losev V.M. Forecast of severe convective weather events in summer // Hydrometeorological research and forecasting. – 2019. – № 4(374). – P. 127–143. (in Russian).
333. Kalinin, N.A., Shikhov, A.N., Bykov, A.V. et al. Conditions for the Appearance and Short-Time Prediction of Strong Squalls and Tornadoes in the European Part of Russia. Atmos Ocean Opt 32, 334–344 (2019). https://doi.org/10.1134/ S1024856019030114.
334. Kalmykova, O.V., Shershakov, V.M., Novitskii, M.A. et al. Automated Forecasting of Waterspouts off the Black Sea Coast of Russia and Its Performance Assessment. Russ. Meteorol. Hydrol. 44, 764–771 (2019). https://doi.org/ 10.3103/S1068373919110062.

335. Toropova M.L., Rusin I.N. Reproducing of atmospheric stratification in order to predict convective phenomena using the WRF-ARW model // Transactions on MGO. – 2019. – № 593. – P. 160–176. (in Russian).
336. Alekseeva A.A. Methods to estimate maximum convective velocity for the diagnosis and forecasting of severe convective weather events // Hydrometeorological research and forecasting. – 2020. – № 2(376). – P. 6–22. – DOI 10.37162/2618-9631-2020-2-6-22. (in Russian).
337. Gubenko I.M., Rubinstein K.G. Analysis of comprehensive forecast of lightning activity // Atmospheric and Oceanic Optics. – 2020. – T. 33, № 12(383). – P. 949–957. – DOI 10.15372/AOO20201208. (in Russian).
338. Dementyeva, S.O., Il'in, N.V., Shatalina, M.V. et al. Forecast of Convective Events and Its Verification against Atmospheric Electricity Observations. Izv. Atmos. Ocean. Phys. 56, 123–129 (2020). https://doi.org/10.1134/S0001433820020036.
339. Kagermazov A.Kh., Sozaeva L.T. Hail forecast on the output data of the global atmospheric model with tree-day advance time // Transactions on MGO. – 2020. – № 598. – P. 204–214. (in Russian).
340. Kalinin, N.A., Shikhov, A.N., Bykov, A.V. et al. Formation Conditions and Short-Term Forecast of Convective Hazardous Weather Events in the Ural Region in the Warm Period of 2020. Atmos Ocean Opt 34, 250–262 (2021). https://doi.org/10.1134/S1024856021030064.
341. Kagermazov A.Kh., Fedchenko L.M., Sozaeva L.T., Zhaboeva M.M. Medium-range hail forecast based on global atmospheric model output data // Science. Innovations. Technologies. – 2021. – № 2. – P. 91–108. – DOI 10.37493/2308-4758.2021.2.6. (in Russian).
342. Aniskina O.G., Stognieva V.V., Tolstobrova N.B. Prediction of thunderstorms using mesoscale hydrodynamic models // Transactions of Mozhaiskiy academy. – 2022. – № S685. – P. 6–10. (in Russian).
343. Kagermazov A.Kh., Sozaeva L.T. Hail prediction and size estimation based on a global mathematical model of the atmosphere // Transactions of Mozhaiskiy academy. – 2022. – № S685. – P. 133–140. (https://www.elibrary.ru/item.asp?id=50202058) (in Russian).
344. Kagermazov A.Kh., Sozaeva L.T. Hail forecast and estimation of its maximum size on the output data of the global atmospheric model with tree-day lead time // Science. Innovations. Technologies. – 2022. – № 2. – P. 103–120. – DOI 10.37493/2308-4758.2022.2.6. (https://www.elibrary.ru/item.asp?id=49161216) (in Russian).
345. Toropova M.L. et al. Ensemble forecast of the development of thunderstorms in the north-west of european part of russia and verification of modeling results // Transactions on MGO. – 2022. – № 606. – P. 7–31. (in Russian).
346. Kostromitinov A.V., Yaremenko I.A. Fog prediction method using convolutional neural networks // Transactions of Mozhaiskiy academy. – 2022. – № S685. – P. 186–193. (in Russian).
347. Ignatov, R.Y., Rubinshtein, K.G. & Yusupov, Y.I. Numerical Experiments on Forecasting Glaze Phenomena. Atmos Ocean Opt 33, 682–689 (2020). https://doi.org/10.1134/S1024856020060202.
348. Ignatov, R.Y., Rubinshtein, K.G. & Yusupov, Y.I. Forecasting the Maximum Thickness of Ice Accretions. Atmos Ocean Opt 35, 541–549 (2022). https://doi.org/10.1134/S102485602205013X.

349. Kiselnikova V.Z. Object-oriented assessment of COSMO-Ru2 precipitation forecast quality for the warm season (may-september) in 2016-2020 // Hydrometeorological research and forecasting. – 2021. – № 2(380). – P. 43–51. – DOI 10.37162/2618-9631-2021-2-43-51. (in Russian).
350. Kalinin, N.A., Bykov, A.V. & Shikhov, A.N. Object-Oriented Estimation of the Short-Term Forecast of Convective Hazardous Weather Events in Perm Krai by the WRF Model. Atmos Ocean Opt 35, 423–433 (2022). https://doi.org/10.1134/S1024856022040054.
351. Malkarova A.M. Development of weather modification activities in the Hydrometeorological Service of Russia. Meteorology and Hydrology. 2022. No. 7, P. 5–10. (in Russian).
352. Korneev, V.P., Koloskov, B.P., Bychkov, A.A. et al. Cloud Seeding for Improving Weather in Megacities. Russ. Meteorol. Hydrol. 47, 523–529 (2022). https://doi.org/10.3103/S1068373922070056.
353. Danelyan B.G., Kirin D.V., Kolokutin G.E., Sprygin A.A. Resource cloudiness for active impacts in the main areas of agricultural production in the European part of Russia. Proceedings of International Scientific Conference "Problems of Atmospheric Physics, Climatology and Environmental Monitoring" NCFU, Stavropol, 08–10 of Sept. 2021.
354. Danelyan B.G., Kolokutin G.E., Kirin D.V., Strunin A.M., Petrov V.V. Some results of experimental work on increasing precipitation in the Stavropol Territory in May-June 2020. Proceedings of International Scientific Conference "Problems of Atmospheric Physics, Climatology and Environmental Monitoring". Nalchik. 08–10 Sept. 2021. .
355. Doronin A.P., Kozlova N.A., Petrochenko V.M. Estimations of suitability of the supercooled cloudiness to dissipation over the central area of the European territory of Russia to solve of applied tasks. Proseeding Mozhaisky Academy. 2019. No. 671, pp. 163–171. (in Russian).
356. Doronin A.P., Petrochenko V.M., Goncharov I.V., Didyk O.I., Kozlova N.A. Assessment of suitability to the scattering of stratus and undulatus clouds in the North-Western region of the European territory of Russia in the interests of hydrometeorological support. Proseeding Mozhaisky Academy 2020. № 59, cc. 70–80 (in Russian).
357. Drofa A.S. About the effectiveness of modifying a convective cloud with ice-forming agents. Proceedings of MGO, 2020. No. 597, pp. 34-50. (in Russian).
358. Drofa, A.S., Kozlov, S.V. & Sprygin, A.A. Forecast of Resource Convective Clouds for Weather Modification. Russ. Meteorol. Hydrol. 47, 516–522 (2022). https://doi.org/10.3103/S1068373922070044.
359. Abshaev, A.M., Abshaev, M.T., Sin'kevich, A.A. et al. Studying an Effect of Glaciogenic Seeding on Lightning Activity of Convective Clouds. Russ. Meteorol. Hydrol. 47, 604–612 (2022). https://doi.org/10.3103/S1068373922080064.
360. Bekkiev, K.M., Lesev, V.N., Shapovalov, V.A. et al. Mathematical Model of a Convective Cloud in Hail Suppression Activities. Russ. Meteorol. Hydrol. 47, 499–506 (2022). https://doi.org/10.3103/S1068373922070020.
361. Sosnikova E.V., Danelyan B.G., Valtzifer V.A., Averkina A.S. Study of the effectiveness of powder crystallizing reagents AgI–SiO2. Proceedings of International Scientific Conference "Problems of Atmospheric Physics, Climatology and Environmental Monitoring" . NCFU, Stavropol, 23–25 of May 2022 г., pp. 132–136.

362. Khuchinaev B.M., Baisiev H.-M. KH., Gekkieva S.O., Budaev A.KH. Experimental research of the ice-forming efficiency of the AD1 pyrotechnic composition with zinc additions. Proceedings of MGO. 2020. No. 597, P. 51–60. (in Russian).
363. Shilin A.G. The efficacy of autonomous pyrotechnic generators of ice-forming aerosol under various conditions. Proceedings of MGO. 2021. No. 602, pp. 79–91 (in Russian).
364. Shilin A.G., Khuchunaev B.M., Budaev A.KH. Influence of soluble iodine compounds on the efficiency of ice-forming aerosol. Proceedings of MGO. 2021. No. 602, pp. 92–103. (in Russian).
365. Shilin A.G. Study of the functioning of ice forming means of active influences under real conditions of application. News of higher educational institutions. North-Caucasian region. Series: Natural Sciences. 2021. No. 4 (212), P. 69–73 DOI: 10.18522/1026-2237-2021-4-69-73 (in Russian).
366. Shilin A.G., Khuchunaev B.M. Possibilities of increasing the efficiency of pyrotechnical generators of ice-forming aerosol. Science. Technology. No. 1. 2022, pp. 87–110 DOI: 10.37493/2308-4758.2022.1.5 (in Russian).
367. Khuchunaev B.M., Baisiev H.-M. KH. Laboratory studies of increasing the ice forming efficiency of pyrotechnical compositions based on AD1. Science. Technology. No. 2. 2021, pp. 125–140. DOI: 10.37493/2308-4758.2021.2.7 (in Russian).
368. Khuchunaev B.M., Gekkieva S.O., Budaev A.KH. Methods for determining the ice-forming effectiveness of anti-hail products in laboratory facilities. Science. Innovation. Technology. 2021. No. 3, pp. 105–118. DOI: 10.37493/2308-4758.2021.3.7 (in Russian).
369. Khuchunaev B.M., Gekkieva S.O., Budaev A.KH. Laboratory studies of the influence of the electric field strength on the specific charge on the particles of the reagent formed during the sublimation of pyrotechnic compositions. Science. Innovation. Technology. 2021. No. 4, pp. 209–226. DOI: 10.37493/2308-4758.2021.4.12 (in Russian).
370. Shilin, A.G., Shilina, A.S., Andreev, Y.V. et al. Investigation of Adsorption Modes of Molecular Iodine and a Possibility of Modifying Ice-forming Characteristics of Silicate and Aluminosilicate Aerosol with Iodine Compounds. Russ. Meteorol. Hydrol. 47, 542–547 (2022). https://doi.org/10.3103/S1068373922070081.
371. Sin'kevich A.A., Boe B., Michailovsky Yu. P., Bogdanov E.V. Electrification changes within cumulus due to airborne seeding with glaciogenic reagent. Proceedings of MGO. 2020. No. 596, pp.131–147 (in Russian).
372. Sin'kevich A.A., Mikhailovskii Y.P., Kurov A.B., Boe B., Pawar S., Gopalakrishnan V. Investigation of radar and electrical characteristics of thunderclouds seeded with a glaciogenic reagent in Karnataka, India. Russian Meteorology and Hydrology. 2021. V. 46. No. 8, P. 545–552. DOI: 10.3103/S1068373921080069.
373. Bychkov, A.A., Petrunin, A.M., Chastukhin, A.V. et al. Prospects of Using Ground-based Generators in Cloud Seeding. Russ. Meteorol. Hydrol. 47, 535–541 (2022). https://doi.org/10.3103/S106837392207007X.
374. Beryulev G.P., Danelyan B.G. Precipitation enhancement: the results of studies and operational activities Russian Meteorology and Hydrology. 2021. V. 46. No 9, P. 579–587. DOI: 10.3103/S106837392109003X.
375. Kovalev N.A., Netyagin O.V., Sazhin I.V. Experience of rainmaking to extinguish wildfires in siberia and the Far East in 2017-2021: preliminary results and

performance assessment issues. Meteorology and Hydrology. 2022. No.7, pp. 71–77. Aerial Forest Protection Service (Avialesookhrana) DOI: 10.52002/0130-2906-2022-7-71-77.
376. Abshaev, M.T., Abshaev, A.M., Malkarova, A.M. et al. Hail Suppression to Protect Crops in the North Caucasus. Russ. Meteorol. Hydrol. 47, 487–498 (2022). https://doi.org/10.3103/S1068373922070019.
377. Liev K.B., Kushchev S.A. Analysis of economic efficiency of anti-hail work in the Russian Federation. Proceedings of MGO. 2021. No. 602, pp. 124–133. (in Russian).
378. Potapov E.I., Zasavitskii E.A. Variability of Summer and Autumn Total Precipitation in the Area of Long-term Hail Suppression Activities in the Republic of Moldova // Russian Meteorology and Hydrology. – 2019. – Vol. 44, No. 8. – P. 555–563. – DOI 10.3103/S1068373919080077.
379. Beituganov M.N., Chochaev KH.KH. Prevention and interruption of hail by the combined method "reagent plus artificially initiated lightning". Proceedings of Mozhaisky Academy. 2022. No. 685, pp. 19–26 (in Russian).
380. Shilin, A.G., Khuchunaev, B.M. Features of Ice-forming Aerosol Generation during the Combustion of Pyrotechnic Composition in the Path of the De Laval Nozzle. Russ. Meteorol. Hydrol. 47, 548–552 (2022). https://doi.org/10.3103/S1068373922070093.
381. Mikhailovsky Yu. P., Sinkevich A.A., Boe B., Abshaev A.M., Toropova M.L. On methods of influencing electrical processes in clouds. Proceedings of MGO. 2021. No. 602, pp. 6–22. (in Russian).
382. Alita S.L., Borisova N.A. The development of the concept of using mobile stations of impact on hail processes. Proceedings of MGO. 2020. No. 599, pp. 151–181. (in Russian).
383. Zharashuev M.V. Opportunities for optimizing the order of radar observations during anti-hail operations. Proceedings of MGO. 2022. No. 605, cc. 164-172. (in Russian).
384. Kuznetsov A.D., Kryukova S.V., Simakina T.E. Modeling size of hydrometeors at artificial cloud modification. Proceedings of MGO. 2019. No. 595, pp. 132–144. (in Russian).
385. Adzhiev, A.K., Dokukin, M.D., Kondrat'eva, N.V. et al. Active Avalanche Control: Results of Research and Operational Activities. Russ. Meteorol. Hydrol. 47, 576–581 (2022). https://doi.org/10.3103/S1068373922080027.
386. Chernous, P.A. Experience of Artificial Avalanche Release: Problems and Prospects. Russ. Meteorol. Hydrol. 47, 582–589 (2022). https://doi.org/10.3103/S1068373922080039.
387. Bobrova D.A., Kazakova E.N.The history of avalanche research on Sakhalin Island. Meteorology and Hydrology. 2022. No. 8, pp. 112–119. DOI: 10.52002/0130-2906-2022-8-112-119 (in Russian).
388. Bolgov, Y.V. Mathematical Modeling of Snow Avalanche Dynamics Using Cellular Automata. Russ. Meteorol. Hydrol. 47, 590–595 (2022). https://doi.org/10.3103/S1068373922080040.
389. Danelyan B.G., Bankova N.Yu., Khizhnyak A., Lomakin I.V. Analysis of the frequency of days with fogs at large airports in the south of Russia for planning and deployment of work on active actions (fog dissipation, precipitation regulation). Proceedings of International Scientific Conference "Problems of Atmospheric Physics, Climatology and Environmental Monitoring" NCFU, Nalchik, 08–10 of Sept. 2021г. pp. 298–302. (in Russian).

390. Bazzaev T.V., Vladimirov C.A., Kochetov N.M., Sosnikova E.V. Khizhnyak A. A method for enlarging particles of hygroscopic reagents generated by pyrotechnic products for the tasks of scattering warm fogs. Proceedings of International Scientific Conference "Problems of Atmospheric Physics, Climatology and Environmental Monitoring" NCFU, Stavropol, 08–10 of Sept. 2021г. pp. 302–308. (in Russian).
391. Khizhnyak A., Bankova N.Yu., Bazzaev T.V., Pozdeev V.N. Basic provisions in the development of an automated system for dispersing supercooled fogs using refrigerants (liquid nitrogen, liquid carbon dioxide). Proceedings of International Scientific Conference "Problems of Atmospheric Physics, Climatology and Environmental Monitoring" NCFU, Stavropol, 08–10 of Sept. 2021г. pp. 313–318. (in Russian).
392. Alekseeva, A.V., Davydov, V.E., Zinkina, M.D. et al. A Laboratory Experiment to Study Ion Wind Effects on the Warm Fog in an Enclosed Volume. Russ. Meteorol. Hydrol. 47, 637–640 (2022). https://doi.org/10.3103/S10683 73922080106.
393. Mostandi S., Predybaylo E., Jsipov E., Zolina O., Gulev S., Parajuli S., Stenchikov G. Sea Breeze Geoengineering to Increase Rainfall over the Arabian Red Sea Coastal Plains. Journal of Hydrometeorology. AMS. 01.01.2022. Vol. 23. Issue 1. P. 3–24. https://journals.ametsoc.org/view/journals/hydr/23/1/JHM-D-20-0266.1.xml.
394. Abshaev M.T., Zakinyan R.G., Abshaev Ali M., Zakinyan A.R., Ryzhkov R.D., Wehbe Y., Al Mandous A. Atmospheric conditions favorable for the creation of artificial clouds by a jet saturated with hygroscopic aerosol. Atmospheric Research. 2022. Vol. 277, 15 October, 106323 https://doi.org/10.1016/j.atmosres. 2022.106323.
395. Flossmann A.I., Manton M., Abshaev A., Bruintjes R., Murakami M., Prabhakaran T. Yao Z. Review of Advances in Precipitation Enhancement Research. Bulletin of the American Meteorological Society. 01 Aug 2019? pp. 1465–1480 DOI: https://doi.org/10.1175/BAMS-D-18-0160.1.
396. Liang H., Abshaev M.T., Abshaev A.M., Huchunaev B.M., Griffiths S., Zou L. Water vapor harvesting nanostructures through bioinspired gradient-driven mechanism. Chemical Physics Letters. Volume 728, August 2019, pp. 167–173. https://doi.org/10.1016/j.cplett.2019.05.008.
397. Abshaev M.T., Abshaev Ali M., Zakinyan R.G. Arthur R. Zakinyan, Youssef Wehbe, Latifa Yousef , Sufian Farrah, Abdulla Al Mandous Investigating the feasibility of artificial convective cloud creation. Atmospheric Research. Volume 243, 1 October 2020, 104998 https://doi.org/10.1016/j.atmosres. 2020.104998.
398. Abshaev M.T., Abshaev A.M., Aksenov A.A., Fisher I.V., Shchelyaev A.E., Al Mandous A., Wehbe Y. & El-Khazali R. CFD simulation of updrafts initiated by a vertically directed jet fed by the heat of water vapor condensation. Scientific Reports. Volume 12, Article number: 9356 (2022) Published: 07 June 2022.

Dynamic Meteorology

I.A. Repina
A.M. Obukhov Institute of Atmospheric Physics RAS
repina@ifaran.ru

Introduction

Scientific work in the field of dynamical meteorology, which has been carried out by the Russian researchers in 2019–2022 and will be discussed in this review can conditionally be related to the following topics: “General dynamics of the atmosphere”, “Large-scale processes and the weather forecast”, “Mesoscale processes”, “Small-scale motions and turbulence in the atmospheric boundary layer”, “Dynamical interaction between lower, middle and high atmosphere”, “Mathematical problems of climate and ecology”. The review structure follows basically the previous review report over 2015–2018 (Kurgansky and Krupchatnikov, 2019).

General dynamics of the atmosphere

Regular all-Russian conference with international participation “Turbulence, atmosphere and climate dynamics”, dedicated to the memory of Academician A.M. Obukhov, took place twice from in November 2020 and 2022. The conference discussed key issues related to one of the most relevant areas in the Earth sciences, namely the research in the field of atmospheric physics, climate and environment. Selected papers from the conference were published in the collection (Turbulence, Atmospheric and Climate Dynamics, 2022). Among the Russian conferences devoted to the dynamics of the atmosphere, it is also worth noting the annual conferences ENVIROMIS and International Symposium "Atmospheric and Ocean Optics. Atmospheric Physics". Symposium "Atmospheric and Ocean Optics. Atmospheric Physics" The conference is held annually in Moscow or Tomsk in the following areas: Molecular Spectroscopy and Atmospheric Radiation Processes, Optical Radiation Propagation in the Atmosphere and Ocean, Optical Investigation of Atmosphere and Ocean, Physics of the troposphere, Physics of the middle and upper atmosphere (Romanovski, Kharchenko, 2022). The multidisciplinary Conference ENVIROMIS (even years in Tomsk, odd years (CITIC) in Moscow) comprising elements of Early Career Scientists School devoted to the state-of-the-art and usage of modern environmental observation techniques, computational and information technologies for assessment, modeling and mitigation of Northern Eurasia environment variations under natural and anthropogenic pressures including those caused by the Global Climate

Change. It is aimed at filling the gap between basic science achievements and their practical applications in this domain. It also addresses a critically important issue –facilitation of professional skill growth of young scientists. To this end a number of invited lectures devoted to the state-of-the-art in the environmental research will be presented by leading specialists, which will allow young participants to get first-hand information on hot topics in Earth System Sciences and attract them professionally to this very important research area (Gordov et al., 2020).

During the reporting period, several monographs were published that relate to the dynamics of the atmosphere.

In this book G.S. Golitsyn (Golitsyn, 2021), on the basis of Kolmogorov's theory, earthquakes with their similarity parameter, the spectra of sea wind waves, the energy spectrum of cosmic rays are considered, the nature of the reliefs of the surfaces of celestial bodies (Kaula's rule) is explained, the nature of hurricanes and similar eddies is explained with an estimate of their power, the laws of flooding by precipitation of the earth surface, the derivation of the basic laws of convection, including in a rotating fluid, is given. These patterns remained empirical for decades, but the use of the laws of probability theory elevates them to the rank of laws of nature.

The principal focus of this book (Polonsky, 2019) is the physical processes in the World Ocean which regulate the interannual-to-multidecadal natural variability of the climate system, and some key atmospheric and marine manifestations of this variability. It analyses a number of Atlantic and Indo-Pacific signals and describes their regional atmospheric and marine manifestations. The role of the Ocean in the recent hiatus of global warming and the probability of abrupt climate change due to thermohaline catastrophe are also assessed. The book pays special attention to the change of parameters of synoptic atmospheric disturbances over the Northern Hemisphere and its subregions in different phases of the natural quasi-periodical climatic signals.

The book Arctic Climate: processes and changes (ed. Mokhov and Semenov, 2022) presents the results of research into the climate of the Arctic, carried out at the Institute of Atmospheric Physics RAS in cooperation with other scientific institutions and organizations. The first part presents the results of the analysis of empirical data for various components of the Arctic climate system: the atmosphere, sea ice, ocean and land, with an assessment of current trends in change. The second part considers the characteristic processes and feedbacks in the Arctic climate system that are important for the formation of long-term climate anomalies in the Arctic, as well as the mechanisms of the impact of climate change in the Arctic on atmospheric circulation in the middle latitudes of the Northern Hemisphere. The third part presents estimate of possible future climate changes in the Arctic based on the results of numerical calculations with climate models under scenarios of an-

thropogenic impact, as well as the impact of these changes on the duration of maritime navigation along the Northern Sea Route, sea waves, characteristics of permafrost soils, and decay of near-bottom methane hydrates.

The book “Study of the natural environment of the high-latitude Arctic on the research station Ice Base Cape Baranova" (Ed. Makshtas, and Sokolov) is devoted to studies of the natural environment of the Bolshevik Island of the Severnaya Zemlya archipelago and the adjacent waters of the Shokalsky Strait, resumed in 2013 at the research station "Ice base Cape Baranov" of the Arctic and Antarctic Research Institute of Roshydromet. The results of meteorological, radiation, aerological, geophysical observations, measurement data of greenhouse gases and aerosol concentrations, results of studying the chemical composition of sediments, data of oceanographic observations in the Shokalsky Strait, results of studies of the morphological and physical and mechanical properties of fast ice, including a description of the technology for observing the characteristics of the ice cover are presented. The results of hydrological, glaciological, and paleogeographic studies on the territory of Bolshevik Island adjacent to the station are presented. The book is intended to show the state of the natural environment of this high-latitude region in the rapidly changing climate of the Arctic.

The book The Republic of Adygea Environment (ed. Bedanokov, Lebedev, Kostianoy, 2022) outlines the current status of the environment in the Republic of Adygea in Russia. The book assesses the environmental conditions, ecological state, climate and vegetation change, anthropogenic loads to soil, water and atmosphere as well as highlighting the potential of water resources, renewable energy and development of tourism, agriculture and industry in this region. It also presents the mechanisms of legal, ecological and economic regulation and environmental insurance in the Republic of Adygea. This book introduces the Republic of Adygea to readers who are not familiar with the Republic and its beautiful landscapes, history and people. It offers a valuable source of information for a broad readership, from students and scientists interested in environmental sciences, to policymakers and practitioners working in the fields of environmental policy and management.

The atmospheric dynamics of the polar regions traditionally attracts the attention of researchers.

Monthly mean data of the ERA-Interim reanalysis (1979–2014) are used to estimate the lapse rate g in the Northern Hemisphere high-latitude troposphere (Akperov et al., 2019. The relationship between the lapse rate and surface air temperature Ts is analyzed in terms of interannual variability for different seasons. The study analyzes the ability of the HIRHAM5 regional climate model to simulate the features of lapse rate distribution in the Arctic troposphere and the parameter of its sensitivity to the variation in surface air temperature dg/dTs that were derived from reanalysis data. The regional fea-

tures of the link between the vertical stratification of tropospheric temperature and the Arctic Oscillation are revealed. The estimates obtained from reanalysis data and model simulations are especially significant as the Arctic climate has higher variability and sensitivity under global changes that is characterized by so called Arctic amplification.

The influence of the oceanic heat inflow into the Barents Sea on the sea ice concentration and atmospheric characteristics, including the atmospheric static stability during winter months, is investigated on the basis of the results of ensemble simulations with the regional climate model HIRHAM/NAOSIM for the Arctic (Akperov et al., 2019). The staticstability of the atmosphere is the important indicator of the spatial and temporal variability of polar mesocyclones in the Arctic region. The results of the HIRHAM/NAOSIM regional climate model ensemble simulations (RCM) for the period from 1979 to 2016 were used for the analysis. The initial and lateral boundary conditions for RCM in the atmosphere were set in accordance with the ERA-Interim reanalysis data. An analysis of 10 ensemble simulations with identical boundary conditions and the same radiation forcing for the Arctic was performed. Various realizations of ensemble simulations with RCM were obtained by changing the initial conditions for integrating the oceanic block of the model. Different realizations of ensemble simulations with RCM are obtained by changing the initial conditions of the model oceanic block integration. The composites method was used for the analysis, i.e. the difference between the mean values for years with the maximum and minimum inflow of oceanic water into the Barents Sea. The statistical significance of the results (at a significance level of $p < 0.05$) was estimated using Student's t-test. In general, the regional climate model reproduces the seasonal changes in the inflow of the oceanic water and heat into the Barents Sea reasonably well. There is a strong relationship between the changes in the oceanic water and ocean heat inflow, sea ice concentration, and surface air temperature in the Barents Sea. Herewith, the increase in the oceanic water inflow into the Barents Sea in winter leads to a decrease in static stability, which contributes to changes in regional cyclonic activity. The decrease of the static stability is most pronounced in the southern part of the Barents Sea and also to the west of Svalbard.

A global analysis of geographical features of vertical profiles of specific air humidity and concentrations of sulfur dioxide and sulfate aerosols is carried out based on the CAMS reanalysis data, as well as the height of the planetary boundary layer (PBL) based on the ERA5 reanalysis data for 2003–2020 (Eliseev et al., 2022). The scale height HY, i.e., the height at which the concentration of the substance Y decreases by a factor of e, is used as a characteristic of the aforesaid profiles. The maximal heights of the upper PBL boundary are observed in regions of the prevailing cyclonic gyre – in storm

tracks and in regions of monsoonal circulation in summer. For the vertical scale of the specific humidity profile, minima are identified in the regions of the subtropical gyre with prevailing large-scale subsidence of air masses. The scale height of SO2 is characterized by spatial minima associated with oxidation of this substance. For HSO4, a spatial minimum over the ocean near southeast Asia is found. A statistically significant negative correlation between the PBL thickness and the vertical scale of the specific humidity profile in humid regions of the tropics is revealed, as well as a positive correlation between scale heights of sulfur dioxide and sulfates, most significantly manifested in regions with acute pollution of the lower troposphere by these substances.

The response of Northern Hemisphere storm tracks (North Atlantic and North Pacific) to climate change and to the strengthening and weakening of the stratospheric polar vortex is investigated in simulations of the Institute of Numerical Mathematics of the Russian Academy of Sciences Climate Model version 5 (INM-CM5) under phase 6 of the Coupled Model Intercomparison Project for the moderate (SSP2-4.5) and severe (SSP5-8.5) greenhouse gas emission scenarios (2015–2100) (Martynova et al., 2022). A significant northward shift of both storm tracks and some strengthening of the North Pacific and weakening of the North Atlantic storm track are expected by the late 21st century under SSP2-4.5. In SSP5-85, the response of both storm tracks manifests itself mainly through amplification and, to a lesser extent, through a poleward. Moreover, there is a difference in the response of the North Pacific and North Atlantic storm tracks to the strengthening and weakening of the stratospheric polar vortex under different climate conditions. Changes in the storm tracks associated with eddy moisture flux demonstrate a character comparable to changes in their intensity, both due to an increase in greenhouse gas concentrations and due to changes in the stratospheric polar vortex.

In paper (Makhotina et al., 2021) the results of an analysis of ceilometer measurements at North Pole (NP) drifting station 37, 39, and 40 were presented. The frequencies of the total cloud amount (in tenth) and the cloud base heights (CBHs) are calculated for the period of the polar night. A comparison of the cloud-cover scores according to the ceilometer data with the visual observation data showed good agreement. However, the value of the correlation coefficient depends on the interpretation of the ceilometer data. In general, a bimodal distribution of the cloudcover scores with the highest frequency of clear sky and overcast clouds are characteristic for indicated stations. The analysis of the frequency of the CBH showed that the most characteristic CBHs are below 600 m. In November, cloud heights in the range of 1000–2000 m are also observed, while their frequency decreases during the winter. Cloudiness during the polar night is characterized by a strong positive

radiative forcing, which has a warming effect on the surface temperature of ice and air. However, cloud radiative forcing, as well as the cloudiness frequency and its effect on the temperature regime, varies significantly from station to station. These differences may become the subject of further research on the interrelation of cloud characteristics with other processes in the Arctic climate system. These statistical estimates significantly supplement the available data on the cloud cover of the Central Arctic.

The North Atlantic is one of the key regions, where low-frequency climate variability is formed. However, despite numerous studies related to this topic, some issues still remain unsolved. One of them is the ambiguous cross-correlation of the North Atlantic Sea surface temperature (SST) and the intensity of Atlantic Meridional Overturning Circulation (AMOC). A widely accepted concept suggests that the long-term climate variability is a result of the atmospheric stochastic forcing transformed by the inertial ocean. Existence of negative and positive feedback mechanisms suggests that the long-term North Atlantic dynamics may be considered as a damped stochastically forced oscillator in which both SST and AMOC are the elements of the same process. In the study (Bekryaev et al., 2019) the cross-correlation functions of the main North Atlantic climatic indexes derived from a simple box-like stochastic model were analyzed. The random forcing simulates the air-sea interface heat fluxes and excites both the SST and the AMOC. Stochastic excitation of the meridional circulation implies the leading AMOC and stochastic forcing of SST implies the leading Atlantic Multidecadal Oscillation (AMO). Connection of the AMOC and AMO indexes depends on the principal oceanic feedbacks and the dissipation intensity.

Forming of the North Atlantic multidecadal variability (MDV) remains quite enigmatic. Some studies connect the long-term North Atlantic oceanic variability to transform of the stochastic atmospheric forcing. On the other hand, the intense heat fluxes directed from ocean to atmosphere precede the large-scale positive sea surface temperature (SST) anomalies in the region (and vice versa). The last phenomenon puts some doubts on the stochastic theory and let to suggest that surface heat fluxes play just a passive role as a response to ocean dynamical processes. Analyzing a toy box model and CMIP5 control experiments Bekryaev (2019) demonstrated that observed phase shifts between SST and surface heat fluxes do not contradict a stochastic theory. The North Atlantic long-term variability can be induced via a transform of the atmospheric random forcing. However, the role of the ocean circulation processes remains crucial for the MDV forming. Specifically, the stochastic excitation of the meridional overturning circulation reproduces observed and model generated MDV. Direct atmospheric impact on SST cannot induce correctly the phase shift between input and output signals.

In paper (Bekryaev, 2022) statistical aspects of the quantitative estimation of the climate change polar amplification (PA) are considered. A theoretical study is provided of the distribution density for the PA sample coefficient defined as the ratio of the linear trend coefficients of spatially averaged surface air temperature. It is shown that heavy tails of the distribution lead to instability of the PA sample estimates. A statistically valid quantification of the PA can be obtained from the results of the ensemble modeling of climate change based on the Fieller's method. The applicability of the method in the case of a non-stationary climate system response to external forcing is considered.

Quantitative estimates of changes in wind energy resources in the Arctic were obtained using the RCA4 regional climate model under the RCP4.5 and RCP8.5 climate change scenarios for 2006-2099 (Akperov et al., 2022). The wind power density proportional to cubic wind speed was analyzed. The procedure for the model near-surface wind speed bias correction using ERA5 data as a reference with subsequent extrapolation of wind speed to the turbine height was applied to estimate the wind power density (WPD). According to the RCA4 simulations for the 21st century under both anthropogenic forcing scenarios, a noticeable increase in the WPD was noted, in particular, over the Barents, Kara, and Chukchi seas in winter. In summer, a general increase in the WPD is manifested over the Arctic Ocean. The changes are more significant under the RCP8.5 scenario with high anthropogenic forcing for the 21st century. According to model projections, an increase in the interdaily WPD variations does not generally lead to the deviations of wind speed to the values at which the operation of wind generators is unfeasible.

The paper (Demichev et al., 2020) presents the results of verification of the surface air temperature values of the ERA-Interim and ERA-5 reanalyses based on data obtained from drifting buoys, ground-based weather stations, and also, for the first time, according to measurements made at the North Pole drifting stations. The latter were not assimilated in any of the considered reanalyses, which provides a rare opportunity for independent validation. Based on the results of comparison with the SP data, it was found that the average errors for the cold season in the Arctic Basin are: 2.25 °C for ERA-I and 3.92 °C for ERA5. Comparison with data from drifting buoys allows us to make an assumption about the reason for such large errors in the reanalyses. Part of the buoys was installed from the air by dropping onto the ice from the aircraft. At the same time, the temperature sensor of the buoy was, with a high degree of probability, buried in the snow cover, which shielded it from the cold atmosphere and contributed to heating due to the heat flow from the underlying layer of sea water. The assimilation of such data is likely to lead to an overestimation of air temperature over drifting ice by reanalyses. Based on the numerical simulation of water circulation in the Sea of Okhotsk

in 1986 to 2015, the impact of deep cyclones on the circulation off the northeastern coast of Sakhalin is studied (Diansky et al., 2022). The circulation in the Sea of Okhotsk is simulated with the COSMO-Ru-INMOM-CICE model configuration, where the COSMO-Ru and INMOM resolve explicitly the mesoscale atmosphere and ocean dynamics and the CICE resolves the ice cover evolution. The extreme atmospheric events associated with the intensive cyclone activity over the Sea of Okhotsk during the cold season are classified. It is found that high velocity is typical of the cyclones coming to the sea from Sakhalin, and wind speed on the periphery is higher for the cyclones coming to the Sea of Okhotsk from the south and southwest. The analysis of water circulation response off the northeastern coast of Sakhalin demonstrates that the meridional current velocity on the shelf increased by several times from the sea surface to the bottom for all types of cyclones. On the edge of the shelf, southern currents intensified in the surface and bottom layers during the passage of cyclones and at the intermediate depths during the passage of fronts. On the continental slope, southern currents intensified in the surface, intermediate, and bottom layers depending on the type of extreme events.

In papers (Ingel, Makosko 2021 a,b) a theoretical problem on linear stationary disturbances introduced by spatial inhomogeneities of gravity field into the background geostrophic flow of the stratified rotating medium (atmosphere) is considered. For the first time, the three-dimensional analytical model is considered (Ingel, Makosko 2021 a). The results imply that inhomogeneities of the gravity field can lead to ordered perturbations of the velocity field of atmospheric currents in large areas. Three-dimensional model allows us to understand and analyse some of the simplest mechanisms and patterns of generation of such disturbances and to make some estimates. The amplitude of the disturbances for the velocity horizontal components can reach values of the order of buoyancy frequency multiplied by the amplitude of deviations of the geoid. This result agrees with the estimates obtained previously for a substantially different disturbances mechanism caused by gravity field inhomogeneities. The heterogeneities of the gravity field (HGF) deform the fields of air pressure, density, and temperature and affect the temperature regime of the boundary layer of the atmosphere, as well as the heat exchange between the air and the underlying surface. The work (Ingel, Makosko 2021b) considers a stationary analytical model intended for estimation of the amplitudes of these effects, which resulted in analytical expressions for profiles of temperature disturbances and amplitudes of deviations of the vertical heat fluxes on the surfaces. Besides the amplitudes of the HGF, the latter most strongly depend on the ambient background stratification. In highly anomalous regions, the amplitudes of deviations of heat fluxes can reach and exceed 1 W/m^2, which gives grounds to take into account the HGF in climate calculations and numerical models of the atmosphere.

Particular attention is paid to satellite methods for studying atmospheric processes. In paper (Sterlyadkin et al., 2022), based on a new method of satellite radiothermovision, which allows, based on the analysis of the reconstructed dynamics of precipitable water vapor (PWV) fields, calculating water vapor fluxes over the oceans, the accuracy of reconstructing PWV fields over land in the Amur River catchment area is estimated. The estimates make it possible to calculate the balance of atmospheric water over a selected area: the water vapor stored above the surface, the amount of water that entered or exited through the boundaries of the catchment area, and to determine the amount of precipitation for any selected time interval. The relative error of such measurements depends not only on the measurement errors of water vapor and the accuracy of radio thermal imaging methods in restoring the field of horizontal flows of atmospheric moisture, but also on the size of the river basin, the intensity and duration of precipitation. For example, for a territory that makes 20 % of the Amur basin with an average amount of precipitation of 60 mm for 10 days, the relative error of the proposed radiometric method for measuring precipitation, according to our estimates, will be about 22 %. Methods are proposed for checking the accuracy of the developed method by comparing it with data from ground-based radiosonde measurements, ground-based meteorological stations that measure the amount of precipitation, and data from ground-based meteorological radars. The analysis performed shows that it is quite possible to determine the amount of precipitation over the territory of the basin of large rivers based on multichannel radiometric microwave measurements from space.

The atmospheric advection of water vapor is one of the most important components of the planetary hydrological cycle. Radiosondes are a means for regular observations of water vapor fluxes. However, their data are sparse in space and time. A more complete picture is provided by reanalysis assimilating these data. However, a statistically representative check of the reanalysis estimates of the water vapor fluxes far from regularly operating weather stations is difficult. The previously proposed and developed method of satellite radiothermovision makes it possible to reconstruct the vertically integrated advective water vapor fluxes from satellite microwave radiometry. In paper (Ermakov et al., 2021), for the first time, the results of direct comparisons of long (5 year) time series of zonal vertically integrated daily water vapor fluxes based on the data of radiosondes, reanalysis, and satellite radiothermovision are performed and presented. It is shown that all the data series are statistically reliably correlated (at a confidence level of 0.995). The regression factor between the fluxes from reanalysis and satellite radiothermovision was close to 1, but with a noticeable bias (the latter were about 60 kg/(m·s) less on average). Grounds are given for the hypothesis that calculations based on satellite radiothermovision mainly characterize water vapor fluxes in the

lower troposphere (up to heights of about 4 km). Its verification, as well as the analysis of the noted cases of violation of the correlation between the fluxes from satellite radiothermovision and reanalysis, requires further research.

In paper (Ermakov et al., 2019) an algorithm is presented for constructing global ocean– atmosphere radiothermal fields with high spatiotemporal sampling by satellite microwave measurements. Attention is focused on the construction of the daily reference images of high spatial resolution. The construction of such reference maps is an important preparatory step for the further application of the earlier proposed and implemented technique of the authors of spatiotemporal interpolation. The software, which implements the described algorithm, makes it possible to obtain global animated radiothermal fields with a time step of 1.5 h and spatial resolution of 0.2°. These parameters are essential for an analysis of complex, fast, and energyintensive processes occurring in the ocean–atmosphere system, such as the formation and evolution of tropical cyclones.

A number of articles discussed the theoretical issues of atmospheric dynamics.

An analytical approach to the determination of optimal disturbances is developed (Kalashnik, Chkhetiani, 2020a). The approach, suitable for flows with piecewise-constant vorticity distributions, is based on the equation of disturbance energy balance and explicit expressions for the growth rate of the energy or the final-to-initial energy ratio. The corresponding expressions are functions of the initial parameters and the optimal disturbance parameters are determined from an extremization of these functions. Within the framework of the approach the classical Rayleigh problem of the free shear layer instability and the problem of the instability of a system consisting of two counterstreaming jet flows in a rotating shallow water layer are considered. The parameters of the optimal disturbances are compared with those of growing normal modes. Baroclinic instability of a flow with a constant vertical shear in a zonal channel has been studied (Kalashnik, Chkhetiani, 2020b). The maximally truncated SQG model was used to describe the dynamics of flow disturbances. A dynamic system describing nonlinear interactions between unstable counterpropagating Rossby waves with one zonal wave number and a neutral mode independent of zonal coordinate has been formulated within the framework of this model. Both analytical and numerical solutions of the system show that exponentially increasing disturbances at the linear stage of instability development give way to nonlinear oscillations (vacillations). The occurrence of such oscillations is caused by the law of conservation of surface potential energy. According to numerical estimates, the period of oscillations is of the order of a month, which is in agreement with measurement data obtained for the winter atmosphere.

As an index of interannual climatic variability of the atmosphere, it is proposed to calculate the weighted average over the hemisphere area (to the pole from latitude 20°) of the vertical helicity flux across the upper boundary of the planetary boundary layer, which is determined by the product of the Coriolis parameter and the square of the wind speed at this boundary (Kurgansky et al., 2020). In practical calculations, the data of reanalyses ERA-Interim and ERA-20C on the wind speed at the isobaric level of 850 hPa were used. The statistical distribution of the Earth's surface area on the helicity flux values, as well as the informational entropy of this distribution, are calculated. It is shown that the introduced index usefully characterizes the interannual climate variability of the atmosphere in both hemispheres.

In the paper (Kalashnik et al., 2021) new vertically discrete versions of the surface quasigeostrophic (SQG) model with two boundaries are formulated. For any number of partition levels, the equations of the discrete model are written in the form of conservation laws for two Lagrangian invariants, which have the meaning of buoyancy distributions at the horizontal boundaries of the fluid layer. The values of the invariants are expressed in terms of the values of the stream function at two internal levels and contain higher order elliptic operators. The use of discrete models greatly simplifies the solution of problems of the linear theory of hydrodynamic stability and provides high accuracy even with a small number of vertical discrete levels. Using the two-level version of the SQG model, which is similar to the classical two–layer Phillips model, we investigated the linear stability of jet flows induced by piecewise constant boundary distributions of buoyancy. For these flows, analytical expressions for the growth rate of perturbations have been obtained and it is shown that the most unstable perturbation has a wavelength of the order of the Rossby baroclinic radius of deformation. Flows with vertical shear induced by smooth and slowly varying boundary buoyancy distributions are also considered. The instability of these flows is found to be absolute, that is, independent of the velocity profile horizontal structure.

The possible existence of distinct regimes of barotropic circulation in closed annular channels at the same external parameters governing the flow dynamics is investigated both experimentally and numerically (Gledzer et al., 2021). Transitions between the regimes are realized by means of varying the value of the main parameter determining the velocity field energy (for example, the current controlling the Ampere force in the case of MHD generation of a velocity field) with subsequent reconstruction of the former parameter value. Depending on the channel rotation period or the configurations of magnet locations in the case of MHD generation or sources and sinks in numerical experiments the following results are possible. (1) The initial and final regimes differ quantitavely in the number of cyclonic or anticyclonic vortices generated. (2) The number of vortex formations does not change but

their localization in space, for example, the angular coordinates of their centers, varies. (3) After the change and reconstruction of the original value of the governing parameter the flow returns to the regime almost undistinguishable from the original regime. The flow patterns and the corresponding diagrams for laboratory experiments and numerical simulations based on shallow water equations are presented.

The paper (Kalashnik, 2019) investigates the stability of a jet flow with a piecewise linear velocity profile in a rotating stratified atmosphere. The linearized set of perturbation equations is reduced to one longitudinal-velocity amplitude equation with turning points. An asymptotic solution of the equation, valid at small Rossby numbers, is derived in terms of the Airy functions. A flow that is stable in a quasi-geostrophic approximation is shown to become unstable due to the emission of inertia–gravity waves. An analytic expression for the growth increment of the perturbations is derived.

Baroclinic instability is that of flows in a rotating stratified fluid with a vertical velocity shear. The generation of large-scale vortical flows in the atmospheres of Earth and other planets is associated with this instability (Kalashnik et al., 2022). The review presents modern theoretical approaches dealing with this instability. They include a description of baroclinic instability through the interaction of edge Rossby waves, the study of the problem of optimal perturbations, i.e., those characterized by the largest growth of energy or other functionals, and an analysis of the nonlinear dynamics of perturbations that relies on a low-mode approximation of the Galerkin method. Classical energy criteria for the stability of zonal flows obtained by the direct Lyapunov–Arnold method are also considered. The results presented may be of interest to specialists in the field of continuum mechanics and astrophysics.

In paper (Kalashnik, 2020) surface quasi-geostrophic (SQG) flows with a much larger horizontal scale than the Rossby radius of deformation are considered. A new version of the SQG model with two boundaries, which is reduced to a nonlinear system of partial differential equations, is proposed to describe the dynamics of such flows. This system describes the interaction between the barotropic and baroclinic components of the stream function and generalises the two-dimensional Euler equations for flows with a vertical velocity shear. The laws of conservation of both total and surface potential energies, which follow from this system, have been formulated. The solutions of a number of problems in the theory of baroclinic instability, which are in agreement with already known solutions, have been obtained within the framework of this system. It is shown that vertical shear flows are absolutely unstable, i.e. their instability is independent of the horizontal velocity profile structure. A generalised system of the SQG model equations, which additionally takes into account the β-effect and the Ekman bottom friction, has also been proposed. The transformation of jet flows due to the bottom friction and

the influence of the β-effect on the stability of shear flows have been studied based on this system.

Within the framework of SQG model with two levels, the hydrodynamic stability of a spatially periodic flow with sinusoidal velocity profile (Kolmogorov flow) is investigated. Such spatially quasi-periodic flows are often observed in the atmospheres of the giant planets and in the Southern Ocean (Kalashnik et al., 2022). To describe the dynamics of perturbations, the Galerkin method with three basis trigonometric functions was used. It provides a tool to study both the linear and nonlinear perturbation dynamics. Analytical expressions are obtained for the growth rates of perturbations in the linear theory of stability, and it is shown that the fastest growing perturbations have a wavelength on the order of the spatial period of the main flow. Using the Galerkin method, it is also shown that the exponential growth of perturbations at the linear stage of development is replaced by the stage of stable nonlinear oscillations. Such oscillations are analogous to the nonlinear fluctuations, or vacillations, found in R. Hide's laboratory experiments. In terms of elliptic integrals, an analytical expression for the period of nonlinear oscillations is obtained, and it is shown that for typical values of the parameters relevant to the Earth's atmosphere, the period of oscillations is about one month. The paper also proposes a long-wavelength version of the discrete SQG model, which describes the dynamics of perturbations with a horizontal scale much larger than the baroclinic Rossby radius of deformation. It is shown that the use of this version simplifies the study of stability and leads to asymptotically correct results. Within the framework of this model, the problems of linear and nonlinear stability of zonal spatially periodic flows are considered (Kalashnik et al., 2020). To study the linear stability of flows with one boundary, two approaches are used. In the first approach, the solution is sought by decomposing into a trigonometric series, and the growth rate of the perturbations is found from the characteristic equation containing an infinite continued fraction. In the second approach, few-mode Galerkin approximations of the solution are constructed. It is shown that both approaches lead to the same dependence of the growth increment on the wavenumber of perturbations. The existence of instability with a preferred horizontal scale on the order of the wavelength of the main flow follows from this dependence. A similar result is obtained within the framework of the SQG model with two horizontal boundaries. The Galerkin method with three basis trigonometric functions is also used to study the nonlinear dynamics of perturbations, described by a system of three nonlinear differential equations similar to that describing the motion of a symmetric top in classical mechanics. An analysis of the solutions of this system shows that the exponential growth of disturbances at the linear stage is replaced by a stage of stable nonlinear oscillations

(vacillations). The results of numerical integration of full nonlinear SQG equations confirm this analysis.

In paper (Kalashnik, Kulichkov, 2019) the problem of perturbations of the surface pressure caused by a moving nonstationary frontal heat source (localized along one horizontal coordinate) is considered. Pressure disturbances are associated with internal gravity waves (IGWs). It is shown that when a source moves in a finite-height atmospheric layer (atmospheric waveguide) when a discrete set of vertical IGW modes is excited, there are three types of temporal variation of surface pressure at a fixed observation point. These types correspond respectively to the time signal with amplitude modulation, the signal with frequency modulated Doppler type and the signal that occurs only after passing through the source. Each type is implemented for specific values of the oscillation frequency of the source and the Mach number (the ratio of the speed of the source to the phase velocity of the IGW). At Mach numbers less than one, an oscillating source always excites wave precursors disturbances observed before the source arrives. The movement of the source in a semi-infinite atmosphere leads to additional excitation of waves that transfer energy to the upper layers of the atmosphere.

The influence of the Ekman friction on the dynamics of zonal flows (ZFs) has been studied within the framework of a quasigeostrophic model of the atmosphere with two horizontal boundaries (the underlying surface and the tropopause) (Kalashnik, 2020). It is assumed that these flows have zero potential vorticity and are caused by specified buoyancy distributions at the boundaries. It is shown that, in the case of periodic distributions, the oppositely directed vertical velocity profile of ZFs transforms into a unidirectional profile with a maximum velocity at the upper boundary and zero velocity at the lower boundary. During this transformation, the velocity at the upper boundary increases; i.e., the upper tropospheric ZFs intensify due to the Ekman friction. A similar intensification occurs also in the case of initial distributions of buoyancy of the frontal type, which induce a system of two oppositely directed jet flows located in the upper and lower halves of the atmospheric layer. Due to the Ekman friction, the axial velocity of the lower flow drops to zero and the velocity of the upper flow, gradually covering the entire troposphere, doubles. The resulting flow is a jet pressed against the upper boundary, which may be considered a prototype of a western upper tropospheric jet flow. The important structural features of such a jet, which are established within the framework of a complete nongeostrophic model, are associated with horizontal jet asymmetry and the formation of fronts (discontinuity surfaces) adjacent to the upper boundary.

The hydrodynamic instability of a system of vertical motions initiated by spatially periodic distributions of heat sources is investigated (Kalashnik, Kurgansky 2020). The Galerkin method with three basis trigonometric func-

tions is used to describe the perturbation dynamics. The nonlinear system of equations for finding the expansion coefficients is formulated. It is found that the vertical motions are unstable in the absence of dissipation if the Richardson number is less than one eighth. A weakly nonlinear model of inviscid instability is developed. It is shown that the loss of stability in the presence of dissipation can lead to formation of either steady-state or timeoscillating secondary flow with nontrivial streamline topology.

The path equations are derived to describe the nonlinear evolution of thin jets generated by temperature fronts (Goncharov, 2021a). An approximate approach is based on the thermal rotating shallow-water model that accounts for the effect of the temperature gradient and uses the variational principle of least action. The dynamics of jets is shown to be effectively described by a nonlinear system of two (1+1)-dimensional partial differential equations. Particular solutions are found in the form of a steady-state meandering jet, a cusped jet, and a two-armed spiral.

A shallow-water model with horizontally nonuniform density is used to study the dynamics of jet flows that arise under the influence of buoyancy and the Coriolis force (Goncharov, 2021b). Within this approach, the jet is described by a self-similar compactly-localized solution and interpreted as a band of shear flow having a temperature contrast with the ambient fluid. In addition to stationary states, the dynamics of such jets admit cyclonic rotation with a constant angular velocity and transverse nonlinear pulsations. The phase portrait corresponding to this model shows that regimes with pulsating jets develop along closed trajectories bounded by the separatrix loop. The theory predicts that the period for warm jet pulsations is longer than the inertial oscillation period caused by the Earth's rotation, while for cold jet pulsations, it is shorter. Thus, only warm jets can have a noticeable effect on the atmospheric dynamics in the synoptic range. In particular, they may well be responsible for additional spectral peaks that appear in this range of wind speed fluctuations.

Laboratory experiments with a rotating cylindrical annulus are reported that reveal a prograde jet, which is adjacent to a (longitudinally) librating inner straight cylindrical wall (Kurgansky et al., 2020). Here, wall libration is realised as a time-harmonic modulation of the inner cylinder's rotation rate. The outer cylindrical wall and bottom and top lids rotate with constant angular velocity. The main purpose of this study is to contribute to a qualitative and quantitative understanding of nonlinearities that are present in oscillating, but centrifugally stable, vertical boundary layers frequently encountered in rotating wallbounded flows. A problem that is in a sense complementary to that of previous works that focused on oscillating Ekman layers but neglected the vertical Stokes−Stewartson layers was considered. A simple analytical model is proposed that is able to predict the magnitude and spatial

structure of the emerging prograde nearwall jet in terms of nonlinearity inherent in the inner cylinder's boundary layer dynamics.

Linear and non-linear inertial stability of a Kolmogorov flow in a rotating viscous fluid of uniform density is investigated using the method of continued fractions and the low-order Galerkin approximations (Kurgansky, 2021). A necessary condition for instability is the violation of the criterion of inviscid inertial stability, and the sufficient condition of instability is formulated in terms of the Reynolds criterion. The existence of stable secondary stationary regimes in the problem is shown, developing in a context of loss of stability of the main flow and having the form of rolls (cloud streets in the atmosphere) oriented along it. Stable density stratification is taken into account within the same low-order model framework when the direction of gravity coincides with the direction of rotation of the fluid. In this case, the necessary condition for the inertial instability of the main flow remains the same, but the critical Reynolds number for the instability depends on two additional dimensionless parameters that appear in the problem: the stratification parameter and the Prandtl number. The case of Prandtl numbers less than or equal to unity has been studied in greater detail, when there exists a secondary stationary regime, which may be unstable – in contrast to the case of a fluid that is uniform in density – and stable density stratification is a destabilizing factor.

The symmetric (inertial) parametric instability of time-periodic flows with a linear velocity profilehas been investigated, with a complete account for the Coriolis force in the problem (Kurgansky, 2022b). The possibility of instability is shown at velocity shears smaller than those indicated by the criterion of inertial stability of a stationary flow with the same velocity amplitude. The most significant results are obtained in the limit of weak density stratification of the medium, which is characteristic of well-mixed vertically convective layers of the atmosphere, in the deep layers of the ocean, and can also be directly related to a laboratory experiment.

The problem of the linear stability of the stratified Kolmogorov flow driven by a sinusoidal in space force in a viscous and diffusive Boussinesq fluid is re-visited using the Floquet theory, Galerkin approximations and the method of (generalized) continued fractions (Kurgansky, 2022c). Numerical and analytical arguments are provided in favor of a conjecture that an ideal stratified Kolmogorov flow is prone to short-wave instability for Richardson numbers markedly greater than the critical Richardson number Ri=¼ that appears in the Miles–Howard theorem. The short-wave instability of the stratified Kolmogorov flow is conjectured to be due to a resonance amplification of the Doppler-shifted internal gravity wave modes, in the presence of critical levels of the main flow that are ignored in the proof of the Miles–Howard theorem, but it is emphasized that the complete resolution of the above para-

dox is a task for future research. The inertial parametric instability of a time-dependent spatially periodic flow (Kolmogorov flow) of a rotating stratified Boussinesq fluid is studied, taking fully into account the Coriolis force in the problem and with the possibility that the flow has an arbitrary orientation in the horizontal plane ((Kurgansky, 2022d). The existence of instability is shown for velocity shears less than those indicated by the criterion of inertial stability of a steady flow with the same spatial period and velocity amplitude. In particular, the instability estimates are obtained for weakly stratified geophysical media, for example for the deep layers of the ocean, and it is suggested that the possible applications of the theory can also be directly related to a laboratory experiment. Two different theoretical scenarios of inclusion of the full Coriolis force account in the problem are considered, and in both cases this leads to a reduction in the degree of inertial instability of the basic flow.

In the paper (Zagumennyi, Chashechkin, 2019) flow structure and dynamics are studied numerically around a horizontal and tilted plate at transient vortex flow regime for both stratified and homogeneous fluids at various geometrical modifications of the leading and trailing edges and different tilt angles of the plate to horizon. The study is based on the high-accuracy and fineresolving numerical simulation of the fundamental system of equations which allows computing flows of both stratified and homogeneous viscous fluids in a single formulation. Unsteady patterns of vorticity, pressure and density gradient fields, as well as values of forces and torques acting on the plate surface, are analyzed at different tilt angles and values of radius of the plate's leading edge rounding and sharpness ratio of its trailing one. The calculated pressure field patterns consist of multiscale spotted structures with negative pressure which correspond to locations of vortex flow elements with spatial and temporal scales, geometrical features, manifestation level, and dissipation rate, being essentially dependent on tilt angle of the plate to horizon, geometrical modification of the its edges and fluid type, as well. A particular attention is paid to studying the flow fine structure around the leading edge of the plate, which is the most multiscale flow region where both large- and small-scale vortex elements are formed and interact actively with each other and with the free stream.

Wave and vortex fine structure of unsteady stratified flows were studied numerically based on the system of fundamental equations for non-homogeneous incompressible fluid with no-slip and no-flux boundary conditions, and experimentally using high-resolution Schlieren visualization techniques (Chashechkin, Zagumennyi, 2019). Different flow regimes, including creeping, wave and vortex ones, which are widespread in the ocean and atmosphere, were investigated in the single problem formulation, starting from the slowest diffusion-induced flows up to the fastest and unsteady ones. A

classification of flow components is proposed, which contains waves, vortices, and ligaments, which manifest themselves in the form of extended interfaces with their transverse scales being determined by the dissipative properties of a fluid and the flow dynamics. Due to interrupting the molecular flux of a stratifying agent on a motionless obstacle, fine structural diffusion-induced flows are formed around the obstacle in the form of a multilevel set of vortex cells which are transformed near the edges into horizontally extended streaky structures. A moving body in a stratified fluid produces upstream disturbances, groups of attached internal waves, leading-edge vortices, and a vortex street in the wake, which coexist in the stratified flow as an organic whole and are separated with ligaments. In the unsteady vortex flow regime, the shape of the bluff body essentially affects the flow structure, determining whether it will consist of a quasisteady chain of vortices with a quite regular vortex shedding structure, or leading-edge vortices and vortex street would evolve into a much more complex and multi-scale vortex evolution. The numerical and experimental visualizations of diffusion-induced flows, internal waves, vortex streets, and fine structural ligaments, are in a qualitative agreement with each other.

On the basis of the fundamental system, which includes equations of continuity, momentum, and substance transfer with a linearized equation of state, methods of experimental and numerical study are developed for visualizing the flow perturbation fields generated by uniform horizontal movement of a vertical plate in a stratified medium (Chashechkin, Zagumennyi, 2020). The stratified flows were visualized in the laboratory tank by the highsensitive and high-resolution Schlieren instrument IAB-458 at the stand 'Laboratory Mobile Tank' of the Unique Research Facility 'HPC IPMech RAS' and numerically calculated within the frame of the open source CFD utility OpenFOAM using computing resources of cluster systems and supercomputers. Both the computation results and the laboratory visualization data show that a vertical plate uniformly moving in a stratified fluid generates flow patterns which contain complex systems of internal waves, including upstream, attached and short ones, and thin interfaces, such as ligaments, formed due to the combined influence of the stratification and dissipation effects. Increase in the velocity of the plate movement leads to an essential restructuring of the wake flow past the plate, where typical vortex elements, such as vortex dipoles and 'vortex bubbles', are formed in the divergence zones of the phase surfaces of internal waves. All the flow structural components evolve and actively interact with each other and with the free stream. The observation and calculation results are in a good qualitative and quantitative agreement with each other. The experimental study has been supported by high-resolution videos of the flow (as seen from above and from the side) (Chashechkin, 2020). The evolution of ejecta, spikes, droplets spray, cavity,

splash, secondary cavity, streamer, secondary droplets and sequence of capillary waves is reported accordingly. In particular, perturbations of the smoothed free surface with transverse dimensions from 0.03 cm to 0.15 cm have been observed in the center of the cavity and at the head of a growing splash. The formation of fine flows components is associated with the release of available potential energy and the conservation of perturbations in a thin "double layer" located in proximity to the original contact surfaces.

The interaction of a falling drop (diluted aqueous solution of ink in various concentrations) with a target fluid (partially degassed tap water) has been tracked by means of high-resolution video recording and photography (Chashechkin, Ilynykh, 2020). The experimental setup has carefully been prepared in order to preserve the axial symmetry of initial conditions. An extensive set of data is reported to support understanding of the observed dynamics and their repeatability and reproducibility. The overall study has been carried out with the express intent to spur the future development of detailed mathematical models and numerical methods suited for this kind of problems.

Based on the numerical and experimental visualization methods, the flow patterns around a uniformly moving plate located at an arbitrary angle of attack are studied (Chashechkin, Zagumennyi, 2021). The study is based on the fundamental equations of continuity, momentum and stratifying substance transport for the cases of strong and weak stratified fluids, as well as potential and actually homogeneous ones. The visualization technique and computation codes were compiled bearing in mind conditions of internal waves, vortices, upstream, and downstream wakes registration, as well as the resolution of ligaments in the form of thin interfaces in schlieren flow images. The analysis was carried out in a unified mathematical formulation for a wide range of plate motion parameters, including slow diffusion-induced flows and fast transient vortex flows. The patterns of formation and subsequent evolution of the basic structural components, such as upstream disturbances, downstream wake, internal waves, vortices, and ligaments, are described both at start of motion and subsequent uniform movement of the plate. Calculations of forces acting on the obstacle in the flow were carried out to study effects of variations in fluid properties, flow conditions and plate parameters on the dynamic characteristics of the obstacle. The numerical and experimental results on the flow patterns around a plate are in a good agreement with each other for different flow regimes.

The problem of generating beams of periodic internal waves in a viscous, exponentially stratified fluid by a band oscillating along an inclined plane is considered by the methods of the theory of singular perturbations in the linear and weakly nonlinear approximations (Chashechkin, 2021). The complete solution to the linear problem, which satisfies the boundary conditions on the

emitting surface, is constructed taking into account the previously proposed classification of flow structural components described by complete solutions of the linearized system of fundamental equations without involving additional force or mass sources. The estimates made show that the amplitudes of such waves are large enough to be observed under laboratory conditions.

Large-scale processes and the weather forecast

In the paper (Ivanova et al., 2022) a method is proposed for in-flight icing prediction up to 12 hours based on the output of the COSMO-Ru configuration of the COSMO model with a grid step of 6.6 km for the Russian Federation area. The calculation of the simplified forecast icing potential (SFIP) using model microphysics data versus AIREP Speci information allowed determining a threshold value of SFIP=0.2, the exceeding of which is an icing criterion. An overview of works devoted to the issues of icing influencing the operation of air transport is presented in (Ivanova, 2021). The problems of ground icing, which lead to a deterioration in the condition of the runways and the complication of pre-flight aerodrome operations, are discussed. The reasons of aircraft icing in flight, means and methods of icing observation, approaches to forecasting icing in clouds and precipitation are considered. Methods for predicting icing of aircraft engines in areas of high concentration of ice crystals are analyzed.

Several papers were presented to estimate features of the atmospheric centers of action (ACA) in the Northern and Southern hemispheres using different long-term reanalysis data. In (Mokhov et al., 2020) the variability of ACAs and their relation to the hemispheric temperature and key climatic modes, including the El Niño–Southern Oscillation, Atlantic Multidecadal Oscillation, and Pacific Decadal Oscillation is analyzed. According to long-term data, it is found that the centennial hemispheric warming is accompanied by a significant weakening of the polar highs and the Greenland High that is more significant in summer. The deepening of the Icelandic Low, especially in summer, and the Aleutian Low, especially in winter, is shown. A significant weakening of the winter Siberian and North American highs and a deepening of the summer North American Low are also revealed. In the Southern Hemisphere, all three subpolar oceanic lows and the Mascarene High significantly intensify under warming conditions, while the summer Australian and South African lows weaken. It is determinate (Mokhov et al., 2022) that regional features of global climate changes are significantly related to the regimes of atmospheric centers of action (ACA) and their variability. The analysis of the expected ACA changes in the Northern Hemisphere was carried out using simulations with ensembles of modern climate models of the international projects CMIP5 and CMIP6 under the scenarios of anthropogenic forcing RCP8.5 and SSP5-8.5 in the 21st century. The most con-

sistent estimates based on simulations with the ensembles of the CMIP5 and CMIP6 models were obtained for the weakening tendencies of the winter North American High and the summer Asian Low. For the winter Siberian High, a weakening trend was found to be more significant according to simulations with the CMIP6 ensemble of climate models. In a comparative analysis of ACAs detected by model simulations and ERA5 reanalysis data, in particular for the base period of 1981-2005, it was noted that, in general, the intensities of subtropical anticyclonic ACAs over the Atlantic and Pacific oceans are larger for summer than for winter according to both reanalysis data and model simulations. For the intensity of subpolar cyclonic ACAs over the Atlantic and Pacific oceans, the opposite peculiarity is noted: their intensity is generally higher for winter than for summer. At the same time, the interannual variability of the intensity of ACAs, characterized by a standard deviation, is generally greater in winter than in summer.

The regional features of the formation of extreme atmospheric and hydrological, climatic, and ecological regimes in connection with the manifestations of the Pacific Decadal Oscillation (PDO) against the background of the general warming of recent decades are estimated (Mokhov et al., 2021). In particular, the record Amur flood in 2013 and the Kamchatka "red tide" in 2020 were formed due to positive temperature anomalies in the western Pacific Ocean in the Northern Hemisphere, which corresponded to the negative PDO phase. Large-scale climatic variations, like the "climate shift" in the second half of the 1970s, are associated with PDO; their connection with the peculiarities of atmospheric blockings is noted. In particular, the frequency of summer atmospheric blockings, maximal over the European territory of Russia, is especially high during a negative PDO phase. The record-long atmospheric blocking period over the European Russia in summer 2010, with record heat and fires, fell precisely on a negative PDO phase.

A two-zone model of the atmospheric circulation over a hemisphere is considered (Kurgansky, 2021c). The latitude φ of the boundary between the zone of the Rossby circulation regime at mid and high latitudes and the zone of the Hadley circulation regime at low latitudes serves as a model variable. The principle of maximum of the (information) entropy of the eddy regime within the Rossby regime zone is used to determine a statistical (climatic) equilibrium value of φ. Based on the proposed model, the question of atmospheric blocking action over the hemisphere is addressed. An attempt has been made to represent a blocking phenomenon as a necessary attribute of the atmospheric circulation in statistical equilibrium. The model suggests that long-term climate change related either to the (significant) global warming or to the (significant) global cooling, both respective to the current climate state, and quantified in terms of changes in latitude φ, leads to an increase in the probability of blocking action.

In the paper (Serykh, Sonechkin, 2021) the predictability of El Nino and La Nina is investigated. In this case, the recently discovered so-called global atmospheric oscillation (GAO) is considered. Assuming GAO to be the main mode of short-term climatic variability, this study defines an index that characterizes the dynamics and relationships of the extratropical components of the GAO and El Nino – Southern Oscillation (ENSO). Due to the general propagation of the GAO's spatial structure from west to east, another index – predictor of ENSO is defined. The crosswavelet analysis between both of these indices and the Oceanic Nino Index (ONI) is performed. This analysis reveals a range of timescales within which the closest relationship between the GAO and ONI takes place. Using this relationship, it is possible to predict El Nino and La Nina with a lead-time of approximately 12 months.

In connection with modern climatic changes, special attention is paid to atmospheric blockings. The estimates of changes in the frequency of atmospheric blocking based on the CMIP5 ensemble simulations with modern climate models of general circulation are obtained using various criteria of atmospheric blocking detection and different RCP scenarios of anthropogenic forcing for the 21st century (Mokhov, Timazhev, 2019). To assess the quality of the model simulation of atmospheric blocking characteristics, the meridional seasonal distributions of the blocking frequency are compared with reanalysis data. The results demonstrate that the choice of the ensembles of the best models (in terms of the blocking simulation for the modern climate) is important. For the best models, a risk of the blocking frequency increase in the warming climate is noted, which is not observed in the results for the full ensemble. A global blocking climatology published by this group for events that occurred during the late 20th century examined a comprehensive list of characteristics that included block intensity (BI). In addition to confirming the results of other published climatologies, they found that Northern Hemisphere (NH) blocking events (1968–1998) were stronger than Southern Hemisphere (SH) blocks and winter events are stronger than summer events in both hemispheres (Lupo et al., 2019). This work also examined the interannual variability of blocking as related to El Niño and Southern Oscillation (ENSO). Since the late 20th century, there is evidence that the occurrence of blocking has increased globally. A comparison of blocking characteristics since 1998 (1998–2018 NH; 2000–2018 SH) shows that the number of blocking events and their duration have increased significantly in both hemispheres. The blocking BI has decreased by about six percent in the NH, but there was little change in the BI for the SH events. Additionally, there is little or no change in the primary genesis regions of blocking. An examination of variability related to ENSO reveals that the NH interannual-scale variations found in the earlier work has reversed in the early 21st century. This could either be the result of interdecadal variability or a change in the climate. In-

terdecadal variations are examined as well. Regional anomalies in the frequency of atmospheric blockings in the Northern Hemisphere detected on the basis of reanalysis data since 1979 during different phase transitions of El Niño phenomena in different phases of the Pacific Decadal and Atlantic Multidecadal Oscillations are estimated – in particular, the regional frequency of summer blockings associated with extreme phases of El Niño phenomena and transitions between them (Mokhov, Timazhev, 2022a). Significant differences are noted for the El Niño phenomena detected with the use of different indices characterizing different process types. A new integral index is proposed for describing the total activity of atmospheric blocking over extended areas at different time intervals (Mokhov, Timazhev, 2022b). The integral index, which characterizes the proportion of the area with atmospheric blocking in a particular region during a certain time interval, is used in two versions – one-dimensional and, more detailed, two-dimensional. Estimates of how strongly Russian regions and the Northern Hemisphere (NH) as a whole are exposed to atmospheric blockings in different seasons and on average for the year are obtained from reanalysis data for four decades (1979–2018). The highest values of the integral index, which depends on the frequency, duration, and size of atmospheric blockings, for Russia and the entire NH are estimated for the summer season. The largest interannual variability is observed in winter seasons. Significant differences in the coherence of interannual variations in the integral index for Russian regions and for the NH as a whole for different seasons were found using cross-wavelet analysis. Their coherence is significant for the longest (interdecadal) variations in the seasonal values of the integral index, except for spring seasons. In paper (Mokhov, 2022) the analysis of winter atmospheric blocking events in the Northern Hemisphere (NH) under climate changes in 1980–2018 was carried out. The results of this analysis indicate a significant increase in the total duration of winter atmospheric blocking events τ in the NH in recent decades. The noted trend was revealed against the background of a rapid increase in the NH surface air temperature T in winter seasons. The parameter of sensitivity of the duration of atmospheric blocking events to changes in the NH surface air temperature in winter seasons for the period 1980–2018 was estimated. The statistically significant estimate obtained means an increase in τ by more than one-and-a-half times with an increase in the mean winter surface air temperature of the NH by 1 K. A more significant relationship with T was obtained for values of τ above the average value of τm for the period 1980–2018, while at $\tau < \tau m$, the relationship was found to be statistically insignificant. The noted features are associated with differences in different phases of the key modes of climatic variability. In particular, the mean value of the surface air temperature of the NH in winter in the positive phase of the Atlantic Multidecadal Oscillation (AMO) within the analyzed period 1980–2018 significantly exceeded

the corresponding mean value of T in the negative phase of AMO. At the same time, it was found that the mean value of the duration of winter blocking events in the NH in the positive AMO phase is one-and-a-half times longer than in the negative AMO phase. For winter seasons, the estimates of the relationship between τ and the intensity of the Arctic anticyclonic center of action depending on the AMO phase were obtained.

Estimates of the probability of warm and cold winters in regions of Northern Eurasia are obtained from data for eight decades, depending on El Niño phenomena (Mokhov, 2020). The features of anomalously warm and anomalously cold winters in different Russian regions in the phases of El Niño and La Niña and in the neutral phase are noted. Features of anomalous winters under El Niño phenomena of different types are compared. Seasonal anomalies of surface air temperature were analyzed for the North Eurasian regions in mid-latitudes using long-term data from the end of the 19th century with an assessment of El Niño Southern Oscillation (ENSO) effects (Mokhov, Timahzev, 2022). In particular, temperature anomalies in the spring–summer months for the European (ER) and Asian (AR) Russian regions for different phase transitions of the ENSO phenomena were estimated using the Niño3, Niño3.4 and Niño4 indices. The largest frequency of the extremely high-temperature and drought conditions in spring–summer months in ER was detected for years starting in the El Niño phase with the transition to the La Niña phase at the end of the year. Such conditions were realized in ER in summer 2010 ("Russian heatwave"). The corresponding largest frequency of high temperature in AR was obtained for conditions with the continuation of the El Niño phase during the whole year. Such conditions in AR were noted, in particular, in the summer of 2015, with an extremely high temperature and extremely low precipitation in the Lake Baikal basin.

Changes in the characteristics of cyclone activity (frequency, depth and size) in the Arctic are analyzed based on simulations with state-of-the-art regional climate models (RCMs) from the Arctic-CORDEX initiative and global climate models (GCMs) from CMIP5 under the Representative Concentration Pathway (RCP) 8.5 scenario (Akperov et al., 2019). Most of RCMs show an increase of cyclone frequency in winter (DJF) and a decrease in summer (JJA) to the end of the 21st century. However, in one half of the RCMs, cyclones become weaker and substantially smaller in winter and deeper and larger in summer. RCMs as well as GCMs show an increase of cyclone frequency over the Baffin Bay, Barents Sea, north of Greenland, Canadian Archipelago, and a decrease over the Nordic Seas, Kara and Beaufort Seas and over the sub-arctic continental regions in winter. In summer, the models simulate an increase of cyclone frequency over the Central Arctic and Greenland Sea and a decrease over the Norwegian and Kara Seas by the end of the 21st century. The decrease is also found over the high-latitude conti-

nental areas, in particular, over east Siberia and Alaska. The sensitivity of the RCMs' projections to the boundary conditions and model physics is estimated. In general, different lateral boundary conditions from the GCMs have larger effects on the simulated RCM projections than the differences in RCMs' setup and/or physics. Paper (Akperov et al, 2021) hypothesizes that biogeophysical feedbacks (BF) over the land, here mainly referring to the albedo-induced warming in spring and evaporative cooling in summer, may have the potential to significantly change cyclone activity in the Arctic. Based on a regional Earth system model (RCA-GUESS) which couples a dynamic vegetation model and a regional atmospheric model and an algorithm of cyclone detection and tracking, this study assesses for the first time the impacts of BF on the characteristics of Arctic cyclones under three IPCC Representative Concentration Pathways scenarios (i.e. RCP2.6, RCP4.5 and RCP8.5). Our analysis focuses on the spring- and summer time periods, since previous studies showed BF are the most pronounced in these seasons. We find that BF induced by changes in surface heat fluxes lead to changes in land-sea thermal contrast and atmospheric stability. This, in turn, noticeably changes the atmospheric baroclinicity and, thus, leads to a change of cyclone activity in the Arctic, in particular to the increase of cyclone frequency over the Arctic Ocean in spring. This study highlights the importance of accounting for BF in the prediction of Arctic cyclones and the role of circulation in the Arctic regional Earth system.

In paper (Durneva, Chkhetiani, 2021) the analysis of monthly mean locations of the planetary upper-level frontal zone in the Euro-Atlantic sector in summer during 1990–2019 is presented. Specific positions for the summer months (June, July, and August) are noted, and maximum northward displacements from the climatological normal for 1961–1990 are found in the years with the formation of the atmospheric blocking. The values of standard deviations of the displacements relative to the normal position were calculated for the summer period of each year both for the North Atlantic, Europe, and the European part of Russia and for the Euro-Atlantic sector. On the basis of linear regression, a tendency is revealed toward an increase in the meridional displacements of the planetary upper-level frontal zone over the recent thirty years and toward the occurrence of maximum deviations over the last decade.

In paper (Kurgansky, 2020c) the response of large-scale atmospheric circulation to the anomalous Barents and Kara Sea ice free surface heating, which has been observed over the past two decades, is considered. For this purpose, a simplified two-dimensional baroclinic atmospheric model obtained by averaging hydrothermodynamic equations over height is used, as well as its two-layer analogue with the effect of anomalous heating and, hence, of horizontal baroclinicity being concentrated within the surface-

adjacent 1- to 2-km-thick atmospheric layer, which fits Arctic conditions more closely. Quasi-geostrophic approximations are derived for both models; for a single-layer model (in the adiabatic and inviscid approximation), the formulation is also given in terms of Nambu mechanics. Both models demonstrate the appearance of a center of increased surface air temperature over the area of anomalous heating; a slight decrease in surface pressure there; and, finally, anticyclonic circulation in the bulk of the atmosphere. The model results are shown to be extremely sensitive to the parameterization of the Ekman boundary layer.

The study (Rivin et al., 2020) presents the new system for operational short-range numerical weather prediction with the grid spacing of 1 km for the Moscow region that considers the features of urbanized surface and is based on the COSMO-Ru1M model configuration. This system is implemented in the Hydrometcenter of Russia. The results of the trial testing of the optimum model configuration for the Moscow region using observations from the dense network of weather stations and MTP-5 temperature profilers are presented. High prediction capabilities of the new forecasting system are demonstrated. The approaches to the minimization of the time of calculations for the technology chain implemented at the Roshydromet supercomputer are described. A case study of modeling with the grid spacing of 500 m versus 1000 m for summer convective weather events in the Moscow region has been analyzed.

The study (Ivanov et al., 2019) is focused on the specific features of ocean–air interaction in the Laptev Sea, in the late summer, on the basis of recurrent measurements during four expeditions in the 2000s and 2010s, atmospheric reanalysis products, and satellite ice concentration data. It was established that in the "icy" years, the accumulation of heat in the upper ocean layer is insignificant for the subsequent ice formation. In the "ice-free" years, the accumulated heat storage in the upper mixed layer depends on the duration of open water and the distance of the point of interest to the nearest ice edge. In a broader context, we considered possible links between the average ice area/extent in the August–September–October (ASO) period, and in the December–January–February (DJF) period, for two representative Arctic regions; that is, the Eurasian segment, defined within the bounds 60–120E, 65–80N, and the American segment, defined within the bounds 150E–150W, 65–80N. Significant "seasonal memory", characterized by the consistent change of the ice cover parameters in sequential seasons, was revealed in the Eurasian segment between 2007 and 2017. No linkage on a seasonal time scale was found in the American segment. A possible explanation for the distinguished contrast between the two geographical regions is proposed.

Mesoscale processes

In the paper (Ivanova, 2019) the overview of papers dealing with the history of development and the current state of thunderstorm nowcasting technologies is presented. A role of information on thunderstorms obtained from different sources (satellites, radars, lightning detectors, ground-based microwave radiometers) and the significance of output data of numerical weather prediction models for thunderstorm nowcasting are shown. The features of thunderstorm nowcasting systems used in the national meteorological services are discussed.

Significant attention was paid for tornadoes and linear windstorm climatology.

The paper (Chernokulsky et al., 2020) introduces a new database of tornadoes in NE that spans from the tenth century to 2016. The database, compiled using various sources, contains 2879 tornado cases over land and water and includes tornado characteristics. Tornadoes are common for most regions of NE, with a density reaching four cases per 104 km2 in 1900–2016 in some regions. Tornadoes over land have distinct annual and diurnal cycles: they form mostly in May– August, with a maximum in June, and during daytime, with a maximum at 1700–1800 local time. Waterspouts form in all months with a maximum in late summer and mostly at 0900–1300 local time. Most tornadoes are weak and short lived. The Fujita-scale intensity is ≤F1 for 80% and ≥F3 for 3% out of all rated tornadoes. Half last less than 10 min. The average annual number of all tornadoes over land is around 150, including 10 and 2 tornadoes with ≥F2 and ≥F3 intensity, respectively. Annually, 1–2 tornadoes lead to casualties and result in 2.9 fatalities and 36.3 injuries. Despite the incompleteness of the dataset, our results show that tornadoes in NE, although being rare, are not as extremely rare as has been thought before. The results illustrate the substantial underestimation of tornado threat by the general public, researchers, and meteorologists, and unambiguously indicate the need for systematic assessments and forecasting of tornadoes by national weather services.

Paper (Shikhov et al., 2020) presents a new geographic information system (GIS) database of stand-replacing windthrow events in the forest zone of European Russia (ER) for the 1986– 2017 period. The delineation of windthrow areas was based on the full Landsat archive and two Landsat-derived products on forest cover change, namely the Global Forest Change and the Eastern Europe's forest cover change datasets. Subsequent verification and analysis of each windthrow was carried out manually to determine the type of related storm event, its date or date range, and geometrical characteristics. The database contains 102 747 elementary areas of damaged forest that were combined into 700 windthrow events caused by 486 convective or noncon-

vective storms. The database includes stand-replacing windthrows only with an area > 0.05 and > 0.25 km2 for the events caused by tornadoes and other storms, respectively. Additional information such as weather station reports and event descriptions from media sources is also provided. The total area of stand-replacing windthrows amounts to 2966 km2, which is 0.19 % of the forested area of the study region. Convective windstorms contribute 82.5 % to the total winddamaged area, while tornadoes and non-convective windstorms are responsible for 12.9 % and 4.6 % of this area, respectively. Most of the windthrow events in ER happened in summer, which is in contrast to Western and Central Europe, where they mainly occur in autumn and winter. Due to several data and method limitations, the compiled database is spatially and temporally inhomogeneous and hence incomplete. Despite this incompleteness, the presented database provides a valuable source of spatial and temporal information on windthrow in ER and can be used by both science and management.

New data are presented on tornadoes over land in Russia for the period of 1900–2018 based on various sources (Chernokulsky et al., 2021). In total, information on 1763 tornadoes was collected, including 993 tornadoes from eyewitness reports on tornado passage and/or associated impacts and 770 tornadoes from satellite data on tornado-induced windthrows. Both single tornadoes and tornado outbreaks, the cases of formation of several tornadoes within one meso- or synoptic-scale system, were reported. On average for 2009–2018, more than 100 tornadoes are observed in Russia per year, including 15 significant tornadoes (with a wind speed >50>50 m/s) and one intense tornado (with a wind speed >70>70 m/s). In some years, these rates can be significantly higher and reach 342, 52, and three tornadoes per year, respectively. Tornadoes are observed on about 41 days per year, up to 68 days per annum in some years. The frequency of occurrence of tornadoes of different categories and the probability of their passage over a point on the ground were estimated. These estimates can be further used to assess a risk of tornadohazardous situations. The general underestimation of the number of tornadic events in routine meteorological observations and existent statistics is discussed.

In paper (Chernokulsky et al., 2022) the spatial and temporal distribution of windthrows in the forest zone of Western Siberia for the period 2001–2020 is considered. Windthrow data are obtained from Landsat and Sentinel-2 satellite images, Global Forest Change project data, and high spatial resolution images from open mapping services. Data from the network of weather stations, images from meteorological satellites, and information on hazardous weather events observed in the region are used to specify dates and time of storm events. The compiled database includes 25 774 elementary damaged areas, which refer to 265 different windthrows. These windthrows were

caused by 158 different storm events. The total area of windthrows is 508.3 km^2 or 0.04% of the total forested area, which is four times less than in the European Russia (ER) for the same period. More than 67% of windthrows included in the database were caused by tornadoes. They also account for 25.4% of the total area, which is much more than in the ER. Squall-induced windthrows account for 30% of cases and 40% of the total area, and windthrows caused by nonconvective events account for 2.5% of cases and 34.5% of the total area. The maximum density of windthrows is found in the Kemerovo oblast, as well as in the west of Tomsk oblast and in the southeast of the Khanty-Mansi autonomous okrug. The largest number of windthrows was recorded in 2007 and 2010. Tornadoes and squalls, which cause windthrows, are most often observed in June, and windthrows caused by nonconvective events were observed in October– November in the Ural and Kuznetsk Alatau mountains. Several large outbreaks of squalls and tornadoes are identified. However, with respect to the area of forest damage, they are 10–15 times less than the largest similar events on ER. The area of windthrows in Western Siberia is 77.5 times less than the area of burns during the same period, with a ratio of 3.5/1 for ER.

The case studies of tornadoes and line windstorm and formation environment analysis were carried out (Chernokulsky et al., 2020). Strong tornadoes are common for the European part of Russia but happen rather rare east of the Urals. June 2017 became an exceptional month when two tornado outbreaks occurred in the Ural region of Russia, yielded $3 million damage, and resulted in 1 fatality and 14 injuries. In (Chernokulsky et al., 2020) detailed analysis of these outbreaks with different data was performed. Tornadoes and tornado-related environments were diagnosed with news and eyewitness reports, ground-based meteorological observations, sounding data, global numerical weather prediction (NWP) models data, synoptic charts, satellite images, and data of specially conducted aerial imaging. The accuracy of short-term forecasting of outbreaks with the WRF-ARW mesoscale atmospheric model, which was run in convection-permitting mode also was estimated. Authors determined the formation of 28 tornadoes during the first outbreak (3 June 2017) and 9 tornadoes during the second outbreak (18 June 2017). They estimated their intensity using three different approaches and confirmed that, based on the International Fujita scale (IF), one of the tornadoes had the IF4 intensity, being the first IF4 tornado in Russia in the 21st century and the first-ever IF4 tornado reported beyond the Ural Mountains. The synopticscale analysis revealed the similarity of two outbreaks, which both formed near the polar front in the warm part of deepening southern cyclones. Such synoptic conditions yield mostly weak tornadoes in European Russia; however, our analysis indicates that these conditions are likely favorable for strong tornadoes over the Ural region. Meso-scale analysis indicates that the environ-

ments were favorable for tornado formation in both cases, and most severe-weather indicators exceeded their critical values. Analysis demonstrates that for the Ural region, like for other regions of the world, combined use of the global NWP model outputs indicating high values of severe-weather indices and the WRF model forecast outputs explicitly simulating tornadic storm formation could be used to predict the high probability of strong tornado formation. For both analyzed events, the availability of such tornado warning forecast could help local authorities to take early actions on population protection.

In paper (Kalinin et al., 2021) the environments of 53 severe squalls and tornadoes that caused large-scale windthrows in the forest zone of European Russia and the Ural in 1989–2019 are analyzed. The CFSR and ERA-5 reanalyses and sounding data were used to estimate characteristics of the environments including convective instability indices. It was found that the substantial temperature gradient on the atmospheric front (9.6°C/500 km on average) and the jet stream presence in the lower or middle troposphere oriented along the frontal zone are important factors to estimate environments of the formation of severe squalls and tornadoes. In most cases, squalls and tornadoes require a combination of high precipitable water content (40 mm on average), moderate or high convective instability (CAPE>1000CAPE>1000J/kg), and moderate or strong wind shear. High precipitable water content and strong convective instability are important for the formation of squalls, while low-level wind shear plays a principal role for the tornado generation.

Severe convective windstorms and tornadoes regularly hit the territory of Russia causing substantial damage and fatalities (Shikhov et al., 2021). An analysis of the climatology and formation environments of these events is essential for risk assessments, forecast improvements and identifying of links with the observed climate change. In this paper, we present an analysis of severe convective windstorms, i.e., squalls and tornadoes reported between 1984 and 2020 in the Perm region (northeast of European Russia), where a local maximum in the frequency of such events was previously found. The analyzed database consists of 165 events and includes 100 squalls (convective windstorms), 59 tornadoes, and six cases with both tornadoes and squalls. We used various information to compile the database including weather station reports, damage surveys, media reports, previously presented databases, and satellite images for windthrow. We found that the satellite images of damaged forests are the main data source on tornadoes, but their role is substantially lower for windstorm events due to the larger spatial and temporal scale of such events. Synoptic-scale environments and associated values of convective indices were determined for each event with a known date and time. Similarities and differences for the formation conditions of

tornadoes and windstorms were revealed. Both squalls and tornadoes occur mostly on rapidly moving cold fronts or on waving quasi-stationary fronts, associated with low-pressure systems. Analyses of 72-h air parcel backward trajectories shows that the Caspian and Aral Seas are important sources of near-surface moisture for the formation of both squalls and tornadoes. Most of these events are formed within high CAPE and high shear environments, but tornadic storms are generally characterized by a higher wind shear and helicity. We also differentiated convective storms that caused forest damage and those did not. We found the composite parameter WMAXSHEAR is the best discriminator between these two groups. In general, storm events causing windthrow mainly occur under conditions more favorable for deep well-organized convection. Thus, forest damage can be considered as an indicator of the storm severity in the Perm region and in adjacent regions with forest-covered area exceeding 50%.

In the summer of 2010, European Russia experienced an unprecedented high air temperature, catastrophic wildfires, heavy air pollution, but also several severe convective storms. Two of them occurring on June 27 and July 29 had a particularly high intensity and resulted in unprecedented forest damage. In study (Chernokulsky et al., 2021) storm-related forest damage using Landsat images and analyse the synoptic-scale and mesoscale peculiarities of these storms formation and evolution using satellite and reanalyses data, surface observations, and mesoscale numerical simulation were estimated. The total area of stand-replacing windthrow caused by these two storms amounts to 1250 km2. We found for both events that dark-coniferous and pine forests were more impacted than deciduous and re-grown forests. Damage track length exceeds 500 km for one storm and 600 km for another; therefore, we classify them as derecho events, which are documented for the first time in Russia. Formation of both derecho-producing mesoscale convective systems (MCSs) was triggered by fast-moving waves formed on the polar front under conditions of substantial temperature gradients on a western flank of long-lived blocking anticyclones in their termination dates. Backward trajectories analysis shows that advection from the Caspian Sea was one of the sources of high atmospheric water content during the MCSs formation. Both MCSs developed within environments of moderate to strong convective instability and extremely high wind shear due to strong midlevel jet stream. We performed convectionpermitting simulation of storms using the WRF model started with the initial data of CFSR and ERA5 reanalysis. For the event of June 27, the simulations with both initial conditions underestimate the maximum wind gusts since the model reproduces only a squall line without dominating derecho-producing storm. For the event of July 29, the ERA5 based simulation successfully reproduced the main features of the storm life cycle, while the CFS-based simulation substantially underestimated the wind gusts and

the storm-affected area. Our results highlight the importance of the atmospheric blocking influence on the convective severe storms formation and development, which deserves further research.

In paper (Shikhov et al, 2022) the applicability of satellite data to the estimation of atmospheric instability and precipitable water for the cases of severe convective events occurring over European Russia and the Ural region was considered. The initial sample includes 305 squalls, tornadoes, and large hail events. We assess the instability parameter Lifted Index (LI) and precipitable water (PW) using MODIS Atmospheric Profile Product data and the ERA5 reanalysis data. It is found that the median values of LI and PW retrieved from MODIS and ERA5 data are close, while the extreme values are substantially different. Local areas with very strong instability and high PW are identified from MODIS data, but not detected by the reanalysis data. The MODIS data are found to be significantly limited because of the low frequency of imagery and the lack of information on the instability parameters for cloudy pixels; therefore, the sample size was reduced from 305 to 95 cases.

Peculiarities were studied of formation of severe convective events, including a long-lived squall and several tornadoes observed over the European territory of Russia on May 15, 2021 (Chernokulsky et al., 2022). The event became one of the most destructive in the forest zone of the region over the past 35 years, with the total area of stand-replacing windthrows exceeding 152 km^2. The event was formed at a relatively low moisture content, but other conditions were exceptionally favorable for the formation of strong squalls and tornadoes characterized by a combination of high convective instability and strong wind shear. This resulted in the formation of several supercells and a mesoscale convective complex. The characteristics of cloud systems that caused squalls and tornadoes were analyzed based on satellite and radar data. Several characteristic signatures were identified at the cloud top, including long-lived overshooting tops that coincide with the area of destruction. The maximum reflectivity in some clusters exceeded 60 dBZ, the presence of a mesocyclone was noted in the radial velocity field during the tornado generation. Numerical experiments were performed to reproduce the event using the WRF regional atmospheric model with different initial conditions, which, however, cannot be considered successful.

In paper (Mokhov et al., 2020) the results of an analysis of detailed wind speed measurements during the heaviest squalls in Moscow on May 29, 2017, and April 21, 2018, are presented. The hurricane wind speed was detected in the surface layer in squalls in the Moscow region for the first time. Features of coherent changes of different wind speed components due to extreme squalls have been revealed using cross-wavelet analysis. The features that indicate the possibility of predictive risk assessments of extreme squalls are noted.

A number of papers were devoted to the structure of a tornado, namely, the dynamics of particles in atmospheric vortices (Ingel, 2020, 2021, 2022). The motion of inertial particles in intense vortices with a vertical axis in the field of gravity has been analytically studied (Ingel, 2020). In this problem, the nonlinear nature of the hydrodynamic resistance – its dependence on the modulus of the particle's velocity relative to the medium – is essential. Different components of the movement interact with each other, since each of them affects the coefficient of resistance. An effective method for an approximate solution of the problem is found. A number of general laws of particle dynamics are established. In particular, a regime is characteristic in which their tangential velocity is close to the velocity of the medium, while the radial velocity is substantially smaller (it is close in order of magnitude to the geometric mean of tangential velocity of the particle and the difference between the latter and the tangential velocity of the medium). The movement of inertial particles in intense vortices with a vertical axis in a gravity field and dynamics of the concentration of inertial particles in intense vortex flows were analyzed analytically (Ingel, 2021, 2022). In this problem, the nonlinear nature of the hydrodynamic resistance is essential: its dependence on the modulus of the particle velocity relative to the medium. The different components of the movement interact with each other, since each of them affects the coefficient of resistance. An effective method for an approximate analytical solution of the problem has been found. A number of general laws of particle dynamics have been established. A comparison of the results with some numerical calculations available in the literature confirms the adequacy of the model for Reynolds numbers up to about 10^3. In some respects, satisfactory agreement can be stated for more massive particles as well. The distance of transport of heavy particles outside the region of intense winds has been estimated. An adequate description of the motion of particles can be important for correctly interpreting the results of radar sounding of tornadoes, for assessing the associated hazards, and, possibly, for modeling the dynamics of the tornadoes themselves. The found analytical solutions demonstrate the significant role of nonlinear effects, since the effective drag coefficients differ from the previously studied case of Stokes particles by at least tens of times.

In paper (Kalmykova et al., 2019) the automated forecasting of waterspouts off the Black Sea coast is considered. The technique for the short-range forecasting of waterspout-risk situations and for the detection of waterspout-risk areas based on weather radar data in real time are presented. The results of the author's testing of the technique for the period from August 2017 to October 2018 are given. A possibility of the automated preparation of waterspout warnings is substantiated. The prospects of using the experience gained for the development of the automated tornado forecasting system for the European part of Russia are analyzed.

The paper (Kalmykova et al., 2021) presents the results of analyzing synoptic conditions that lead to the waterspouts outbreak over the Black Sea on July 16, 2019. It is found that during the analyzed day, the Black Sea region was influenced by the mesocyclone and the atmospheric front with wave perturbations. The dynamics of characteristics of the waterspout parent cloud formed near Lazarevskoe are described, which, unlike the others, dissipated not over the sea but off the coastal line and induced the squall. It is shown based on weather radar data that the cloud did not differ from the non-waterspout clouds formed on that day near the coast. It is noted that the forecast of an extremely high risk of waterspouts off the entire coast of the Krasnodar krai was issued for the analyzed day, which indicated a possibility of the waterspouts outbreak.

Assessment technique of waterspouts risk occurrence developed in RPA "Typhoon" allow to form forecasts about waterspout-risk areas within the eastern part of the Black Sea, to recognize clouds with possible risk of waterspout formation, and to give forecasts about waterspouts occurrence near the various parts of the Russian Black Sea coast (Kalmykova, 2021). The technique is implemented in a form of automated technology that operates in a continuous mode. Output calculated by technique are presented in the form of interactive maps, graphical and tabular forms using a specially developed web application. By the decision of CMKP of Roshydromet developed technology for the purpose of form waterspout risk forecasts is embedded in operation in FSBI "STSGMS CHAM" and FSBI ""North Caucasian UGMS" as an advisory method for forecasting waterspouts.

In paper (Chechin at al, 2019) a simple analytical model of the atmospheric boundary layer (ABL) coupled to sea ice is presented. It describes clear-sky cooling over sea ice during polar night in the presence of leads. The model solutions show that the sea ice concentration and wind speed have a strong impact on the thermal regime over sea ice. Leads cause both a warming of the ABL and an increase of stability over sea ice. The model describes a sharp ABL transition from a weakly stable coupled state to a strongly stable decoupled state when wind speed is decreasing. The threshold value of the transition wind speed is a function of sea ice concentration. The decoupled state is characterized by a large air–surface temperature difference over sea ice, which is further increased by leads. In the coupled regime, air and surface temperatures increase almost linearly with wind speed due to warming by leads and also slower cooling of the ABL. The cooling time scale shows a nonmonotonic dependency on wind speed, being lowest for the threshold value of wind speed and increasing for weak and strong winds. Theoretical solutions agree well with results of a more realistic single-column model and with observations performed at the three Russian ''North Pole'' drifting stations (NP-35, -37, and -39) and at the Surface Heat Budget of the Arctic

Ocean ice camp. Both modeling results and observations show a strong implicit dependency of the net longwave radiative flux at the surface on wind speed.

The driving mechanisms of mesoscale processes and associated heat transport in the Japan/East Sea (JES) from 1990 to 2010 were examined using eddy-resolving ocean model simulations (Stepanov et al., 2022). The simulated circulation showed correctly reproduced JES major basin-scale currents and mesoscale dynamics features. We show that mesoscale eddies can deepen isotherms/isohalines up to several hundred meters and transport warm and low salinity waters along the western and eastern JES boundaries. The analysis of eddy kinetic energy (EKE) showed that the mesoscale dynamics reaches a maximum intensity in the upper 300 m layer. Throughout the year, the EKE maximum is observed in the southeastern JES, and a pronounced seasonal variability is observed in the southwestern and northwestern JES. The comparison of the EKE budget components confirmed that various mechanisms can be responsible for the generation of mesoscale dynamics during the year. From winter to spring, the baroclinic instability of basinscale currents is the leading mechanism of the JES mesoscale dynamics' generation. In summer, the leading role in the generation of the mesoscale dynamics is played by the barotropic instability of basin-scale currents, which are responsible for the emergence of mesoscale eddies, and in autumn, the leading role is played by instabilities and the eddy wind work. We show that the meridional heat transport (MHT) is mainly polewards. Furthermore, we reveal two paths of eddy heat transport across the Subpolar Front: along the western and eastern (along 138E) JES boundaries. Near the Tsugaru Strait, we describe the detected intensive westward eddy heat transport reaching its maximum in the first half of the year and decreasing to the minimum by summer.

An analytical description of turbulent flows is given in the papers (Ingel, 2019-2022). The known nonlinear integral model of a turbulent thermal is generalized to the case of the presence of the horizontal component of its motion relative to the surrounding medium (for example, the floating-up of a thermal in a shear flow) (Ingel, 2019 a). The solution describes, in particular, the nonlinear effect of the interaction of the horizontal and vertical components of the thermal motion, since each of the components affects the rate of entrainment of the surrounding medium, i. e., the growth rate of the thermal size and, hence, its mobility. The simplest linear model of convection driven by double diffusion in a rotating medium is considered in paper (Ingel, 2019 b). The possibility of a contribution of such effects to the concentration of vorticity during tornado formation is discussed. In (Ingel, 2021) a linear model of the convection caused by double diffusion in a rotating medium is considered. In elaboration of the previous work of the author, a much more

complex problem is considered with account for the temperature stratification of the medium. Differential diffusion makes possible the vertical motions and concentration of vorticity despite the negative feedbacks, caused by the background stable stratification of density. By using the methods of scale analysis, dimensional analysis, and of the symmetry of differential equations, the dynamics of buoyant convective jets connected with stationary, local sources of a weightless heat-releasing impurity in a neutrally stratified medium was investigated (Ingel 2019). The laws of motion of turbulent thermals connected with instantaneous sources of the impurity are given that follow from the considerations of dimensionality and similarity. A well-known simplified model of turbulent convection from local sources of buoyancy and/or momentum acting for a short time has been developed and generalized in a number of directions. The features of the dynamics of convection from finite-size sources are considered (Ingel, 2021). The solutions describe, in particular, the nonlinear interaction of various components of the thermal's motion velocity, since each of them affects the environmental entrainment and, therefore, the thermal size and mobility. A two-dimensional stationary linear model of flows arising in a stably (neutral) stratified medium over a thermally inhomogeneous flat inclined surface was analyzed analytically (Ingel, 2022). An appropriate criterion for distinguishing these flows is established. The Prandtl model of slope flows (convection in a stratified medium near an inclined surface) has been generalized to the case of the presence of bulk heat sources/sinks oriented in parallel with the slope (Ingel, 2021). The properties of the analytical solutions found are nontrivial in some respects. For example, the intensity of stationary slope flows may increase with decrease in the inclination angle of the lower boundary. Numerical estimates show the possibility of generation of noticeable atmospheric slope flows in the presence of an aerosol that influences the radiation balance. Horizontal inhomogeneities of the exchange coefficients in a stratified medium lead to inhomogeneities of the vertical diffusion flow of buoyancy and its horizontal distribution and, consequently, to the emergence of horizontal inhomogeneities of hydrostatic pressure and the generation of currents (Ingel, 2022). The appearance of ordered flows in a temperature (density) stratified turbulent medium in a gravity field near an inclined surface is considered as an example. A stationary nonlinear analytical model of the Ekman-type boundary layer with anisotropic resistance was developed (Ingel, 2021). The results show that the effects of anisotropy can be noticeable.

It is shown that the hydrodynamics equations for a thin spherical liquid layer are satisfied by the stream function of a pair of antipodal point vortices (APVs), in contrast to the stream function of a single point vortex on a sphere with a background of a uniform opposite sign vorticity (Mokhov et al., 2020). A simple zero solution of the equation of the absolute vorticity conservation

is used for bypassing the well-known nonlinear problem of a point vortices interaction with a regular vorticity field, and an exact solution for the APV dynamics problem on a rotating sphere is obtained. Due to this, a new stable stationary solution for the dynamics of APV is obtained, which can model the dynamics of the global vortex structures, such as atmospheric centers of action.

A number of exact and asymptotic solutions of two-dimensional hydrodynamic equations describing nonstationary vortex streets have been constructed (Kalashnik, Chkhetiani, 2019). It is shown that the superposition of the flow with a constant horizontal shear and its perturbations in the form of a nonmodal wave provides an exact solution that describes a nonstationary vortex street with rotating elliptic current lines. The width of the zone occupied by such a vortex street has been determined. The equation of separatrix separating vortex cells with closed current lines from an external meandering flow has been obtained. The influence of the quasi-two-dimensional compressibility and beta effect on the dynamics of vortex streets has been studied based on the potential vorticity transport equation. The solutions describing the formation of vortex streets during the development of an unstable zonal periodic flow and a free shear layer have been constructed using a longwave approximation.

An investigation into mesoscale roll circulation and its transport characteristics in the atmospheric boundary layer (ABL) is carried out (Kosyakov et al., 2019). The case study of July 28, 2007, in Kalmykia, monitored during an expedition from the Obukhov Institute of Atmospheric Physics, is considered using the WRF-ARW model. The development of circulation with considerable asymmetry in the positive and negative components of the velocity field and helicity is recorded. The quasi-2D roll structures are characterized by an intensification of the dust capture and accumulation from the underlying terrain and, along with intensive vortices with a vertical axis, are a significant source of atmospheric impurities. Captured finely dispersed aerosols can be transported at long distances and form aerosol layers.

An investigation into mesoscale roll circulation and its transport characteristics in the atmospheric boundary layer (ABL) is carried out (Vazaeva et al., 2019). The case study of July 28, 2007, in Kalmykia, monitored during an expedition from the Obukhov Institute of Atmospheric Physics, is considered using the WRF-ARW model. The development of circulation with considerable asymmetry in the positive and negative components of the velocity field and helicity is recorded. The quasi-2D roll structures are characterized by an intensification of the dust capture and accumulation from the underlying terrain and, along with intensive vortices with a vertical axis, are a significant source of atmospheric impurities.

Helicity is inherent in many circulating motions and structures in the atmospheric boundary layer, where it is continuously reproduced due to the

combined action of the Earth's rotation and friction, which also is closely related to the phenomena of the inverse cascade and large-scale restructuring of flows. The helicity factor should be correctly considered during the construction of atmosphere models, and, accordingly, the knowledge of the helicity distribution in the ABL and its relation to dynamic atmospheric processes is required. In study (Vazaeva et al., 2021) the helicity of the circulation structures of various spatial and temporal scales in the ABL is determined from an analysis of field measurement data. A qualitative and quantitative comparison with the observed values is carried out on the basis of results of numerical simulations using the quasi-twodimensional model and a WRF-ARW mesoscale atmospheric nonhydrostatic model, in particular, WRF-LES. A good agreement with the observed spatial distributions of circulating motions is obtained. A link between the turbulent characteristics and helicity of the structures under study is shown. The helicity estimates for circulation structures of various scales in the ABL and in the free atmosphere are compared.

In the paper (Davydova et al., 2022), we consider two reasonable approaches to the problem of numerical simulation of the concentration distribution of a finely dispersed aerosol in spiral vortex structures (rolls) at the atmospheric boundary layer in order to estimate the contribution of vortex structures to the transport of aerosols through the boundary layer. Using the methods of perturbation theory, an approximate solution of a stationary spatially periodic singularly perturbed problem of the reaction–diffusion–advection type, which models the distribution of an aerosol in vortices, is obtained, the residual term is estimated, and a method for numerically solving the zero-approximation problem is proposed. As an alternative approach to the problem of numerical modeling of an aerosol-concentration field in rolls, implementation of the method of evolutionary factorization is considered. Using model data, an estimate of the amount of an aerosol carried by vortex structures is obtained.

A theoretical approach based on the Abel transform is proposed to infer the statistical distribution of the pressure drop in the center of convective vortices, including dust devils, based on measurements of peak pressure drops at a ground-based meteorological station, when the vortices pass over or near the barometric sensor. Paper (Kurgansky, 2019) shows that if the pressure inside the vortex is modeled realistically, then the statistics of observed pressure drops is related to the statistics of pressure drops in vortex centers of the subpopulation of vortices detected by the pressure sensor. This relationship holds for an arbitrary size-frequency distribution of dust devils. The relationship between the observed statistics of pressure drops and the statistics of central pressure drop values for the whole population of vortices depends on the correlation between the dust-devil diameter (defined either

optically or as twice the radius of the maximum circumferential velocity in the vortex) and the maximum pressure drop in its center. If the observed statistics can be approximated with a truncated power-law distribution then this approximating distribution is generally biased toward overestimation of the contribution from vortices with larger pressure drops. In a case of no apparent correlation between the vortex diameter and the maximum pressure drop in its center, the measurements provide an unbiased power-law estimate of the actual central pressure drop-frequency distribution. These theoretical results are applied to three sets of observations of Martian convective vortices, including dust devils. This technique has been applied with success to Mars Science Laboratory (MSL) convective vortices. In contrast to the previous work, it enables one to infer not only the mean vortex diameter, but also the whole size-frequency distribution of MSL vortices (Kurgansky, 2020b). A number density of convective vortices (a number of vortices per km2) at the InSight landing site on Mars is estimated as a metric of vortex activity, using a theoretical expression that relates this number density to the recorded number of nearby passages of vortices experienced by the InSight Mars lander (Kurgansky, 2021b). A very high estimate, i.e. 56 vortices per km2, of the average, over the whole period of observed vortex activity, number density of the vortices was obtained. Taking into account all the uncertainties involved in this quantity estimate, the latter can be reduced by a factor of about two, at most, but still remains at an unprecedented high level. For the sake of comparison, this methodology also applies to the Mars Science Laboratory and the Phoenix Lander vortices. The theoretical foundations of the exponential and power-law analytical formulations forthe size–frequency and intensity–frequency distributions of the convective vortices, including dust devils, are reexamined. Jaynes' general statistical arguments based on Shannon's entropy maximum principle leading to an exponential distribution are supplemented by Rényi's maximum entropy principle which is shown to lead to a power-law distribution (Kurgansky, 2022). In both cases, a key ingredient of the theory is the a priori knowledge of a first finite moment of the distribution. Applications to statistics of convective vortices, including dust devils, on Earth and Mars are discussed. The existence of a finite expectation value of the vortex diameter related to the absolute value of the Obukhov length scale in the atmospheric boundary layer allows a quantitative explanation of a burst of convective vortex activity observed at the InSight landing site in northern autumn on Mars.

In paper (Kurgansky, 2020) the hydrodynamic instability of monochromatic inertia-gravity waves (IGWs) of finite amplitude, propagating at small angles either to the vertical or horizontal, is studied. In both cases, the corresponding angle serves as a small parameter in the problem, and instability is investigated using the Galerkin method. For IGWs that propagate at a small

angle to the vertical, it is shown that stable density stratification is a stabilizing factor, and fluid rotation is destabilizing. The opposite is true for IGWs that propagate at a small angle to the horizontal. Previous analysis of the short wave instability of the monochromatic internal gravity waves of finite amplitude that propagate at small angles to the vertical is generalised to the case of the IGW. As an auxiliary but methodologically useful problem, the stability of a monochromatic inertial wave of finite amplitude in a fluid of uniform density is investigated in the same mathematical formulation. In study (Harlander, Kurgansky, 2021) a low-order IGW beam model is used to delineate both linear and so called non-modal transient instability. In the first part of the study, linear normal mode instability of a wave beam consisting of two finite amplitude plane monochromatic IGWs with the same frequency and parallel wave vectors of different magnitude is investigated using the Galerkin method. It is concluded that the wave beam is linearly more unstable than its constituent plane waves, taken separately. The degree of instability increases with the separation of the constituent waves in the wave number space, that is, with the wavebeam concentration in the physical space. The narrower a wave beam is, the more linearly unstable it is. In its turn, transient instability typically occurs for linearly stable flows or before linear instability can set in (subcritical instability) if the governing system matrix is nonnormal. In the second part of the paper, first the non-normality of the linear system matrix of the wave beam model is examined by computing measures like the Henrici number, the pseudospectrum, and the range of the matrix. Subsequently, the robustness of the transient growth is studied when the initial condition for optimal growth is randomly perturbed. It is concluded that for full randomisation, in particular, shallow wave beams can show subcritical growth when entering a turbulent background field. Such growing and eventually breaking wave beams might add turbulence to existing background turbulence that originates from other sources of instability. However, the robustness of transient growth for wave beam perturbations depends strongly on the strength of randomisation of the initial conditions, the beam angle and the perturbation wavelength.

The phase-screen (split-step) method is widely used for modeling wave propagation in inhomogeneous media (Gorbunov et al., 2020). The method of plane phase screens is best known. However, for modeling a 2D problem of radio occultation sounding of the Earth's atmosphere, the method of cylindrical phase screen was developed many years ago. In this paper, we propose a further generalization of this method for the 3D problem on the basis of spherical phase screens. In the paraxial approximation, we derive the formula for the vacuum screen-to-screen propagator. We also infer the expression for the phase thickness of a thin layer of anisotropic random media. We describe a numerical implementation of this method and give numerical examples of

its application for modeling a diverging laser beam propagating on a 25-km-long atmospheric path.

In the paper (Kan et al., 2020) a method for reconstructing the parameters of internal gravitational waves (IGWs) in the stratosphere from amplitude fluctuations in satellite radiooccultation observations are discussed. In the formation of radio-signal fluctuations, IGWs play the main role in these observations, while the contribution of isotropic turbulence is negligible. We consider methodological issues: (1) the choice of a model for the spatial spectrum of internal waves, (2) the derivation of relations connecting the statistical parameters of the IGW spectra and amplitude fluctuations in the approximation of a phase screen and weak fluctuations, (3) the development of a reconstruction algorithm, and (4) the estimation of possible errors. The reconstructed parameters are the outer or dominant scale and the structural characteristic of the vertical IGW spectrum, which determines the spectral amplitude in the saturation mode. The operating range covers altitudes from 28 km to the upper boundary of the tropopause. The error estimates for the reconstruction algorithm are 10–20% for the outer scale and 20–40% for the structural characteristic. The method of reconstructing the global distribution of statistical parameters of internal gravity waves in the atmosphere has been tested using the data of amplitude fluctuation measurements of a radio signal in satellite radio occultation (RO) observations (Kan et al., 2020b). In our previous work, for the chosen model of the spatial IGW spectrum, its relationship with the spectra of amplitude fluctuations was obtained, an algorithm for reconstructing the model parameters was developed, and the reconstruction errors were estimated. The reconstructed parameters of the vertical IGW spectrum are the external scale, which separates the unsaturated large-scale waves from saturated small-scale waves, and the structural characteristic, which determines the spectral amplitude of saturated waves. These parameters are used to calculate the variance of temperature fluctuations and the potential energy of the waves. This article presents the altitude–latitude distribution of IGW parameters in the stratosphere according to the measurements of the COSMIC experiment in 2011. The characteristic features of these distributions are noted, and the results are compared with the data of other measurements.

By now, a series of advanced wave optical approaches to the processing of radio occultation (RO) observations are widely used. In particular, the canonical transform (CT) method and its further developments need to be mentioned. The latter include the full spectrum inversion (FSI) method, the geometric optical phase matching (PM) method, and the general approach based on the Fourier integral operators (FIOs), also referred to as the CT type 2 (CT2) method. The general idea of these methods is the application of a canonical transform that changes the coordinates in the phase space from time

and Doppler frequency to impact parameter and bending angle. For the spherically symmetric atmosphere, the impact parameter, being invariant for each ray, is a unique coordinate of the ray manifold. Therefore, the derivative of the phase of the wave field in the transformed space is directly linked to the bending angle as a single-valued function of the impact parameter. However, in the presence of horizontal gradients, this approach may not work. Here we introduce a further generalization of the CT methods in order to reduce the errors due to horizontal gradients. In paper (Gorbunov et al., 2021) the modified CT2 method, denoted CT2A, which complements the former with one more affine transform: a new coordinate that is a linear combination of the impact parameter and bending angle are described. The linear combination coefficient is a tunable parameter. We derive the explicit formulas for the CT2A and develop the updated numerical algorithm. For testing the method, we performed statistical analyses based on RO retrievals from data acquired by the Constellation Observing System for Meteorology, Ionosphere, and Climate (COSMIC) and collocated analysis profiles of the European Centre for Medium-Range Weather Forecasts (ECMWF). We demonstrate that it is possible to find a reasonably optimal value of the new tunable CT2A parameter that minimizes the root mean square difference between the RO retrieved and the ECMWF refractivity in the lower troposphere and allows the practical realization of the improved capability to cope with horizontal gradients and serve as the basis of a new quality control procedure.

The paper (Nerushev et al, 2019) presents the results of an investigation into the spatiotemporal variability of the main characteristics of jet streams (JSs) in the upper troposphere of the Northern and Southern hemispheres in the field of view of European geostationary meteorological satellites for the period of 2007–2017. Most attention is paid to their relationship with tropospheric temperature, the sea-ice area, and large-scale atmospheric phenomena. The general patterns and significant differences in the interannual variability of the main characteristics of JSs in the Northern and Southern hemispheres are established. Annual variations in the sea-ice area (Sice) and S occur in both hemispheres mostly in phase, while the variations in Sice and φ in both hemispheres are close to antiphase. The feature of annual variations of the Sice and S series in the Northern Hemisphere was found.

In paper (Nerushev et al., 2021b) a statistical model of the temporal variability of the characteristics of high-altitude jet streams in the Northern Hemisphere for 2007–2019 was present. The area of Arctic sea ice, tropospheric temperatures at various levels and their differences between low and high latitudes, and various indices of large-scale processes characterizing climatic variability were used as predictors for constructing a multiple linear regression model. The sea-ice area and a group of predictors associated with variations in tropospheric temperature are shown to make the greatest contribution

to the variations in the characteristics of jet currents. The maximal contribution of the indices of large-scale atmospheric processes to the model quality does not exceed 10%. In general, the multiple linear regression model can describe up to 50–70% of the variability in the average area, maximal velocity, and latitudinal position of the jet stream center. The relationships between monthly mean surface air temperature at 147 meteorological stations in Europe and 53 stations in the European territory of Russia (ETR) and the characteristics of high-altitude jet streams determined from the measurements of the SEVIRI radiometer on board European geostationary satellites in the water vapor channel of 6.2 microns were discussed (Nerushev et al., 2021c). An algorithm for calculating the annual variation of the monthly mean anomalies of the jet stream center latitude under the influence of changes in the temperature of the upper troposphere and the area of the Arctic sea ice, which qualitatively reflects the main features of the variations of jet stream latitude observed from satellite data in 2017–2019 is proposed.

Traditionally, many papers are devoted to tropical cyclogenesis. An animated analysis of the data of global radiothermal satellite monitoring carried out in August 2000 has been applied to study the processes of evolution of tropical cyclones in the Northern Hemisphere (Ermakov et al., 2019). The crucial role of tropospheric advective latent heat fluxes within the rapid intensification of the tropical cyclone has been identified and confirmed by existing examples. The main disturbing factor that introduces significant errors into the evaluations by this approach is the proximity of large landmasses; hence a deeper analysis requires a preliminary selection of tropical cyclones moving over the ocean-water space away from the shoreline as objects of study. Proposals for further improving the analysis technique aimed at a detailed investigation of individual phases of a tropical cyclone evolution using large arrays of radiothermal remote data are formulated.

Results from an analysis of the frequency of tropical cyclones, the probability of their transformation into extratropical cyclones, and their trends in different oceanic basins of the Northern and Southern Hemispheres on the basis of observations over the period from 1970 to 2019 are presented. Significant trends in the increase in the transformation frequency of tropical cyclones into extratropical for the Earth as a whole have been noted (Mokhov et al., 2020). The specific features of different oceanic basins of the Northern and Southern Hemispheres are manifested. In particular, a significant increase in the frequency of the transformation events was observed for the northwestern water area of the Pacific Ocean, where the cyclones hit in the coastal extratropical regions of Eurasia, including the Far East. Against the background of this general trend, significant variations are manifested for different phases of the El Niño phenomenon. To evaluate the integral energetic effect of tropical cyclones, a special characteristic was used – an action

with the dimension [energy] × [time] (Mokhov, Poroshenko, 2020). Estimates of changes in the total action of tropical cyclones in the northwestern Pacific Ocean (NWPO) are obtained from observations for the period of 1951–2019. A significant increase in the interannual variability of the action of tropical cyclones in recent decades has been noted against the background of an increase in average values. There are also tendencies of an increase in the action of tropical cyclones and typhoons reaching extratropical latitudes, with significant interannual variations. In paper (Mokhov, Poroshenko, 2021) statistical estimates of the relationship between the duration and intensity of tropical cyclones using RSMC data for the period of 1951–2019 are presented. A good correspondence is noted between the duration of tropical cyclones, including the most powerful ones (typhoons), and their maximum intensity for the Northwest Pacific expressed in the form of power-law dependence. The similar dependences are obtained for the tropical cyclones transitioned into extratropical ones.

In the paper (Sukhanovskii, Popova, 2020) laboratory study is focused on the role of convective rolls in enhancement of the heat flux from the sea and triggering of the process of rapid intensification of tropical cyclones. The appearance of coherent convective structures such as thermals and rolls are registered by different optical techniques and temperature measurements. Two-dimensional velocity fields are used for the study of the structure and characteristics of the flow. The heat flux from the heating plate to the fluid is measured directly. Obtained results clearly show that rapid intensification of a laboratory analog of a tropical cyclone is tightly linked with the heat transfer process in the boundary layer. Formation of secondary convective structures strongly increases the heat transfer and intensity of convective circulation. Intensity of radial inflow is a crucial aspect for the intensification of cyclonic vortex, hence rapid variation of the heat transfer is a factor that has a substantial influence on the dynamics of a laboratory vortex. Time series of maximal radial and azimuthal velocities are in a good qualitative agreement with the ones from a theoretical model. It is shown that the mean square of velocity depends linearly on temperature difference between the inflow and the heating surface.

Numerical simulations of a laboratory model of a tropical cyclone are carried out for different rotation rates. Particular attention is paid to the nonstationary stage of intensive cyclonic vortex formation (Evgrafova, Sukhanovskii, 2022 b). The transfer of angular momentum plays a key role in the formation of cyclonic and anticyclonic flows; therefore, a detailed analysis of the redistribution and variation of angular momentum is given. The time evolution of angular momentum fluxes and total angular momentum strongly depend on the rotation rate. It is shown that intensive cyclonic motion with velocity exceeding initial values substantially (ten or more times) is a result

of accumulation in the center of a small fraction of global angular momentum of a fluid layer (from 0.25% at fast rotation to 2% at slow rotation). The integral angular momentum of the anticyclonic flow is significantly larger than that of the cyclonic flow, mainly because of the relatively large fluid volume of the anticyclonic flow. Another important result is that the rotating fluid layer very quickly adapts to new boundary conditions (heating and cooling). Approximately two rotation periods are required to reach a quasi-stationary state. The application of the obtained results to the evolution of real tropical cyclones is discussed.

An original approach is proposed for determining the exact time of the onset of tropical cyclogenesis (Levina, 2022). This approach includes a combined analysis of satellite images of cloudiness and the corresponding data of cloud-resolving numerical modeling for the region of developing vortex disturbance. The theoretical basis is the fundamental hypothesis of a turbulent vortex dynamo. The theory provides quantitative criteria that determine the excitation of largescale vortex instability in the atmosphere. Atmospheric numerical modeling makes it possible to accurately determine the moment of time at which the necessary conditions for the onset of instability are realized. This moment is interpreted as the beginning of cyclogenesis. The specific configurations of vortical cloud convection found in the work, which correspond to the initial stage of cyclogenesis, can be used in operational meteorological diagnostics when analyzing satellite images of cloudiness. The approach is illustrated by the example of diagnostics of tropical cyclogenesis.

Polar mesocyclones, also known as polar lows (PLs), are important maritime mesoscale (horizontal diameter up to 1000 km) weather systems at high latitudes, forming to the pole from the polar front. Statistical estimates of the relationship between the characteristic sizes and lifetime of polar lows (PLs) are obtained using the Sea Surface Temperature and Altimeter Synergy for Improved Forecasting of Polar Lows (STARS) data for 2002–2010 (Mokhov, Poroshenko, 2021). The features of their nonlinear relationship are noted. A model explanation of the power and exponential (linear in the simplest case) relationship for the largest-scale and longest-lived PLs is proposed. In paper (Vazaeva et al., 2020) the possible prognostic criteria of the PLs, in particular, the kinematic helicity as a squared characteristic related to the integral vortex formations and kinematic vorticity number is considered. To calculate such characteristics, we use reanalysis data and the results of numerical modeling with the WRF-ARW model for the PLs over the Nordic (Norwegian and Barents) seas. For comparison, experimental data are used. Our estimation of the helicity is based on its remarkable property – the connection of integral helicity content in the Ekman layer with the geostrophic wind velocity. Criteria associated with vorticity and helicity manifested through the PL genesis and development quite clearly. These criteria can be used to increase

the efficiency and accuracy of complex forecasting techniques. The cases of polar lows over the Norwegian and Barents seas in 2013, in the vicinity of Severnaya Zemlya in 2015, and in the near-edge zone of the Laptev Sea in 2021 were analyzed using the reanalysis and the WRFARW model simulations (Vazaeva et al., 2022). A combination of criteria was selected that are sufficient for identifying PLs and analyzing their size and intensity in a convenient and understandable form. These criteria are the estimates of helicity as an integral characteristic related to integral vortex formations and a kinematic vorticity number. Such criteria can be used to simplify the time-consuming procedure for collecting primary data on PL cases for machine learning.

Orographic wind circulations have been considered in a number of works. The paper (Shestakova, Debolskiy, 2022) considers the influence of the Novaya Zemlya bora on the turbulent heat exchange between the atmosphere and the ocean and on processes in the ocean. Another goal of this study is to demonstrate the sensitivity of simulated turbulent fluxes during bora to model coupling between atmosphere, ocean and sea waves. In this regard, a high-resolution numerical simulation of one winter bora episode was carried out using the COAWST (Coupled-OceanAtmosphere-Wave-Sediment Transport) modeling system, which includes the atmospheric (WRFARW model), oceanic (ROMS model), and sea waves (SWAN model) components. As shown by the simulation results, in the fully coupled experiment, turbulent heat exchange is enhanced in comparison with the uncoupled experiment (by 3% on average over the region). This is due to the atmosphere-sea-waves interaction, and the results are highly sensitive to the choice of roughness parameterization. The influence of the interaction of the atmospheric and oceanic components on turbulent fluxes in this episode is small on average. Bora has a significant impact on the processes in the ocean directly near the coast, forming a strong coastal current and making a decisive contribution to the formation of dense waters. In the open sea, the bora, or rather, the redistribution of the wind and temperature fields caused by the orography of Novaya Zemlya, leads to a decrease in ocean heat content losses due to a decrease in turbulent heat exchange in comparison with the experiment with flat topography.

The article (Shestakova et al., 2022) presents a comprehensive analysis of the foehn episode which occurred over Svalbard on 30–31 May 2017. This episode is well documented by multiplatform measurements carried out during the Arctic CLoud Observations Using airborne measurements during polar Day (ACLOUD) and Physical feedbacks of Arctic PBL, Sea ice, Cloud And AerosoL (PASCAL) campaigns. Both orographic wind modification and foehn warming are considered here. The latter is found to be primarily produced by the isentropic drawdown, which is evident from observations and mesoscale numerical modeling. The structure of the observed foehn warming

was in many aspects very similar to that for foehns over the Antarctic Peninsula. In particular, it is found that the warming was proportional to the height of the mountain ridges and propagated far downstream. Also, a strong spatial heterogeneity of the foehn warming was observed with a clear cold footprint associated with gap flows along the mountain valleys and fjords. On the downstream side, a shallow stably stratified boundary layer below a well-mixed layer formed over the snow-covered land and cold open water. The foehn warming downwind of Svalbard strengthened the north–south horizontal temperature gradient across the ice edge near the northern tip of Svalbard. This suggests that the associated baroclinicity might have strengthened the observed northern tip jet. A positive daytime radiative budget on the surface, increased by the foehn clearance, along with the downward sensible heat flux provoked accelerated snowmelt in the mountain valleys in Ny-Ålesund and Adventdalen, which suggests a potentially large effect of the frequently observed Svalbard foehns on the snow cover and the glacier heat and mass balance.

The article (Shestakova, 2021) considers the reasons for the underestimation of the wind speed by the WRF-ARW model when simulating downslope windstorms in the Russian Arctic. Simulation results for the Tiksi windstorm, for which sensitivity tests were carried out, appeared to be weakly dependent on the initial and boundary conditions, topography resolution, and boundary layer parameterization. Wind speed underestimation was mostly related to improper land use and the highly overestimated roughness length, which are used in the model. Reduction of the roughness length in accordance with the observations leads not only to a quantitative change in the wind speed in the boundary layer, but to qualitative changes in the dynamics of the flow. Wind underestimation in simulations with the overestimated roughness was caused by the jet stream unrealistically jumping over the lee slope and wake formation in the station area, while jet stream stayed near the surface and propagated to the station area in simulations with the modified roughness length. Modification of land use and roughness length in Tiksi and other regions where downslope windstorms are observed (Novaya Zemlya, Pevek, Wrangel Island) led to a decrease in wind speed modelling error by more than 2.5 times.

The paper (Shestakova, Repina, 2021) presents the results of a case-study of lake-effect circulation over Lake Baikal in December 2012, when the lake surface was still almost free from ice. The most spectacular manifestation of lake effect was a mesoscale vortex over the northern part of the lake. The analysis of this phenomenon is based on satellite observations, in-situ measurements, as well as on mesoscale numerical modeling with the WRF-ARW model. The model reproduced well the time and location of the vortex observed, correctly featuring cloud structures and time course of meteorological

parameters near the surface, though it was less accurate reproducing precipitation due to some space shift between observed and simulated landfall location. Sensitivity experiments revealed the role of the warm lake surface and orography in the vortex generation and intensification. Unlike vortices over the American Great Lakes, where orography is small and the main reasons of vortex formation are breeze circulation and diabatic heat fluxes from the surface, considered Baikal vortex was formed primarily due to orographyinduced convergence. Orography generated conducive conditions for local winds and breeze circulation and to a large extent formed unstable temperature stratification due to partial blocking of the incoming flow.

The paper (Shestakova et al., 2020) investigates for the first time sea waves during Novaya Zemlya bora – a downslope windstorm on the western coast of the archipelago during eastern winds – using a statistical and case-study approach. Statistical analysis of altimeter data off the western coast of Novaya Zemlya during bora shows that, despite strong wind forcing, the frequency of hazard wave heights was low due to the limited fetch. This result was confirmed by the high-resolution numerical simulations of two severe bora episodes. However, the influence of bora on sea waves in some cases was significant: bora increased wave height at a distance from shore greater than 200 km and wave height anomaly was up to 2–3 m. The influence of the wind input parametrization choice during bora is great in the coastal region; however, parametrizations with fetch-limited modifications and strong-wind adopted aerodynamic drag coefficient do not improve the modeling results in the open sea where altimeter data are available.

The paper (Shestakova, Toropov, 2021) presents the results of numerical modelling of extreme precipitation on the southern coast of the Caspian sea using the WRF-ARW model with realistic and idealised conditions aimed at evaluating the orographic and lake effects.Verified against the observational data, this model reproduces the spatial distribution and the total amount of precipitation in selected episodes reasonably well, with a certain set of physical parametrizations. Sensitivity tests showed that the lake effect is evident only in the presence of orography. The total contribution of the warm Caspian sea and orography to the amount of precipitation is, on average, 50%.

On the basis of satellite data and the results of a numerical simulation with the WRF-ARW model, cases of mesoscale circulation over Lake Uvs-Nuur, Mongolia, in November 2016 were analyzed (Vazaeva et al., 2022). During this period of time, when the surface of the lake was not yet completely covered with ice, a stable mesoscale vortex was observed for several days – a clear evidence of the lake effect. Regardless of the initial data, the adapted model reproduced the time and location of the observed vortex with a good accuracy, correctly representing the structure of clouds and the time course of meteorological parameters near the surface, although it reproduced

precipitation somewhat less accurately. Sensitivity experiments revealed the role of the warm lake surface and orography in the formation and enhancement of vortex. The orography near Uvs-Nuur is sufficient to create favorable conditions for local wind and breeze circulation, and it largely formed unstable temperature stratification due to partial blocking of the oncoming flow, playing a predominant role in the genesis of the vortex due to orographically induced convergence.

Small-scale motions and turbulence in the atmospheric boundary layer

In 1982 Lovejoy has published an illustration to Mandelbrot proposal how to characterize the area-perimeter ratio of complicated planar forms and it was found that exponent β for the satellite- and radar-determined cloud and rain areas of such a fractal is 1.35 close to 4/3. Later on, it was notified that the same exponent was found also for noctilucent clouds. Such a value might be related to classic turbulence theory of 1941. Paper (Golitsyn at al., 2022) demonstrates this relation using two basic papers by Kolmogorov and Obukhov. The role of prefractal multipliers is revealed, they form a couple of the peculiar invariants for cloud fields and a non-dimensional selfsimilarity numbers for these fields of sizes $1-10^6$ km^2. The peculiarity is in their dimensional dependence and in the presence of few invariants, not usual invariants in cloud forms. Further research on random walk of a fluid particle in the 6D phase-space may lead to new discoveries.

In paper (Kuznetsov, Mikhailov 2022) the process of breaking of inviscid incompressible flows along a rigid body with slipping boundary conditions is studied. Such slipping flows may be considered compressible on the rigid surface, where the normal velocity vanishes. It is the main reason for the formation of a singularity for the gradient of the velocity component parallel to rigid border. Slipping flows are studied analytically in the framework of two- and three-dimensional inviscid Prandtl equations. Criteria for a gradient catastrophe are found in both cases. For 2D Prandtl equations breaking takes place both for the parallel velocity along the boundary and for the vorticity gradient. For three-dimensional Prandtl flows, breaking, i.e. the formation of a fold in a finite time, occurs for the symmetric part of the velocity gradient tensor, as well as for the antisymmetric part – vorticity. The problem of the formation of velocity gradients for flows between two parallel plates is studied numerically in the framework of two-dimensional Euler equations. It is shown that the maximum velocity gradient grows exponentially with time on a rigid boundary with a simultaneous increase in the vorticity gradient according to a double exponential law.

In paper (Vulfson and Nikolaev, 2022) approximations of the turbulent moments of the atmospheric convective boundary layer are constructed based on a variant of the local similarity theory. As the basic parameters of this theory, the second moment of vertical velocity and the "spectral" Prandtl mixing length are used. This specific choice of the basic parameters allows us to consider the coefficient of turbulent transfer and the dissipation of kinetic energy of the Prandtl turbulence theory as the forms of the local similarity. Therefore, the obtained approximations of the turbulent moments should be considered as natural complementation to the semiempirical turbulence theory. Moreover, within the atmospheric surface layer, the approximations of the new local similarity theory are identical to the relations of the Monin–Obukhov similarity theory (MOST). Therefore, the proposed approximations should be considered as a direct generalization of the MOST under free-convection conditions. The new approximations are compared with the relations of the known local similarity theories. The advantages and limitations of the new theory are discussed. The comparison of the approximations of the new local similarity theory with the field and laboratory experimental data indicates the high effectiveness of the proposed approach.

Direct numerical simulations of the directional sea surface gravity waves are carried out within the framework of the primitive potential equations of hydrodynamics (Slunyaev, Kokorina, 2020; Slunyaev, 2020). The data obtained for conditions of deep water, the JONSWAP spectrum, and various wave intensities and directional spectrum widths are processed with the focus on the statistical and spectral wave characteristics, and on the extreme events. The dynamic kurtosis (i.e., produced by the free wave component) is shown able to contribute essentially to the abnormally large values of the surface displacement kurtosis when the waves are intense and the directional spectrum is relatively narrow (Slunyaev, 2020). In this situation the free wave stochastic dynamics is strongly non-Gaussian, and extreme events last for abnormally long times – up to several tens of characteristic wave periods (Slunyaev, Kokorina, 2020). The long-lived coherent patterns, where most of extreme waves occur, may be revealed using the proposed windowed InverseScattering-Technique approach (Slunyaev, 2021). The physical mechanisms of the rogue wave generation and the corresponding mathematical models; the available field data; results of the direct numerical simulation and of laboratory experiments; new approaches to modeling and forecasting extreme sea waves have been reviewed and discussed (Slunyaev, 2020).

The theory for nonlinear self-modulation is developed for flexural-gravity waves on a water surface covered by a compressed ice sheet of given thickness and density in a basin of a constant depth. Some inconsistencies in the previous fundamental works have been fixed. The domains of instability are presented in the planes of governing physical parameters; the shapes of the

domains exhibit fairly complicated patterns. It is shown that, under certain conditions, the modulational instability can develop from shorter groups and for fewer wave periods than in the situation of deep-water gravity waves on a free water surface (Slunyaev, Stepanyants, 2022).

A simple model for the development of submesoscale perturbations in the atmospheric boundary layer (ABL) is proposed (Chkhetiani, Vazaeva, 2019). The growth of perturbations is associated with the shear algebraic instability of the wind velocity profile in the ABL. Seeking optimum values of such perturbations (streaks) allows one to solve the problem of estimating their scales, which turn out to be about 100–200 m vertically and 300–600 m horizontally. Similar scales are also revealed for experimental data on the structure of the wind field in the lower part of the ABL; the data were obtained in 2017 and 2018 in summer at the Tsimlyansk Scientific Station of the Obukhov Institute of Atmospheric Physics during acoustic sounding of the atmosphere with a high-resolution three-component Doppler minisodar.

In the paper (Shishov et al., 2021) the results of multipoint measurements of wind-direction pulsations and air temperature in the surface layer on the basis of the Tsymljansk Scientific Station of the Obukhov Institute of Atmospheric Physics, Russian Academy of Sciences (RAS), generalized over several years, are considered. The characteristic sizes of vortex and thermal structures, as well as the ratio of these sizes under various conditions, have been determined. The previously found dependence of the characteristic sizes of structures on the conditions of thermal stratification is confirmed. Visualizations of two-dimensional fields of temperature and wind direction are presented.

The relationship between the concentration of an arid aerosol 0.2–0.4 microns in size and the electric field strength is investigated using field measurements carried out on a desert territory in Kalmykia in 2020 (Malinovskaya, Chkhetiani, 2021). It is shown that the increase and decrease in the electric field strength is associated with a change in the wind velocity and the its direction relating to the dune ridges. An increase in the electric field strength occurs at wind velocity close to the threshold value and when the wind direction is close to the tangent to the crest line of the dune. According to an analytical estimate, the relative change in the electric field strength is proportional to the square of the number of microparticles generated. Free microparticles, pushed up by the electric field from the saltation layer, appear at the moment of accumulation of a critical charge on the saltation particle. Particle charging occurs faster with small bounces of particles, as in the tangential direction or when the wind velocity is close to the threshold. The influence of aeolian ripples on the motion and the height of the jumps of the saltating particles is noted at wind directions of 25 –45 to the crest line, as a weakening of the electric field with an increase in the number of microparticles.

DNS LES and modeling is widely used to describe turbulent processes in the atmosphere. Data of a numerical simulation of a stably stratified turbulent Couette flow are analyzed for various values of the Richardson number (Glazunov et al., 2019) . Two different methods are used: direct numerical simulation (DNS) and large-eddy simulation (LES). It is shown that the flow contains large organized structures, along with chaotic turbulence, regardless of the simulation method. These structures appear as inclined layers in the temperature field with weakly stable stratification, separated by very thin layers with large temperature gradients. The existence of such layered structures in nature is indirectly confirmed by the analysis of data from field measurements on the meteorological mast, where temperature gradient histograms are found to be far from the normal distribution and similar to temperature gradient probability distributions obtained in numerical model data. The simulations indicate an increase in the turbulent Prandtl number with an increase in the gradient Richardson number. It is likely that the identified structures serve as efficient barriers for vertical turbulent heat flux without blocking the momentum transfer. We propose a hypothesis that it is these structures which serve as a physical mechanism for maintaining turbulence under supercritically stable stratification.

A relaxation equation for turbulence wavenumber in semi-empirical turbulence closures was considered (Mortikov et al., 2019). It is shown that the well-known phenomenological equation for the dissipation rate of turbulent kinetic energy can be related to this relaxation equation as a close approximation of the latter for stably stratified quasi-stationary flows. The proposed approach makes possible clarification of turbulent closures in the boundary layers of the atmosphere and ocean by specifying the equilibrium states and relaxation relations consistent with the direct and large eddy simulation data.

The problem of modelling 2D isotropic turbulence in a periodic rectangular domain excited by the forcing pattern of prescribed spatial scale is considered (Perezhogin et al., 2019). This setting could be viewed as the simplest analogue of the large scale quasi-2D circulation of the ocean and the atmosphere. Since the direct numerical simulation (DNS) of this problem is usually not possible due to the high computational costs we explore several possibilities to construct coarse approximation models and corresponding subgrid closures (deterministic or stochastic). The necessity of subgrid closures is especially important when the forcing scale is close to the cutoff scale of the coarse model that leads to the significant weakening of the inverse energy cascade and large scale component of the system dynamics. The construction of closures is based on the a priori analysis of the DNS solution and takes into account the form of a spatial approximation scheme used in a particular coarse model. We show that the statistics of a coarse model could be significantly improved provided a proper combination of deterministic and stochas-

tic closures is used. As a result we are able to restore the shape of the energy spectra of the model. In addition the lagged auto correlations of the model solution as well as its sensitivity to external perturbations fit the characteristics of the DNS model much better.

The paper (Debolskiy et al., 2019) discusses approaches to constructing bulk convective boundary layer (CBL) models based on the concept of complete mixing. Large-eddy simulation (LES) results are used to test the basic similarity hypotheses. The empirical constants of the bulk CBL model that are obtained from LES data for the case of free convection agree well with previously published data from laboratory experiments. It is also shown that the flux of kinetic energy from the upper CBL boundary transported by gravity waves is small compared with other components of the balance of turbulence kinetic energy (TKE) in the convective layer. The parametrization of TKE generation for the case of a sheared CBL in terms of the friction velocity and the average wind velocity in the CBL is derived; all dimensionless constants of the theoretical model are obtained from LES data. The results allow us to formulate an integral model of the sheared CBL suitable for practical use.

Large-Eddy Simulation (LES) numerical experiments of neutrally-stratified turbulent flow over an urban-type surface and passive scalar transport by this flow are performed (Glazunov et al., 2022). A simple parameterization of the turbulent length scale containing only one empirical constant is proposed. Multilayer Reynolds-Averaged Navier-Stokes (RANS) model of turbulent flow and turbulent scalar diffusion is constructed. The results of the RANS model are compared with the LES experiments. It is shown that the proposed approach allows predicting the average flow velocity and the scalar concentration inside and above the urban canopy.

The study (Tkachenko et al., 2022) presents the results of large-eddy simulation (LES) of the evening transition in the atmospheric boundary layer in the case of free convection and in the presence of geostrophic wind. The turbulent kinetic energy (TKE) balance and the dispersion dynamics of the velocity components are analyzed. It is shown that fast and slow decay periods can be distinguished within the transition. The differences in TKE anisotropy between these two periods are demonstrated. During the fast decay period, the majority of the energy within the vertical component is consumed due to thermals inertial movement after the cease of convection. This is followed by the TKE redistribution into large-scale horizontal components, which leads to the formation of quasi-horizontal turbulence, where the TKE dissipation is significantly slower in comparison to the isotropic state. It is shown that one-dimensional boundary-layer model, in which turbulent fluxes are parameterized by means of a two-equation closure, does not reproduce evening transition dynamics. In particular, the use of the gradient approximation in the one-

dimensional model leads to the preservation of the convective distribution of the heat flux along the vertical during the transition period and additional TKE generation in the boundary layer due to the action of buoyancy forces. The use of the phenomenological equation for the dissipation rate leads to decreased TKE decay rate during the fast decay period and increased TKE decay rate during the slow decay period. Possible approaches toward modification of the Reynolds-averaged Navier– Stokes (RANS) closures in order to correctly reproduce transition periods of the atmospheric boundary layer are discussed.

Turbulence is ever produced in the low-viscosity/large-scale fluid flows by velocity shears and, in unstable stratification, by buoyancy forces. It is commonly believed that both mechanisms produce the same type of chaotic motions, namely, the eddies breaking down into smaller ones and producing direct cascade of turbulent kinetic energy and other properties from large to small scales toward viscous dissipation. The conventional theory based on this vision yields a plausible picture of vertical mixing and has remained in use since the middle of the twentieth century in spite of increasing evidence of the fallacy of almost all other predictions. The paper (Zilitinkevich et al., 2021) reveals that in fact buoyancy produces chaotic vertical plumes, merging into larger ones and producing an inverse cascade toward their conversion into the self-organized regular motions. Herein, the velocity shears produce usual eddies spreading in all directions and making the direct cascade. This new paradigm is demonstrated and proved empirically; so, the paper launches a comprehensive revision of the theory of unstably stratified turbulence and its numerous geophysical or astrophysical applications.

In paper (Zasko et al., 2022) optimal disturbances of a turbulent stably stratified plane Couette flow in a wide range of Reynolds and Richardson numbers are studied. These disturbances are computed based on a simplified system of equations in which turbulent Reynolds stresses and heat fluxes are approximated by isotropic viscosity and diffusivity with the coefficients obtained from results of direct numerical simulation. Three types of disturbances are considered: large-scale streamwise-elongated rolls converting into streamwise streaks; large-scale vortical structures, inclined in the vertical plane, changing the inclination to the opposite in process of their evolution; near-wall rolls converting into streaks. Large-scale rolls and streaks predominate at neutral or weakly stable stratification while the inclined structures begin to dominate at moderately stable stratification. Near-wall rolls and streaks appear at any stratification and their spanwise size in wall length units does not depend on the values of Reynolds and Richardson numbers. It is shown that the development of inclined optimal disturbances is due to the coupled action of the lift-up effect and the inviscid Orr mechanism. The energetics of the optimal disturbances is discussed. It is shown that inclined optimal disturbances dissipate rapidly after reaching maximum energy amplification.

In paper (Glazunov et al., 2022) large-eddy simulations (LES) of neutrally and stably stratified turbulent flows over urban-type surfaces with relatively low plan area ratios are presented. Numerical experiments were performed for different shapes of streamlined objects and at different static stability. A new method for setting up a numerical experiment aimed at studying the heat and momentum transfer within the roughness layer and investigating the thermal and dynamic interaction between the turbulent flow and the surface as a whole has been proposed. This method enables us to obtain an equilibrium state for values of parameters determining the characteristics of the external turbulent flow chosen beforehand. A strong dependence of the thermal roughness length on stratification was found. We also discuss the physical mechanisms that lead to the maintenance of turbulence above the canopy when the ground surface is strongly cooled.

Several works are devoted to new methods of experimental studies of atmospheric turbulence.

The capabilities of a quadcopter in the hover mode for low-altitude sensing of atmospheric turbulence with high spatial resolution in urban areas characterized by complex orography are investigated in the paper (Shelekhov at al., 2022). The studies were carried out in different seasons (winter, spring, summer, and fall), and the quadcopter hovered in the immediate vicinity of ultrasonic weather stations. The DJI Phantom 4 Pro quadcopter and AMK-03 ultrasonic weather stations installed in different places of the studied territory were used in the experiment. The smoothing procedure was used to study the behavior of the longitudinal and lateral spectra of turbulence in the inertial and energy production ranges. The longitudinal and lateral turbulence scales were estimated by the least-square fit method with the von Karman model as a regression curve. It is shown that the turbulence spectra obtained with DJI Phantom 4 Pro and AMK-03 generally coincide, with minor differences observed in the highfrequency region of the spectrum. In the inertial range, the behavior of the turbulence spectra shows that they obey the Kolmogorov–Obukhov "5/3" law. In the energy production range, the longitudinal and lateral turbulence scales and their ratio measured by DJI Phantom 4 Pro and AMK-03 agree to a good accuracy. Discrepancies in the data obtained with the quadcopter and the ultrasonic weather stations at the territory with complex orography are explained by the partial correlation of the wind velocity series at different measurement points and the influence of the inhomogeneous surface.

The paper (Shelekhov at al., 2021a) demonstrates the possibility of using the telemetry of small unmanned aerial vehicles (UAVs) to monitor the state of atmospheric turbulence. The turbulence spectrum is determined from data on the roll, pitch, and yaw angles of the DJI Mavic Mini quadcopter and then compared with measurements of AMK-03 autonomous sonic weather station.

The measurements are carried out at the Basic Experimental Complex (BEC) of the Zuev Institute of Atmospheric Optics, Siberian Branch, Russian Academy of Sciences (SB RAS) (Tomsk, Russia), the territory of which has a nearly smooth and uniform surface, on July 24 and August 12, 2020. It has been found that the turbulence spectra obtained with AMK-03 and the DJI Mavic Mini are generally identical with minor discrepancies in the high-frequency spectral range from Hz. For the data obtained in July, the turbulence spectra in the inertial range obey the 5/3 law, and the relation of measured turbulence spectra of the longitudinal and transverse velocity components corresponds to the Kolmogorov–Obukhov isotropic turbulence. As for the data obtained in August, a slight deviation from the 5/3 law was observed in both AMK-03 and DJI Mavic Mini measurements. The longitudinal and transverse turbulence scales were estimated by the least-square fit method with the von Karman model as a regression curve. The turbulence scales calculated from the July and August data of AMK-03 and the DJI Mavic Mini coincide, and the condition describing the relation between the longitudinal and transverse scales in the isotropic atmosphere stays true to a good accuracy.

The paper (Shelekhov at al., 2021b) shows the possibility of using small UAVs with a rotary wing to monitor the state of atmospheric turbulence at different altitudes. The measurements were carried out at the Basic Experimental Observatory of the V.E. Zuev Institute of Atmospheric Optics SB RAS. The turbulence spectra at 4, 10, and 27 m, as well as turbulence scale profiles obtained with three DJI Mavic Mini and one DJI Mavic Air quadcopters are reported. The turbulence spectra measured at different altitudes and turbulence scale profiles are compared with the data obtained from three AMK-03 automated meteorological systems installed at the 4-m and 30-m meteorological towers. It has been found that the turbulence spectra obtained with the AMK03 and quadcopters are generally in a good agreement with some differences observed in the highfrequency spectral region nearby $f \sim 1$ Hz. During the experiment, Kolmogorov turbulence was observed in the atmosphere in a wide frequency range at all altitudes. This type of turbulence was confirmed by both the AMK-03 and quadcopter data. When determining the longitudinal and lateral turbulence scales at altitudes of 4, 10, and 27 m, the least square fit method was used with the von Karman model as the regression curve. The turbulence scales calculated from AMK-03 and quadcopter data are shown to agree well. The condition describing the relation between the longitudinal and lateral scales in an isotropic atmosphere is true to sufficient accuracy.

The paper (Evgrafova, Sukhanovskii, 2022) presents results of a laboratory modeling of heat transfer processes in the idealized urban landscape conditions. As an experimental model, we used a three-dimensional layout of the central part of Perm city (the area of five square kilometers) at the scale

of 1:4000. The estimation of governing parameters was done using eddy transfer coefficients which are common for the atmospheric boundary layer. The process of cooling of the city model surface after prolonged heating by infrared radiation was studied. The key issue is the time dependence of the surface temperature on the type of urban structure. We focused on the influence of building density and artificial relief on the cooling process of the layout surface. Two separate stages of cooling were revealed, namely, relatively short period of a fast cooling and longtime relaxation period. On the base of correlation coefficients, it was shown that a buildings density has substantial influence on the fast stage and during this stage the correlation coefficient is larger than 0.4. The correlation at the late stage of cooling is weak. The duration of the fast cooling stage shows even stronger correlation (above 0.5) with building density.

In paper (Repina, Artamonov, 2020) the results of direct measurements of turbulent fluxes at Bellingshausen station (the Antarctic) in the summer of 2002, 2003, 2007, and 2009 are considered. The features of energy exchange are studied for these seasons. The interannual and intraseasonal variability of energy exchange characteristics is investigated. It is found that heat fluxes depend on the surface state and on the wind direction. Also, as a rule, they have a clear diurnal course with negative or near-zero values at night and with positive values in the daytime, when intensive convective fluxes are observed over open ground. The momentum flux is defined by the wind direction and wind speed and by stratification conditions. The main factors affecting energy exchange between the atmosphere and the surface in the Antarctic coastal zone are synoptic conditions and the surface state (snowless season duration and moss cover presence).

The structure of atmospheric turbulence over urban areas has been actively studied. The paper (Drozd et al., 2022) considers the conditions for the applicability of the Monin-Obukhov similarity theory to the calculation of turbulent fluxes over a heterogeneous urban landscape.

A new 21-meter eddy covariance tower is installed in the Meteorological observatory of Moscow State University in November 2019. The mast is located inside the urban area and makes it possible to analyze the structure of atmospheric turbulence in a heterogeneous urban condition. The measurement data from November 2019 to May 2020 are processed. Turbulent fluctuations of the wind velocity components are found to increase with height within 20 meters above the surface. The turbulent kinetic energy is proportional to the square of the averaged horizontal wind speed. The drag coefficient is determined by the type of footprint surface, with a value of 0.08 and 0.05 for urbanized and vegetated surfaces, respectively. The turbulent flux of heat flux is reasonably well predicted by diagnostic relation with heat flux, skewness and standard deviation of vertical speed, suggesting significant

contribution of coherent structures to turbulent fluxes. The daily amplitude of the temperature variance increases with the daily amplitude of the average temperature. In the paper (Barskov et al., 2022) the results from the multi-level mast eddycovariance measurements conducted over flat grassland and over complex urban terrain composed of trees and small buildings are presented. Relationships between the stability parameter and turbulent statistical properties were analysed. Over flat grassland, non-dimensional turbulent moments up to the third-order obey Monin–Obukhov similarity theory. Third-order moments increase for increasing instability, indicating nonlocal turbulent transport of heat flux due to convective motions, and in this case, the relationship between the third- and second-order moments obtained using the framework of the mass-flux approach might be applicable. In stable conditions, the turbulent transport of heat flux is positive and does not demonstrate an explicit dependence on stability but might be associated with large eddies and sweep motions transporting downwards the heat flux originating near the top of a stable boundary layer. Such a downward transport of negative heat flux by large eddies makes applicable the mass-flux approach even in stable boundary layers at higher levels. Over the urban landscape, for all wind directions the third moment corresponds well with the theoretical curve in cases of stable and unstable stratification, but there is a wide spread of data in near-neutral conditions. Skewness of the vertical velocity component is negative over the urban landscape and its value depends on wind direction. At lower levels, the standard deviation of the vertical velocity component is increasing withstability faster than expected from the theoretical curve. Over the urban landscape, large roughness elements do not affect the performance of the mass-flux approach in the convective boundary layer. Furthermore, there is a link between the second and third moments even in stable boundary layers over heterogeneous landscape.

In paper (Barskov et al., 2019) experimental results of turbulent heat exchange between a small frozen lake surrounded by forest and the atmospheric boundary layer are presented. Heat fluxes are measured at three levels using the eddy-covariance method and estimated by Monin–Obukhov similarity theory (MOST). In addition, we estimate the heat flux due to non-local turbulent transport of heat by coherent structures originating at the forest/lake transition, given the measured skewness of w and w w T, using a bimodal bottom-up–top-down model or the massflux models appropriate to the convective boundary layer. Two heat-flux-formation regimes in the surface layer are clearly distinguished. When the flow is from the vast forest, wind shear at the tree height leads to increased turbulent kinetic energy above the centre of the lake. Under conditions of simultaneous horizontal advection of warm air in the boundary layer above the canopy, a downward turbulent diffusion of negative heat flux leads to increased negative sensible heat flux in the surface

layer, accompanied by an increasing third moment w w T. Since MOST does not account for this mechanism, MOST-based fluxes poorly correspond to the eddycovariance data in this case. At the same time the contribution of coherent structures increases. In contrast, when the flow is from the gap connecting the lake with the wide clearing, the effects of landscape inhomogeneity significantly reduce. In this case the turbulent transport of the heat flux from the upper part of the boundary layer vanishes, w w T is negligible, and the heat flux is now primarily determined by the wind speed and temperature differences between the surface and nearsurface atmosphere. This is a surface-flow regime for which MOST has been developed, and MOST-based fluxes correlate well with eddy-covariance data.

Dynamical interaction between lower, middle and high atmosphere

Dynamical processes in the Arctic stratosphere in the winter of 2017/2018 are analyzed using data of the NCEP reanalysis and SABER and MLS satellite measurements . The following features are revealed: the downward propagation of wave activity from the stratosphere to troposphere over Canada in late December and early January, the major sudden stratospheric warming with the zonal wind reversal in February 2018 accompanied by the stratospheric polar vortex splitting, the propagation of stratospheric circulation anomalies to the lower troposphere, the mesospheric cooling, the stratopause height change, and the cooling in the tropical lower stratosphere (Vargin, Kiryushov, 2019).

In (Vargin at al., 2022, 2021) presented that Arctic stratosphere winter season of 2021– 2022 was characterized by a stable, cold stratospheric polar vortex with a volume of polar stratospheric clouds (PSC) close to the maximum values since 1980, before the beginning of minor sudden stratospheric warming (SSW) events in the late February and early March and major SSW on 20 March. Analysis of dynamical processes of the Arctic stratosphere using reanalysis data indicates that the main reasons for the strengthening of the stratospheric polar vortex in January– February are the minimum propagation of planetary wave activity from the troposphere to the stratosphere over the past 40 years and its reflection in the upper stratosphere–lower mesosphere in the second half of January. The first minor SSW was limited to the upper polar stratosphere, whereas the second one propagated to the middle and lower stratosphere and led to the disappearance of the PSC, which prevented significant ozone depletion. Both minor and major SSW events led to a weakening of the residual meridional circulation in the upper Arctic stratosphere and its intensification in the middle and lower stratosphere, which contributed to additional warming of the subpolar region and weakening of

the polar vortex. After the SSW, which persisted for about 3 weeks, and until the end of the winter season, the lower stratosphere temperature inside the stratospheric polar vortex remained higher than required for the formation of polar stratospheric clouds.

Paper (Lukyanov et al., 2021) presents the results of applying the Lagrangian methods to study the fine dynamic structure of the stratospheric polar vortex in the winter–spring of 2019–2020. Characteristics of the vortex structure for this winter are compared with those of a strong polar vortex and the winter of 2018–2019, when the vortex was weak. Due to the low activity of planetary waves, the polar vortex in 2019–2020 remained stable until the end of April, which created the conditions for record ozone destruction in the Arctic. We present variations of the horizontal dynamic structure obtained using reverse domain filling (RDF) and the vortex strength represented as an M function depending on time and altitude. Variations in ozone and thermodynamic parameters averaged over the ensemble of trajectories inside the vortex using the ERA5 reanalysis data are also presented.

Five 50-year simulations for the 5th version of the climate model of the Marchuk Institute of Numerical Mathematics, Russian Academy of Science (INM RAS), are used to analyze the interannual variability of Arctic stratospheric polar vortex and dates of spring breakup events (springtime transition) in comparison with reanalysis data (Vargin et al., 2020). Early spring breakup events are accompanied by stronger wave activity in comparison with late ones. Winter seasons with the maximal air volume in the polar stratosphere and conditions sufficient for the formation of polar stratospheric clouds are characterized by relatively early spring breakup events. The model is employed to analyze the Northern Hemisphere storm track characteristics in the winter season. The results show similar features of the North Atlantic and North Pacific storm tracks that dominate in the Northern Hemisphere in the model simulations and reanalysis data (Vargin et al, 2019). A composite analysis of the weakening /strengthening of Arctic stratospheric polar vortex events with their influence on the troposphere shows an equatorward/poleward shift in the North Atlantic storm track. As a response to the recent Arctic amplification, a poleward shift in the Pacific storm track and weakening of the North Atlantic storm track have been revealed when comparing two periods: 1998-2014 and 1980-1997. Also, simulations for the period from 2015 to 2100 under moderate (SSP2-4.5) and severe (SSP5-8.5) scenarios of greenhouse gases growth are analyzed to investigate changes of Arctic polar stratospheric vortex, planetary wave propagation, Sudden Stratospheric Warming frequency, Final Warming dates, and meridional circulation. Strengthening of wave activity propagation and a stationary planetary wave number 1 in the middle and upper stratosphere, acceleration of meridional circulation, an increase of winter means polar stratospheric volume

(Vpsc) and strengthening of Arctic stratosphere interannual variability after the middle of 21st century, especially under a severe scenario, were revealed (Vargin et al., 2022). March monthly values of Vpsc in some winters could be about two times more than observed ones in the Arctic stratosphere in the spring of 2011 and 2020, which in turn could lead to large ozone layer destruction. Composite analysis shows that "warm" winters with the least winter mean Vpsc values are characterized by strengthening of wave activity propagation from the troposphere into the stratosphere in December but weaker propagation in January– February in comparison with winters having the largest Vpsc values.

The response of the Arctic stratosphere to El Nino is studied with account of its Eastern and Central Pacific types for the period of 1950–2005. The study is based on the regression and composite analysis using the simulations with six CMIP5 coupled climate models and reanalysis data (Kolennikova et al., 2021). Also five 50-year simulations with version 5 of the INM RAS coupled climate model revealed that the winters with El Niño are characterized by higher Arctic stratospheric temperature as compared to the seasons with La Niña. Lower stratospheric temperature in the Arctic regions as compared to the seasons with negative sea surface temperature (SST) anomalies corresponds to the winter seasons with positive SST anomalies in the North Pacific (Vargin et al., 2021).

Dynamical processes and changes in the ozone layer in the Arctic stratosphere during the winter of 2019–2020 were analyzed using numerical experiments with a chemistry-transport model (CTM) and reanalysis data (Smyshlyaev et al., 2021). The results of numerical calculations using CTM with Dynamic parameters specified from the Modern Era Retrospective analysis for Research and Applications, version 2 (MERRA-2) reanalysis data, carried out according to several scenarios of accounting for the chemical destruction of ozone, demonstrated that both Dynamic and chemical processes contribute significantly to ozone changes over the selected World Ozone and Ultraviolet Radiation Data Centre network stations, both in the Eastern and in the Western hemispheres. Based on numerical experiments with the CTM, the specific Dynamic conditions of winter–spring 2019–2020 described a decrease in ozone up to 100 Dobson Units (DU) in the Eastern Hemisphere and over 150 DU in the Western Hemisphere. In this case, the photochemical destruction of ozone in both the Western and Eastern Hemispheres at a maximum was about 50 DU with peaks in April in the Eastern Hemisphere and in March and April in the Western Hemisphere. Heterogeneous activation of halogen gases on the surface of polar stratospheric clouds, on the one hand, led to a sharp increase in the destruction of ozone in chlorine and bromine catalytic cycles, and, on the other hand, decreased its destruction in nitrogen catalytic cycles. Analysis of wave activity using 3D Plumb fluxes showed

that the enhancement of upward wave activity propagation in the middle of March over the Gulf of Alaska was observed during the development stage of the minor sudden stratospheric warming (SSW) event that led to displacement of the stratospheric polar vortex to the north of Canada and decrease of polar stratospheric clouds' volume. The variability of parameters of the Antarctic ozone anomaly is studied using data of the TOMS/OMI satellite monitoring of the ozone layer, MERRA-2 reanalysis, and balloon sounding of the vertical distribution of ozone and temperature at the South Pole (Vargin et al., 2020). The dynamic processes in the Antarctic stratosphere which define conditions for the significant ozone layer destruction are analyzed. Despite the decrease in the concentration of ozone-depleting substances, the significant ozone loss in the recent 8 years was observed in the Antarctic in 2011 and 2015.

Three-dimensional (3D) planetary wave analysis can provide more regionalized information on stratospheric-tropospheric dynamic interactions (Wei et al., 2021). The upward wave flux from the troposphere to the stratosphere is maximized above northeastern Eurasia, while the downward flux occurs mainly over the North America and North Atlantic (NANA) region, which is much stronger during mid-to-late winter. This distribution is determined by the wavewave interactions between the different wavenumbers of planetary waves, especially between wavenumber 1 and wavenumber 2. The upward wave flux anomalies in early winter are negatively correlated with the strength of the stratospheric polar vortex (SPV). During the mid-to-late winter months, the strength of the SPV is positively correlated with the first mode of the 3D wave flux and has a leading relationship of approximately one month. The stronger SPV corresponds to a stronger upward wave flux above northern Eurasia and stronger downward flux over the NANA region. The interannual variations in wave flux during early winter are closely associated with the Scandinavian wave train pattern. In contrast, the wave flux variations are related to the circulation anomaly corresponding to the Arctic Oscillation during mid-to-late winter, which causes climate anomalies across the Northern Hemisphere, especially coherent temperature changes in northern Europe, eastern United States and northeastern China.

The paper (Vyazankin et al., 2020) presents the prognostic capabilities of the SOCOL global climate model. A correction of the trajectory is proposed by supplementing the algorithms of the nominal control of the return vehicle with the atmospheric parameters at altitudes of 40–80 km obtained as a result of prognostic calculations. The estimates of chemical ozone depletion in winter – spring sea sons are given for the Arctic stratosphere based on long-term observations of the vertical distribution of ozone in paper (Tsvetkova et al., 2021). The features and possible causes for an un usually strong and stable stratospheric polar vortex in the Arc tic in the winter 2019/2020, that led to a

record ozone loss in recent years, and the dynamic processes associated with this polar vortex are analyzed. The TRACAO trajectory model and ERA5 reanalysis are used for the comparative analysis of ozone depletion in the polar vortex in the winter – spring seasons 2010/2011 and 2019/2020. To achieve better agreement of simulated Arctic winter stratospheric dynamic with observations assimilation procedure nudging was incorporated in CCM SOCOL ((Tsvetkova et al., 2020). Trajectories based on SOCOL output winds demonstrate the reasonable agreement with trajectories based on reanalysis data inside the polar vortex and can be used for analysis and forecast of ozone related processes in winter-spring seasons. Obtained results of several recent major Arctic SSW events analysis show that CCM SOCOL could be used for SSW forecast over the period up to 8 days.

The paper (Lukyanov et al., 2021) presents a short description and some applications of trajectory and dispersion models developed for studies of the stratospheric and tropospheric transport. The trajectory model TRACAO was applied to investigate the processes related to ozone depletion in the polar stratosphere, stratosphere – troposphere exchange and for analysis of balloon and aircraft (M-55, YAK-42) observations. Then based on TRACAO the dispersion model GLADIM with eddy diffusion parameterization was developed and applied for the simulation of volcanic ash dispersion and the carbon dioxide profiles reconstruction. The model validation was conducted by comparisons with results of widely used FLEXPART model. Nowadays these models are used in the regional center of information and analysis «Middle atmosphere». Based on the results of simulations with the TRACAO trajectory model, the comparative analysis of stratospheric polar vortex evolution in winters of 2015/2016 and 2018/2019 is performed (Vargin et al., 2020).

The variability of Arctic total ozone in the winter of 2015/2016 is studied using the data of the national network equipped with M-124 filter ozonometers and satellite monitoring (Nikiforova et al., 2019). The first ozone minihole that emerged in the first half-year over the whole history of observations (developed at the end of January 2016) is analyzed. The reasons for the total ozone variability over Russia in the first quarter of 2016 are analyzed, and the comparison with the significant Arctic ozone anomalies in 1996/1997 and 2010/2011 is presented.

The papers (Nerushev, Ivangorodsky, 2019; Nerushev et al., 2020) present the method of determining the turbulence zones in the upper troposphere that is based on measurements of atmospheric self-radiation from geostationary meteorological satellites and uses extremal correlation algorithms. The features of the method applied to the determination of clear air turbulence (CAT) from the SEVIRI radiometer water vapor 6.2 μm channel measurements of European geostationary meteorological satellites of the second generation are considered. The results of the calculations of average monthly

space turbulence zones with different values of the coefficient of horizontal mesoscale turbulent diffusion for 2007–2017 in the satellite view zone are presented. It is shown, that for the past 11 years there has been a significant increase in the area of zones occupied by relatively weak and moderate turbulence and a slight decrease in the area of zones with strong and very strong turbulence. A close relationship was revealed between the interannual variability of the monthly area means of turbulence zones and the corresponding variability of the characteristics of jet streams. Significant with a probability of more than 95 % annual variations of area of turbulence zones and most of the characteristics of jet stream have been identified. The most pronounced are in phase annual variations of the turbulence areas with the jet stream area and the velocity gradient and counterphase variations with the latitude and longitude of the centre of the jet stream. The connection between the variability of turbulence and the temperature variability of the upper troposphere is revealed. In this case, the effect of temperature on turbulence manifests itself indirectly through the characteristics of jet stream.

According to known experiments both the zonal and meridional components of the wind demonstrate a clear increase in amplitude, starting from heights of 80–85 km, and the maximum amplitudes, which are reached at altitudes of 100–110 km. With a further increase in altitude, a gradual decrease in amplitudes begins. The wind maximum amplitudes turn out to be much larger than predicted by the theory of tidal movements in the ionosphere or the empirical Horizontal Wind Model (HWM). In paper (Chkhetiani, Shalimov, 2022) a simple two-dimensional model to indicate the cause of abnormal amplitudes of wind motion in the lower ionosphere is proposed. The model is based on the existence of a well-established Ekman wind profile at the heights of the mesosphere-thermosphere.

Numerical modeling of climate

Climate changes in 2015–2100 have been simulated with the use of the INM-CM5 climate model following four scenarios: SSP1-2.6, SSP2-4.5, and SSP5-8.5 (single model runs) and SSP3-7.0 (an ensemble of five model runs) (Volodin, Gritsun 2020). Changes in the global mean temperature and spatial distribution of temperature and precipitation are analyzed. The global warming predicted by the INM-CM5 model in the scenarios considered is smaller than that in other CMIP6 models. It is shown that the temperature in the hottest summer month can rise more quickly than the seasonal mean temperature in Russia. An analysis of a change in Arctic sea ice shows no complete Arctic summer ice melting in the 21st century under any model scenario. Changes in the meridional streamfunction in atmosphere and ocean are studied.

In paper (Vorobyeva, Volodin, 2021) The study of winter seasonal predictability with the climate model INM-CM5-0 is presented. Initial conditions were produced using ERA-Interim reanalysis data for atmosphere, SODA3.4.2 reanalysis data for ocean and the bias-correction algorithm. The seasonal 5-month reforecasts consisting of 10 ensemble members with small initial condition perturbations for each year over the 35-yr period are conducted. A comparison of the multiyear mean winter averaged anomaly correlation for basic variables in several regions with similar results of SLAV model was conducted. An increase in the anomaly correlation for the years with El Nino and La Nina events was shown. The predictability of NAO and PNA indices was studied. INM-CM5-0 provides very high skill in predicting the winter NAO (correlation coefficient of 0.71 with ERA Interim reanalysis and 0.68 with instrumental CRU data for 1991– 2010). It was shown, that the stratospheric variability provides a significant contribution, although potentially is not the only cause of model high skill in NAO index predictability. Correlation coefficients for PNA index in December-February is 0.60. In the years of the most pronounced El Nino the values of PNA index have significantly positive values, and for La Nina years they are noticeably less than zero.

Current climate models demonstrate large discrepancy in equilibrium climate sensitivity (ECS) (Volodin, 2021). The effects of cloudiness parameterization changes on the ECS of the INM-CM4-8 climate model were investigated. This model shows the lowest ECS among CMIP6 models. Reasonable changes in the parameterization of the degree of cloudiness yielded ECS variability of 1.8–4.1 K in INM-CM4-8, which was more than half of the interval for the CMIP6 models. The three principal mechanisms responsible for the increased ECS were increased cloudiness dissipation in warmer climates due to the increased water vapor deficit in the non-cloud fraction of a cell, decreased cloudiness generation in the atmospheric boundary layer in warm climates, and the instantaneous cloud response to CO2 increases due to stratification changes.

The analysis is carried out for changes in runoff of the Amur and Selenga rivers in the 21st century according to the CMIP6 (Coupled Model Intercomparison Project, Phase 6) climate model ensemble simulations using the Bayesian approach versus stream gage data on annual runoff and GPCP-2.3 dataset on annual precipitation over catchments on different timescales (Lipavskii et al., 2022). For both catchments, significant intermodel differences are associated with the projections of multiyear mean runoff and interannual variability. The intermodel distribution of Bayesian weights indicates a high role of uncertainty related to initial conditions for model simulations. There is a positive trend in total runoff in the Amur River basin in the 21st century under all analyzed anthropogenic forcing scenarios. For total runoff

of the Selenga River, there are no trends in the 21st century for all analyzed scenarios. No significant trends for the Amur and Selenga surface runoff were revealed for all algorithms for considering Bayesian weights and all anthropogenic forcing scenarios. At the same time, significant interdecadal variations in the interannual variability of runoff were found.

The duration of the navigation period (DNP) on the Northern Sea Route (NSR) and in some parts of it in the twenty-first century has been analyzed based on the models of the CMIP5 ensemble (Coupled Models Intercomparison project, phase 5) under the RCP 8.5 scenario using Bayesian averaging methods (Parfenova et al., 2022). According to the study results, differences in the quality of the DNP models and in DNP variations are greater in the western part of the NSR than in the eastern part. The DNP ensemble average was obtained in the range of 3–4 months in the middle of the twenty-first century and increasing to about six months by the end of the century. The ensemble average estimates of variations in DNP are generally robust for the choice of assumptions used for calculating the Bayesian weights. The joint consideration of the quality of modeled climate characteristics on all time scales (long-term average, interannual variations, and linear trend) in comparison with the satellite data makes it possible to reduce the intermodel standard deviation by two times for the western part of the NSR and one and a half times for the eastern part.

In paper (Denisov et al., 2022) model estimates of the contribution of anthropogenic and natural fluxes of greenhouse gases from the territories of different countries to global climate change in the 21st century under different scenarios of anthropogenic forcing were obtained. Quantitative estimates were made for the effect of changes in regional climatic conditions on the intensity of the greenhouse gas exchange between the atmosphere and natural ecosystems over different time horizons in comparison with anthropogenic emissions. For Russia, China, Canada, and the United States, the CO2 uptake by natural ecosystems in the second half of the 21st century decreases under all scenarios of anthropogenic forcing, with a weakening of the corresponding climate-stabilizing effect. At the same time, the methane emission to the atmosphere by wetlands in the analyzed regions increases significantly in the 21st century according to the model estimates. As a consequence, the cumulative effect of natural fluxes of greenhouse gases into the atmosphere for some regions may accelerate the warming.

A stationary, computationally efficient scheme ChAP 1.0 (Chemical and Aerosol Processes, version 1.0) for the sulfur cycle in the troposphere is developed (Eliseev et al., 2021). This scheme is designed for Earth system models of intermediate complexity (EMICs). The scheme accounts for sulfur dioxide emissions into the atmosphere, its deposition to the surface, oxidation to sulfates, and dry and wet deposition of sulfates on the surface. The calcula-

tions with the scheme are forced by anthropogenic emissions of sulfur dioxide into the atmosphere for 1850–2000 adopted from the CMIP5 dataset and by the ERA-Interim meteorology assuming that natural sources of sulfur into the atmosphere remain unchanged during this period. The ChAP output is compared to changes of the tropospheric sulfur cycle simulations with the CMIP5 data, with the IPCC TAR ensemble, and with the ACCMIP phase II simulations. In addition, in regions of strong anthropogenic sulfur pollution, ChAP results are compared to other data, such as the CAMS reanalysis, EMEP MSC-W, and individual model simulations. Our model reasonably reproduces characteristics of the tropospheric sulfur cycle known from these information sources. In our scheme, about half of the emitted sulfur dioxide is deposited to the surface, and the rest is oxidised into sulfates. In turn, sulfates are mostly removed from the atmosphere by wet deposition. The lifetimes of the sulfur dioxide and sulfates in the atmosphere are close to 1 and 5 d, respectively. The limitations of the scheme are acknowledged, and the prospects for future development are figured out. Despite its simplicity, ChAP may be successfully used to simulate anthropogenic sulfur pollution in the atmosphere at coarse spatial scales and timescales.

The paper (Eliseev et al., 2019) updates the results obtained earlier with the climate model developed at the A.M. Obukhov Institute of Atmospheric Physics of the Russian Academy of Sciences (IAP RAS CM) and describing the impact of atmospheric sulfur dioxide on the terrestrial carbon cycle. Since no global data are available for the near-surface SO2 concentration, a statistical model was used to reconstruct its concentration from appropriate data on surface sulfate concentrations; the coefficients of this model were tuned by using the output of the RAMS-CMAQ atmospheric chemistry and transport model. The results obtained in this study are generally consistent with data reported earlier. Specifically, the most significant SO2 impact on the terrestrial carbon cycle was found to be for southeastern North America and for Europe. However, this impact for southeastern Asia obtained in this study is considerably weaker than the value obtained earlier, which can be explained by the excessive moisture content in the atmosphere used in the IAP RAS CM for this region.

Concluding remarks

In this report, we overviewed the articles belonging to the field of dynamical meteorology, or closely related to it, which are authored or co-authored by Russian scientists and have been published in 2019–2022 in peer-reviewed journals indexed in WoS and/or Scopus databases. The review would not have been possible without participation and support of a large number of Russian scientists, to whom all we are sincerely grateful.

References

1. Akperov M., Rinke A., Mokhov I.I. et al. Future projections of cyclone activity in the Arctic for the 21st century from regional climate models (Arctic-CORDEX) // Glob. Planet. Change. 2019. V. 182. P. 103005.
2. Akperov M., Zhang W., Miller P.A., Mokhov I.I., Semenov V.A., Matthes H., Rinke A. Responses of Arctic cyclones to biogeophysical feedbacks under future warming scenarios in a regional Earth system model // Environmental Research Letters. 2021. V. 16. №. 6. P. 064076.
3. Akperov M.G. Mokhov I.I., Dembitskaya M.A., Parfenova M.R., Rinke A. Lapse rate peculiarities in the Arctic from reanalysis data and model simulations // Russian meteorology and hydrology. 2019. V. 44. P. 97-102.
4. Akperov M.G., Eliseev A.V., Mokhov I.I., Semenov V.A., Parfenova M.R., Koenigk T. Wind energy potential in the arctic and subarctic regions and its projected change in the 21st century according to regional climate model simulations // Russian Meteorology and Hydrology. 2022. DOI: 10.52002/0130-2906-2022-6-18-29.
5. Akperov M.G., Semenov V.A., Mokhov I.I., Parfenova M.R., Dembitskaya M.A., Bokuchava D. D., Dorn W. The influence of ocean heat transport in the Barents Sea on the regional sea ice and the atmospheric static stability // Ice and Snow. 2019. V. 59. №. 4. P. 529–538.
6. Arctic Climate: processes and changes // Ed. V. Semenov and I. Mokhov. M: Fizmatkniga, 2022. 360 p.
7. Barskov K. , Chechin D. , Drozd I., Repina I. et al. Relationships between second and third moments in the surface layer under different stratification over grassland and urban landscapes // Boundary-Layer Meteorology. 2022.
8. Barskov K., Stepanenko V., Repina I., Artamonov A., Gavrikov A. Two regimes of turbulent fluxes above a frozen small lake surrounded by forest // Boundary-Layer Meteorology. 2019. V. 173. P. 311–320.
9. Bekryaev R.V. Interrelationships of the North Atlantic multidecadal climate variability characteristics // Russian Journal of Earth Sciences. 2019. V. 19(3). P. ES3004.
10. Bekryaev R.V. One mystery of the North Atlantic multidecadal variability. An attempt of simple explanation // IOP Conference Series: Earth and Environmental Science. 2019. V. 231, No. 1. P. 012008.
11. Bekryaev R.V. Statistical Aspects of Quantitative Estimation of Polar Amplification. Part 1: The Ratio of Trends // Russian Meteorology and Hydrology. 2022. V. 47, No. 6. P. 419–427.
12. Chashechkin Y.D. Conventional partial and new complete solutions of the fundamental equations of fluid mechanics in the problem of periodic internal waves with accompanying ligaments generation // Mathematics. 2021. V. 9(6). No. 586.
13. Chashechkin Y.D., Zagumennyi I.V. Formation of waves, vortices and ligaments in 2D stratified flows around obstacles // Physica Scripta. 2019. V. 94. No. 5 P. 1–17. doi:10.1088/1402-4896/ab0066.
14. Chashechkin Yu.D. Fast superfine components and sound packets in flows induced by a drop impact on a target fluid at rest // Fluid Dynamics & Material Processing (FDMP). 2020. V. 16, No. 4. P. 773–800. DOI:10.32604/fdmp.2020.09001.

15. Chashechkin Yu.D., Ilynykh A.Yu. Complete Coalescence, Partial Bounce and Rebound: Different Regimes Resulting from the Interaction of a Free Falling Drop with a Target Fluid // Fluid Dynamics & Material Processing (FDMP). 2020. V. 16, No. 4. P. 801–811. DOI:10.32604/fdmp.2020.09168.
16. Chashechkin Yu.D., Zagumennyi I.V. 2D hydrodynamics of a plate: from creeping flow to transient vortex regimes // Fluids. 2021. V. 6(9). P. 310. https://doi.org/10.3390/fluids6090310.
17. Chechin D.G., Makhotina I.A., Lüpkes C., Makshtas A.P. Effect of Wind Speed and Leads on Clear-Sky Cooling over Arctic Sea Ice during Polar Night. Journal of the atmospheric science. 2019. V. 76. P. 2481–2503. https://doi.org/10.1175/JAS-D-18-0277.1.
18. Chernokulsky A., Kurgansky M., Mokhov I., Shikhov A., Azhigov I. Selezneva E., Zakharchenko D., Antonescu B., Kühne T. Tornadoes in Northern Eurasia: from the Middle Age to the Information Era // Monthly Weather Review, 2020, Vol. 148, No 8, P. 3081–3110, DOI: 10.1175/MWR-D-19-0251.1
19. Chernokulsky A., Shikhov A., Bykov A., Azhigov, I. Satellite-based study and numerical forecasting of two tornado outbreaks in the Ural region in June 2017 // Atmosphere. 2020. V. 11. No. 11. P.1146. DOI: 10.3390/atmos11111146.
20. Chernokulsky A., Shikhov A., Bykov A., Kalinin N., Kurgansky M., Sherstyukov B., Yarinich Yu. Diagnosis and modelling of two destructive derecho events in European Russia in the summer of 2010 // Atmospheric Research. 2022. Vol. 267. P. 105928 DOI: 10.1016/j.atmosres.2021.105928
21. Chernokulsky A.V., M.V. Kurgansky, I.I. Mokhov, A.N. Shikhov, I.O. Azhigov, E. V. Selezneva, D. I. Zakharchenko, B. Antonescu, and T. Kuhne Tornadoes in the Russian Regions // Russian Meteorology and Hydrology, 2021, V. 46, No 2, P. 69–82, DOI: 10.3103/S1068373921020023.
22. Chernokulsky A.V., Shikhov A.N., Azhigov I.O., Eroshkina N.A., Korenev D.P., Bykov A.V., Kalinin N.A., Kurgansky M.V., Pavlyukov Yu.B., Sprygin A.A., Yarinich Yu.I. Squalls and Tornadoes over the European Territory of Russia on May 15, 2021: Diagnosis and Modeling // Russian Meteorology and Hydrology. 2022. V. 47. N. 11. P. 859–873. doi: 10.3103/S1068373922110073.
23. Chkhetiani O.G., Shalimov S.L. On anomalous wind amplitudes in the lower ionosphere // Journal of Atmospheric and Solar-Terrestrial Physics. 2022. V. 240. P.105960.
24. Chkhetiani O.G., Vazaeva N.V. On algebraic perturbations in the atmospheric boundary layer // Izvestiya, Atmospheric and Oceanic Physics. 2019. V. 55. No 5. P. 432-445.
25. Davydova M.A., Chkhetiani O.G., Levashova N.T., Nechaeva A.L. On estimation of the contribution of secondary vortex structures to the transport of aerosols in the atmospheric boundary layer // Fluid Dynamics. 2022. Vol. 57. No. 8. P. 998–1007.
26. Debolskiy A.V., Stepanenko V.M., Glazunov A.V., Zilitinkevich S.S. Bulk models of sheared boundary layer convection // Izvestiya – Atmospheric and Oceanic Physics. 2019. Vol. 55, no. 2. P. 139–151. DOI: 10.1134/s000143381902004x.
27. Demchev D.M., Kulakov M.Y., Makshtas A.P., Makhotina I.A., FilChuk K.V., Frolov I.E. Verification of ERA-Interim and ERA5 reanalyses data on surface air temperature in the Arctic // Russian Meteorology and Hydrology. 2020. V. 45. P. 771–777.

28. Denisov S.N., Eliseev A.V., Mokhov I.I. Model Estimates for Contribution of Natural and Anthropogenic CO2 and CH4 Emissions into the Atmosphere from the Territory of Russia, China, Canada, and the USA to Global Climate Change in the 21st Century // Russian Meteorology and Hydrology. 2022. V. 47. №. 10. P. 735–747.
29. Diansky N.A., Stepanov D.V., Fomin V.V. and Chumakov M.M. Water Circulation Off the Northeastern Coast of Sakhalin during the Passage of Three Types of Deep Cyclones over the Sea of Okhotsk // Russian Meteorology and Hydrology. 2020. V. 45(1). P. 29–38. https://doi.org/10.3103/S1068373920010045.
30. Durneva E.A., Chkhetiani O.G. Planetary upper-level frontal zone in the euro-Atlantic sector in summer in 1990–2019 // Russian Meteorology and Hydrology. 2021. V. 46. No 6. P. 365371.
31. Eliseev A.V., Gizatullin R.D., Timazhev A.V. ChAP 1.0: a stationary tropospheric sulfur cycle for Earth system models of intermediate complexity // Geoscientific Model Development. 2021. V. 14. №. 12. P. 7725–7747.
32. Eliseev A.V., Timazhev A.V., Jimenez P.L. Scale Heights of Water Vapor and Sulfur Compounds in the Lower Troposphere // Atmospheric and Oceanic Optics. 2022. V. 35. №. 6. P. 782–792.
33. Eliseev A.V., Zhang M., Gizatullin R.D., Altukhova A.V., Perevedentsev Y.P., Skorokhod A.I. Impact of sulfur dioxide on the terrestrial carbon cycle / /Izvestiya, Atmospheric and Oceanic Physics. 2019. V. 55. P. 38–49.
34. Ermakov D., Kuzmin A., Pashinov E., Sterlyadkin V., Chernushich A., Sharkov E. Comparison of Vertically Integrated Fluxes of Atmospheric Water Vapor According to Satellite Radiothermovision, Radiosondes, and Reanalysis // Remote Sens. 2021. V. 13. P. 1639. https://doi.org/10.3390/rs13091639.
35. Ermakov D.M., Raev M.D., Chernushich A.P., Sharkov E.A. Algorithm for construction of global ocean-atmosphere radiothermal fields with high spatiotemporal sampling based on satellite microwave measurements // Izvestiya, Atmospheric and Oceanic Physics. 2019. Vol. 55. No. 9. P. 1041–1052. doi: 10.1134/S0001433819090159.
36. Ermakov D.M., Sharkov E.A., Chernushich A.P. Role of tropospheric latent heat advective fluxes in the intensification of tropical cyclones // Izvestiya, Atmospheric and Oceanic Physics. 2019. V. 55, No. 9. P. 1254–1265. doi: 10.1134/S0001433819090172.
37. Evgrafova A., Sukhanovskii A. Angular momentum transfer in direct numerical simulations of a laboratory model of a tropical cyclone // Geophysical & Astrophysical Fluid Dynamics. 2022b. Vol. 116, N. 3. P.185–205. doi: 10.1080/0309 1929.2022.2066659.
38. Evgrafova A., Sukhanovskii A. Impact of complex relief on heat transfer in urban area // Urban Climate. 2022. V. 43. P. 101177. https://doi.org/10.1016/ j.uclim.2022.101177.
39. G.S. Golitsyn Probabilistic structures of the macroworld: earthquakes, hurricanes, floods... Moscow: Fizmatlit, 2021. 174 p.
40. Glazunov A., Mortikov E., Debolskiy A. Studies of Stable Stratification Effect on Dynamic and Thermal Roughness Lengths of Urban-Type Canopy Using Large-Eddy Simulation // J. Atmos. Sci. 2022. V. 80. P. 31–48. https://doi.org/ 10.1175/JAS-D-22-0044.1.
41. Glazunov A.V., Debolskiy A.V., Mortikov E.V. Turbulent Length Scale for Multilayer RANS Model of Urban Canopy and Its Evaluation Based on Large-Eddy

Simulations // Supercomputing Frontiers and Innovations. 2022. V. 8(4). P. 100–116. https://doi.org/10.14529/jsfi210409.
42. Glazunov A.V., Mortikov E.V., Barskov K.V. et al. Layered structure of stably stratified turbulent shear flows // Izvestiya – Atmospheric and Oceanic Physics. 2019. Vol. 55, no. 4. P. 312–323. DOI: 10.1134/s0001433819040042.
43. Gledzer A.E., Gledzer E.B., Khapaev A.A., Chkhetiani O.G. Multiplicity of flow regimes in thin fluid layers in rotating annular channels // Fluid Dynamics. 2021. V. 56. No 4. P. 587599.
44. Golitsyn G.S., Chkhetiani O.G., Vazaeva N.V. Clouds and Turbulence Theory: Peculiar Self-Similarity, 4/3 Fractal Exponent and Invariant // Izvestiya, Atmospheric and Oceanic Physics, 2022. V. 58. No. 6. P. 645–648.
45. Goncharov V.P. Dynamics of thin jets generated by temperature fronts // Physical Review Fluids. 2021a. V. 6. No. 10. P. 103801.
46. Goncharov V.P. Nonlinear pulsations of horizontal jets // Dynamics of Atmospheres and Oceans. 2021b. V. 95. P. 101237.
47. Gorbunov M.E., Kirchengast G., Lauritsen K.B. Generalized Canonical Transform Method. Atmospheric Measurement Techniques. 2021. Vol. 14, No. 2. P. 853–867. doi: 10.5194/amt14-853-2021.
48. Gorbunov M.E., Koval O.A., Mamontov A.E. Method of Spherical Phase Screens for Modeling the Propagation of Diverging Beams in Inhomogeneous Media // Izvestiya, Atmospheric and Oceanic Physics. 2020. Vol. 56. No. 1. P. 52–60, doi: 10.1134/S0001433820010041.
49. Gordov E.P. et al. Multidisciplinary ENVIROMIS conference: new experience //IOP Conference Series: Earth and Environmental Science. – IOP Publishing, 2020. V. 611. №. 1. P. 012063.
50. Harlander U., Kurgansky M.V. Two-dimensional internal gravity wave beam instability. Linear theory and subcritical instability // Geophysical and Astrophysical Fluid Dynamics. 2021. V. 115. No. 5–6. P. 612–647. DOI: 10.1080/03091929.2021.1943379.
51. Ingel L.K. Initiation of vortex flows induced by double diffusion. Journal of Engineering Physics and Thermophysics. 2021. V. 94. N 3. P. 648–653. https://doi.org/10.1007/s10891021-02340-7.
52. Ingel L.K. On the theory of slope flows over a thermally inhomogeneous surface // Journal of Applied Mechanics and Technical Physics. 2022. Vol. 63. No. 5. P. 843–850.
53. Ingel L.K. Slope flows produced by bulk heat release // Journal of Engineering Physics and Thermophysics. 2021. V. 94. N 1. P. 160–164. https://doi.org/10.1007/s10891-021-02284y.
54. Ingel L.Kh. Ekman-type boundary layer over the anisotropic underlying surface // Fundamentalnaya I Prikladnaya Gidrofizika. 2021. V. 14. N 1. P. 63–66.
55. Ingel L.Kh. On the dynamics of inertial particles in an intensive atmospheric vortex // Izvestiya, Atmospheric and Oceanic Physics. 2021. Vol. 57, No. 6. P. 551–558. DOI: 10.1134/S0001433821060062.
56. Ingel L.Kh. On The Dynamics of the Concentration of Heavy Particles in Intensive Vortex Flows // Izvestiya, Atmospheric and Oceanic Physics. 2022. Vol. 58. No. 4. P. 340–345. DOI: 10.1134/S0001433822040053.
57. Ingel L.Kh. On the limiting laws of buoyant convective jets and thermals from local sources of a heat releasing impurity // Journal of Engineering Physics and Thermophysics. 2019. V. 92. No. 6. P. 1481–1488. DOI 10.1007/s10891-019-02067-6.

58. Ingel L.Kh. On the nonlinear dynamics of massive particles in tornadoes // Technical Physics. 2020. Vol. 65. No. 6. P. 860–864. DOI: 10.1134/S10637842 20060122.
59. Ingel L.Kh. On the nonlinear dynamics of turbulent thermals in the shear flow // Russian Journal of Nonlinear Dynamics. 2019a. V. 15. № 1. P. 35–39. DOI: 10.20537/nd190104
60. Ingel L.Kh. Some problems of nonlinear dynamics of turbulent thermals // Radiophysics and Quantum Electronics. 2021. V. 64. N. 3. P. 205–213. DOI 10.1007/ s11141-021-10124-5.
61. Ingel L.Kh. Stratified flows due to spatial inhomogeneities of exchange coefficients // Izvestiya, Atmospheric and Oceanic Physics, 2022. Vol. 58. No. 1. P. 18–21. DOI: 10.1134/S0001433822010042.
62. Ingel L.Kh., Makosko A.A. Estimation of the impact of gravity heterogeneities on the heat regime of the boundary layer of the atmosphere // Doklady Earth Sciences. 2021. Vol. 500. Part 1. P. 777–780. DOI: 10.1134/S1028334X21090117.
63. Ingel L.Kh., Makosko A.A. Geostrophic flow disturbances influenced by inhomogeneities of gravity field. 3D analytical model // Geophysical and Astrophysical Fluid Dynamics. 2021a. Vol. 115. N 1. P. 35–43. DOI: 10.1080/03091929.2020.1762080.
64. Ivanov V., Varentsov M., Matveeva T., Repina I., Artamonov A., Khavina E. Arctic Sea Ice Decline in the 2010s: The Increasing Role of the Ocean – Air Heat Exchange in the Late Summer // Atmosphere. 2019. V. 10. №. 4. P. 184.
65. Ivanova A.R. Icing Effects on Air Transport Operation: State-of-the-art and Prediction Problems // Russian Meteorology and Hydrology. 2021. V. 46. No. 7. P. 461–473.
66. Ivanova A.R. International practices of thunderstorm nowcasting // Russian Meteorology and Hydrology. 2019. V. 44 (11). P. 756–763.
67. Ivanova A.R., Skriptunova E.N., Komasko N.iI., Zavyalova A.A. Application of the COSMO-Ru System for Aircraft Icing Prediction over the Russian Federation Area // Russian Meteorology and Hydrology. 2022. V.47. No.6. P.437–448.
68. Kalashnik M.V. Ekman friction and the formation of upper tropospheric zonal flows // Izvestiya, Atmospheric and Oceanic Physics. 2020. V. 56. No 5. P. 448–457.
69. Kalashnik M.V. Long-wave instabilities in the SQG model with two boundaries // Geophysical and Astrophysical Fluid Dynamics. 2020. 115(4):1–19.
70. Kalashnik M.V. Radiative instability of a barotropic jet flow in a rotating stratified atmosphere // Izvestiya, Atmospheric and Oceanic Physics. 2019. V. 55. No 3. P. 229–234.
71. Kalashnik M.V., Chkhetiani O.G. Baroclinic instability and nonlinear oscillations in the truncated SQG model // Quarterly Journal of the Royal Meteorological Society. 2020b. V. 146. No 732. P. 3534–3547.
72. Kalashnik M.V., Chkhetiani O.G. Nonstationary vortex streets in shear flows // Izvestiya, Atmospheric and Oceanic Physics. 2019. V. 55. No 6. P. 602–611.
73. Kalashnik M.V., Chkhetiani O.G. Optimal disturbances in the development of the instability of a free shear layer and a system of two counter-streaming jet flows // Fluid Dynamics. 2020a. V. 55. No 2. P. 171–184.
74. Kalashnik M.V., Chkhetiani O.G., Kurgansky M.V. Discrete SQG models with two boundaries and baroclinic instability of jet flows // Physics of Fluids. 2021. V. 33. No 7. P. 076608.

75. Kalashnik M.V., Kulichkov S.N. On pressure perturbations caused by a moving heat source of frontal type (hydrostatic mode) // Izvestiya, Atmospheric and Oceanic Physics. 2019. V. 55. No 5. P. 423–431.
76. Kalashnik M.V., Kurgansky M.V. Hydrodynamic instability of vertical motions excited by spatially periodic distributions of heat sources // Fluid Dynamics. 2020. V. 55. No 4. P. 554565.
77. Kalashnik M.V., Kurgansky M.V., Chkhetiani O,G, Baroclinic instability in geophysical fluid dynamics // Physics-Uspekhi. 2022. V. 65 (10). P. 1039-1070.
78. Kalashnik M.V., Kurgansky M.V., Kostrykin S.V. Instability of surface quasigeostrophic spatially periodic flows // Journal of the Atmospheric Sciences. 2020. V. 77. No 1. P. 239255.
79. Kalinin N.A., Shikhov A.N., Chernokulsky A.V., Kostarev S.V., Bykov A.V. Environments of Formation of Severe Squalls and Tornadoes Causing Large-scale Windthrows in the Forest Zone of European Russia and the Ural // Russian Meteorology and Hydrology. 2021. V.46. No 2. P. 83–93, DOI: 10.3103/S1068373921020035.
80. Kalmykova O.V. Assessment technique of waterspouts risk occurrence near the Russian Black Sea coast and results of its testing // Information collection "Results of testing new and improved technologies, models and methods of hydrometeorological forecasts". 2021. N. 48. P. 42–61.
81. Kalmykova O.V., Fedorova V.V., Fadeev R.O. Analysis of occurrence conditions of the waterspouts outbreak over the Black Sea on July 16, 2019 and forecast skill assessment // Hydrometeorological Research and Forecasting. 2021. N. 1 (379). P. 112–129.
82. Kalmykova O.V., Shershakov V.M., Novitskii M.A., Shmerlin B.Ya. Automated Forecasting of Waterspouts off the Black Sea Coast of Russia and Its Performance Assessment // Russian Meteorology and Hydrology. 2019. V. 44. P. 764–771.
83. Kan V., Gorbunov M.E., Fedorova O.V., Sofieva V.F. Latitudinal Distribution of the Parameters of Internal Gravity Waves in the Atmosphere Derived from Amplitude Fluctuations of Radio Occultation Signals // Izvestiya, Atmospheric and Oceanic Physics. 2020 b. Vol. 56, No. 6. P. 564–575. doi: 10.1134/S0001433820060055.
84. Kan V., Gorbunov M.E., Shmakov A.V., Sofieva V.F. The Reconstruction of the Parameters of Internal Gravity Waves in the Atmosphere from Amplitude Fluctuations in the Radio Occultation Experiment // Izvestiya, Atmospheric and Oceanic Physics. 2020. Vol. 56, No. 5. P. 435–447, doi: 10.1134/S0001433820050072.
85. Kolennikova M.A., Vargin P.N., Gutchina D.Y. Interrelations between El Nino Indices and Major Characteristics of Polar Stratosphere According to CMIP5 Models and Reanalysis // Russian Meteorology and Hydrology. 2021. Vol. 46. No. 6. P. 351–364.
86. Kosyakov S.I., Kulichkov S.N., Chkhetiani O.G., Tsybul'skaya N.D. On the effect of weak attenuation of acoustic waves from high-altitude explosions // Acoustical Physics. 2019. V. 65. No 6. P. 731–741.
87. Kurgansky M.V. A simple model of blocking action over a hemisphere // Theoretical and Applied Climatology. 2021c. V. 147. No. 1–2. P. 65–71. DOI: 10.1007/s00704-021-03782y.
88. Kurgansky M.V. An estimate of convective vortex activity at the InSight landing site on Mars // Icarus. 2021b. V. 358. P. 114200. DOI: 10.1016/j.icarus.2020.114200.

89. Kurgansky M.V. Atmospheric circulation response to heat flux anomalies in a twodimensional baroclinic model of the atmosphere // Izvestiya – Atmospheric and Oceanic Physics. 2020c. V. 56. No. 1. P. 33–42. DOI: 10.1134/s0001433820010053.
90. Kurgansky M.V. Inertial instability of the Kolmogorov flow in a rotating stratified fluid // Fluid Dynamics Research. 2021. V. 53. P. 035502. DOI: 10.1088/1873-7005/abfaf0.
91. Kurgansky M.V. Inertial instability of the time-periodic Kolmogorov flow in a rotating fluid with the full account of the Coriolis force // Fluid Dynamics Research. 2022d. V. 54. No. 5. P. 055504. DOI: 10.1088/1873-7005/ac963d.
92. Kurgansky M.V. On determination of the size-frequency distribution of convective vortices in pressure time-series surveys on Mars // Icarus. 2020 b. V. 335. P. 113389. DOI: 10.1016/j.icarus.2019.113389.
93. Kurgansky M.V. On short-wave instability of the stratified Kolmogorov flow // Theoretical and Computational Fluid Dynamics. 2022c. V. 36, No. 4. P. 575–595. DOI: 10.1007/s00162022-00613-2.
94. Kurgansky M.V. On the instability of finite-amplitude inertia-gravity waves // Fluid Dynamics Research. 2020. V. 52. P. 035503. DOI: 10.1088/1873-7005/ab9070.
95. Kurgansky M.V. On the statistical distribution of pressure drops in convective vortices: Applications to martian dust devils // Icarus. 2019. V. 317. P. 209–214. DOI: 10.1016/j.icarus.2018.08.004.
96. Kurgansky M.V. On the theory of symmetric instability of time-periodic flows with a complete account for the Coriolis force // Izvestiya – Atmospheric and Oceanic Physics. 2022b. V. 58, No. 4. P. 329-339. DOI: 10.1134/s0001433822040077.
97. Kurgansky M.V. Statistical distribution of atmospheric dust devils on Earth and Mars // Boundary-Layer Meteorology. 2022. V. 184. No. 3. P. 381–400. DOI: 10.1007/s10546-02200713-w.
98. Kurgansky M.V., Maksimenkov L.O., Chkhetiani O.G. Vertical helicity flux as an index of interannual atmospheric variability // IOP Conf. Ser.: Earth Environ. Sci. 2020. V. 606. P. 012028.
99. Kurgansky M.V., Seelig T., Klein M., Will A., Harlander U. Mean flow generation due to longitudinal librations of sidewalls of a rotating annulus // Geophysical and Astrophysical Fluid Dynamics. 2020. V. 114. No. 6. P. 742–762. DOI: 10.1080/03091929.2019.1692829.
100. Kuznetsov E. A., Mikhailov E.A. Slipping flows and their breaking //Annals of Physics. 2022. V. 447. P. 169088.
101. L. Kh. Ingel, Vortex motion driven by differential diffusion // Izvestiya, Atmospheric and Oceanic Physics. 2019b. Vol. 55. No. 3. P. 257–260.
102. Levina G.V. Application of the Turbulent Vortex Dynamo Theory for Early Diagnostics of the Tropical Cyclone Genesis // Fundamental and Applied Hydrophysics. 2022. V. 15. (2). P. 47–59. doi:10.48612/fpg/vaxg-xdmv-11pn. Drozd I., Repina I., Gavrikov A. et al. Atmospheric turbulence structure above urban nonhomogeneous surface // Russian Journal of Earth Sciences. 2022. Vol. 22, no. 5. P. ES01SI11.
103. Lipavskii A.S., Eliseev A.V., Mokhov I.I. Bayesian projections of the amur and selenga river runoff changes in the 21st century based on cmip6 model ensem-

ble simulations // Russian Meteorology and Hydrology. 2022. Vol. 47, no. 5. P. 370–384.
104. Lukyanov A.N., A. V. Ganshin, V. A. Yushkov, and A. S. Vyazankin, Trajectory Modeling of the Middle Atmosphere // Russian Meteorology and Hydrology. 2021. Vol. 46. No. 9. P. 34–39.
105. Lukyanov A.N., Vargin P.N., Yushkov V.A. Lagrange Studies of Anomalously Stable Arctic Stratospheric Vortex Observed in Winter 2019–2020 // Izvestiya, Atmospheric and Oceanic Physics. 2021. Vol. 57/ No. 3. P. 247–253.
106. Lupo A.R., Jensen A.D., Mokhov I.I., Timazhev A., Eichler T., Efe B. Changes in global blocking character during recent decades // Atmosphere. 2019. V. 10. No. 2. P. 92. https://doi.org/10.3390/atmos10020092.
107. Makhotina I.A., Chechin D.G., Makshtas A.P. Cloud Radiative Forcing over Sea Ice in the Arctic during the Polar Night According to North Pole-37, -39, and -40 Drifting Stations // Izvestiya, Atmospheric and Oceanic Physics. 2021. Vol. 57. No. 5. P. 451–460.
108. Malinovskaya E.A., Chkhetiani O.G. On conditions for the wind removal of soil particles // Journal of Applied Mechanics and Technical Physics. 2021. V. 62. No 7. P. 1117–1131.
109. Martynova Yu.V., Vargin P.N., Volodin E.M. Variation of Northern Hemispheric Wintertime Storm Tracks under Future Climate Change in INM-CM5 Simulations // Izvestiya, Atmospheric and Oceanic Physics. 2022. V. 58, No 3. P.208–218.
110. Mokhov I.I. Anomalous winters in regions of northern Eurasia in different phases of the El Niño phenomena // Doklady Earth Sciences. 2020. V. 493. P. 649–653.
111. Mokhov I.I. Extreme atmospheric and hydrological phenomena in Russian regions: Relationship with the Pacific Decadal Oscillation // Doklady Earth Sciences. 2021. V. 500. P. 861–865.
112. Mokhov I.I. Winter Atmospheric Blocking Events in the Northern Hemisphere under Climate Changes in Recent Decades (1980–2018) // Doklady Earth Sci. 2022. V. 507 (2). P. 334–339.
113. Mokhov I.I., Chefranov S.G., Chefranov A.G. Point vortices dynamics on a rotating sphere and modeling of global atmospheric vortices interactions // Phys. Fluids. 2020. V. 32. 106605. https://doi.org/10.1063/5.0026014.
114. Mokhov I.I., Chernokulsky A.V., Osipov A.M. Atmospheric Centers of Action in the Northern and Southern Hemispheres: Features and Variability // Russian Meteorology and Hydrology. 2020. V. 45. N.11. P.749–761. DOI: 10.3103/S1068373920110011.
115. Mokhov I.I., Makarova M.E., Poroshenko A.G. Tropical cyclones and their transformation into extratropical: estimates of the half-century trends // Doklady Earth Sciences. 2020. V. 493. P. 552–557.
116. Mokhov I.I., Osipov A.M., Chernokulsky A.V. Atmospheric Centers of Action in the Northern Hemisphere: Current Features and Expected Changes in the 21st Century Based on Simulations with the CMIP5 and CMIP6 Ensembles of Climate Models // Doklady Earth Sciences. 2022. Vol. 507, No. 2. P. 1132–1139. DOI: 10.1134/S1028334X2260089X.
117. Mokhov I.I., Poroshenko A.G. Action as an Integral Characteristic of Atmospheric (Climatic) Structures: Estimates for Tropical Cyclones // Izvestiya, Atmospheric and Oceanic Physics. 2020. V. 56. P. 539–544.

118. Mokhov I.I., Poroshenko A.G. Statistical and model estimates of the relationship between the intensity and duration of tropical cyclones // Russian meteorology and hydrology. 2021. V. 46. №. 5. P. 302–306.
119. Mokhov I.I., Poroshenko A.G. Statistical and Model Estimates of the Relationship between the Size and Lifetime of Polar Lows // Moscow University Physics Bulletin. 2021. V. 76. №. 6. P. 477–481.
120. Mokhov I.I., Timazhev A.V. Atmospheric blocking and changes in its frequency in the 21st century simulated with the ensemble of climate models //Russian Meteorology and Hydrology. 2019. V. 44. P. 369–377.
121. Mokhov I.I., Timazhev A.V. Frequency of summer atmospheric blockings in the Northern Hemisphere in different phases of El Niño and Pacific decadal and Atlantic multidecadal oscillations //Izvestiya, Atmospheric and Oceanic Physics. 2022a. V. 58. №. 3. P. 199–207.
122. Mokhov I.I., Timazhev A.V. Integral Index of Atmospheric Blocking Activity in the Northern Hemisphere in Recent Decades // Izvestiya, Atmospheric and Oceanic Physics. 2022b. V. 58. №. 6. P. 545–552.
123. Mokhov I.I., Timazhev A.V. Seasonal Temperature Extremes in the North Eurasian Regions Depending on ENSO Phase Transitions // Atmosphere. 2022. V. 13. №. 2. P. 249.
124. Mokhov I.I., Yushkov V.P., Timazhev A.V., Babanov B.A. Squalls with a hurricane wind in Moscow // Moscow University Physics Bulletin. 2020. V. 75. P. 712–716.
125. Mortikov E.V., Glazunov A.V., Debolskiy A.V. et al. Modeling of the dissipation rate of turbulent kinetic energy // Doklady Earth Sciences. 2019. Vol. 489. P. 1440–1443. DOI: 10.1134/S1028334X19120067.
126. Nerushev A.F., Ivangorodsky R.V. Determination of turbulence zones in the upper troposphere based on satellite measurements// Sovremennye problemy distantsionnogo zondirovaniya Zemli iz kosmosa. 2019. Vol. 16. No 1. P. 205–215. DOI: 10.21046/20707401-2019-16-1-205-215.
127. Nerushev A.F., Visheratin K.N., Ivangorodsky R.V. Statistical Model of the Time Variability of the Characteristics of High-Altitude Jet Currents in the Northern Hemisphere Based on Satellite Measurements // Izvestiya, Atmospheric and Oceanic Physics. 2021b. Vol. 57. No. 4. pp. 354–364. DOI: 10.1134/S0001433821040198.
128. Nerushev A.F., Visheratin K.N., Ivangorodsky R.V. Dynamics of High-Altitude Jet Streams from Satellite Measurements and Their Relationship with Climatic Parameters and LargeScale Atmospheric Phenomena // Izvestiya, Atmospheric and Oceanic Physics. 2019. Vol. 55. No. 9. P. 1198–1209. DOI: 10.1134/S0001433819090329.
129. Nerushev A.F., Visheratin K.N., Ivangorodsry R.V. Turbulence in the upper troposphere according to long-term satellite measurements and its relationship with climatic parameters // Sovremennye problemy distantsionnogo zondirovaniya Zemli iz kosmosa. 2020. Vol. 17. No. 6. P. 82–86. DOI: 10.21046/2070-7401-2020-17-6-82-86.
130. Nerushev A.F., Visheratin K.N., Kulizhnikova L.K., Ivangorodsky R.V. The relationship of surface air temperature anomalies and the characteristics of high-altitude jet streams// Sovremennye problemy distantsionnogo zondirovaniya Zemli iz kosmosa. 2021c. Vol. 18. No.1. P. 199–209. DOI: 10.21046/2070-7401-2021-18-1-199-20.

131. Nikiforova M.P., Vargin P.N, Zvyagintsev A.M**.** Ozone Anomalies over Russia in the Winter-Spring of 2015/2016 // Russian Meteorology and Hydrology. 2019. V. 44, No 1. P. 23–32.
132. Parfenova M.R., Eliseev A.V., Mokhov I.I. Changes in the Duration of the Navigation Period in Arctic Seas along the Northern Sea Route in the Twenty-First Century: Bayesian Estimates Based on Calculations with the Ensemble of Climate Models // Doklady Earth Sciences. 2022. V. 507. №. 1. P. 952–958.
133. Perezhogin P.A., Glazunov A.V., Gritsun A.S. Stochastic and deterministic kinetic energy backscatter parameterizations for simulation of the two-dimensional turbulence // Russian Journal of Numerical Analysis and Mathematical Modelling. 2019. Vol. 34. no. 4. P. 197–213. DOI: 10.1515/rnam-2019-0017.
134. Polonsky A.B. The Ocean's Role in Climate Change. Cambridge Scholars Publishing, Newcastle, UK, 2019, 294 p.
135. Repina I.A., Artamonov A.Y. Air – Surface Turbulent Heat Exchange in the Antarctic Coastal Zone Derived from Instrumental Observations // Russian Meteorology and Hydrology. 2020. V. 45. P. 81–86.
136. Rivin G.S., Rozinkina I.A., Vilfand R.M., Kiktev D.B., Tudrii K.O., Blinov D.V., Repina I.A., Artamonov A.Y. Development of the high-resolution operational system for numerical prediction of weather and severe weather events for the Moscow region // Russian Meteorology and Hydrology. 2020. V. 45. P. 455–465.
137. Romanovskii O.A., Kharchenko O.V. Atmospheric and Ocean Optics: Atmospheric Physics III //Atmosphere. 2022. V. 13. №. 11. P. 1912.
138. Serykh I.V., Sonechkin D.M. El Niño forecasting based on the global atmospheric oscillation // International Journal of Climatology. 2021. Vol. 41. P. 3781–3792. https://doi.org/10.1002/joc.6488.
139. Shelekhov A.P. et al. Low-Altitude Sensing of Urban Atmospheric Turbulence with UAV // Drones. 2022. V. 6, no. 3. P. 61. https://doi.org/10.3390/drones6030061.
140. Shelekhov A.P. et al. Profiling the turbulence from spectral measurements in the urban atmosphere using UAVs // Proc. SPIE 11864, Remote Sensing Technologies and Applications in Urban Environments VI, 118640B (12 September 2021b); doi: 10.1117/12.2597992.
141. Shelekhov A.P. Using Small Unmanned Aerial Vehicles for Turbulence Measurements in the Atmosphere // Izvestiya, Atmospheric and Oceanic Physics. 2021a. Vol. 57, No. 5. P. 533–545, doi: 10.1134/S0001433821050133.
142. Shestakova A. A., Debolskiy A.V. Impact of the Novaya Zemlya Bora on the OceanAtmosphere Heat Exchange and Ocean Circulation: A Case-Study with the Coupled Model // Atmosphere. 2022. V. 13. №. 7. P. 1108.
143. Shestakova A. A., Myslenkov S. A., Kuznetsova A. Influence of Novaya Zemlya Bora on sea waves: Satellite measurements and numerical modeling // Atmosphere. 2020. V. 11. №. 7. P. 726.
144. Shestakova A.A. Chechin D.G., Lüpkes C., Hartmann J., Maturilli M. The foehn effect during easterly flow over Svalbard // Atmospheric Chemistry and Physics. 2022. V. 22. №. 2. P. 1529–1548.
145. Shestakova A.A. Impact of land surface roughness on downslope windstorm modelling in the Arctic // Dynamics of Atmospheres and Oceans. 2021. V. 95. P. 101244.

146. Shestakova A.A., Repina I.A. Mesoscale vortex over Lake Baikal: A case-study // Russian Journal of Earth Sciences. 2021. V. 21. №. 5. P. 1.
147. Shestakova A.A., Toropov P.A. Orographic and lake effect on extreme precipitation on the Iranian coast of the Caspian sea: a case study // Meteorology and Atmospheric Physics. 2021. V. 133. P. 69–84.
148. Shikhov A., Chernokulsky A., Azhigov I., Semakina A. A satellite-derived database for stand-replacing windthrows in boreal forests of the European Russia in 1986–2017 // Earth System Science Data, 2020, V. 12, P. 3489–3512, DOI: 10.5194/essd-12-3489-2020.
149. Shikhov A., Chernokulsky A., Kalinin N., Bykov A., Pischalnikova E. Climatology and Formation Environments of Severe Convective Windstorms and Tornadoes in the Perm Region (Russia) in 1984–2020. // Atmosphere. 2021. Vol. 12, No. 11, P. 1407. DOI: 10.3390/atmos12111407.
150. Shikhov A.N., Chernokulsky A.V. Sprygin A.A., Yarinich Yu.I. Estimation of Convective Atmospheric Instability during Squalls, Tornadoes, and Large Hail Events from Satellite Observations and ERA5 Reanalysis Data // Atmospheric and Oceanic Optics. 2022. Vol. 35. No. 6. P. 793–801. DOI: 10.1134/S102485 6022060227.
151. Shikhov A.N., Chernokulsky A.V., Azhigov, I. O. Spatial and Temporal Distribution of Windthrows in the Forest Zone of Western Siberia in 2001–2020 // Cosmic Research. 2022. V. 60(Suppl 1). P. S91–S103.
152. Shishov E.A., Solenaya O.A., Chkhetiani O.G., Azizyan G.V., Koprov V.M. Multipoint measurements of temperature and wind in the surface layer // Izvestiya, Atmospheric and Oceanic Physics. 2021. V. 57. No 3. P. 254–263.
153. Slunyaev A., Kokorina A. Numerical Simulation of the Sea Surface Rogue Waves within the Framework of the Potential Euler Equations // Izvestiya, Atmospheric and Oceanic Physics. 2020. V. 56, No. 2. P. 179–190. DOI: 10.1134/S0001433820020127.
154. Slunyaev A.V. Effects of coherent dynamics of stochastic deep-water waves // Phys. Rev. E. 2020. V. 101. P. 062214. DOI: 10.1103/PhysRevE.101.062214.
155. Slunyaev A.V. Persistence of hydrodynamic envelope solitons: detection and rogue wave occurrence // Physics of Fluids. 2021. V. 33. P. 036606. doi: 10.1063/5.0042232.
156. Slunyaev A.V., Stepanyants Y.A. Modulation property of flexural-gravity waves on a water surface covered by a compressed ice sheet // Phys. Fluids. 2022. V. 34. P. 077121. Doi: 10.1063/5.0100179.
157. Smyshlyaev S.P., Vargin P.N., Motsakov M.A. Numerical modeling of ozone loss in the exceptional Arctic stratosphere winter-spring of 2020 // Atmosphere. 2021. V. 12. P. 1470.
158. Stepanov D., Fomin V., Gusev A., Diansky N. Mesoscale Dynamics and Eddy Heat Transport in the Japan/East Sea from 1990 to 2010: A Model-Based Analysis // Journal of Marine Science and Engineering. 2022. V. 10(1). P. 33. https://doi.org/10.3390/jmse10010033
159. Sterlyadkin V.V., Ermakov D.M., Kuzmin A.V., Pashinov E.V. Flood prediction on major rivers from radiometric microwave measurements from space. Is it possible? // Sovremennyye problemy distantsionnogo zondirovaniya Zemli iz kosmosa (Current problems of remote sensing of the Earth from space). 2022. V. 19. N. 5. P. 40–52. DOI: 10.21046/2070-7401-2022-19-5-40-52.

160. Study of the natural environment of the high-latitude Arctic on the research station "Ice Base Cape Baranova" // Ed. A.P. Makshtas and V.T. Sokolov. St. Petersburg: AARI, 2021. 260 p. ISBN 978-5-98364-103-7.
161. Sukhanovskii A., Popova E. The Importance of Horizontal Rolls in the Rapid Intensification of Tropical Cyclones // Boundary-Layer Meteorology. 2020. Vol. 175. P. 259–276. https://doi.org/10.1007/s10546-020-00503-2
162. The Republic of Adygea Environment // Ed. Kostianoy A.G., Bedanokov M.K., Lebedev S.A. Springer International Publishing AG, 2020. 714 p.
163. Tkachenko E.V., Debolskiy A.V., Mortikov E.V. et al. 2022) Large-Eddy Simulation and Parameterization of Decaying Turbulence in the Evening Transition of the Atmospheric Boundary Layer. // Izv. Atmos. Ocean. Phys. 58, 219–236. https://doi.org/10.1134/S0001433822030112.
164. Tsvetkova N.D., Vargin P.N., Lukyanov A.N., Kirushov B.M., Yushkov V.A., Khattatov V.U. Investigation of chemistry ozone loss and Arctic stratosphere dynamical processes in the winter 2019–2020 // Russian Meteorology and Hydrology. 2021. V. 46. No 9. P. 606615.
165. Tsvetkova N.D., Vyzankin A.S., Vargin P.N., Lukyanov A.N., Yushkov V.A. Investigation and forecast of Sudden Stratospheric Warming events with chemistry climate model SOCOL // IOP Conf. Series, Earth Environmental Science. 2020. V. 606. P. 012062, doi:10.1088/1755-1315/606/1/012062.
166. Turbulence, Atmosphere and Climate Dynamics //IOP Conference Series: Earth and Environmental Science. IOP Publishing, 2022. V. 1040.
167. Vargin P., Lukyanov A., Kiryushov B. Dynamical processes of Arctic stratosphere in the winter 2018–2019 // Russian Meteorology and Hydrology. 2020. V. 45. P. 387–397.
168. Vargin P., Martynova Y., Volodin E., Kostrykin S. Investigation of boreal storm tracks in historical simulations of INM CM5 and reanalysis data // IOP Conf. Series, Earth Environmental Science. 2019. V. 386. P. 012007, doi:10.1088/1755-1315/386/1/012007.
169. Vargin P.N., Guryanov V.V., Lukyanov A.N., Vayzankin A.S. Dynamic Processes of the Arctic Stratosphere in the 2020–2021 Winter // Izvestiya, Atmospheric and Oceanic Physics. 2021. V. 57, No 6, p. 568–580.
170. Vargin P.N., Kiryushov B.M. Major Sudden Stratospheric Warming in the Arctic in February 2018 and Its Impacts on the Troposphere, Mesosphere, and Ozone Layer // Russian Meteorology and Hydrology. 2019. Vol. 44. No. 2. P. 112–123.
171. Vargin P.N., Kolennikova M.A., Kostrykin S.V., Volodin E.M. Impact of Sea Surface Temperature Anomalies in the Equatorial and North Pacific on the Arctic Stratosphere According to the INMCM5 Climate Model Simulations // Russian Meteorology and Hydrology. 2021. Vol. 46. No. 1. P. 1–9.
172. Vargin P.N., Koval A.V., Guryanov V.V. Arctic Stratosphere Dynamical Processes in the Winter 2021–2022 // Atmosphere. 2022. V. 13, 1550.
173. Vargin P.N., Nikiforova M.P., Zvyagintsev A.M**.** Variability of the Antarctic Ozone Anomaly in 2011–2018 // Russian Meteorology and Hydrology. 2020. Vol. 45. No. 2. P. 20–34.
174. Vargin P.N., Kostrykin S.V., Rakushina E.V., Volodin E.M., Pogoreltzev A.I. Study of the Variability of Spring Breakup Dates and Arctic Stratospheric Polar Vortex Parameters from Simulation and Reanalysis Data // Izvestiya, Atmospheric and Oceanic Physics. 2020. Vol. 56. No 5. P. 458–469.

175. Vargin, P.N.; Kostrykin, S.V.; Volodin, E.M.; Pogoreltsev, A.I.; Wei, K. Arctic Stratosphere Circulation Changes in the 21st Century in Simulations of INM CM5 // Atmosphere. 2022. V. 13. P. 25.
176. Vazaeva N.V., Chkhetiani O,G., Durneva E.A. Criteria to Identify Polar Lows // Russian Meteorology and Hydrology. 2022. V. 47, No 4. P. 262–271.
177. Vazaeva N.V., Chkhetiani O.G., Kurgansky M.V. On integral characteristics of Polar Lows // IOP Conf. Ser.: Earth Environ. Sci. 2020. V. 606 P. 012065.
178. Vazaeva N.V., Chkhetiani O.G., Kurgansky M.V., Kallistratova M.A. Helicity and turbulence in the atmospheric boundary layer // Izvestiya, Atmospheric and Oceanic Physics. 2021. V. 57. No 1. P. 29–46.
179. Vazaeva N.V., Chkhetiani O.G., Maksimenkov L.O. Organized roll circulation and transport of mineral aerosols in the atmospheric boundary layer // Izvestiya, Atmospheric and Oceanic Physics. 2019. V. 55. No 2. P. 152–166.
180. Vazaeva N.V., Repina I.A., Shestakova A.A., Ganbat G. Mesoscale vortex over Uvs-Nuur: analysis and numerical simulation // Modern problems of remote sensing of the Earth from space. 2022. V. 19. No 4. S. 306–317.
181. Volodin E. The Mechanisms of Cloudiness Evolution Responsible for Equilibrium Climate Sensitivity in Climate Model INM-CM4-8 // Geophysical Research Letters. 2021. V. 48. P. e2021GL096204. https://doi.org/10.1029/2021GL096204.
182. Volodin E., Gritsun A. Simulation of Possible Future Climate Changes in the 21st Century in the INM-CM5 Climate Model // Izvestia. Atmospheric and oceanic physics. 2020. V. 56. N3. P. 255–266.
183. Vorobyeva V., Volodin E. Evaluation of the INM RAS climate model skill in climate indices and stratospheric anomalies on seasonal timescale // Tellus A. 2021. V. 73. P. 1892435. https://doi.org/10.1080/16000870.2021.1892435.
184. Vulfson A., Nikolaev P. Local Similarity Theory of Convective Turbulent Layer Using “Spectral” Prandtl Mixing Length and Second Moment of Vertical Velocity // Journal of the atmospheric science. V. 79. P. 101–118.
185. Vyazankin A.S., Tsvetkova N.D., Vargin P.N., Yushkov V.A. Atmospheric Modeling for Controlling the Motion of a Return Vehicle // Solar System Research. 2020. Vol. 54. No. 7. P. 679–684.
186. Wei K., Chen W., Vargin P. Longitudinal peculiarities of planetary waves-zonal flow interaction and its role in stratosphere-troposphere dynamical coupling // Climate Dynamics. 2021. https://doi.org/10.1007/s00382-021-05842-5.
187. Zagumennyi Y.V., Chashechkin Y.D. Numerical Analysis of Flows of Stratified and Homogeneous Fluids near Horizontal and Inclined Plates // Fluid Dyn. 2019. V. 54. P. 958– 969. doi:10.1134/S0015462819070152.
188. Zasko G.V., Glazunov A.V., Mortikov E.V. et al. Optimal Energy Growth in Stably Stratified Turbulent Couette Flow // Boundary-Layer Meteorol. 2022. https://doi.org/10.1007/s10546-022-00744-3.
189. Zilitinkevich S., Kadantsev E., Repina I., Mortikov E., Glazunov A. Order out of Chaos: Shifting Paradigm of Convective Turbulence // J. Atmos. Sci. 2021. V. 78. P. 3925–3932. https://doi.org/10.1175/JAS-D-21-0013.1.

Middle Atmosphere

A.A. Krivolutsky[1], *S.V. Veretenenko*[2], *I.A. Mironova*[3]
[1] Central Aerological Observatory, Dolgorudny, Russia
[2] Ioffer Institute, Russia Academy of Science, St. Petersburg, Russia
[3] Institute of Physics, St. Petersburg, Russia

The results obtained by russian scientists in mentioned period may be grouped into the following sections: winds, temperature, composition, solar activity forcing. Presented results were published as for Russian as foreing journals. Corresponding papers were found in next journals: Advances in Space Research, Journal of Atmospheric and Solar-Terrestral Physics, Atmosphere, Geomagnetism and Aeronomy, Meteorologia and Gidrologia, Optics of Atmosphere and Gidrosphere, Physics of Atmosphere and Ocean.

Advances in Space Research

1. Korotyshkin D., Merzlyakov E., Sherstyukov O., Valiullin F. Mesosphere/lower thermosphere wind regime parameters using a newly installed SKiYMET meteor radar at Kazan (56°N, 49°E). Advances in Space Research. 2019. V. 63, Issue 7. P. 2132–2143.

New meteor radar (MR) horizontal wind data obtained during 2015–2018 at Kazan (56°N, 49°E) are presented. The measurements were carried out with a state-of-the-art SKiYMET meteor radar. Monthly mean vertical profiles of zonal and meridional components of the prevailing wind speeds, also amplitudes and phases of the components of diurnal (DT) and semidiurnal tide (SDT) winds are displayed as contour plots for a mean calendar year over the four recent years and compared with distributions of these parameters provided by the previous multiyear (1986–2002) meteor radar (MR) measurements at Kazan and by the recent HWM07 empirical model. The analysis shows that the SKiYMET zonal and meridional prevailing wind speeds are generally in good agreement, sharing the same seasonal features, with the earlier MR seasonal winds. Comparisons with the HWM07 model are not favourable: eastward solstitial cells as modelled are significantly larger, >30 m/s compared to 15–20 m/s. Also, reversal lines are too variable with height, and the positions of modelled cells (positive and negative) are unlike those of either MRs at Kazan or other MLT radars. Both MR systems provide the large SDT amplitudes, approximately 30 m/s and vertical wavelengths, approximately 55 km, for both components at middle latitudes in winter. They also show the well known strong SDT September feature (heights

85–100 km, the vertical wavelength ~55–60 km), and the weak summer SDT for 80–91 km. HWM07 shows unrealistic amplitudes and phases above 90 km by height and month: minimal amplitudes in equinoxes and no September feature.

The weak DT of middle to high latitudes provide similar amplitude and phase structures from both MRs, 1986–2002 and 2015–2017: largest amplitudes (10–12 or 8–10 m/s) for the evanescent meridional tide in summer, peaking in late July; weakest (0–2, 2–4 m/s) at 80 to 92–96 km, when the tide is vertically propagating (January, February, November, December) with a vertical wavelength near 40 km. Again, HWM07 differs in amplitude and phase structures: showing peak amplitudes in equinoxes: April, 15 m/s at 88 km; October, 21 m/s at 89 km.

Coupling of the MR wind parameters with the ERA5 wind parameters is studied for a case in 2016. It is shown that the prevailing winds and DT amplitudes and phases of both datasets can be simply linked together, but that the ERA5 SDT amplitudes are significantly underestimated at the top model levels of the ERA5 reanalysis project.

2. Korotyshkin D., Merzlyakov E., Jacobi C., Lilienthal F., Wu Q. Longitudinal MLT wind structure at higher mid-latitudes as seen by meteor radars at central and Eastern Europe (13°E/49°E). Advances in Space Research. 2019. V. 63, Issue 10. P. 3154–3166.

The mid-latitude mesosphere and lower thermosphere (MLT) wind speeds measured by two SKiYMET meteor radars (MRs) at Collm (51°N, 13°E) and Kazan (56°N, 49°E) during 2016–2017 were analyzed to study longitudinal wind structures. The differences between monthly mean prevailing wind speeds and tidal amplitudes were compared with the corresponding differences obtained from TIMED/TIDI satellite winds and gradient wind speeds from the AURA/MLS instrument. It is shown that the MR wind difference between the two sites is statistically significant. The difference of the horizontal prevailing winds can be explained by a superposition of the background zonal flow, which is different at the two latitudes, with stationary planetary waves of different origin. Non-migrating tides contribute significantly to the difference of the semidiurnal tidal winds between the two sites.

3. Veretenenko S., Ogurtsov M. Manifestation and possible reasons of ~60-year oscillations in solar-atmospheric links. Advances in Space Research. 2019. V. 64, Issue 1. P. 104–116.

In this work we continue studying possible reasons for temporal variability observed in correlation links between characteristics of the lower atmosphere and solar activity phenomena at the multidecadal time scale. Temporal variations of correlation coefficients between troposphere pressure at extratropical latitudes and sunspot numbers are compared with the evolution of the

large-scale circulation forms according to the Vangengeim-Girs classification, as well as the characteristics of the stratospheric polar vortex and global temperature anomalies. The results obtained show that temporal variability of solar activity/galactic cosmic ray (SA/GCR) effects on troposphere pressure (the development of extratropical baric systems) is characterized by a roughly 60-year periodicity and closely related to changes in the regime of large-scale circulation which accompany transitions between the different states of the polar vortex. It was suggested that the character of SA/GCR effects depends on the polar vortex strength influencing the troposphere-stratosphere coupling. It was shown that the evolution of the polar vortex may be associated with global temperature variations, with a possible reason for these variations being long-term changes of total solar irradiance.

4. Yankovsky V., Vorobeva E., Manuilova R. New techniques for retrieving the [O(3P)], [O_3] and [CO_2] altitude profiles from dayglow oxygen emissions: Uncertainty analysis by the Monte Carlo method. Advances in Space Research. 2019. V. 64, Issue 10. P. 1948–1967.

This study presents methods for retrieving the altitude profiles of atomic oxygen, [$O(^3P)$], ozone, [O_3], and carbon dioxide, [CO_2], concentrations in the daytime mesosphere and lower thermosphere (MLT) in the framework of the YM2011 model of the electronic-vibrational oxygen kinetics. The emissions of singlet oxygen molecules $O_2(b^1\Sigma^+_g,\ v \le 2)$, $O_2(a^1\Delta_g,\ v = 0)$ and the $O(^1D)$ atom are used as proxy of the [$O(^3P)$], [O_3] and [CO_2]. For all the proposed techniques, we compare the uncertainty values of the retrieved [$O(^3P)$], [O_3] and [CO_2], obtained by the Monte Carlo method, with estimations obtained by the sensitivity analysis method in the earlier works. For all the above mentioned methods for retrieving the [$O(^3P)$], [O_3] and [CO_2] profiles, we obtained analytical expressions that include the concentrations of excited substances considered as proxies. In addition, the optimal altitude ranges for using these remote sensing methods were determined based on the results of numerical experiments by the Monte Carlo method.

5. Tolmacheva A.V., Bakhmetieva N.V., Grigoriev G.I., Egerev M.N. Turbopause range measured by the method of the artificial periodic irregularities. Advances in Space Research. 2019. V. 64, Issue 10. P. 1968–1974.

A new opportunity for estimating the level of the turbopause is presented. It is based on the method of determining atmospheric parameters using artificial periodic irregularities of the ionosphericplasma (the API techniques). The obtained data show the presence of variations of the level of the turbopause. Experiments were carried out using SURA heating facility (56.1°N, 46.1°E) for API creation. Above the observation point the turbopause region occupies the altitude interval between 94 and 106 km. There are changes in the level of the turbopause during the day: in the evening hours the turbo-

pause level can go down. Temporal variations of the turbopause level are observed. They are compared with variations in the atmospheric parameters at these heights.

6. Merzlyakov E., Solovyova T., Yudakov A., Korotyshkin D., Jacobi Ch., Lilienthal F. Some features of the day-to-day MLT wind variability in winter 2017–2018 as seen with a European/Siberian meteor radar network. Advances in Space Research. 2020. V. 65, Issue 6. P. 1529–1543.

We present results of wind measurements near the mesopause carried out with meteor radars (MRs) at Collm (51°N, 13°E), Obninsk (55°N, 37°E), Kazan (56°N, 49°E), Angarsk (52°N, 104°E) and Anadyr (65°N, 178°E) from October 1, 2017 till March 31, 2018. The Collm and Kazan MRs are SKiYMET radars with vertical transmission and radio echo height finding, while the other radars operate with horizontal transmission and without height finding. We paid particular attention to the meridional wind variability with periods of 4–6 days and 9–11 days. The waves with these periods are seen as spots of the wave activity in the wavelet spectra and include oscillations with different periods and different discrete zonal wavenumbers. These wave packets successively propagate as a group of waves from one site to another one in such a way that they are observed at one site and almost disappear at the previous one. The 4–6 wave group includes planetary-scale oscillations (individual spectral components) which have eastward phase velocities and mostly zonal wavenumbers 2 and 3, and the vertical wavelength exceeds 70 km at middle latitudes. The source of the oscillations is the polar jet instability. The wave group itself propagates westward, and the amplitudes of wind oscillations are approximately 5–6 m/s as obtained from the wind data averaged over the meteor zone. The 9–11 day wave set propagates westward as a group and mainly consists of spectral components which have westward phase velocity and zonal wavenumber 1. Amplitudes of these wind perturbations strongly vary from station to station and can reach, approximately, 8 m/s. The vertical wavenumber is 0.014 km^{-1} as taken from the Kazan and 0.05 km^{-1} according to the Collm data. We obtained a global view on the waves by using the AURA MLS geopotential data. We found a good correspondence between wave features obtained from the MR wind measurements and the MLS data. To our knowledge, such a wave propagation of planetary wave in the mesosphere/lower thermosphere (MLT) region has so far not obtained much attention.

7. Merzlyakov E., Solovyova T., Yudakov A., Korotyshkin D., Jacobi Ch., Lilienthal F. Amplitude modulation of the semidiurnal tide based on MLT wind measurements with a European/Siberian meteor radar network in October – December 2017. Advances in Space Research. 2020. V. 66, Issue 3. P. 631–645.

We present results on temporal and longitudinal modulations of semidiurnal tide amplitudes in the mesosphere and lower thermosphere winds. The wind data were obtained during October – December 2017 when six meteor radars operated simultaneously. The radar network covers latitudes from 51°N to 72°N and longitudes from 13°E to 178°E. The results show a clear tidal 8–9 day amplitude modulation, which significantly changes with latitude. Evidence is provided for a non-linear interaction between the semidiurnal tide and eastward and westward propagating planetary waves as a source of the modulation. The modulation from the interaction with eastward propagating waves of zonal wavenumber 1 is observed at high latitudes (65°–72°N). A modulation in correspondence with non-linear interaction with a westward propagating wave of zonal wavenumber 1 replaces the first one at middle latitudes (51°–52°N). Furthermore, we found a significant statistical link between the upper stratosphere zonal jet oscillations and the longitudinal difference in tidal amplitudes obtained at the Collm and Angarsk mid-latitude stations. The correlation coefficients are about 0.61 and 0.55 for zonal and meridional amplitudes, respectively. The difference between tidal winds taken at different longitudes grows in amplitude for both wind components at middle latitudes during the increase of stationary planetary wave 1 activity in December. TIDI upper mesospheric wind data indicate a semidiurnal westward propagating tide with wavenumber 3 as the leading source of this effect. The difference between tidal winds at high-latitudes shows different behaviour for the zonal and meridional wind components in December.

8. Merzlyakov E., Korotyshkin D., Jacobi Ch., Lilienthal F. Long-period meteor radar temperature variations over Collm (51°N, 13°E) and Kazan (56°N, 49°E). Advances in Space Research. 2021. V. 67, Issue 10. P. 3250–3259.

We have estimated temperatures from meteor radar measurements using the gradient method and the full width at half maximum method over Kazan (56°N 49°E) and Collm (51°N, 13°E). The time series cover the period 2016–2019. The temperature gradient model is constructed from SABER temperature observations. We demonstrate that annual mean, amplitudes and phases of the annual and semiannual oscillations of the radar temperatures are close to those of the MLS and SABER temperatures. The annual mean temperatures over Kazan and Collm differ non-significantly. The seasonal variability of the radar temperature is mostly due to the annual cycle which tends to grow with latitude. The gradient method produces temperatures which agree with the SABER temperatures better than with the MLS ones. The harmonics of the annual oscillations from periods of 73 days up to periods of about 40 days are the most significant day-to-day temperature oscillations and have zonal wavenumber zero. Their periods and phases are in good correspondence with those of the MLS and SABER ones. We also show some results

which demonstrate that at 56°N the FWHM method is not as robust as the gradient method.

9. Veretenenko S. Effects of Solar Proton Events of January 2005 on the middle atmosphere dynamics in the Northern hemisphere. Advances in Space Research. 2021. V. 68, Issue 4. P. 1814–1824.

In January 2005, a series of strong Solar Proton Events (SPEs) associated with an enhancement of flare activity on the Sun occurred resulting in a considerable increase of ionization in the polar atmosphere. In this work an impact of these events on the middle atmosphere circulation in the Northern hemisphere is investigated on the base of daily values of western wind velocity at different stratospheric levels taken from NCEP-DOE reanalysis-2 archive. A noticeable increase of western wind velocity in the latitudinal belt 60–80°N at all the stratospheric levels was revealed in the course of SPEs under study. The detected effects provide evidence for intensification of the stratospheric polar vortex which plays an important part in the mechanism of solar-atmospheric links. It was shown that ionization changes associated with powerful SPEs and, possibly, auroral phenomena may influence the state of the stratospheric polar vortex on the day-to-day time scale. A possible reason for the polar vortex intensification seems to be temperature variations which may be associated with changes of chemical composition of the polar atmosphere caused by ionization increase, as well as with radiative forcing of cloud changes.

10. Kulikov M.Yu., V. Belikovich M.V., Grygalashvyly M., Sonnemann G.R., Feigin A.M. Retrieving daytime distributions of O, H, OH, HO_2, and chemical heating rate in the mesopause region from satellite observations of ozone and OH* volume emission: The evaluation of the importance of the reaction $H + O_3 \rightarrow O_2 + OH$ in the ozone balance. Advances in Space Research. 2022. V. 69, Issue 9. P. 3362–3373.

Based on data from the SABER (Sounding of the Atmosphere using Broadband Emission Radiometry) instrument onboard the TIMED (Thermosphere Ionosphere Mesosphere Energetics and Dynamics) satellite observations 2003–2015, we retrieved atomic oxygen and atomic hydrogen distributions in the mesopause region (~77 km–100 km) for daytime conditions taking into account the reaction of the ozone with atomic hydrogen in the ozone balance equation (OBE). Subsequently we calculated daytime distributions of OH, HO_2, and the corresponding total chemical heating rate (CHR) from seven exothermic chemical reactions. The novelty of our approach is that we consider, to the best of our knowledge, the reaction $H + O_3 \rightarrow O_2 + OH$ in the daytime OBE for the retrieving procedure for the first time. It is shown that neglecting this reaction has little effect on H distributions, but it leads to O and CHR underestimations (up to ~ 35–40%) and HO_2 and OH overestimations (up to ~ 50–85%).

Journal of Atmospheric and Solar-Terrestrial Physics

1. Koval A.V., Gavrilov N.M., Pogoreltsev A.I., Drobashevskaya E.A. Numerical simulation of the mean meridional circulation in the middle atmosphere at different phases of stratospheric warmings and mountain wave scenarios. Journal of Atmospheric and Solar-Terrestrial Physics. 2019. V. 183. P. 11–18.

In this study, numerical simulations have been performed to estimate the transformation of the mean meridional circulation in altitude range 0–100 km at different phases of simulated stratospheric warming (SW) events in January–February including and excluding impact of mesoscale orographic gravity waves (OGWs). To obtain an ensemble of 12 pairs of model runs with and without a parameterization of OGW effects, the numerical middle and upper atmosphere model (MUAM) has been used. Obtained results demonstrate weakening of the zonal mean meridional circulation at altitudes up to 100 km during and after simulated SWs compared to the time interval before SWs. At altitudes below 50 km, southward mean meridional winds decrease (up to 15%) before and after simulated SWs. OGW effects may increase the mean northward wind at altitudes above 60 km up to 10–15%. The most significant changes of the meridional circulation in the middle atmosphere are detected at the middle and high latitudes of the Northern Hemisphere: the southward meridional circulation increases at altitudes above 40 km and decreases below 40 km. Thus, the global-scale mean meridional circulation in the middle atmosphere may significantly depend on different phases of SW events during the northern winter season. It is also quite sensitive to the dynamical and thermal OGW impacts.

2. Medvedeva I.V., Semenov A.I., Pogoreltsev A.I., Tatarnikov A.V. Influence of sudden stratospheric warming on the mesosphere/lower thermosphere from the hydroxyl emission observations and numerical simulations. Journal of Atmospheric and Solar-Terrestrial Physics. 2019. V. 187. P. 22–32.

We present the results of studying the behavior of temperature and of the atomic oxygen concentration in the mesopause region during the 2013 January major Sudden Stratospheric Warming (SSW). The data on the hydroxyl molecule OH(6-2), 834.0 nm emission intensity and rotational temperature were analyzed. These data were obtained through spectrometric measurements at the Geophysical Observatory of the Institute of Solar-Terrestrial Physics of the Siberian Branch of the Russian Academy of Sciences (51.8°N, 103.1°E, Tory), and at the Zvenigorod Station at the Obukhov Institute of Atmospheric Physics of the Russian Academy of Sciences (55.7°N, 36.8 E°). We calculated the concentration of atomic oxygen and its variations by using the data of the OH emission measurements. We revealed, that the response of the mesopause characteristics for two longitudinally spaced mid-latitude re-

gions essentially differs. Thus, from the Tory Station data, the maximal increase in the OH emission intensity (by a factor of ∼2) and in the concentration [O] (by a factor of ∼3) occurred during the sudden stratospheric warming (SSW) evolution, whereas, from the Zvenigorod Station data, the OH emission intensity increase (by a factor of ∼3) and the concentration [O] increase (by a factor of ∼3.5) was observed at the SSW recovery phase. As a result of numerical modeling using the Middle and Upper Atmosphere Model (MUAM), it was shown, that the cause for the revealed effect may probably be longitudinal differences in the diurnal variation in the vertical wind at the mesopause heights over the indicated stations during the SSW. One may elucidate these differences through the generation of non-migrating tides due to a non-linear interaction between the intensified stationary planetary wave 1 (SPW1) and migrating tides and forcing a set of high-frequency PWs at the stratospheric heights. All these waves are capably of propagating into the MLT region and produce observed changes in behavior of the OH emission intensity, temperature and atomic oxygen concentration over Tory and Zvenigorod.

3. Shpynev B.G., Khabituev D.S., Chernigovskaya M.A., Zorkal'tseva O.S. Role of winter jet stream in the middle atmosphere energy balance. Journal of Atmospheric and Solar-Terrestrial Physics. 2019. V. 188. P. 1–10.

We consider physical mechanisms responsible for forming plain-layered jet streams in the winter stratosphere. Unlike the conventional notion about the balance between the energy of the solar UV radiation energy absorbed by the stratospheric ozone within the Hartley band and the energy of loss due to infrared emission from CO_2, O_3, and H_2O molecules, such a balance is shown not to persist. It is shown that the bias of these energies observed in satellite experiments can be explained by dynamic mechanism increasing the air gravity potential in the tropical stratosphere and forming equator/winter pole baroclinic instability, which generates the jet stream. Jet streams transport energy and pulse from equatorial to polar region and facilitate the descending part of the Brewer-Dobson global circulation. Potential energy release, when the stratospheric jet stream lowers, is $\sim 10^{18}$ W/day; the air mass transported by the jet stream to the winter tropopause region is estimated as being $\sim 10^{14}$ kg/day. Based on the ECMWF ERA-Interim reanalysis data, we analyzed the temporal characteristics of the stratospheric air motion from the region of gravity potential abundance generation in the summer tropical stratosphere to the polar winter tropopause altitudes, where the stratospheric air ends its motion, thus participating in cyclogenesis. Duration of the descending part of the Brewer-Dobson circulation in the winter stratosphere/troposphere averages 50–70 days.

4. Zuev V.V., Savelieva E. The cause of the strengthening of the Antarctic polar vortex during October–November periods. Journal of Atmospheric and Solar-Terrestrial Physics. 2019. V. 190. P. 1–5.

The stratospheric polar vortex strength in spring determines to a great extent the duration and intensity of ozone depletion in the polar regions. The size of the Antarctic ozone hole usually reaches its maximum in September, and then drops off during October and November. However, in 1987, 1998, 1999, 2001, 2006, 2011 and especially in 2015, a significant increase in the ozone hole area relative to climatological mean values was observed in October and November under strong polar vortex conditions. Furthermore, in these years it occurred simultaneously with a temperature increase in the subtropical lower stratosphere in the Southern Hemisphere. Based on the ERA-Interim reanalysis temperature and zonal wind data, we reveal a high correlation between interannual variations of the subtropical temperature and the zonal wind at 60° S in October and November (the Pearson correlation coefficients r equal 0.71 and 0.82, respectively). Thus, a temperature increase in the subtropical lower stratosphere from October to November can strengthen the Antarctic polar vortex in this period.

5. Belyaev A.N. Local temperature changes in the mesosphere due to a "horizontally propagating" turbulent patch. Journal of Atmospheric and Solar-Terrestrial Physics. 2019. V. 190. P. 62–63.

In this study, we model thermal changes in the background atmosphere due to a horizontally" moving" turbulent patch. We divide the process of mutual adjustment of the turbulent patch and the background atmosphere into the two stages: (i) Fast high-to-low transition of the atmospheric stability within the turbulent patch induced by strong adiabatic mixing within the "moving" turbulent patch. (ii) Slow adjustment of the ambient background atmosphere to a quasi-stabilized, near-adiabatic thermal stratification within the turbulent patch. Within the framework of the first stage, assuming the existence of a background downward heat flux, we developed a boundary value problem for a non-homogeneous heat equation that accounts for turbulent dissipative heating and mixing. This two-point boundary value problem was solved analytically by applying the Fourier method (separation of variables) to the thickness of the turbulent patch. The solution obtained tends towards equilibrium as the distance from the front border of the "moving" turbulent patch increases. Within the scope of the second stage, we solved the problem of thermal coupling of the two heat-transfer domains, one of which is characterized by a high coefficient of heat transfer. Solving this problem is the basis of our proposing that the thermal structure of a turbulent patch does not change under the influence of an ambient atmosphere, while the ambient atmosphere is cooled slowly above the turbulent patch and warmed slowly

below it. Consequently, it is shown that the model temperature profiles demonstrate the same features as those observed in mesospheric inversion layers (MILs): temperature inversions and a near-adiabatic lapse rate between them.

6. Zuev V.V., Savelieva E. Arctic polar vortex splitting in early January: The role of Arctic sea ice loss. Journal of Atmospheric and Solar-Terrestrial Physics. 2019. V. 195. 105137.

The Arctic stratospheric polar vortex usually forms in autumn, reaches its peak intensity in mid-winter and decays in spring. The polar vortex strength and persistence in the winter–spring period play an important role in stratospheric ozone depletion with the return of solar radiation in late winter. The polar vortex breakdown in most cases occurs under the influence of vertically propagating planetary Rossby waves. The increased activity of planetary waves was observed in 1984/1985, 1998/1999 and 2012/2013 and led to the polar vortex breakdown in mid-winter, after which it was not observed for more than a month. In this study, Arctic sea ice loss is considered as the most likely cause of the increased activity of planetary waves resulting in the unusual weakening of the Arctic polar vortex. Arctic sea ice extent was a record low in autumn 1984, 1998 and 2012 in the Beaufort Sea, the Canadian Arctic Archipelago and the Central Arctic.

7. Shevchuk N., Pertsev N., Dalin P., Perminov V. Wave-induced variations in noctilucent cloud brightness: model and experimental studies. Journal of Atmospheric and Solar-Terrestrial Physics. 2020. V. 203. 105257.

The paper describes a dynamical (geometrical) model of gravity-wave-induced noctilucent cloud (NLC) brightness. NLC brightness dependences on gravity wave parameters are presented. Results of the inverse-problem solution are addressed as well. It is shown that relative variations of NLC brightness are mainly dependent on the amplitude of a gravity wave, its horizontal wavelength and unperturbed thickness of an NLC layer. It is also shown that the model can be used for determining a geometric amplitude of a perturbing wave from a relative brightness distribution (inverse problem) and that the uncertainty of the geometric wave amplitude is mainly defined by an uncertainty of the cloud layer thickness.

8. Popov A.A., Gavrilov N.M, Perminov V.I., Pertsev N.N., Medvedeva I.V. Multiyear observations of mesoscale variances of hydroxyl nightglow near the mesopause at Tory and Zvenigorod. Journal of Atmospheric and Solar-Terrestrial Physics. 2020. V. 205. 105311.

Digital difference filters were used for the analysis of data of the spectral observations of the rotational temperature and emission intensity of vibrationally excited hydroxyl (OH*) at altitudes 85–90 km at observatories

Zvenigorod (56° N, 37° E) for 2004–2016 years and Tory (52° N, 103° E) for 2012–2017. The monthly-average values and standard deviations of mesoscale perturbations of the OH* emission characteristics with periods 0.8–11 h are obtained. These mesoscale perturbations may reflect internal gravity waves (IGWs) in the mesopause region. To filter out mesoscale perturbations, differences between the sequential values of the OH* emission characteristics, averaged over the intervals by duration from 0.5 h to 2 h, were obtained. The average monthly variances of mesoscale perturbations in the OH* rotational temperature obtained at Tory are larger compared to Zvenigorod ones. Average seasonal changes of relative mesoscale variances demonstrate maxima in winter and in summer, with the summer maximum shifted closer to spring months for the Tory station. The reasons for the differences could be different orography and jet streams in the lower and middle atmosphere, also different spectra of IGW horizontal wavelengths due to different geometry of observations at Tory and Zvenigorod.

9. Gabis. I.P. Quasi-biennial oscillation of the equatorial total ozone: A seasonal dependence and forecast for 2019–2021. Journal of Atmospheric and Solar-Terrestrial Physics. 2020. V. 207. 105353.

The interannual variability of the total ozone (TOZ) in the equatorial region (5°S – 5°N) has been studied using the satellite daily and monthly data in 1978–2018. The coupling of the equatorial TOZ changes to the quasi-biennial oscillation (QBO) of the zonal wind in the equatorial stratosphere has long been known. However, the detailed analysis of the daily deseasonalized TOZ data over the course of 15 complete wind QBO cycles convincingly showed some new important features of the ozone QBO (ΔTOZ). The key points of the equatorial ΔTOZ variations are clearly linked with the certain time moments during the downward propagation from ~10 to ~70 hPa of the easterly and westerly regimes of the wind QBO. The equatorial ΔTOZ distinctly maximizes when the westerly regime reaches ~70 hPa and the easterly regime appears at ~10 hPa, which occur simultaneously. The times of minima of the equatorial ΔTOZ are less obvious due to the westerly regime appearance at ~10 hPa on the background of the unfinished descent of the easterly regime. Furthermore, the seasonal regularities of the wind QBO causes the seasonal dependence of the ozone QBO in the equatorial region. Maxima of the equatorial ΔTOZ are definitely observed near solstice months (June or December). This result contradicts to the general belief about lack of the seasonal synchronization of the equatorial ozone QBO in contrast to the seasonally synchronized extratropical ozone. However, the coincidence of the equatorial ΔTOZ maxima with solstices and, consequently, their recurrence every 2 or 2.5 years allow a prediction of the equatorial TOZ, based on the long-

term forecast of the wind QBO. The ozone QBO forecast for subsequent about two years (2019–2021) is presented.

10. Gavrilov N.M., Kshevetskii S.P., Koval A.V. Thermal effects of nonlinear acoustic-gravity waves propagating at thermospheric temperatures matching high and low solar activity. Journal of Atmospheric and Solar-Terrestrial Physics. 2020. V. 208. 105381.

Numerical high-resolution modeling of nonlinear acoustic-gravity waves (AGWs) generated at the Earth's surface and propagating to the thermosphere shows that wave characteristics are depending on modifications in the mean density, temperature, molecular dissipation and composition due to variations of solar activity (SA). Amplitudes of temperature wave perturbations are generally larger at high SA at altitudes above 150 km, due to larger mean temperature and smaller molecular heat conductivity. Increasing kinematic coefficients of molecular heat conduction and viscosity result in stronger decreasing AGW amplitudes at altitudes larger 150 km at low SA. Dissipating AGWs generally produce heating at altitudes below 120 km. At larger heights, AGWs generally heat the thermosphere at low SA and cool it at high SA. Wave enthalpy fluxes are mainly upwards below 120 km altitude and downwards above 150 km at high SA, where they may have directions opposite to the upward wave energy fluxes. Downward wave enthalpy fluxes correspond to AGW cooling the upper atmosphere at high SA. Nonlinear dissipating AGWs may produce upward and downward transport of atmospheric mass. These mass flows may produce adiabatic heat influxes in the upper atmosphere. Mainly positive residual wave-induced mass flows at altitudes higher 150 km may contribute to the wave cooling of the upper atmosphere. Wave breaking and interactions between waves and the mean flow in the nonlinear model are stronger at higher amplitudes of AGW excitation at the ground, which lead to bigger energy losses for larger-amplitude waves. At high SA, resulting effects in the thermosphere depend on the balance between, on one hand, increases in wave amplitudes, caused by weaker molecular dissipation and smaller transfer of the wave energy to the wave-induced jet flows, and, on the other hand, decreases in the amplitudes due to higher density and larger AGW reflection. The thermal effects of waves in the upper atmosphere may depend on competitions between heating due to dissipation of the upward wave energy flux and cooling due to divergence of the downward wave entropy (or potential enthalpy) flux. At high SA, larger mean temperatures and larger temperature perturbations might increase magnitudes of downward wave entropy fluxes, which may result in more frequent downward wave enthalpy fluxes and wave cooling of the upper atmosphere.

Atmosphere

1. Medvedev A.V., Ratovsky K.G., Tolstikov M.V., VasilyevR.V., Artamonov M.F. Method for Determining Neutral Wind Velocity Vectors Using Measurements of Internal Gravity Wave Group and Phase Velocities. Atmosphere. 2019. V. 10. Issue 9. 546; doi:10.3390/atmos10090546

This study presents a new method for determining a neutral wind velocity vector. The basis of the method is measurement of the group velocities of internal gravity waves. Using the case of the Boussinesq dispersion relation, we demonstrated the ability to measure a neutral wind velocity vector using the group velocity and wave vector data. An algorithm for obtaining the group velocity vector from the wave vector spectrum is proposed. The new method was tested by comparing the obtained winter wind pattern with wind data from other sources. Testing the new method showed that it is in quantitative agreement with the Fabry–Pérot interferometer wind measurements for zonal and vertical wind velocities. The differences in meridional wind velocities are also discussed here. Of particular interest were the results related to the measurement of vertical wind velocities. We demonstrated that two independent methods gave the presence of vertical wind velocities with amplitude of ~20 m/s. Estimation of vertical wind contribution to plasma drift velocity indicated the importance of vertical wind measurements and the need to take them into account in physical and empirical models of the ionosphere and thermosphere.

2. Bakhmetieva N.V., Kulikov Y.Y., Zhemyakov I.N., Mesosphere Ozone and the Lower Ionosphere under Plasma Disturbance by Powerful High-Frequency Radio Emission, Atmosphere. 2020. V. 11. Issue 11. 1154. doi: 10.3390/ atmos11111154.

We present the results of experiments on the Earth's lower ionosphere at mesospheric heights by creating artificial periodic irregularities (APIs) of the ionospheric plasma and simultaneous measurement of the atmospheric emission spectrum in the ozone line by ground-based microwave radiometry when the ionosphere was disturbed by powerful high-frequency radio emission from the midlatitude SURA heating facility (56.15° N; 46.11° E). The diagnostics of the ionosphere was carried out on the basis of measuring amplitudes and phases of signals scattered by periodic irregularities in the altitude range of 50–130 km. For each heating session lasting 30 min, two ozone spectra were measured. These spectra were compared with the measured spectra the periods when heating was turned off. During the heating session of the ionosphere, a decrease in the intensity of the microwave radiation of the atmosphere in the ozone line was observed. The lower ionosphere was characterized by intense dynamics. Rapid variations in the amplitude of the

scattered signal and the relaxation time of artificial periodic irregularities were observed. The velocity of a regular vertical movement in the D-region of the ionosphere constantly varied direction with average minute values up to 4–5 m/s. We assume the decrease in the ozone emission spectrum at the altitude of 60 km can be explained by an increase in the coefficient of electron attachment to oxygen molecules during heating sessions. The lower boundary of the region enriched with atomic oxygen was estimated from the height profile of the API relaxation time.

3. Grigoriev G.I., Lapin V.G., Kalinina E.E., Generation of Internal Gravity Waves in the Thermosphere during Operation of the SURA Facility under Parametric Resonance Conditions. Atmosphere. 2020. V. 11. Issue 11. 1169, doi: 10.3390/atmos11111169.

The problem of excitation of internal gravity waves (IGWs) in the upper atmosphere by an external source of a limited duration of operation is investigated. An isothermal atmosphere was chosen as the propagation environment of IGWs in the presence of a uniform wind that changes over time according to the harmonic law. For the vertical component of the displacement of an environment, the Mathieu equation with zero initial conditions was solved with the right part simulating the effect of a powerful heating facility on the ionosphere. In the case of a small amplitude of the variable component of the wind, the time dependence of the vertical displacement under parametric resonance conditions using the perturbation method is obtained. The obtained dependence of the solution of the differential equation on the parameters allows us to perform a numerical analysis of the problem in the case of variable wind of arbitrary amplitude. For practical estimations of the obtained values, data on the operating modes of the SURA heating facility (56.15° N, 46.11° E) with periodic (15–30 min) switching on during of 2–3 h for ionosphere impact were used.

4. Jakovlev A.R., Smyshlyaev S.P., Galin V.Y. Interannual Variability and Trends in Sea Surface Temperature, Lower and Middle Atmosphere Temperature at Different Latitudes for 1980–2019. Atmosphere. 2021 V. 12. Issue 4. 454. doi: 10.3390/atmos12040454.

The influence of sea-surface temperature (SST) on the lower troposphere and lower stratosphere temperature in the tropical, middle, and polar latitudes is studied for 1980–2019 based on the MERRA2, ERA5, and Met Office reanalysis data, and numerical modeling with a chemistry-climate model (CCM) of the lower and middle atmosphere. The variability of SST is analyzed according to Met Office and ERA5 data, while the variability of atmospheric temperature is investigated according to MERRA2 and ERA5 data. Analysis of sea surface temperature trends based on reanalysis data revealed that a

significant positive SST trend of about 0.1 degrees per decade is observed over the globe. In the middle latitudes of the Northern Hemisphere, the trend (about 0.2 degrees per decade) is 2 times higher than the global average, and 5 times higher than in the Southern Hemisphere (about 0.04 degrees per decade). At polar latitudes, opposite SST trends are observed in the Arctic (positive) and Antarctic (negative). The impact of the El Niño Southern Oscillation phenomenon on the temperature of the lower and middle atmosphere in the middle and polar latitudes of the Northern and Southern Hemispheres is discussed. To assess the relative influence of SST, CO2, and other greenhouse gases' variability on the temperature of the lower troposphere and lower stratosphere, numerical calculations with a CCM were performed for several scenarios of accounting for the SST and carbon dioxide variability. The results of numerical experiments with a CCM demonstrated that the influence of SST prevails in the troposphere, while for the stratosphere, an increase in the CO2 content plays the most important role.

5. Smyshlyaev S.P., Vargin P.N., Motsakov M.A. Numerical Modeling of Ozone Loss in the Exceptional Arctic Stratosphere Winter–Spring of 2020. Atmosphere. 2021. V. 12. Issue 11. 1470. doi: 10.3390/atmos12111470

Dynamical processes and changes in the ozone layer in the Arctic stratosphere during the winter of 2019–2020 were analyzed using numerical experiments with a chemistry-transport model (CTM) and reanalysis data. The results of numerical calculations using CTM with Dynamic parameters specified from the Modern Era Retrospective analysis for Research and Applications, version 2 (MERRA-2) reanalysis data, carried out according to several scenarios of accounting for the chemical destruction of ozone, demonstrated that both Dynamic and chemical processes contribute significantly to ozone changes over the selected World Ozone and Ultraviolet Radiation Data Centre network stations, both in the Eastern and in the Western hemispheres. Based on numerical experiments with the CTM, the specific Dynamic conditions of winter–spring 2019–2020 described a decrease in ozone up to 100 Dobson Units (DU) in the Eastern Hemisphere and over 150 DU in the Western Hemisphere. In this case, the photochemical destruction of ozone in both the Western and Eastern Hemispheres at a maximum was about 50 DU with peaks in April in the Eastern Hemisphere and in March and April in the Western Hemisphere. Heterogeneous activation of halogen gases on the surface of polar stratospheric clouds, on the one hand, led to a sharp increase in the destruction of ozone in chlorine and bromine catalytic cycles, and, on the other hand, decreased its destruction in nitrogen catalytic cycles. Analysis of wave activity using 3D Plumb fluxes showed that the enhancement of upward wave activity propagation in the middle of March over the Gulf of Alaska was observed during the development stage of the minor sudden stratospheric

warming (SSW) event that led to displacement of the stratospheric polar vortex to the north of Canada and decrease of polar stratospheric clouds' volume.

6. Vargin P.N., Kostrykin S.V., Volodin E.M., Pogoreltsev A.I., Wei K. Arctic Stratosphere Circulation Changes in the 21st Century in Simulations of INM CM5. Atmosphere. 2022. V. 13. Issue 1. 25. doi: 10.3390/atmos13010025.

Simulations of Institute of Numerical Mathematics (INM) coupled climate model 5th version for the period from 2015 to 2100 under moderate (SSP2-4.5) and severe (SSP5-8.5) scenarios of greenhouse gases growth are analyzed to investigate changes of Arctic polar stratospheric vortex, planetary wave propagation, Sudden Stratospheric Warming frequency, Final Warming dates, and meridional circulation. Strengthening of wave activity propagation and a stationary planetary wave number 1 in the middle and upper stratosphere, acceleration of meridional circulation, an increase of winter mean polar stratospheric volume (Vpsc) and strengthening of Arctic stratosphere interannual variability after the middle of 21st century, especially under a severe scenario, were revealed. March monthly values of Vpsc in some winters could be about two times more than observed ones in the Arctic stratosphere in the spring of 2011 and 2020, which in turn could lead to large ozone layer destruction. Composite analysis shows that "warm" winters with the least winter mean Vpsc values are characterized by strengthening of wave activity propagation from the troposphere into the stratosphere in December but weaker propagation in January–February in comparison with winters having the largest Vpsc values.

7. Kolennikova M., Gushchina D. Revisiting the Contrasting Response of Polar Stratosphere to the Eastern and Central Pacific El Niños. Atmosphere. 2022 V. 13. Issue 5. 682. doi: 10.3390/atmos13050682.

El Niño Southern Oscillation (ENSO) invokes the release of a large amount of heat and moisture into the tropical atmosphere, inducing circulation anomalies. The circulation response to ENSO propagates both horizontally poleward and vertically into the stratosphere. Here, we investigate the remote response of the polar stratosphere to ENSO using reanalysis data, along with composite and regression analysis. In particular, we focus on inter-event variability resulting from two ENSO types (the Eastern Pacific (EP) and the Central Pacific (CP) El Niño) and the inter-hemispheric difference in the ENSO responses. Consistent with previous results, we show that ENSO is associated with a weakening in the stratospheric polar vortex but emphasize that the polar stratosphere response strongly depends on the ENSO types, differs between the hemispheres, and changes from the lower to middle stratosphere. The main inter-hemispheric asymmetry manifests in response to the

EP El Niño, which is not significant in the Southern Hemisphere, while CP events are associated with pronounced weakening in the polar vortex in both hemispheres. The weakening in the stratospheric polar vortex arguably results from the intensification in the wave flux from the troposphere into the stratosphere and is accompanied by increased heat transport. The latter causes stratospheric warming in the Artic and Antarctic and slows zonal currents. The response of the lower stratosphere circulation to ENSO is approximately the opposite to that of the middle stratosphere.

8. Veretenenko S. Stratospheric Polar Vortex as an Important Link between the Lower Atmosphere Circulation and Solar Activity. Atmosphere. 2022. V. 13. Issue 7. 1132. doi: 10.3390/atmos13071132

The stratospheric polar vortex is a large-scale cyclonic circulation that forms in a cold air mass in the polar region and extends from the middle troposphere to the stratosphere. The polar vortex is implicated in a variety of atmospheric processes, such as the formation of ozone holes, the North Atlantic and the Arctic Oscillations, variations in extratropical cyclone tracks, etc. The results presented in this work show that the vortex plays an important part in the mechanism of solar activity influence on lower atmosphere circulation, with variations in the vortex intensity being responsible for temporal variability in the correlation links observed between atmospheric characteristics and solar activity phenomena. In turn, the location of the vortex is favorable for the influence of ionization changes associated with charged particle fluxes (cosmic rays, auroral and radiation belt electrons) that affect the chemical composition and temperature regime of the polar atmosphere as well as its electric properties and cloudiness state. In this work, recent results concerning solar activity effects on the state of the stratospheric polar vortex as well as its role in solar–atmospheric links are discussed.

9. Koval A.V., Gavrilov N.M., Didenko K.A., Ermakova T.S., Savenkova E.N. Sensitivity of the 4–10-Day Planetary Wave Structures in the Middle Atmosphere to the Solar Activity Effects in the Thermosphere. Atmosphere. 2022. V. 13. Issue 8. 1325. doi: 10.3390/atmos13081325.

Numerical simulation of the general atmospheric circulation was performed to estimate changes in amplitudes of the westward-travelling planetary waves (PWs) at altitudes from the Earth's surface up to 300 km under different solar activity (SA) levels. The three-dimensional nonlinear mechanistic model of circulation of the middle and upper atmosphere "MUAM" was used. The atmospheric general circulation and PW amplitudes were calculated based on ensembles containing 16 model runs for conditions corresponding to low and high SA. PWs having periods of 4–10 days were considered. Comparison with the data of digital ionosondes showed that the MUAM

model is capable of reproducing the considered PW modes at thermospheric heights. It is shown that under high SA conditions, PW amplitudes are significantly larger in the thermosphere and smaller in the middle atmosphere. The observed PW structures are influenced not only by changes in atmospheric refractive index and Eliassen–Palm flux but also by varying PW reflection in the lower thermosphere, which can change proportions of the wave energy transferred from the lower atmosphere to the upper layers and reflected downwards.

10. Bakhmetieva N.V., Grigoriev G.I. Study of the Mesosphere and Lower Thermosphere by the Method of Creating Artificial Periodic Irregularities of the Ionospheric Plasma. Atmosphere. 2022. V. 13. Issue 9. 1346. doi: 10.3390/atmos13091346

This article presented a brief review of studies of the Earth's ionosphere at the heights of the mesosphere and lower thermosphere by a method based on the creation of artificial periodic inhomogeneities (APIs) of the ionospheric plasma by high-frequency radiation from powerful thermal installations. APIs are created by a standing wave due to the interference between upward-propagating radio waves and those reflected from the ionosphere. API studies of the ionosphere were based on Bragg scattering of probing impulse signals from an artificial periodic structure. The method makes it possible to measure the parameters of the neutral and ionized components of the Earth's atmosphere. Note that, despite the fact that the API method assumes an artificial perturbation of the ionospheric plasma, the parameters of the mesosphere and lower thermosphere are determined at the stage of inhomogeneity relaxation and characterize the undisturbed medium. To date, periodic inhomogeneities have been observed at the heating points of Zimenki and Sura ionospheric heating facility (SURA, Vasilsursk, Russia), Gissar (Tajikistan), Arecibo (Puerto Rico, USA), High Power Auroral Stimulation Observatory (HIPAS) and High Frequency Active Auroral Research Program (HAARP, Gakona, AK, USA), and European Incoherent Scatter (EISCAT, Tromso, Norway). Most of the API studies of the ionosphere were carried out at the SURA mid-latitude heating facility (56.1° N; 46.1° E). The review presented the main results of determining the parameters of the ionosphere and neutral atmosphere at altitudes of 60–120 km and studies of the atmosphere during sunrise and sunset events and solar eclipses. In fact, the review is far from a complete illustration of the possibilities of using the API method to study the mesosphere and lower thermosphere.

11. Vargin P.N., Koval A.V., Guryanov V.V. Arctic Stratosphere Dynamical Processes in the Winter 2021–2022. Atmosphere. 2022. V. 13. Issue 10. 1550. doi: 10.3390/atmos13101550

The Arctic stratosphere winter season of 2021–2022 was characterized by a stable, cold stratospheric polar vortex with a volume of polar stratospheric clouds (PSC) close to the maximum values since 1980, before the beginning of minor sudden stratospheric warming (SSW) events in the late February and early March and major SSW on 20 March. Analysis of dynamical processes of the Arctic stratosphere using reanalysis data indicates that the main reasons for the strengthening of the stratospheric polar vortex in January–February are the minimum propagation of planetary wave activity from the troposphere to the stratosphere over the past 40 years and its reflection in the upper stratosphere–lower mesosphere in the second half of January. The first minor SSW was limited to the upper polar stratosphere, whereas the second one propagated to the middle and lower stratosphere and led to the disappearance of the PSC, which prevented significant ozone depletion. Both minor and major SSW events led to a weakening of the residual meridional circulation in the upper Arctic stratosphere and its intensification in the middle and lower stratosphere, which contributed to additional warming of the subpolar region and weakening of the polar vortex.

12. Ermakova T.S., Koval A.V., Smyshlyaev S.P., Didenko K.A., Aniskina O.G., Savenkova E.N., Vinokurova E.V. Manifestations of Different El Niño Types in the Dynamics of the Extratropical Stratosphere. Atmosphere. 2022. V. 13. Issue 12. 2111. doi: 10.3390/atmos13122111.

The behavior of planetary waves and their influence on the global circulation of the Northern Hemisphere during different El Niño types is studied. Three sets of five boreal winters were chosen for each El Niño type: Modoki I and II and canonical El Niño. Based on data of the Japanese 55-year Reanalysis and the Modern-Era Retrospective Analysis for Research and Applications, the spatio-temporal structure of planetary waves and the residual mean circulation were analyzed. The results show that the canonical El Niño type is characterized by the weakest wave activity in March. It is also demonstrated that warming of the polar stratosphere, accompanied by maximizing wave activity and weakening of the zonal wind, may lead to earlier stratospheric polar vortex collapse and the early spring transition under Modoki I conditions. This study is the next step in understanding of the so-called long-range teleconnections, consisting of the propagation of a signal from the tropical El Niño Southern Oscillation source into the polar stratosphere.

Geomagnetism and Aeronomy

1. Kandieva K.K., Aniskina O.G., Pogoreltsev A.I., Zorkaltseva O.S., Mordvinov V.I. Effect of the Madden–Julian Oscillation and Quasi-Biennial Oscillation on the Dynamics of Extratropical Stratosphere. Geomagnetism and Aeronomy. 2019.V. 59, № 1, P. 105–114.

The effects of the Madden–Julian oscillation and quasi-biennial oscillation in the equatorial stratosphere on the dynamic processes in the extratropical stratosphere has been studied with the use of a model of the middle and upper atmospheric circulation. The heat source of the Madden–Julian oscillation in tropics is specified as a longitude-modulated wave perturbation with a zonal wavenumber of $m = 2$ and a period of about $T = 45$ days that propagates eastward with a phase speed of ~5 m/s. Ensemble calculations were carried out independently for the westerly and easterly phases of the quasi-biennial oscillation. Analysis of the results has shown that both phenomena strongly affect the circulation of the winter extratropical stratosphere, the polar vortex decay, and sudden stratospheric warming events; the character of the effect depends on the combination of their phases. The good agreement between the simulation results and the reanalysis of data confirms our results.

2. Kropotkina E.P., Rozanov S.B., Lukin A.N., Solomonov S.V., Ignat'ev A.N. Characteristics of changes in the ozone content in the upper stratosphere over Moscow during the cold half-years of 2014–2015 and 2015–2016. Geomagnetism and Aeronomy. 2019. V. 59. № 2. P. 212–220.

The results of ground-based microwave measurements of the stratospheric ozone profiles over Moscow during the cold half-years of 2014–2015 and 2015–2016 are presented. The causes of the observed changes in the ozone in the upper stratosphere are considered. Increased planetary wave activity, strong temperature decreases in the beginning of winter, and decreased temperatures from January to March were detected during the winter of 2014–2015. The polar vortex was long-lived but not deep; the cold air of the vortex was over Moscow in February–March. This led to a strong negative correlation of the measured ozone content with the temperature. The highest ozone content at the 2-mb level was observed in mid-March. Conversely, an intense polar vortex formed in November–December 2015 under lower planetary wave activity; it was completely destroyed by the major final warming in the beginning of March 2016. The ozone variations in the upper stratosphere over Moscow in December 2015 and January 2016 were related to the alternation of air masses of the vortex and regions outside the vortex. Higher temperatures (as compared to those in the beginning of 2015) led to a decreased ozone content in the beginning of 2016. The interannual difference in the ozone content in the first half of March exceeded 40% of the monthly mean value.

3. Veretenenko S.V., Ogurtsov M.G. 60-year cycle in the Earth's climate and dynamics of correlation links between solar activity and circulation of the lower atmosphere: new data. Geomagnetism and Aeronomy. 2019. T. 59. № 7. P. 908–917.

In this work we continue studying possible reasons for a roughly 60-year periodicity in the evolution of correlation links between pressure in the lower atmosphere and solar activity. New data providing evidence for influence of the atmospheric circulation regime on the formation of effects of solar activity (galactic cosmic ray fluxes) on tropospheric pressure variations (the development of extratropical baric systems) are presented. It is shown that, in turn, changes in the circulation regime are associated with variations of the intensity of the stratospheric polar vortex, which are also characterized by a ~60-year periodicity. Dominant harmonics with periods of ~80 and ~60 years were revealed in variations of total solar irradiance according to the updated Hoyt–Schatten reconstruction. This allows us to consider variations of solar irradiance as one of possible reasons for changes in the state of the polar vortex and the corresponding changes in large-scale circulation.

4. Kulikov Y.Y., Ryskin V.G., Poberovskii A.V., Yushkov V.A. Detection of large fluctuations in ozone content in the middle atmosphere during sudden stratospheric warmings and subpolar latitudes of the Arctic. Geomagnetism and Aeronomy. 2020. V. 60. № 2. P. 254–262.

The results of microwave radiometry studies of the ozone-content dynamics in the middle atmosphere above Peterhof during stratospheric warmings of two winters, 2015–2016 and 2016–2017, are presented. Ground-based observations employed mobile microwave ozone-measuring instrument (operating frequency is 110.8 GHz). The vertical ozone distribution in the altitude range of 22–60 km is estimated. The results are compared to satellite-borne data on the total ozone content, to vertical profiles of the ozone and temperature in the middle atmosphere, and to data from an ozone-measuring sounder. In the middle atmosphere above Peterhof, there have been significant variations (by several times) in the ozone content at heights of 40–60 km due to minor stratospheric warming.

5. Danilov A.D., Konstantinova A.V. Long-term variations in the parameters of the middle and upper atmosphere and ionosphere (review). Geomagnetism and Aeronomy. 2020. V. 60. № 4. P. 397–420.

The article reviews the main publications from the last eight years on long-term trends in the parameters of the middle atmosphere, thermosphere, and ionosphere. It is shown that the negative temperature trends in the middle atmosphere have been reliably established based on observations by various methods. An analysis of satellite orbits in the thermosphere showed negative density trends at heights of ~400 km. Unexpectedly high negative trends in ion temperature *Ti* above ~220 km obtained with the incoherent-scatter method. The same measurements high positive trends in *Ti* at the heights of the *F*1 layer. There are discrepancies in the estimates of the absolute value of

the negative trends in the critical frequency and height of the *F*2 layer; however, these trends are high in the opinion of the authors.

6. Ginzburg E.A., Krivolutsky A.A., Kukoleva A.A., Myagkova I.N. Calculation of the ionization rate in the atmosphere in the polar region during solar proton events. Geomagnetism and Aeronomy. 2020. V. 60. № 5. P. 570–576.

The results of a comparative analysis of the fluxes and spectra of solar protons measured in September 2017 by satellites at different orbits (ELECTRO-L No. 2, GOES 13, and METEOR-3 No. 2) and the results of modeling of the ionization rate in the polar atmosphere based on data from these experiments are presented. It is found based on data from Russian and US satellites that the proton spectra are sufficiently close to each other and are exponential. Calculations of the ionization rate in the polar atmosphere based on data from the three experiments showed close results, except for those at low altitudes.

7. Veretenenko S.V., Ogurtsov M.G. Influence of solar-geophysical factors on the state of the stratospheric polar vortex. Geomagnetism and Aeronomy. 2020. V. 60. № 7. P. 570–576.

The stratospheric polar vortex is one of the most important connecting links between solar activity and circulation of the lower atmosphere at extratropical latitudes. In this work, the changes in the vortex intensity (western wind velocity in the high latitude stratosphere) are studied in relation to various phenomena caused by solar activity. A significant increase in wind velocity was detected at all stratospheric levels during the powerful solar proton events of January 15–20, 2005. It has been shown that auroral activity may also contribute to the intensification of the polar vortex on a daily time scale. On a multidecadal time scale, geomagnetic activity is one of possible factors of the polar vortex intensity. A significant strengthening of the vortex during the period of increased occurrence of magnetic storms with gradual commencements (~1980–2000) and a weakening during a decrease of occurrence of these storms (~1950–1980) were detected. The results of the study confirmed an important role of the stratospheric polar vortex in the mechanism of solar influence on the Earth's atmosphere.

8. Pertsev N.N., Perminov V.I., Dalin P.A. Lunar tides in the mesopause region obtained from summer temperature of the hydroxyl emission layer. Geomagnetism and Aeronomy. 2021. V. 61. № 2. P. 259–265.

The summer mesopause region (altitudes of 82–92 km) is the coldest place in the Earth's atmosphere; it is influenced by external effects, including lunar tides. In this study, we isolate the lunar tidal harmonics from the temperature series of the hydroxyl emission layer (OH*) obtained from spectrophotometric measurements at the Zvenigorod scientific station of the Obu-

khov Institute of Atmospheric Physics, Russian Academy of Sciences, in the summer seasons of 2000–2016. The OH* temperatures are the weighted average in a layer of ~9 km thick, which has a maximum at an altitude of ~87 km. The analysis made it possible to distinguish lunar oscillations, among which two harmonics in the temperature of the mesopause region are identified for the first time. These oscillations are recognized as the second harmonic of the anomalistic lunar tide (the mean period is ~13.78 days) and the lunar tide with a period of 8 h 17 min, or, interpreting alternatively, the third harmonic of the lunar synodic month (~9.84 days).

9. Danilov A.D., Berbeneva N.A. Some applied aspects of the study of trends in the upper and middle atmosphere. Geomagnetism and Aeronomy. 2021. V. 61. № 4. P. 578–588.

It is shown that that there are currently trends in the parameters of the middle and upper atmosphere and ionosphere that are already leading or may lead in the near future to changes in these spheres. The trends in these parameters, which, in our opinion, can already be used in applied problems, are indicated. The increase in water vapor in the middle atmosphere could influence the state of the ozone layer. This increase explains also the increase in the number of the polar summer mesospheric echoes, which trouble military organizations. There is also a change in the wind system and intensification of the penetration to the ionosphere by internal gravity waves. The latter should lead to a substantial intensification of the "meteorological control" (coupling from below) of the ionosphere. The density trends at satellite altitudes are already leading to an increase in the lifetime of space-debris objects and an increase in the probability of their collisions with space vehicles. The negative trend in the amount of atomic oxygen in the thermosphere most likely indicates intensification of the eddy diffusion. Apparently, this will require the correction of thermospheric models used in many applied problems. The negative trends in the ion temperature in the ionosphere can already influence the operation of global positioning systems. The trends in the total electron content and the "slab thickness" of the ionospheric are related to the correction of the positioning systems and other similar systems. A "descending" of the levels of constant values of *Ne* in the *D* region has been detected. This should be taken into account in systems using the propagation of very low-frequency and low-frequency radio waves. The trends in the *F*2-layer critical frequency may lead in the near future to changes in *foF*2, which, as the calculations show, substantially influence the parameters of the shortwave radio paths.

10. Kirillov A.S., Belakhovsky V.B., Maurchev E.A., Balabin Y.V., Germanenko A.V., Gvozdevskiy B.B. Luminescence of molecular nitrogen and molecular oxygen in the Earth's middle atmosphere during the precipitation of high-energy protons. Geomagnetism and Aeronomy. 2021. V. 61. № 6. P. 864–870.

The intensity profiles of the bands of the first and second positive N_2 systems and the infrared atmospheric and atmospheric O_2 systems were calculated based on models of the electronic kinetics of triplet states of molecular nitrogen and singlet states of molecular oxygen for the middle Earth's atmosphere in the case of the precipitation of high-energy protons into the Earth's atmosphere during the ground-level enhancement (GLE) (no. 69) on January 20, 2005. Calculations have shown that there is a significant contribution from the quenching of the $B^3\Pi_g$ state during molecular collisions over nearly all of the considered altitude range of 20–80 km. The kinetics of O_2 singlet states at altitudes of the middle atmosphere during proton precipitation is considered. Both direct excitation by high-energy particles and intermolecular processes of electron-excitation transfer are taken into account. It is shown that the quenching of the $b^1\Sigma_g^+$ state during inelastic molecular collisions leads to a significant decrease in the intensities of the bands of the atmospheric system at the heights of the middle atmosphere.

11. Veretenenko S.V. Effects of energetic solar proton events of solar cycle 23 on intensity of the stratospheric polar vortex. Geomagnetism and Aeronomy. 2021. V. 61. № 7. P. 985–992.

In this work we continue studying the effects of energetic solar proton events on variations in intensity of the stratospheric polar vortex, which plays an important part in solar–atmospheric relations. It was shown that during strong solar proton events in January 2005 and December 2006, which were accompanied by an increase in the fluxes of particles with energies of more than several hundred MeV, there was a noticeable intensification in zonal western flow in the latitude range of 50°–75° N (the region of the polar vortex formation) at all levels of the stratosphere. A study of the effects of solar proton events with particle energies of >100 MeV which occurred during the 23rd solar cycle (1996–2008) showed that the intensification of the polar vortex associated with the studied events is observed mainly in the western phase of quasi-biennial oscillations of the atmosphere. It was found that an increase in western wind velocity at different stratospheric levels correlates to the greatest extent with changes in ionization rate at altitudes of ~50 km. The obtained results allow suggesting that the detected variations in intensity of the stratospheric polar vortex are caused by changes in the radiation-thermal balance of the polar atmosphere, which are due to changes in its chemical composition.

12. Korshunov V.A., Zubachev D.S. Manifestation of solar activity effects in lidar observations of stratospheric aerosol. Geomagnetism and Aeronomy. 2021. V. 61. № Suppl. 1. P. S67–S74.

An analysis of lidar observations at wavelengths of 532 and 355 nm conducted in the layer 13–23 km over Obninsk (55° N) from 2014 to 2018 has revealed the effect of solar activity factors on stratospheric aerosol. The time

interval from 2016 to 2018 is characterized by a decrease in aerosol backscattering by a few percent 0 to 2 days after the commencement of Forbush decreases in the galactic cosmic ray flux. In 2014–2017, solar proton events with a delay of 3–8 days are followed by an increase of 20% to 70% in aerosol backscattering. This effect has been shown to occur predominantly during the transport of stratospheric air to the observation point from the region of high latitudes.

13. Popov A.A., Gavrilov N.M., Perminov V.I., Pertsev N.N. Statistical correction of mesoscale variances of the upper atmospheric temperature based on observations of the night hydroxyl emission in Zvenigorod. Geomagnetism and Aeronomy. 2021. V. 61. № Suppl. 1. P. S127–S133.

Temporally coherent mesoscale perturbations of the rotational temperature of excited hydroxyl (OH*) are often used as an indicator of wave processes in the mesosphere and lower thermosphere. Digital filters are used in this study to determine the mesoscale component with periods of 0.8–11 h, based on the differences in measured values shifted in time by fixed intervals varying from 10 min to 2 h. The average monthly intensity of mesoscale variations is proportional to the variance of the indicated differences recorded in each calendar month of measurements. These variances contain both information about coherent mesoscale processes and also temporally incoherent noise of an instrumental and turbulent nature. A statistical method for the analysis of the structural functions of the analyzed characteristics of nighttime airglow was developed and applied to estimate the variance of incoherent random noise. These estimates are subtracted from the measured monthly mean variances of mesoscale differences in order to obtain information on the intensity of coherent mesoscale processes near the mesopause. Subtraction of the variance of incoherent noise does not change the character of seasonal variations in all spectral intervals, but it decreases the values of mesoscale standard deviations by 10–20%. The proposed correction makes it possible to better determine the features of seasonal and interannual changes in coherent mesoscale disturbances in different ranges of the frequency spectrum.

14. Kurdyaeva Yu.A., Kshevetsky S.P., Borchevkina O.P., Karpov M.I. Wind effects in the thermosphere during the propagation of atmospheric waves generated by a tropospheric heat source. Geomagnetism and Aeronomy. 2022. V. 62. № 4. P. 453–459.

The results of a numerical study of the processes of propagation into the thermosphere of internal gravity waves excited by heat sources in the troposphere are presented. The results of numerical experiments have shown that thermospheric disturbances from such sources arise ~30 min after the onset of their action. The reason for the appearance of a fast reaction of the thermosphere is the infrasonic waves excited during the generation of internal gravi-

ty waves. It is shown that the thermospheric wind significantly affects the spatiotemporal structure of wave disturbances in the upper atmosphere. This influence manifests itself in an increase in the amplitudes and a decrease in the spatial scales of waves that propagate against the thermospheric wind. For waves that propagate in the direction of the thermospheric wind, a decrease in amplitudes and an increase in spatial scales are noted.

15. Veretenenko S.V. Effects of Solar Proton Events of January 2005 on the Middle Atmosphere Circulation in the Southern Hemisphere. Geomagnetism and Aeronomy. 2022. V. 62. № 7. P. 924–931.

In this paper, we study the effects of solar proton events (SPEs) of January 2005 on the stratosphere circulation in the Southern Hemisphere according to the NCEP-DOE (National Centers for Environmental Prediction-Department of Energy) reanalysis (R-2) data. It was found that in the course of the considered events, in the upper stratosphere (30–10 hPa), where eastern transport of air masses dominates in the whole hemisphere in summer season (December–February), eastern winds noticeably weakened at middle and high latitudes (>40° S), while they strengthened at lower latitudes. In the lower stratosphere (100–50 hPa), where circulation is characterized by a western zonal flow at middle latitudes, a weakening of eastern winds took place only in the polar region (>60° S), with a maximum of the western zonal flow being shifted to higher latitudes. The effects of SPEs of January 2005 observed in the stratosphere circulation of the Northern and Southern Hemispheres were compared. It has been shown that in the Northern (winter) Hemisphere the SPE effects observed in variations of zonal wind velocity are more pronounced than those in the Southern (summer) Hemisphere. It is supposed that the circulation disturbances, which were detected in both hemispheres during the studied SPEs, may be caused by changes in the temperature regime of the polar atmosphere due to variations in its chemical composition (ozone depletion) associated with a considerable increase in the ionization rate.

Optics of Atmosphere and Ocean

1. Korshunov V. A., Merzlyakov E. G., Yudakov A. A. Observations of meteoric aerosol in the upper stratosphere–lower mesosphere by the method of two-wavelength lidar sensing. Atmospheric and Oceanic Optics. 2019. V. 32, № 1. P. 45–54.

We present the results of two-wavelength lidar sensing of the middle atmosphere in the altitude range from 30 to 60 km over Obninsk (55.1° N, 36.6° E) in 2012–2017. Monthly average values of the ratio of aerosol and Rayleigh backscattering coefficients (RARC) at a wavelength of 532 nm, averaged over the layers of 40–50 km and 50–60 km, vary from 0 to 0.02,

while the average peak RARC levels in these layers vary from 0.1 to 0.2. Short-term (shorter than 1 month) and long-term (half-year and longer) variations in backscattering are observed. Short-term variations are time concurrent with the occurrence of meteor showers. Long-term enhancements of backscattering in the layer of 50–60 km were observed in 2013 after the Chelyabinsk meteorite fall, as well as in the first half of 2016. In 2014–2015, the monthly average RARC was zero within measurement errors at altitudes from 40 to 60 km. We analyzed the possibility for meteoric aerosol to manifest in backscattering, taking into account the fluxes of meteoric material, gravitational sedimentation of aerosol, and the effect of vertical wind. The flux of visible meteors with masses larger than 10^{-6} kg and bolides is shown to be insufficient for a long-term enhancement of backscattering in the layer of 50–60 km. It is hypothesized that the enhancement in backscattering is most likely to be due to the occurrence of an enlarged fraction of meteoric smoke particles, formed by ablation of radio meteors and penetrating into the upper stratosphere in the region of the stratospheric polar vortex. In early 2016, this was favored by the formation of an extremely strong stratospheric polar vortex and its shift toward Eurasia.

2. Gerasimov V.V., Zuev V.V., Savelieva E.S. Traces of Canadian pyrocumulonimbus clouds in the stratosphere over Tomsk in June-July, 1991. Atmospheric and Oceanic Optics. 2019. V. 32, № 3. P. 316–323.

We revise the results of lidar measurements of stratospheric aerosol over Tomsk that were made from June 29 to July 14, 1991, and initially interpreted as aerosol layers after the Pinatubo eruption. Using the NOAA HYSPLIT trajectory model, we show that the aerosol layers detected at altitudes of 12 and 14.2 km on June 29 and July 11, respectively, were the stratospheric smoke plume from massive forest fires occurring in Quebec, Canada, in June 1991. Biomass burning products reached the stratosphere via convective ascent within a pyrocumulonimbus (pyroCb) cloud that was detected at 100 km to the west of Baie-Comeau (Quebec, Canada) on June 19. The aerosol layers observed at altitudes between 11 and 16.5 km on July 8, 9, and 14 represented superpositions of the smoke plume from the Quebec pyroCb and first traces of the Pinatubo eruption.

3. Bazhenov O.E., Nevzorov A.A., Nevzorov A.V., Dolgii S.I., Makeev A.P. Disturbance of the stratosphere over Tomsk during winter 2017/2018 using lidar and Aura MLS/OMI observations. Atmospheric and Oceanic Optics. 2020. V. 33. № 6. P. 622–628.

Lidar observations at Siberian Lidar Station (SLS) of the Institute of Atmospheric Optics, Siberian Branch, Russian Academy of Sciences, in Tomsk (56.5° N; 85.0° E) showed the presence of stratospheric aerosol layers, descent of air masses, and deficit of ozone over the city during winter

2017–2018. Aura OMI/MLS data indicated that the total ozone (TO) content and NO_2 content in the stratosphere over northern Eurasia, as well as the temperature in the stratosphere, were significantly lower than normal in December 2017–January 2018. Analysis of back trajectories and integrated (over profile) TO showed that the dynamic disturbance of the Arctic stratosphere in December 2017 led to the extrusion of cold air masses with excessive reactive chlorine content (in view of NO_2 deficit) beyond the Arctic circle and their intrusion into the stratosphere of Tomsk. Seemingly, they were exposed to solar radiation in the stratosphere over Tomsk and, staying spatially isolated, became chemically disturbed. This state is similar to the state of the springtime Arctic stratosphere, where ozone is intensely destroyed until the final warming.

4. Zuev V.V., Borovko I.V., Savelieva E.S. Influence of the temperature of the lower subtropical stratosphere on Antarctic polar vortex dynamics. Atmospheric and Oceanic Optics. 2020. V. 33. № 6. P. 708–711.

Stability of the stratospheric polar vortex in the winter–spring period is one of key factors of the duration and scales of stratospheric ozone depletion in a polar region. The Arctic polar vortex attains its peak intensity in winter, whereas the Antarctic vortex usually strengthens in early spring. As a result, large-scale ozone depletion occurs every year from August to November over the Antarctic, and short-term ozone loss occasionally occurs from January to March over the Arctic. In this work, we analyze the reason for the high strength and stability of the Antarctic polar vortex in the winter–spring period. A good agreement between the seasonal variations in the temperature of the subtropical lower stratosphere and in the zonal wind in the lower subpolar and polar stratosphere in the Southern Hemisphere is shown on the basis of ERA-Interim reanalysis data. The results of numerical simulations with the PlaSim-ICMMG-1.0 model show acceleration of zonal wind in the subpolar region with an increase in the temperature of the subtropical stratosphere. Thus, the winter–spring strengthening of the Antarctic polar vortex occurs due to an increase in the stratospheric equator-to-pole temperature gradient caused by the seasonal increase in the temperature of the lower subtropical stratosphere in this period.

5. Nevzorov A.V., Bazhenov O.E., Elnikov A.V., Loginov V.A. Comparison of time series of integrated aerosol content in the stratosphere and total ozone content. Atmospheric and Oceanic Optics. 2021. V. 34. № 5. P. 411–416.

We present the decadally averaged time series of the total ozone content and integrated aerosol backscattering coefficient over Tomsk in the period of 2000–2016, obtained using the M-124 ozonometer and lidar method, respectively. The relationship between them is studied. The time series for the period of time, considered here, were used to create the annual behaviors in the

form of decadal values (36 points in all) of the parameters studied. These time series were analyzed to identify their differences and similarities.

6. Bazhenov O.E. Ozone anomaly during winter–spring 2019–2020 in the Arctic and over the north of Eurasia using satellite (Aura MLS/OMI) observations. Atmospheric and Oceanic Optics. 2021. V. 34. № 6. P. 643–648.

In winter–spring 2019–2020 there was the strongest ozone anomaly in the Arctic in the total history of the observations. It was due to an extraordinarily strong and long-lived polar vortex, entailing unprecedented chemical ozone destruction. Analysis of Aura OMI/MLS data showed that the total ozone content steadily decreased to 230 DU on March 18 at the Alert site, 222 DU on March 18 at Eureka, 229 DU on March 20 at Thule, and 226 DU on March 18 at Resolute. The minimal temperature was 9–10% below normal from December to April in the stratosphere over Tomsk and the Arctic. The ozone concentration decreased to 4% and 6% of the long-term average at an altitude of 20 km on March 27 for Eureka and at an altitude of 19 km on April 16 for Ny-Ålesund. This event is within the context of climate changes, leading to cooling of the stratosphere. Until the level of ozone-depleting substances in the stratosphere of the Arctic is above the values expected from implementation of the Montreal Protocol, there will be a danger that these events will recur in the future. The 2020 vortex was exceptionally isolated, which appreciably mitigated its effect in midlatitudes.

7. Cheremisin A.A., Marichev V.N., Bochkovskii D.A., Novikov P.V., Romanchenko I.I. Stratospheric aerosol of Siberian forest fires according to lidar observations in Tomsk in August 2019. Atmospheric and Oceanic Optics. 2022. V. 35. № 1. P. 57–64.

The frequency of forest fires has recently increased. Combustion aerosol can enter the stratosphere, which can have noticeable consequences for the climate. In this work, we examine the transport of combustion aerosol into the stratosphere in summer 2019, when numerous wildfires occurred in Siberia, Canada, and Alaska. According to lidar observations at the stratospheric lidar station of the V.E. Zuev Institute of Atmospheric Optics, Siberian Branch, Russian Academy of Sciences, in Tomsk in August 2019, layers of aerosol scattering were pronounced in the lower stratosphere. The analysis of back air mass trajectories calculated on the basis of satellite radiometric information about fires in the Northern Hemisphere and CALIPSO lidar data allows a conclusion that the aerosol layers observed result from transfer of the combustion products of Siberian wildfires into the stratosphere.

8. Zuev V.V., Savelieva E.S., Pavlinsky A.V. Features of stratospheric polar vortex weakening prior to breakdown. Atmospheric and Oceanic Optics. 2022. V. 35. № 2. P. 183–186.

We consider the features of the weakening of a stratospheric polar vortex, which precedes its breakdown. To analyze the abnormal dynamics of polar vortices, we used the method for estimating the main vortex parameters by delineating its edges using the geopotential values determined from the maximal temperature gradient and maximal wind speed according to the ERA5 reanalysis data. As a result, we show the criteria for the abnormal weakening of the polar vortex preceding its breakdown: a decrease in the vortex area to less than 10 million km^2 and a subsequent decrease in the mean wind speed along the vortex edge below 30 and 45 m/s in the lower and middle stratosphere, respectively. In this case, the polar vortex becomes a small cyclone (characterized by high temperatures and the absence of a dynamic barrier) and collapses within three weeks.

9. Nikitenko A.A., Timofeev Yu.M., Virolainen Ya.A., Nerobelov G.M., Poberovskii A.V. Comparison of stratospheric CO_2 measurements by ground- and satellite-based methods. Atmospheric and Oceanic Optics. 2022. V. 35. № 4. P. 341–344.

We compared the measurements of the CO_2 content in the lower stratosphere (12–18 km altitude layer) using a ground-based Bruker 125HR Fourier-transform spectrometer and ACE satellite measurements in 2009–2019. The analysis of the two types of measurements showed a good agreement between them. On the average, the ground-based CO_2 measurements exceed the satellite data by 2.8 ppm (less than 1%), the standard deviations being ~5.0 ppm. The correlation coefficient between the measurements by the two methods is 0.77. The ground-based and satellite CO_2 measurements show weak seasonal variations, opposite to those in tropospheric CO_2: the CO_2 content in the lower stratosphere is maximal in summer and minimal in winter.

10. Zuev V.V., Zueva N.E., Savelieva E.S., Korotkova E.M., Pavlinsky A.V. The role of large volcanic eruptions in stratospheric ozone depletion and degradation of coniferous forests. Atmospheric and Oceanic Optics. 2022. V. 35. № 4. P. 355–358.

A large amount of volcanic aerosol is emitted into the stratosphere as a result of large eruptions of tropical volcanoes and contributes to the formation of positive temperature and negative ozone anomalies in the lower tropical stratosphere. Large eruptions with VEI $\geq$ 5 can cause global ozone depression. A volcanic increase in the temperature of the lower tropical stratosphere increases the stratospheric meridional temperature gradient and thus strengthens the polar vortex. Polar ozone depletion occurs under the conditions of the winter–spring strengthening of the vortex. Stratospheric ozone anomalies due to an increase in the UV-B irradiation can manifest themselves in the degradation of coniferous forests, which serve a biospheric indicator of

climate changes. Mass focal drying of dark coniferous forests has been observed in the mountain regions of southern Siberia since the middle 1990s under an increase in the surface UV-B radiation as a result of ozone depletion after the eruption of Mount Pinatubo.

11. Korshunov V.A., Zubachev D.S. Increase in the aerosol backscattering ratio in the lower mesosphere in 2019–2021 and its effect on temperature measurements with the Rayleigh method. Atmospheric and Oceanic Optics. 2022. V. 35. № 4. P. 366–370.

The results of aerosol backscattering sounding at two wavelengths of 355 and 532 nm in the lower mesosphere at Rosgydromet lidar stations from 2012 to 2021 are presented. A significant increase in the backscattering ratio R has been observed in the altitude range 50–70 km since 2018. In 2019–2020, the average R attained 1.25 at an altitude of 70 km. The Rayleigh measurements at 532 nm overestimated the temperature by up to +20 K in that period. The two-wavelength temperature measurement technique eliminates this error.

12. Kashkin V.B., Odintsov R.V., Rubleva T.V. On the effects of a nuclear explosion on stratospheric ozone. Atmospheric and Oceanic Optics. 2022. V. 35. № 4. P. 402–406.

In our nuclear era, suspicions exist about the fate of the Earth's ozone layer: both large- and local-scale conflicts, using nuclear weapons, are thought to be able to destroy the ozone layer for years to come. On September 22, 1979, an officially unidentified state covertly performed the nighttime nuclear weapon test in a desolate region of the World Ocean. This event is conventionally called the Vela Incident. In this work, we used ozone data obtained by the NASA satellite *Nimbus-7* 16 min and 44 s after the explosion. It is shown that the shock wave left a "trace" in the ozone layer. No decrease in the ozone amount is noticed. The coordinates of the explosion site are determined from the trace.

13. Bazhenov O.E. Ozone anomalies in the stratosphere of the Arctic and North Eurasia: Comparison of the 2011 and 2020 events using TEMIS and Aura MLS data. Atmospheric and Oceanic Optics. 2022. V. 35. № 5. P. 517–523.

In winter–spring of 2019–2020 and 2010–2011 the strongest ozone anomalies in the Arctic in the entire satellite era were observed. They were due to extraordinarily strong and long-lasting stratospheric polar vortices, entailing unprecedented chemical ozone destruction. The analysis of the TEMIS data indicates that the relative total ozone content (TOC) deviations from the multiyear (2003–2019 except 2011) average were 37–44% in 2011 and 45–55% in 2020 at Arctic sites; and 27–36% in 2011 and 27–32% in 2020 at subarctic latitudes. Based on Aura MLS data, the minimal temperatures over the Arctic were 8–12% below normal in 2011 and 8–13% below

normal in 2020. The ozone concentration for Alert station dropped to 23% of the multiyear average at the altitude of 20 km on March 22, 2011, and to 6% at the altitude ~19 km on April 15, 2020. A detailed correlation analysis showed that deviations in concentrations of water vapor and ozone, water vapor and temperature, and ozone and temperature from multiyear averages correlate stronger in 2020 than 2011. The correlations decrease toward the vortex periphery owing to the exchange of air masses between the Arctic and middle latitudes, until becoming weakly significant outside the Arctic circle.

Russian Meteorology and Hydrology

1. Shashkin V.V., Tolstykh M.A., Volodin E.M. Stratospheric circulation modeling with the SL-AV semi-Lagrangian atmospheric model. Russian Meteorology and Hydrology. 2019. V. 44. № 1. P. 1–12.

The article describes the development of the version of the SL-AV global semi-Lagrangian atmospheric model with high spatial resolution in the stratosphere. The new model version uses the vertical grid of 100 levels, grid spacing of 500 m in the layer between 100 and 10 hPa, and the upper lid at 0.04 hPa. The parameterization of the non-orographic gravity wave drag is implemented. Numerous modifications are introduced in the block for the numerical solution of dynamical equations to enhance model stability. The experiment on atmospheric dynamics modeling for 28 years is carried out. It is shown that the SL-AV model reproduces the main features of stratospheric circulation, such as the polar night stratospheric jet formation and sudden stratospheric warming. The quasi-biennial oscillation of equatorial wind is reproduced with realistic period and amplitude.

2. Nikiforova M.P., Vargin P.N., Zvyagintsev A.M. Ozone anomalies over Russia in the winter-spring of 2015/2016. Russian Meteorology and Hydrology. 2019. V. 44. № 1. P. 23–32.

The variability of Arctic total ozone in the winter of 2015/2016 is studied using the data of the national network equipped with M-124 filter ozonometers and satellite monitoring. The first ozone mini-hole that emerged in the first half-year over the whole history of observations (developed at the end of January 2016) is analyzed. The reasons for the total ozone variability over Russia in the first quarter of 2016 are analyzed, and the comparison with the significant Arctic ozone anomalies in 1996/1997 and 2010/2011 is presented.

3. Vargin P.N., Kiryushov B.M. Major sudden stratospheric warming in the Arctic in February 2018 and its impacts on the troposphere, mesosphere, and ozone layer. Russian Meteorology and Hydrology. 2019. V. 44. № 2. P. 112–123.

Dynamical processes in the Arctic stratosphere in the winter of 2017/2018 are analyzed using data of the NCEP reanalysis and SABER and MLS satel-

lite measurements. The following features are revealed: the downward propagation of wave activity from the stratosphere to troposphere over Canada in late December and early January, the major sudden stratospheric warming with the zonal wind reversal in February 2018 accompanied by the stratospheric polar vortex splitting, the propagation of stratospheric circulation anomalies to the lower troposphere, the mesospheric cooling, the stratopause height change, and the cooling in the tropical lower stratosphere.

4. Cheremisin A.A., Marichev V.N., Novikov P.V., Pavlov A.N., Shmirko K.A., Bochkovskii D.A. Assessing the transport of volcanic aerosol in the stratosphere over Tomsk and Vladivostok from lidar data. Russian Meteorology and Hydrology. 2019. V. 44. № 5. P. 345–354.

The transport of volcanic aerosol in the atmosphere after the eruptions of the Grimsvotn and Nabro volcanoes in 2011 is analyzed using the method of Lagrangian particle trajectories. It was impossible to identify volcanic aerosol after the Grimsvotn eruption using data of lidar observations over Tomsk and Vladivostok against the existing background aerosol. At that time there was strong horizontal mixing in the Northern Hemisphere atmosphere. Volcanic aerosol formed after the Nabro eruption was clearly manifested in the form of aerosol scattering peaks over Vladivostok and Tomsk. This is proved by data of the CALIPSO space lidar and by the satellite observations of sulfur dioxide with GOME-2. The dynamics of the eruptive aerosol cloud formation over the Northern Hemisphere is traced.

5. Perevedentsev Y.P., Shantalinskii K.M., Gur'yanov V.V., Vasil'ev A.A. Thermal regime of the troposphere, stratosphere, and lower mesosphere in the Northern Hemisphere in 1979–2016. Russian Meteorology and Hydrology. 2019. V. 44. № 8. C. 501–512.

The characteristics of spatiotemporal variability of air temperature and ozone mass mixing ratio at 26 levels from the ground to the altitude of 64 km are considered using the ERA-Interim reanalysis data for 1979–2016. Differences are revealed in the distribution of air temperature trends between seasons and latitude zones, between the Atlantic-European, Asian-Pacific, and American sectors of the Northern Hemisphere mid-latitudes, and between the thermal regime over the land and ocean. The correlations between the layers and atmospheric circulation patterns in different seasons are assessed.

6. Jakovlev A.R., Smyshlyaev S.P. Numerical simulation of world ocean effects on temperature and ozone in the lower and middle atmosphere. Russian Meteorology and Hydrology. 2019. V. 44. № 9. V. 594–602.

The description of the ocean-atmosphere coupling is presented. The paper analyzes the data of MERRA, JRA, ERA-Interim, and ERA-20Century reanalyses and the re suits of CCM chemistry-climate model simulations based on monthly mean values of air temperature and ozone mixing ratio at the

levels of 925 and 20 hPa during 1980–2015. The comparison with data on sea surface temperature is provided. The results of simulation are in good agreement with reanalysis data for the atmospheric surface layer, whereas essential differences for the stratosphere require a more detailed analysis. According to the model results, air temperature rises in the surface layer, and air temperature and ozone mixing ratio decrease in the stratosphere. Reanalysis data do not contradict simulation results for the troposphere but differ significantly for the stratosphere.

7. Vargin P.N., Nikiforova M.P., Zvyagintsev A.M. Variability of the Antarctic ozone anomaly in 2011–2018. Russian Meteorology and Hydrology. 2020. V. 45. № 2. P. 63–73.

The variability of parameters of the Antarctic ozone anomaly is studied using data of the TOMS/OMI satellite monitoring of the ozone layer, MERRA-2 reanalysis, and balloon sounding of the vertical distribution of ozone and temperature at the South Pole. The dynamic processes in the Antarctic stratosphere which define conditions for the significant ozone layer destruction are analyzed. Despite the decrease in the concentration of ozone-depleting substances, the significant ozone loss in the recent 8 years was observed in the Antarctic in 2011 and 2015.

8. Smyshlyaev S.P., Blakitnaya P.A., Motsakov M.A. Numerical modeling of the influence of physical and chemical factors on the interannual variability of Antarctic ozone. Russian Meteorology and Hydrology. 2020. V. 45. № 3. P. 153–160.

The variability of Antarctic total column ozone in 1980–2018 is considered. The study analyzes trends in Antarctic total column ozone during the study period as well as the physical and chemical processes affecting the seasonal variability of total column ozone. The main attention is paid to the influence of dynamical processes on the stability of the Antarctic polar vortex, to the formation of polar stratospheric clouds, and to the influence of gas-phase and heterogeneous processes on the surface of polar stratospheric clouds and sulfate aerosol. The method of research is the analysis of the results of ground and satellite observations and numerical modeling of physical and chemical processes over the Antarctic using a global chemistry transport model with the dynamical parameters specified from reanalysis data.

9. Vargin P.N., Luk'yanov A.N., Kiryushov B.M. Dynamic processes in the Arctic stratosphere in the winter of 2018/2019. Russian Meteorology and Hydrology. 2020. V. 45. № 6. P. 387–397.

The major dynamic processes in the Arctic stratosphere in the winter of 2018/2019 and their impact on the troposphere, mesosphere, and ozone layer are analyzed using the NCEP reanalysis and MLS satellite data. Based on the

results of simulations with the TRACAO trajectory model, the comparative analysis of stratospheric polar vortex evolution in winters of 2015/2016 and 2018/2019 is performed.

10. Vargin P.N., Kolennikova M.A., Kostrykin S.V., Volodin E.M. Impact of sea surface temperature anomalies in the equatorial and North Pacific on the Arctic stratosphere according to the INMCM5 climate model simulations. Russian Meteorology and Hydrology. 2021. V. 46. № 1. P. 1–9.

Five 50-year simulations with version 5 of the INM RAS coupled climate model revealed that the winters with El Niño are characterized by higher Arctic stratospheric temperature as compared to the seasons with La Niña. Lower stratospheric temperature in the Arctic regions as compared to the seasons with negative sea surface temperature (SST) anomalies corresponds to the winter seasons with positive SST anomalies in the North Pacific.

11. Gochakov A.V., Krupchatnikov V.N., Martynova Y.V., Antokhina O.Y. Method for identifying and clustering Rossby wave breaking events in the Northern hemisphere. Russian Meteorology and Hydrology. 2021. V. 46. № 1. P. 10–18.

Many large-scale dynamic phenomena in the Earth's atmosphere are associated with the processes of propagation and breaking of Rossby waves. A new method for identifying the Rossby wave breaking (RWB) is proposed. It is based on the detection of breakings centers by analyzing the shape of the contours of potential vorticity or temperature on quasimaterial surfaces: isentropic and iserthelic (surfaces of constant Ertel potential vorticity (PV)), with further RWB center clustering to larger regions. The method is applied to the set of constant PV levels (0.3 to 9.8 PVU with a step of 0.5 PVU) at the level of potential temperature of 350 K for 12:00 UTC. The ERA-Interim reanalysis data from 1979 to 2019 are used for the method development. The type of RWB (cyclonic/anticyclonic), its area and center are determined by analyzing the vortex geometry at each PV level for every day. The RWBs obtained at this stage are designated as elementary breakings. Density-Based Spatial Clustering of Applications with Noise algorithm (DBSCAN) was applied to all elementary breakings for each month. As a result, a graphic dataset describing locations and dynamics of RWBs for every month from 1979 to 2019 is formed. The RWB frequency is also evaluated for each longitude, taking into account the duration of each RWB and the number of levels involved, as well as the anomalies of these parameters.

12. Marichev V.N., Bochkovskii D. Monitoring the variability of the stratospheric aerosol layer over Tomsk in 2016–2018 based on lidar data. Russian Meteorology and Hydrology. 2021. V. 46. № 1. P. 43–51.

The results of observations of the features of interannual variability for the vertical structure of background aerosol in the stratosphere over Western

Siberia in 2016–2018 are presented and analyzed. Experimental data were obtained at the lidar complex of Zuev Institute of Atmospheric Optics (Siberian Branch, Russian Academy of Sciences) with a receiving mirror diameter of 1 m. The objective of the study is to investigate the dynamics of background stratospheric aerosol, since during this period there were no volcanic eruptions leading to the transport of eruptive aerosol into the stratosphere. The results of the study confirm a stable interannual cycle of maximum aerosol filling of the stratosphere in winter, a decrease in spring to the minimum, practical absence in summer, and an increase in autumn. At the same time, the variability of stratification and aerosol filling is observed for different years. It was found that aerosol is concentrated in the layer up to 30 km all year round, except for the winter period. It is shown that the vertical aerosol stratification is largely determined by the thermal regime of the troposphere–stratosphere boundary layer. The absence of a pronounced temperature inversion at the tropopause contributes to an increase in the stratosphere–troposphere exchange and, as a result, to the aerosol transport to the stratosphere. This situation is typical of the cold season. For the first time, data on the quantitative content of stratospheric aerosol (its mass concentration) were obtained from single-frequency lidar data.

13. Gabis I.P. Quasi-biennial oscillation of zonal wind in the equatorial stratosphere and its influence on interannual fluctuations in the depth of the Antarctic ozone hole. Russian Meteorology and Hydrology. 2021. V. 46. № 5. P. 287–294.

The Antarctic ozone hole is observed annually in spring due to the complex influence of photochemical and dynamical processes. The increased concentration of ozone-depleting substances in the atmosphere causes a long-term negative trend in total ozone (TO). Intense interannual fluctuations in TO against a background of the long-term trend associated with dynamic atmospheric processes do not allow assessing definitely the direction of the trend (growth/decline) in the recent years. Studying the dependence of interannual fluctuations in the ozone hole intensity on the equatorial quasi-biennial oscillation (QBO) allows identifying natural causes of variations and assessing the trend due to anthropogenic factors. The long-term QBO forecast allows predicting different phenomena that depend on the QBO.

14. Kolennikova M.A., Gushchina D.Y., Vargin P.N. Interrelations between El Niño indices and major characteristics of polar stratosphere according to CMIP5 models and reanalysis. Russian Meteorology and Hydrology. 2021. V. 46. № 6. P. 351–364.

The response of the Arctic stratosphere to El Niño is studied with account of its Eastern and Central Pacific types for the period of 1950–2005. The study is based on the regression and composite analysis using the simulations with six CMIP5 coupled climate models and reanalysis data.

15. Kuminov A.A., Yushkov V.A., Gvozdev Y.N., Shtyrkov O.V., Lykov A.D., Balugin N.V. Meteorological rocket sounding for atmospheric research and geophysical monitoring. Russian Meteorology and Hydrology. 2021. V. 46. № 9. P. 571–578.

The brief description of technical specification of meteorological rockets used at Roshydromet stations, including the exposition of the MERA new meteorological rocket with a lift up to 100 km, MRS 100 rocketsonde, onboard measuring and service equipment, is presented. The technique for measuring atmospheric parameters and the results of investigating long-term variability of temperature and wind in the stratosphere and mesosphere according to long-term (1969–1995) data of meteorological rocket sounding at Volgograd station are considered. It is shown that in the altitude range from 25 to 75 km, trends in temperature and wind speed over Volgograd station for 1969–1995 are nonlinear and, at most altitudes, nonmonotonic. An increase with altitude in the range of trend variations in the analyzed parameters during the surveyed period is discovered: up to 15–19 K in the lower and middle mesosphere for temperature, up to 15 m/s at the stratopause for the zonal component of wind speed, up to 10 m/s in the lower mesosphere for its meridional component.

16. Krivolutskii A.A., V'yushkova T.Y., Cherepanova L.A., Banin M.V., Repnev A.I., Kukoleva A.A. Numerical global models of the ionosphere, ozonosphere, temperature regime, and circulation for altitudes of 0–130 km: results and prospects. Russian Meteorology and Hydrology. 2021. V. 46. № 9. P. 596–605.

An overview of the work on the development and use of global numerical models of the atmosphere, that has been carried out in the Laboratory for Atmospheric Chemistry and Dynamics (Central Aerological Observatory), is presented. The models were created in the framework of the Roshydromet plans.

17. Tsvetkova N.D., Vargin P.N., Lukyanov A.N., Kiryushov B.M., Yushkov V.A., Khattatov V.U. Studying chemical ozone depletion and dynamic processes in the Arctic stratosphere in the winter 2019/2020. Russian Meteorology and Hydrology. 2021. V. 46. № 9. P. 606–615.

The estimates of chemical ozone depletion in winter-spring seasons are given for the Arctic stratosphere based on long-term observations of the vertical distribution of ozone. The features and possible causes for an unusually strong and stable stratospheric polar vortex in the Arctic in the winter 2019/2020, that led to a record ozone loss in recent years, and the dynamic processes associated with this polar vortex are analyzed. The TRACAO trajectory model and ERA5 reanalysis are used for the comparative analysis of ozone depletion in the polar vortex in the winter-spring seasons 2010/2011 and 2019/2020.

18. Lukyanov A.N., Gan'shin A.V., Yushkov V.A., Vyazankin A.S. Trajectory modeling of the middle atmosphere. Russian Meteorology and Hydrology. 2021. V. 46. № 9. P. 624–630.

A short description and some applications of the trajectory and dispersion models developed in Central Aerological Observatory (CAO) for studying the stratospheric and tropospheric transport of pollutants are presented. The TRACAO trajectory model is applied to investigate the processes related to the ozone depletion in the winter polar stratosphere, in order to study the mid-latitude stratosphere–troposphere exchange, as well as to analyze balloon and aircraft (M55 "Geophysics," Yak-42D "Roshydromet") observations. Then based on the TRACAO, the GLADIM dispersion model that simulates trajectories of the set of particles with the eddy diffusion parameterization and determines the pollutant concentration at the regular grid points, was developed. The dispersion model was applied to simulate volcanic ash dispersion and carbon dioxide profile reconstruction. The model validation was done by comparisons with the results of the widely used FLEXPART model. Nowadays these models are used at the "Middle Atmosphere" Regional Information and Analytic Center established in CAO.

19. Timofeev Y.M., Nerobelov G.M., Polyakov A.V., Virolainen Y.A. Satellite monitoring of the ozonosphere. Russian Meteorology and Hydrology. 2021. V. 46. № 12. P. 849–855.

The importance of controlling total ozone (TO) and surface ultraviolet irradiance is a reason for continuous monitoring of the ozonosphere using various ground-based and satellite methods and instruments. The global monitoring of TO has been carried out with the Russian instrument IKFS-2 on the Meteor-M No. 2 satellite since 2015. These measurements are conducted during the whole day and in polar night conditions. The developed algorithm based on using artificial neural networks and OMI satellite instrument measurements is periodically updated and allows determining TO with an average total error of 3–5%. The IKFS-2 measurements can be used for analyzing spatial and temporal (seasonal, interannual) variations in ozone, its long-term trends, verifying modern numerical stratospheric models, studying ozone anomalies, etc. The examples of analyzing TO in autumn-spring periods and TO anomalies in winter and spring of 2020 are given. They clearly demonstrate advantages of satellite TO measurements with the thermal radiation method.

20. Kulikov Yu.Yu., Kirillov A.S., Poberovskii A.V., Imchasin Ch.Ch. Microwave monitoring of middle atmosphere ozone in Apatity and Peterhof in the winter of 2021/2022. Russian Meteorology and Hydrology. 2022. V. 47. № 12. P. 969–975.

Results of synchronous microwave monitoring of middle atmosphere ozone in Apatity (67° N, 33° E) and Peterhof (60° N, 30° E) during the win-

ter and spring of 2021/2022 are presented. Identical mobile microwave spectrometers with an observation frequency of 110.8 GHz were used for ozone measurements. These instruments have identical techniques for observations and estimation of ozone profiles at the altitudes of 22–60 km. The main attention was given to changes in ozone (daily variations) in the mesosphere during the polar night and dynamic disturbances. To interpret the mesospheric ozone (60 km) behavior, MLS/Aura satellite data on the vertical distribution of temperature in the middle atmosphere over Apatity were used.

Solar activity forcing

Over the past years, from 2019 to 2022, some progress has been made in assessing the role of the impact of energetic particle precipitating (EPP) on the state of the middle atmosphere. The correct estimation of EPP ion production and spectra for the computation of ionization rates is an important issue for estimating atmosphere and climate forces. A series of works by Mironova et al in 2019-2022 was devoted inverstigation of spectra and ionization rates induced by energetic elctron precipitation (EEP). In the papers by Mironova et al. 2019, 2019a the variability in the ionization rate above the Murmansk region, Russia, in 1961–2019 using the balloon observations of secondary bremsstrahlung initiated by EEP was studied. The ionization rates in the atmosphere induced by energetic electron precipitation from balloon observations in the polar atmosphere compare them against ionization rates recommended for the Phase 6 of the Coupled Model Intercomparison Project (Mironova et al. 2019). As the main results it is shown that simulations with one-dimentional radiative-convective model with interactive neutral and ion chemistry demonstrate the difference of the Phase 6 of the Coupled Model Intercomparison Project and balloon-based ionization rate that can lead to underestimation of the NOx enhancement by more than 100% and ozone loss up to 25% in the mesosphere. The paper by Mironova et al 2021 proposes a favorable method for the computation of ionization rates using the new parameterization of ion production and a new spectrum shape, which allow one to take into account the range of precipitating particles from tens of keV to several MeV. Look-up tables with ion production/yield function for isotropically precipitating monoenergetic electrons can be easily used for the computation of ionization rates and can further be used by atmospheric and chemistry-climate models for accurate quantification of atmospheric parameters during EEP.

There are many studies where the contribution of energetic particles during solar proton events has been widely examinated to the formation of hydrogen oxide radicals and ozone loss. However, there was no solid evidence that the reduction in galactic cosmic ray fluxes during a magnetic storm,

known as Forbush-effect, directly and noticeably affects the polar-night stratospheric chemistry. Mironova et al. 2021a investigated the impact of the Forbush decrease on the behavior of hydrogen oxide radicals using the three-dimentional chemistry-climate model SOCOLv2 (SOlar Climate Ozone Links). It was found that hydrogen oxide radical lost about half of its concentration over the polar boreal night stratosphere owing to a reduction in ionization rates induced by Forbush decreases after solar proton events. The robust response in ozone was not found.

In the papers by Karagodin et al. 2019, 2022 the ionospheric potential as well as hypothezy that the IMF By fluctuation can modulate the atmospheric global electric circuit (GEC) over the polar regions and affect surface meteorology (named as Mansurov effect) were deep investigated by chemistry-climate models. The examination of the Mansurov effect over the period 1999–2002 using ensemble experiments modeled with the chemistry-climate model SOCOLv3 was performed by Karagodin et al. 2020. Using observed IMF By, Karagodin et al. model its effect on ground-level air pressure and temperature to examine one of the proposed GEC-cloud hypotheses: that surface meteorology response on IMF By fluctuations occurs through the Jz-associated intensification of cloud droplet coalescence rate. The results showed that anomalies in surface air pressure and temperature from the control run, where IMF By is omitted, do not robustly differ from experiments in which the dependence of cloud droplet coalescence rate on IMF By is included.

Exceptionally strong high-energy electron precipitation event detected by balloon measurements in geomagnetic midlatitudes, with ionization rates locally comparable to strong solar proton events was study by Mironova et al. 2022. This electron precipitation was possibly caused by wave–particle interactions in the slot region between the inner and outer radiation belts, connected with still poorly understood natural phenomena in the magnetosphere. Satellite observations of odd nitrogen and nitric acid are consistent with widespread electron precipitation into magnetic midlatitudes and simulations with three-dimentional chemistry–climate model HAMMONIA indicate the almost complete destruction of ozone in the upper mesosphere over the region where high-energy electron precipitation occurred.

Pikulina et al. 2022 examined the response of the middle atmosphere to increased radiation following several powerful X-class solar flares during September 2017. Both flares caused an increase of the solar irradiance in extreme ultraviolet and soft X-ray spectral regions, and Ly-α line. The empirical FISM2 model was used to obtain data on the radiation fluxes from solar flares. The HAMMONIA chemistry–climate model was used to analyze the effect of radiation on the neutral atmosphere. It was shown a significant increase in the concentrations of the reactive nitrogen and hydrogen oxides in the equatorial latitudes and southern high latitudes. This increase did not af-

fect the change in the ozone content in the tropical stratosphere because the ozone destruction by nitrogen oxides is not effective in the upper mesosphere and there are no persistent downward motions, which can transport extra NOx down to the stratosphere. Hydrogen oxides do not have major influence on the ozone during the considered seasons, however, some small ozone depletion correlated with HOx increase is simulated in the southern hemisphere.

The paper of Grankin et al. 2023 estimated ozone destruction during EEP events using one-dimensional photochemical radiation-convective models, taking into account both parameterization and ion chemistry as well as provided an estimation of electron density during these periods. It was shown that during geomagnetic disturbances, there is an increase in the concentration of reactive oxides of nitrogen and hydrogen relative to calm conditions, reaching significant values for intense EEP events. An increase in the concentration of radicals leads to the destruction of the ozone at the heights of the mesosphere during the day, with a maximum destruction of about 14 to 25% at a height of about 75 km for intense events. The effects obtained for events of medium intensity depend on the method of accounting for ion chemistry.

The incease of the concentration of nitrogen oxide in the atmosphere at altitudes of 64–90 km during EEP in the period 2002–2012 was estimated by Makhmutov et al. 2021 with NO measurements with the SCIAMACHY spectrometer installed onboard the European ENVISAT satellite .

During 2019–2022 years some progress has been done in high-resolution numerical simulations of non-stationary, nonlinear acoustic–gravity waves (AGWs) propagating upwards from surface wave sources are performed for different temporal intervals relative to activation and deactivation times of the wave forcing. Gavrilov et al. 2022 estimated the decay times of this wave noise produced by slow residual, quasi-standing and secondary AGW spectral components. The standard deviations of the wave noise are larger for the case of sharp activation and deactivation of the wave forcing compared to the steep processes. These results showed that transient wave sources may create long-lived wave perturbations, which can form a background level of wave noise in the atmosphere. Gavrilov et al. 2022 suggsted that this should be taken into account in parameterizations of atmospheric AGW impacts. Koval et al. 2019, 2022 examined the effect of changes in solar activity on amplitudes of long-period planetary waves.

Recently results of ozone observations and ozone modelling lead a new light on modern ozone layer variabiity. The paper by Nerobelov et al. 2022 demonstrated that total ozone column variations near St. Petersburg measured by different methods are in good agreement with respect to Dobson measurements constitute which is close to the actual requirements of the quality of total ozone content (TOC) measurements. The results showed the pronounced

TOC seasonal cycle with the maximum in spring and minimum in autumn and significant positive TOC trend near St. Petersburg (~0.4 ± 0.1 DU per year) from all datasets considered for 2004–2021years. Smyshlyaev et al. 2021 analyzed ozone variability using numerical experiments with a chemistry-transport model (CTM) and reanalysis data. The results of numerical calculations demonstrated that dynamic conditions of winter–spring 2019–2020 described a decrease in ozone up to 100 Dobson Units (DU) in the Eastern Hemisphere and over 150 DU in the Western Hemisphere.

References

1. Mironova, I.A., Artamonov, A.A.,Bazilevskaya, G., Rozanov, E., Kovaltsov, G.A., Makhmutov, V.S., et al. Ionization of the polaratmosphere by energetic electronprecipitation retrieved from balloonmeasurements.*Geophysical Research Letters*, **2019**, 46, 990–996. https://doi.org/10.1029/2018GL079421.
2. Mironova, I.A.; Bazilevskaya, G.A.; Kovaltsov, G.A.; Artamonov, A.A.; Rozanov, E.V.; Mishev, A.; Makhmutov, V.S.; Karagodin, A.V.; Golubenko, K.S. Spectra of high energy electron precipitation and atmospheric ionization rates retrieval from balloon measurements. *Sci. Total Environ.* **2019a**, *693*, 133–242.
3. Mironova, I.; Kovaltsov, G.; Mishev, A.; Artamonov, A. Ionization in the Earth's Atmosphere Due to Isotropic Energetic Electron Precipitation: Ion Production and Primary Electron Spectra. *Remote Sens.* **2021**, *13*, 4161. https://doi.org/10.3390/rs13204161.
4. Mironova I, Karagodin-Doyennel A and Rozanov E. The Effect of Forbush Decreases on the Polar-Night HOx Concentration Affecting Stratospheric Ozone. *Front. Earth Sci*., **2021a**, 8:618583. doi: 10.3389/feart.2020.618583.
5. Karagodin, A.; Rozanov, E.; Mareev, E.; Mironova, I.; Volodin, E.; Golubenko, K. The representation of ionospheric potential in the global chemistry-climate model SOCOL. *Sci. Total. Environ.* **2019**, *697*, 134172.
6. Karagodin, A.; Rozanov, E.; Mironova, I. On the Possibility of Modeling the IMF B_y-Weather Coupling through GEC-Related Effects on Cloud Droplet Coalescence Rate. *Atmosphere* **2022**, *13*, 881. https://doi.org/10.3390/atmos13060881
7. Mironova, I., Sinnhuber, M., Bazilevskaya, G., Clilverd, M., Funke, B., Makhmutov, V., Rozanov, E., Santee, M. L., Sukhodolov, T., and Ulich, T.: Exceptional middle latitude electron precipitation detected by balloon observations: implications for atmospheric composition, Atmos. Chem. Phys., **2022**, 22, 6703–6716, https://doi.org/10.5194/acp-22-6703-2022.
8. Pikulina, P.; Mironova, I.; Rozanov, E.; Karagodin, A. September 2017 Solar Flares Effect on the Middle Atmosphere. *Remote Sens.* **2022**, *14*, 2560. https://doi.org/10.3390/rs14112560.
9. Grankin, D.; Mironova, I.; Bazilevskaya, G.; Rozanov, E.; Egorova, T. Atmospheric Response to EEP during Geomagnetic Disturbances. *Atmosphere* **2023**, *14*, 273. https://doi.org/10.3390/atmos14020273.
10. Makhmutov, V.S., Bazilevskaya, G.A., Mironova, I.A. *et al.* Atmospheric Effects during the Precipitation of Energetic Electrons. *Bull. Russ. Acad. Sci. Phys.*, **2021**, **85**, 1310–1313 https://doi.org/10.3103/S1062873821110228.

11. Gavrilov, N.M., Kshevetskii, S.P., and Koval, A.V.: Decay times of atmospheric acoustic–gravity waves after deactivation of wave forcing, *Atmos. Chem. Phys.,* **2022**, 22, 13713–13724, https://doi.org/10.5194/acp-22-13713-2022.
12. Koval A.V. Statistically significant estimates of influence of solar activity on planetary waves in the middle atmosphere of the Northern Hemisphere as derived from MUAM model data. *Solar-Terrestrial Physics.* **2019**. Vol. 5. I. 4. P. 53–59. DOI: 10.12737/stp-54201907.
13. Koval, A.V., Gavrilov, N.M., Didenko, K.A., Ermakova, T.S., Savenkova, E.N. Sensitivity of the 4–10-Day Planetary Wave Structures in the Middle Atmosphere to the Solar Activity Effects in the Thermosphere. *Atmosphere* **2022**, 13, 1325. DOI: 10.3390/atmos13081325.
14. Nerobelov, G.; Timofeyev, Y.; Virolainen, Y.; Polyakov, A.; Solomatnikova, A.; Poberovskii, A.; Kirner, O.; Al-Subari, O.; Smyshlyaev, S.; Rozanov, E. Measurements and Modelling of Total Ozone Columns near St. Petersburg, Russia. *Remote Sens.* **2022**, *14*, 3944. https://doi.org/10.3390/rs14163944.
15. Smyshlyaev, S.P.; Vargin, P.N.; Motsakov, M.A. Numerical Modeling of Ozone Loss in the Exceptional Arctic Stratosphere Winter–Spring of 2020. *Atmosphere* **2021**, *12*, 1470. https://doi.org/10.3390/atmos12111470.

Ozone

B.D. Belan
V.E. Zuev Institute of atmospheric Optics SB RAS
bbd@iao.ru

Keywords: atmospheric ozone, ozone layer, atmospheric composition, minor gases, air quality, ozone chemistry, atmospheric transport processes

1. Tropospheric ozone and its precursors

1.1. Observations

The Russian network for monitoring of the surface concentrations of ozone and its precursors has partially changed over the past four years as compared to the previous period [1].

According to the assignment of responsibilities between departments, the main information about the ozone content in the surface air layer should be provided by Rosgidromet (Russian Federal Service on Hydrometeorology and Monitoring of the Environment), which monitors the air composition in more than 240 Russian cities. However, annual Rosgidromet issues provide no ozone data [2, 3], although the Rosgidromet network has been modernized in recent years.

The two largest Russian cities, St. Petersburg and Moscow, have monitoring systems for ground-level ozone and other pollutants that are comparable to foreign analogs. The environmental monitoring network of the State Environmental Budgetary Institution (GPBU "Mosecomonitoring"), a specially authorized organization for state environmental monitoring, has been operating in Moscow since 2002 [4]. Regular measurements of the ground-level ozone concentration are carried out at 17 stations for automatic monitoring of atmospheric pollution (ASKZA) every hour around the clock. Values averaged for 20 minutes are recorded in the database. The measurements at the Mosecomonitoring network in Moscow are carried out with gas analyzers of three types operating on the basis of the ultraviolet photometry method: Casella Monitor ME 9810B, Environnement S.A. O3 42M, HORIBA Ltd APXA-370 APOA-370, and one OPSIS AB AR500 device based on the method of differential optical absorption spectroscopy (DOAS). These devices are included in the State Register of Measuring Instruments and verified by the State Metrological Service. Analytical materials on the state of the urban environment in Moscow are published in the annual report [5] and partly included in quarterly reviews [6–21].

In the rest territory of the Russian Federation, ozone observations are carried out on an initiative basis, mainly by scientific or university organiza-

tions. The established informal consortium of such stations began to publish reports on the ozone concentration in the troposphere over the territory of Russia [22–24].

According to the information published in the reports, the ozone measurements in the period under consideration were carried out at the Kislovodsk High-mountain Scientific Station (KVNS), in the Karadagsky State Nature Reserve, at a 300-meter tower in Obninsk (Taifun Scientific-Production Association), at 3 stations in St. Petersburg: ORTES-N located nearby the Alexander Nevsky Lavra, ORTES-P at Vasilyevsky Island, and ORTES-PR in the Leningrad region, at the Gromovo station of the Priozersky district, at the station for monitoring of ground-level ozone, its precursors, and basic meteorological parameters at the Peoples' Friendship University of Russia with participation of the A.M. Prokhorov Institute of General Physics RAS within the Third Traffic Ring at Ordzhonikidze Street, 3, at the Vyatskiye Polyany station located in the south of the Kirov region, at the TOR station and the Fonovaya Observatory in the Tomsk region, and in the suburbs of Ulan-Ude. Then, the additional stations were put in operation in Apatity (Murmansk region) and Boyarsky (Republic of Buryatia). In 2021, measurements were restored at the Slyudyanka station (Irkutsk Region) and in Tarusa (Kaluga Region), and the OPTEK station (Republic of Karelia) was opened. The stations are equipped with network instruments recommended by the Global Atmosphere Watch (GAW WMO). All instruments are regularly calibrated.

In addition to stationary measurements, expeditionary studies of ozone and components of the ozone cycle were carried out at the territory of Lake Baikal and the adjacent territory [25–29], as well as in the Arctic region.

The vertical distribution of gases in the troposphere was measured with the Tu-134 Optik flying laboratory. The current equipment of the Optik flying laboratory is described in [31]. During the entire period under consideration, monthly flights were performed over the southern regions of Western Siberia. A unique experiment to measure the gas composition of atmospheric air, including ozone, over all the seas of the Russian sector of the Arctic was carried out in September 2020. Another experiment was conducted in September 2022. It consisted in measuring the composition of air in the meridional direction. The route started near 56° N and ended over the waters of the Kara Sea, where the near-surface measurements were supported by the *Akademik Mstislav Keldysh* research vessel.

Measurements of the vertical distribution of ozone in the upper troposphere – lower stratosphere were carried out in Tomsk with a differential absorption lidar. The lidar operates at wavelengths of 299–341 nm and 308–353 nm and allows measurements of the vertical ozone distribution in the 5–45 km layer [32].

1.2. Distribution and variability

The data reported in reviews [22-24] indicate a significant variability in the ozone concentration in the surface air layer in different geographical regions of Russia. As an example, Figure 1 shows the annual average and maximum ozone concentrations in 2021.

It can be seen from Fig. 1a that the annual average values of the surface ozone concentration (SOC) differ by a factor of 2.5. The highest values are recorded at the high-mountain station in Kislovodsk, in the Crimea, and on the shore of Lake Baikal, while the smallest values are observed at the city station in Obninsk.

The maximum ozone concentrations (Fig. 1b) are observed in large cities, where there are additional emissions of ozone precursor gases. In this case, the order of the stations in the histogram changes.

It follows from Fig. 1 that there is no longitudinal or latitudinal dependence for the annual average SOC values. Possibly, here we see the effect of local sources of ozone precursors and anthropogenic factors. Another version is the long-term interannual variability of the ozone concentration, due to which the average annual concentration can vary up to 4 times [33]. To answer this question, a separate study is required.

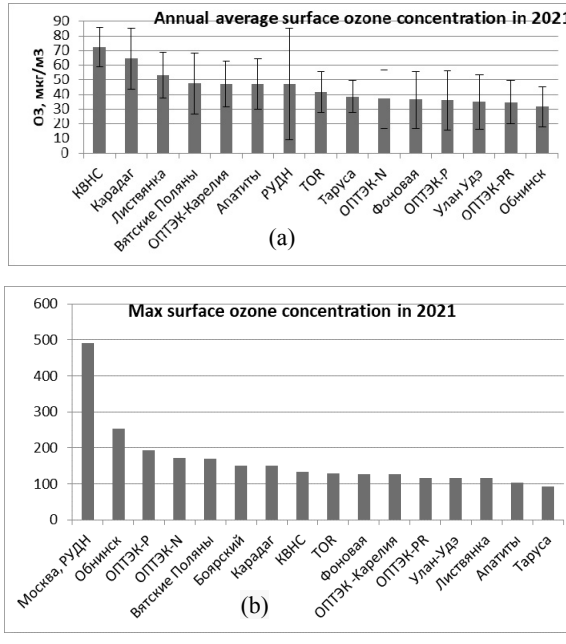

Fig. 1. Annual average (a) and maximum (b) surface ozone concentration in 2021 in Russia

Possible reasons for high annual average ozone concentrations at KVNS were examined in detail in [24] using the 7-day back trajectory analysis of incoming air masses as described in [23]. About 17 000 trajectories (less than in 2020 due to gaps in the 2021 measurements for technical reasons) have been simulated. In urban environments, ozone drops to very low levels are indicators of severe nitrogen oxide pollution. To the contrary, KVNS is located in a clean high-mountain area and above the atmospheric boundary layer. The abnormally low values of the ozone concentration at KVNS are associated more likely with the dry deposition onto the ground surface rather than with long-range transport. This process is most active in a stationary air mass, when the analyzed air contacts with the surface covered with vegetation for the longest time. As shown in [34], the pollutant transport from the lower levels from the city of Kislovodsk (altitude of 750–850 m above sea level) on days with conditions favorable for the development of mountain-valley circulation leads, to the contrary, to a slight increase in the daily ozone maximum. In addition, fog contributes to a decrease in the ozone concentration. In this connection, back trajectories for days characterized by high humidity (more than 80%) at the trajectory end point (KVNS) were excluded from the analysis. The results obtained indicate that extremely high anomalies of surface ozone at KVNS were associated with air transport from the south, while extremely low values were associated with air transport from the north-west.

Features of ozone generation in the Karadag region were analyzed in [35-38]. It was found that highest SOCs are observed in dry hot weather and have an advective nature. The trajectory analysis showed that air masses move over the Black Sea from Ukraine, Turkey, Romania, and Bulgaria in spring and over land mainly from Ukraine and southern Russian regions in summer. The ozone concentration is also significantly affected by breeze circulation and by nighttime slope winds.

Features of ozone dynamics in seven cities of the Baikal region (southeast of Siberia) were analyzed in [39]. It was found that significant differences in the spatial and temporal variability of the daily average ozone concentration depend on various anthropogenic loads. In large cities with heavy industry located in the valley of the Angara River, ozone concentrations were minimal and changed only slightly during the year: lower than 5 $\mu g/m^3$ in Angarsk and 20–30 $\mu g/m^3$ in Irkutsk. In towns of a less polluted area (the Selenga River valley), ozone concentrations were significantly higher and the annual ozone variability was typical for Eastern Siberia: maximum in spring (60-70 $\mu g/m^3$) and minimum in fall and winter (10 to 30 $\mu g/m^3$). The maximum ozone concentrations, up to 80–100 $\mu g/m^3$ in the period of the spring maximum, were observed in rural areas (Listvyanka station).

1.3. Role of atmospheric processes and phenomena in ozone variations

The correlation between the concentrations of CH_4, CO, CO_2, NO, NO_2, O_3, SO_2 and the aerosol particle number density for particles larger than 0.4 μm in diameter and the following weather parameters: air temperature, atmospheric pressure, wind direction and speed, total solar radiation and ultraviolet radiation in the range of 295–320 nm, relative humidity, and water vapor pressure was studied in [40]. This study used the data of air composition monitoring (for the period of 1993–2018) at the TOR station located in Tomsk Akademgorodok. From analysis of monthly average data, it was found that ozone has a significant positive or negative correlation with almost all analyzed weather parameters, except for only the wind direction. High negative correlations were observed between the carbon dioxide concentration and the solar and UV-B radiation, air temperature, and water vapor pressure. Nitrogen dioxide has not only a positive correlation with atmospheric pressure, but also two significant negative correlations with the air temperature and wind speed. Atmospheric aerosol, as well as minor gases, has a stable positive correlation with the air pressure and negative correlations with solar radiation, UV-B radiation, air temperature and water vapor pressure. No significant correlations between weather parameters and such minor gases as SO_2, CO, and NO have been revealed.

The effect of water aerosol on the ozone content in the atmospheric air was studied in [41]. In field experiments, a sharp decrease in the ozone content in the surface atmosphere was observed during a short-term heavy rain in a big city. The process of ozone destruction in the presence of water was also analyzed under laboratory conditions in the reaction chamber. It has been shown that the ozone destruction in air proceeds with a higher rate at high values of relative humidity, as well as in the presence of water aerosol. The ozone destruction rate depends on the size of aerosol particles: the smaller the particles, the higher the destruction rate. This may indicate a significant role of heterogeneous binding processes on the surface of aerosol particles.

In [42], no such stable correlation was found. The study showed that both an increase and a decrease in the surface ozone concentration can occur during precipitation, regardless of the precipitation type, intensity, and measurement area. The greatest changes are associated with frontal precipitation and reflect a stepwise change in concentrations at the alternation of air masses. In intramass precipitation, the sign of the change in the ozone content depends on the period of a day, when precipitation is observed. If precipitation is observed during the growth in the diurnal O_3 profile, then in the most cases this leads to an increase in the ozone content. If precipitation falls during a decrease in the diurnal O_3 variation, then a decrease in the ozone content is recorded.

The role of absolute humidity in the ozone formation was studied in [43]. The analysis revealed a neutral dependence at positive temperatures and unexpectedly strong alternating-sign variability at negative temperatures. Absolute humidity has a negative effect on the ozone formation in the surface air layer, causing a decrease in the ozone concentration at temperatures of 0–30°C. At the very low temperatures (below -30°C), the effect changes to a positive one, with a significant increase in the contribution of absolute humidity.

The role of solar radiation in photochemical generation of ground-level ozone was examined in [44]. According to the reported data, the photochemical generation begins in the morning when the radiation intensity reaches the level higher than 200 W/m^2 and continues until the same level in the evening. That is why the ozone maximum usually lags several hours behind the maximum in the daily solar radiation.

The contributions of CO and 15 volatile organic compounds (VOCs) to the formation of ozone in the surface air layer in summer seasons of 2011–2013 in Moscow were analyzed in [45, 46]. The highest O_3 concentration (up to 210 $\mu g/m^3$) was observed in daytime periods under anticyclonic meteorological conditions with weak mixing of the atmospheric boundary layer and high temperatures. To the contrary, the content of NO_x, CO and benzene decreased from 8 am to 17–18 pm Local Time. The high positive correlation of daytime O_3 with secondary VOCs confirmed the important role of photochemical O_3 production in Moscow. The main sources of anthropogenic VOCs in Moscow were local emissions from traffic. Nevertheless, only about 5% of observed isoprene was classified as anthropogenic, indicating a significant contribution from biogenic sources to the total levels ozone precursors. The contribution of various anthropogenic and biogenic VOCs to the measured ozone values was estimated. The ozone forming potential (OFP) of total VOCs averaged 31–67 $\mu g/m^3$ and exceeded 100 $\mu g/m^3$ in 10% of high ozone events, reaching 136 $\mu g/m^3$. Gases such as acetaldehyde, 1,3-butadiene and isoprene have the highest ozone forming potential in Moscow as compared to other measured VOCs.

The conditions for the formation of ozone near the 300-m tower in Zotino are considered in [47]. High levels of O_3 and NO_X are observed there in the air coming from the industrial regions of Western Siberia and the Ural Mountains, while the background air comes from remote regions of Northern Eurasia within 55°–70° N. Ozone in the continental air has a distinct maximum in April, as well as in mid-latitudes of the Northern Hemisphere. In spring and early summer, under hot weather conditions, regional anthropogenic and forest fire emissions are important sources of ozone in the continental boundary layer over southern and central Siberia. For the rest part of the year, central northern Eurasia is a hemispheric sink of tropospheric ozone.

Large-scale measurements of ozone and its cycle components are used in [48] to assess the impact of the two dominant sectors of anthropogenic emissions (traffic and power industry) and plant fires on ground-level concentrations of NO_x and O_3 over Siberia and the Russian Arctic. The results suggest that regional ozone is more sensitive to anthropogenic emissions, especially in the traffic sector. The contribution from fire emissions is observed in June and is largely limited to latitudes south of 60°N. The effect of fires on dry ozone deposition within the region under study is small compared to anthropogenic emissions and negligible north of 60°N. These results indicate that ground-level ozone in the studied region is controlled by the interplay between seasonality in atmospheric transport models, dry deposition on vegetation, and dominant emissions from traffic and power industry.

The long-term variability of the total content (TC) of carbon monoxide as one of the ozone precursors and meteorological parameters is studied in [49]. The characteristics of carbon monoxide accumulation in the atmospheric boundary layer on calm days in Moscow were obtained. A decrease in the average annual TC of CO in 2000–2018 in Moscow (–2.56 ± 0.52%/year) and at Zvenigorod Research Station (ZRS) (–1.15 ± 0.37%/year) was revealed. However, the rate of decrease at the both sites in different seasons and periods is different. After 2007–2008, the rate of decrease in CO TC reduced at the both sites. In the period 2008–2018, ZRS recorded an increase in CO TC in the summer and fall months at a rate of about 0.7%/year. An increase in the wind speed at a rate of 0.4–1.6%/year in the atmospheric boundary layer was observed in Moscow in different periods of 2000–2018. At the same time, no statistically significant changes were found in the Kaluga region. The occurrence of calm days in Moscow in 2006–2017 decreased (–7.06 ± 3.96%/year) with a decrease in the anthropogenic part of the CO content in the same period (–6.72 ± 3.48%/year). The results obtained indicate the influence of climatic (meteorological) factors on the air quality, including ozone, in Moscow.

The dry deposition of ozone in the Baikal region was studied in [50]. The ozone flows and dry deposition of ozone on the underlying surface were estimated from experimental data for various environments (grasslands, forests) based on the vortex covariance and gradient methods, including the aerodynamic gradient method, the modified Bowen method, and the modified gradient method. The average rate of dry ozone deposition was equal to 0.37 cm/s at night (00–03 Local Time) and 0.91 cm/s in daytime (12–18 Local Time). The ozone flow was 0.24 μg m^{-2} s^{-1} in nighttime and 0.72 μg m^{-2} s^{-1} in daytime. Quantitative estimates demonstrate the higher absorption capacity of forests compared to soil vegetation.

The weekly cycle and the weekend effect on the concentrations of O_3, NO, NO_2, CO, CH_4, SO_2, NMHC and PM10 were studied in Moscow

through field measurements from January 1, 2005 to December 31, 2014 at 49 stations of the Moscow Environmental Monitoring Network [51]. The diurnal cycle of O_3 is typical for big cities. On workdays, the ozone concentration is minimum in predawn at 7:30 LT and maximum at 15:00–16:00 LT. On weekend, there is no predawn minimum, since lower NO_x emissions from traffic reduce ozone depletion at this time. Daily fluctuations in CO, NOx, NMHC, and PM10 concentrations depend mainly on traffic emissions and the vertical stratification of the atmospheric boundary layer. A characteristic feature of Moscow is the coincidence of peak hours in time and the inversion of surface temperature in the cold season, which leads to the accumulation of pollutants in the surface layer of the atmosphere. Near-ground concentrations of pollutants (except for ozone and methane) have been found to decrease on weekends. Workday (Tuesday-Friday)-Sunday differences in the daily (08:00-22:00 LT) concentrations of NO, NO_2, CO, SO_2, NMHC, and PM10 relative to the workday concentrations averaged over all stations for 2005-2014 were 23.9±5.8, 16.7±2.8, 13.6±3.3, 7.6±6.5, 6.3±2.2 and 14.5±5.1%, respectively. The ozone concentration increased by 16.5±4.8% on Sunday. The weekend effect on all the pollutant concentrations was reduced within the green zone around Moscow. In different sectors of Moscow, the impact of pollutants (except for SO_2) on weekends was approximately the same. The vertical structure of the weekend effects of NO, NO_2, and CO was analyzed from the data obtained in measurements on a 500-m TV tower. The weekend effects decreased nonlinearly with altitude. Estimates obtained for the main criteria for the activity of photochemical processes that determine the formation of the weekly ozone cycle and the weekend effect of ozone (the NMHC/NO_x ratio, the fraction of radical losses due to the chemical action of NO_x, the O_x concentration) show that the chemical composition with a limited content of VOCs is typical for Moscow.

1.4. Anomalies and extreme events

Undoubtedly, the COVID-19 coronavirus pandemic was an extreme event in the period under study. Changes in the atmospheric composition in different periods of 2020 in Moscow associated with measures to prevent the coronavirus pandemic and the corresponding decrease in pollutant emissions were studied in [52]. Near-ground concentrations of nitrogen dioxide NO_2, carbon monoxide CO, ozone O_3, PM10 aerosol, and meteorological parameters in different periods of 2020 are compared with similar data for the previous five years. An analysis of ground-based measurements and high-resolution satellite data on the CO and NO_2 distributions indicates that the content of the main pollutants and its spatial distribution in the Moscow region were significantly affected by both the restrictive measures and abnormal weather conditions in 2020.

The results of monitoring of ground-level ozone in the atmosphere of Moscow in 2020 and 2021 under severe restrictions associated with the COVID-19 pandemic are reported in [53]. These two years distinguished significantly in weather conditions and the anthropogenic load on the environment. In 2020, a relatively low level of O_3 surface concentrations for a big city was observed in Moscow. The average annual value was 28 $\mu g/m^3$, and the year maximum was 185 $\mu g/m^3$. This is due to a combination of relatively cold summer weather with the low levels of pollutants in the air. In the summer of 2021, intense heat waves were observed under conditions of a blocking anticyclone, and daytime temperatures rose up to 35°C. Combined with higher air pollution, this resulted in unusually high O_3 concentrations. The annual average ozone concentration was 48 $\mu g/m_3$, and the maximum value was 482 $\mu g/m_3$.

Abnormally low ozone concentrations in the surface atmosphere of central Russia were recorded in the spring of 2020 [54]. An increase in the ozone content, which is typical for spring due to a seasonal increase in temperature and irradiation, was replaced with a monotonic decrease. The monthly averaged maximum daily values of the observed concentrations in April 2020 were three times lower than those recorded at the same period in 2019. Both a decrease in the regional background ozone concentrations in the surface atmosphere and a decrease in the intensity of photochemical ozone formation were observed. The authors believe that the most probable reason for the observed phenomenon is the decrease in atmospheric emissions of combustion products in China, Europe, and Russia associated with the COVID-19 pandemic.

1.5. Simulation of surface ozone formation and transformation processes

The sensitivity of the O_3 field to the total emissions of ozone precursors was calculated in [55–57] with the GEOS-Chem global transport-chemical model using the databases on anthropogenic (EDGAR) and biogenic (MEGAN, GFED) emissions for 2007–2012 with application of the reduction approach. Detailed quantitative estimates of the influence of individual factors that determine seasonal variations in the surface ozone content in Central Siberia have been obtained. The anthropogenic and biogenic signals in measured O_3 concentrations were estimated quantitatively with the GEOSChem global chemical transport model taking into account all the main ozone sources and sinks. The influence of climatically significant regional sources of emissions of nitrogen oxides ($NOx \equiv NO+NO_2$), CO, and biogenic volatile organic compounds (VOCs) on the photochemical generation of ground-level ozone (O_3) in European and Siberian regions has been studied. It was found that the value of photochemical ozone production in the summer months cor-

relates well with the air mass age determined from the relation to the total reactive nitrogen, with an average contribution of regional sources of ~10–15 ppb. The obtained quantitative estimates of the production efficiency are in good agreement with the conclusions of the photochemical theory of tropospheric ozone for conditions of slightly polluted air.

The relative importance of isoprene and monoterpenes in formation of ground-level ozone in Russian cities along the Trans-Siberian Railway was evaluated in [58, 59]. Toward this end, the ozone forming potential (OFP) in daytime was calculated. The calculated OFPs for isoprene and monoterpenes along the Trans-Siberian Railway average 15±13 and 18±25 ppb ozone, respectively. In most cities along the Trans-Siberian Railway, where high concentrations of NO_x (10–20 ppm) were observed along with high daytime temperatures (>25°C), monoterpenes were the major contributors to the formation of tropospheric ozone. Only in the Far Eastern cities, where the largest deciduous vegetation of the Trans-Siberian Railway is located, isoprene played a major role in the formation of tropospheric ozone.

The measurements of ozone and nitrogen oxide concentrations at the Zotino Tall Tower Observatory (ZOTTO) in Central Siberia were used to estimate the rates of ozone generation (P) and destruction (L), as well as the content of peroxide radicals (OX) with the photostationary approximation [60, 61]. The diurnal profiles of these parameters peaked at ~ 6 ppb/h (P), 1.4 ppb/h (L), and 115 ppt ([OX]) in the period from 11:00 to 15:00 LT. In the range of measured NO_x concentrations from 0.2 to 0.8 ppm, there is a linear dependence of P on [NOx], corresponding to NO_x-limiting ozone production, with a proportionality coefficient $P(O_3)/[NO_x]$ ~ 13 (ppb /h)/ppb. The high content of peroxide radicals along with the condition P >> L indicates the processes of intense oxidation of biogenic VOCs and photochemical generation of ozone. The estimates obtained reveal the significant role of regional NO_x emissions in the balance of ground-level ozone and the need to take this factor into account when predicting environmental risks in Siberian regions that are traditionally classified as environmentally friendly.

The agreement between the results of chemical transport simulation of NO_2 with the SILAM and COSMO-ART models in the Moscow region and measurements by the DOAS method is being investigated in a series of publications [62–65]. The simulated ground-level concentrations were compared with the observed ones and the DOAS results in [64], and corrections to the spatial distribution and power of sources in Moscow were proposed to improve model estimates of air quality in Moscow.

The sources of emission of ozone precursors were refined in [66–71]. To optimize the spatial distribution of sources and the values of emissions in Moscow, the fields of ozone and other pollutants for the summer and winter months were calculated with the SILAM and COSMO-ART chemical

transport models using both calculated emissions and those borrowed from the TNO inventory database. Comparison of the observations obtained in the Moscow Environmental Monitoring Network (MEMN) with the results of numerical simulation based on the SILAM chemical transport model showed that errors in determining the concentrations of ozone and other substances in the urban atmosphere have a more complex structure than those assumed in ordinary data assimilation algorithms.

The Russian Hydrometeorological Center is working on creation and improvement of pollutant (including ozone) concentration forecasting technology based on chemical transport models (CTMs) [72, 73]. At the initial stage, the calculation technology using the open access CHIMERE chemical model with assimilation of data of the WRF-ARW model was implemented. At the next stage, the CHIMERE CTM calculations with data of the COSMO-Ru07 numerical model of the atmosphere were provided to ensure the stability and efficiency of the calculation. Owing to computational modernization and development of the numerical model of the atmosphere, pollutant concentration fields are calculated now in the experimental mode using the CHIMERE-COSMO-Ru2,2 CTM for a part of the Central European region of Russia (36.6–44.2°E and 55.1–56.5°N). In addition, COSMO-Ru2.2-ART (COnsortium for Small-scale MOdelling) CTM calculations are performed for the Moscow region on a grid with a horizontal step of 2 km. A specific feature of COSMO-Ru2.2-ART (unlike CHIMERE CTM) is the joint calculation of meteorological parameters and chemical transformations at every time step, which makes it possible to take into account the feedback effect of aerosols and gases on radiation processes and the meteorological conditions of the atmosphere. The very important point in the functioning of the automated air quality forecasting technology based on the CHIMERE-COSMO-Ru2.2 and COSMO-Ru2.2-ART CTMs is the verification of models against pollution observation data. The verification showed overestimation of concentrations in CHIMERE CTM and their underestimation in COSMO-ART. The both CTMs mostly underestimate pollution in transport-type areas. The correlation coefficient (R) between the model and measured average concentrations of NO_2 and CO was 0.6–0.7. For the calculations of the O_3 concentration, CHIMERE provides R=0.7–0.8 and COSMO-Ru2ART gives R=0.4–0.5. Seasonal variability of model deviations with sign alternation for each model and each pollutant was revealed. The largest model deviations were observed under abnormal weather conditions: during heat waves in summer and during advection of dusty air in spring. With allowance for the model errors of each CTM, recommendations for compiling an operational consolidated forecast with the integration of the calculations provided by the two CTMs are formulated.

1.6 Ozone and health

An increase in the ozone content in the surface air due to changing global climate and increasing atmospheric pollution can lead to an increase in morbidity and mortality in the population. The correlation between abnormally high SOC in Moscow and morbidity and mortality in different age groups of the population in summer of 2010 and the frequency of cardiovascular diseases and mortality in a low-urbanized area in the south of Kirov region was investigated in [74]. It was shown that a statistically significant correlation is observed in the groups of men and women aged 31–60 years and older and is lacking in the corresponding age groups of 15–30 years. In the south of the Kirov region, when the average daily maximum allowable ozone concentration (MAC) was exceeded for several days, the frequency of calls associated with cardiovascular diseases to first aid teams significantly increased. This confirms the validity of the Russian domestic MAC for ozone equal to 30 $\mu g/m^3$.

It was assumed [75] that in the COVID-19 period, when ozone enters a body with inhaled air, it can adversely affect the main body systems: cardiovascular, nervous, respiratory, and immune ones. In particular, ozone, as a strong oxidizing agent, can cause the formation of free radicals in the respiratory tract, provoking lipid peroxidation and suppressing immunity.

The further studies showed [76] that in summer of 2021, a rare combination of the new wave of SARS-CoV-2 (delta strain) infection and meteorological conditions conducive to the formation of abnormally high ground-level ozone concentrations was observed in Moscow. In addition to the high frequency of infections, the highest death rate due to this virus during the pandemic was recorded in Moscow in that period. The correlation coefficients between infection and mortality rates with ground-level ozone concentration were ~0.59 ($p < 0.01$) and ~0.60 ($p < 0.01$), respectively. The observed correlation may be due to the combined pathological effects of high concentrations of ozone and the SARS-CoV-2 virus on the respiratory and circulatory organs. This effect can lead to both easier transmission of infection and more severe disease and increased mortality.

In [77], the same scientific team draws attention to the fact that the surface concentrations of ozone observed in Russia significantly exceed the thresholds for a negative impact on vegetation.

2. Stratospheric ozone

2.1. Observations

To monitor the total ozone content (TOC) in Russia, the State monitoring system has been created and is functioning. The State monitoring system continues to ensure the operation of the ground-based Rosgidromet ozonometric

network. Observations at 28 stations have been conducted since 1973. Long-term data series allow analyzing the spatial and temporal variability and revealing the correlations between anomalies in the TOC field and the general circulation of the lower stratosphere and upper troposphere. The results of assessing long-term changes in the thickness of the protective ozone layer, the main trends and tendencies, as well as the current state of the ozone layer are reported in annual "Reviews of the state and pollution of the environment in the Russian Federation" [78–81]. A separate analysis is carried out for stations in the Arctic region. Measurements of erythemal UV radiation continue at 12 stations. Calibration of the measuring equipment plays a significant role in providing ground-based measurements. The instruments are referred to the world scale via regular calibrations according to the standard of the Rosgidromet ozonometric network (Dobson spectrophotometer No. 108).

Works to re-equip the Rosgidromet ozonometric network continue. In the trial operation of UV ozone spectrometers (UVOSs) designed for complex measurements of the spectral composition of the total UV radiation and total ozone content, the software and methods for calibration and calculation of TOC were improved. For several instruments, series of parallel observations with M-124 ozonometers have been accumulated with satisfactory consistency and homogeneity. Zenith spectrometers for TOC measurements in regions with severe climatic conditions were made in 2022, and their tests begin in 2023.

In 2022, The State monitoring system and the Arctic and Antarctic Research Institute (AARI) started joint work to organize a network of regular automatic observations of UV radiation with high temporal resolution at polar (Arctic and Antarctic) stations and AARI research ships. The TOC dataset is updated annually with data from the Mirny, Novolazarevskaya, and Vostok Russian Antarctic stations and AARI research vessels. Until the early 2000s, a steady trend of a decrease in the total ozone content in the Antarctic spring was observed at the Antarctic stations. Now, the ozone content demonstrates a tendency of return to values characteristic of the period preceding the ozone hole effect [82].

Observations of the integral optical density of the atmosphere, which started in the 1970s, continue. The results of data analysis are reported in the annual issues of "Reviews of the state and pollution of the environment in the Russian Federation" [83–86]. The character of the interannual variability of the integral optical density of the atmosphere allows one to see consequences of powerful volcanic eruptions, periods of self-purification of the atmosphere due to reduction in industrial activity in the post-perestroika years, and a decrease in optical turbidity of the atmosphere. Since the early 2000s, a relatively calm state of the atmosphere is observed, no statistically significant trends in the optical density of the atmosphere were revealed.

Observations of the aerosol optical depth of the atmosphere in Antarctica continue as well. The values obtained from the results of direct spectral solar photometric measurements and the integrated optical thickness determined from the data of standard actinometric observations of the direct solar radiation are indicators of the optical state of the atmosphere. Comparison of the data obtained with estimates for other natural regions and conditions indicates that in the periods without the influence of volcanic eruptions, the levels of aerosol turbidity in the atmosphere in Antarctica over the past decades are minimal on the planet and can be considered as global background characteristics [87].

Keeping in mind the tangible climate changes on the planet as a whole, databases and archives of data on the main climate-forming characteristics of the atmosphere collected over long periods of time in different regions of the globe and, in particular, in the polar regions acquire a particular importance. The total solar radiation is one of the most important parameters affecting the energy balance of the Earth-atmosphere system. A database of hourly and daily sums of total radiation at Russian stations in Antarctica is described in [88]. This database is designed to study the radiation conditions in the Antarctic from the beginning of actinometric observations to the present. It has passed the state registration procedure and is registered with No. 2020621401. The information contained in this database was used to estimate the variability characteristics of daily, monthly and annual total radiation at Bellingshausen, Vostok, Mirny, Novolazarevskaya, and Progress stations for the entire observation period through 2019. The results of analysis of these data are indicative of the absence of significant changes in the total solar radiation influx to the Antarctic surface over more than a sixty-year period of actinometric observations.

In previous years, at the initiative of the WMO Ozone Commission, observations of the total ozone content were carried out at the KVNS, Obninsk, and Tomsk stations equipped with Brewer spectrophotometers. The data from these stations were regularly transmitted to the World Ozone and Ultraviolet Radiation Data Centre (WOUDC). The spectrophotometers were regularly calibrated using a Brewer No. 17 mobile spectrophotometer standard [89]. By political reasons, the next calibration did not take place. Therefore, the reliability of the data obtained is questionable now.

In addition to the State and international networks, the TOC and components of the ozone cycles were studied at the territory of Russia in university and research centers, such as St. Petersburg State University, Institute of Atmospheric Physics (IAP) RAS, Institute of Atmospheric Optics (IAO) SB RAS, etc.

Thus, the Department of Atmospheric Physics and the Laboratory for the Study of the Ozone Layer and Upper Atmosphere of the St. Petersburg State

University employ satellite and ground-based equipment to study spatiotemporal variability of ozone. Information processing methods are being improved. An original algorithm for solving the inverse problem is proposed to obtain the total ozone content from the spectra measured by the IKFS-2 Fourier spectrometer at the Russian Meteor-M N2 satellite [90-92]. The algorithm is based on the method of artificial neural networks, the method of principal components, and TOC measurements by the OMI instrument at the Aura satellite. The error of TOC determination is about 3%. The method allows analyzing the global TOC distribution, in particular, in the absence of solar radiation, for example, during polar nights. To determine TOC, the authors apply the DOAS differential spectroscopy technique to interpret the data measured by the ground-based ultraviolet ozone spectrometer (UVOS) [93]. Comparison of the calculated TOC values with the data of independent measurements revealed their systematic discrepancy, which can be eliminated with a more accurate adaptation of the DOAS algorithm to the conditions of the problem and the UVOS characteristics. An improved technique for processing ground-based spectral measurements of the Bruker 125HR Fourier spectrometer to obtain information on TOC and other stratospheric gases is presented in [94]. In addition, it is demonstrated how ground-based measurements can be used to interpret processes occurring in the ozonosphere [94].

The contents of NO_2 and other components of the ozone cycles in the vertical atmospheric column are closely related to TOC and necessary to study changes in the state of the ozone layer. These characteristics were measured every day at KVNS, ZRS and in Tomsk. The Institute of Atmospheric Physics (IAP) RAS continued to develop and improve the ground-based method of multi-angle differential spectroscopy (DOAS) for determining the content of NO_2, H_2CO and other reactive gases in the atmospheric boundary layer (ABL). In 2016, the IAP RAS team took part in international intercomparison of the instruments and methods for measuring NO_2 and other gases by the DOAS – CINDI-2 method. The CINDI-2 comparison involved 36 spectral instruments from 26 different scientific teams. The results of comparison of the methods for retrieval of such chemically active substances affecting ozone chemistry as NO_2, O_4, O_3, H_2CO, HNO_2 are reported in [95, 96]. The results were used to draw recommendations on measurement modes and parameters for processing of data obtained by the DOAS method.

The Siberian lidar station of the V.E. Zuev Institute of Atmospheric Optics (IAO) SB RAS in Tomsk (56.5 N, 85.0 E) continued vertical sensing to study the ozone dynamics in the tropopause and to track global changes in the ozonosphere [97]. The sensing is based on the differential absorption at 299/341 and 308/353 nm wavelength pairs with allowance for the temperature and aerosol corrections. The lidar system covers the height range ~ 5–45 km. Testing and selection of optimal sets of absorption cross sections

for retrieving the vertical ozone distribution in the upper layers of the troposphere-stratosphere were carried out [98]. A temperature correction technique that improves the accuracy of data acquisition has been developed [99].

Measurements of the vertical ozone distribution by a microwave spectroradiometer over Nizhny Novgorod continued [100]. These measurements covered the height range of 25–60 km.

The results of ground-based TOC measurements with different equipment are regularly intercompared. This allows evaluating the homogeneity of data series and the reliability of the obtained information. The results of ground-based TOC measurements with a Dobson spectrophotometer, an M-124 filter ozonometer, and a Bruker 125HR Fourier spectrometer located near St. Petersburg at a distance of about 50 km from each other are compared in [101]. Comparison of daily average values showed that the spread in data between different sets of TOC measurements does not exceed the measurement errors of the used methods. Time series of monthly average TOC obtained from three sets of ground-based measurements in the St. Petersburg area revealed no clear year-to-year increase or decrease in the gas content over the period 2009–2020.

Information about the spatiotemporal changes in TOC obtained with different methods and observation models can differ significantly due to measurement and modeling errors, differences in ozone search algorithms, etc. That is why data obtained by various methods should be checked regularly. Comparison of TOC data series obtained by ground-based instruments (Bruker IFS 125 HR, Dobson and M-124), satellite (OMI, TROPOMI and IKFS-2) instruments and models (ERA5 and EAC4 reanalysis, EMAC and INM RAS – RSHU models) near St. Petersburg (Russia) from 2009 to 2020 show good consistency (correlation coefficients of 0.95–0.99). All datasets demonstrate a pronounced seasonal TOC profile with a maximum in spring and a minimum in fall. The period of 2004–2021 is characterized by a significant positive TOC trend near St. Petersburg (~ 0.4 ± 0.1 units per year) for all the datasets [102].

TOC data are periodically compared at the IAO SB RAS and IMCES SB RAS with other instruments. TOC measurements by the M-124 instruments and the Aura OMI satellite sensor were compared in [103, 104]. The comparison showed that they correlate well in terms of pronounced variations that occur in time profiles, but the amplitudes of these variations differ. In general, it can be noted that the IAO SB RAS instrument exceeds the data of the other two instruments, while the Aura OMI TOC values are the smallest.

MLS/Aura and IASI/MetOp satellite and LiDAR data on ozone in the stratosphere are compared in [105,106]. It is shown that the average relative difference between the LiDAR and MLS/Aura measurements is negative in the height range of 16–38 km and reaches measurements is positive in the

height range of 6–18 km, where it reaches 43.68% at 16.80 km, and negative above this range, where it reaches –43.86% at 20 km.

Measurements of TOC profiles in the atmosphere of St. Petersburg with a ground-based Bruker 125HR Fourier spectrometer and a satellite microwave limb sounder (MLS) for 2018–2020 were compared in [107]. The vertical profile of the discrepancy between the two types of ozone profile measurers was analyzed. The comparison showed satisfactory results.

One of the main tasks of ground-based measurements is to ensure the validation of satellite equipment. Satellite methods of remote contribute significantly to analysis of the spatial distribution and evolution of the ozone content and its anomalies. The technique developed at St. Petersburg State University makes it possible to determine TOC from measurements by IKFS-2 (infrared Fourier spectrometer) installed onboard the Meteor-M N_2 satellite [108]. Comparison of the results of satellite measurements with ground-based observations in 2019–2020 demonstrated the consistency of the IKFS-2 global TOC fields with OMI measurements, ECMWF ERA5 reanalysis data, and ground-based measurements.

Regular satellite measurements of nitrogen dioxide content are conducted now with the TROPOMI, OMI, and GOME-2 instruments. The horizontal spatial resolution achieved by them with global coverage is tens of kilometers, which is sufficient for studying stratospheric NO_2. In 2016–2017, the IAP RAS team conducted the first experiments on highly detailed sensing of tropospheric NO_2. The measurements with the hyperspectral GSA spectrometer installed on Resurs-P spacecraft were involved. The results obtained were used to develop the first world-class algorithm for determining the integral content of NO_2 in the troposphere with a spatial resolution of about 2.4 km at a 120-m grid with a measurement error of 10^{15} mol/cm^2 typical of satellite methods. To validate the large-scale structures revealed in the reconstructed NO_2 distribution fields, the data were compared with TROPOMI and OMI findings [109–111]. The comparison confirmed the reliability of the results obtained.

The potential of GOME-2 products is assessed in [112, 113]. It is found that the averaged values of ground-based measurements and satellite estimates are in good agreement for an averaging period from thirty days. It is also shown that satellite estimates suit for describing regional pollution and plausibly represent both the annual and the spatial variation of the concentration. However, there are some limitations on the use of these estimates to describe instantaneous concentration, as well as direct urban pollution.

2.2. Study of stratospheric ozone dynamics

The results of long-term measurements of the temporal variability of the total content of O_3 and NO_2 at the Kislovodsk high-mountain (KVNS) and Zvenigorod (ZRS) research stations of IAP RAS are reported in a large series

of papers [114–123]. The long-term variability of data was analyzed using the method of multiple linear regression. Annual and seasonally dependent estimates of linear trends in O_3 and NO_2 are obtained. A common feature of long-term observations of TOC at KVNS and NO_2 content at ZRS and KVNS is pronounced trends in the winter-spring period. They are negative at the both stations and more intense at KVNS than at ZRS. The TOC tendency was positive in 1989–2002 (1.6% per decade) and negative in 2003–2020 (–1.2% per decade). The obtained characteristics of ozone variability testify to the particular character of the interannual and long-term evolution of TOC over the North Caucasus. In particular, the TOC trends in the North Caucasus region are opposite to those of the zonal average TOC values. Dependent estimates of linear trends and interannual variations in total ozone associated with the effects of the 11-year solar cycle, the Quasi-Biennial Oscillation (QBO) in the equatorial stratosphere, North Atlantic Oscillation (NAO), and El Nino-Southern Oscillation (ENSO) were obtained. Changes in total ozone during the 11-year solar cycle in the Caucasus are especially significant in summer and amount to about 4%. QBO-related interannual fluctuations in total ozone with amplitude of about 6% manifest themselves in the cold season. General ozone fluctuations due to NAO are pronounced in the winter-spring period. The ENSO effect on total ozone is marked in summer and lags the regional sea surface temperature variation by about a year, so that total ozone decreases after El Nino events and increases after La Nino events. The obtained characteristics of the total ozone variability are indicative of a particular character of long-term total ozone variations in the North Caucasus.

The observations at ZRS of IAP RAS and at IAO SB RAS (Tomsk) were used to estimate the temporal variability of the integral content of formaldehyde H_2CO [124]. It is shown that the integral formaldehyde content is characterized by a statistically significant positive trend depending on the temperature at $T > 5$°C at the both sites. The observed positive trend is likely associated with an increase in biogenic emissions of isoprene and other non-methane VOCs with increasing temperature, as well as in areas of forest and peat fires. Air masses arriving at ZRS from Moscow have a stable excess of integral formaldehyde content on average by $0.4\pm0.1\times10^{16}$ mol/cm^2 at positive temperatures and by $0.8\pm0.2\times10^{16}$ mol/cm^2 at negative temperatures. Despite the significant distance from Moscow, the integral formaldehyde content values observed at ZRS are generally 10% higher than those observed in Tomsk.

The aerosol and ozone distributions were studied by the lidar method with satellite information invoked for interpretation of the results in a cycle of IAO SB RAS publications [125–133]. Lidar measurements at the Siberian Lidar Station showed the presence of stratospheric aerosol layers and a TOC deficit over the city in the winter of 2017–2018. Aura OMI/MLS data indi-

cated that in December 2017 – January 2018, the total ozone and NO_2 content in the stratosphere over northern Eurasia, as well as the temperature in the stratosphere, were significantly below normal. An analysis of back trajectories and the profile-integral TOC revealed that the dynamic disturbance of the Arctic stratosphere in December 2017 led to the displacement of cold air masses with an excess content of aggressive chlorine (due to NO_2 deficiency) beyond the Arctic Circle and their invasion into the Tomsk stratosphere.

The effect of high humidity in the Arctic stratosphere on the level of ozone depletion was studied in [134]. An analysis of the Aura MLS data showed that the temperature in the Arctic stratosphere was much lower than normal in the entire period of January–March 2011 in the height range of 20–35 km. This resulted in a significant spread of polar stratospheric clouds (PSCs), which formed most intensively at heights and in periods of minimum temperatures (maximum temperature drop below the PSC formation threshold). The main ozone losses were observed in March. This was facilitated by the photochemical release of chlorine, which avoided deactivation due to nitrogen deficiency caused by denitrification during frequent dehydration events, as evidenced by fluctuations in the height of the maximum humidity deviation from the long-term norm. The high humidity in the stratosphere increased the PSC formation threshold temperature for PSCs that were observed until the end of March. As a result, the activation threshold for chlorine was increased and thus chlorine deactivation was delayed. This further increased the level of total ozone losses in March 2011.

The results of ground-based microwave measurements of the evolution of the vertical ozone content in the middle atmosphere over Nizhny Novgorod (56°20′ N, 44° E) in the winter of 2017–2018 are reported in [135]. These data are compared with Aura MLS satellite data and with ERA5 reanalysis data. In particular, the degree of dependence of the ozone content in the stratosphere on the position of the polar vortex boundary at different heights relative to the observation site was determined. It was observed that in January 2018 the polar vortex approached Nizhny Novgorod. Further, until the vortex destruction on February 12, its boundary oscillated over the city, so that different altitude ranges alternately appeared inside or outside the vortex. This vortex dynamics affected most noticeably the evolution of the stratospheric ozone maximum, whose position followed the vortex boundary and changed quasi-periodically in the altitude range of 30–35 km. The results of ground-based microwave sensing give, on average, the lower relative ozone content than the MLS data with a maximum systematic discrepancy of ~0.8 ppm at a height of 38-39 km. Nevertheless, the analysis of ground-based measurements allowed observing the clearer ozone response to changes in the structure of the polar vortex over Nizhny Novgorod than the analysis of satellite data and reanalysis data did.

A nonlinear photochemical response to diurnal variations in solar illumination at the second subharmonic of this effect was recorded experimentally for the first time in the Earth's atmosphere by the research team of the Institute of Applied Physics RAS [136]. As a result of a theoretical study of two-day photochemical oscillations of the components of the odd oxygen O_x (O, $O(^1D)$, O_3) and hydrogen HO_x (H, OH, HO_2) families at mesopause heights (80–90 km) with models of different complexity, indicators of the presence of this phenomenon in the spacecraft sensing data were determined. The most pronounced feature of these oscillations is a significant (by several orders of magnitude) difference between two successive values of the H concentration at the end of the night. In addition, it was found that the necessary conditions for the manifestation of these oscillations in the H profile before sunrise are certain restrictions on the lifetimes of the HO_x and O families at the corresponding instants of local time. Processing of the data of the SABER/TIMED satellite campaign allowed obtaining the first experimental evidence for the existence of two-day photochemical oscillations at mesopause heights.

The atmosphere continues to be deficient in ozone over the polar regions [137]. This makes the study of ozone holes urgent, and this issue is touched numerous publications.

The studies [138, 139] for the Antarctic showed that the hypothesis of a possible relation between the quasi-biennial oscillation and the state of the Antarctic ozone hole is most likely unfounded. The variability of parameters of the Antarctic ozone anomaly was studied based on the data of TOMS/OMI satellite monitoring of the ozone layer, MERRA-2 reanalysis, and balloon sounding of the vertical distribution of ozone and temperature at the South Pole. Despite the reduction in the concentrations of ozone-depleting substances, the intense depletion of the ozone layer was observed in the Antarctic in 2011 and 2015. The dynamic processes in the Antarctic stratosphere, which determine the conditions for this depletion over the past 8 years, are analyzed.

The ozone anomaly in the Arctic was analyzed in [140] and its characteristic features were determined.

Ozone in the Arctic region was studied by Russian investigators in cooperation with colleagues from the European institutes. An analysis of ground-based observations at 38 European stations allowed assessing the response of the ozone layer over Europe to extreme ozone depletion in the Arctic in 2020 [141]. The effect spread to the middle latitudes of Europe, but with a decrease in amplitude and a time delay of up to 20 days. The development of the situation was similar to that observed after the significant depletion of the ozone layer in the Arctic in 2011.

The largest ever observed Arctic ozone anomaly took place in winter-spring 2019–2020 [142, 143]. It was driven by an unusually strong and pro-

longed polar vortex that caused unprecedented chemical destruction of ozone. The analysis of the Aura OMI/MLS data showed that the total ozone content steadily decreased and amounted to 230 DU on March 18 at Alert, 222 DU on March 18 in Eureka, 229 DU on March 20 in Tula, and 226 DU on March 18 at Resolute. The minimum temperature was 9–10% below normal from December to April in the stratosphere over Tomsk and the Arctic. The ozone concentration decreased to 4 and 6% of the long-term average at an altitude of 20 km on March 27 at the Eureka site and at an altitude of 19 km on April 16 at the Ny-Ålesund site, respectively. This phenomenon fits into the context of climate changes leading to the cooling of the stratosphere.

In [144], the appearance of the ozone hole is associated with the blocking process. The TOC anomaly was mainly due to a decrease in the ozone content in the lower stratosphere, reaching 50% near the 70 hPa level. With the key contribution of atmospheric dynamic processes to the formation of an ozone mini-hole, the possibility of a contribution from ozone destruction in heterogeneous reactions on the surface of polar stratospheric clouds due to a strong reduction in temperature in the stratosphere above the blocking region was noted.

Stratospheric warmings are among the interesting phenomena observed in the middle atmosphere. One of them is described in [145]. It was observed over Canada in late December 2017 – early January 2018. The main sudden stratospheric warming in February 2018 was accompanied by a change in the direction of the zonal wind, separation of the stratospheric polar vortex, spread of stratosphere circulation anomalies to the lower troposphere, cooling in the mesosphere, change in the stratopause height, and a decrease in the temperature of the lower stratosphere in the tropics.

2.3. Simulation of processes in the ozonosphere

Works on development and use of global numerical models of the atmosphere in the Laboratory of Chemistry and Atmospheric Dynamics of the Central Aerological Observatory (CAO) are reviewed [146]. Some of them are relevant to the topic of this paper.

To study the variability and correlations of polar ozone content from the data on polar temperature at levels of 30, 70, 100 hPa and on the mean zonal wind at latitudes of 45–75° and at levels of 10, 70 hPa, a model of polar ozone in the Arctic and Antarctic for winter -spring period was constructed in [147]. The model was tested against measurements 1979–2020, and the errors in calculation of polar ozone were estimated.

Dynamic processes and changes in the ozone layer in the Arctic stratosphere in winter of 2019–2020 are analyzed in [148,149] using numerical experiments with a chemical transport model (CTM) and reanalysis data. The dynamic conditions of winter-spring 2019–2020 described an ozone decrease

down to 100 DU in the Eastern Hemisphere and over 150 DU in the Western Hemisphere. The photochemical destruction of ozone both in the Western and Eastern hemispheres was about 50 DU at a maximum with peaks in April in the Eastern Hemisphere and in March-April in the Western Hemisphere. On the one hand, heterogeneous activation of halogen gases on the surface of polar stratospheric clouds resulted in a sharp increase in ozone destruction in the catalytic cycles of chlorine and bromine. On the other hand, it reduced its destruction in nitrogen catalytic cycles. Analysis of wave activity with 3D Plumb fluxes showed that an increase in the spread of upwelling wave activity in mid-March over the Gulf of Alaska was observed at the stage of development of a minor sudden stratospheric warming event. This warming led to a shift of the stratospheric polar vortex to the north of Canada and a decrease in the volume of polar stratospheric clouds. Due to the low activity of planetary waves, the polar vortex in 2019–2020 remained stable until the end of April. This formed the conditions favorable for record ozone depletion in the Arctic.

The issues of model testing and improvement are considered in [150–152]. Using the data of five 50-year calculations by the INM RAS Version 5 climate model for modern conditions, the interannual variability of the characteristics of the stratospheric polar vortex in the Arctic and the dates of the spring restructuring of the stratospheric circulation are analyzed in comparison with the reanalysis data. Early restructuring of the stratospheric circulation is accompanied by stronger wave activity than the late one. Winter seasons with the maximum air volume in the polar stratosphere and conditions sufficient for the formation of polar stratospheric clouds are, on average, characterized by early spring restructuring. Numerical seasonal temperature forecasts were obtained using two interactively operating numerical global models: the CAO CHARM photochemical model (0–90 km) and the GMC/INM RAS PLAV seasonal forecast model (0–30 km). The forecast results are compared with the reanalysis data. It was found that the new combined FOROZ (Forecast with Ozone) model showed stability in realization of numerical scenarios. The seasonal predictive temperature fields of the PLAV model and the combined FOROZ model are similar with reanalysis data in the lower troposphere and differ in the stratosphere. The combined FOROZ model provides better temperature prediction in the upper troposphere and stratosphere.

To study the changes in the Arctic polar stratospheric vortex in the near future, the simulation by INM RAS Version 5 climate model was carried out for the period of 2015–2100 with two SSP2-4.5 and SSP5-8.5 scenarios of an increase in the concentration of greenhouse gases [153]. The simulation revealed an increase in the spread of wave activity and stationary planetary wave number 1 in the middle and upper stratosphere, an acceleration of me-

ridional circulation, an increase in the winter average polar stratospheric volume (Vpsc) and an increase in the interannual variability of the Arctic stratosphere after the middle of the 21st century, especially according to the SSP5-8.5 scenario. March monthly Vpsc values in some winters can be about twice as large as those observed in the Arctic stratosphere in the spring of 2011 and 2020. This, in turn, can lead to large ozone depletion. A comprehensive analysis shows that "warm" winters with the lowest average Vpsc values are characterized by an increase in the spread of wave activity from the troposphere to the stratosphere in December, but weaker spread in January-February as compared to winters with the highest Vpsc values.

The behavior of the ozone layer in the past and future is actively simulated in St. Petersburg State University based on the earlier developed SOCOL [154] and HAMMONIA [155] chemistry and climate models, as well as the new SOCOL4 [156] model of the global system including the interactive ocean, dynamic vegetation, atmospheric chemistry and sulfate aerosol microphysics. To further improve the models, the possible effect of iodine-containing pollutants on the ozone layer was studied [156]. It has been shown that the destruction of ozone by natural iodine-containing pollutants exerts some effect on the climatology of the ozone layer, which is more noticeable in the troposphere. At the same time, doubling of current emissions of iodine-containing pollutants that is expected in the future has a little effect on the ozone layer in the lower stratosphere and reduces the total ozone content in the atmospheric column by 1.5–2.5%. The results obtained demonstrate a relatively low sensitivity of atmospheric ozone to iodine chemistry for future periods, but the uncertainty remains high because of to the deficit of observations on iodine compounds. Thus, the evolution of the ozone layer from 1980 to 2100 was calculated by the basic version of the SOCOL4 model ignoring iodine-containing pollutants [156]. Changes in the ozone layer for the historical period were calculated using the observed parameters for all significant factors, such as the concentrations of greenhouse and ozone depleting gases, emission of gases from various sources, solar radiation, and volcanic eruptions. The calculated trends were compared with the results of the analysis of ozone changes obtained from the BASIC and MSRv2 multisensor composite data and the MERRA-2 and ERA-5 reanalysis data. Trend analysis was performed separately for the periods of ozone depletion (1985–1997) and recovery of the ozone layer (1998–2018). In the period 1998–2018, SOCOLv4 shows statistically significant positive trends of ozone content in the mesosphere, upper and middle stratosphere and a steady increase in tropospheric ozone. The SOCOLv4 results [158] also indicate some negative trends in the lower layers of the tropical and mid-latitude stratosphere. These results are not consistent with the BASIC data in terms of magnitude and statistical significance. Despite the somewhat lower significance and scale of the simulat-

ed results, the authors conclude that modern CCMs, such as SOCOLv4, are generally capable of reconstructing the observed changes in the ozone concentration. This conclusion justifies the use of such models to predict the future evolution of the ozone layer.

The future evolution of the ozone layer was estimated by the SOCOLv4 model using scenarios of changes in the concentration of greenhouse and ozone-depleting gases, emissions of gases from various sources, solar radiation, and volcanic eruptions [159]. Modeling was performed based on two potential IPCC scenarios: SSP2-4.5 and SSP5-8.5. In the both scenarios, the model shows future depletion of tropospheric ozone. This depletion will start in the 2030s in SSP2-4.5 and after the 2060s in SSP5-8.5 and is associated with the decreasing concentrations of ozone precursors such as NO_x and CO. The results also indicate a very probable increase of the ozone content in mesosphere, upper and middle stratosphere, and lower stratosphere at high latitudes. According to SSP5-8.5, stratospheric ozone increases in the stratosphere due to stronger cooling (> 1 K per decade) caused by greenhouse gases, which slows down cycles of catalytic ozone destruction. To the contrary, ozone concentrations in the tropical lower stratosphere decrease, but increase over the middle and high latitudes of the both hemispheres due to an increase in meridional transport, which is stronger for the SSP5-8.5 scenario. The SOCOLv4 model proposes that the evolution of stratospheric ozone over the 21st century will be largely determined not only by reduction of halogen concentrations, but also by future greenhouse gas emissions. Therefore, although the problem of anthropogenic halogen emissions has now been brought under control, future changes in ozone on a global and regional scale are still unclear and largely depend on the development of future human activities.

The resulting generally optimistic estimates of the future evolution of the ozone layer contrast sharply with a situation if measures to protect the ozone layer would not be taken. New estimates by the SOCOLv4 model [160], which includes the interactive ocean and dynamic vegetation, confirmed the dramatic ozone depletion in that case, as was calculated earlier with less sophisticated models. In addition, it was shown that due to restrictions on production of ozone-depleting pollutants, additional warming of the global climate by more than 2 K was prevented.

Much attention was paid to the impact of factors associated with the space weather on the ozone layer. The use of the HAMMONIA chemical-climatic model [155] allowed estimation of the effect of solar flares in September 2017 on the chemical composition of the atmosphere [161]. It is shown that solar flares in early September 2017 led to a significant increase in the concentrations of active nitrogen and hydrogen oxides at equatorial and southern high latitudes. However, this increase did not change the ozone content in the tropical stratosphere, because the process of ozone destruction by nitrogen

oxides (NO_x) is not efficient in the upper mesosphere and there are no downward air flows that could transport additional NO_x into the stratosphere. Hydrogen oxides (HO_x) do not exert a significant effect on ozone in the considered seasons. However, some small ozone depletion correlated with an increase in HO_x is simulated in the southern hemisphere. The conclusion of a weak effect of electromagnetic radiation on the Earth's atmosphere during solar flares is drawn. As was shown in [162] and [163], energetic electron precipitation from the magnetosphere can have a much greater effect on ozone.

Simulation of consequences of an extreme event over Moscow in December 2009 with the HAMMONIA model showed almost complete destruction of the ozone layer in the mesosphere and lower thermosphere of the northern hemisphere. The energetic electron precipitation over the city of Apatity was considered in [163], and the changes in the concentrations of ozone, electrons, and nitrogen and hydrogen oxides caused by these events were calculated. For the events of October 9, 1998, and September 1, 2000, the calculated drop in the ozone concentration was 14 and 30% at an altitude of 75 km. The results obtained indicate the potentially significant effect of energetic electrons on the chemistry of the atmosphere.

The condition of chemical equilibrium for nighttime ozone is widely used to reconstruct the spatiotemporal distributions of nighttime O, H, and some other characteristics in the altitude range of 80–100 km from satellite data. The boundary below which the equilibrium of nighttime ozone is significantly disturbed was found in [164] using the previously determined analytical criterion. The annual (for 2004) SABER/TIMED database of simultaneous nighttime measurements of temperature, pressure, ozone concentration profiles and the OH* volume emission rate near 2 μm as a result of (9–7) and (8–6) transitions in the altitude range of 75 -100 km was processed. It was found, first, that the position of the nighttime ozone equilibrium boundary varies in the range of 77–86 km depending on the season and latitude, which generally confirms the conclusions of theoretical studies [165, 166]. In addition, this boundary was found to be a sensitive indicator of the evolution of the middle atmosphere. In particular, the results of SABER data processing in 2003-2005 showed that the anomalous latitude dependence of the position of the ozone equilibrium boundary above 60ºN in January-March 2004 is associated with very unusual dynamics of the stratospheric polar vortex during the Arctic winter of 2003-2004, which was “remarkable winter in the 50-year record of meteorological analyses” and was accompanied by an elevated (up to 80 km) stratopause [167]. Second, the spatiotemporal distributions of O and H nighttime concentrations were retrieved from SABER data for 2004. It was found that the application of the ozone equilibrium condition below its equilibrium boundary leads to a significant (up to 5–8 times) under-

estimation of the O concentration in the altitude range of 80–86 km, but practically does not affect the quality of H retrieval. In a recent paper [168], this criterion was improved, and the position of the nighttime ozone equilibrium boundary found with the improved criterion almost perfectly matches the results of chemical transport simulation. In addition, this paper presents the general theory of photochemical/chemical equilibrium of minor atmospheric gases and derives rigorously mathematically a set of conditions that ensure that the concentration of a particular gas is close to its instantaneous equilibrium value.

In [169], a new source of $O(^1D)$ in the region of mesopause due to the process $OH(v\geq5) + O(^3P) \rightarrow OH(0\leq v'\leq v-5) + O(^1D)$ is first applied to retrieve the spatiotemporal distribution of nighttime $O(^1D)$ from SABER/TIMED data for 2003-2005. Using the condition of the nighttime chemical equilibrium of ozone, it is shown that during a year, depending on the month, the average monthly distributions of $O(^1D)$ have from two to four maxima with values up to 340 m^{-3}, which fall in the altitude range of ~ 92–96 km and the latitude range of ~20–40°S,N and ~60–80°S,N. The annual average distributions in 2003–2005 have one weak maximum at ~93 km and ~65°S with values of 150–160 cm^{-3} and three pronounced maxima (with values up to 230 cm^{-3}) at ~ 95 km and ~35°S, ~94 km and ~40°N, and ~93 km and ~65–75°N. In general, the content of $O(^1D)$ in the northern hemisphere is slightly higher than that in the southern hemisphere. The results obtained represent a currently unique database for the subsequent assessment of the effect of nighttime $O(^1D)$ on the chemical composition of the mesopause region.

An analytical study of the mechanism of generation of reaction-diffusion waves in the mesopause region (80–90 km) was performed for the first time in [170]. These waves are nonlinear phase fronts of oscillations in the concentrations of O, O_3, H, OH, and HO_2 with a period of 2 days that move in the zonal direction (strictly to the east) at a constant speed. They appear when the photochemistry of the mesosphere subharmonically (with a period of 2 days) responds to diurnal variations in solar radiation (external periodic impact) with allowance for the horizontal turbulent diffusion. The photochemical system in the mesopause region is a non-linear oscillator, which is described by a system of two differential non-autonomous equations with power-law non-linearity derived in the earlier papers of the authors. It was found that the reaction-diffusion waves are caused by a specific “wind” type transfer that occurs in the equations for the amplitudes of two-day photochemical fluctuations in O and H concentrations due to the zonal inhomogeneity of the external impact. The resulting equation for the wave propagation velocity fully confirmed the previously obtained numerical results that the velocity is proportional to the diffusion coefficient and the phase gradient of the external impact. The direction of wave propagation is determined by spe-

cific phase relationships and depends only on the internal parameters of the system. This study is of fundamental importance, for example, from the viewpoint of predicting the occurrence of similar phenomena in the photochemistry of the atmosphere in other regions due to both diurnal variations in solar radiation and the presence of many other periodic effects. From the practical point of view, this result allows determining the main indicators of reaction-diffusion waves necessary for their subsequent experimental detection under actual conditions of the mesopause and estimating the horizontal turbulent diffusion coefficient, one of the most important but unmeasured transport parameters at altitudes of a given atmospheric region.

The quality of retrieval of the daytime distributions of O, H, OH, HO_2 and the chemical heating rate at altitudes of 77–100 km was analyzed using the long-term (2003–2015) SABER/TIMED database with the photochemical equilibrium condition for daytime ozone [171]. It is found that the generally accepted rejection of the reaction $O_3 + H \rightarrow O_2 + OH$ in this condition leads to underestimation (up to 35–40%) of the O concentration and the chemical heating rate and significant overestimation (up to ~50–85%) of the HO_2 and OH concentrations. In a subsequent paper [172], an improved model of excited OH with constants corresponding to published data was applied to retrieve the daily distributions of O, H, OH, HO_2 from the same SABER/TIMED data. It was found that changes in the parameters of the retrieval procedure lead to a noticeable (up to 80%) increase in the concentration of O below 85–86 km, to a significant (up to 170%) increase in the concentrations of H, OH and HO_2 below 90 km, and a marked (up to 40%) decrease in them nearby 100 km.

To reduce the uncertainty in determining the resonant frequency of the ozone emission line near 110.836 GHz (rotational transition J = 61.5 – 60.6), which is widely used for passive measurement of vertical profiles of ozone concentration at heights of the stratosphere and lower mesosphere, the results of long-term ground-based measurements of the spectra of atmospheric microwave radiation in this spectral range were analyzed in [173]. The use of the modernized equipment developed in the Institute of Applied Physics RAS with high spectral resolution (~12 kHz) allowed determination of the resonant frequency of this ozone emission line with previously inaccessible accuracy. This frequency turned out to be 110835.909 ± 0.016 MHz. It was shown that the Doppler shift of the frequency by the horizontal wind, as well as variations in tropospheric absorption, do not affect the result obtained. The determined value is 130 kHz lower than the laboratory value and differs from the results of calculations by modern spectroscopic models, but is close to the results of the first semi-empirical calculations carried out more than 40 years ago.

3. Techniques and instrumentation

The methods applied to study ozone have already been touched above, except only for the methods developed for data processing.

Based on the NOAA HYSPLIT_4 trajectory model and NCEP/NCAR reanalysis, the team of the A.M. Obukhov Institute of Atmospheric Physics RAS has developed a method for calculation of super-large sets (millions of trajectories) of forward and backward trajectories [174]. Fields of potential sources of aerosol particles and gases are detected using datasets and trajectory methods. The distributions of potential sources of ammonium nitrate, ammonium sulfate, and silicate contributing to ground aerosol, as well as tropospheric formaldehyde and stratospheric nitrogen dioxide at the Zvenigorod scientific station, stratospheric ozone at the Kislovodsk high-mountain scientific station, aerosol column at the AERONET stations in Tomsk and Ussuriysk have been analyzed. The method is also used to identify hard-to-reach zones associated with anomalies in winter surface air temperature in Moscow and precipitation anomalies in the Lake Baikal basin.

A method for taking into account serial correlation (autocorrelation) of data in the problem of multiple linear regression is proposed in [175, 176]. The method is effective in the analysis of long-term trends and temporal variations in atmospheric constituents. It allows the autocorrelation of data to be taken into account at large scales. The residual series is represented as an autoregressive process, whose order k can be much greater than unit, and the autocorrelation function of the process is calculated by solving the system of Yule-Walker equations. The autocorrelation function is used to construct the autocorrelation matrix, which is a component of equations for estimating the regression coefficients and their standard errors. The efficiency of the method is demonstrated with the multiple regression analysis of data of 26-year measurements of the total NO_2 content at the Zvenigorod scientific station of the Institute of Atmospheric Physics. Estimates of the regression coefficients and their errors depend on the autoregression order k. Initially, the error increases as k increases. Then it reaches a maximum and then begins to decrease. In the case of NO_2, the maximum error more than doubles its initial value. The decrease in the error after reaching the maximum stops if k reaches a value, at which the autoregressive process allows describing important features of the autocorrelation function of the residual series. Estimates of seasonally dependent trends and effects of natural factors, such as the 11-year solar cycle, quasi-biennial cycle, the North Atlantic Oscillation, and others, on NO_2 are obtained.

A new approach to processing of long data series of ozone monitoring in the surface atmosphere referred to as Data Parallel Processing in Block Streams is described in [177]. The proposed method is based on the division

of a sequential series of initial data into blocks filled with the results of ground-level ozone monitoring during one day. Further, these blocks form a chain, whose length is determined by the total duration of the observation process. The parallel processing of the initial data aimed at smoothing out fast fluctuations is performed along this chain of blocks. The smoothed data is then used to determine the daily production of ozone due to photochemical reactions, its minimum nighttime levels, as well as the magnitude of nighttime maxima. The potential of the proposed approach is demonstrated with analysis of ground-level ozone monitoring data in Moscow in 2020 taken as an example.

A new lidar for measuring tropospheric ozone and aerosol was developed at the Institute of Atmospheric Optics SB RAS [178]. The lidar system is based on a QX 500 laser (SOLAR LS, Belarus) and a Cassegrainian telescope with a receiving mirror 0.35 m in diameter and of 0.7 m in a focal length. It operates at wavelengths of 299/341 nm and should cover the altitude range from ~0.1 to 12 km. In addition, the capability of monitoring UV solar radiation at the Fonovaya Observatory was significantly expanded [179], and a new UV radiation detector was developed [180].

A singlet oxygen gas analyzer was created in OPTEK JSC (St. Petersburg, Russia) [181]. The operating principle of this device is based on the chemiluminescent reaction of 9,10-defilantracene. The new gas analyzer is designed to solve a wide range of fundamental and applied problems related to processes and phenomena at an interface between biogenic and abiogenic nature. Its capabilities have been demonstrated in the monitoring of pollutant concentrations in the atmospheric air, in vivo and in vitro experiments on detection of singlet oxygen on the snow surface and near plants infected with a pathogenic fungus, and in tests of photocatalytic materials developed for use in medicine and in protection of architectural and sculptural monuments from biodeterioration.

Conclusions

The studies of atmospheric ozone by the Russian state monitoring services and initiative groups in universities and scientific organizations at the territory of Russia continued in 2019–2022. The network of stations that measure ground-level ozone concentrations has noticeably expanded. The publication of reviews on the ozone content in the Russian Federation has begun.

Data processing methods have been improved, and new devices have been developed. A large amount of research into the spatiotemporal variability of the ozone concentration and the factors that determine it has been carried out.

The numerical simulation has been used to estimate the components of ozone cycles, as well as trends in ozone changes until 2100.

To be noted is the release of a monograph on the history of ozone research, covering the period from discovery of oxygen to the present days [182].

References

1. Elanskii N.F. Russian studies of atmospheric ozone and its precursors in 2015–2018 // Izv. RAN. Fiz. Atmos. Okeana, 2020, V. 56, No. 2, p. 170–185.
2. Review of the state and pollution of the environment in the Russian Federation for 2020. Rosgidromet, 2021. 205 pp.
3. Review of the background state of the environment in the territory of the CIS countries for 2021. Yu.A. Israel Institute of Global Climate and Ecology, 2022. 115 pp.
4. https://mosecom.mos.ru/
5. https://www.mos.ru/eco/documents/doklady/view/
6. Ivanova N.S., Kruchenitskii G.M., Kuznetsova I.N., Lapchenko V.A. Statnikov V.A. Ozone Content over the Russian Federation in 2018 // Russian Meteorol. Hydrol. 2019. V. 44, No. 2. P. 152–158.
7. Ivanova N.S., Kruchenitskii G.M., Kuznetsova I.N., Lapchenko V.A., Shirotov V.V. Ozone Content over the Russian Federation in the First Quarter of 2019 // Russian Meteorol. Hydrol. 2019. V. 44, No. 6. P. 424–429.
8. Ivanova N.S., Kruchenitskii G.M., Kuznetsova I.N., Lapchenko V.A. Shirotov V.V. Ozone Content over the Russian Federation in the Second Quarter of 2019 // Russian Meteorol. Hydrol. 2019. V. 44, No. 9. P. 639–642.
9. Ivanova N.S., Kruchenitskii G.M., Kuznetsova I.N., Lapchenko V.A., Shirotov V.V. Ozone Content over the Russian Federation in the Third Quarter of 2019 //Russian Meteorol. Hydrol. 2019, V. 44, No. 12, P. 844–849.
10. Ivanova N.S., Kruchenitskii G.M., Kuznetsova I.N., Shalygina I.Yu., Lapchenko V.A. Demin V.I. Ozone Content over the Russian Federation in 2019 // Russian Meteorol. Hydrol. 2020. V. 45, No. 3. P. 211–218.
11. Ivanova N.S., Kruchenitskii G.M., Kuznetsova I.N., Lapchenko V.A., Demin V.I. Ozone Content over the Russian Federation in the First Quarter of 2020 // Russian Meteorol. Hydrol. 2020. V. 45, No. 6. P. 447–454.
12. Ivanova N.S., Kruchenitskii G.M., Kuznetsova I.N. Ozone Content over the Russian Federation in the Second Quarter of 2020 // Russian Meteorol. Hydrol. 2020. V. 45, No. 8. P. 599–605.
13. Ivanova N.S., Kruchenitskii G.M., Kuznetsova I.N. Ozone Content over the Russian Federation in the Third Quarter of 2020 // Russian Meteorol. Hydrol. 2020, V. 45, No. 11, P. 814–818.
14. Ivanova N.S., Kuznetsova I.N., Shalygina I.Yu., Lezina E.A. Ozone Content over the Russian Federation in 2020// Russian Meteorol. Hydrol. 2021. V. 46, No. 2. P. 129–137.
15. Ivanova N.S., Kuznetsova I.N., Lezina E.A. Ozone Content over the Russian Federation in the First Quarter of 2021 // Russian Meteorol. Hydrol. 2021. V. 46, No. 6. P. 416–421.

16. Ivanova N.S., Kuznetsova I.N., Lezina E.A. Ozone Content over the Russian Federation in the Second Quarter of 2021 // Russian Meteorol. Hydrol. 2021. V. 46, No. 8. P. 553–559.
17. Ivanova N.S., Shalygina I.Yu., Lezina E.A. Ozone Content over the Russian Federation in the Third Quarter of 2021 // Russian Meteorol. Hydrol. 2021, No. 11, P. 799–804.
18. Ivanova N.S., Kuznetsova I.N., Lezina E.A. Ozone Content over the Russian Federation in 2021 // Russian Meteorol. Hydrol. 2022. V. 47, No. 3. P. 241–249.
19. Ivanova N.S., Kuznetsova I.N., Lezina E.A. Ozone Content over the Russian Federation in the First Quarter of 2022 // Russian Meteorol. Hydrol. 2022. V. 47, No. 6. P. 137–143.
20. Ivanova N.S., Kuznetsova I.N., Lezina E.A. Ozone Content over the Russian Federation in the Second Quarter of 2022 // Meteorol. Gidrol. 2022. No. 8. P. 138–142 [in Russian].
21. Ivanova N.S., Kuznetsova I.N., Lezina E.A. Ozone Content over the Russian Federation in the Third Quarter of 2022 // Meteorol. Gidrol. 2022. No. 11. P. 138–142 [in Russian].
22. Andreev V.V., Arshinov M.Yu., Belan B.D., Davydov D.K., Elansky N.F., Zhamsueva G.S., Zayakhanov A.S., Ivlev G.A., Kozlov A.V., Kotel'nikov S.N., Kuznetsova I.N., Lapchenko V.A., Lezina E.A., Postylyakov O.V., Savkin D.E., Senik I.A., Stepanov E.V., Tolmachev G.N., Fofonov A.V., Chelibanovi I.V., Chelibanov V.P., Shirotov V.V. Surface Ozone Concentration over Russian Territory in the First Half of 2020 // Atmospheric and Oceanic Optics, 2020, Vol. 33, No. 6, pp. 671–681.
23. Andreev V.V., Arshinov M.Yu., Belan B.D., Davydov D.K., Elansky N.F., Zhamsueva G.S., Zayakhanov A.S., Ivlev G.A., Kozlov A.V., Kotel'nikov S.N., Kuznetsova I.N., Lapchenko V.A., Lezina E.A., Postylyakov O.V., Savkin D.E., Senik I.A., Stepanov E.V., Tolmachev G.N., Fofonov A.V., Chelibanovi I.V., Chelibanov V.P., Shirotov V.V., Shukurov K.A. Surface Ozone Concentration in Russia in the Second Half of 2020 // Atmospheric and Oceanic Optics, 2021, Vol. 34, No. 4, pp. 347–356.
24. Andreev V.V., Arshinov M.Yu., Belan B.D., Belan S.B., Davydov D.K., Demin V.I., Dudorova N.V., Elansky N.F., Zhamsueva G.S., Zayakhanov A.S., Ivlev G.A., Kozlov A.V., Konovaltseva L.V., Kotel'nikov S.N., Kuznetsova I.N., Lapchenko V.A., Lezina E.A., Obolkin V.A., Postylyakov O.V., Potemkin V.L., Savkin D.E., Senik I.A., Stepanov E.V., Tolmachev G.N., Fofonov A.V., Khodzher T.V., Chelibanov I.V., Chelibanov V.P., Shirotov V.V., Shukurov K.A. Tropospheric Ozone Concentration on the Territory of Russia in 2021 // Atmospheric and Oceanic Optics, 2022, Vol. 35, No. 6, pp. 741–757.
25. Zayakhanov A.S., Zhamsueva G.S., Tsydypov V.V., Balzhanov T.S., Balin Yu.S., Penner I.E., Kokhanenko G.P., Nasonov S.V. Specific features of transport and transformation of atmospheric aerosol and gas admixtures in the coastal zone of Lake Baikal // Atmospheric and Oceanic Optics. 2019. V. 32, No. 2. P. 158–164. DOI: 10.1134/S1024856019020192.
26. Khodzher T.V., Zhamsueva G.S., Zayakhanov A.S., Dementeva A.L., Tsydypov V.V., Balin Yu.S., Penner I.E., Kokhanenko G.P., Nasonov S.V., Klemasheva M.G., Golobokova L.P. and Potemkin V.L. Ship-Based Studies of Aerosol-Gas Admixtures over Lake Baikal Basin in Summer 2018 // Atmospheric and Oceanic Optics, 2019, V. 32. No. 04. pp. 434–441.

27. Tcydypov V.V., Zayakhanov A.S., Zhamsueva G.S., Dementeva A.L., Balzhanov T.S., Sungrapova I.P., Naguslaev S.A. Features of the spatial distribution of gaseous impurities in the atmosphere of the South-Eastern coast of Lake Baikal by route measurements in the summer period 2018–2019 // Limnology and Freshwater Biology. 2020. No. 4. P. 892–893 doi: 10.31951/2658-3518-2020-A-4-892.
28. Zhamsueva G., Zayakhanov A., Tcydypov V., Dementeva A., Balzhanov T. Spatial-Temporal Variability of Small Gas Impurities over Lake Baikal during the Forest Fires in the Summer of 2019 // Atmosphere. 2021. V. 12, No.1. DOI: 10.3390/atmos12010020.
29. Zhamsueva, G.; Zayakhanov, A.; Khodzher, T.; Tcydypov, V.; Balzhanov, T.; Dementeva, A. Studies of the Dispersed Composition of Atmospheric Aerosol and Its Relationship with Small Gas Impurities in the Near-Water Layer of Lake Baikal Based on the Results of Ship Measurements in the Summer of 2020 // Atmosphere 2022, 13, 139. https://doi.org/10.3390/atmos13010139.
30. Pankratova N.V., Belikov I.B., Belousov V.A., Kopeikin V.M., Skorokhod A.I., Shtabkin Yu.A., Malafeev G.V., Flint M.V. Concentration of methane, ozone, black carbon, nitrogen and carbon oxides, and δ13CCH4 content over seas of the Russian Arctic (ship observations) // Okeanologiya. 2020, V. 60, No. 5, p. 685–695 [in Russian].
31. Belan B.D., Ancellet G., Andreeva I.S., Antokhin P.N., Arshinova V.G., Arshinov M.Y., Balin Y.S., Barsuk V.E., Belan S.B., Chernov D.G., Davydov D.K., Fofonov A.V., Ivlev G.A., Kotel'nikov S.N., Kozlov A.S., Kozlov A.V., Law K., Mikhal'chishin A.V., Moseikin I.A., Nasonov S.V., Nédélec P., Okhlopkova O.V., Ol'kin S.E., Panchenko M.V., Paris J.-D., Penner I.E., Ptashnik I.V., Rasskazchikova T.M., Reznikova I.K., Romanovskii O.A., Safatov A.S., Savkin D.E., Simonenkov D.V., Sklyadneva T.K., Tolmachev G.N., Yakovlev S.V., Zenkova P.N. Integrated airborne investigation of the air composition over the Russian sector of the Arctic // Atmos. Meas. Tech., 2022, v. 15, N 13, p.3941–3967.
32. Matvienko G.G., Babushkin P.A., Bobrovnikov S.M., Borovoi A.G., Bochkovskii D.A., Galileiskii V.P., Grishin A.I., Dolgii S.I., Elizarov A.I., Kokarev D.V., Konoshonkin A.V., Kryuchkov A.V., Kustova N.V., Nevzorov A.V., Marichev V.N., Morozov A.M., Oshlakov V.K., Romanovskii O.A., Sukhanov A.Ya., Trifonov D.A., Yakovlev S.V., Sadovnikov S.A., Nevzorov A.A. and Kharchenko O.V. Laser and Optical Sounding of the Atmosphere // Atmospheric and Oceanic Optics, 2020, V. 33. No. 01. P. 51–68.
33. Antokhin P.N., Arshinov M.Yu., Belan B.D., Belan S.B., Sklyadneva T.K., Tolmachev G.N. Many-year variability of ozone and aerosol near Tomsk and justification of the ten-year prediction of their yearly average concentrations . // Optika Atmosfery i Okeana. 2010. V. 23. No. 09. P. 772–776 [in Russian].
34. Senik I.A., Elansky N.F., Belikov I.B., Lisitsyna L.V., Galaktionov V.V., Kortunova Z.V. Main regularities of the temporal variability of near-surface ozone at altitudes of 870 and 2070 m nearby Kislovodsk // Izv. RAN Fiz. Atmos. Okeana, 2005, V. 41, No. 1, p. 78–91 [in Russian].
35. Shalygina I.Yu., Kuznetsova I.N., Lapchenko V.A. Near-surface ozone at the Karadag station in Crimea according to observations in 2009–2018 // Gidrometeorol. Issled. Prognozy, 2019, No.2 (372), p. 102–113 [in Russian].

36. Lapchenko V.A., Kuznetsova I.N., Monitoring of near-surface ozone in Karadagsky natural reserve in the period of 2017–2021 // Gidrometeorol. Issled. Prognozy, 2022, No. 2 (384), p. 113–125 [in Russian].
37. Fedorova E.I., Lapchenko V.A., Elanskii N.F., Skorokhod A.I. Variations of surface ozone in Karadagsky natural reserve // Proc. IV All-Russia Conference with international participation dedicated to the memory of Academician A.M. Obukhov "Turbulence, dynamics of the atmosphere, and climate 2022,", Moscow, November 22–24 (2022).
38. Borisov D.V., Shalygina I.Yu., Lezina E.A. Study of seasonal and diurnal variability of the surface ozone concentration // Gidrometeorol. Issled. Prognozy, 2020, No.3 (377), p. 122–135 [in Russian].
39. Obolkin, V., Potemkin V., Khuriganova O., Khodzher T. Ozone Monitoring in the Baikal Region (East Siberia): Spatiotemporal Variability under the Influence of Air Pollutants and Site Conditions // Atmosphere 2022, v. 13, 519. https://doi.org/10.3390/ atmos13040519.
40. Antokhin P.N., Antokhina O.Yu., Antonovich V.V., Arshinova V.G., Arshinov M.Yu., Belan B.D., Belan S.B., Davydov D.K., Dudorova N.V., Ivlev G.A., Kozlov A.V., Pestunov D.A., Rasskazchikova T.M., Savkin D.E., Simonenkov D.V., Sklyadneva T.K., Tolmachev G.N., Fofonov A.V. Interrelation between Dynamics of Gas Composition and Meteorological Parameters in the Region of Tomsk // Atmospheric and Oceanic Optics, 2020, Vol. 33, No. 6, pp. 629–637.
41. Kotelnikov S.N., Stepanov E.V. Role of water aerosol in the ozone destruction in the surface atmosphere // Kratkie Soob. po Fizike FIAN, V. 46, No. 9, 2019, P. 23–30 [in Russian]. DOI: 10.3103/S1068335619090045
42. Arshinova V.G., Belan B.D., Lapchenko V.A., Lapchenko E.V., Rasskazchikova T.M., Savkin D.E., Sklyadneva T.K., Tolmachev G.N., Fofonov A.V. Changes in Surface Ozone Concentration during Precipitation // Atmospheric and Oceanic Optics, 2019, Vol. 32, No. 6, pp. 671–679.
43. Belan B.D., Savkin D.E. The Role of Air Humidity in Variations of Near-Surface Ozone Concentration // Atmospheric and Oceanic Optics, 2019, Vol. 32, No. 5, pp. 586–589.
44. Khuriganova O., Obolkin V., Akimoto H., Ohizumi T., Khodzher T., Potemkin V., Golobokova L. Long-Term Dynamics of Ozone in Surface Atmosphere at Remote Mountain, Rural and Urban Sites of South-East Siberia, Russia // Open Access Library Journal, 2022*, v.* 3: e2578. http://dx.doi.org/10.4236/oalib.1102578.
45. Berezina E.V., Moiseenko K.B., Skorokhod A.I., Pankratova N.V., Belikov I.B., Belousov V.A., Elansky N.F. Impact of VOCs and NOx on ozone formation in Moscow // Atmosphere 2020, v.11, 1262; doi:10.3390/atmos11111262.
46. Berezina, E.; Moiseenko, K.; Vasileva, A.; Pankratova, N.; Skorokhod, A.; Belikov, I.; Belousov, V. Emission Ratios and Source Identification of VOCs in Moscow in 2019–2020. // Atmosphere 2022, 13, 257. https://doi.org/10.3390/ atmos13020257.
47. Moiseenko K.B., Vasileva A.V., Skorokhod A.I., Belikov I.B.,Repin A.Y., Shtabkin Y.A. Regional Impact of Ozone Precursor Emissions on NO_X and O_3 Levels at ZOTTO Tall Tower in Central Siberia // Earth and Space Science, 2021, v. 8, N 7, e2021EA001762, DOI:10.1029/2021EA001762.

48. Thorp T., Arnold S.R., Pope R.J., Spracklen D.V., Conibear L., Knote C., Arshinov M., Belan B., Asmi E., Laurila T., Skorokhod A.I., Nieminen T., and Petäjä T. Late-spring and summertime tropospheric ozone and NO2 in western Siberia and the Russian Arctic: regional model evaluation and sensitivities // Atmos. Chem. Phys., 21, 4677–4697, https://doi.org/10.5194/acp-21-4677-2021, 2021.
49. Rakitin V.S., Elanskii N.F., Skorokhod A.I., Dzhola A.V., Rakitina A.V., Shilkin A.V., Kirillova N.S., Kazakov A.V. Long-term trends in the total content of carbon monoxide in the atmosphere of the Moscow metropolis // Izv. RAN. Fiz. Atmos. Okeana, 2021, V. 57, No. 1, P. 126–136. DOI: 10.31857/S0002351521010107.
50. Zayakhanov A.S.; Zhamsueva G.S.; Tcydypov V.V.; Balzhanov T.S.; Dementeva A.L.; Khodzher T.V. Investigation of Transport and Transformation of Tropospheric Ozone in Terrestrial Ecosystems of the Coastal Zone of Lake Baikal // Atmosphere 2019, v.10, 739. https://doi.org/10.3390/atmos10120739.
51. Elansky N.F., Shilkin A.V., Semutnikova E.G., Zaharova P. V., Rakitin V.S., Ponomarev N. A., Verevkin Y. M., Weekly Cycle of Pollutant Concentrations in Near-Surface Air over Moscow // Atmospheric and Oceanic Optics, 2019, Vol. 32, N1, p. 85–93.
52. Skorokhod A.I., V.S. Rakitin, and N.S. Kirillova. Impact of COVID-19 Pandemic Preventing Measures and Meteorological Conditions on the Atmospheric Air Composition in Moscow in 2020. // Russian Meteorol. Hydrol. 2022, Vol. 47, No. 3, pp. 183–190.
53. Stepanov, E.V., Andreev, V.V., Konovaltseva, L.V., *et al.* Surface Ozone in the Atmosphere of Moscow during the COVID-19 Pandemic // Atmos Ocean Opt., 2022, v. 35, N 6, p. 732–740. https://doi.org/10.1134/S1024856022060252
54. Kotelnikov, S.N., Stepanov, E.V. Anomalous Dynamics of Tropospheric Ozone in the Spring of 2020 in Central Russia // Bull. Lebedev Phys. Inst., 2021, v. 48, p. 92–96. https://doi.org/10.3103/S1068335621030076.
55. Shtabkin Yu.A., Moiseenko K.B., Skorokhod A.I., Berezina E.V., Natural and anthropogenic factors of seasonal variability of ground-level ozone in Central Siberia // Proceedings of V International scientific and practical conference "Fundamental and applied aspects of geology, geophysics and geoecology using modern information technologies," Maikop, Russia, May 20–24 (2019), p. 291–298.
56. Shtabkin Yu.A., Moiseenko K.B., Skorokhod A.I., Berezina E.V. Seasonal variations of the ground-level ozone content in Northern Eurasia: observations and numerical simulation // Abstracts of Reports at All-Russia Conference with international participation dedicated to the memory of Academician A.M. Obukhov "Turbulence, dynamics of the atmosphere, and climate," Moscow, November 10–12, 2020 (Fizmatkniga, Moscow, 2020), p. 133.
57. Shtabkin Yu.A., Moiseenko K.B., Skorokhod A.I., Berezina E.V. Васильева А.В. Influence of long-range transport of air masses on seasonal variations and regional balance of tropospheric ozone // Abstracts of Reports at All-Russia Conference with international participation dedicated to the memory of Academician A. M. Obukhov "Turbulence, dynamics of the atmosphere, and climate," Moscow, November 10-12, 2020 (Fizmatkniga, Moscow, 2020), p.134.
58. Berezina E., Moiseenko K., Skorokhod A., Elansky N., Belikov I., Pankratova N. Isoprene and monoterpenes over Russia and their impacts in tropospheric

ozone formation // Geography, Environment, Sustainability, 2019, Vol. 12, No 1, p. 63–74, DOI-10.24057/2071-9388-2018.
59. Safronov A.N., Shtabkin Yu.A., Berezina E.V., Rakitin V.S., Skorokhod A.I., Belikov I.B., Elansky N.F. Isoprene, methyl vinyl ketone and methacrolein from TROICA-12 measurements and WRF-CHEM and GEOS-CHEM simulations in the Far East region // Atmosphere .2019. V. 10, 152. doi:10.3390/atmos100 30152.
60. Moiseenko K.B., Berezina E.V., Vasileva A.V., Shtabkin Yu.A., Skorokhod A.I., Elansky N. F., Belikov I.B., NO_x-limiting mode of photochemical ozone generation in slightly polluted convective boundary layer: observations at ZOTTO high tower in Central Siberia in 2007–2015 // Dokl. Akad Nauk. 2019. V. 487. No 6. p. 669–673.
61. Moiseenko K.B., Vasilieva A.V., Skorochod A.I., Shtabkin Yu.A., Belikov I.B., Repin A.Yu. O_3–NO–NO_2 photostationary state and near-surface ozone generation from ZOTTO Tower data (central Siberia) // Optika Atmosfery i Okeana. 2022. V. 35. No. 10. P. 850–857. DOI: 10.15372/AOO20221008 [in Russian].
62. Borovski A.N., Elansky N.F., Ponomarev N.A., Postylyakov O.V. Comparison of measured and simulated by SILAM NO2 integral content in atmospheric boundary layer in Moscow region // Proc. SPIE, 11152, 111520P, 2019, doi:10.1117/12.2535492.
63. Postylyakov O., Borovski A., Kirsanov A., Vasileva A., Elansky N. Comparison of measured and simulated NO2 integral content in the lower troposphere in Moscow region // IOP Conference Series: Earth and Environmental Science, 2020, 489, 012035, doi: doi:10.1088/1755-1315/489/1/012035.
64. Ponomarev, N.A., Elansky, N.F., Kirsanov, A.A., Postylyakov, O.V., Borovski, A.N., Verevkin, Y.M. Application of Atmospheric Chemical Transport Models to Validation of Pollutant Emissions in Moscow. Atmospheric and Oceanic Optics, 2020, 33, 362–371, doi:1134/S1024856020040090.
65. Borovski A.N., Elokhov A.S., Kirsanov A.A., Postylyakov O.V. Measured and simulated integral content of NO2 in the atmospheric boundary layer in Moscow region in summer // Proc. SPIE 11531, 1153108, 2020, doi:10.1117/12.2571724.
66. Ponomarev N.A., Elansky N.F., Zakharov V.I., Verevkin Ya.M. Optimization of pollutant emissions for simulation of air quality in Moscow // Processy v Geosredakh, 2019, No. 1 (19), p. 65–73.
67. Elansky N.F., Shilkin A.V., Ponomarev N.A., Semutnikova E.G., Zakharova P.V. Weekly patterns and weekend effects of air pollution in the Moscow megacity. Atmospheric Environment. 2020. V. 224. 117303. http://www.elsevier.com/locate/atmosenv; https://doi.org/10.1016/j.atmosenv.2020.117303
68. Ponomarev N., Yushkov V., Elansky N. Air Pollution in Moscow Megacity: Data Fusion of the Chemical Transport Model and Observational Network // Atmosphere 2021, v.12, 374. https://doi.org/10.3390/atmos12030374.
69. Lokoshchenko M.A., Bogdanovich A.Yu., Elansky N.F., Lezina E.A. Temperature inversions in Moscow and their effect on the surface air composition // Izv. RAN. Fiz. Atmos. Okeana , 2021, V. 57, No. 6, p. 641–650. DOI: 10.31857/S0002351521060080.
70. Zakharova S.A., Elansky N.F., Verevkin Y.M., Davydova M.A. Determination of Emissions in the City by the Rate of Change in the Integral Content of Impurities in the Atmospheric Boundary Layer // Doklady Earth Sciences, 2022,

Vol. 504, Part 1, pp. 326–331. © Pleiades Publishing, Ltd., 2022. DOI: 10.1134/S1028334X22050191.

71. Elansky N.F., Shilkin A.V., Ponomarev N.A., Zakharova P.V., Kachko M.D., Polykov T.I. Spatiotemporal variations of pollutant content and Moscow air basin and pollutant emissions // Izv. RAN. Fiz. Atmos. Okeana, 2022, V. 58, No. 1, p. 92–108. DOI: 10.31857/S0002351522010023.
72. Kuznetsova I.N., Nakhaev M.I., Kirsanov A.A., Borisov D.V., Tkacheva Yu.V., Rivin G.S., Lezina E.A. Testing and potential of the technology for prediction of air pollution with CHIMERE and COSMO-Ru2ART chemical transport models // Gidrometeorol. Issled. Prognozy 2022. No. 4 (386). P. 147–170. DOI: https://doi.org/10.37162/2618-9631-2022-4-147-170.
73. Nakhaev M.I., Kuznetsova I.N., Shalygina I.Yu., Borisov D.V., Kirsanov A.A., Prediction of pollutant concentrations with chemical transport models. Abstracts of reports at Scientific-Practical Conference on Problems of Hydrometeorological Forecasts, Ecology, and Climate of Siberia, Novosibirsk. October 20–22, 2021.
74. Kotelnikov S.N., Stepanov E.V., Ivashkin V.T., Aboveground Ozone Concentration and the Health Status in Various Age Groups of Muscovites in Summer 2010 // Izvestiya Atmospheric and Oceanic Physics, 2019, Vol. 55, No. 11, p. 1602–1613. DOI: 10.1134/S0001433819110070
75. Ivashkin V.T., Kotelnikov S.N., Stepanov E.V., Possible increase in severity of COVID-19 due to the combined action of the Sars-CoV-19 virus and ozone at a seasonal increase in the ozone content in the surface atmosphere // Ecologiya i

82. Sibir E.E., Radionov V.F., Rusina E.N. Results of long-term observations of total ozone in Antarctica and over the Atlantic and Southern Oceans // Russian Meteorol. Hydrol. 2020. T. 45. No. 3. P. 161–168.
83. Rusina E.N., Bobrova V.K. – 2.3.1. Optical density and transparency of the atmosphere // Review of the State and Pollution of the Environment in the Russian Federation for 2021, 2022, pp. 31–34.
84. Rusina E.N., Bobrova V.K. – 2.3.1. Optical density and transparency of the atmosphere // Review of the State and Pollution of the Environment in the Russian Federation for 2021, 2022, pp. 31–34.
85. Rusina E.N., Bobrova V.K. – 2.3.1. Optical density and transparency of the atmosphere // Review of the State and Pollution of the Environment in the Russian Federation for 2021, 2022, pp. 31–34.
86. Rusina E.N., Bobrova V.K. Optical density and transparency of the atmosphere in the Arctic zone of the Russian Federation // Review of the State and Pollution of the Environment in the Russian Federation for 2021, 2022, pp. 184–185.
87. Radionov V.F., Rusina E.N., Sibir E.E Long-term variability of integral and spectral transparency of the atmosphere at Mirny observatory, Antarctica, 2020, Russian Meteorol. Hydrol. 2020, V. 45, No.2, p. 74–80.
88. Sibir E.E., Radionov V.F., Rusina E.N. Database of hourly and daily sums of total radiation at Russian antarctic stations: analysis of changes in total radiation for the entire period of observations in Antarctica // Arctic and Antarctic Research. 2021;67(3):249–260. (In Russ.) https://doi.org/10.30758/0555-2648-2021-67-2-249-260
89. Dorokhov V., Yushkov V., Makshtas A., Ivlev G., Tereb N., Savinykh V., Shepelev D., Nakajima H., McElroy C.T., Tarasick D., Goutail F., Pommereau J.-P., Pazmino A. Brewer, SAOZ and ozonesonde observations in Siberia // Atmosphere-Ocean. 2015. V. 53. No. 1. P. 14–18. https://doi.org/10.1080/07055900.2013.830078.
90. Polyakov, A.V., Timofeyev, Y.M., Virolainen, Y.A. , Kozlov D.A. Atmospheric Ozone Monitoring with Russian Spectrometer IKFS-2 // J Appl Spectrosc 86, 650–654 (2019). https://doi.org/10.1007/s10812-019-00873-7.
91. Timofeyev Yu.M., Nerobelov G.M., Polyakov A.V., Virolainen Ya.A. Satellite monitoring of the ozonosphere // Russian Meteorol. Hydrol. 2021, V. 46, No. 12, p. 71–79.
92. Polyakov A., Virolainen Ya., Nerobelov G., Timofeyev Yu., Solomatnikova A., Total ozone measurements using IKFS-2 spectrometer aboard Meteor M N2 satellite in 2019–2020 // Int. J. Rem. Sens., 2021, v. 42, N 22, p. 8709–8733. https://doi.org/10.1080/01431161.2021.1985741.
93. Ionov D.V. and Privalov V.I. The Differential Spectroscopy Technique DOAS in the Problem of Determining the Total Ozone Content from Measurements of Ground-Based UV Spectrometer UFOS // Atmospheric and Oceanic Optics, 2022, V. 35. No. 01. pp. 1–7. https://doi.org/10.15372/AOO20211102.
94. Virolainen Ya.A. , Polyakov A.V., Timofeyev Yu.M., Analysis of variations of stratospheric gases from data of ground-based spectroscopic measurements in the region of St. Petersburg // Izv. RAN, Fiz. Atmos. Okeana, 2021, V. 57, No. 2, p. 163–174. DOI: 10.31857/S0002351521010132.
95. Kreher K., Van Roozendael M., Hendrick F., Apituley A., Dimitropoulou E., Frieß U., Richter A., Wagner T., Lampel J., Abuhassan N., Ang L., Anguas M., Bais A., Benavent N., Bösch T., Bognar K., Borovski A., Bruchkouski I.,

Cede A., Chan K. L., Donner S., Drosoglou T., Fayt C., Finkenzeller H., Garcia-Nieto D., Gielen C., Gómez-Martín L., Hao N., Henzing B., Herman J. R., Hermans C., Hoque S., Irie H., Jin J., Johnston P., Khayyam Butt J., Khokhar F., Koenig T. K., Kuhn J., Kumar V., Liu C., Ma J., Merlaud A., Mishra A.K., Müller M., Navarro-Comas M., Ostendorf M., Pazmino A., Peters E., Pinardi G., Pinharanda M., Piters A., Platt U., Postylyakov O., Prados-Roman C., Puentedura O., Querel R., Saiz-Lopez A., Schönhardt A., Schreier S. F., Seyler A., Sinha V., Spinei E., Strong K., Tack F., Tian X., Tiefengraber M., Tirpitz J.-L., van Gent J., Volkamer R., Vrekoussis M., Wang S., Wang Z., Wenig M., Wittrock F., Xie P.H., Xu J., Yela M., Zhang C., Zhao X. Intercomparison of NO2, O4, O3 and HCHO slant column measurements by MAX-DOAS and zenith-sky UV–visible spectrometers during CINDI-2 // Atmos. Meas. Tech., 13, 2169–2208, doi:10.5194/amt-13-2169-2020, 2020.

96. Wang Y., Apituley A., Bais A., Beirle S., Benavent N., Borovski A., Bruchkouski I., Chan K.L., Donner S., Drosoglou T., Finkenzeller H., Friedrich M.M., Frieß U., Garcia-Nieto D., Gómez-Martín L., Hendrick F., Hilboll A., Jin J., Johnston P., Koenig T. K., Kreher K., Kumar V., Kyuberis A., Lampel J., Liu C., Liu H., Ma J., Polyansky O. L., Postylyakov O., Querel R., Saiz-Lopez A., Schmitt S., Tian X., Tirpitz J.-L., Van Roozendael M., Volkamer R., Wang Z., Xie P., Xing C., Xu J., Yela M., Zhang C., Wagner T. Intercomparison of MAX-DOAS measurements of tropospheric HONO slant column densities and vertical profiles during the CINDI-2 campaign // Atmos. Meas. Tech., 13, 5087–5116, https://doi.org/10.5194/amt-13-5087-2020, 2020.
97. Dolgii S.I., Nevzorov A.A., Nevzorov A.V., Romanovskii O.A., Kharchenko O.V. Lidar differential absorption system for measuring ozone in the upper troposphere–stratosphere // Journal of Applied Spectroscopy. 2019. V. 85. No. 6. P. 1114 – 1120. DOI 10.1007/s10812-019-00767-8.
98. Dolgii S.I., Nevzorov A.V., Nevzorov A.A., Gridnev Yu.V., Romanovskii O.A., Kharchenko O.V. Influence of Absorption Cross-Sections on Retrieving the Ozone Vertical Distribution at the Siberian Lidar Station // Atmosphere. 2022. V. 13. Issue 2. P. 293. https://doi.org/10.3390/atmos13020293.
99. Dolgii S.I., Nevzorov A.A., Nevzorov A.V., Gridnev Yu.V., Kharchenko O.V. Temperature Correction of the Vertical Ozone Distribution Retrieval at the Siberian Lidar Station Using the MetOp and Aura Data // Atmosphere 2020. V. 11. Issue 11. P. 1139. https://doi.org/10.3390/atmos11111139.
100. Ryskin, V.G., Zinchenko, I.I., Krasil'nikov, A.A. et al. Stratospheric ozone distribution features from the results of simultaneous ground-based microwave measurements in Nizhni Novgorod and Kyrgyzstan. // Russian Meteorol. Hydrol. 2012, v. 37, p. 659–665. https://doi.org/10.3103/S1068373912100032.
101. Nerobelov G.M., Al-Subari O.H., Timofeyev Yu.M., Violainen Ya.A., Poberovskii A.V., Solomatnikova A.A. Comparison of results of ground-based measurements of the total ozone content near St. Petersburg // Izv. RAN, Fiz. Atmos. Okeana, 2022, V. 58, No. 5, p. 1–7.
102. Nerobelov G., Timofeyev Yu., Virolainen Y., Polyakov A., Solomatnikova A., Poberovskii A., Kirner O., Al-Subari O., Smyshlyaev S., Rozanov E. Measurements and Modelling of Total Ozone Columns near St. Petersburg, Russia // Remote Sensing, 2022, V. 14, N16, 3944. https://doi.org/10.3390/rs14163944.
103. Bazhenov O.E., Nevzorov A.V., Smirnov S.V., Elnikov A.V., Loginov V.A. Comparison of total ozone observations over Tomsk (2006-2020) with three

spectrophotometers // Proc. XXVIII International Symposium “Atmospheric and Ocean optics. Atmospheric Physics,” Tomsk, Russia, July 4–8, 2022 (IAO SB RAS, Tomsk, 2022).
104. Bazhenov O.E., Nevzorov A.V., Smirnov S.V., Elnikov A.V., Loginov V.A. Comparison of observations of total ozone content over Tomsk (2006-2020) obtained using three spectrophotometers // Proceedings of SPIE. 2022. V. 12341. https://doi.org/10.1117/12.2643481
105. Dolgii S.I., Nevzorov A.A., Nevzorov A.V., Romanovskii O.A., Kharchenko O.V. Comparison of ozone vertical profiles in the upper troposphere–stratosphere measured over Tomsk, Russia (56.5° N, 85.0° E) with DIAL, MLS, and IASI // International Journal of Remote Sensing. 2020. V. 41. N. 22. P. 8590–8609. doi: 10.1080/01431161.2020.1782506. https://doi.org/10.1080/01431161.2020.1782506.
106. Dolgii S.I., Nevzorov A.A., Nevzorov A.V., Gridnev Yu.V. Kharchenko O.V. Measurements of Ozone Vertical Profiles in the Upper Troposphere–Stratosphere over Western Siberia by DIAL, MLS, and IASI // Atmosphere. 2020. V. 11. Issue 2. P. 196. https://doi.org/10.3390/atmos11020196.
107. Bordovskaya Yu.I., Virolainen Ya.A., Timofeev Yu.M. Comparison of ground-based and satellite methods for determination of vertical ozone profiles // Sovr. Probl. Dist. Zondir. Zemli ia Kosmosa, 2022, v. 19, No. 2, p. 225–231.
108. Polyakov A., Ya. Virolainen, G. Nerobelov, Yu. Timofeyev, A. Solomatnikova,: Total ozone measurements using IKFS-2 spectrometer aboard MeteorM N2 satellite in 2019–2020 // Int. J. Rem. Sens., 2021, v. 42, No. 22, p. 8709–8733.
109. Postylyakov O.V., Borovski A.N., Elansky N.F., Davydova M.A., Zakharova S.A., Makarenkov A.A. Comparison of space high-detailed experimental and model data on tropospheric NO_2 distribution // Proc. SPIE, 11208, 112082S, 2019, doi:10.1117/12.2540770.
110. Postylyakov O.V., Borovski A.N., Davydova M.A., Makarenkov A.A. Preliminary validation of high-detailed GSA/Resurs-P tropospheric NO_2 maps with alternative satellite measurements and transport simulations // Proc. SPIE, 11152, 111520F, 2019, doi:10.1117/12.2535487.
111. Postylyakov O.V., Borovski A.N., Shukurov K.A., Mukhartova I.V., Davydova M.A., Makarenkov A.A. On validation high-detail mapping of tropospheric NO_2 using GSA/Resurs-P observations with simulated data // Proc. SPIE 11531, 1153109, 2020, doi:10.1117/12.2574240.
112. Chan K.L., Valks P., Heue K.-P., Lutz R., Hedelt P., Loyola D., Pinardi G., Van Roozendael M., Hendrick F., Wagner T., Kumar V., Bais A., Piters A., Irie H., Kanaya Y., Takashima H., Choi Y., Park K., Chong J., Cede A., Frieß U., Richter A., Ma J., Benavent N., Holla R., Postylyakov O., Cárdenas R, C., Wenig M. Global Ozone Monitoring Experiment-2 (GOME-2) Daily and Monthly Level 3 Products of Atmospheric Trace Gas Columns // Earth Syst. Sci. Data Discuss. 2022, doi:10.5194/essd-2022-315.
113. Trifonova-Yakovleva A.M., Gromov S.A., Khodzher T.V., Potemkin V.L., Obolkin V.A. Assessment of the possibility of using the GOME-2 high-resolution ozone profile to estimate the ground-level ozone concentration // Sovr. Probl. Dist. Zondir. Zemli ia Kosmosa. 2017. V. 14. No. 5. p. 239–247. DOI: 10.21046/2070-7401-2017-14-5-2.
114. Gruzdev A.N., Arabov A.Ya., Elokhov A.S., Savinykh V.V., Senik I.A., Borovskii A.N., Elanskii N.F. Long-term observations of stratospheric species at

the A.M. Obukhov Institute of Atmospheric Physics, Russian Academy of Sciences: analysis of trends and interannual variations in the total contents of O_3 and NO_2 // Izvestiya, Atmospheric and Oceanic Physics. 2022. V. 58. No 3. P. 270–283. DOI: 10.1134/S0001433822030069.

115. Gruzdev A.N., Elansky N.F., Arabov A.ya., Elokhov A.S., Savinykh V.V., Senik I.A., Borovski A.N., Manifestation of 11-year solar cycle in total content of O_3 and NO_2 from long-term measurements at research stations of the A.M. Obukhov Institute a atmospheric Physics RAS // Abstract of Reports at 17th Annual Conference "Physics of Plasma in the Solar System," February 7–11, 2022, Moscow (Institute of Space Studies RAS, Moscow, 2022). p. 207. DOI 10.21046/20DZZconf-2022a.
116. Savinykh V.V., Elansky N.F., Gruzdev A.N. Interannual variations and long-term trends in total ozone over the North Caucasus // Atmospheric Environment. 2021. V. 251. 118252. P. 1–10. DOI: 10.1016/j.atmosenv.2021.118252. https://doi.org/10.1016/j.atmosenv.2021.118252.
117. Savinykh V.V., Gruzdev A.N., Elansky N.F. Trends and variations in total ozone over the North Caucasus // Proceedings of SPIE. 2021. V. 11916. P. 119162S. ISSN: 1996-756X. DOI: 10.1117/12.2602435.
118. Gruzdev A.N., Elansky N.F., Elokhov A.S., Savinykh V.V., Arabov A.Ya., Borovski A.N., Senik I.A. Long-term measurements of total NO_2 and O_3 column contents at stations of the A.M. Obukhov Institute of Atmospheric Physics, Russian Academy of Sciences: Observational methods, long-term trends and interannual variations of the species // Proceedings of SPIE. 2022. Vol. 12341. P. 1234172-1–1234172-6. doi: 10.1117/12.2643897.
119. Gruzdev A.N., Elokhov A.S. Changes in the column content and vertical distribution of NO_2 according to the results of 30-year measurements at the Zvenigorod Scientific Station of the A. M. Obukhov Institute of Atmospheric Physics, Russian Academy of Sciences. Izvestiya, Atmospheric and Oceanic Physics. 2021. V. 57. No 1. P. 91–103. DOI: https://doi.org/10.1134/S0001433821010084.
120. Gruzdev A.N., Elokhov A.S. Trends in total, tropospheric and stratospheric NO_2 contents based on results of ground-based and satellite (OMI) measurements // Proceedings of SPIE. 2022. Vol. 12341. P. 123412G-1–123412G-6. doi: 10.1117/12.2644393.
121. Gruzdev A.N., Elokhov A.S. Comparison of the results of ground-based and satellite (OMI) measurements of the NO_2 contents in the stratosphere and troposphere over Zvenigorod: Sensitivity to cloud cover and tropospheric pollution // Proceedings of SPIE. 2021. V. 11916. P. 1191628. ISSN: 1996-756X. DOI: 10.1117/12.2601814.
122. Gruzdev A.N., Elokhov A.S. Long-term trends and interannual variations of the NO_2 contents in the troposphere and stratosphere of the western Moscow region according to results of remote spectrometric measurements of the vertical NO_2 profile // Proceedings of SPIE. 2021. V. 11916. P. 1191627. ISSN: 1996-756X. DOI: 10.1117/12.2601812.
123. Gruzdev A.N., Elokhov A.S. Three decades of remote sensing of NO_2 vertical distribution and column content at the A. M. Obukhov Institute of Atmospheric Physics // IOP Conf. Ser. Earth Environ. Sci. 2022. V. 1040. 012027. P. 1–8. doi:10.1088/1755-1315/1040/1/012027. https://iopscience.iop.org/article/10.1088/1755-1315/1040/1/012027/pdf.

124. Bruchkouski I., Borovski A., Dzhola A., Elansky N., Postylyakov O., Bazhenov O., Romanovskii O., Sadovnikov S., Kanaya Y. Observations of Integral Formaldehyde Content in the Lower Troposphere in Urban Agglomerations of Moscow and Tomsk Using the Method of Differential Optical Absorption Spectroscopy // Atmos. Ocean. Opt, 2019, 32, 248–256. doi:10.1134/S1024856019030047.
125. Bazhenov O.E., Nevzorov A.V., Dolgii S.I., Elnikov A.V., Sysoev S.M., Analysis of annual variations of the total ozone content and integral aerosol backscattering coefficient in stratosphere over Tomsk // Abstracts of Reports at XXV International Symposium "Atmospheric and Ocean Optics. Atmospheric Physics," (IAO SB RAS, Tomsk, 2019). P. 145. ISBN 978-5-94458-175-4. https://symp.iao.ru/ru/aoo/25/progpdf
126. Nevzorov A.V., Bazhenov O.E., Dolgii S.I., Elnikov A.V., Sysoev S.M., Analysis of annual variations in total ozone content and integrated aerosol backscattering coefficient in the stratosphere over Tomsk // Proc. SPIE 2019. V. 11208. P. 112088P-1–112088P-4.
127. Nevzorov A.V., Bazhenov O.E., Elnikov A.V. and Loginov V.A. Comparison of Time Series of Integrated Aerosol Content in the Stratosphere and Total Ozone Content // Atmospheric and Oceanic Optics, 2021, V. 34. No. 05. pp. 411–416.
128. Nevzorov A.V., Bazhenov O.E., Elnikov A.V., Loginov V.A. Interaction of the integral aerosol content in the stratosphere and the total ozone content //// Abstracts of Reports at XXVII International Symposium "Atmospheric and Ocean Optics. Atmospheric Physics" (IAO SB RAS, Tomsk, 2021). P. 46. ISBN 978-5-94458-186-0. https://symp.iao.ru/ru/aoo/27/progpdf .
129. Nevzorov A.V., Bazhenov O.E., Elnikov A.V., Loginov V.A. Interaction of integrated aerosol content in the stratosphere and total ozone content // Proceedings of SPIE. 2021. V. 11916. CID: 11916 29.
130. Bazhenov O.E., Nevzorov A.A., Nevzorov A.V., Dolgii S.I. and Makeev A.P. Disturbance of the Stratosphere over Tomsk during Winter 2017/2018 Using Lidar and Aura MLS/OMI Observations // Atmospheric and Oceanic Optics, 2020, V. 33. No. 06. pp. 622–628.
131. Bazhenov O.E., Nevzorov A.A., Nevzorov A.V., Dolgii S.I., Makeev A.P. Disturbance of the Stratosphere over Tomsk prior to the 2018 Major Sudden Stratospheric Warming: Effect of ClO Dimer Cycle // Optical Memory and Neural Networks (Information Optics) 2021. V. 30. No. 2. P.146–156.
132. Bazhenov O.E., Nevzorov A.A., Nevzorov A.V., Dolgii S.I., Makeev A.P. Disturbance of the Stratosphere over in winter 2017/2018 from data of lidar and satellite (Aura MLS) observations // Abstracts of Reports at XXVII International Symposium "Atmospheric and Ocean Optics. Atmospheric Physics" (IAO SB RAS, Tomsk, 2021). P. 54. ISBN 978-5-94458-186-0. https://symp.iao.ru/ru/aoo/27/progpdf
133. Bazhenov O.E., Nevzorov A.A, Nevzorov A.V., Dolgii S.I., Makeev A.P. Disturbance of the stratosphere over Tomsk in winter 2017-2018 using lidar and satellite (Aura MLS) observations // Proceedings of SPIE. 2021. V. 11916. P. 119162J-1–119162J-6.
134. Bazhenov O.E. Increased humidity in the stratosphere as a possible factor of ozone destruction in the Arctic during the spring 2011 using Aura MLS observations // International Journal of Remote Sensing. 2019. Vol. 40. No. 9. P. 3448–3460.

135. Belikovich M.V., Ryskin V.G., Kulikov M.Yu., Krasilnikov A.A., Shvetsov A.A., Feigin A.M. Microwave observations of atmospheric ozone over Nizhny Novgorod in winter of 2017-2018 // Radiophysics and Quantum Electronics, 2021, v.63, p.191–206, https://doi.org/10.1007/s11141-021-10045-3.
136. Kulikov M.Y., Belikovich M. V., Feigin A.M. The 2-day photochemical oscillations in the mesopause region: the first experimental evidence? // Geophysical Research Letters. 2021, V. 48. e2021GL092795. https://doi.org/10.1029/2021GL092795 .
137. Kiselev A.A. Ozone deficiency shows itself // Ros. Polar. Issled., No. 2 (40), 2020, p. 52–54. http://old.aari.ru/misc/publicat/rpr_arh_jour.php?idpub=229&arh=2.
138. Vargin, P.N., Nikiforova, M.P. , Zvyagintsev, A.M. Variability of the Antarctic Ozone Anomaly in 2011–2018. // Russian Meteorol. Hydrol. 2020, V. 45, p. 63–73. https://doi.org/10.3103/S1068373920020016.
139. Frolkis V.A., Karol' I.L., Kiselev A.A. Is there a correlation between quasi-biennial atmospheric variations and changes in ozone and temperature in Antarctica? // Trudy GGO, Issue 601, 2021, p. 19–34. http://voeikovmgo.ru/images/stories/publications/2021/%D0%A2%D1%80%D1%83%D0%B4%D1%8B%20%D0%93%D0%93%D0%9E,%20%D0%B2%D1%8B%D0%BF.%20601.pdf
140. Nikiforova, M.P., Vargin, P.N., Zvyagintsev, A.M. Ozone Anomalies over Russia in the Winter-Spring of 2015/2016. // Russian Meteorol. Hydrol. 2019, V.44, p. 23–32. https://doi.org/10.3103/S1068373919010035
141. Petkov B. H., Vitale V., Di Carlo P., Drofa O., Mastrangelo D., Smedley A. R. D., Solomatnikova A.A., Pavlova K. G. An unprecedented Arctic ozone depletion event during spring 2020 and its impacts across Europe. //Journal of Geophysical Research: Atmospheres, 2023, v.128, e2022JD037581 https://doi.org/10.1029/2022JD037581.
142. Bazhenov O.E. Ozone Anomaly during Winter–Spring 2019–2020 in the Arctic and over the North of Eurasia Using Satellite (Aura MLS/OMI) Observations // Atmospheric and Oceanic Optics, 2021, V. 34. No. 06. pp. 643–648. DOI: 10.15372/AOO20210706.
143. Tsvetkova, N.D., Vargin, P.N., Lukyanov, A.N., Kiryshov B.M., Yushkov V.A., Khattatov V.U. Studying Chemical Ozone Depletion and Dynamic Processes in the Arctic Stratosphere in the Winter 2019/2020. // Russian Meteorol. Hydrol. 2021, V. 46, p. 606–615. https://doi.org/10.3103/S1068373921090065.
144. Sitnov S.A., Mokhov I.I. Correlation of ozone mini-hole over Siberia in January 2016 with atmospheric blocking // Doklady AN. 2021. V. 500. No. 1. p. 90–95. DOI: 10.31857/S2686739721090176.
145. Vargin, P.N., Kiryushov, B.M. Major Sudden Stratospheric Warming in the Arctic in February 2018 and Its Impacts on the Troposphere, Mesosphere, and Ozone Layer. // Russian Meteorol. Hydrol. 2019, V.44, No. 2, p. 112–123. https://doi.org/10.3103/S1068373919020043
146. Krivolutskii, A.A., V'yushkova, T.Y., Cherepanova, L.A., Banin M.V., Repnev A.I., Kukoleva A.A., Numerical Global Models of the Ionosphere, Ozonosphere, Temperature Regime, and Circulation for Altitudes of 0–130 km: Results and Prospects. // Russian Meteorol. Hydrol. 2021, V. 46, No. 9, p. 596–605. https://doi.org/10.3103/S1068373921090053

147. Ivanova, N.S. A Statistical Model of Winter/Spring Polar Ozone. // Russian Meteorol. Hydrol. 2021. V. 46, No. 5, p. 295–301. https://doi.org/10.3103/S10683 73921050022.
148. Smyshlyaev S.P., Vargin P.N., Motsakov M. A. Numerical modeling of ozone loss in the exceptional Arctic stratosphere winter-spring of 2020 // Atmosphere, 2021, v.12, 1470. https://doi.org/10.3390/atmos12111470**.**
149. Lukyanov, A.N., Vargin, P.N., Yushkov V.A. Study of abnormally stable arctic stratospheric vortex observed in winter 2019/2020 with Lagrange methods// Izv. RAN. Fiz. Atmos. Okeana . 2021, V. 57, No. 3, p. 278–285.
150. Vargin P.N., Kostrykin S.V., Rakushina E.V., Volodin E.M., Pogoreltsev A.I. Study of variations of the date of spring restructuring of the stratospheric circulation and the volume of polar stratospheric clouds in the Arctic from model and reanalysis data // Izv. RAN. Fiz. Atmos. Okeana . 2020, V. 56, No. 5, p. 1–13.
151. Tsvetkova N.D., Vyzankin A.S., Vargin P.N., Lukyanov A.N., Yushkov V.A. Investigation and forecast of Sudden Stratospheric Warming events with chemistry climate model SOCOL // IOP Conf. Series, Earth Environmental Science. 2020, 606, 012062, doi:10.1088/1755-1315/606/1/012062.
152. Krivolutskii A.A., Vyushkova T.Yu., Banin M.V., Tolstykh M.A. Experimental global forecasts of atmospheric parameters based on experimental technology that takes into account ozone photochemistry (FOROZ model) // Geomagnetism i Aerologiya, 2020, No. 2, p. 250–260.
153. Vargin P.N.; Kostrykin S.V.; Volodin E.M.; Pogoreltsev A.I.; Wei K. Arctic Stratosphere Circulation Changes in the 21st Century in Simulations of INM CM5 // Atmosphere, 2022, *13*, 25. https://doi.org/10.3390/atmos13010025.
154. Muthers S., Anet J.G., Stenke A., Raible C.C., Rozanov E., Brönnimann S., Peter T., Arfeuille F.X., Shapiro A.I., Beer J., Steinhilber F., Brugnara Y., Schmutz W. The coupled atmosphere–chemistry–ocean model SOCOL-MPIOM // Geosci. Model Dev., 2014, v.7, p. 2157–2179, doi:10.5194/gmd-7-2157-2014.
155. Schmidt H., Brasseur G.P., Charron M., Manzini E., Giorgetta M.A., Diehl T., Fomichev V.I., Kinnison D., Marsh D., Walters S. The HAMMONIA Chemistry Climate Model: Sensitivity of the Mesopause Region to the 11- Year Solar Cycle and CO_2 Doubling // J. Climate, 2006, v. 19, 3903, https://doi.org/ 10.1175/JCLI3829.1.
156. Sukhodolov T., Egorova T., Stenke A., Ball W. T., Brodowsky C., Chiodo G., Feinberg A., Friedel M., Karagodin-Doyennel A., Peter T., Sedlacek J., Vattioni S., Rozanov E. Atmosphere-Ocean-Aerosol-Chemistry-Climate Model SOCOLv4.0: description and evaluation // Geosci. Model Dev., 2021, v. 14, p. 5525–5560, doi: 10.5194/gmd-14-5525-2021.
157. Karagodin-Doyennel A., Rozanov E., Sukhodolov T., Egorova T., Saiz-Lopez A., Cuevas C.A., Fernandez R.P., Sherwen, T. Volkamer R., Koenig T.K., Giroud T., Peter T. Iodine chemistry in the chemistry–climate model SOCOL-AERv2-I // Geosci. Model Dev., 2021, v.14, p.6623–6645,. doi: 10.5194/gmd-14-6623-2021.
158. Karagodin-Doyennel A., Rozanov E., Sukhodolov T., Egorova T., Sedlacek J., Ball W., Peter T. The historical ozone trends simulated with the SOCOLv4 and their comparison with observations and reanalyses // Atmospheric Chemistry and Physics, 2022, v. 22, N 23, p. 15333–15350. doi:10.5194/acp-22-15333-2022.

159. Karagodin-Doyennel A., Rozanov E., Sukhodolov T., Egorova T., Sedlacek J., Peter T., The future ozone trends in changing climate simulated with SOCOLv4, Atmospheric Chemistry and Physics Discuss., 2022. https://doi.org/10.5194/egusphere-2022-1260.
160. Egorova T., Sedlacek J., Sukhodolov T., Karagodin-Doyennel A., Zilker F., Rozanov E. Montreal Protocol's impact on the ozone layer and climate, Atmospheric Chemistry and Physics Discuss., 2022. https://doi.org/10.5194/acp-2022-730.
161. Pikulina P., Mironova I., Rozanov E., Karagodin A. September 2017 Solar Flares Effect on the Middle Atmosphere // Remote Sens., 2022, v. 14, 2560. doi:10.3390/rs14112560.
162. Mironova I., Sinnhuber M., Bazilevskaya G., Clilverd M., Funke B., Makhmutov V., Rozanov E., Santee M., Sukhodolov T., Ulich T. Exceptional middle latitude electron precipitation detected by balloon observations: implications for atmospheric composition // Atmos. Chem. Phys., 2022, v. 22, p. 6703–6716, 2022. doi:10.5194/acp-22-6703-2022.
163. Grankin D., Mironova I., Bazilevskaya G., Rozanov E., Egorova T. Atmospheric Response to EEP during Geomagnetic Disturbances // Atmosphere, 2023, v. 14, 273. https://doi.org/10.3390/atmos14020273.
164. Kulikov M.Yu., Nechaev A.A., Belikovich M.V., Vorobeva E.V., Grygalashvyly M., Sonnemann G.R., Feigin A. M. Boundary of nighttime ozone chemical equilibrium in the mesopause region from SABER data: Implications for derivation of atomic oxygen and atomic hydrogen // Geophysical Research Letters, 2019, v. 46, N 2, p. 997–1004. https://agupubs.onlinelibrary.wiley.com/doi/abs/10.1029/2018GL080364.
165. Belikovich M.V., Kulikov M.Y., Grygalashvyly M., Sonnemann G.R., Ermakova T.S., Nechaev A.A., Feigin A.M. Ozone chemical equilibrium in the extended mesopause under the nighttime conditions // Advances Space Research, v. 61, N 1, p. 426-432, 2018. https://doi.org/10.1016/j.asr.2017.10.010.
166. Kulikov M.Yu., Belikovich M.V., Grygalashvyly M., Sonnemann G.R., Ermakova T.S., Nechaev A.A., Feigin A.M. Nighttime ozone chemical equilibrium in the mesopause region // Journal of Geophysical Research Atmospheres, doi:10.1002/2017JD026717, 2018. https://agupubs.pericles-prod.literatumonline.com/doi/10.1002/2017JD026717 .
167. Manney G.L., Santee M.L., Froidevaux L., Hoppel K., Livesey N.J., Waters J.W. EOS MLS observations of ozone loss in the 2004–2005 Arctic winter // *Geophys. Res. Lett.*, 2006, v.33, L04802, doi:10.1029/2005GL024494.
168. Kulikov M.Yu., Belikovich M.V., Chubarov A.G., Dementeyva S.O., Fegin A.M., Boundary of nighttime ozone chemical equilibrium in the mesopause region: improved criterion of determining the boundary from satellite data // Advances in Space Research, 2023, V. 71, N 6, P. 2770–2780, https://doi.org/10.1016/j.asr.2022.11.005.
169. Kulikov M.Yu., Belikovich M.V. Nighttime O(^{1}D) distributions in the mesopause region derived from SABER data // Ann. Geophys., 38, 815–822, https://doi.org/10.5194/angeo-38-815-2020, 2020.
170. Kulikov M.Yu., Belikovich M.V., Fegin A.M. Analytical investigation of the reaction-diffusion waves in the mesopause photochemistry // Journal of Geophysical Research Atmospheres, 2020, v. 125, doi: 10.1029/2020JD033480. https://agupubs.pericles-prod.literatumonline.com/doi/10.1029/2020JD033480.

171. Kulikov M.Yu., Belikovich M.V., Grygalashvyly M., Sonnemann G.R., Fegin A.M. Retrieving daytime distributions of O, H, OH, HO2, and chemical heating rate in the mesopause region from satellite observations of ozone and OH* volume emission: The evaluation of the importance of the reaction $H+O_3$ ->O_2+OH in the ozone balance // Advances in Space Research, 2022, v. 69, N 9, p. 3362–3373. https://doi.org/10.1016/j.asr.2022.02.011.
172. Kulikov M.Y., Belikovich M.V., Grygalashvyly M., Sonnemann G.R., Fegin A.M. The revised method for retrieving daytime distributions of atomic oxygen and odd-hydrogens in the mesopause region from satellite observations // Earth Planets Space, 2022, v.74, 44. https://doi.org/10.1186/s40623-022-01603-8.
173. Kulikov M.Yu., Krasil'nikov A.A., Belikovich M.V., Ryskin V.G., Shvetsov A.A., Feigin A.M., High precision measurements of resonance frequency of ozone rotational transition J = $6_{1,5}$ – $6_{0,6}$ in the real atmosphere // Remote Sensing, 2023 (in press).
174. Shukurov K.A., Postylyakov O.V., Borovski A.N., Shukurova L.M., Gruzdev A.N., Elokhov A.S., Savinykh V.V., Mokhov I.I., Semenov V.A,. Chkhetiani O.G., Senik I.A. Study of transport of atmospheric admixtures and temperature anomalies using trajectory methods at the A.M. Obukhov Institute of Atmospheric Physics // IOP Conference Series: Earth and Environmental Science, 2019, v.231(1), 012048. https://doi.org/10.1088/1755-1315/231/1/012048.
175. Gruzdev A.N. Accounting for autocorrelation in the linear regression problem by an example of analysis of the atmospheric column NO_2 content // Izvestiya, Atmospheric and Oceanic Physics, 2019, v. 55, no 1, pp. 65–72. DOI: 10.1134/S0001433819010043.
176. Gruzdev A.N. Accounting for long-term serial correlation in a linear regression problem // IOP Conf. Ser. Earth Environ. Sci. 2019. V. 231. 012020. P. 1–10. doi:10.1088/1755-1315/231/1/012020. https://iopscience.iop.org/article/10.1088/1755-1315/231/1/012020/meta.
177. Stepanov E.V. Data parallel processing in block streams for analysis of long-term series of ozone content in ground atmosphere // Laser Phys., 2022, v. 32 No. 8 084011. https://doi.org/10.1088/1555-6611/ac7336
178. Nevzorov A.A., Nevzorov A.V., Kharchenko O.V., Makeev A.P. Development of mobile lidar system for monitoring of tropospheric ozone and aerosol // Proceedings of SPIE. 2022. V. 12341.
179. Belan B.D., Ivlev G.A., Kozlov A.V., Pestunov D.A., Sklyadneva T.K., Fofonov A.V. Solar radiation measurements at the Fonovaya observatory. Part I Methodical aspects and specifications . // Optika Atmosfery i Okeana. 2022. V. 35. No. 09. P. 759–765. DOI: 10.15372/AOO20220909 [in Russian]. DOI: 10.15372/AOO20220909.
180. Tentyukov M.P., Lyutoev V.P., Belan B.D., Simonenkov D.V., Golovataya O.S. Ultraviolet Radiation Detector Based on Artificial Periclase Nanocrystals (MgO) // Atmospheric and Oceanic Optics, 2022, Vol. 35, No. 1, pp. 89–96.
181. Iasenko E.A., Marugin A.M., Chelibanov V.P., Chelibanov I.V., Frank-Kamenetskaya O.V., Pinchuk O A. Chapter 8 Singlet Oxygen in the Lower Atmosphere: Origin, Measurement and Participation.// In Processes and Phenomena at the Boundary Between Biogenic and Abiogenic Nature. Springer Nature Switzerland AG, 2019, p. 137–153.
182. Larin I.K. History of Ozone (RAN, Moscow, 2022), 478 pp.

Planetary Atmospheres

O.I. Korablev
Space Research Institute RAS
korab@cosmos.ru

A review of the studies on planetary atmospheres performed by Russian scientists in 2019–2022 prepared in the Commission on planetary atmospheres of the National Geophysical Committee for the National Report on Meteorology and Atmospheric Science to the XXVIII General Assembly of the International Union of Geodesy and Geophysics is presented.

1. Introduction

The report of the Commission on planetary atmospheres of the National Geophysical Committee includes studies of planetary atmospheres completed in 2019–2022. This period of four years, longer than usual, was marked by massive publication of results from ESA-Roscosmos ExoMars Trace Gas Orbiter (TGO). Launched in October 2016, this spacecraft has orbited Mars and completed the aerobraking orbit-forming campaign in March 2018. Since then, it performs regular measurements related to Mars atmospheric composition and climate with the Russian-led instrument, the Atmospheric Chemistry Suite (ACS) (Korablev et al., 2018). Also, like before (Korablev 2016; 2020), many results were obtained from the analysis of data of European Mars Express and Venus Express spacecraft equipped with instruments with Russian participation. Mars Express remains operational during more than 19 years; the Venus Express spacecraft operated in 2006–2014 and its long data series continues to inspire new publications.

The report is based on the results related to neutral planetary atmospheres and planetary climates authored or co-authored by scientists affiliated with Russian institutions and published in the peer-reviewed literature. It follows the repartition by planets, and includes a brief account for spectroscopy related to planetary atmospheres. Recent advancements in detection and understanding the nature of extra-solar planets and their atmospheres often fall close to modelling of the solar system objects, the latter serving as well-studied reference (e.g., Forget et al. 2021). It is a new, rapidly developing branch of atmospheric science. Still, we considered not to discuss such studies in the report on Meteorology and Atmospheric Science at this moment.

The investigations related to atmospheric circulation and chemistry of Venus mesosphere are considered in Section 2; multiple studies of Mars' atmosphere, including water vapor and isotopic ratios measurements and their implications for escape, the atmospheric structure and circulation, at-

mospheric circulation and aerosols are combined in Section 3; few results on circulation and composition of Saturn, Titan and Pluto atmospheres are presented in Section 4; finally, a selection of findings and amendments in molecular spectroscopy related to or originated from the planetary atmospheres are summarized in Section 5.

2. Venus

2.1. Atmospheric circulation

The thick cloud layer of Venus rotates in the westward direction at approximately 100 m/s for the altitudes of 65–70 km (upper cloud level), a phenomenon known as retrograde superrotation (e.g., Imamura et al., 2020). Its analysis using tracking of cloud features at different altitudes has been continued. Khatuntsev et al (2022b) have analyzed ≥250,000 wind vectors derived from the visible (VIS) (513 nm) images captured by the Venus Monitoring Camera (VMC) onboard Venus Express. This spectral range corresponds to 60±3 km altitude level, in between the previously analyzed VMC datasets in the ultraviolet (UV) range (365 nm; 70 ± 2 km) and near-infrared (NIR) (965 nm; 55 ± 2 km) (Khatuntsev et al., 2013; 2017). At 60 km, middle and low clouds the mean zonal wind was decreasing from 76.5 to 61.5 m/s at 30°–65°S. The meridional wind was opposite to that derived from UV observations at the cloud top, an equatorward flow of up to 7 m/s.

The previous analysis of the UV (365 nm) VMC images was complemented with similar Akatsuki JAXA dataset. The joint analysis (Khatuntsev et al., 2022a) enabled characterization of the cloud top circulation over the period 2006–2021 with ~2.5-y gap between Venus Express and Akatsuki missions in 2014–2016. Over the equatorial latitudes (0–20°S) the annual mean zonal wind was −98.6 ± 1.3 m/s varying with the period of 12.5 ± 0.5 y and an amplitude of ~10. m/s. The mean meridional poleward wind was −2.3 ± 0.2 m/s, also varying with an amplitude of 3.4 ± 0.3 m/s. To explain the observed periodicity, Khatuntsev et al. (2022a) invoked correlated periodical changes in the UV albedo or the 11-y solar cycle. Both factors could influence the radiative balance; the solar cycle might also affect the mesospheric chemistry.

Observing near-infrared thermal emissions from the warmer atmosphere below clouds and surface on the nightside give access to the lowermost cloud layer. Gorinov et al. (2021) tracked the displacement of cloud features observed by Visible and InfraRed Thermal Imaging Spectrometer (VIRTIS-M) instrument in the spectral window of 1.74 μm to derive the wind speed at 44–48 km. Superrotation with a westward mean velocity of 60–63 m/s at 0–60°S latitudes was observed. Meridional component was significantly weaker 0–2 m/s; equatorward at ≥20°S and poleward at 0–20°S, with increasing wind speed.

Gubenko et al. (2021) analyzed small-scale (~1 km vertical length) fluctuations of the received signal from several radio-occultation profiles of Venera-15 and 16 spacecraft. The spectrum of the variations occurring above 61.5 km pointed to vertically propagating internal gravity waves. The intrinsic frequencies of these waves were (3.5–9.5) × 10^{-4} rad/s, and the ratio of horizontal to vertical wavelength was 21–57.

Summarizing, the cloud tracking provided data at four levels within the Venus' cloud layer, approximately 48 (1.74 μm), 55 (NIR), 60 (VIS) and 70 km (UV). The height difference between the VIS and NIR layers was changing during the mission. It was less than 1 km at the beginning of the mission (solar cycle minimum) and grow up to 8.5 km with the increasing solar activity. The motion of the observed cloud features can be associated with the atmosphere dynamics at these altitudes. The mean zonal flow (the superrotation speed) depends on local solar time and latitude and is affected by large-scale topography (Bertaux et al., 2016; Patsaeva et al., 2019; Khatuntsev et al., 2022a). The surface effect is most pronounced in the UV and NIR data. In the lowermost layer, no significant correlation with surface topography was seen. The meridional wind direction and speed can point to configuration of the cloud-level Hadley circulation, yet the available data still remains incomplete for formal description. In the south hemisphere, the poleward (direct) branch of the main cloud Hadley cell was observed at 70 km. The return branch was in the region of the lower cloud boundary (55 km), where the flow was directed towards the equator. In low latitudes, the 1.74-μm dataset might have probed a fragment of the poleward branch of the lower cloud Hadley cell.

2.2. Mesosphere composition and chemistry

Following the first detection of ozone (O_3) at 90–100 km on the nightside (Montmessin et al., 2011), Marcq et al (2019) reported another, permanent ozone layer on Venus from the analysis of the whole SPICAV-UV/Venus Express nadir dataset. Ozone was found at high latitudes (≥50° in both hemispheres) at the upper cloud level (70 km). The O_3 mixing ratio peaked at 10–20 ppbv, comparable to Mars values. Simulations using 3D-photochemical model (Lebonnois et al., 2010; called PCM since 2022) suggest that the observed ozone layer resulted from downward transport of O_2 molecules over the poles by the meridional circulation.

The same SPICAV-UV nadir dataset was reprocessed in order to retrieve SO_2 abundance at the cloud tops (70 km) through the duration of the Venus Express mission (2006–2014). This study confirmed and extended the previous analysis (Marcq et al., 2013). A large long-term variations of low-latitude SO_2, from ~100 ppbv (2007, 2009) to ≤ 10 ppbv (2014) were observed (see also Fig. 2 in Korablev 2016). The sulfur dioxide was depleted toward the

pole and near the sub-solar point, reflecting balance between advection and photo-chemical destruction. An enhancement of SO_2 and UV brightness above Aphrodite Terra, consistent with Bertaux et al. (2016) supply mechanism through orographic gravity waves was also noted. However, the observational selection might as well tie this result to the long-term variability.

Leveraging on improved calibrations of the SPICAV-UV stellar occultation dataset (Evdokimova et al., 2020), Evdokimova et al. (2021) retrieved vertical profiles of nighttime ozone and SO_2 through the mission lifetime. Following the discovery of the ozone layer in the mesosphere by Montmessin et al. (2011), 132 new detections over the 8-y observing period were reported. In the rare detections, the peak abundances of O_3 were 10^7 to 10^8 molec·cm^{-3} at 85–110 km. A mean ozone profile evolves from 10–30 ppbv at 85–90 km to ~100 ppbv at 100 km. The work also provided an improved sequel to the mesosphere sulfur dioxide survey by Belyaev et al. (2017). On average, the SO_2 content was 135 ± 21 ppbv between 85 and 100 km. Variations in individual profiles prevented from concluding on any time or space pattern of SO_2.

The photochemical modeling study by Pinto et al. (2021) targeted the abundance of SO dimers $(SO)_2$ in the upper atmosphere of Venus as a candidate component of the unknown ultraviolet absorber. The shape of the $(SO)_2$ spectral absorption fitted the unknown absorber, however their abundance was found to be insignificant. The photolysis and/or reaction products of the dimers were considered, such as S_2O, higher order S_nO species and polysulfur, S_n. All these species, in the aerosol or gas phase absorb in the range of interest. Prospects for identifying the ultraviolet absorber on Venus by different *in-situ* techniques on the future descent probes were discussed.

3. Mars

3.1. Water vapor and escape

The fate of water is a key issue in the history of Mars. Its losses as a result of photodissociation and subsequent dissipation of hydrogen depend on solar radiation from above and the rise of water from below. The higher the water molecule rises in the atmosphere, the more efficient the escape process is. Solar occultation observations of the Martian atmosphere by the Russian SPICAM IR and ACS instruments aboard the Mars Express and ExoMars TGO spacecraft, covering eight Martian years and two global dust storms (GDS), made it possible to study the distribution of water up to altitudes of 100–120 km (Fedorova et al., 2020; 2021; 2023; Belyaev et al., 2021).

The studied SPICAM/Mars Express dataset (2005 to March, 2019) covered eight Martian years (MY) from MY27 to MY35. Water vapor reached altitudes of 70–90 km during the southern summer (Ls = 240–300°; the peri-

helion season). In this season, years without GDS showed elevated water of ~100 ppmv in the southern hemisphere. The two observed GDS, in MY28 and MY34, differed regarding the water vapor response. The MY28 GDS, coincident with the southern summer solstice, created a larger water increase in both hemispheres at >80 km (Fedorova et al., 2021).

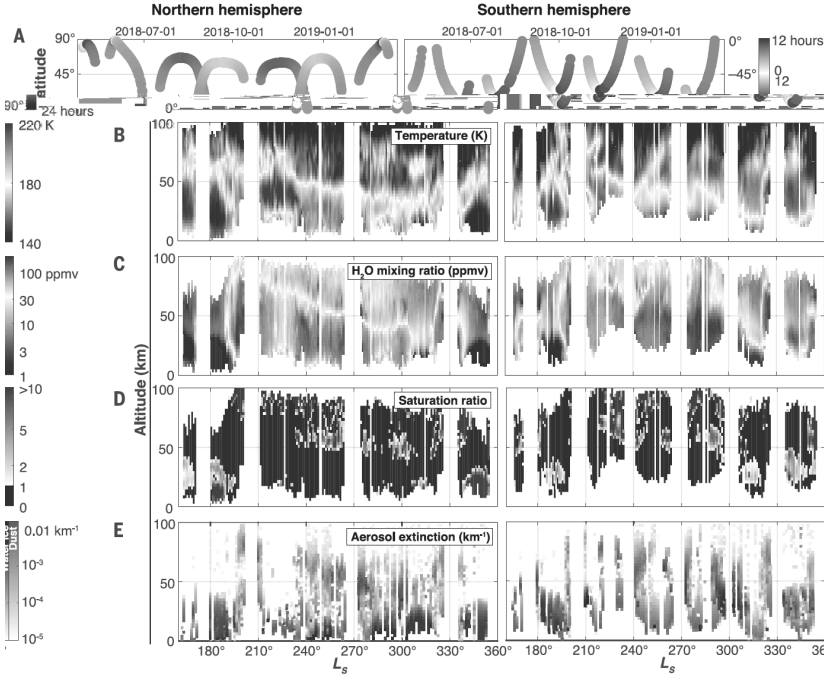

Fig. 3.1. Atmospheric properties' profiles (temperature, water vapor mixing ratio, saturation ratio, dust and cloud extinction) derived during the dusty season of MY34 from ACS/TGO occultation data. The latitudes and local time of occultations are shown in the upper panel (Figure from Fedorova et al., 2020)

The ACS dataset spanned two Martian years from Ls = 163° of MY34 to Ls = 170° of MY36. The profiles of water vapor, temperature profiles of the atmosphere, dust, and clouds were simultaneously retrieved. Using temperature derived from the CO_2 density in hydrostatic equilibrium Fedorova et al. (2020, 2023) has found a widespread and deep supersaturation of water vapor above aerosol layers, often observed simultaneously with clouds. In aphelion, the water mixing ratio above 40 km was below 3 ppmv and yet was found to be supersaturated. In perihelion, water was supersaturated above 60 km with a mixing ratio of 30–50 ppmv. Saturation varied between the evening and morning terminators in response to thermal tides. This ACS data set revealed

that supersaturation is nearly ubiquitous, particularly during the dust season, thereby promoting water escape on an annual average.

The solar occultation datasets are restricted to terminator, where specific temperature conditions could affect the saturation state. To understand supersaturation and water loss, a global distribution of water was investigated through an assimilation analysis unifying water, temperature and dust retrievals from several instruments on multiple spacecraft including ACS and the companion TGO instrument, NOMAD (Aoki et al., 2021) throughout MY 34 with a global circulation model (Holmes et al., 2022). During the dusty season of MY 34, they modeled substantial supersaturation above 60 km across all latitudes. Lower altitudes showed more diurnal variation resulting in discrete layers of supersaturation. Holmes et al. (2022) also found evidence of supersaturated water vapor breaking into the northern winter polar vortex. The MY34 GDS and southern summer regional dust storm forced water vapor at all latitudes in a supersaturated state up to 60–90 km where it is more likely to escape from the atmosphere.

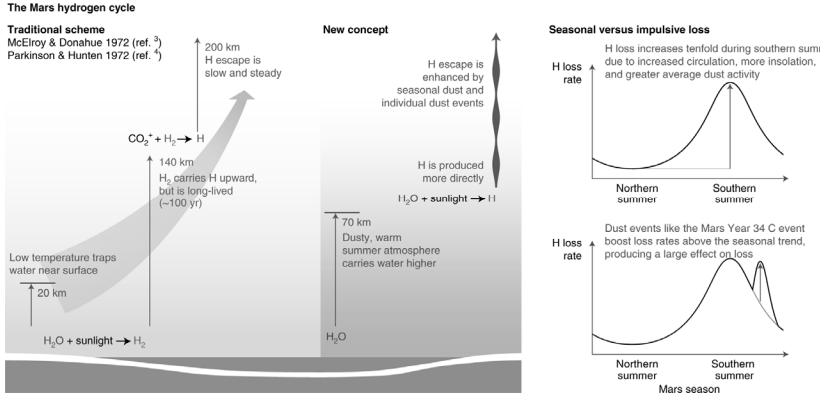

Fig. 3.2. A concept of direct supply of H to photodissociation altitudes by water vapor explaining the seasonally-modulated flux of escaping H (Figure from Chaffin et al., 2021)

Observations during multiple Martian years confirmed the effectiveness of dust storms in the rise of water and revealed that in the southern hemisphere, atmospheric water reaches high altitudes during the entire perihelion season. The efficiency of the dissociation process was confirmed for the first time by simultaneous observations of the hydrogen corona onboard the MAVEN spacecraft during a regional dust event (Chaffin et al., 2021). A gap in the TGO occultations during the peak of this regional dust event was filled using the general circulation model (GCM) with assimilation by Holmes et al. (2021).

Following previous SPICAM UV and HST observations of H Lyman-alpha (Chaffin et al., 2014) the new datasets confirm a new paradigm of H loss from Mars. In the traditional scheme, water vapor was assumed to be captured below the mesopause and H supply to the upper atmosphere was regulated by the slow diffusion of H_2. In the new paradigm for H loss (Fig. 3.2), seasonal or impulsive changes in dust and therefore the atmospheric temperature and circulation let water to high altitude where it can directly dissociate and boost escape.

Summarizing the above results, we may conclude that the cold tropopause region that prevents water from entering the upper atmosphere on the Earth does not really work on Mars, and water escapes from Mars easier than previously thought.

The discussed observations of H Lyman-alpha and the elevated water vapor have initiated multiple modelling efforts. Krasnopolsky (2019) used a 1D photochemical model of the neutral and ion composition at 80–300 km, with varying solar activity. They have found a hydrogen escape of $\approx 1.9 \times 10^8$ cm^{-2} s^{-1} at 250 km out of perihelion. The dayside-mean water abundances required to account for the observed high hydrogen escape up to 10^9 cm^{-2} s^{-1} in perihelion were $\leq$60 ppm at 80 km, in line with SPICAM IR observations. The photolysis of H_2O is the most effective at 160–180 nm and weakly depends on solar activity. The H_2O photolysis proceeds near 100 km, and just a small fraction of the resulting hydrogen can escape. The hydrogen escape flux at 250 km may be approximated as Φ_H (cm^{-2} s^{-1}) = $1.6 \times 10^8 + 1.4 \times 10^7 f_{H2O}$ (ppm), where f_{H2O} is the H_2O mixing ratio at 80 km.

Montmessin et al. (2021) have built a simplified 1D air parcel transport model to show that in addition to the formation of atomic hydrogen from water photolysis above 80 km, a major fraction of the exospheric hydrogen is formed at altitudes ~60 km and is then directly advected to the upper atmosphere. Comparing the injection of water from global dust storm, perihelion periods, and regional storm as documented by ACS observations (Belyaev et al., 2021), they conclude that on the long-term southern spring/summer the most efficiently controls H production and further ascent into the upper atmosphere.

Shaposhnikov et al. (2022a) employed the MAOAM GCM (also known as Max Planck Institute Mars GCM) to simulate Mars' hydrological cycle during the MY 28 and MY 34 dust storm seasons. Considering the water photodissociation at the Lyman-alpha wavelength, they noted the effect of dust storms on both the total water vapor content and its vertical distribution. The supply of water vapor into the upper atmosphere during dust storms results in intense photodissociation (up to 6.5 tons per second for the whole atmosphere). The photodissociation peaked at 50–80 km during the MY34 GDS

and 70–80 km in MY28. The model results were compared with ACS/TGO water profiles.

Shaposhnikov et al. (2019; 2021) have used the MAOAM GCM to investigate how the dynamics of the middle and upper atmosphere affects the water vapor rise. In the 2019 paper they have invoked the effect of the seasonal water "pump". In their simulation the upward branch of the meridional circulation located at perihelion above 60°S is particularly strong. There, a combination of the mean vertical flux and solar tides perturbations allowed water to penetrate through the mesopause minimum at approximately 60 km. The meridional circulation then transported water across the globe to the north. The intensity of the circulation was controlled by dust amount, and the water contents in the upper atmosphere strongly increased during dust events. Shaposhnikov et al. (2022b) further detailed the water "pump" mechanism by considering the gravity wave forcing. They found that molecular diffusion played little role in water transport in the middle atmosphere and across the mesopause and studied the effect of gravity waves during GDS and equinoxes.

One more study of Mars water vapor used Mars Express nadir datasets acquired in the near-IR (1.38 μm) and thermal IR (20–40 μm) spectral domains (Knutsen et al., 2022). The absorption by water vapor at these wavelengths is formed at different atmospheric levels and their joint analysis allows not only to decipher the total column abundance but to put constraints on the vertical distribution. The synergy can differentiate between the near-surface content below 5 km and the rest of the column. Overall, they have found that water was strongly confined near the surface, and not evenly mixed in the boundary layer. The retrieved distribution differed from the LMD Mars Climate Database (MCD) especially at low and middle latitudes where the synergy produced a stronger near-surface confinement. Current knowledge of the water distribution in the lowermost layer of the atmosphere is mainly based on GCMs, whereas significant discrepancies between MCD and the synergy indicated that the mechanisms shaping the vertical distribution are not completely understood.

3.2. Isotopic ratios and escape

Isotope ratios impose important constraints on the stability and evolution of planetary atmospheres: in the long term, they can point to total volatile losses, out of the atmospheric reservoir or other reservoirs exchanging with the atmosphere. On the other hand, the measured isotopic ratios are affected by the physical and chemical processes in the modern atmosphere (isotopic fractionation due to diffusion, condensation or photolysis). The isotopic abundances in the Martian atmosphere were mostly measured by means of ground-based spectroscopy. The deuterium to hydrogen (D/H) ratio is widely used to assess the past inventory of water on Mars and its evolution through

ages of the water cycle, yet the mechanisms controlling present-day HDO behavior are poorly understood. The ExoMars TGO spectrometers, observing solar occultations through the atmosphere with high spectral resolution, permitted the first profiling of water and CO_2 isotopologues, shedding light on the fractionation processes at different atmospheric levels.

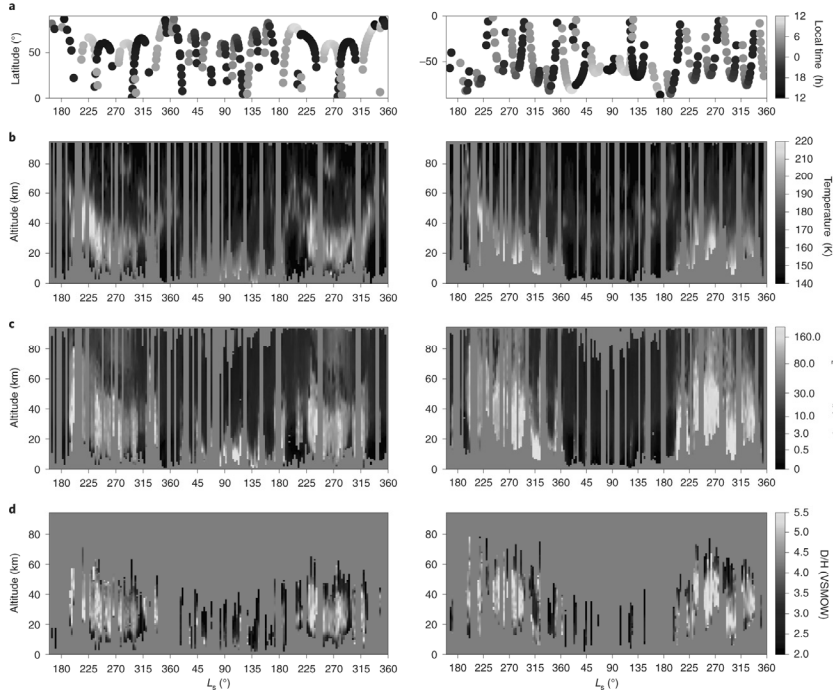

Fig. 3.3. Vertical profiles retrieved from ACS/TGO data in function of altitude and solar longitude for the northern (left) and southern (right) hemispheres:

a) latitudes and local time of solar occultation observations; b) atmospheric temperature; c) water vapor volume mixing ratio (VMR); d) D/H ratio in water vapor with uncertainties lower than 1 Vienna Standard Mean Ocean Water (VSMOW) (Figure from Alday et al. 2021a)

The first TGO publication on the HDO/H_2O ratio profile (Vandaele et al., 2019) described measurements of dust, water and semi-heavy water (HDO) at the onset of a MY34 GDS by NOMAD and ACS instruments onboard the ExoMars TGO. The vertical distribution of the HDO/H_2O ratio (D/H) was obtained from the planetary boundary layer up to ~80 km. One of the first, this publication documented an abrupt increase in the abundances of H_2O and HDO at 40–80 km resulting from warmer temperatures during the GDS (see Section 3.1). Analyzing a much longer ACS dataset, from the beginning of the TGO science observations (Ls=174° MY34) to the end of MY35,

Alday et al. (2021a) retrieved high-resolution HDO and H_2O profiles at 0–80 and 0–100 km, respectively. Combining the profiles with expected photolysis rates, they have found the prevalence of the perihelion season for the formation of atomic H and D at the escape altitudes. The have also established that, while condensation-induced fractionation is the main driver of variations of D/H in water vapor, the differential photolysis of HDO and H_2O is a more important factor in isotopic abundance of dissociated D and H. The results contribute to estimates of total water loss from Mars based on the ratio of deuterium to hydrogen.

Krasnopolsky (2021) observed latitudinal variations of the HDO/H_2O ratio in the Martian northern midsummer using CSHELL at NASA IRTF. The data for seven seasonal points are combined into a map of HDO/H_2O seasonal-latitudinal variations. The observation showed good correlation between HDO/H_2O and the mean temperature in the lowest scale height, that might be caused by the temperature-dependent isotope fractionation. However, the quantitative assessment of the correlation and its variations remain uncertain, the authors conclude that the HDO/H_2O variations across the Martian globe are too complicated to be described by unique activation energy.

Measurements of oxygen isotope ratios in H_2O are even more challenging given the weakness of the relevant spectral lines and high spectral resolution required to separate them within the dense H_2O absorption band. Yet they provide important constraints on the history of the Martian volatile system, reflecting several fractionation processes, such as atmospheric loss into space or interaction with the surface. The infrared measurements of the with the mid-infrared channel (MIR) of ACS/TGO enabled observation of several absorption lines of $H_2{}^{16}O$, $H_2{}^{18}O$, and $H_2{}^{17}O$, and, for the first time, the measurement of vertical profiles of the $^{18}O/^{16}O$ and $^{17}O/^{16}O$ ratios in atmospheric water vapor (Alday et al., 2019). The observed ratios were enriched as $\delta^{18}O = 200 \pm 80$‰ and $\delta^{17}O = 230 \pm 110$‰ wr.r.t. VSMOW. The vertical profiles of the ratios did not show any notable features.

The isotopic composition of O and C ratios in CO_2 were monitored between 70 and 130 km for more than half a Martian year using ACS/TGO solar occultations (Alday et al., 2021b). The vertical trends of the isotopic ratios were generally consistent with diffusive separation of isotopologues above the homopause, with Earth-like fractionation ($\delta^{13}C = -3 \pm 37$‰; $\delta^{18}O = -29 \pm 38$‰; and $\delta^{17}O = -11 \pm 41$‰) below. The authors suggested a lower limit to the escape of primordial C on Mars, ≥20%–40%. The total losses of C lost from the atmosphere, due to carbonate formation or other sinks, were certainly larger. Also, to explain the larger enrichment in the $^{18}O/^{16}O$ ratio in H_2O than in CO_2, they have invoked a photochemical transfer of light O from H_2O to CO_2.

The above observations, in particular the availability of the first vertically-resolved D/H profiles have initiated modelling efforts aimed on the refinement of the existing 3D global climate models. Significant variations of the D/H ratio over the globe, consisting of lower HDO/H_2O ratios in the colder regions and related to the condensation fractionation, were first predicted on the basis of a 3D global climate model (Montmessin et al, 2005) and later confirmed by ground-based observations (e.g., Krasnopolsky 2021). The Laboratoire de Météorologie Dynamique Mars Global Climate Model (LMD MGCM or PCM) was updated to include a detailed account for formation water ice clouds and an improved formulation of the fractionation by condensation (Vals et al., 2022). The simulations were compared with the ACS/TGO observations (Rossi et al., 2022) showing that the model well reproduced the temperature, water vapor and HDO fields (Fedorova et al., 2020; Alday et al., 2021a), offering a good basis for representing the D/H ratio cycle. The comparison also emphasized the importance of modeling the supersaturation state (see section 3.1), resulting from the microphysical processes of water ice clouds, to correctly account for the water vapor and the D/H ratio. Rossi et al. (2021) used the model to explore the impact of the MY34 GDS on HDO. Simulations showed that HDO is on average 40% more abundant at 100 km during the MY34 GDS year than during a regular year, with likely important consequences for the escape flux of water.

The following block of studies is related to thermosphere-to-exosphere transition atmosphere region boundary region and the oxygen escape. Shematovich (2021) considered the processes of formation, kinetics, and transport of suprathermal oxygen atoms during proton aurorae on Mars. According to the MAVEN observations, these aurorae are sporadic events induced by precipitation of energetic hydrogen atoms. To determine the sources of suprathermal oxygen atoms, Shematovich (2021) accounted for the penetration of protons into the daytime atmosphere due to charge exchange in the hydrogen corona (Shematovich et al., 2021). Collisions, as an additional source of hot oxygen atoms accompanied by the momentum and energy transfer from precipitating high-energy particles H/H^+ to atomic oxygen were also accounted for in a set of the Monte-Carlo kinetic models (Shematovich et al., 2019; Shematovich and Kalinicheva, 2020). The estimated losses of atomic oxygen during the proton aurorae were within $(3.5–5.8) \times 10^7$ cm^{-2} s^{-1}, comparable to the oxygen loss due to photochemical reactions. Therefore, the precipitation-induced flux of escaping hot oxygen atoms may become dominant during extreme solar events, solar flares or coronal mass ejections and play an important role in the atmospheric loss at the long time scales.

3.3. The Atmospheric Structure and Circulation

The ACS instrument onboard the ExoMars TGO has a capacity to monitor the temperature and density of Martian atmosphere in different infrared spectral ranges. The thermal infrared channel of ACS in honor of professor Vassilii Ivanovich Moroz (ACS TIRVIM) acquired nadir spectra in the spectral range 7.7–16.7 μm (600–1,300 cm^{-1}) from March 2018 to December 2019, covering almost a complete MY. An advantage of the TGO orbit is the capacity to resolve from nadir observations the diurnal cycle over a 54-sol period. Inversion of measured spectra, notably in the CO_2 15-μm band, permitted retrievals of vertical temperature profiles from the surface up to 60 km, surface temperatures and column aerosol optical depths (dust at ~9 μm and water ice at ~12 μm). Vlasov et al. (2022) reported the atmospheric thermal structure and the column dust content during the MY34 GDS, monitored at L_s = 182–212°. They captured the evolution of the GDS and the response of the atmospheric thermal structure to the changing dust loading. The storm caused asymmetric atmosphere heating, predominantly in the southern hemisphere, and changed diurnal contrast of thermal structure. A reduced diurnal contrast of surface temperatures at the peak of the GDS was also noted.

Guelret et al. (2021) described an alternative retrieval algorithm for the analysis of ACS TIRVIM spectra. Similarly, they retrieved vertical profile of atmospheric temperature up to 50 km, surface temperature, and integrated optical depth of dust and water ice clouds. They noted an ambiguity in estimation of the desired atmospheric quantities at different times of day: the 54-sol observation cycle mixed the diurnal signal with the seasonal changes. The retrieval algorithm was tested regarding its robustness and different sorts of biases, in particular, related to the aerosol retrieval. A cross-validation of retrieved atmospheric temperature and dust integrated opacity with thousands of collocated Mars Climate Sounder (MCS) profiles was performed. The found differences between TIRVIM and MCS temperatures were attributed to different vertical resolution of the methods. Daytime dust opacities from TIRVIM and MCS were well consistent, while TIRVIM often failed to produce the correct dust opacity over the cold surface (cases with low temperature contrast between the surface and the atmosphere).

Fan et al. (2022) used the atmospheric profiles resolved over full local time from Guerlet at al. (2021) to study the thermal tides in the Martian atmosphere. The data were selected near the northern summer solstice at Ls=75°–105° MY 35. Wave mode decomposition of the daily temperature anomalies showed a pronounced diurnal tide, important semi-diurnal tide and diurnal Kelvin wave, with maximal amplitudes of 5, 3, and 2.5 K, respectively, in the pressure range from tens to hundreds of Pa. The results generally

agreed with the LMD MGCM (PCM), but with noticeable earlier phases of diurnal (~1 hr) and semi-diurnal (~3 hr) tides.

Young et al. (2022) have used the ACS TIRVIM nadir dataset for assimilation into the Mars Planetary Climate Model. The assimilation period was Ls = 182°–211° MY34, covering the onset and peak of the 2018 GDS. First, they assimilated TIRVIM temperature profiles to update temperature and dust profiles, followed by dust column optical depths to update the total column dust abundance. Assimilation showed a reasonable agreement with in-sample TIRVIM observations, MCS/MRO temperature and dust profiles, and with the surface pressure diurnal cycle measured by Curiosity. The assimilation allowed for retrieval of winds. At the peak of the storm, the meridional circulation strengthened, an 125 m/s asymmetry developed in the midlatitude zonal jets, the diurnal tide weakened at the equator and strengthened to 10–15 K at midlatitudes, and the semi-diurnal tide strengthened everywhere.

Solar occultation spectroscopy in the CO_2 infrared absorption bands offers another source of pressure-temperature profiles. One way of obtaining the profile is to retrieve the CO2 number density profile and then derive the atmospheric profile hydrostatic approximation, as it was done by Alday et al. (2021a) with ACS/TGO spectra in the 2.7-μm range. More accurate estimation of the profile was used by Fedorova et al. (2020, 2023) in the 1.43-μm band and Belyaev et al. (2021; 2022) at 2.7 μm. In these studies, first the density profile was first derived from the absorption, simultaneously temperature was estimated from rotational structure of the CO_2 bands, to define pressure at the best-defined atmospheric level. This pressure serves to reconstruct the profile under the hydrostatic equilibrium assumption on the second step. The atmospheric mean molecular mass was taken from the Mars Climate Database (MCD 5.3).

Using a strong CO_2 absorption band near 2.7 μm observed by ACS MIR onboard TGO, Belyaev et al (2022) obtained the atmospheric thermal structure in an unprecedentedly large altitude range, from 20 to 180 km during 1.5 MY, from the middle of MY34 to the end of MY35. They presented the latitudinal and seasonal climatology of the thermal structure and studied the seasonal variation of the mesopause minimum (observed at 70 to 145 km) and homopause, changing from 90 to 100 km at aphelion to 120–130 km at perihelion. The homopause altitude was estimated assuming constant eddy mixing of 10^7 cm^2/s at 35 km.

Two studies have considered the impact of the MY 34 GDS on the dynamics of the Martian atmosphere via MGCM simulations relying on assimilation of the ACS temperature fields. Streeter et al. (2021) studied the behavior of polar vortices: powerful westerly jets isolating the cold polar from dust, water, and chemical tracers. They assimilated the MCS/MRO and ACS/TGO (Fedorova et al., 2020) temperature profiles into MGCM. The dust storm had

asymmetrical hemispherical impacts, with the southern vortex substantially diminished in its intensity. They concluded that the modification of vortex enhanced transport into Mars' southern and not northern polar region and modified transport of dust and chemical species over longitudes. Rajendran et al. (2021) modeled the effect of the MY 34 GDS on Mars superrotation. This phenomenon is crucial for understanding the atmospheric dynamics of slow-rotating planets such as Venus and Titan (see Sections 2.1 and 5). The Martian atmosphere is also a candidate for superrotation, in particular, dust-driven heating can excite a superrotating jet. In MGCM simulation with the same MCS and ACS temperature profiles assimilation. They found that superrotation increased by a factor of two at the peak of the GDS, as compared to the same period in the previous MY. This enhanced circulation was shown to have commenced 40 sols before the onset of the GDS. Strong eastern winds formed above 60 km, as a result of momentum transport by thermal tides due to dust lifting in the southern mid-latitudes and tropics.

3.4. Atmospheric Composition and Chemistry

Methane

The main findings of ACS/TGO regarding methane and detection of minor species were reviewed by Korablev (2021). Reports on the detection of methane in the Martian atmosphere motivated numerous studies aiming to confirm or explain its presence on a planet where it might imply a biogenic or geophysical origin. Overall, detections reported so far showed methane relative abundances ranging from 0.2 (SAM-TLS/Curiosity; Webster et al., 2018) to 45 ppbv (Earth-based; Mumma et al. 2009) and were characterized by strong variability. For Gale in particular, the picture of a crater hosting or traversed by intermittent methane releases combined with a continuous outgassing has emerged (e.g., Moores et al., 2019). However, no part of this global methane picture has been so far supported by TGO measurements.

With its spectral resolving power of $\lambda/\Delta\lambda \approx 30{,}000$ and signal-to-noise ratio for unattenuated spectra of $\geq$10,000, ACS MIR channel offers the best characteristics to detect minor gases in solar occultations. The first ACS MIR spectra in the wavelength range where the strongest methane features should be found (Fig. 3.4) lowered the upper limit to an order of magnitude below the SAM-TLS background values. The spectra showed faint absorption lines of water vapor and other atmospheric components (see below) but not the neighboring features of methane. The first ACS publication has established an upper limit of 0.05 ppbv (Korablev et al. 2019), followed by 0.06 ppbv according to the NOMAD/TGO (Knutsen et al. 2021). A more extensive ACS data set covering two Martian years MY34–35 resulted in an improved upper limit of 0.02 ppbv (Montmessin et al. 2021). The TGO measurements

in the vicinity of Gale Crater are assigned the highest priority; there ACS always operates and tuned to measure methane. Unfortunately, aerosols impede measurements at altitudes where the maximum sensitivity could be achieved. The most stringent upper limits were obtained at aphelion season when dust activity on Mars is minimal. Condensation clouds in the equatorial latitudes of Mars, where Curiosity measures, reduce the ability to constrain methane when observing solar occultations. The best upper limits established by ACS near Gale were 65–150 ppbv.

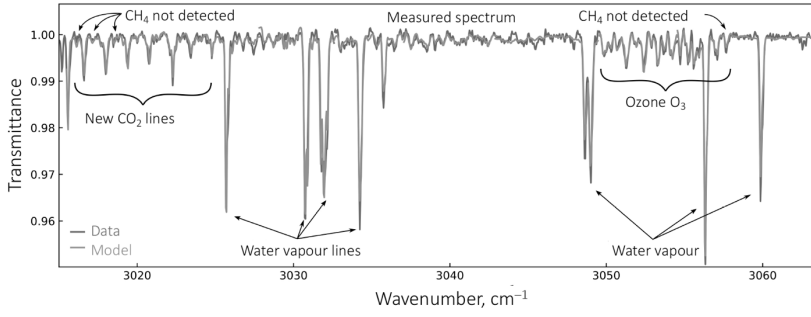

Fig. 3.4. An ACS MIR/TGO spectrum composed of several diffraction orders showing the absence of methane and newly detected lines of CO_2 and ozone. After Olsen et al. (2020), Trokhimovskiy et al. (2020). Credit ESA

The main difficulty of the methane problem lies in the apparent contradiction between the "background" level of methane, recorded by Curiosity, and the upper limits by TGO, an order of magnitude lower. With a lifetime of 100–300 years, methane must accumulate in the atmosphere, while atmospheric mixing must spread it in a few months. Assuming the Gale crater an only source on the planet, an implausible scenario, and only the background methane (0.41 ppbv), Korablev et al. (2019) estimated the accumulation time after which TGO should detect methane at 24 years. Accounting for multiple potential sources, the spikes recorded by Curiosity and other assets and the improved TGO upper limit makes the accumulation time even shorter. Mesoscale simulations of the dilution of seeping methane under the TGO constraints suggest that not only Gale is the single source on the planet, but a particular location of the putative source within the crater rim can solely explain the observed background and spikes (Webster et al., 2021; Luo et al., 2021). Another hypothesis (Moores et al. 2019) invoked a lowering of the planetary boundary layer at night (when SAM-TLS/curiosity measures), limiting mixing and leading to the accumulation of methane. The recent (MY35) daytime TLS measurements tend to confirm this inference (Webster et al., 2021). This scenario would increase the accumulation time of methane or the allowable seepage area. Still, to comply with the TGO upper limits, an as yet

unknown mechanism for the rapid methane destruction, which does not affect the reasonably well-established chemistry of other active species of the Martian atmosphere (CO, O_3, see below) is needed. Overall, the question of methane on Mars remains open.

Ozone and CO

Ozone (O_3) is an important indicator of the Martian atmospheric chemistry. Early measurements established that the atmosphere is remarkably deficient in dissociation products of CO_2 (CO, O_2, O_3, O), which is readily dissociated by sunlight at wavelengths ≤200 nm. The firts photochemical models found that the recombination of carbon dioxide is catalyzed by trace amounts of water, various forms of odd hydrogen (H, OH, HO_2). Yet, balancing the carbon dioxide production has proven difficult suggesting that heterogeneous chemistry could have an important impact on the composition of the Martian atmosphere. Modern, more sophisticated models (e.g., Daerden et al., 2019; Lefèvre et al., 2021) called for detailed observations of the Martian atmosphere, simultaneous and collocated measurements of dissociation products (O_3, CO) and water vapor. Such measurements were provided by SPICAM/Mars Express and ACS/TGO.

In the atmosphere of Mars, O_3 is produced by the CO_2 photolysis and destroyed by the hydrogen radicals (HO_x) released by the photolysis and oxidation of water vapor. As a result, an anti-correlation between ozone and water vapor is expected. Lefèvre et al. (2021) used the SPICAM/Mars Express simultaneous nadir observations of both species during four MY and compared the measurement against LMD MGCM with photochemistry (PCM). A distinct anti-correlation of O_3 and H_2O columns was found at high latitudes, while they were uncorrelated near the equator. The model with the gas-phase chemistry underpredicted the observed ozone by about a factor of 2, a bias which was not solved by including low-temperature CO_2 absorption cross sections, or adjusting kinetics rates. Taking into account heterogeneous processes of HO_x loss on ice clouds improved the match at high northern latitudes.

The SPICAM/Mars Express UV spectrometer performed both stellar and solar occultations during four MY with good spatial and seasonal coverage to obtain the vertical distribution of O_3 (Määttänen et al., 2022). Stellar occultations were performed in the nightside atmosphere, whereas solar occultations belong to terminator, enabling the study of the diurnal changes of this photochemically active species. The low- and midlatitude ozone layer forming during northern spring was mapped in both hemispheres and its night–terminator variations probed with the combination of stellar and solar occultations. The southern polar winter vortex showed hints of the mid-altitude ozone layer already seen in the SPICAM data previously. During the northern

polar spring, SPICAM observed the top of the lower atmosphere ozone layer above 10 km.

The lowermost part of the ozone profiles was systematically studied from the data of ACS MIR/TGO spectrometer, which registered the infrared absorption of O_3 at 3.3 μm as shown in Fig. 3.4, first reported by Olsen et al. (2020). A climatology of ozone profiles covering the second half of MY 34, all of MY 35, and the start of MY 36 was published by Olsen et al. (2022). Around the equinoxes in both hemispheres and over the southern winters, they regularly observed 200–500 ppbv of O_3 below 30 km. During the warm and wet southern summers, at perihelion, O_3 was not detectable. During the northern summers, water vapor was restricted to below 10 km, and an O_3 was seen at 20–30 km. A comparison to vertical profiles of water vapor and temperature confirmed the anticorrelation of H_2O and O_3. Comparing to LMD MGCM (PCM) showed the observed O_3 abundance larger by factor 2–6, indicating important differences in the rate of odd-hydrogen photochemistry. The lack of modeled ozone means that the HO_x-catalyzed photochemistry in simulations was found too efficient, in line with the long-standing underestimation of CO in Mars photochemical models. Similar difficulties occur when modeling O_3 and HO_x in the Earth's upper stratosphere and mesosphere.

The ACS/TGO reported the first CO altitude profiles. Carbon monoxide does not condense and its relative content changes as the main component (CO_2) seasonally condenses and sublimes into and from the polar caps. Photochemical production of CO is balanced by its loss reaction with OH, which recycles CO into CO_2. CO is therefore a sensitive tracer of the OH-catalyzed chemistry that contributes to the stability of CO_2. Before, only the vertically integrated column of CO has been measured, ignoring the upper atmosphere, where CO is produced. Profiling of CO by the MIR channel in the 2.35 μm band from 10 to 120 km before and during MY34 GDS showed a marked decrease in CO, indicating CO oxidation under wetter GDS conditions boosting OH abundance at high altitudes (Olsen et al., 2021a).

A full climatology of CO vertical profiles from 0 to 80 km was obtained in a weak NIR band at 1.6 μm (Fedorova et al., 2022). Seasonal and latitudinal changes in the altitudinal distribution of CO were studied for the first time. The following new features were observed: This study showed 1) an enriched CO layer at 10-20 km in the southern polar regions at the end of winter, indicating active processes of CO_2 condensation in these regions; 2) an increase in the relative content of 4–5 times above 50 km at the equinox, evidence of CO-enriched air transport; 3) reduction of CO during the MY34 GDS associated with the effect of water vapor on the CO loss rate and its conversion to CO_2. The mean CO content was ~950 ppmv, higher than Curiosity measurements and closer to other remote results.

The Hydrogen Chloride (HCl) Discovery and Other Trace Gases

For the first time since the methane detection, a new chemical species has been discovered in the atmosphere of Mars. Hydrogen chloride (HCl) was confidently identified by 12 lines in the ACS MIR spectrum (Fig. 3.5; Korablev et al. 2021). The detection was supported by NOMAD. Its relative content reaches four ppbv, significantly higher than upper limits previously established by the Earth-based and out-of-atmosphere astronomy (≤0.3 ppbv). The hydrogen chloride appeared after the global dust storm of MY34, while outside the dusty season, its content remained below 0.1 ppbv, resolving the apparent contradiction.

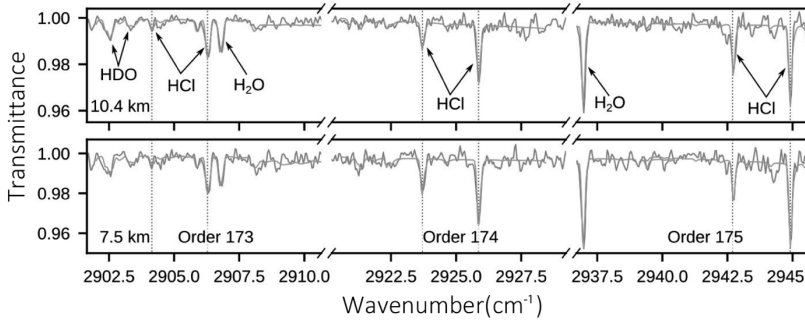

Fig. 3.5. ACS/TGO spectra at two tangent altitudes demonstrating the detection of HCl lines (adapted from Korablev et al. 2021)

Chlorine is abundant at the surface of Mars in the form of NaCl or perchlorates and is identified within the surface dust. Both forms can be lifted into the lower atmosphere during a dust storm, where they might serve as a source of Cl. Possible mechanisms for the HCl formation may include 1) gas-surface oxidation processing of the dust aerosols with the increase of oxidants such as OH and HO_2 during the GDS; 2) Chlorine release from dust via acidic oxidation, analogous to terrestrial processes; 3) mobilization of dust grains that have not been previously exposed to UV by saltation processes during the GDS; 4) volatilization of chloride minerals by electrical discharges in the dust storm.

Longer record of HCl monitoring by ACS, covering two perihelion seasons of MY34-35 (Olsen et al., 2021b) showed that HCl reappeared in similar quantities during the next Martian year MY35, although dust activity was much lower and no GDS was observed. Also, few trustable detections in aphelion (Ls = 120°, at low dust amount) challenge the correlation with dust and might even point to surface degassing. The NOMAD dataset showed a similar seasonal behavior but no aphelion detection (Aoki et al., 2021). From

the gas chemistry viewpoint, HCl should be a stable chlorine reservoir in the lower atmosphere of Mars (Krasnopolsky, 2022). The observed variability suggests an unexplained chemical or physical chlorine loss. Perhaps this is due to the absorption of HCl on the surface of water ice clouds, present throughout the dusty period, when HCl was observed (Luginin et al., 2020; see Section 3.5). Overall, the questions about the sources and sinks of HCl, as well as its role in the Martian atmosphere chemistry remains open calling for new laboratory research and model simulations needed to quantify the rate of formation and destruction of HCl. Peak HCl concentrations on Mars are comparable to those in the Earth's upper stratosphere and mesosphere. The ozone depletion cycle, well known in the Earth's stratosphere, would be effective on Mars as well. The discovery of hydrogen chloride suggests the photochemistry of Mars be revisited to account for new heterogeneous reactions.

The high fidelity of the collected spectra makes it possible to estimate the ratio of $H^{37}Cl$ and $H^{35}Cl$ isotopologues (Trokhimovskiy et al. 2021). Unlike for other volatiles on Mars, the $^{37}Cl/^{35}Cl$ ratio fell close to the terrestrial value. On average, the atmosphere of Mars may be slightly depleted in ^{37}Cl (–7±20‰), similarly to the Martian surface. This result confirmed the idea of the formation of HCl from chlorine-containing dust and suggested that the chlorine isotopes were not involved in any long-term surface-atmosphere cycle.

The ACS MIR high-resolution spectra in the range of 2.2–4.2 μm were checked for the presence of other yet undetected species on Mars. The search for sulfur-bearing gases, including SO_2, which might point to volcanic degassing (Braude et al., 2021) during MY34–35 was negative. The 1σ upper limits on their concentration established for the most optimal sensitivity conditions were $SO_2 \leq 20$ ppbv (2481–2492 cm^{-1} range), $H_2S \leq 15$ ppbv (3827–3833 cm^{-1}), and $OCS \leq 0.4$ ppbv (3460–3500 cm^{-1}), the latter notably improving the previous searches. Also, an upper limit for phosphine, whose claimed detection on Venus have recently attracted much attention and raised heated debates, was searched on Mars. The ACS spectral range includes several absorption lines of PH_3 with line strengths comparable to CH_4 lines. The signature of PH_3 in the range 2395–2406 cm^{-1} was not observed over one MY, with upper limits being 0.1–0.6 ppbv (Olsen et al., 2021c).

3.5. Dust and Clouds

In 2018, six orbiters and two rovers observed the most recent MY 34 global dust storm. Many studies dedicated to this enigmatic feature of Mars climate were gathered in a topical collection in JGR-Planets edited, among others, by A.A. Fedorova (Guzewich et al., 2020). The ACS/TGO datasets

have contributed to this effort by observing solar occultations with all channels the evolution of dust and water ice clouds profiles (Fedorova et al., 2020; see Fig. 3.1; Stcherbinine et al., 2020), determining the properties of dust and ice particles (Luginin et al., 2020) and by monitoring the development of the dust event in nadir by ACS TIRVIM (Vlasov et al., 2022).

Fedorova et al. (2020) have retrieved aerosol concentrations from ACS TIRVIM solar occultation data with addition, where available, of NIR and MIR channels data. Extinction profiles were obtained at 19 wavelengths in the overall spectral range 2–6 μm, outside of strong gas absorption bands. The characteristic 3-μm spectral band of water ice allows to disentangle the condensate clouds from the mineral dust and to constrain an intermediate case with a unimodal or bimodal distribution of the particle size (in Mie approximation). During the GDS, dust reached above 60 km, while clouds were observed up to 100 km, overlaying dust. The ACS MIR solar occultation spectra, including the 3-μm range where water ice absorbs, before and during the MY34 GDS were used by Stcherbinine et al. (2020). ACS MIR was sensitive to mean particle size ≤2 μm. They also note a shift in water ice cloud maximum altitudes from ~60 km before the GDS to above 90 km during the storm. At these extreme altitudes, small-sized (≤0.3 μm) particles were more frequent. Generally, particle size decreased with altitude. During the GDS, the presence of large water ice particles (≥1.5 μm) was noted at 50–70 km. Luginin et al. (2020) used a broader spectral range of 0.7–6 μm combining solar occultations by all three channels of ACS to constrain the particle size distribution for both types of aerosol. They have retrieved the effective radius, effective variance, number density, and mass loading through the GDS period. The effective radius of dust and water ice particles was within 0.1−3.5 μm and 0.1–5.5 μm, respectively. The largest aerosol particles (> 2.5 μm for dust and > 3.5 μm for water ice) were detected below 10 km before the onset and during the GDS decay phase. During the peak of the GDS, dust reached maximum altitudes of 85 km; the effective radius was 1–2 μm with 0.1–1 cm^{-3} number density and 0.1 effective variance. Detached layers of water ice 0.1–1 μm particles were often detected at 50–100 km. Below 50 km dust was mixed with ice. The above results suggested that GDS impacted significantly the formation and properties of high-altitude water ice clouds as compared to the usual perihelion dust activity.

Along with the atmospheric and surface temperature, Vlasov et al. (2022) have mapped the dust loading from the 9-μm silicate absorption band in ACS TIRVIM nadir spectra to track the development of the storm (Fig. 3.6). The maximum thermal IR optical depth exceeded 3 and the storm extended up to 60° both north and south.

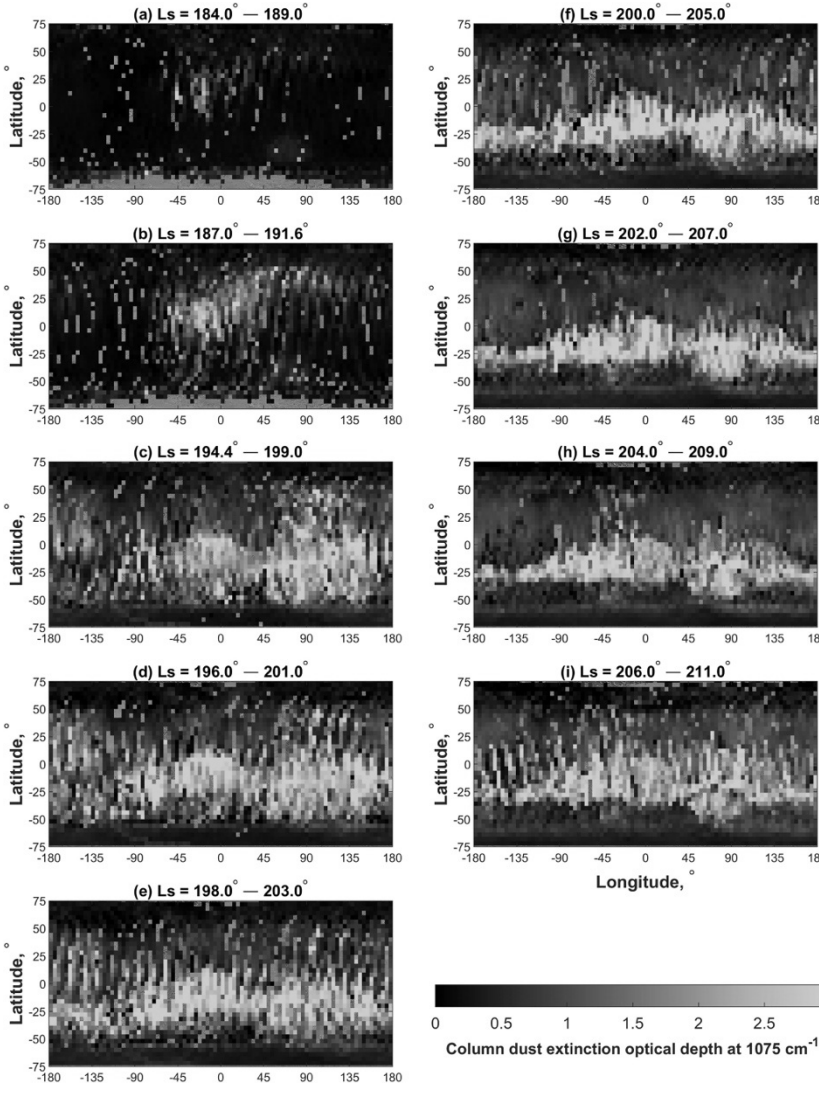

Fig. 3.6. The evolution of the global dust storm of MY 34 retrieved from ACS TIRVIM dataset. The diurnally averaged maps of column dust extinction optical depth at 1,075 cm^{-1} in nine 5° of Ls periods. (Figure from Vlasov et al., 2022)

Monitoring of aerosols over a longer period covering two MY was continued in follow-up papers on water vapor supersaturation and water ice clouds. Stcherbinine et al. (2022) have extended the analysis of ACS MIR data over the period from the beginning of the mission $L_s = 163°$ in MY 34

to $L_s = 180°$ in MY 36. A typical altitude of clouds varies between summer and winter by 20–40 km. During summer in the midlatitudes they extended up to 80 km. Using the latitude drift of solar occultations within certain campaigns, they found that clouds in the polar regions were generally by 20–40 km lower than in the midlatitudes. The MY 34GDS was also compared to the same season in MY 35, to find higher clouds during the GDS and a flattening of the latitudinal pattern. Comparison with PCM showed that the model underestimates the vertical extent of the cloud by 10–20 km. Fedorova et al. (2023) built dust and ice clouds optical depths profiles vs latitude to support the supersaturation study (see Section 3.1). The cross-sections were obtained following the same method as in Fedorova et al. (2020) for 30° of Ls bins from Ls=180° MY34 through the end of MY35.

A series of studies tackled the issue of dust devils on Mars, including theoretical assessment, lander's data interpretation and the statistical analysis. Kurgansky (2019) related the statistics of pressure drops observed by a surface meteorological station to the actual statistics of central pressure drops in convective vortices to provide an estimate of the distribution for the whole population of vortices. Application of this statistics to InSight data (Kurgansky 2021) revealed an unprecedentedly high number of convective vortices per km^2 at the InSight landing site. Kurgansky (2020) considered the radial extent of a convective vortex/dust devil from single-station pressure records to infer the whole size-frequency distribution of Curiosity-observed vortices. The theoretical foundations of the exponential and power-law analytical formulations for the size–frequency and intensity–frequency distributions of the convective vortices, and their application to Earth and Mars are discussed were studied by Kurgansky (2022). A relationship between the vortex diameter and the Obukhov length scale in the planetary boundary layer allowed to describe a burst of convective vortex activity observed at the InSight landing site in northern autumn. Izvekova et al. (2020) considered the hydrodynamic similarity of convective vortices in the terrestrial and Martian atmospheres.

4. Outer Planets

A general circulation model used previously for Venus was adapted for the atmosphere of Titan (Mingalev et al. 2019). The model is based on numerical integration with a fine spatial resolution of the complete system of gas dynamics equations. The relaxation approximation is used to calculate the rates of heating and cooling. The spatial resolution, a factor of 3–5 better than in previous Titan atmosphere models allowed to study mesoscale circulation details and various wave processes, in particular, internal gravity (buoyancy) waves (GW). A simulation of the Titan general circulation at equinox was analyzed.

In the study by Brown et al. (2022) the internal gravity waves in the Saturn's atmosphere were extracted using the method described for Mars (Section 3.3) from temperature profiles observed by Cassini UV spectrometer. An upward propagation of GW packets, their saturation, and breaking was observed. The analysis suggested that the GW drag induced equatorward flows facilitating transport of heat away from the auroral zones and redistributing energy across latitudes. The results help to explain why Saturn's (and the other outer planets') thermosphere is hotter than what follows from radiative balance.

Krasnopolsky (2020a) have adapted their previous model developed for the atmosphere and ionosphere of Titan to Pluto observed during the New Horizons mission fly-by. The input data were the surface pressure of 11.5 μbar and temperature profile from the radio and UV solar/stellar occultations. The model included over 400 reactions and extended up to exobase at 1600 km. The results include the effect of the dayside ionosphere on neutral composition, estimates of hydrogen and methane escape, condensation and polymerization of hydrocarbons and nitriles. Seasonal variations of methane found to alter the photochemistry of Pluto and Triton. A follow-up study (Krasnopolsky 2020b) aimed to bring the photochemical model into agreement with the detection of methylacetylene C_3H_4 and to develop on the $^{14}N/^{15}N$ ratio in HCN, whose much larger value $HC^{14}N/HC^{15}N > 125$ on Pluto looked puzzling compared to 60 on Titan. The analysis confirmed the predissociation of N_2 at 80–100 nm being the main process of nitrogen isotope fractionation. The observed twofold difference is partially caused by the diffusive depletion of the heavy isotope in HCN and in the predissociation of N_2. On Pluto, both processes occur well above the homopause at ~100 km, while on Titan $HC^{14}N/HC^{15}N$ wre observed at 100–500 km, the predissociation occurs ≤1000 km, both below the homopause at 1000 km, and diffusive depletion does not occur. Krasnopolsky (2020b) have also estimated the lifetime of N_2 in Pluto's atmosphere with the current loss primarily due to photodestruction. The calculated isotope fractionation in the N_2 ice accounts for the formation and condensation of nitriles, diffusive separation, and fractionation during thermal escape.

5. Spectroscopy Related to Planetary Atmospheres

A high-resolution spectroscopic observation of the Martian atmosphere, serving as a gigantic laboratory cell, helped to improve the knowledge of CO_2 spectroscopy. New absorbers discovered in the of ACS MIR spectra in the range used for methane search (2900–3300 cm^{-1}; see Section 3.4) and hindering the sensitive methane detections, were attributed to ozone (Olsen et al., 2020) and to CO_2 lines missing from spectroscopic databases (Trokhimovsky et al., 2020), see Fig. 3.4.

The frequencies of 30 observed lines coincided with the theoretically calculated P-, Q-, and R-branches of the magnetic dipole or electroquadrupole band of the main CO_2 isotopologue (Perevalov et al., 2021). This $\nu_2+\nu_3$ band, which is forbidden for electric dipole absorption, has never been observed before and has not been calculated numerically. The relative depth of the branches testified to its magnetic dipole nature (Trokhimovsky et al., 2020). The discovery of the forbidden system has initiated follow-up studies. Yachmenev et al. (2021) published more theoretical predictions for the electroquadrupole band and assigned a few weak features in the ACS MIR spectra. Borkov et al. (2021) measured the line intensities of the discovered band in the laboratory spectra to find values ~2 times smaller than those recovered from the Martian spectra. Similar measurements were completed by the Grenoble group (Fleurbaey et al., 2021), who have measured both the intensities of the magnetic dipole and electroquadrupole systems in the laboratory to find a good agreement with Borkov et al. (2021) regarding the magnetic dipole. Following these studies, the $\nu_2+\nu_3$ magnetic dipole system was included into the HITRAN 2020 edition (Karlovets et al., 2021; Gordon et al., 2022).

Considering vibrational magnetism in symmetric linear molecule, Kazakov and Vigasin (2021) questioned the magnetic-dipole nature of the band measured in the Mars atmosphere or in the laboratory, because its integrated intensity exceeded the theoretically expected value. Chistikov (2023) have resolved the controversy, attributing the excess intensity to the electroquadrupole system, many of whose lines overlap with those of magnetic dipole.

We shall also note multiple further improvements of HITRAN 2020 regarding planetary atmospheres, including line broadening parameters due to pressure of CO_2, H_2 and He, update of the collision-induced absorption (Karman et al., 2019; see also Finenko et al., 2022), amendment of ethane, phosphine, SO and other line lists of planetary significance, improvement of the high-temperature representation, etc.

More spectroscopic studies include Deichuli et al. (2022), who have measured H_2O near-IR line parameters in CO_2, the linelist already implemented for the Mars' atmospheric water analysis (Fedorova et al., 2023). Gamache et al. (2022) presented computation of internal vibrational and rotational partition functions needed for NLTE analysis of nine molecules that are often observed in NLTE conditions in planetary atmospheres: H_2O, CO_2, O_3, N_2O, CO, CH_4, NO, NO_2, and OH.

6. Conclusions

The studies of planetary atmospheres in the period 2019-2022 have largely benefited from the results of ExoMars TGO, Mars Express, Venus Express and Akatsuki space projects. A number of them, all led by Russian scientists,

have been marked as the most important yearly results of Space Research Institute (IKI) RAS or by The Science Council on Astronomy of RAS. We briefly list these results below, citing also some follow-up studies:

- Venus' atmospheric dynamics at multiple levels from Venus Express and Akatsuki multiwavelength observations (Patsaeva et al., 2019; Gorinov et al.,2021; Khatuntsev et al., 2022ab). The cloud tracking provided wind fields at four levels within the Venus' cloud layer, approximately 48, 55, 60 and 70 km. The height difference between the levels varied with latitude and was changing during the mission. The superrotation speed was found to depend on local solar time and latitude and reflect large-scale topography. The meridional wind direction and speed can point to configuration of the cloud-level Hadley circulation, yet the available data still remains incomplete for formal description. In the south hemisphere, the poleward (direct) branch of the main cloud Hadley cell was observed at 70 km. The return branch was in the region of the lower cloud boundary (55 km). In low latitudes, the 1.74-μm (48 km) dataset might have probed a fragment of the poleward branch of the lower cloud Hadley cell.
- Low upper limit on methane in the Martian atmosphere established from ExoMars TGO observations and contradicting to measurements at the surface by Curiosity (Korablev et al., 2019; Montmessin et al., 2021). From the ACS TGO observations the upper limit on methane was 0.02–0.05 ppbv, an order of magnitude below the SAM-TLS background values (0.48 ppbv average). The TGO solar occultations probe altitudes above 3–15 km, and the best upper limits are obtained in polar areas where the atmosphere is cleaner. Measurements in the vicinity of Gale Crater (near the equator) are impeded by aerosols and the bets upper limits near Gale were 65–150 ppbv. The atmospheric mixing time is within 1–3 months, while the methane lifetime is ≥300 y, so the methane should add up to be eventually detected by TGO. The only way to reconcile the two datasets is the yet undefined process of rapid methane destruction, which does not affect other reactive atmospheric species.
- Distribution and supersaturation of atmospheric water on Mars from ExoMars TGO and Mars Express observations and implications for water escape through the planet's history (Fedorova et al., 2020; 2021; 2023; Belyaev et al., 2021; Montmessin et al., 2022; Shaposhnikov et al., 2019; 2022). The loss of water on Mars is the result of its photodissociation followed by hydrogen dissipation into space. The higher the water molecule reaches in the atmosphere, the more efficient this process is. ACS TGO observations provided the first vertical distribution of water up to high altitudes (≤120 km). Simultaneous measurements of temperature, dust, and clouds allowed to study the water vapor saturation state. In the southern hemisphere,

water reached high altitudes during the entire perihelion season, including a global dust storm and a regional storm. Widespread supersaturation of water vapor, often observed simultaneously with clouds, has been detected. It means that the cold tropopause region that prevents water from entering the upper atmosphere on Earth does not work on Mars, and the dissipation of water from Mars goes easier than previously thought.

- Discovery and study of hydrogen chloride in the atmosphere of Mars from ExoMars TGO observations (Korablev et al., 2021; Olsen et al, 2021b; Trokhimovskiy et al., 2021). In the ACS TGO spectra, 12 hydrogen chloride (HCl) lines, a new gas in the Mars' atmosphere, were confidently identified. HCl was recorded in the amount of 1–4 ppbv during the MY 34 GDS, and gradually disappeared after it ended. Gas re-appeared during the next, 35 MY, although there was no global dust storm. Outside of the dusty season, upper limits were ≤0.1 ppbv, in agreement with previous ground-based and space observatory upper limits. HCl is produced annually during the dusty season, likely through heterogeneous reactions involving dust and water vapor. Sources on the surface are not excluded. Unlike for other gases, enriched in heavy isotopes due to atmospheric losses, the isotopic ratio $H^{37}Cl/H^{35}Cl$ was nearly terrestrial, suggesting that chlorine in HCl is not involved in any long-term surface-atmosphere process.
- Carbon monoxide (CO) distribution and chemistry, and the vertical structure of Mars' atmosphere from ExoMars TGO data (Olsen et al., 2021a; Fedorova et al., 2022; Belyaev et al, 2022, Starichenko yet al., 2021). ACS TGO measurements provided the first ever climatology of the vertical distribution of carbon monoxide (CO) in the Martian atmosphere. CO relative content changes as the main component of the Martian atmosphere (CO_2) condenses and sublimes seasonally. The following features were observed for the first time: 1) an enriched CO layer of 10-20 km in the southern polar regions at the end of winter, indicating active atmospheric condensation, 2) an increase in the relative content of 4–5 times above 50 km at the equinox, evidence of transport of CO-enriched air, 3) depletion of CO during the MY 34 GDS associated with elevated water vapor affecting the rate of CO loss and conversion to CO_2. The vertical distribution of density and temperature was retrieved in a record altitude range 10–180 km. Seasonal variations in the mesopause and homopause altitudes were obtained. For the first time, wave effects with a characteristic damping of the wave in the homopause region were revealed along the entire atmospheric column.

The ExoMars 2022 Rover-Surface Platform ESA-Roscosmos cooperation was terminated in 2022 following reasons unrelated to science or technical issues. It is a big loss for Russian space science and planetary meteorology in particular. The fate of Russian science instruments from this project is yet to be decided. On the positive side, the ExoMars TGO cooperation continues,

and the mission is expected to last long. In June 2023 the Mars Express mission shall celebrate its 20th anniversary and a series of papers summarizing its findings is being prepared at this moment. The Mars Express operations have been recently extended to 2026 with possible further prolongation. Beyond these two ongoing projects, there are no confirmed investigations in planetary atmospheric science before 2029–2031. These are the target launch dates for the ambitious Venera-D Roscosmos mission (Zasova et al., 2020), which includes an instrumented orbiter, a lander with a possibility to perform the atmospheric measurements during the descent down to the surface, and atmospheric floating probes targeting, among other goals, the assessment of the habitability of Venus' cloud layer (Limaye et al., 2021).

We thank all the authors that supported papers discussed within this report.

References

1. Alday J., Wilson C.F., Irwin P.G.J., et al. Oxygen isotopic ratios in Martian water vapour observed by ACS MIR on board the ExoMars Trace Gas Orbiter Astron. Astrophys. 630, A91 (2019) https://doi.org/10.1051/0004-6361/201936234
2. Alday J., Trokhimovskiy A., Irwin P.G.J., et al. Isotopic fractionation of water and its photolytic products in the atmosphere of Mars. Nature Astron. 5, 943 (2021a) https://doi.org/10.1038/s41550-021-01389-x
3. Alday J., Wilson C.F., Irwin P.G.J., et al. Isotopic Composition of CO2 in the Atmosphere of Mars: Fractionation by Diffusive Separation Observed by the ExoMars Trace Gas Orbiter J. Geophys. Res. (Planets) 126, e06992 (2021b) https://doi.org/10.1029/2021JE006992
4. Aoki S., Daerden F., Viscardy S., et al. Annual Appearance of Hydrogen Chloride on Mars and a Striking Similarity With the Water Vapor Vertical Distribution Observed by TGO/NOMAD Geophys. Res. Lett. 48, e92506 (2021) https://doi.org/10.1029/2021GL092506
5. Aoki S., Vandaele A. C., Daerden F., et al. Global Vertical Distribution of Water Vapor on Mars: Results From 3.5 Years of ExoMars-TGO/NOMAD Scienceence Operations J. Geophys. Res. (Planets) 127, e07231 (2022) https://doi.org/10.1029/2022JE007231
6. Belyaev D.A., Fedorova A.A., Trokhimovskiy A., et al. Revealing a High Water Abundance in the Upper Mesosphere of Mars With ACS Onboard TGO Geophys. Res. Lett. 48, e93411 (2021) https://doi.org/10.1029/2021GL093411
7. Belyaev D.A., Fedorova A.A., Trokhimovskiy A., et al. Thermal Structure of the Middle and Upper Atmosphere of Mars From ACS/TGO CO_2 Spectroscopy J. Geophys. Res. (Planets) 127, e2022JE007286 (2022) https://doi.org/10.1029/2022JE007286
8. Bertaux J.-L., Khatuntsev I.V., Hauchecorne A., et al. Influence of Venus topography on the zonal wind and UV albedo at cloud top level: The role of stationary gravity waves J. Geophys. Res. (Planets) 121, 1087 (2016) https://doi.org/10.1002/2015JE004958

9. Borkov Y.G., Solodov A.M., Solodov A.A., Perevalov V.I. Line intensities of the 01111-00001 magnetic dipole absorption band of 12C16O2: Laboratory measurements J. Molec. Spectr. 376, 111418 (2021) https://doi.org/10.1016/j.jms.2021.111418
10. Braude A.S., Montmessin F., Olsen K.S., et al. No detection of SO_2, H_2S, or OCS in the atmosphere of Mars from the first two Martian years of observations from TGO/ACS Astron. Astrophys. 658, A86 (2022) https://doi.org/10.1051/0004-6361/202142390
11. Brown Z.L., Medvedev A.S., Starichenko E.D., et al. Evidence for Gravity Waves in the Thermosphere of Saturn and Implications for Global Circulation Geophys. Res. Lett. 49, e97219 (2022) https://doi.org/10.1029/2021GL097219
12. Chaffin M.S., Chaufray J.-Y., Stewart I., et al. Unexpected variability of Martian hydrogen escape Geophys. Res. Lett. 41, 314 (2014) https://doi.org/10.1002/2013GL058578
13. Chaffin M.S., Kass D.M., Aoki S., et al. Martian water loss to space enhanced by regional dust storms. Nature Astron. 5, 1036 (2021) https://doi.org/10.1038/s41550-021-01425-w
14. Chistikov D.N. Magnetic dipole and quadrupole transitions in the ν2 + ν3 vibrational band of carbon dioxide, J. Chem. Phys. 158, 134307 (2023) https://doi.org/10.1063/5.0144201
15. Daerden F., Neary L., Viscardy S., et al. Mars atmospheric chemistry simulations with the GEM-Mars general circulation model Icarus 326, 197 (2019) https://doi.org/10.1016/j.icarus.2019.02.030
16. Deichuli V.M., Petrova T.M., Solodov A.M., et al. Water vapor absorption line parameters in the 6760-7430 cm-1 region for application to CO_2-rich planetary atmosphere J. Quant. Spectr. Rad. Transf. 293, 108386 (2022) https://doi.org/10.1016/j.jqsrt.2022.108386
17. Evdokimova D., Belyaev D., Montmessin F., et al. Improved calibrations of the stellar occultation data accumulated by the SPICAV UV onboard Venus Express P&SS 184, 104868 (2020) https://doi.org/10.1016/j.pss.2020.104868
18. Evdokimova D., Belyaev D., Montmessin F., et al. The Spatial and Temporal Distribution of Nighttime Ozone and Sulfur Dioxide in the Venus Mesosphere as Deduced From SPICAV UV Stellar Occultations J. Geophys. Res. (Planets) 126, e06625 (2021) https://doi.org/10.1029/2020JE006625
19. Fan S., Guerlet S., Forget F., et al. Thermal Tides in the Martian Atmosphere Near Northern Summer Solstice Observed by ACS/TIRVIM Onboard TGO Geophys. Res. Lett. 49, e97130 (2022) https://doi.org/10.1029/2021GL097130
20. Fedorova A.A., Montmessin F., Korablev O., et al. Stormy water on Mars: The distribution and saturation of atmospheric water during the dusty season Science 367, 297 (2020) https://doi.org/10.1126/science.aay9522
21. Fedorova A., Montmessin F., Korablev O., et al. Multi-Annual Monitoring of the Water Vapor Vertical Distribution on Mars by SPICAM on Mars Express J. Geophys. Res. (Planets) 126, e06616 (2021) https://doi.org/10.1029/2020JE006616
22. Fedorova A., Montmessin F., Trokhimovskiy A., et al. A Two-Martian Years Survey of the Water Vapor Saturation State on Mars Based on ACS NIR/TGO Occultations J. Geophys. Res. (Planets) 128, e2022JE007348 (2023) https://doi.org/10.1029/2022JE007348

23. Fedorova A., Trokhimovskiy A., Lefèvre F., et al. Climatology of the CO Vertical Distribution on Mars Based on ACS TGO Measurements J. Geophys. Res. (Planets) 127, e07195 (2022) https://doi.org/10.1029/2022JE007195
24. Fleurbaey H., Grilli R., Mondelain D., Kassi S., Yachmenev A., Yurchenko S.N., Campargue A., Electric-quadrupole and magnetic-dipole contributions to the ν2+ ν3 band of carbon dioxide near 3.3 μm. J. Quant. Spectrosc. Radiat. Transfer 266, 107558 (2021). https://doi.org/10.1016/j.jqsrt.2021.107558
25. Forget F., Korablev O., Venturini J., et al. Editorial: Topical Collection on Understanding the Diversity of Planetary Atmospheres Space Sci. Rev. 217, 51 (2021) https://doi.org/10.1007/s11214-021-00820-z
26. Gamache R. R., Vispoel B., Rey M., et al. Partition sums for non-local thermodynamic equilibrium conditions for nine molecules of importance in planetary atmospheres Icarus 378, 114947 (2022) https://doi.org/10.1016/j.icarus.2022.114947
27. Gordon I.E., Rothman L.S., Hargreaves R.J., et al. The HITRAN2020 molecular spectroscopic database J. Quant. Spectr. Rad. Transf. 277, 107949 (2022) https://doi.org/10.1016/j.jqsrt.2021.107949
28. Gorinov D.A., Zasova L.V., Khatuntsev I.V., et al. Winds in the Lower Cloud Level on the Nightside of Venus from VIRTIS-M (Venus Express) 1.74 μm Images. Atmosphere 12, 186 (2021) https://doi.org/10.3390/atmos12020186
29. Gubenko V.N., Kirillovich I.A., Gubenko D.V., et al. Activity of Small-Scale Internal Waves in the Northern Polar Atmosphere of Venus by Radio Occultation Measurements of Signal Intensity (Λ = 32 cm) from Venera-15 and -16 Satellites Solar Syst. Res. 55, 1 (2021) https://doi.org/10.1134/S0038094621010044
30. Guerlet S., Ignatiev N., Forget F., et al. Thermal Structure and Aerosols in Mars' Atmosphere From TIRVIM/ACS Onboard the ExoMars Trace Gas Orbiter: Validation of the Retrieval Algorithm J. Geophys. Res. (Planets) 127, e07062 (2022) https://doi.org/10.1029/2021JE007062
31. Guzewich S. D., Fedorova A. A., Kahre M. A., Toigo A. D. Studies of the 2018/Mars Year 34 Planet-Encircling Dust Storm J. Geophys. Res. (Planets) 125, e06700 (2020) https://doi.org/10.1029/2020JE006700
32. Holmes J.A., Lewis S.R., Patel M.R., et al. Enhanced water loss from the martian atmosphere during a regional-scale dust storm and implications for long-term water loss Earth Planet. Sci. Lett. 571, 117109 (2021) https://doi.org/10.1016/j.epsl.2021.117109
33. Holmes J.A., Lewis S.R., Patel M.R., et al. Global Variations in Water Vapor and Saturation State Throughout the Mars Year 34 Dusty Season J. Geophys. Res. (Planets) 127, e2022JE007203 (2022) https://doi.org/10.1029/2022JE007203
34. Imamura T., Mitchell J., Lebonnois S., et al. Superrotation in Planetary Atmospheres Space Sci. Rev. 216, 87 (2020) https://doi.org/10.1007/s11214-020-00703-9
35. Izvekova Y.N., Popel' S.I., Izvekov O.Y. On the Question of Calculating the Parameters of Vortices in the Near-Surface Atmosphere of Mars. Solar Syst. Res. 53, 423 (2020) https://doi.org/10.1134/S0038094619050058
36. Karlovets E.V., Gordon I.E., Rothman L.S., et al. The update of the line positions and intensities in the line list of carbon dioxide for the HITRAN2020 spec-

troscopic database J. Quant. Spectr. Rad. Transf. 276, 107896 (2021) https://doi.org/10.1016/j.jqsrt.2021.107896
37. Karman T., Gordon I.E., van der Avoird A., et al. Update of the HITRAN collision-induced absorption section Icarus 328, 160 (2019) https://doi.org/10.1016/j.icarus.2019.02.034
38. Kazakov K.V., Vigasin A.A. Vibrational magnetism and the strength of magnetic dipole transition within the electric dipole forbidden v2 + v3 absorption band of carbon dioxide, Molec. Phys. 119:12 (2021) https://doi.org/10.1080/00268976.2021.1934581
39. Khatuntsev I.V., Patsaeva M.V., Titov D.V., et al. Cloud level winds from the Venus Express Monitoring Camera imaging Icarus 226, 140 (2013) https://doi.org/10.1016/j.icarus.2013.05.018
40. Khatuntsev I.V., Patsaeva M.V., Titov D.V., et al. Twelve-Year Cycle in the Cloud Top Winds Derived from VMC/Venus Express and UVI/Akatsuki Imaging. Atmosphere 13, 2023 (2022b) https://doi.org/10.3390/atmos13122023
41. Khatuntsev I.V., Patsaeva M.V., Titov D.V., et al. Winds in the Middle Cloud Deck From the Near-IR Imaging by the Venus Monitoring Camera Onboard Venus Express J. Geophys. Res. (Planets) 122, 2312 (2017) https://doi.org/10.1002/2017JE005355
42. Khatuntsev I.V., Patsaeva M.V., Zasova L.V., et al. Winds From the Visible (513 nm) Images Obtained by the Venus Monitoring Camera Onboard Venus Express J. Geophys. Res. (Planets) 127, e07032 (2022a) https://doi.org/10.1029/2021JE007032
43. Knutsen E.W., Montmessin F., Verdier L., et al. Water Vapor on Mars: A Refined Climatology and Constraints on the Near-Surface Concentration Enabled by Synergistic Retrievals J. Geophys. Res. (Planets) 127, e07252 (2022) https://doi.org/10.1029/2022JE007252
44. Knutsen E.W., Villanueva G.L., Liuzzi G., et al. Comprehensive investigation of Mars methane and organics with ExoMars/NOMAD Icarus 357, 114266 (2021) https://doi.org/10.1016/j.icarus.2020.114266
45. Korablev O.I. Studies of planetary atmospheres in Russia (2011–2014). Izv. Atmos. Ocean. Phys. 52, 483–496 (2016). https://doi.org/10.1134/S0001433816050066
46. Korablev O.I. Studies of Planetary Atmospheres in Russia (2015-2018) Izv. Atmos. Ocean. Phys. 56, 130 (2020) https://doi.org/10.1134/S0001433820020061
47. Korablev O.I. Trace species in planetary atmospheres: Some results of TGO ExoMars Astron. Astrophys.T 32, 289 (2021)
48. Korablev O., Montmessin F., Trokhimovskiy A., et al. The Atmospheric Chemistry Suite (ACS) of Three Spectrometers for the ExoMars 2016 Trace Gas Orbiter Space Sci. Rev. 214, 7 (2018) https://doi.org/10.1007/s11214-017-0437-6
49. Korablev O., Olsen K. S., Trokhimovskiy A., et al. Transient HCl in the atmosphere of Mars Science Advances 7, eabe4386 (2021) https://doi.org/10.1126/sciadv.abe4386
50. Korablev O., Vandaele A. C., Montmessin F., et al. No detection of methane on Mars from early ExoMars Trace Gas Orbiter observations Nature 568, 517 (2019) https://doi.org/10.1038/s41586-019-1096-4

51. Krasnopolsky V.A. Photochemistry of water in the martian thermosphere and its effect on hydrogen escape Icarus 321, 62 (2019) https://doi.org/10.1016/j.icarus.2018.10.033
52. Krasnopolsky V.A. A photochemical model of Pluto's atmosphere and ionosphere Icarus 335, 113374 (2020a) https://doi.org/10.1016/j.icarus.2019.07.008
53. Krasnopolsky V.A. On the methylacetylene abundance and nitrogen isotope ratio in Pluto's atmosphere P&SS 192, 105044 (2020b) https://doi.org/10.1016/j.pss.2020.105044
54. Krasnopolsky V.A. Photochemistry of HCl in the martian atmosphere Icarusus 374, 114807 (2022) https://doi.org/10.1016/j.icarus.2021.114807
55. Krasnopolsky V.A. Seasonal and latitudinal variations of the HDO/H2O ratio in the martian atmosphere P&SS 208, 105345 (2021) https://doi.org/10.1016/j.pss.2021.105345
56. Kurgansky M.V. On the statistical distribution of pressure drops in convective vortices: Applications to Martian dust devils Icarus 317, 209 (2019) https://doi.org/10.1016/j.icarus.2018.08.004
57. Kurgansky M.V. On determination of the size-frequency distribution of convective vortices in pressure time-series surveys on Mars Icarus 335, 113389 (2020) https://doi.org/10.1016/j.icarus.2019.113389
58. Kurgansky M.V. An estimate of convective vortex activity at the InSight landing site on Mars Icarusus 358, 114200 (2021) https://doi.org/10.1016/j.icarus.2020.114200
59. Kurgansky M.V. Statistical Distribution of Atmospheric Dust Devils on Earth and Mars Boundary-Layer Meteorology 184, 381 (2022) https://doi.org/10.1007/s10546-022-00713-w
60. Lebonnois S., Hourdin F., Eymet V., et al. Superrotation of Venus' atmosphere analyzed with a full general circulation model J. Geophys. Res. (Planets) 115, E06006 (2010) https://doi.org/10.1029/2009JE003458
61. Lefèvre F., Trokhimovskiy A., Fedorova A., et al. Relationship Between the Ozone and Water Vapor Columns on Mars as Observed by SPICAM and Calculated by a Global Climate Model J. Geophys. Res. (Planets) 126, e06838 (2021) https://doi.org/10.1029/2021JE006838
62. Limaye S. S., Zelenyi L., Zasova L. Introducing the Venus Collection – Papers from the First Workshop on Habitability of the Cloud Layer Astrobiology 21, 1157 (2021) https://doi.org/10.1089/ast.2021.0142
63. Luginin M., Fedorova A., Ignatiev N., et al. Properties of Water Ice and Dust Particles in the Atmosphere of Mars During the 2018 Global Dust Storm as Inferred From the Atmospheric Chemistry Suite J. Geophys. Res. (Planets) 125, e06419 (2020) https://doi.org/10.1029/2020JE006419
64. Luo Y., Mischna M.A., Lin J.C., et al. Mars Methane Sources in Northwestern Gale Crater Inferred From Back Trajectory Modeling Earth Space Sci. 8, e01915 (2021) https://doi.org/10.1029/2021EA001915
65. Määttänen A., Lefèvre F., Verdier L., et al. Ozone vertical distribution in Mars Years 27-30 from SPICAM/MEX UV occultations Icarus 387, 115162 (2022) https://doi.org/10.1016/j.icarus.2022.115162
66. Marcq E., Baggio L., Lefèvre F., et al. Discovery of cloud top ozone on Venus Icarus 319, 491 (2019) https://doi.org/10.1016/j.icarus.2018.10.006

67. Marcq E., Lea Jessup K., Baggio L., et al. Climatology of SO2 and UV absorber at Venus' cloud top from SPICAV-UV nadir dataset Icarus 335, 113368 (2020) https://doi.org/10.1016/j.icarus.2019.07.002
68. Mingalev I.V., Rodin A.V., Orlov K.G. Numerical Modeling of the General Circulation of the Atmosphere of Titan at Equinox Solar Syst. Res. 53, 278 (2019) https://doi.org/10.1134/S0038094619040051
69. Montmessin, F., Fouchet, T., & Forget, F. Modeling the annual cycle of HDO in the Martian atmosphere. Journal of Geophysical Research 110(E3), E10004 (2005). https://doi.org/10.1029/2004JE002357
70. Montmessin F., Bertaux J.-L., Lefèvre F., et al. A layer of ozone detected in the nightside upper atmosphere of Venus Icarus 216, 82 (2011) https://doi.org/10.1016/j.icarus.2011.08.010
71. Montmessin F., Korablev O.I., Trokhimovskiy A., et al. A stringent upper limit of 20 pptv for methane on Mars and constraints on its dispersion outside Gale crater Astron. Astrophys. 650, A140 (2021) https://doi.org/10.1051/0004-6361/202140389
72. Montmessin F., Belyaev D.A., Lefèvre F., et al. Reappraising the Production and Transfer of Hydrogen Atoms From the Middle to the Upper Atmosphere of Mars at Times of Elevated Water Vapor J. Geophys. Res. (Planets) 127, e07217 (2022) https://doi.org/10.1029/2022JE007217
73. Moores J.E., King P.L., Smith C.L., et al. The Methane Diurnal Variation and Microseepage Flux at Gale Crater, Mars as Constrained by the ExoMars Trace Gas Orbiter and Curiosity Observations Geophys. Res. Lett. 46, 9430 (2019) https://doi.org/10.1029/2019GL083800
74. Mumma M.J., Villanueva G.L., Novak R.E., et al. Strong Release of Methane on Mars in Northern Summer 2003 Science 323, 1041 (2009) https://doi.org/10.1126/science.1165243
75. Olsen K.S., Lefèvre F., Montmessin F., et al. First detection of ozone in the mid-infrared at Mars: implications for methane detection Astron. Astrophys. 639, A141 (2020) https://doi.org/10.1051/0004-6361/202038125
76. Olsen K.S., Lefèvre F., Montmessin F., et al. The vertical structure of CO in the Martian atmosphere from the ExoMars Trace Gas Orbiter Natue Geosci. 14, 67 (2021a) https://doi.org/10.1038/s41561-020-00678-w
77. Olsen K.S., Trokhimovskiy A., Montabone L., et al. Seasonal reappearance of HCl in the atmosphere of Mars during the Mars year 35 dusty season Astron. Astrophys. 647, A161 (2021b) https://doi.org/10.1051/0004-6361/202140329
78. Olsen K.S., Trokhimovskiy A., Braude A.S., et al. Upper limits for phosphine (PH3) in the atmosphere of Mars Astron. Astrophys. 649, L1 (2021c) https://doi.org/10.1051/0004-6361/202140868
79. Olsen K.S., Fedorova A.A., Trokhimovskiy A., et al. Seasonal Changes in the Vertical Structure of Ozone in the Martian Lower Atmosphere and Its Relationship to Water Vapor J. Geophys. Res. (Planets) 127, e2022JE007213 (2022) https://doi.org/10.1029/2022JE007213
80. Patsaeva M.V., Khatuntsev I.V., Zasova L.V., et al. Solar-Related Variations of the Cloud Top Circulation Above Aphrodite Terra From VMC/Venus Express Wind Fields J. Geophys. Res. (Planets) 124, 1864 (2019) https://doi.org/10.1029/2018JE005620

81. Perevalov V.I., Trokhimovskiy A.Y., Lukashevskaya A.A., et al. Magnetic dipole and electric quadrupole absorption in carbon dioxide J. Quant. Spectr. Rad. Transf. 259, 107408 (2021) https://doi.org/10.1016/j.jqsrt.2020.107408
82. Pinto, J.P., Li J., Mills F.P., Marcq E., Evdokimova D., Belyaev D., Yung,Y.L. Sulfur monoxide dimer chemistry as a possible source of polysulfur in the upper atmosphere of Venus. Nature Communications, 12(1), 1–6 (2021). https://doi.org/10.1038/s41467-020-20451-2
83. Rajendran K., Lewis S.R., Holmes J.A., et al. Enhanced Super-Rotation Before and During the 2018 Martian Global Dust Storm Geophys. Res. Lett. 48, e94634 (2021) https://doi.org/10.1029/2021GL094634
84. Rossi L., Vals M., Montmessin F., et al. The Effect of the Martian 2018 Global Dust Storm on HDO as Predicted by a Mars Global Climate Model Geophys. Res. Lett. 48, e90962 (2021) https://doi.org/10.1029/2020GL090962
85. Rossi L., Vals M., Alday J., et al. The HDO Cycle on Mars: Comparison of ACS Observations With GCM Simulations. Journal of Geophysical Research: Palnets 127, e07201 (2022) https://doi.org/10.1029/2022JE007201
86. Shaposhnikov D.S., Medvedev A.S., Rodin A.V., Hartogh P. Seasonal Water "Pump" in the Atmosphere of Mars: Vertical Transport to the Thermosphere Geophys. Res. Lett. 46, 4161 (2019) https://doi.org/10.1029/2019GL082839
87. Shaposhnikov D.S., Medvedev A.S., Rodin A.V. Simulation of Water Vapor Photodissociation during Dust Storm Season on Mars Solar Syst. Res. 56, 23 (2022a) https://doi.org/10.1134/S0038094622010051
88. Shaposhnikov D.S., Medvedev A.S., Rodin A.V., et al. Martian Dust Storms and Gravity Waves: Disentangling Water Transport to the Upper Atmosphere J. Geophys. Res. (Planets) 127, e07102 (2022b) https://doi.org/10.1029/2021JE007102
89. Shematovich V.I. Atmospheric Loss of Atomic Oxygen during Proton Aurorae on Mars Solar Syst. Res. 55, 324 (2021) https://doi.org/10.1134/S0038094621040079
90. Shematovich V.I. and Kalinicheva E.S., Atmospheric escape of oxygen atoms during the proton aurorae at Mars, Astron. Rep., 2020, vol. 64, pp. 628–635.
91. Shematovich, V.I., Bisikalo, D.V., Gerard, J.-C., and Hubert, B., Kinetic Monte Carlo model of the precipitation of high-energy proton and hydrogen atoms into the Martian atmosphere with taking into account the measured magnetic field, Astron. Rep., 2019, vol. 63, pp. 835–845.
92. Shematovich, V.I., Bisikalo, D.V., and Zhilkin, A.G., Effects of column density variations of extended hydrogen corona of mars on the charge exchange efficiency with solar wind protons, Astron. Rep., 2021, vol. 65, pp. 203–208.
93. Starichenko E.D., Belyaev D.A., Medvedev A.S., et al. Gravity Wave Activity in the Martian Atmosphere at Altitudes 20–160 km From ACS/TGO Occultation Measurements J. Geophys. Res. (Planets) 126, e06899 (2021) https://doi.org/10.1029/2021JE006899
94. Stcherbinine A., Vincendon M., Montmessin F., et al. Martian Water Ice Clouds During the 2018 Global Dust Storm as Observed by the ACS-MIR Channel Onboard the Trace Gas Orbiter J. Geophys. Res. (Planets) 125, e06300 (2020) https://doi.org/10.1029/2019JE006300
95. Stcherbinine A., Montmessin F., Vincendon M., et al. A Two Martian Years Survey of Water Ice Clouds on Mars With ACS Onboard TGO J. Geophys. Res. (Planets) 127, e2022JE007502 (2022) https://doi.org/10.1029/2022JE007502

96. Streeter P.M., Lewis S.R., Patel M.R., et al. Asymmetric Impacts on Mars' Polar Vortices From an Equinoctial Global Dust Storm J. Geophys. Res. (Planets) 126, e06774 (2021) https://doi.org/10.1029/2020JE006774
97. Trokhimovskiy A., Perevalov V., Korablev O., et al. First observation of the magnetic dipole CO2 absorption band at 3.3 μm in the atmosphere of Mars by the ExoMars Trace Gas Orbiter ACS instrument Astron. Astrophys. 639, A142 (2020) https://doi.org/10.1051/0004-6361/202038134
98. Trokhimovskiy A., Fedorova A.A., Olsen K.S., et al. Isotopes of chlorine from HCl in the Martian atmosphere Astron. Astrophys. 651, A32 (2021) https://doi.org/10.1051/0004-6361/202140916
99. Vals M., Rossi L., Montmessin F., et al. Improved Modeling of Mars' HDO Cycle Using a Mars' Global Climate Model J. Geophys. Res. (Planets) 127, e07192 (2022) https://doi.org/10.1029/2022JE007192
100. Vandaele A.C., Korablev O., Daerden F., et al. Martian dust storm impact on atmospheric H2O and D/H observed by ExoMars Trace Gas Orbiter Nature 568, 521 (2019) https://doi.org/10.1038/s41586-019-1097-3
101. Vlasov P., Ignatiev N., Guerlet S., et al. Martian Atmospheric Thermal Structure and Dust Distribution During the MY 34 Global Dust Storm From ACS TIRVIM Nadir Observations J. Geophys. Res. (Planets) 127, e07272 (2022) https://doi.org/10.1029/2022JE007272
102. Webster C.R., Mahaffy P.R., Atreya S.K., et al. Background levels of methane in Mars' atmosphere show strong seasonal variations Science 360, 1093 (2018) https://doi.org/10.1126/science.aaq0131
103. Webster C.R., Mahaffy P.R., Pla-Garcia J., et al. Day-night differences in Mars methane suggest nighttime containment at Gale crater. Astron. Astrophys. 650, A166 (2021) https://doi.org/10.1051/0004-6361/202040030
104. Yachmenev A., Campargue A., Yurchenko S.N., et al. Electric quadrupole transitions in carbon dioxide J. Chem. Phys. 154, 211104 (2021) https://doi.org/10.1063/5.0053279
105. Young R. M. B., Millour E., Guerlet S., et al. Assimilation of Temperatures and Column Dust Opacities Measured by ExoMars TGO-ACS-TIRVIM During the MY34 Global Dust Storm J. Geophys. Res. (Planets) 127, e07312 (2022) https://doi.org/10.1029/2022JE007312
106. Zasova L.V., Gorinov D.A., Eismont N.A., et al. Venera-D: A Design of an Automatic Space Station for Venus Exploration. Solar Syst. Res. 53, 506 (2020) https://doi.org/10.1134/S0038094619070244

Polar Meteorology

A.V. Klepikov
Arctic and Antarctic Research Institute
klep@aari.ru

This section is a review of the results of Russian polar meteorological and climate studies performed in 2019–2022. The review is based on material prepared by the Commission on Polar Meteorology of the National Geophysical Committee, Russian Academy of Sciences, and included into the National Report on Meteorology and Atmospheric Sciences to the XXVIII General Assembly of the International Union of Geodesy and Geophysics, Berlin, Germany, July 11–20, 2023.

Arctic meteorology studies

Description of the current state of the Arctic climate is presented in the monograph [1]. The book presents the results of research into the climate of the Arctic, carried out at the Institute of Atmospheric Physics of the Russian Academy of Sciences. The results of the analysis of empirical data for various components of the Arctic climate system: the atmosphere, sea ice, ocean and land are presented with an assessment of current trends in change. Typical processes and feedbacks in the Arctic climate system that are important for the formation of long-term climate anomalies in the Arctic, as well as the mechanisms of the impact of climate change in the Arctic on atmospheric circulation in the middle latitudes of the Northern Hemisphere, are considered. Estimates of possible future climate changes in the Arctic are given based on the results of numerical calculations with climate models under scenarios of anthropogenic impact, as well as the impact of these changes on the duration of maritime navigation along the Northern Sea Route, sea waves, characteristics of permafrost soils, and the decay of near-bottom methane hydrates.

The features of present-day rapid climate changes in the Arctic and their consequences are presented in review [2]. An assessment is made of the relative contribution of natural and anthropogenic factors to the formation of temperature trends at different time horizons in the Arctic. In view of the rapid changes of the Arctic climate, the prospects of the Northern Sea route are examined. According to the estimates obtained, the dominant role of radiative forcing is manifested in the Arctic latitudes on time scales of about half a century or more. New climatic phenomena (in particular, the formation of craters in the Yamal Peninsula under the conditions of melting permafrost) and new effects (including the change in the trends of changes in sea waves

in the waters of the Arctic basin) indicate the achievement of a certain critical level of regional and global warming, comparable to the warming of the Holocene Climate Optimum. At the same time, modern climate models can not only reproduce the key features of current climatic regimes and their variability, but also provide adequate predictive estimates even for complex processes in the Arctic [2]. Analytical conditions for the formation of the Arctic amplification in the Earth's climate system are presented in [3].

The results of verification of data on the near-surface air temperature of the ERA-Interim and ERA-5 reanalyses based on the results of measurements obtained from drifting buoys, ground-based meteorological stations, and also, for the first time, according to measurements performed at the ice drifting stations "North Pole", are presented in [4]. The latter were not assimilated in any of the considered reanalyses, which provides a rare opportunity for independent validation. Based on the results of comparison with data from the North Pole stations, it was found that the average error for the cold season in the Arctic basin is 2.25°C for ERA-Interim and 3.92°C for ERA-5. Comparison with data from drifting buoys allows us to make an assumption about the reason for such large errors in the reanalyses. Part of the buoys was installed from the air by dropping onto the ice from the aircraft. At the same time, the temperature sensor of the buoy was, with a high degree of probability, buried in the snow cover, which shielded it from the cold atmosphere and contributed to heating due to the heat flow from the underlying layer of sea water. The assimilation of such data is probably one of the reasons for the overestimation of air temperature over drifting ice by reanalyses.

Based on the monthly average data of the ERA-Interim reanalysis (1979–2014), estimates of the vertical temperature gradient g in the high-latitude troposphere of the Northern Hemisphere were obtained in [5] with an analysis of its relationship with the near-surface temperature Ts in interannual variability for different seasons. We also analyzed the ability of the HIRHAM5 regional climate model to reproduce the features of the distribution of the vertical temperature gradient in the troposphere in the Arctic latitudes and the parameter of sensitivity to changes in surface temperature dg/dTs, identified from the reanalysis data. Regional features of the relationship between the vertical temperature stratification in the troposphere and the Arctic oscillation are noted. The estimates obtained from the reanalysis data and model calculations are of particular importance due to the higher variability and sensitivity of the climate of the Arctic latitudes to global changes, which is characterized by the so-called Arctic amplification.

Changes in the characteristics of cyclone activity (frequency, depth and size) in the Arctic are analyzed in [6] based on simulations with state-of-the-art regional climate models (RCMs) from the Arctic-CORDEX initiative and global climate models (GCMs) from CMIP5 under the Representative Con-

centration Pathway (RCP) 8.5 scenario. Most of RCMs show an increase of cyclone frequency in winter (DJF) and a decrease in summer (JJA) to the end of the 21st century. However, in one half of the RCMs, cyclones become weaker and substantially smaller in winter and deeper and larger in summer. RCMs as well as GCMs show an increase of cyclone frequency over the Baffin Bay, Barents Sea, north of Greenland, Canadian Archipelago, and a decrease over the Nordic Seas, Kara and Beaufort Seas and over the sub-arctic continental regions in winter. In summer, the models simulate an increase of cyclone frequency over the Central Arctic and Greenland Sea and a decrease over the Norwegian and Kara Seas by the end of the 21st century. The decrease is also found over the high-latitude continental areas, in particular, over East Siberia and Alaska. The sensitivity of the RCMs' projections to the boundary conditions and model physics is estimated. In general, different lateral boundary conditions from the GCMs have larger effects on the simulated RCM projections than the differences in RCMs' setup and/or physics.

The impact of the Atlantic water (AW) inflow into the Barents Sea on the regional cyclone activity in winter is analyzed in [7] with 10 ensemble simulations of the coupled Arctic atmosphere-ocean-sea ice model HIRHAM-NAOSIM for the 1979–2016 period. The model shows a statistically robust connection between AW inflow and climate variability in the Barents Sea. The analysis reveals that anomalously high AW inflow leads to changes in static stability and wind shear in the lower troposphere, and thus favorable conditions for cyclogenesis in the Barents/Kara Seas. The frequency of occurrence of cyclones, but particularly of intense cyclones, is increased over the Barents Sea. Furthermore, the cyclones in the Barents Sea become larger (increased radius) and stronger (increased intensity) in response to an increased AW inflow into the Barents Sea, compared to years of anomalously low AW inflow.

Arctic cyclones, as a prevalent feature in the coupled dynamics of the Arctic climate system, have large impacts on the atmospheric transport of heat and moisture and deformation and drifting of sea ice. Studies based on historical and future simulations with climate models suggest that Arctic cyclogenesis is affected by the Arctic amplification of global warming, for instance, a growing land-sea thermal contrast. The authors of [8] hypothesize that biogeophysical feedbacks (BF) over the land, here mainly referring to the albedo-induced warming in spring and evaporative cooling in summer, may have the potential to significantly change cyclone activity in the Arctic. Based on a regional Earth system model (RCA-GUESS) which couples a dynamic vegetation model and a regional atmospheric model and an algorithm of cyclone detection and tracking, the study [8] assesses for the first time the impacts of BF on the characteristics of Arctic cyclones under three IPCC Representative Concentration Pathways scenarios (i.e. RCP2.6,

RCP4.5 and RCP8.5). Analysis focuses on the spring- and summer time periods, since previous studies showed BF are the most pronounced in these seasons. It was found that BF induced by changes in surface heat fluxes lead to changes in land-sea thermal contrast and atmospheric stability. This, in turn, noticeably changes the atmospheric baroclinicity and, thus, leads to a change of cyclone activity in the Arctic, in particular to the increase of cyclone frequency over the Arctic Ocean in spring. The study highlights the importance of accounting for BF in the prediction of Arctic cyclones and the role of circulation in the Arctic regional Earth system.

The parameterization of ocean/sea-ice/atmosphere interaction processes is a challenge for regional climate models (RCMs) of the Arctic, particularly for wintertime conditions, when small fractions of thin ice or open water cause strong modifications of the boundary layer. Thus, the treatment of sea ice and sub-grid flux parameterizations in RCMs is of crucial importance. However, verification data sets over sea ice for wintertime conditions are rare. In the paper [9], data of the ship-based experiment Transarktika 2019 during the end of the Arctic winter for thick one-year ice conditions are presented. The data are used for the verification of the regional climate model COSMOCLM (CCLM). In addition, Moderate Resolution Imaging Spectroradiometer (MODIS) data are used for the comparison of ice surface temperature (IST) simulations of the CCLM sea ice model. CLM is used in a forecast mode (nested in ERA5) for the Norwegian and Barents Seas with 5 km resolution and is run with different configurations of the sea ice model and sub-grid flux parameterizations. The use of a new set of parameterizations yields improved results for the comparisons with in-situ data. Comparisons with MODIS IST allow for a verification over large areas and show also a good performance of CCLM. The comparison with twice-daily radiosonde ascents during Transarktika 2019, hourly microwave water vapor measurements of first 5 km in the atmosphere and hourly temperature profiler data show a very good representation of the temperature, humidity and wind structure of the whole troposphere for CCLM.

In 2014/2015 a one-year field campaign at the Tiksi observatory in the Laptev Sea area was carried out using Sound Detection and Ranging/Radio Acoustic Sounding System (SODAR/RASS) measurements to investigate the atmospheric boundary layer (ABL) with a focus on low-level jets (LLJ) during the winter season. In addition to SODAR/RASS-derived vertical profiles of temperature, wind speed and direction, a suite of complementary measurements at the Tiksi observatory was available. In [10] data of a regional atmospheric model were used to put the local data into the synoptic context and two case studies of LLJ events are presented. The statistics of LLJs for six months show that in about 23% of all profiles LLJs were present with a mean jet speed and height of about 7 m/s and 240 m, respectively. In 3.4% of

all profiles LLJs exceeding 10 m/s occurred. The main driving mechanism for LLJs seems to be the baroclinicity, since no inertial oscillations were found. LLJs with heights below 200 m are likely influenced by local topography.

Measurements of the atmospheric boundary layer (ABL) structure performed for three years (October 2017–August 2020) at the Russian observatory "Ice Base Cape Baranova" (79.280 N, 101.620 E) using SODAR are discussed in [11]. In addition to SODAR-derived vertical profiles of wind speed and direction, a suite of complementary measurements at the observatory was available. ABL measurements were used for verification of the regional climate model COSMO-CLM (CCLM) with a 5 km resolution for 2017–2020. The CCLM was run with nesting in ERA5 data in a forecast mode for the measurement period. SODAR measurements were mostly limited to wind speeds <12 m/s since the signal was often lost for higher winds. The SODAR data showed a topographical channeling effect for the wind field in the lowest 100 m and some low-level jets (LLJs). The verification of the CCLM with near-surface data of the observatory showed good agreement for the wind and a negative bias for the 2 m temperature. The comparison with SODAR data showed a positive bias for the wind speed of about 1 m/s below 100 m, which increased to 1.5 m/s for higher levels. In contrast to the SODAR data, the CCLM data showed the frequent presence of LLJs associated with the topographic channeling in Shokalsky Strait. Although SODAR wind profiles are limited in range and have a lot of gaps, they represent a valuable data set for model verification. However, a full picture of the ABL structure and the climatology of channeling events could be obtained only with the model data. The climatological evaluation showed that the wind field at Cape Baranova was not only influenced by direct topographic channeling under conditions of southerly winds through the Shokalsky Strait but also by channeling through a mountain gap for westerly winds. LLJs were detected in 37% of all profiles and most LLJs were associated with channeling, particularly LLJs with a jet speed _ 15 m/s (which were 29% of all LLJs). The analysis of the simulated 10 m wind field showed that the 99%-tile of the wind speed reached 18 m/s and clearly showed a dipole structure of channeled wind at both exits of Shokalsky Strait. The climatology of channeling events showed that this dipole structure was caused by the frequent occurrence of channeling at both exits. Channeling events lasting at least 12 h occurred on about 62 days per year at both exits of Shokalsky Strait.

A simple analytical model of the atmospheric boundary layer (ABL) coupled to sea ice is presented in [12]. It describes clear-sky cooling over sea ice during polar night in the presence of leads. The model solutions show that the sea ice concentration and wind speed have a strong impact on the thermal regime over sea ice. Leads cause both a warming of the ABL and an increase

of stability over sea ice. The model describes a sharp ABL transition from a weakly stable coupled state to a strongly stable decoupled state when wind speed is decreasing. The threshold value of the transition wind speed is a function of sea ice concentration. The decoupled state is characterized by a large air–surface temperature difference over sea ice, which is further increased by leads. In the coupled regime, air and surface temperatures increase almost linearly with wind speed due to warming by leads and also slower cooling of the ABL. The cooling time scale shows a nonmonotonic dependency on wind speed, being lowest for the threshold value of wind speed and increasing for weak and strong winds. Theoretical solutions agree well with results of a more realistic single-column model and with observations performed at the three Russian "North Pole" drifting stations (NP-35, NP-37, and NP-39) and at the Surface Heat Budget of the Arctic Ocean ice camp. Both modeling results and observations show a strong implicit dependency of the net longwave radiative flux at the surface on wind speed.

In [13] the authors present the results of an analysis of ceilometer measurements at North Pole (NP) drifting station 37, 39, and 40. The frequencies of the total cloud amount (in tenth) and the cloud base heights (CBHs) are calculated for the period of the polar night. A comparison of the cloud-cover score according to the ceilometer data with the visual observation data showed good agreement. However, the value of the correlation coefficient depends on the interpretation of the ceilometer data. In general, a bimodal distribution of the cloud-cover scores with the highest frequency of clear sky and overcast clouds are characteristic for indicated stations. The analysis of the frequency of the CBH showed that the most characteristic CBHs are below 600 m. In November, cloud heights in the range of 1000–2000 m are also observed, while their frequency decreases during the winter. Cloudiness during the polar night is characterized by a strong positive radiative forcing, which has a warming effect on the surface temperature of ice and air. However, cloud radiative forcing, as well as the cloudiness frequency and its effect on the temperature regime, varies significantly from station to station. These differences may become the subject of further research on the interrelation of cloud characteristics with other processes in the Arctic climate system. These statistical estimates significantly supplement the available data on the cloud cover of the Central Arctic.

The influence of the oceanic heat inflow into the Barents Sea on the sea ice concentration and atmospheric characteristics, including the atmospheric static stability during winter months, is investigated in [14] on the basis of the results of ensemble simulations with the regional climate model HIRHAM/NAOSIM for the Arctic. The static stability of the atmosphere is the important indicator of the spatial and temporal variability of polar mesocyclones in the Arctic region. The results of the HIRHAM/NAOSIM regional

climate model ensemble simulations (RCM) for the period from 1979 to 2016 were used for the analysis. The initial and lateral boundary conditions for RCM in the atmosphere were set in accordance with the ERA-Interim reanalysis data. An analysis of 10 ensemble simulations with identical boundary conditions and the same radiation forcing for the Arctic was performed. Various realizations of ensemble simulations with RCM were obtained by changing the initial conditions for integrating the oceanic block of the model. Different realizations of ensemble simulations with RCM are obtained by changing the initial conditions of the model oceanic block integration. The composites method was used for the analysis, i.e. the difference between the mean values for years with the maximum and minimum inflow of oceanic water into the Barents Sea. The statistical significance of the results (at a significance level of $p < 0.05$) was estimated using Student's t-test. In general, the regional climate model reproduces the seasonal changes in the inflow of the oceanic water and heat into the Barents Sea reasonably well. There is a strong relationship between the changes in the oceanic water and ocean heat inflow, sea ice concentration, and surface air temperature in the Barents Sea. Herewith, the increase in the oceanic water inflow into the Barents Sea in winter leads to a decrease in static stability, which contributes to changes in regional cyclonic activity. The decrease of the static stability is most pronounced in the southern part of the Barents Sea and also to the west of Svalbard [14].

The analysis of the characteristics of sea wave activity in the Arctic Basin carried out using the WAWEWATCH III model and the results of calculations of sea ice and wind in the atmosphere with the ensemble of global climate models CMIP5 are discussed in [15]. The relative role of wind waves and swell in the overall activity of sea waves in the Arctic Basin is estimated according to model calculations in comparison with those obtained using reanalysis and satellite data. Estimates of possible changes in sea waves accompanying a significant decrease in the extent of sea ice in the Arctic are obtained according to model calculations for the 21st century under different scenarios of anthropogenic impacts. The features of various regimes of sea waves in the Arctic Basin are noted with an assessment of the role of wind waves, swell, their interaction, modes of chaotic waves such as wave crush.

Coastal and fast ice polynyas in the Arctic seas can have a noticeable effect on the Arctic climate, increasing the temperature of the cold air which coming from continental Siberia in winter to these seas and in the Arctic basin. In [16] this paper the effect of polynyas on surface air temperature and on the meridional heat and moisture transfers is studied according to field observations and ERA-Interim reanalysis. According to the results of field observations carried out in the 1990s, estimates of heat inflows from the surface of the polynya were calculated. From reanalysis, meridional heat transfers were

obtained through 70° N, air temperature profiles, wind speed in the region of the Laptev Sea (100–140° E.), and polynya which located in the Laptev Sea (120–130° E). It is confirmed that winter transfers of cold air from the mainland do not have a cooling effect on the average winter air temperature north of 70° N due to the heating effect of polynya.

Quantitative estimates of the relationship between intra-annual and interannual variations of snow cover extent in Eurasia and changes of surface air temperature in the Northern Hemisphere were obtained in [17] based on satellite data and reanalysis data for the period 1979–2020. Estimates of parameters of the sensitivity of the snow cover extent in Eurasia to the temperature changes for the last four decades (1980–2019) are compared with the estimates obtained for the last fifteen years (2005–2019). Seasonal features of the relationship between the snow cover extent and the temperature regime are noted, particularly during the formation of the snow cover in autumn. The results of the correlation and cross-wavelet analysis indicate a general significant coherence and a negative correlation with the surface temperature of the snow cover extent in Eurasia as a whole, not only in the annual cycle, but also in interannual variability for most months. An increase in the absolute value of the parameter of the sensitivity of the snow cover extent to changes in the surface temperature for Eurasia was noted by using annual-mean data for the period 2005–2019, with their generally statistically insignificant negative correlation for the last four decades [17].

Quantitative estimates of the relationship between the snow cover and sea ice extension in the Northern Hemisphere with the surface air temperature in the annual cycle and interannual variability are obtained in [18] on the basis of modern satellite data and reanalysis data for the period 1979–2020. The results obtained indicate a general significant coherence and negative correlation with the surface air temperature of the snow cover and sea ice extent not only in the annual cycle, but also for most months in interannual variability. At the same time, peculiarities appear in the autumn months, associated with regional features of the variability of the temperature conditions and the snow cover extent during the season of its formation in Eurasia and North America. For the winter months, an increase in the absolute value of the parameters of the sensitivity of the snow cover and sea ice extent to temperature variations in recent decades and the coefficients of their correlation was noted, and for the warm months of the year, the opposite changes were observed. Along with a statistically significant negative correlation of the total snow cover and sea ice extent with variations in the hemispheric surface air temperature in the annual cycle, cross-wavelet analysis revealed a statistically significant negative correlation for the longest interdecadal variations with the manifestation in recent years of significant anticorrelation for interannual variations, in particular for variations with a periods typical for El Niño events [18].

The results of measurements of the physical and chemical characteristics of atmospheric aerosol (aerosol optical depth, aerosol and black carbon concentrations, elemental and ion compositions of aerosol, organic and elemental carbon contents in aerosol, isotopic composition of carbon in the aerosol and snow samples) in the region of Cape Baranov (the Severnaya Zemlya archipelago) are discussed in [19]. It is shown that the average values of most aerosol characteristics, measured in April–June 2018, are a little lower than in the Arctic settlement Barentsburg (Spitsbergen archipelago) and several-fold smaller than in the south of Western Siberia in the same period.

The results of comparison of the average physicochemical aerosol characteristics in neighboring regions: in the Arctic settlement Barentsburg (Spitsbergen Archipelago) and over the Barents Sea are presented in [20]. A small (less than 0.02) excess of the atmospheric aerosol optical depth in the island area over the maritime region is noted. The aerosol microphysical characteristics in the near-ground layer differ strongly: the black carbon concentrations are (a factor of 4) larger in Barentsburg, and particle concentrations are (a factor of 2.4) larger over the sea. The absolute concentrations of ions in the atmosphere of Barentsburg are several-fold smaller than over the sea. However, with respect to the relative content, Na^+, Cl^- and NH_4^+, SO_4^{2-} ions predominate in both regions, indicating equivalent contributions of continental and maritime sources.

The chemical composition (ions, elements, polycyclic aromatic hydrocarbons) of atmospheric aerosol in various regions of the Northern Arctic, the European and Russian parts of the Arctic Ocean, the seas of northern latitudes and the Far East is considered in [21]. The studies were carried out from sea vessels along their routes (R/V Akademik Mstislav Keldysh, R/V Akademik Treshnikov, R/V Professor Multanovsky). Air samples were taken according to the methodology adopted in the international networks of atmospheric monitoring programs in Southeast Asia (EANET) and Europe (EMEP). The average sum of concentrations of ions and individual ions in aerosol over the seas of the North Atlantic and the European part of the Arctic Ocean is consistent with measurements in the Laptev and Kara Seas in 2018 and 2019. Elevated values of PAHs in the aerosol of the seas and the Arctic Ocean in the central part of the Russian Arctic coincide with the increased concentrations of ions and microelements in the aerosol. There is a difference in the distribution of trace element concentrations in the composition of aerosols from the seas of the North Atlantic and the central region of the Russian Arctic, which may indicate different sources of these components.

The results from studies of aerosol in the Arctic atmosphere including the aerosol optical depth (AOD), the concentrations of aerosol and black carbon, and chemical composition of the aerosol are presented in [22]. The average aerosol characteristics, measured during nine expeditions (2007–2018) in the

Eurasian sector of the Arctic Ocean, had been 0.068 for AOD (0.5 μm); 2.95 cm^{-3} for particle number concentrations; 32.1 ng/m^3 for black carbon mass concentrations. Approximately two–fold decrease of the average characteristics in the eastern direction (from the Barents Sea to Chukchi Sea) is revealed in aerosol spatial distribution. The average aerosol characteristics over the Barents Sea decrease in the northern direction: black carbon concentrations by a factor of 1.5; particle concentrations by a factor of 3.7. These features of the spatial distribution are caused mainly by changes in the content of fine aerosol, namely: by outflows of smokes from forest fires and anthropogenic aerosol. Authors considered separately the measurements of aerosol characteristics during two expeditions in 2019: in the north of the Barents Sea (April) and along the Northern Sea Route (July–September). In the second expedition the average aerosol characteristics turned out to be larger than multiyear values: AOD reached 0.36, particle concentration up to 8.6 cm^{-3}, and black carbon concentration up to 179 ng/m^3. The increased aerosol content was affected by frequent outflows of smoke from forest fires. The main (99%) contribution to the elemental composition of aerosol in the study regions was due to Ca, K, Fe, Zn, Br, Ni, Cu, Mn, and Sr. The spatial distribution of the chemical composition of aerosols was analogous to that of microphysical characteristics. The lowest concentrations of organic and elemental carbon (OC, EC) and of most elements are observed in April in the north of the Barents Sea, and the maximal concentrations in Far East seas and in the south of the Barents Sea. The average contents of carbon in aerosol over seas of the Asian sector of the Arctic Ocean are OC = 629 ng/m^3, EC = 47 ng/m^3.

In recent decades, surface air temperature (SAT) data from Global reanalysis points to maximum warming over the northern Barents area. However, a scarcity of observations hampers the confidence of reanalysis in this Arctic hotspot region. In [23] the authors study the warming over the past 20–40 years based on new available SAT observations and a quality controlled comprehensive SAT dataset from the northern archipelagos in the Barents Sea. Statistically significant record – high annual warming of up to 2.7 °C per decade with a maximum in autumn of up to 4.0 °C per decade was identified. The results are compared with the most recent global and Arctic regional reanalysis data sets, as well as remote sensing data records of sea ice concentration (SIC), sea surface temperature (SST) and high-resolution ice charts. The warming pattern is primarily consistent with reductions in sea ice cover and confirms the general spatial and temporal patterns represented by reanalysis. However, our findings suggest even a stronger rate of warming and SIC-SAT relation than was known in this region until now.

Electronic archives of data from standard meteorological observations (mean daily/monthly surface air temperatures – SAT) at the meteorological

stations at Bukhta Tikhaya (Hooker Island, 1929–1960) and Krenkel Observatory (Hayes Island, 1957–2017) on Franz Josef Land (FJL) are presented in [24]. Parallel data series of SAT made in 1958 and 1959 on both meteorological stations were analyzed. Linear regression equations used for extrapolation of observational data representative for Krenkel Observatory for the period 1929–1957 are also presented. The assessment of long-term changes in SAT on FJL was carried out based on the analysis of the obtained series (1929–2017). The main conclusions are: total warming in the FJL archipelago was 1.6–1.8°C (0.2°C/decade) for the entire available period of instrumental observations (1929–2017); highest rates of warming were recorded in March-April and amounted to 0.6°C/decade; particular strong warming has been observed since the 1990s; annual temperature increased by 6.3°C (2.2°C/decade) for the period 1990–2017 and 5.2°C (2.9°C/decade) for the period 2000–2017; for the period 1990–2017 the maximum rate of warming occurred between October to February with 4.4°C/decade; for the period 2000–2017 the maximum rate of warming occurred between January to April and from November to December with 5.6°C/decade; dominant seasons of the year are winter (November–April), spring (May), summer (June-September) and autumn (October); over the entire observation period the largest temperature increase was observed in the winter season; during the period of modern warming (1990–2017), the largest temperature increase was observed in winter and autumn.

The article [25] discusses the regional features of the Svalbard climate based on the data of regular meteorological observations obtained at Norwegian, Russian and Polish stations. Attention is paid to the spatial features of the multi-year regime of surface air temperature (SAT). Climatic norms (1961–1990, WMO recommendations) calculated from all meteorological stations, as well as long-term changes in the spatial gradients of the SAT and estimates of the range of annual fluctuations, revealed stations (area) with a "*continental*" and "*marine*" type of climate, as well as trends in spatial heterogeneities of the Svalbard climate. The rate of "*modern*" climate warming (1990–2016) was, on average, three times higher compared with the period after II World War (1948–2016). The continentality and abnormality of the climate are analyzed. Conclusions are formulated about a regular change in the spatial features of the climate (SAT) and the manifestation of its anomalous nature in different periods (1960–1970, 1988 and 2005–2014).

The Svalbard archipelago in the Arctic North Atlantic is experiencing rapid changes in the surface climate and sea ice distribution, with impacts for the coupled climate system and the local society. This study [26] utilizes observational data of surface air temperature (SAT) from 1980–2016 across the whole Svalbard archipelago, and sea ice extent (SIE) from operational sea ice charts to conduct a systematic assessment of climatologies, long-term chang-

es and regional differences. The proximity to the warm water mass of the West Spitsbergen Current drives a markedly warmer climate in the western coastal regions compared to northern and eastern Svalbard. This imprints on the SIE climatology in southern and western Svalbard, where the annual maxima of 50–60% area ice coverage are substantially less than 80–90% in the northern and eastern fjords. Owing to winter-amplified warming, the local climate is shifting towards more maritime conditions, and SIE reductions of between 5% to 20% per decade in particular regions are found, such that a number of fjords in the west have been virtually ice-free in recent winters. The strongest decline is motivated by SAT forcing and occurs over the most recent 1–2 decades in all regions; while in the 1980s and 1990s, enhanced northerly winds and sea ice drift can explain 30–50% of SIE variability around northern Svalbard, where they had correspondingly lead to a SIE increase. With an ongoing warming, it is suggested that both the meteorological and cryospheric conditions in eastern Svalbard will become increasingly similar to what is already observed in the western fjords, namely suppressed typical Arctic conditions.

The results of studying the temporal variability of atmospheric circulation in the Western Arctic (the Norwegian and Barents seas) are presented in [27]. The daily dataset of Girs–Vangengeim E, W, and C circulation forms for the period of 1891–2016 is used to describe atmospheric circulation. Special attention is given to the estimation of differences in weather conditions during the modern period of warming (1985–2015) and in the period of the first Arctic warming (1920–1950). For the cold (November–March) and warm (April–October) seasons, the trends in the frequency of occurrence of the circulation forms are determined. The occurrence of the number of consecutive days with the same atmospheric circulation form which can be considered as a characteristic of weather stability during the analyzed period of warming is computed for both seasons. The prevalence of the E circulation form during the warm season is typical of both periods. The modern period of warming in the study area, as compared to the period of the first warming, is characterized by an increase in the occurrence of the C circulation form with a short duration. It is found that the current climate regime is characterized by an increase in surface air temperature against a background of less stable weather conditions.

The article analyzes [28] the common features and differences of "*earlier*" and "*modern*" warming observed. The longest-period series of meteorological observations made on the Svalbard archipelago are used. The phases of growth of surface air temperature are studied. It has been shown that "*earlier*" warming was more significant in comparison with "*modern*" warming. The most significant anomalies are observed in the winter months in "*early*" warming, while "*modern*" warming is recorded throughout the year.

In 2016–2017, during Russian Arctic Expedition on Svalbard the authors of [29] have collected the samples of atmospheric precipitation, terrestrial waters, snow and ice on Spitsbergen island in the vicinity of Grønfjorden. The measurements of stable water isotope content ($\delta^{18}O$ and δD) in the atmospheric precipitation has allowed to draw the Local Meteoric Water Line ($\delta D = 6{,}93\delta^{18}O - 0{,}35$) and to analyze the relationship between the isotopic content and condensation temperature. Aside from this, the d-excess values in precipitation ($dexc = \delta D - 8\delta^{18}O$) was interpreted as a marker of the moisture source. It has been demonstrated that the isotopic content of the surface waters (lakes and rivers) clearly points to the dominating type of feeding (atmospheric, ground) of these hydrological objects. We have discovered the interannual variability of the isotopic composition of Lake Kongress water during 2 years and defined the sources of waterin its tributes: 13 of them have atmospheric source and 9 – ground source. In general, isotopic content of water in the vicinity of Grønfjorden (mean values are: $\delta^{18}O$ = -10,3‰, δD = -72,5‰) is higher than in other regions of Svalbard.

The chemical composition (ions, elements, polycyclic aromatic hydrocarbons) of aerosol and gaseous impurities (SO_2, HNO_3, HCl, NH_3) in the surface layer of the atmosphere in Barentsburg, located on the Western Svalbard island (Svalbard archipelago), is analyzed in [30]. Atmospheric aerosol and gaseous impurities brought to the Arctic from middle latitudes and deposited on snow and ice not only interact with various natural objects, but also spread to long distances with melting dirty snow and ice. Air sampling was carried out following to methodology adopted by the international networks of the atmospheric monitoring programs in South-East Asia (EANET) and Europe (EMEP). In 2011–2015, the observations of the chemical composition of the atmospheric ground layer were performed daily during the light season (April–September), and monthly from April 2016 to 2018. The largest total ion concentrations were observed in 2011–2012. Seasonal variability of ion concentrations in the aerosol was characterized by high values in the cold period (October–February) and low values in the warm one (May–June). High values of the coefficient of correlation between ions Na^+ and Cl^- (r = 0,93) as well as between Mg^{2+} and Cl^- (r = 0,81) throughout the year show that the main source of the aerosol is the sea surface. The significant correlation between ions K^+, NO_3^-, NH_4^+, SO_4^{2-}, K^+, SO_4^{2-} in the polar night point to the influence of local sources: coal mining at the mine and its combustion at thermal power plants. Emission of polycyclic aromatic hydrocarbons and the gaseous impurities (SO_2, HNO_3) into the atmosphere, especially during the polar night, is also influenced by local sources. Among the elements the maximum enrichment of the aerosol was revealed for As, Cr, Zn, Mo, Cd, Sn, Sb, W, and Pb with a low content of Cd, Sn, Sb, W, and Pb in the coal, sludge and on the underlying surface. On the basis of the elemental

composition of the aerosol and the back-trajectory analysis, it was shown that the air masses enriched in heavy metals come to the area of the Barentsburg settlement from middle latitudes.

The book [31] contains materials on topical issues of determining the impact of methane on climate change. The sources and sinks of methane are considered, quantitative estimates of the ratio of natural (natural) and anthropogenic emissions of methane into the atmosphere in Russia and in the world are presented. An analysis of the role of methane in atmospheric photochemical processes was performed with an assessment of modern changes in the concentration of methane in the atmosphere and their causes. Particular attention is paid to methane emissions in the Arctic zone, including methane emissions from permafrost swamps in Russia. The results of a comparative analysis of the systems of coefficients used in determining methane emissions into the atmosphere in national inventories are presented. Including the corresponding coefficients for the production processes of the oil and gas industry. New metrics for estimating greenhouse gas emissions are considered. Particular attention is paid to the factors influencing global and regional climate changes with an assessment of the role of anthropogenic methane emissions into the atmosphere, including using models of the Earth system.

In recent years, new geophysical phenomena have been observed in the high-latitude regions of continental permafrost. Since 2014 new craters 10–20 m in diameter have been found within the Yamal Peninsula and neighboring regions. They are associated with the emissions of gases, which could have been formed during dissociation of relict gas hydrate deposits due to increases in soil temperature. The paper [32] presents the results of numerical modeling of the thermal regime of permafrost in the north of Western Siberia with the assessment of methane hydrate stability zone under climate changes over the past 130,000 years. According to the results obtained, the upper boundary of the methane hydrate stability zone in Yamal could have reached the surface within the periods of glacial maxima (about 90,000 and 60,000 years ago). It is shown that at present in Yamal permafrost above the modern boundary of the stability zone, relic methane hydrates are likely to exist at depths of up to 100–150 m, they could have "survives" warming during the Holocene optimum about 6,000 years ago and remain in permafrost rocks under negative temperatures even under transgression and increased geothermal flux conditions.

Estimates of the intra- and intersentennial degradation of permafrost at different depths and conditions of methane hydrate stability on the Yamal Peninsula under warming were obtained in [33] on the basis of the heat transfer model in soil using simulations with global climate models. The results of the simulations with the climate model of intermediate complexity for the last 130 thousand years ago were used along simulations with general circulation

climate models of the Coupled Model Intercomparison Project Phase 6 (CMIP6) ensemble (ScenarioMIP) from 1850 to the end of the 21st century under different SSP scenarios of anthropogenic forcings, in particular, the SSP5-8.5 scenario. The limiting conditions for the existence of permafrost at different depths and conditions for the methane hydrate stability were estimated for the global warming scenarios extended up to 2300 in accordance with the CMIP6 protocol as well as for the next 15 millennia with the use of the SSP5-8.5 scenario of anthropogenic forcing up to 2100.

Arctic tundra is facing unprecedented warming, resulting in shifts in the vegetation, thaw regimes, and potentially in the ecosystem–atmosphere exchange of carbon (C). However, the estimates of regional carbon dioxide (CO_2) and methane (CH_4) budgets are highly uncertain. The authors of [34] measured CO_2 and CH_4 fluxes, vegetation composition and leaf area index (LAI), thaw depth, and soil wetness in Tiksi (71 N, 128 E), a heterogeneous site located within the prostrate dwarf-shrub tundra zone in northeastern Siberia. Using the closed chamber method, the authors determined the net ecosystem exchange (NEE) of CO_2, ecosystem respiration in the dark (ER), ecosystem gross photosynthesis (Pg), and CH_4 flux during the growing season. The authors applied a previously developed high-spatial-resolution land cover map over an area of 35.8 km^2 for spatial extrapolation. Among the land cover types varying from barren to dwarf-shrub tundra and tundra wetlands, the NEE and Pg at the photosynthetically active photon flux density of 800 μmol m^{-2} h^{-1} (NEE800 and Pg800) were greatest in the graminoid-dominated habitats, i.e., streamside meadow and fens, with EE800 and Pg800 of up to -21 (uptake) and 28 μmol m^{-2} h^{-1}, respectively. Vascular LAI was a robust predictor of both NEE800 and Pg800 and, on a landscape scale, the fens were disproportionately important for the summertime CO_2 sequestration. Dry tundra, including the dwarf-shrub and lichen tundra, had smaller CO_2 exchange rates. The fens were the largest source of CH_4, while the dry mineral soil tundra consumed atmospheric CH_4, which on a landscape scale amounted to ~9% of the total CH_4 balance during the growing season. The largest seasonal mean CH_4 consumption rate of 0.02 μmol m^{-2} h^{-1} occurred in sand- and stone-covered barren areas. The high consumption rate agrees with the estimate based on the eddy covariance measurements at the same site. The uncertainty involved in spatial extrapolations due to a small number of replicates per land cover type is acknowledged. This study highlights the need to distinguish different land cover types including the dry tundra habitats to account for their different CO_2 and CH_4 flux patterns, especially the consumption of atmospheric CH_4, when estimating tundra C exchange on a larger spatial scale [34].

The paper [35] describes the characteristics of atmospheric surface layer and heat balance components of snow-ice cover during drift of R/V “Akademik Treshnikov” to the north of the archipelagos Franz Josef Land and Sval-

bard, in the area 80–82 N, 30–45 E, in comparison with observations at drifting station "North Pole-35", worked in the same area in April 2008, and "Ice Base Cape Baranova" in April 2019. Characteristics of atmospheric surface layer and the energy exchange processes during the drift of the expedition "Transarctica-2019" were significantly affected by the presence of clouds and the state of the ice cover. The influence of these factors led to a decrease in the radiative cooling of the surface, the formation of a warmer and wetter ABL and to a weakening of the turbulent exchange between the atmosphere and the snow-ice cover. Comparison of energy exchange characteristics, calculated for the Bolshevik Island (79° N) and for expedition "Transarctica 2019" area shows good agreement between the monthly averaged values and trends in heat fluxes, despite the fact that in the first case the underlying surface was sea ice cover, and in the second it was the land surface.

For the first time experience was gained with the operation of Russian equipment for water content and temperature remote sensing of the lower atmosphere in the Arctic. The comparison the results of measurements by radiometric systems with data of radiosoundings in wide range of meteorological conditions is presented in [36]. It is shown that mean difference between integral atmospheric water content, measured by water vapor radiometer WVR, and calculated from radiosoundings data does not exceed 6 % with standard deviation 0.54 kg/m^2 and significant correlation coefficient 0,92. Analysis the data of meteorological temperature profiler MTR-5 allows to conclude that in general its adequately reproduce air temperature profiles in the atmospheric lower 1000 m layer. Some deviations take place only in cases of large temperature gradients. Preliminary analysis of WVR data showed that monthly mean value of integral atmospheric water content in area under study in April 2019 year practically coincides with calculated from radiosoundings, performed in 1983–1988 years at the polar station Barentsburg, nearest to the drift region, 3.61 and 3.62 kg/m^2 respectively. Same time hourly mean values of integral atmospheric water content during drift varied from 2 to 10 kg/m^2, with extreme values recorded between April 15 and April 20, probably due to intensive transport of air masses of the Atlantic origin. Based on MTR-5 data it was concluded that despite differences in sounding technology, the place and time of observations, the statistics of inversions registered during drift correspond well to statistics of inversions, recorded on the Arctic coastal stations and over sea ice cover of the Weddell Sea in winter.

The duration of the navigation period (DNP) on the Northern Sea Route (NSR) and in some parts of it in the twenty-first century has been analyzed [37] based on the models of the CMIP5 ensemble (Coupled Models Intercomparison project, phase 5) under the RCP 8.5 scenario using Bayesian averaging methods. According to the study results, differences in the quality of the DNP models and in DNP variations are greater in the western part of the

NSR than in the eastern part. The DNP ensemble average was obtained in the range of 3–4 months in the middle of the twenty-first century and increasing to about six months by the end of the century. The ensemble average estimates of variations in DNP are generally robust for the choice of assumptions used for calculating the Bayesian weights. The joint consideration of the quality of modeled climate characteristics on all time scales (long-term average, interannual variations, and linear trend) in comparison with the satellite data makes it possible to reduce the intermodel standard deviation by two times for the western part of the NSR and one and a half times for the eastern part.

Every aspect of human activities in the Arctic faces a wide range of risks. By the beginning of the XXI century, mankind had recognized a new class of risks, namely the risks associated with anthropogenic climate change, which is more noticeable in the Arctic, where the rate of warming is twice as high as the world average. The global and especially Arctic climate is likely to continue to change, thereby significantly affecting future socio-economic development, biodiversity, ecosystems and human society. In the [38] the authors consider climate risks associated with socio-economic development of the Russian Arctic, and propose a modelling framework that allows stakeholders to identify and manage climate risks, assess the economic impacts of climate change in the Arctic, and assist in the development of climate change adaptation strategies.

In [39] Quantitative estimates of changes in wind energy resources in the Arctic were obtained using the RCA4 regional climate model under the RCP4.5 and RCP8.5 climate change scenarios for 2006–2099. The wind power density proportional to cubic wind speed was analyzed. The procedure for the model near-surface wind speed bias correction using ERA5 data as a reference with subsequent extrapolation of wind speed to the turbine height was applied to estimate the wind power density (WPD). According to the RCA4 simulations for the 21st century under both anthropogenic forcing scenarios, a noticeable increase in the WPD was noted, in particular, over the Barents, Kara, and Chukchi seas in winter. In summer, a general increase in the WPD is manifested over the Arctic Ocean. The changes are more significant under the RCP8.5 scenario with high anthropogenic forcing for the 21st century. According to model projections, an increase in the interdaily WPD variations does not generally lead to the deviations of wind speed to the values at which the operation of wind generators is unfeasible.

Antarctic meteorology studies

Quantitative estimates of the relationship between interannual variations in the extent of Antarctic and Arctic sea ice and changes in the surface air temperature in the Northern and Southern hemispheres are obtained in [40, 41] using satellite, ground-based, and reanalysis data for the past four dec-

ades (1980–2019). It is shown that the previously noted general increase in the extent of Antarctic sea ice observed until recent years from satellite data (available only since the late 1970s) over the background global warming and a rapid decrease in the extent of Arctic sea ice is associated with a regional decrease in the surface temperature at Antarctic latitudes from the end of the 1970s. This is a result of regional manifestation of natural climate variations with periods of up to several decades against the background of global secular warming with a relatively weak temperature trend over the ocean in the Southern Hemisphere. Since 2016, a sharp decrease in the extent of Antarctic sea ice in the Southern Ocean has been observed. The results of the correlation and cross-wavelet analysis indicate significant coherence and negative correlation with the surface temperature of the extent of sea ice in recent decades, not only in the Arctic, but also in the Antarctic.

Changes in snow cover and sea ice extents associated with temperature changes in the Northern and Southern Hemispheres for the period 1979–2020 are analyzed using monthly-mean satellite and reanalysis data [42]. Quantitative estimates of the relationship between the Antarctic and Arctic sea ice and changes in the surface air temperature were obtained. Overall increase of the Antarctic sea ice extent is associated with the regional manifestation of natural multidecadal climate modes with periods of up to several decades (against the background of global warming and a rapid decrease in the extent of sea ice in the Arctic). The results of correlation and cross-wavelet analyses show significant coherence and negative correlation of the surface air temperature in both Arctic and Antarctic with the respective sea ice extent in recent decades. Seasonal and regional features of the snow cover sensitivity to changes in the temperature regime in the Northern Hemisphere for the past four decades are noted. The features of snow cover variability in Eurasia and North America are presented.

Stable water isotopologues (SWIs) are useful tracers of moist diabatic processes in the atmospheric water cycle. They provide a framework to analyze moist processes on a range of timescales from large-scale moisture transport to cloud formation, precipitation and small-scale turbulent mixing. Laser spectrometric measurements on research vessels produce high-resolution time series of the variability of the water vapour isotopic composition in the marine boundary layer. In the study [43], the authors present a 5-month continuous time series of such ship-based measurements of δ^2H and δ^{18}O from the Antarctic Circumnavigation Expedition (ACE) in the Atlantic and the Southern Ocean in the time period from November 2016 to April 2017. The authors analyze the drivers of meridional SWI variations in the marine boundary layer across diverse climate zones in the Atlantic and Southern Ocean using Lagrangian moisture source diagnostics and relate vertical SWI differences to near-surface wind speed and ocean surface state.

The median values of $\delta^{18}O$, $\delta^{2}H$ and deuterium excess during ACE decrease continuously from low to high latitudes. These meridional SWI distributions reflect climatic conditions at the measurement and moisture source locations, such as air temperature, specific humidity and relative humidity with respect to sea surface temperature. The SWI variability at a given latitude is highest in the extratropics and polar regions with decreasing values equatorwards. This meridional distribution of SWI variability is explained by the variability in moisture source locations and its associated environmental conditions as well as transport processes. The westward-located moisture sources of water vapour in the extratropics are highly variable in extent and latitude due to the frequent passage of cyclones and thus widen the range of encountered SWI values in the marine boundary layer. Moisture loss during transport further contributes to the high SWI variability in the extratropics. In the subtropics and tropics, persistent anticyclones lead to well-confined narrow easterly moisture source regions, which is reflected in the weak SWI variability in these regions. Thus, the expected range of SWI signals at a given latitude strongly depends on the large-scale circulation. Furthermore, the ACE SWI time series recorded at 8.0 and 13.5 m above the ocean surface provide estimates of vertical SWI gradients in the lowermost marine boundary layer. On average, the vertical gradients with height found during ACE are for $\delta^{18}O$, for $\delta^{2}H$ and 0.3 ‰ m^{-1} for deuterium excess. Careful calibration and post-processing of the SWI data and a detailed uncertainty analysis provide a solid basis for the presented gradients. Using sea spray concentrations and sea state conditions, we show that the vertical SWI gradients are particularly large during high wind speed conditions with increased contribution of sea spray evaporation or during low wind speed conditions due to weak vertical turbulent mixing. Although further SWI measurements at a higher vertical resolution are required to validate these findings, the simultaneous SWI measurements at several heights during ACE show the potential of SWIs as tracers for vertical mixing and sea spray evaporation in the lowermost marine boundary layer [43].

The study [44] presents the results of analysis of observational data on total ozone at the Russian Antarctic stations Mirny, Novolazarevskaya, and Vostok for 1975–2019 and on the research vessels for 2005–2019. A steady trend towards the total ozone decrease in Antarctic spring was observed till the early 2000-s. Currently, there is a tendency of returning total ozone values to those typical of the period preceding the manifestation of the ozone hole effect.

Surface layer and upper-air in situ observations from two research vessel cruises and an ice station in the Weddell Sea from 1992 and 1996 are used to validate four current atmospheric reanalysis products: ERA-Interim, CFSR, JRA-55 and MERRA-2 [45]. Three of the observation datasets were not

available for assimilation, providing a rare opportunity to validate the reanalyses in the otherwise datasparse region of the Antarctic against independent data. All four reanalyses produce 2 m temperatures warmer than the observations and the biases vary from +2.0 K in CFSR to +2.8 K in MERRA-2. All four reanalyses are generally too warm also higher up in the atmospheric boundary layer (ABL), with biases up to +1.4 K (ERA-Interim). Cloud fractions are relatively poorly reproduced by the reanalyses, MERRA-2 and JRA-55 having the strongest positive and negative biases of about +30 % and -17 %, respectively. Skill scores of the error statistics reveal that ERA-Interim compares generally the most favorably against both the surface layer and the upper-air observations. CFSR compares the second best and JRA-55 and MERRA-2 have the least favorable scores. The ABL warm bias is consistent with previous evaluation studies in high latitudes, where more recent observations have been applied. As the amount of observations has varied depending on the decade, season and region, the consistency of the warm bias suggests a need to improve the modelling systems, including data assimilation as well as ABL and surface parameterizations [45].

Since 2004, Russian Antarctic Expeditions have carried out yearly measurements of physicochemical aerosol characteristics onboard research vessels at Southern Hemisphere high latitudes (34–72° S; 45° W–110° E). In [46] the authors statistically generalize the results from multiyear (2004–2021) measurements in this area of the aerosol optical depth (AOD) of the atmosphere, concentrations of aerosol and equivalent black carbon (EBC), as well as the ionic composition of aerosol. A common regularity was that the aerosol characteristics decreased with increasing latitude up to the Antarctic coast, where the aerosol content corresponded to the global background level. Between Africa and Antarctica, AOD decreased from 0.07 to 0.024, the particle volume decreased from 5.5 to 0.55 $\mu m^3/cm^3$, EBC decreased from 68.1 to 17.4 ng/m^3, and the summed ion concentration decreased from 24.5 to 2.5 $\mu g/m^3$. Against the background of the common tendency of the latitude decrease in aerosol characteristics, we discerned a secondary maximum (AOD and ion concentrations) or a plateau (aerosol and EBC concentrations). The obtained spatial distribution of aerosol characteristics qualitatively agreed with the model-based MERRA-2 reanalysis data, but showed quantitative differences: the model AOD values were overestimated (by 0.015, on average); while the EBC concentrations were underestimated (by 21.7 ng/m^3). An interesting feature was found in the aerosol spatial distribution in the region of Antarctic islands: at a distance of 300 km from the islands, the concentrations of EBC decreased on average by 29%, while the aerosol content increased by a factor of 2.5 [46].

The aerosol optical depth of the atmosphere obtained from spectral sun photometer measurements and the integral optical depth determined from

standard actinometric observations of direct solar radiation are the parameters of the optical state of the atmosphere. The quantitative estimates of the integral transparency and aerosol optical depth of the atmosphere in Antarctica are presented, their long-term variability over the entire period of observations is analyzed in [47]. The comparison of obtained data with the estimates for other natural regions and conditions revealed that during the periods without the impact of volcanic eruptions, the levels of atmospheric aerosol turbidity in Antarctica over the recent decades are minimal on the planet and can be considered as global background characteristics.

Taking into account the tangible changes in the climate on the planet as a whole, databases and archives of data on the main climate-forming characteristics of the atmosphere, collected over long periods of time in various regions of the globe and, in particular, in the polar regions, acquire a special role. Total solar radiation is one of the most important parameters affecting the energy balance of the Earth-atmosphere system. The authors of [48] have created a database (DB) of hourly and daily sums of total radiation (Q) at the Russian Antarctic stations, designed to study the radiation regime of Antarctic, from the beginning of actinometric observations to 2019. The information presented in the database was collected at five Antarctic stations – Bellingshausen, Vostok Mirny, Novolazarevskaya and Progress. A description of the structure of the DB and the representativeness of information for each station are described in detail in [48]. As an example of using database information, characteristics of the total radiation in the different parts of the Antarctic continent are obtained. It was found that the average monthly amounts of Q in the continental part of Antarctica on the high plateau (Vostok station) in conditions of minimal cloudiness and high transparency during the Antarctic summer are maximum and average 1240 MJ/m^2. At the same time, at the tip of the Antarctic Peninsula (Bellingshausen station) during the same period, the average monthly amounts of Q due to the almost constantly present cloud cover do not exceed 570 MJ/m^2. In the coastal areas at the remaining three stations, the average monthly amounts of total radiation range from 908 MJ/m^2 (Progress) to 950 MJ/m^2 (Mirny). Estimates of variability characteristics of daily, monthly, and annual sums of total radiation at all five stations for the entire observation period up to 2019 were also obtained. The absence of statistically significant long-term trends in the annual and monthly sums of total radiation at all the stations under consideration was noted. The results of their analysis indicate that there are no significant changes in the inflow of total solar radiation to the Antarctic surface over more than sixty years of actinometric observations.

In [49] it is shown that the snow stake measurements in central Antarctica systematically underestimate the value of the snow build-up. Two methods for the calculation of the corresponding correction to the snow stake meas-

urements at Vostok station are developed to take this underestimation into account. The first method is based on the Sorge's law to calculate the rate of compaction of snow layers using the vertical profile of snow density. The second method is based on the direct field measurements of this compaction. Two independent methods for the estimation of the snow accumulation rate in the vicinity of Vostok station are also considered: geodetic data on the rate of snow layer sinking and glaciological data from snow pits. The most reliable estimate of the snow accumulation rate in this region is 2.26 ± 0.10 g/cm^2 per year, that is $8 \pm 4\%$ higher than uncorrected values from snow accumulation measurements [49].

References

1. Climate of the Arctic: processes and changes. Ed. I.I. Mokhov, V.A. Semenov. M.: Fizmatkniga, 2022, 360 p. (In Russ).
2. Mokhov I.I. Features of modern climate changes in the Arctic and their consequences. Problemy Arktiki i Antarktiki. Arctic and Antarctic Research. 2020, 66 (4): 446-462. (In Russ.) https://doi.org/10.30758/0555-2648-2020-66-4-446-462
3. Mokhov, I.I., Analytical conditions for the formation of the Arctic amplification in the Earth's climate system, Dokl. Earth Sciences. 2022, 505, No.1, 102–107. (In Russ).
4. Demchev D.M., Kulakov M.Y., Makshtas A.P., Makhotina I.A., Fil'chuk K.V., Frolov I.E. Verification of ERA-Interim and ERA-5 reanalyses data on surface air temperature in the Arctic. Rus. Meteorol. Hydrol. 2020, 45, No. 11, 771–777.
5. Akperov M.G., Mokhov I.I., Dembitskaya M.A., Parfenova M.R., Rinke A. Peculiarities of temperature stratification and its changes in the troposphere of Arctic latitudes according to reanalysis data and model calculations. Rus. Meteorol. Hydrol. 2019, No. 2, 19–27. (In Russ).
6. Akperov M., Rinke A., Mokhov I.I. et al. Future projections of cyclone activity in the Arctic for the 21st century from regional climate models (Arctic-CORDEX). Glob. Planet. Change. 2019, 182, 103005. doi: 10.1016/j.gloplacha.2019.103005.
7. Akperov M., Semenov V.A., Mokhov I.I., Dorn W., Rinke A. Impact of Atlantic water inflow on winter cyclone activity in the Barents Sea: insights from coupled regional climate model simulations. Environ. Res. Lett., 2020, 15(2), 024009. doi: 10.1088/1748-9326/ab6399.
8. Akperov M., Zhang W., Miller P.A., Mokhov I.I., Semenov V.A., Matthes H., Smith B., Rinke A. Responses of Arctic cyclones to biogeophysical feedbacks under future warming scenarios in a regional Earth system model. Environ. Res., Lett., 2021, 16 (6), 064076. https://doi.org/10.1088/1748-9326/ac0566.
9. Heinemann G., Willmes S., Schefczyk L., Makshtas A., Kustov V., Makhotina I. Observations and Simulations of Meteorological Conditions over Arctic Thick Sea Ice in Late Winter during the Transarktika 2019 Expedition. Atmosphere, 2021, 12, 174. https://doi.org/10.3390/atmos12020174.
10. Heinemann G., Drüe C., Schwarz P., Makshtas A. Observations of Wintertime Low-Level Jets in the Coastal Region of the Laptev Sea in the Siberian Arctic Using SODAR/RASS. Remote Sens., 2021, *13*, 1421. https://doi.org/10.3390/rs13081421

11. Heinemann G., Drüe C., Makshtas A. A Three-Year Climatology of the Wind Field Structure at Cape Baranova (Severnaya Zemlya, Siberia) from SODAR Observations and High-Resolution Regional Climate Model Simulations during YOPP. Atmosphere, 2022, 13, 957. https://doi.org/10.3390/atmos13060957.
12. Chechin D., Makhotina I., Lüpkes C., Makshtas A. Effect of Wind Speed and Leads on Clear-Sky Cooling over Arctic Sea Ice during Polar Night. Journal of the Atmospheric Sciences. 2019, 76 (8). 2481–2503. DOI:10.1175/JAS-D-18-0277.1.
13. Makhotina I.A., D.G. Chechin, A.P. Makshtas. Cloud Radiative Forcing over Sea Ice in the Arctic during the Polar Night According to North Pole-37, -39, and -40 Drifting Stations. Izvestiya, Atmospheric and Oceanic Physics, 2021, Vol. 57, No. 5, 451–460.
14. Akperov M.G., Semenov V.A., Mokhov I.I., Parfenova M.R., Dembitskaya M.A., Bokuchava D.D., Rinke A., Dorn W. The influence of ocean heat transport in the Barents Sea on the regional sea ice and the atmospheric static stability. Led i Sneg. Ice and Snow. 2019, 59 (4), 529–538. (In Russ). https://doi.org/10.15356/2076-6734-2019-4-438.
15. Mokhov I.I., Pogarsky F.A. Changes in sea wave regimes in the Arctic basin according to ensemble model calculations for the 21st century. Dokl. Earth Sciences. 2021, 496. No. 2, 189–193.
16. Prokhorova U.V. and A.V. Urazgildeeva. Effect from polynyas in the Siberian Arctic seas to atmospheric transport of heat and moisture. IOP Conf. Ser.: Earth Environ. Sci., 2020, 606, No. 012047. DOI 10.1088/1755-1315/606/1/012047.
17. Mokhov, I. and M. Parfenova. Changes in the Snow Cover Extent in Eurasia from Satellite Data in Relation to Hemispheric and Regional Temperature Changes. Dokl. Earth Sciences. 2021, 501, 963-968. DOI 10.1134/S1028334X21110106.
18. Mokhov, I. and M. Parfenova. Relationship of snow cover and sea ice extent to temperature changes in the Northern hemisphere based on data for recent decades. Izvestiya, Atmospheric and Oceanic Physics, 2022, Vol. 58, No. 4, 411–423. DOI: 10.31857/S0002351522040101 (In Russ).
19. Sakerin S.M., Golobokova L.P., Kabanov D.M., Kalashnikova D.A., Kozlov V.S., Kruglinsky I.A., Makarov V.I., Makshtas A.P., Popova S.A., Radionov V.F., Simonova G.V., Turchinovich Yu.S., Khodzher T.V., Khuriganova O.I., Chankina O.V., and Chernov D. G. Measurements of physical-chemical characteristics of atmospheric aerosol at research station Ice Base Cape Baranov in 2018. Atmospheric and Oceanic Optics. 2019, Vol. 32, No. 5, 511–520. DOI: 10.1134/S1024856019050130.
20. Sakerin S.M., Golobokova L.P., Kabanov D.M., Kozlov V.S., Pol'kin V.V., Radionov V.F. and Chernov D G. Comparison of Average Aerosol Characteristics in Neighboring Arctic Regions. Atmospheric and Oceanic Optics, 2019, Vol. 32. No. 1, 33–40. DOI: 10.1134/S1024856019010147.
21. Golobokova L.P., Khodzher T.V., Izosimova O.N., Zenkova P.N., Pochufarov A.O., Khuriganowa O.I., Onishyuk N.A., Marinayte I.I., Polkin V.V., Radionov V.F., Sakerin S.M., Lisitzin A.P., Shevchenko V.P. Chemical Composition of Atmospheric Aerosol in the Arctic Region and Adjoining Seas along the Routes of Marine Expeditions in 2018–2019. Atmospheric and Oceanic Optics. 2020, Vol. 33, No. 5, 480–489. DOI: 10.1134/S1024856020050085
22. Sakerin S.M., Kabanov D.M., Makarov V.I., Pol'kin V.V., Popova S.A., Chankina O.V., Pochufarov A.O., Radionov V.F., Rize D.D. Spatial distribution of

atmospheric aerosol physicochemical characteristics in the Russian sector of the Arctic Ocean. Atmosphere, 2020, 11(11), 1170 DOI: 10.3390/atmos11111170.
23. Isaksen, K., Nordli, Ø., Ivanov, B. et al. Exceptional warming over the Barents area. Sci Rep 12, 9371 (2022). https://doi.org/10.1038/s41598-022-13568-5.
24. Ivanov B., Karandasheva T., Demin V., Revina A., Sviashchennikov P., Isaksen K., Førland E.J., Nordli Ø., Gjelten H.M. Assessment of long-term changes surface air temperature from the High Arctic archipelago Franz Joseph Land from 1929 to the present (2017). Czech Polar Report. 2021, №11 (1), 114-133. DOI: 10.5817/CPR2021-1-9.
25. Ivanov B., Prokhorova Y., Sviashchennikov P. Analysis of continentality and anomality of Svalbard climate according to observations of surface air temperature in the second half of the XX century. IOP Conf. Ser.: Earth Environ. Sci., 2021, 606 012021 doi:10.1088/1755-1315/606/1/012021
26. Dahlke S., Hughes N.E., Wagner P.M., Gerland S., Wawrzyniak T., Ivanov B.V., Maturilli M. The observed recent surface air temperature development across Svalbard and concurring footprints in local sea ice cover. Int. J. Climatol., 2020, 40, 5246–5265. https://doi.org/10.1002/joc.6517DAHLKEET AL.5265.
27. Svyaschennikov P.N., U.V. Prokhorova, B.V. Ivanov. Comparison of Atmospheric Circulation in the Area of Spitsbergen in 1920–1950 and in the Modern Warming Period. Rus. Meteorol. Hydrol, 2020, Vol. 45, No. 1, 22–28. DOI: 10.3103/S1068373920010033.
28. Ivanov B.V. Comparing the «earlier» and the «modern» warming in West Arctic on example of Svalbard. IOP Conf. Ser.: Earth Environ. Sci., 2019, 231 12023 doi:10.1088/1755-1315/231/1/012023.
29. Skakun A.A., Chikhachev K.B., Ekaykin A.A., Kozachek A.V., Vladimirova D.O., Veres A.N., Verkulich S.R., Sidorova O.R., Demidov N.E. Stable isotopic composition of atmospheric precipitation and natural waters in the vicinity of Barentsburg (Svalbard). Led i Sneg. Ice and Snow. 2020. 60 (3): 379–394. [In Russ.]. doi: 10.31857/S2076673420030046.
30. Golobokova L.P., Khodzher T.V., Chernov D.G., Sidorova O.R., Khuriganova O.I., Onischuk N.A., Zhuchenko N.A., Marinaite I.I. Chemical composition of the near-surface atmospheric aerosol in Barentsburg (Svalbard) based on the long-term observations. Led i Sneg. Ice and Snow. 2020; 60(1), 85–97. (In Russ.) https://doi.org/10.31857/S2076673420010025
31. Methane and climate change: scientific problems and technological aspects. Moscow: Russian Academy of Sciences, Ed. V.G. Bondur, I.I. Mokhov, A.A. Makosko. 2022, 388 p.
32. Arzhanov M.M., Malakhova V.V., Mokhov I.I. Modeling thermal regime and evolution of the methane hydrates stability zone of the Yamal Peninsula permafrost. Permafrost and Periglacial Processes. 2020, Vol. 31 (4), 487-496. (In Russ).
33. Mokhov I.I., Malakhova V.V., Arzhanov M.M. Model estimates of intra- and intersentennial degradation of permafrost on the Yamal Peninsula under warming. Doklady Earth Sciences, 2022. Vol. 506 (2), 782–789.
34. Juutinen S., Aurela M., Tuovinen J.-P., Ivakhov V., Linkosalmi M., Räsänen A., Virtanen T., Mikola J., Nyman J., Vähä E., Loskutova M., Makshtas A., and Laurila T.. Variation in CO_2 and CH_4 fluxes among land cover types in heterogeneous Arctic tundra in northeastern Siberia. Biogeosciences, 19, 3151–3167, https://doi.org/10.5194/bg-19-3151-2022, 2022.

35. Makhotina I.A., A.P. Makshtas, V Yu. Kustov. Sea ice – Atmosphere heat exchange during expedition “Transarctica-2019”. IOP Conf. Ser.: Earth Environ. Sci., 2020, 606 012032. DOI: 10.1088/1755-1315/606/1/012032.
36. Makshtas A.P., Il’in G.N., Bykov V.Yu., Miller E.A., Troitsky A.V., Kustov V.Yu., Bolshakova I.I., Rize D.D. The experience of remote temperature-water content sounding of atmosphere during drift of R/V “Akademik Tryoshnikov”. Problemy Arktiki i Antarktiki. Arctic and Antarctic Research. 2020; 66 (3): 349–363. (In Russ.) https://doi.org/10.30758/0555-2648-2020-66-3-349-363.
37. Parfenova, M.R., A.V. Eliseev, and I.I. Mokhov, 2022. Changes in the duration of the navigation period in Arctic seas along the Northern Sea Route in the twenty-first century: Bayesian estimates based on calculations with the ensemble of climate models. Doklady Earth Sci., 507, No. 1, 952-958. doi 10.1134/S10283 34X2260058X.
38. Soldatenko S.A. and G.V. Alekseev. Managing climate risks associated with socio-economic development of the Russian Arctic 2020, IOP Conf. Ser.: Earth Environ. Sci. 606 012060 DOI 10.1088/1755-1315/606/1/012060.
39. Akperov M.G., Eliseev A.V., Mokhov I.I., Semenov V.A., Parfenova M.R., Koenigk T. Wind energy potential in the Arctic and Subarctic regions and Its projected change in the 21st century based on regional climate model simulations. Rus. Meteorol. Hydrol. 2022. V. 47. No. 6, 428–436.
40. Mokhov I.I., Parfenova M.R. Peculiarities of Antarctic and Arctic sea ice variability in recent decades against the background of global and regional climate changes. Problems of geography. 2020, No. 150, 304-319. (In Russ.).
41. Mokhov I.I., Parfenova M.R. Relationship of the extent of Antarctic and Arctic sea ice with temperature changes, 1979-2020. Doklady Earth Sci. 2021, V. 496. No. 1, 66-71.
42. Mokhov I.I., Parfenova M.R. Changes of the sea ice and snow cover extent associated with teperature changes in the Northern and Southern Hemispheres in recent decades 2022 IOP Conf. Ser.: Earth Environ. Sci. 1040 012016. DOI 10.1088/1755-1315/1040/1/012016.
43. Thurnherr I., Kozachek A., Graf P., Weng Y., Bolshiyanov D., Landwehr S., Pfahl S., Schmale J., Sodemann H., Steen-Larsen H.C., Toffoli A., Wernli H., and Aemisegger F.: Meridional and vertical variations of the water vapour isotopic composition in the marine boundary layer over the Atlantic and Southern Ocean, Atmos. Chem. Phys., 2020, 20, 5811–5835, https://doi.org/10.5194/acp-20-5811-2020.
44. Sibir E.E., V.F. Radionov, E.N. Rusina Results of Long-term Observations of Total Ozone in Antarctica and over the Atlantic and Southern Oceans. Rus. Meteorol. Hydrol., 2020, Vol. 45, No. 3, 161-168. DOI: 10.3103/S1068373920030036
45. Jonassen M.O., Valisuo I., Vihma T., Uotila P, Makshtas A. P., Launiainen J. Assessment of Atmospheric Reanalyses With Independent Observations in the Weddell Sea, the Antarctic. JGR Atmospheres, 2019, 124, No.23, 12468-12484 DOI**:** 10.1029/2019JD030897
46. Sakerin S.M., Golobokova L.P., Kabanov D.M., Khuriganowa O.I., Pol’kin V.V., Radionov V.F., Sidorova O.R., Turchinovich Y.S. Spatial distribution of aerosol characteristics over the South Atlantic and Southern Ocean using multiyear (2004–2021) measurements from Russian Antarctic Expeditions. Atmosphere, 2022, 13, 427. DOI: 10.3390/atmos13030427

47. Radionov V.F., Rusina E.N., Sibir E.E. Long-term Variability of Integral and Spectral Transparency of the Atmosphere at Mirny Observatory, Antarctica. Rus. Meteorol. Hydrol., 2020, Vol. 45, No.2, 74-80. DOI: 10.3103/S106837 392002002
48. Sibir E.E., Radionov V.F., Rusina E.N. Database of hourly and daily sums of total radiation at Russian antarctic stations: analysis of changes in total radiation for the entire period of observations in Antarctica. Problemy Arktiki i Antarktiki. Arctic and Antarctic Research. 2021, 67 (3): 249–260. (In Russ.). https://doi.org/ 10.30758/0555-2648-2021-67-3-249-260.
49. Ekaykin A.A., Teben'kova N.A., Lipenkov V.Y. et al. Underestimation of Snow Accumulation Rate in Central Antarctica (Vostok Station) Derived from Stake Measurements. Russ. Meteorol. Hydrol., 2020, 45, No.2, 132–140. https://doi.org/10.3103/S1068373920020090

Radiation

Edited by *Timofeev Yu.M.* (SPbU)

Coordinated Lead Authors

Budak V.P. (MPEI), *Chubarova N.E.* (MSU), *Filippov N.N.* (SPbU), *Ptashnik I.V.* (IAO), *Uspenskii A.B.* (SRC "Planeta"), *Virolainen Ya.A.* (SPbU)

Contributing Authors

SPbU: *Mikhailov E.F.*, *Vlasenko S.S.*, *Nagirner D.I.*, *Nerobelov G.M.*

OIAP: *Gorchakov G.I., Vigasin A.A., Postylakov O.V., Rakitin V.S., Grechko E.I.*

IAO: *Astafurov V.G., Belan B.D., Belov V.V., Bobrovnikov S.M., Zhuravleva T.B., Marichev V.N., Panchenko M.V., Simonova A.A., Sinitsa L.N., Chesnokova T.Yu.*

SRC "Planeta": *Kiseleva Yu.B., Rublev A.N.*

RPA "Typhoon": *Nerushev A.F.*

RSHU*: Pokrovskii O.M.*

MGO: *Solomatnikova A.A., Ivahov V.M., Paramonova N.N.*

AARI: *Radionov V.F.*

INSM UFU: *Zakharov V.I.*

IAP: *Feigin A.M.*

List of abbreviations

AARI – Arctic and Antarctic Research Institute

IAO – Zuev V.E. Institute of Atmospheric Optics of the Siberian Branch of the Russian Academy of Sciences

IAP – Institute of Applied Physics of the Russian Academy of Sciences

INM – Marchuk Institute of Numerical Mathematic of the Russian Academy of Science

INSM UFU – Institute of Natural Sciences and Mathematics of Ural Federal University

MGO – Voeikov Main Geophysical Observatory

MPEI – Moscow Power Engineering Institute

MSU – Moscow State University

OIAP – Obukhov A.M. Institute of Atmospheric Physics of the Russian Academy of Sciences

RPA "Typhoon" – Research and Production Association "Typhoon"

RSHU – Russian State Hydrometeorological University

SPbU – St. Petersburg State University

SRC "Planeta" – Scientific Research Center of Space Hydrometeorology "Planeta"

Abstract. The report prepared by the Russian Radiation Commission contains the most significant results of scientific studies in the field of atmospheric radiation during 2019–2022. It is an integral part of the National Report of Russia on Meteorology and Atmospheric Sciences prepared for the International Association of Meteorology and Atmospheric Sciences (IAMAS). During the last four years the Russian Radiation Commission in cooperation with different institutions and organizations organized two international symposiums "Atmospheric Radiation and Dynamics" (ISARD-2019, ISARD-2021). The symposiums were dedicated to actual problems of atmospheric physics: radiation transfer and atmospheric optics, greenhouse gases, clouds and aerosols, ground-based and satellite techniques of remote sensing measurements.

Radiative transfer theory

Two new Monte Carlo algorithms have been developed to calculate the spectral fluxes and brightness fields of thermal radiation with allowance made for the sphericity of the atmosphere and 3D effects of clouds [Zhuravleva et al, 2019]. The algorithms differ in the ways the molecular absorption is considered (the k-distribution method and the randomization method). Realizations of cloud fields are simulated based on a Poisson model of broken clouds. The Poisson model of broken clouds provides for the efficient simulation of many various mesoscale cloud fields, which makes it possible to identify the 3D effects of clouds on outgoing radiation in the upper atmosphere as functions of cloud configuration and optical characteristics in different spectral ranges.

The intensity of transmitted solar radiation in the presence of optically thin cirrus clouds has been simulated statistically for two geometrical sensing schemes of the AERONET photometric network [Zhuravleva, 2021]. Numerical experiments have been performed with different cirrus cloud models, namely, OPAC (hexagonal particles with a smooth surface) and a model proposed by a group of authors B.A. Baum, P. Yang, A.J. Heymsfield et al. (mixture of particles of different shapes, hexagonal columns, and aggregates of hexagonal columns with a very rough surface). It has been found that the absence of brightness peaks in the zones of possible halo appearance does not mean the absence of cirrus clouds in the sky, since the angular structure of the radiation field in the presence of strongly rough hexagonal particles is described by a smooth function of the scattering angle. An analysis of the influence of the microstructure of cirrus clouds on the albedo and diffuse transmission averaged over a set of cloud realizations has shown that the mean value of the uncertainty due to the lack of information about the shape and size of particles is within ~2% [Zhuravleva, 2021]. This value is compa-

rable to the influence of the effects of random cloud geometry in optically thin clouds, while as the optical density increases, the diffuse transmission can be underestimated by more than 10%.

An original algorithm for statistical simulation of solar radiation transfer in the presence of cirrus clouds that are optically anisotropic with respect to the zenith angle of the incident radiation has been developed and successfully tested [Zhuravleva, 2021; Zhuravleva, 2021a]. The results of the numerical experiments indicate that the proposed algorithm adequately considers the properties of optical anisotropy of the environment when simulating the radiation transfer.

In [Firsov et al., 2021], a broadband model for the transfer of short-wave solar radiation in the Earth's atmosphere has been developed. The model is based on the parametrization of radiation transmission functions using modern spectroscopic information in the form of short exponential series, which makes it possible to apply the standard discrete ordinate method to solving the radiation transfer equation for each exponential component.

The study [Fomin, 2021] presents an effective direct calculation line-by-line (LBL) method for fast calculation of compact and accurate spectral search tables for LBL radiation transfer models. The key feature of this method is to obtain and to use efficient grids with inhomogeneous wavenumbers to interpolate the line profile with a given accuracy.

The study [Svetsov V. et al, 2019] is devoted to solving the radiation transfer equation system together with the equations of gas dynamics. The approximation of radiative thermal conductivity was used, or, if the optical depth of the Rosseland radiating volume of gas and steam was less than one, in the approximation of volumetric radiation. The developed algorithm is used for numerical simulation of collisions of cometary bodies with a diameter of 0.3, 1 and 3 km, which enter the atmosphere at different angles.

Soldatenko S. et al. [2021] studied the influence of uncertainties in radiation feedbacks and inertia of the climate system on the power spectrum of fluctuations in the Global Mean Surface Temperature (GMST). It has been shown that in the high-frequency range of the GMST oscillation power spectrum, the influence of the inertia of the climate system is more significant than the influence of feedbacks. In the low-frequency range, on the contrary, the influence of feedbacks on the power spectrum exceeds the influence of climatic inertia.

In the study [Chesnokova et al, 2019], the upward and downward fluxes of solar and thermal radiation are modeled for meteorological conditions typical for summer in the middle latitudes. The balance of atmospheric radiation caused by cirrus clouds of different depths and the sensitivity of radiative forcing to various models of continuum absorption of water vapor are estimated.

In [Timofeev et al, 2020], based on the analysis of the radiation transfer equation in integral form, the causes of changes in the outgoing thermal radiation of the Earth with an increase in atmospheric CO_2 content are investigated.

The study [Kuchma et al, 2020] considered the problem of atmospheric correction of short-wave channels of a low-resolution multispectral scanning radiometer on board the Meteor-M No. 2 satellite. An atmospheric correction algorithm based on special search tables generated by the authors is proposed. The test showed a high correlation with the reference reflection coefficient obtained from the sites for checking the albedo of the surface of the EUMETSAT portal.

In [Silant'ev et al, 2021], radiation transfer equations were obtained for all Stokes parameters of continuous radiation in atmospheres in a homogeneous magnetic field. Explicit formulas for cross-sections and phase shifts are given considering absorption effects. The presented theory is valid for magnetic fields of no more than 1010Gs. In general, the magnetic field consists of an average value and a chaotic part. The system of transfer equations for the four averaged Stokes parameters, I, Q, U and V, decomposes into two independent systems – for the parameters I, Q and V, U.

Balugin et al. [2022] presented a method for assessing the impact of stratospheric aerosol on the radiation balance of the stratosphere based on the data of balloon sensing by an optical aerosol backscattering probe. The assessment methodology is based on the use of a radiation (line-by-line and Monte Carlo) model of solar radiation transfer.

Fomin et al. [2019] discussed the changes in the calculations of line-by-line infrared radiation spectra that occur when replacing HITRAN-2012 with HITRAN-2016 and the Voigt contour with the Hartman-Tran contour.

The study [Chernenkov et al, 2021] estimated the concentration of soot in snow based on the balance model of the snow layer and the SNICAR radiation transfer model. The albedo of snow and the radiation effect from the darkening of snow from the concentration of soot are calculated.

In [Dombrovsky et al, 2020], a model of virus spread by airborne droplets inside water microdrops was proposed. A model of a viral cloud is constructed considering various mechanisms, such as the effect of solar irradiation, dynamic relaxation of moving droplets in the ambient air and gravitational precipitation of droplets. The maximum estimation of the spectral radiation flux in the case of a cloudless sky showed that the contribution of radiation to the evaporation of individual water droplets is insignificant.

The study [del Águila A. et al, 2020] describes a method for accelerating hyperspectral radiation transfer calculation models based on clustering of spectral emissions calculated using a low-flow transfer model and regression analysis performed for low-flow and multi-flow models within each cluster. This approach, which we call the Cluster Low-Streams Regression (CLSR)

method, is used to calculate the emission spectra in the A-band of O_2 at 760 nm and the CO_2 range at 1610 nm for five atmospheric scenarios. The CLSR method is compared with a transfer model based on Principal Component Analysis, demonstrating improvements in accuracy and computational performance.

Zhuravleva [2021] presented an original algorithm for statistical modeling of solar radiation transfer in the presence of clouds of ice crystals optically anisotropic with respect to the zenith angle of incident radiation. Numerical experiments have shown that when using the proposed algorithm, the properties of an optically anisotropic medium are most adequately taken into account when modeling radiation transfer.

In [Kataev M.Yu. et al, 2019, 2021, 2022], image processing algorithms obtained from unmanned aerial vehicles in real time for optical remote sensing of the Earth's surface are analyzed. The use of an analogue of the vegetation index allows to highlight plants in the RGB image, which increases the probability of correct recognition of surface types (plants). The methods of preliminary and thematic image processing necessary for confident recognition of surface types are considered.

An analysis was carried out [Belov et al., 2019a] of the effectiveness of the optical (photo and radiometric) method for detecting oil pollution, based on the difference in the reflective characteristics of clean and oil-contaminated water surfaces, when choosing the wavelength of sensing in the UV, visible, near and middle IR ranges of the spectrum.

In [Belov et al., 2019b], the results of experiments with underwater bistatic optoelectronic communication systems in which scattered laser radiation is a source of information and a useful signal are considered. In the field, information transmission ranges of up to 40 m in lake water were obtained.

Burenkov et al. [2019] have estimated the errors in determining the indicator of light attenuation by sea water by the Monte Carlo method. As a rule, measurements of the attenuation index are carried out with a small base of the device in fairly clear waters. However, in practice, there are cases of very turbid waters (bottom nepheloid layers), where the measurement errors of the attenuation index increase significantly due to multiple scattering within the base of the device. Estimates of such errors are considered in this paper. The influence of the scattering indicatrix on the errors under consideration is considered in the most detail. In addition, the influence of the attenuation of the length of the base of the device and the angle of view of the receiving system on the measurement errors was studied.

In [del Águila A. et al, 2019, 2021], to improve the efficiency of the hyperspectral data processing algorithm, dimensionality reduction methods were analyzed in relation to hyperspectral remote sensing of the atmosphere. When the dimensionality decreases, redundant information is excluded from

the data, and at present, dimensionality reduction is an integral part of high-performance radiation transfer models.

In [Afanas'ev et al, 2019], a comparative analysis of methods for solving the transport equation for radiation and particles is carried out. The physical model of the light field is equivalent to the theory of propagation of beams of elementary particles in the approximation of classical mechanics. Today it is especially important that the accuracy of experiments in particle physics is close to the limit, which makes it possible to test many relations of the theory of the light field in a turbid environment, where such accuracy is not yet achievable. The results of calculations are compared with experimental data on the angular distributions of electrons elastically reflected from two-layer solid-state targets.

The study [Efremenko, 2021] is devoted to the use of artificial neural networks for parameterization of computationally time-consuming radiation transfer models (MPI) in problems of remote sensing of the atmosphere. Although the direct replacement of MPI by neural networks can lead to a multiple increase in performance, this approach has certain disadvantages, such as loss of generality, problems with stability, etc. In this case, the neural network is usually trained for a specific application, for example, for predefined atmospheric scenarios and a given spectrometer. In this paper, a new concept of neural network MPI is considered, in which the neural network does not replace the entire model, but only part of it (the algorithm for calculating eigenvalues), thereby reducing the total calculation time while maintaining the generality of MPI. Dependencies on the observation geometry and the optical thickness of the medium are excluded from the training.

References

1. Afanas'ev V.P., Basov A.Yu., Budak V.P., Efremenko D.S., and Kokhanovsky A.A. Analysis of the Discrete Theory of Radiative Transfer in the Coupled "Ocean–Atmosphere" System: Current Status, Problems and Development Prospects // Journal of Marine Science and Engineering, 1920. Vol. 8. Art. 202
2. Afanas'ev V.P., Budak V.P., Efremenko D.S., and Kaplya P.S. Application of the photometric theory of the radiance field in the problems of electron scattering // Light & Engineering, 2019. Vol. 27, No. 2, pp. 88–96
3. Balugin N.V., Fomin B.A., Lykov A.D. & Yushkov V.A. Stratospheric Radiation Budget According to Optical Balloon Backscatter Probe and Radiation Modeling // (2022) Russian Meteorology and Hydrology, 47 (10), pp. 812 – 817, Cited 0 times.
4. Belov M.L., Vsyakova Y.I., and Gorodnichev V.A. Optical method of detection of oil contamination on water surface in uv spectral range // Light & Engineering, 2019a. Vol. 27, No. 5. P. 88–96
5. Belov V.V., Abramochkin V.N., Gridnev Yu.V., Kudryavtsev A.N., Tarasenkov M.V., and Fedosov A.V. Bistatic underwater optical-electronic commu-

nication: field experiments of 2017–2018 // Light & Engineering, 2019nb. Vol. 27, No. 5. P. 97–102.
6. Burenkov V.I., Sheberstov S.V., Artemiev V.A., and Taskaev V.R. Estimation of measurement error of the seawater beam attenuation coefficient in turbid water of arctic seas // Light & Engineering, 2019. Vol. 27, No. 5. P. 103–111.
7. Chernenkov A.Y., Kostrykin S.V. Estimation of Radiative Forcing from Snow Darkening with Black Carbon Using Climate Model Data // (2021) Izvestiya – Atmospheric and Ocean Physics, 57 (2), pp. 133 – 141, Cited 1 times.
8. Chesnokova T.Y., Firsov K.M., Razmolov A.A. Contribution of the Water Vapor Continuum Absorption to the Radiation Balance of the Atmosphere with Cirrus Clouds // (2019) Atmospheric and Oceanic Optics, 32 (1), pp. 64 – 71, Cited 12 times.
9. Chuprov I.A., Konstantinov D.N., Efremenko D.S., Zemlyakov V.V., and Gao J. Solution of the radiative transfer equation for vertically inhomogeneous media by numerical integration solvers: comparative analysis // Light & Engineering, 2022 Vol. 30, No. 5, pp. 21–30.
10. del Águila A. and Efremenko D.S. Accuracy enhancement of the two-stream radiative transfer model for computing absorption bands at the presence of aerosols // Light & Engineering, 2021. Vol. 29, No. 2. P. 79–86.
11. del Águila A., Efremenko D.S., and Trautmann T. A review of dimensionality reduction techniques for processing hyper-spectral optical signal // Light & Engineering, 2019. Vol. 27, No. 3, pp. 85–98
12. del Águila A., Efremenko D.S., Molina García V., Kataev M.Y. Cluster low-streams regression method for hyperspectral radiative transfer computations: Cases of o2 a-And Co2 bands // (2020) Remote Sensing, 12 (8), art. no. 1250, Cited 4 times.
13. Dombrovsky L.A., Fedorets A.A., Levashov V.Y., Kryukov A.P., Bormashenko E., Nosonovsky M. Modeling evaporation of water droplets as applied to survival of airborne viruses // (2020) Atmosphere, 11 (9), art. no. 965, Cited 23 times.
14. Efremenko D.S. Discrete ordinate radiative transfer model with the neural network based eigenvalue solver: proof of concept // Light & Engineering, 2021. Vol. 29, No. 1, pp. 56–62.
15. Firsov K.M., Chesnokova T.Y., Razmolov A.A. The Influence of Aerosol and Clouds on Underlying Surface Parameters Measured by Sentinel-2A in the Lower Volga Region // (2021) Atmospheric and Oceanic Optics, 34 (4), pp. 335–340, Cited 0 times.
16. Fomin B.A. Efficient line-by-line technique for calculating accurate and compact spectral lookup tables for satellite remote sensing // (2021) International Journal of Remote Sensing, 42 (8), pp. 3074–3089, Cited 0 times.
17. Fomin B.A., Kolokutin G.E. New HITRAN-2016 spectroscopic database for line-by-line models used in remote sensing of the Earth by infrared spectrometry // (2019) Sovremennye Problemy Distantsionnogo Zondirovaniya Zemli iz Kosmosa, 16 (1), pp. 17–24.
18. Kataev M.Yu. and Dadonova M.M. Method of vegetation detection using RGB images made by unmanned aerial vehicles on the basis of colour and texture analysis // Light & Engineering, 2019. Vol. 27, No. 5. P. 55–62.
19. Kataev M.Yu., Dadonova M.M., and Efremenko D.S. Illuminance correction of multi-time rgb images obtained with an unmanned aerial vehicle // Light & Engineering, 2021. Vol. 29, No. 2. P. 50–58.

20. Kataev M.Yu., Kartashov E.Yu., and Karpov R.K. Methodology for assessing the colour quality of brick production based on RGB images // Light & Engineering, 2022. Vol. 30, No. 4, pp. 18–24.
21. Kuchma M.O., Bloshchinskiy V.D. Algorithm for the Atmospheric Correction of Shortwave Channels of the MSU-MR Radiometer of the Meteor-M No. 2 Satellite // (2020) Izvestiya – Atmospheric and Ocean Physics, 56 (9), pp. 909–915, Cited 2 times.
22. Silant'ev N.A., Alekseeva G.A., Ananjevskaja Y.K. Radiative transfer in atmospheres with a large chaotic magnetic field // (2021) Monthly Notices of the Royal Astronomical Society, 506 (4), pp. 4805–4818, Cited 1 times.
23. Soldatenko S., Colman R. Effects of Climate System Feedbacks and Inertia on Surface Temperature Power Spectrum Obtained from CMIP5 and Low-Order Models // (2021) Izvestiya – Atmospheric and Ocean Physics, 57 (6), pp. 659–668, Cited 0 times.
24. Svetsov V., Shuvalov V. Thermal radiation from impact plumes // (2019) Meteoritics and Planetary Science, 54 (1), pp. 126–141, Cited 12 times.
25. Timofeev Y.M., Virolainen Y.A., Polyakov A.V. AUTHOR FULL NAMES: Timofeev Yu. M. (7005435915); Virolainen Ya. A. (55407570200); Polyakov A.V. (7201781002) Estimates of Variations in CO2 Radiative Forcing in the Last Century and in the Future // (2020) Atmospheric and Oceanic Optics, 33 (2), pp. 206–209, Cited 0 times.
26. Zhuravleva T.B. and Nasrtdinov I.M. Effect of Microstructure and Horizontal Inhomogeneity of Broken Cirrus Clouds on Mean Solar Radiative Fluxes in the Visible Wavelength Region: Results of Numerical Simulation // Atmospheric and Oceanic Optics, 2021, V. 34. No. 06. pp. 678–688.
27. Zhuravleva T.B. Effect of Shape and Sizes of Crystal Particles on Angular Distributions of Transmitted Solar Radiation in Two Sensing Geometries: Results of Numerical Simulation // Atmospheric and Oceanic Optics, 2021, V. 34. No. 01. pp. 50–60.
28. Zhuravleva T.B. Simulation of Brightness Fields of Solar Radiation in the Presence of Optically Anisotropic Ice-Crystal Clouds: Algorithm and Test Results // (2021) Atmospheric and Oceanic Optics, 34 (2), pp. 140–147, Cited 9 times.
29. Zhuravleva T.B. Simulation of Brightness Fields of Solar Radiation in the Presence of Optically Anisotropic Ice-Crystal Clouds: Algorithm and Test Results // Atmospheric and Oceanic Optics, 2021, V. 34. No. 02. pp. 140–147.
30. Zhuravleva T.B., Nasrtdinov I.M., Artyushina A.V., Timofeev D.N., Shishko V.A., Konoshonkin A.V., Kustova N.V. Intensity of reflected solar radiation in the presence of optically anisotropic crystal clouds: Results of preliminary calculations // Proceedings of SPIE. 2021a. V. 11916. 1191603. [11916-145].
31. Zhuravleva Tatiana, Nasrtdinov Ilmir, Chesnokova Tatiana, Ptashnik Igor. Monte Carlo simulation of thermal radiative transfer in spatially inhomogeneous clouds taking into account the atmospheric sphericity // J. of Quantative Spectroscopy and Radiative Transfer, 2019, V. 236. pp. 296–305.

Atmospheric spectroscopy

The study in this field was mainly carried out in two directions: the study of the characteristics of spectral lines and bands and the study of continuous absorption. High-precision information on atmospheric gas absorption lines is required for modeling atmospheric radiation transport and remote monitoring of greenhouse gases and atmospheric pollutants. A series of theoretical studies on the lines of the ν_6 CH_3I band was carried out at SPbU jointly with the IAO and the Franche-Comté University (Besançon, France). Interest in the spectroscopic parameters of methyl iodide lines has increased dramatically over the past few years due to its ecological significance (the source of iodine atoms that destroy the ozone layer). The CH_3I self-broadening coefficients were calculated, including their temperature dependence [Troitsyna et al., 2020], nitrogen broadening [Troitsyna et al., 2021a], oxygen and air broadening [Troitsyna et al., 2021b]. Laboratory studies of the IAO include measurements with the Bruker Fourier Transform IR (FTIR) spectrometer and the cavity ring-down spectrometer being unique in Russia. New information on the absorption spectra of such molecules as C_2H_2, O_3, CF_4, CO, CH_3I, NO_2, N_2O, HCl, H_2S has been obtained, which contributes significantly to the popular HITRAN and GEISA spectroscopic databases [Vasilchenko et al., 2022a; Dudaryonok et al., 2022a; Dudaryonok et al., 2022b; Lavrentieva et al., 2022; Serdyukov et al., 2022; Sinitsa et al., 2022; Jacquemart et al., 2022; Vasilchenko et al., 2022b]. A set of low-temperature cells to model various gas environments, including mixtures of greenhouse gases, under the conditions of the upper atmosphere is under development [Serdyukov et al., 2020; Sinitsa et al., 2020].

The influence of spectroscopic information on absorption lines of CH_4, CO, and H_2O in the modern databases on the accuracy of determination of the atmospheric total columns (TCs) of methane, carbon monoxide, and water vapor from mid- and near-IR spectra of direct solar radiation measured by ground-based FTIR spectrometers installed at the St. Petersburg and Kourovka stations has been analyzed [Chesnokova et al., 2019; Chesnokova et al., 2020a; Chesnokova et al., 2020b]. The discrepancies in CH_4, CO, and H_2O TCs due to the use of different versions of HITRAN, GEISA, and ATM databases can reach 4% and higher. To define the strategies for retrieving the CO and CH_4 TCs applied in the NDACC and TCCON international networks for greenhouse gas monitoring based on an integrated approach using a large dataset of FTIR-measurements and statistical criteria for evaluating the solution of the inverse problem, recommendations to use spectroscopic databases on absorption lines in problems of remote sensing of the gas content has been obtained. The use of these databases can improve the accuracy of TC retrieval.

Laboratory air pressure broadened H_2O absorption spectra were recorded in a range of 5900–6100 cm^{-1} at the IFS 125 HR Fourier spectrometer of the IAO. Parameters of H_2O absorption lines were determined for Voigt line profiles and modified Voigt profiles that take into account the broadening dependence on velocities of colliding molecules [Deichuli et al., 2021]. It is shown that the use of new data on the parameters of H_2O absorption lines improves the agreement between the model and measured atmospheric solar spectra as compared to the use of the well-known HITRAN and GEISA spectroscopic databases. As a result, the quality of solution of the inverse problem to determine the content of gases in the atmosphere improves.

A broadband model for calculating the radiation transfer in the Earth's atmosphere in the solar short-wavelength spectral range for the spectral channels of Sentinel-2A radiometers has been developed [Firsov et al., 2021]. This model is based on LBL calculations of absorption spectra with the use of up-to-date spectroscopic information and following parameterization of radiation transmission functions in the form of a short exponential series for application in the discrete ordinate method when solving the radiative transfer equation. For the channels of the Sentinel-2A radiometers, errors in the surface spectral brightness coefficients due to uncertainties in aerosol extinction for typical optical and meteorological conditions of the Lower Volga region have been estimated.

In [Kuzov et al., 2022], a new non-Markovian theory of the evolution of diffuse satellites around allowed (parent) rotation lines perturbed by buffer gases is proposed. As the pressure of the buffer gas increases, the Lorentzian part of the parent lines adjacent to the center of the band decays due to the transfer of intensity to the satellites. Various channels contributing to the attenuation of infrared and Raman lines of linear molecules are considered. Simple estimates of the attenuation constants agree satisfactorily with the experimental data available for the absorption spectra of HCl and HF perturbed by monatomic gases.

Several experimental and theoretical studies have been carried out at the IAP aimed at improving the accuracy of reconstructing atmospheric temperature and humidity profiles using microwave radiometry. This problem was solved mainly by obtaining high-precision experimental data on the shape parameters of the main diagnostic atmospheric lines. A study was made of the water vapor absorption line near 183 GHz [Koshelev et al., 2021a] and the oxygen band in the 60 GHz region [Makarov et al., 2020; Koshelev et al., 2021b; Koshelev et al., 2022]. The data obtained make it possible to model in detail collisional molecular effects (including the dependence of the effective collision cross section on velocity) and form the empirical basis of modern models of millimeter wave propagation in the atmosphere. Belikovich et al. [2022] demonstrated that high-precision modeling of the 60 GHz oxygen

absorption band profile based on the obtained data and the sudden energy correction formalism (Enegry Correction Sudden, ECS) can reduce the error in reconstructing the atmospheric temperature profile from HARTPRO radiometer data to fraction of the brightness temperature of the radiation (K). Based on the results of these and several previous studies of radiation absorption by the atmosphere, a monograph has been published [Tretyakov, 2021].

The absence of a satisfactory theory of magnetic-dipole transitions in polyatomic molecules did not allow to describe the $\nu_2+\nu_3$ band of carbon dioxide, which is forbidden in the electric-dipole approximation, observed in the Martian atmosphere. To overcome this disadvantage, the quantum theory of the magnetic moment of spinless molecules was constructed at the OIAP, including the basic elements of the theory of magnetic-dipole vibrational-rotational transitions [Kazakov at al., 2021]. A method for calculating magnetic dipole spectra was developed and the necessary quantum chemical calculations were performed. Variational calculations of the magnetic-dipole and quadrupole spectra in the region of 3.3 μm of carbon dioxide were carried out. Good agreement between the theoretical spectra and laboratory measurement data obtained using the highly sensitive CRDS method and Fourier spectroscopy [Borkov at al., 2021] is shown.

In the study [Ptashnik at al., 2019], carried out jointly by the staff of the IAO and OIAP, a description of the continuum absorption of water vapor in the regions of 2.7 and 6.25 μm was proposed. The study used the concept of the continuum as the sum of the contributions of bound and quasi-bound dimers of water and the far wings of the vibrational-rotational lines of the spectrum of monomers. In the IAP, experimental studies have been carried out aimed at improving the accuracy of describing continuum absorption in the region of the rotational band of the water molecule [Odintsova et al., 2019; Odintsova et al., 2020; Koroleva et al., 2021]. An approach to physically based modeling of the continuum based on modern concepts of bimolecular absorption and the behavior of the far wings of water vapor resonance lines is proposed [Odintsova et al., 2022].

The effect of water vapor continuum absorption on the CO_2 radiative forcing in the atmosphere has been estimated based on mass calculations of thermal radiation fluxes for the summer months of 2021 in the Lower Volga region [Firsov et al., 2022]. It was shown that as the humidity increases, the CO_2 contribution to the radiative forcing on the ground surface decreases. This leads to the lower surface heating and higher atmospheric heating. In this case, the major contributor is water vapor continuum absorption, rather than selective absorption in H_2O bands.

In cooperation with the Redding University (Great Britain), experimental spectra of water vapor self-continuum absorption in the 1.14 and 0.94 μm absorption bands at the increased temperature (400–430 K) have been rec-

orded for the first time [Simonova et al., 2019; Simonova et al., 2022a; Simonova, 2022b]. The laboratory measurements and the analysis of theoretical calculations allowed to estimate the contribution of the simplest water complexes – dimers – to the water vapor self-continuum in the IR absorption bands as 40 to 90% in the temperature range from 280 to 430 K [Simonova et al., 2022a; Simonova, 2022b]. A semi-empirical model of water dimers has been developed to predict the values and spectral features of water vapor self-continuum in IR absorption bands in the temperature range from 280 to 430 K [Simonova et al., 2022a; Simonova, 2022b; Simonova et al., 2022c].

Separately, it is worth noting the theoretical works that use the method of classical trajectories to calculate the contributions to the continuum absorption. The first studies on using this method to obtain collision-induced spectra of atmospheric molecules began in 2014 almost simultaneously at the OIAP and at SPbU. The successful development of this theoretical approach in [Chistikov et al., 2019; Serov et al., 2020; Chistikov et al., 2021] led to a joint publication [Odintsova et al., 2021]. In this paper, the results of theoretical modeling of the CO_2-Ar rototranslational band obtained at the OIAP and at SPbU, compared with the data available in the literature, as well as with the results of high-precision measurements carried out at the OIAP. It turned out that, despite some differences in the methodology of trajectory calculations carried out at the OIAP and at SPbU, the independently obtained theoretical spectra generally agree well with the measurement data. This made it possible to include the rototranslational absorption spectra of CO_2-Ar and N_2-N_2 obtained at the OIAP in the main block of the HITRAN database [Gordon et al., 2022]. In [Finenko et al., 2022], the CH_4-N_2 rototranslational spectra at temperatures from 70 to 400 K were obtained using the trajectory method at the OIAP. The spectra of CH_4-N_2 and N_2-N_2 were used in this work to interpret the spectral brightness of radiation in the atmosphere of Titan. A very good agreement between the theoretical data and the results of measurements from the Cassini spacecraft is shown. It can be assumed that the binary absorption coefficients for CH_4-N_2 and N_2-N_2 obtained at the OIAP will be useful for modeling radiation processes in some exoplanetary atmospheres, presumably consisting of nitrogen with an admixture of methane. The study [Oparin et al., 2020], carried out at SPbU, proposed a method for calculating the wings of vibrational-rotational bands based on trajectory calculations. The method has been successfully applied to calculate the absorption in the region of the high-frequency wing of the ν_3 CO_2 band in mixtures with noble gases.

References

1. Belikovich M.V., Makarov D.S., Serov E.A., Kulikov M.Yu., Feigin A.M. Validation of atmospheric absorption models within the 20–60 GHz band by simultaneous radiosonde and microwave observations: the advantage of using ECS

formalism // Remote Sensing. 2022. V. 14. P. 6042. https://doi.org/10.3390/rs14236042
2. Borkov Y.G., Solodov A.M., Solodov A.A. and Perevalov V.I., Line intensities of the 01111–00001 magnetic dipole absorption band of $^{12}C^{16}O_2$: Laboratory measurements // Journal of Molecular Spectroscopy. 2021. V. 376. P. 111418.
3. Chesnokova T.Yu., Makarova M.V., Chentsov A.V., Voronina Yu.V., Zakharov V.I., Rokotyan N.V., and Langerock B. Retrieval of Carbon Monoxide Total Column in the Atmosphere from High Resolution Atmospheric Spectra// Atmospheric and Oceanic Optics. 2019. V. 32, N. 4. P. 378–386. DOI: 10.1134/S1024856019040031.
4. Chesnokova T.Yu., Makarova M.V., Chentsov A.V., Kostsov V.S., Poberovskii A.V., Zakharov V.I., Rokotyan N.V. Estimation of the impact of differences in the CH_4 absorption line parameters on the accuracy of methane atmospheric total column retrievals from ground-based FTIR spectra // Journal of Quantitative Spectroscopy & Radiative Transfer. 2020. V. 254. 107187. https://doi.org/10.1016/j.jqsrt.2020.107187
5. Chesnokova T.Yu., Chentsov A.V., Firsov K.M. Impact of spectroscopic information on total column water vapor retrieval in the near-infrared spectral region // Journal of Applied Remote Sensing. 2020. V. 14. N. 3. 034510, doi: 10.1117/1.JRS.14.034510. http://dx.doi.org/10.1117/1.JRS.14.034510
6. Chistikov D.N., Finenko A.A., Lokshtanov S.E., Petrov S.V., and Vigasin A.A. Simulation of collision-induced absorption spectra based on classical trajectories and ab initio potential and induced dipole surfaces. I. Case study of N_2-N_2 rototranslational band // Journal Chemical Physics. 2019. V. 151. P. 194106. https://doi.org/10.1063/1.5125756
7. Chistikov D.N., Finenko A.A., Kalugina Y.N., Lokshtanov S.E., Petrov S.V., Vigasin A.A. Simulation of collision-induced absorption spectra based on classical trajectories and ab initio potential and induced dipole surfaces. II. CO_2–Ar rototranslational band including true dimer contribution // The Journal of Chemical Physics. 2021. V. 155. P. 064301. https://doi.org/10.1063/5.0060779
8. Deichuli V.M., Petrova T.M., Solodov A.M., Solodov A.A., Chesnokova T.Yu. and Trifonova-Yakovleva A.M. H_2O Absorption Line Parameters in the 5900–6100 cm^{-1} Spectral Region // Atmospheric and Oceanic Optics. 2021. V. 34. N. 3. P. 184–189.
9. Dudaryonok A.S., Buldyreva J.A., Lavrentieva N.N., Troitsyna L. Temperature-dependence exponents for CH3I-N2 line-broadening coefficients // J. Quant. Spectrosc. Radiat. Transfer. 2022a. V.277. 107956.
10. Dudaryonok A., Buldyreva J., Lavrentieva N., Troitsyna L. Temperature-dependence parameters for CH3I-O2 and CH3I-air line-broadening coefficients // J. Quant. Spectrosc. Radiat. Transfer. 2022b. V. 277. 108164.
11. Finenko A.A., Bézard B., Gordon I.E., Chistikov D.N., Lokshtanov S.E., Petrov S.V. and Vigasin A.A. Trajectory-based Simulation of Far-infrared Collision-induced Absorption Profiles of CH_4–N_2 for Modeling Titan's Atmosphere // The Astrophysical Journal Supplement Series. 2022. V. 258:33. https://doi.org/10.3847/1538-4365/ac36d3
12. Firsov K.M., Chesnokova T.Yu. and Razmolov A. A. The Influence of Aerosol and Clouds on Underlying Surface Parameters Measured by Sentinel-2A in the Lower Volga Region // Atmospheric and Oceanic Optics. 2021. V. 34. N. 4. P. 335–345. DOI: 10.1134/S1024856021040072.

13. Firsov K.M., Chesnokova T.Yu., Razmolov A.A. Impact of the water vapor continuum absorption on the CO_2 radiative forcing in the atmosphere for Lower Volga Region . // Optika Atmosfery i Okeana. 2022. V. 35. No. 12. P. 1029–1035. DOI: 10.15372/AOO20221210 [in Russian].
14. Fleurbaey, H., Grilli, R., Mondelain, D., Kassi, S., Yachmenev, A., Yurchenko, S.N. and Campargue, A., Electric-quadrupole and magnetic-dipole contributions to the $\nu_2+\nu_3$ band of carbon dioxide near 3.3 μm // J. Quant. Spectrosc. Radiat. Transfer.2021. V. 266. P. 107558.
15. Gordon I.E., Rothman L.S., Hargreaves R.J., Hashemi R., Karlovets E.V., Skinner F.M., et al. The HITRAN2020 molecular spectroscopic database // J. Quant. Spectrosc. Radiat. Transfer. 2022. V. 277. P. 107949. https://doi.org/10.1016/j.jqsrt.2021.107949
16. Jacquemart D., Lyulin O.M., Solodov A.M., Petrova T.M., Solodov A.A. The Q-branch of $\nu_1+\nu_3+3\nu_4$ band of $^{12}C_2H_2$ located at 8330 cm−1 // J. Quant. Spectrosc. Radiat. Transfer. 2022. V.288. 108272.
17. Kazakov K.V., Vigasin A.A. Vibrational magnetism and the strength of magnetic dipole transition within the electric dipole forbidden $\nu_2+\nu_3$ absorption band of carbon dioxide // Molecular Physics. 2021. V. 119. P. e1934581. https://doi.org/10.1080/00268976.2021.1934581
18. Koroleva A.O., Odintsova T.A., Tretyakov M.Yu., Pirali O., Campargue A. The Foreign-Continuum Absorption of Water Vapour in the Far-Infrared (50–500 cm^{-1}) // J. Quant. Spectrosc. Radiat. Transfer. 2021. V. 261. P. 107486.
19. Koshelev M.A., Vilkov I.N., Makarov D.S., Tretyakov M.Yu., Vispoel B., Gamache R.R., Cimini D., Romano F., Rosenkranz P.W. Water Vapor Line Profile at 183 GHz: Temperature Dependence of Broadening, Shifting, and Speed-Dependent Shape Parameters // J. Quant. Spectrosc. Radiat. Transfer. 2021. V. 262. P. 107472. https://doi.org/10.1016/j.jqsrt.2020.107472
20. Koshelev M.A., Vilkov I.N., Makarov D.S., Tretyakov M.Yu., Rosenkranz P.W. Speed-Dependent Broadening of the O_2 Fine-Structure Lines // J. Quant. Spectrosc. Radiat. Transfer. 2021. V. 264. P. 107546.
21. Koshelev M.A., Golubyatnikov G.Yu., Vilkov I.N., Tretyakov M.Yu. Molecular Oxygen Fine Structure with Sub-kHz Accuracy // J. Quant. Spectrosc. Radiat. Transfer. 2022. V. 278. P. 108001.
22. Kouzov A.P., Sokolov A.V., Filippov N.N. Non-Markovian approach to pressure broadening of isolated lines in spectra of light rotators // J. Quant. Spectrosc. Radiat. Transfer. 2022. V. 278. P. 108043. https://doi.org/10.1016/j.jqsrt.2021.108043
23. Lavrentieva N.N., Dudaryonok A.S. Nitrogen dioxide line shift coefficients induced by air pressure // Molecular Physics. 2022. 2052370.
24. Makarov D.S., Tretyakov M.Yu., Rosenkranz P.W. Revision of the 60-GHz Atmospheric Oxygen Absorption Band Models for Practical Use // J. Quant. Spectrosc. Radiat. Transfer. 2020. V. 242. P. 106798.
25. Odintsova T.A., Tretyakov M.Yu., Zibarova A.O., Pirali O., Roy P., Campargue A. Far-Infrared Self-Continuum Absorption of $H_2{}^{16}O$ and $H_2{}^{18}O$ (15–500 cm^{-1}) // J. Quant. Spectrosc. Radiat. Transfer. 2019. V. 227. P. 190–200.
26. Odintsova T.A., Tretyakov M.Yu., Simonova A.A., Ptashnik I.V., Pirali O., Campargue A. Measurement and Temperature Dependence of the Water Vapor Self-Continuum Between 70 and 700 cm^{-1} // J. Mol. Struct. 2020. V. 1210. P. 128046.

27. Odintsova T.A., Serov E.A., Balashov A.A., Koshelev M.A., Koroleva A.O., Simonova A.A., Tretyakov M.Yu., Filippov N.N., Chistikov D.N., Finenko A.A., Lokshtanov S.E., Petrov S.V., Vigasin A.A. CO_2-CO_2 and CO_2-Ar continua at millimeter wavelengths // J. Quant. Spectrosc. Radiat. Transfer. 2021. V. 258. P. 107400.
28. Odintsova T.A., Koroleva A.O., Simonova A.A., Campargue A., Tretyakov M.Yu. The atmospheric continuum in the "terahertz gap" region (15–700 cm^{-1}): Review of experiments at SOLEIL synchrotron and modeling // J. Mol. Spectrosc. 2022. V. 386. P. 111603. https://doi.org/10.1016/j.jms.2022.111603
29. Oparin D.V., Filippov N.N., Grigoriev I.M., Kouzov A.P. Non-empirical calculations of rotovibrational band wings: Carbon dioxide-rare gas mixtures // J. Quant. Spectrosc. Radiat. Transfer. 2020. V. 247. 106950. https://doi.org/10.1016/j.jqsrt.2020.106950
30. Ptashnik I.V., Klimeshina T.E., Solodov A.A., Vigasin A.A., Spectral composition of the water vapour self-continuum absorption within 2.7 and 6.25 μm bands // J. Quant. Spectrosc. Radiat. Transfer. 2019. V. 228, P. 97–105. https://doi.org/10.1016/j.jqsrt.2019.02.024
31. Serdyukov V.I., Sinitsa L.N., Lugovskoy A.A., Emelyanov N.M. Optical cell cooled by liquid nitrogen to study absorption spectra at a Fourier spectrometer // Optika Atmosfery i Okeana. 2020. V. 33. No. 02. P. 146–152. DOI: 10.15372/AOO20200210 [in Russian].
32. Serdyukov V.I., Sinitsa L.N., Emelyanov N.M. Study of the *R*-branch of the $3\nu_3$ band of $^{13}CH_4$ in the 1 μm region // Optika Atmosfery i Okeana. 2022. V. 35. No. 08. P. 619–625. DOI: 10.15372/AOO20220804 [in Russian].
33. Serov E.A., Balashov A.A., Tretyakov M.Yu., Odintsova T.A., Koshelev M.A., Chistikov D.N., Finenko A.A., Lokshtanov S.E., Petrov S.V., Vigasin A.A. Continuum absorption of millimeter waves in nitrogen // J. Quant. Spectrosc. Radiat. Transfer. 2020. V. 242. P. 106774. https://doi.org/10.1016/j.jqsrt.2019.106774
34. Simonova A.A. and Ptashnik I.V. Contribution of Errors in Line Parameters to the Retrieval of the Vapor Continuum Absorption within 0.94- and 1.13-μm Bands // Atmos. Ocean. Opt., 2019, 32(4), 375–377. https://doi.org/10.1134/S1024856019040146
35. Simonova A.A., Ptashnik I.V., Elsey J., McPheat R.A., Shine K.P., Smith K.M. Water vapour self-continuum in near-visible IR absorption bands: Measurements and semiempirical model of water dimer absorption // J. Quant.Spectrosc. Radiat. Transf. 2022, 277, 107957. https://doi.org/10.1016/j.jqsrt.2021.107957.
36. Simonova A.A., Ptashnik I.V. Contribution of water dimers to the water vapor self-continuum absorption in fundamental bending and stretching bands // Atmos. Ocean. Opt., 2022, 35(2), 110–117. https://doi.org/10.1134/S1024856022020117
37. Simonova A.A. Mechanisms of Formation of the Continuum Absorption Spectrum of Water Vapor in the IR Absorption Bands of the Water Molecule: dissertation Phys.-Math. Sciences: 01.04.05. – IAO SB RAS, Tomsk, 2022. [in Russian] https://www.iao.ru/files/iao/theses/thesis112/text.pdf
38. Sinitsa L.N., Serdyukov V.I., Lugovskoy A.A. Low-temperature absorption spectrum of the (0120)–(0000) $^{13}CH_4$ band. Line assignment // Optika Atmosfery i Okeana. 2020. V. 33. No. 09. P. 668–676. DOI: 10.15372/AOO20200902 [in Russian].

39. Sinitsa L.N., Serdyukov V.I., Polovtseva E.R., Bykov A.D., Scherbakov A.P. Led-based fourier spectroscopy of $HD^{17}O$ in the range of 10 000–11 300 cm^{-1}. Analysis of the $3\nu_3$ band. // J. Quant. Spectrosc. Radiat. Transfer. 2022. 294 108409.
40. Tretyakov M.Yu. High Accuracy Resonator Spectroscopy of Atmospheric Gases at Millimetre and Submillimetre Waves. Cambridge Scholars Publ., UK. 2021. 425 p. ISBN 1-5275-7581-0. https://www.cambridgescholars.com/product/978-1-5275-7581-3
41. Troitsyna L., Dudaryonok A., Buldyreva J.V., Filippov N.N., Lavrentieva N. Temperature dependence of CH_3I self-broadening coefficients in the ν_6 fundamental // J. Quant. Spectrosc. Radiat. Transfer. 2020. V. 242. P. 106797. https://doi.org/10.1016/j.jqsrt.2019.106797
42. Troitsyna L., Dudaryonok A., Buldyreva J.V., Filippov N.N., Lavrentiev N.A. Room-temperature CH_3I-N_2 broadening coefficients for the ν_6 fundamental // J. Quant. Spectrosc. Radiat. Transfer. 2021. V. 266. P. 107566.
43. https://doi.org/10.1016/j.jqsrt.2021.107566
44. Troitsyna L., Dudaryonok A., Filippov N.N., Lavrentieva N., Buldyreva J.V. Oxygen- and air-broadening coefficients for the CH_3I ν_6 fundamental at room temperature // J. Quant. Spectrosc. Radiat. Transfer. 2021. V. 273. P. 107839. https://doi.org/10.1016/j.jqsrt.2021.107839
45. Vasilchenko S., Mikhailenko S.N., Campargue A. Cavity ring down spectroscopy of water vapour near 750 nm: a test of the HITRAN2020 and W2020 line lists // Molecular Physics, Volume 120, 2022 – Issue 15-16, Article: e2051762.
46. Vasilchenko S., Barbe A., Starikova E., Kassi S., Mondelain D., Campargue A., Tyuterev V. Cavity-ring-down spectroscopy of the heavy ozone isotopologue $^{18}O_3$: Analysis of a high energy band near 95% of the dissociation threshold // J. Quant. Spectrosc. Radiat. Transfer. 2022. V. 278. P. 108017.

Aerosol and radiative forcing and climate effects

The analysis of dust mineral aerosol was carried out at the OIAP. It was shown that along with the sand fraction and the fraction of mineral dust particles, the wind-sand flux contains an aleurite fraction of particles with sizes from about 10 to 100 μm [Gorchakov et al., 2019a]. Statistical relationships between the concentrations of the aleurite and sand particles in the wind-sand flux with the wind speed in the surface layer of the atmosphere have been established [Gorchakov et al., 2020a]. Approximations of the vertical distributions of the concentrations of aleurite and sand particles in the wind-sand flux under quasi-stationary conditions have been proposed [Gorchakov et al., 2021a; Gorchakov et al., 2021b]. It has been shown that in the upper layer of saltation, in contrast to the lower layer with a thickness of about 9 cm, the vertical gradient of the concentration of saltating particles depends on the wind speed in the surface layer of the atmosphere [Gorchakov et al., 2021a; Gorchakov et al., 2021b]. An empirical model of stratification of the size distribution function of the aleurite and sand particles in a wind-sand flux in the desertified area has been developed [Gorchakov et al., 2021c]. Measure-

ments of vertical turbulent fluxes of dust aerosol were carried out by the correlation method in the desertified area [Gorchakov et al., 2020b, Karpov et al., 2021]. Estimates of the rate of an uplift of the dust aerosol from the underlying surface (up to 6–7 cm/s) have been obtained [Gorchakov et al., 2020b, Karpov et al., 2021]. Low-frequency variations in the density of a turbulent dust aerosol flux are determined by the convectively determined variability of the horizontal and vertical components of the wind speed in the surface layer of the atmosphere [Gorchakov et al., 2020b, Karpov et al., 2021]. The data have shown that the wind-sand flux is characterized by anomalously high electrization [Gorchakov et al., 2022a; Gorchakov et al., 2022b].

The results of measurements of the electric field strength, saltation electric currents, and electric currents due to the transfer of charged dust aerosol particles are presented [Gorchakov et al., 2022a; Gorchakov et al., 2022b]. An estimate of the density of electric charges on the underlying surface (up to +25 nK/m^2) has been obtained. A new mechanism has been proposed for initiating saltation by electric (corona) discharges on the underlying surface, which can provide the escape of saltating particles from the underlying surface at a speed of 1 m/s or more [Gorchakov et al., 2022a; Gorchakov et al., 2022b]. The properties and radiation effects of dust haze on the North China Plain were studied during the advection of dust aerosol from the Taklamakan desert [Gorchakov et al., 2022c]. Using AERONET data in the Beijing region in 2001 – 2021, aerosol optical thicknesses in the visible region of the spectrum reached up to 4.0–4.5, the optical and microphysical characteristics of the dust aerosol are determined by its coarse fraction with a modal radius of particle volume distribution of 2–4 μm with a mass content in the atmosphere up to 10–12 g/m^2. According to monitoring data at the Xinglong and Beijing stations in April 2006 and at the Beijing-CAMS station in March 2021, the imaginary part of the refractive index of the dust aerosol did not exceed 0.003 in most cases under conditions of the optically dense dust haze. It is shown that with intensive dust aerosol drifts to the Beijing region, the efficiency of aerosol radiative forcing reached 85 W/m^2 at the upper boundary of the atmosphere and 135–140 W/m2 at the lower boundary [Gorchakov et al., 2022c]. Using wind field reanalysis data, aerosol optical depth satellite monitoring data (MODIS) and attenuation coefficient vertical distribution (CALIOP), as well as AERONET data, it is shown that the mass flux of dust aerosol from the TaklaMakan Desert to the North China Plain in April 2006 reached 1.5 t/s or about 1.5 million t/day.

The extent of distribution of optically dense haze in Eurasia in July 2016 was estimated, including the record-breaking Siberian haze, which spread over an area of about 16 million km2 due to the eastward transport of air masses [Gorchakov et al., 2019b]. The total mass of smoke aerosol in the

haze on the territory of Northern Eurasia reached approximately 3.2 million tons. The average aerosol radiative forcing during the period of maximum smoke in Siberia was -67 W/m^2 at the upper boundary of the atmosphere and -98 W/m2 at the lower boundary. According to MODIS and AERONET data, the spatial distributions of smog and smoke haze on the North China Plain in June 2007 were established [Gorchakov et al., 2019c]. The similarity of the optical and microphysical characteristics of the smoke aerosol in the large-scale haze in Russia and in the haze in the North China Plain is revealed. It is shown that in the summer smog on the North China Plain the single scattering albedo is on average lower (0.91) than in the large-scale smoky haze on the territory of Russia (0.95–0.98). The efficiency of aerosol radiative forcing at the upper boundary of the atmosphere in smog is 45 W/m^2, which is about 30% less (58–62 W/m^2) than in smoky haze in Russia, and at the lower boundary of the atmosphere, the efficiency of radiative forcing in smog (144 W/m^2) is about 30% more than in smoky haze (102–118 W/m^2).

Using the flying laboratory of the IAO [Panchenko et al.,2020a, Petäjä et al., 2020] the detailed analysis of the aerosol properties was carried out in the atmospheric surface layer and in the troposphere in the background conditions of Western Siberia. As a development of Rozenberg's idea on classification of aerosol states in the atmospheric surface layer for various types of "optical weather," a new version of division of observational datasets into types of "aerosol weather" is proposed. This approach is based on the fact that the basic (“dry”) microphysical composition of particles is formed under the effect of many relatively long processes, while the particle optical characteristics depend strongly on the rapidly varying relative air humidity. Within the framework of this approach, the entire observational dataset can be divided into four types of aerosol weather designated conventionally as background, haze, smog, and smoke haze [Panchenko et al., 2019a]. The analysis showed that the main types of aerosol weather can be reliably distinguished in seasonal datasets of the studied optical and microphysical characteristics [Panchenko et al., 2020b]. The analysis of long-term observations [Pol’kin et al., 2022a., Pol'kin etal, 2022b, Kabanov et al., Panchenko et al., 2021] and the classification of the states of the surface atmosphere according to the types of aerosol weather have significantly reduced the uncertainty of setting the measured input parameters in the empirical model of aerosol optical characteristics of the atmospheric surface layer. This has an important role in development of a modern version of the generalized empirical model of optical characteristics of tropospheric aerosol in Western Siberia [Zenkova et al., 2021].

In 2019–2022, the IAO has continued regular aircraft observations in the background region of Western Siberia [Arshinov et al., 2021]. In the fall seasons of 2020 and 2022, large-scale comprehensive measurements of green-

house gases and aerosols in the Russian sector of the Arctic were carried out with the Optik Tu-134 flying laboratory [Belan et al., 2022]. From the data of airborne sensing of the troposphere obtained during the comprehensive experiment to study the tropospheric composition in the Russian sector of the Arctic in September 2020 over the Barents, Kara, Laptev, East Siberian, Chukchi, and Bering seas, the vertical profiles of the mass concentration of submicron aerosol and absorbing matter (black carbon) were determined [Zenkova et al., 2022]. In the 2020 campaign, we succeeded in carrying out the airborne sensing of aerosol in the Arctic region at the transition from the troposphere to the stratosphere for the first time [Antokhin et al., 2021]. It was found that when crossing the tropopause, the aerosol particle number density increases. Above the tropopause, Si and SO_4^{2-} predominate respectively in the elemental and ionic composition, while terrigenous elements Al, Cu, and Fe dominate in the troposphere [Antokhin et al., 2021].

It should be emphasized that during the airborne campaigns, the IAO in cooperation with the State Scientific Center for Virology and Biotechnology VECTOR has been accumulated the unique dataset on the content of microorganisms in atmospheric aerosol in the troposphere of Western Siberia at altitudes from 0 to 7 km. Comparison of the data obtained in the period of 2006–2008 with the measurements of 2012–2016 indicated that the content of cultivated microorganisms hazardous to human health in atmospheric aerosol in the south of Western Siberia has not changed for ten years (trends are indistinguishable from zero with a confidence probability higher than 95%) [Safatov et al.,2022].

As a member of integrated research campaigns, the IAO continued measurements of aerosol characteristics and summarized the results obtained at polar stations and in marine areas [Sakerin et al., 2019, 2020a, 2020b, 2022a, 2022b; Radionov et al., 2019, 2020; Kabanov et al., 2020; Golobokova et al., 2020]. Based on long-term field studies (2007–2018), it was shown for the first time that the average characteristics of atmospheric aerosol decrease from west to east in the Russian sector of the Arctic Ocean, which indicates the predominance of the export of anthropogenic and natural aerosol from Europe [Radionov et al., 2019, Sakerin et al., 2020a, 2020b]. The analysis of the long-term observation series at the Barentsburg and Ny-Alesund polar stations revealed that the seasonal and year-to-year aerosol optical thickness (AOT) variability is determined by the change in the content of fine aerosol under the significant influence of forest fire smoke emissions. The year-to-year AOT fluctuations at the two stations are consistent [Radionov et al., 2020, Golobokova et al., 2020, Sakerin et al., 2022a]. The long-term studies in 20 Antarctic expeditions revealed features in the spatial distribution of the aerosol optical depth (AOD) of the atmosphere, particle number density, and the content of absorbing matter (black carbon) at high latitudes of the Indo-

Atlantic sector of the ocean. The general trend is the latitudinal decline in combination with the plume of dust and anthropogenic aerosol transported from Africa. It is shown that the spatial distribution is determined by the cyclonic aerosol transport from the continent to the zone of the Subantarctic depression (55°–60°S), the action of the Antarctic anticyclone preventing further air transfer, and the latitudinal change in wind speed and ocean ice cover, which affect the generation of marine aerosol [Sakerin et al., 2022b].

In connection with the growing number of extensive natural fires that spread over vast territories of Siberia and invade the Arctic region, a very urgent task is to correctly determine the radiation effects of such fires [Zhuravleva et al., 2020, Konovalov et al., 2021]. As a part of this task, a new cycle of measurements and simulation of the scattering and absorbing properties of smoke aerosol has been started near a fire source with the emphasis at the day-to-day transformation of aerosol properties [Uzhegov et al., 2022; Zhuravleva et al., 2021, 2022]. The measurements of optical and microphysical characteristics of smokes of various compositions in the Large Aerosol Chamber of the IAO have allowed us to reveal a trend in the brown to black carbon ratio in the mass concentration of mixed smokes at the stage of smoke formation and two to three days of aging under UV irradiation and in the darkness [Uzhegov et al., 2022]. A series of model calculations of the radiative forcing of smoke aerosol depending on the photochemical evolution of its organic component, irradiation conditions, and types of the underlying surface (water, mixed forest, and snow/ice) has shown that an increase in the albedo of the underlying surface and a decrease in the aerosol optical depth can lead to transformation of the cooling/heating effect. It was found that neglecting the variability of the optical characteristics of organic aerosol, one may overestimate or underestimate the radiative forcing at the atmospheric top boundary by several tens of W/m^2 or even obtain incorrectly its sign [Zhuravleva et al., 2019, 2021, 2022]. With the CHIMERE chemical transport model in combination with the WRF meteorological model, the radiative forcing of smoke aerosol in the eastern part of the Arctic was calculated in detail for the period of Siberian superfires of July 16–31, 2016, taken as an example. Model estimates of daily average direct radiative effects of smoke aerosol in the solar spectral range that were obtained from observations at Tiksi station during the period of abnormally high concentration of black carbon in the atmospheric surface layer (July 2014) were obtained [Zhuravleva et al., 2019]. It was shown that the monthly average values of radiative effects due to variability of the optical characteristics of the background aerosol, on the one hand, and short-term BC outflows from forest fires to the observation site, on the other hand, are quite comparable.

The research at the aerosol laboratory of SPbU covered a wide range of research and development [Vlasenko et al., 2019; Volkova et al., 2020; Mi-

khailov and Vlasenko, 2020; Mikhailov et al., 2021]. It includes ground-based monitoring of dispersed characteristics of aerosols, their chemical composition and optical properties near St. Petersburg, an improvement of aerosol equipment and expansion of the list of measured parameters of aerosols, in particular – gravimetric measurements of PM10, determination of organic (OC) and elemental carbon (EC), determination of dispersed parameters of aerosols, measurement of aerosol scattering and absorption coefficients.

The conducted research and development allowed us to study the temporal variability of concentrations of PM10, EC and OC during 2013-2021. It is shown that PM10 concentrations in Peterhof are noticeably lower than the Russian and European maximum permissible concentrations (MPC). A significant decrease in PM10, EC and OC concentrations was observed from April 2020 to June 2021, which is likely due to pandemic restrictions. In general, although the measured concentrations of aerosol substances do not exceed the permissible threshold for PM10, data analysis shows that the St. Petersburg region is experiencing a systematic anthropogenic load. Therefore, in winter, the polluted air masses account for ~ 69% and only ~ 31% refers to background conditions.

In the suburban area of St. Petersburg in Peterhof, where the aerosol station is located, the main sources of aerosol particles are vehicle exhaust gases (proximity to the circular ring road) and biogenic activity in the summer. In the cold seasons (autumn, winter, spring), a high concentration of ultra-small particles (< 100 nm) is maintained by vehicle emissions of combustion products of motor fuel. The relatively high concentration of aerosol particles in the summer season is due to the additional contribution to the aerosol population of biogenic sources producing secondary aerosol as a result of photochemical conversion of volatile organic compounds. The seasonal size distributions of the calculated and volumetric particle concentrations for the period from January 2018 to December 2021 have been studied. The particle number distribution by particles smaller than 0.1 microns is dominated. The aerosol distribution by volume has two modes: accumulative (0.1-1.0 microns) and coarse (>1 microns).

Special attention was paid to the development of the measurement infrastructure and obtaining new data on the size distribution of ultra-small particles (<100 nm). Model calculations were carried out and potential sources of contamination were analyzed using receptor modeling. For the first time in the Russian Federation, monitoring has been established and regular measurements of ultra-small particles (<100 nm), an important component of urbanized territories that affects the health of the population, are carried out.

An important aerosol studies were fulfilled by the scientists from the Institute of Arctic and Antarctic. The estimates of the integral transparency and

aerosol optical depth of the atmosphere in Antarctica were evaluated and their long-term variability over the entire period of observations was analyzed. The comparison of obtained data with the estimates for other natural regions and conditions revealed that during the periods without the impact of volcanic eruptions, the levels of atmospheric aerosol turbidity in Antarctica over the recent decades are minimal on the planet and can be considered as global background characteristics [Radionov et al, 2020]. Given the significant changes in the climate on the planet, databases and archives of data on the main climate-forming characteristics of the atmosphere, collected over long periods of time in various regions of the globe and, in particular, in the polar regions, acquire a special role. Since global solar radiation is one of the most important parameters affecting the energy balance of the Earth-atmosphere system, a database of its hourly and daily sums at five Russian Antarctic stations (Bellingshausen, Vostok Mirny, Novolazarevskaya and Progress) has been created. It includes the data from the beginning of actinometric observations to 2019 [Sibir et al., 2021].

The scientists from MSU in collaboration with Russian Hydrometcenter estimated the urban aerosol pollution over the Moscow megacity region using the COSMO-ART model system and intensive measurement campaigns in 2018 and 2019 [Chubarova et al, 2022b]. The PM10, black carbon (BC), mass concentration, aerosol gas precursors (NOx , SO2, CHx) as well as columnar aerosol parameters for fine and coarse modes as well as an index characterizing the intensity of particle dispersion (IPD) were studied. The correlation of BC with NO2 and PM10 mass concentrations, and a pronounced increase in the BC/PM10 ratio from 0.7 to 5.9%, with the decrease in the IPD index related to the amplification of the atmospheric stratification were shown. An inverse dependence between the BC/PM10 ratio and columnar single-scattering albedo (SSA) for the intense air mixing conditions was obtained. Using long-term parallel AOD in Moscow and background conditions the urban component of AOD (AODurb) has been estimated, which comprised 15 %–19% of the total AOD at 550 nm. A pronounced diurnal cycle of PM10urb and urban BC (BCurb) has been obtained with a strong correlation with the IPD indices. With the IPD index change from 3 to 1 at night, there was about 4 times increase in PM10urb and 3 times increase in BCurb.

The analysis of the changes of aerosol content during COVID-19 lockdown period has been carried out in [Chubarova et al., 2021a]. The decrease in traffic emissions during the lockdown periods from March 30th until June 8th, 2020, played an important role in the decrease (up to 70%) of many gaseous species and aerosol PM10 concentrations and in the increase of surface ozone (up to 18%). The analysis of the pollutant concentrations during the lockdown showed much smoother diurnal cycle for most of the species due to

the reduced intensity of traffic especially during rush hours, compared with that before and after the lockdown. However, the specific meteorological conditions with low temperatures during the lockdown periods as well as the observed smoke air advection have made a considerable contribution to the air quality. The analysis of Pearson partial correlation coefficients with fixed temperature factor has revealed a statistically significant negative correlation between the Yandex self-isolation indices (SII), which can be used as a proxy of traffic intensity, and daily concentrations of all pollutants, except surface ozone, which has a statistically significant positive correlation with SII caused by specific photochemical reactions. In situations with SII>2.5 more favorable conditions for surface ozone generation were observed due to smaller NO_x and the higher O_3/NO_x ratios at the same ratio of VOC/NOx.

The aerosol urban pollution over Moscow was also studied using MODIS/MAIAC satellite data and AERONET ground measurements (Zhdanova et al., 2020). For the ground-based measurements, the AOD urban effect was about 0.02. According to the MAIAC dataset, the urban AOT varied within plus minus 0.01 and was not statistically significant. The urban AOT started decreasing recently due to intensive urban development of the territory around Zvenigorod and the decrease in pollutant emissions in Moscow, which is mainly caused by the environmental regulations. According to the MAIAC dataset, the most pronounced spatial AOT differences over the territory of Moscow were observed at the 5% quantile level, where they reached 0.05–0.06 over several locations and could be attributed to the stationary sources of aerosol pollution, for example, large areas of construction sites, aerosol pollution from roads and highways, or agriculture activities. Over several local areas in Moscow region urban AOD comprises about 0.02–0.04, which could be attributed to the local aerosol sources.

The RPA «Typhoon» has developed a lidar network AK-3 for sounding the parameters of the average atmosphere at wavelengths of 308, 355 and 532 nm [Ivanov et al., 2020]. It is equipped with lidar stations of Roshydromet, based on measurements of which a cycle of studies of the characteristics of the stratospheric aerosol was carried out. In [Korshunov, 2022, Korshunov and. Zubachev, 2021] a study of multiple scattering of laser radiation in cirrus clouds was carried out. A comparison of the results of modeling with experimental data was carried out. The results of measurements of the parameters of cirrus clouds using a two-wave polarizing lidar at wavelengths of 355 and 532 nm in Obninsk (55º N) from 2012 to 2020 are presented in [Grebennikov et al., 2022] the data of lidar measurements of the volcanic aerosol observed in the layer from 13 to 18 km at the lidar stations of Roshydromet in Obninsk, Znamensk, Novosibirsk and Petropavlovsk-Kamchatsky after the explosive eruption of the Raikoke volcano (Kuril Islands, 48.29º N, 153.25º E) in June 2019. The results of the study of the effect of solar activity

on the aerosol of the middle atmosphere according to lidar observations at wavelengths of 532 and 355 nm in Obninsk from 2014 to 2018 are given in [Korshunov and Zubachev, 2022]. In the lower stratosphere, an average slight (~7%) decrease in backscattering was detected in the period from 0 to 2 days after the magnetic storm, which is associated with a Forbush decrease in the flow of galactic cosmic rays. Solar-proton events with a lag of 3–8 days are followed by an increase in aerosol backscattering ranging from 20 to 70%. The results of lidar observations at a wavelength of 532 nm in Obninsk for the period from 2012 to 2021 are presented in [Korshunov, 2021]. They demonstrated that aerosol maxima associated with volcanic eruptions and wildfires. It is noted that in some episodes, the addition of biomass burning aerosol to the optical layer thickness of 10-30 km in relation to the spherical sulfuric acid aerosol is from 50 to 150%. At the same time, in average annual terms, this additive on average for 2014-2021 is about 10%.

The indirect aerosol effects play an important role in aerosol –cloud interaction and has a significant influence on radiation budget. They have been thoroughly studied using COSMO mesoscale model as well as ground-based and satellite data during typical [Shatunova et al., 2020] and COVID-19 lockdown conditions [Shuvalova et al., 2022] by the researchers from MSU and Russian Hydrometcenter. They showed that during the lockdown period, with similar northern advection conditions, there was a reduction of particle number concentration on 40–50 cm^{-3} (or 14–16%), with the increase in droplet effective radius by 8% and cloud optical thickness reduction by 5%, in contrast to the values in typical conditions observed in 2018–2019. According to the numerical experiments using COSMO model, the observed reduction in cloud droplet concentration by 50 cm^{-3} provides a 5–9 W/m^2 (or 9–11%) increase in global irradiance at ground in overcast cloud conditions with liquid water path of 200–400 g/m^2.

The indirect aerosol effects were also studied using the INMCM48 model in collaboration between the MSU and the INM [Poliukhov et al., 2022]. The parameterization of aerosol–cloud interaction has been updated in the INMCM48 model. The impact of sulfate aerosol inclusion on the cloud droplet number concentration, cloud cover, net radiation at the top of the atmosphere, and cloud transmission of solar radiation has been assessed. It is shown that including sulfate aerosol in the parameterization of the aerosol–cloud interaction provides correct reproducing of changes in cloud transmission from 1980 to 2005 in the INMCM48 model compared to the ERA-Interim reanalysis and the data from the solar radiation reconstruction model for several stations located in northern Eurasia, where strong changes in the content of sulfate aerosol are observed. According to preliminary estimates, the average global radiative forcing due to the aerosol indirect aerosol effect is –0.13 W/m^2 for 2005 relative to 1850.

Some improvements were made in sulfate aerosol from natural dimethyl sulfide (DMS) emissions in the climate model of the INM, which provide a better agreement between new model estimates of AOT and the Copernicus Atmosphere Monitoring Service (CAMS) reanalysis data [Chubarova et al., 2021b]. These data and the latest recommended emissions are used to estimate radiative forcing effects (RFEs) of the sulfate aerosol of different origin at the top of the atmosphere. The maximum (in absolute values) radiative effect of natural sulfate aerosol is observed due to high DMS emissions over the marine coast of Antarctica, where the annual mean RFE is –0.14 W m^{-2} (up to –0.45 W m^{-2} in January). The average global annual RFE of sulfate aerosol for 2005 is –0.36 W m^{-2} with small seasonal changes. Overall, the fraction of the RFE from natural sulfate aerosol is 20%, but there are significant variations in this value from month to month, with a maximum in January, when this fraction reaches 37%.

Radiation climate and the features of natural illuminance in Moscow has been studied according to long-term measurements at the MSU Meteorological Observatory [Gorbarenko, 2019, 2020]. Further development of high-quality measurements at MSU Meteorological Observatory since 2021 has been carried out by using a new RAD-MSU(BSRN) robotic radiation station, which has been modernized by self-developed software for visualization and processing of measurement data, including evaluation of data quality criteria [Chubarova et al., 2022a].

A new reconstruction model of shortwave solar radiation has been developed [Volpert, Chubarova, 2021]. The analysis of the solar radiation temporal variability due to various factors over the territory of Northern Eurasia (40–80N; 10W–180E) revealed that in most cases there is a tendency to its increase since 1979, which has been mainly explained by changes in effective cloud amount, with the exception of the polluted regions of Siberia and China and several sites in Northern Europe, where the effect of aerosol factor was dominating in some cases.

Temporal variability in erythemal ultraviolet radiation (Eery) over Northern Eurasia (40–80N, 10W–180E) due to ozone TCs (X) and cloudiness was assessed by using retrievals from ERA-Interim re-analysis, TOMS/OMI satellite measurements, and INM-RSHU chemistry–climate model (CCM) for the 1979–2015 period [Chubarova et al., 2020]. For clear-sky conditions during spring and summer, consistent trends in erythemal daily doses (Eery) up to +3%/decade, attributed to decreases in X, were calculated from the three datasets. Model experiments suggest that anthropogenic emissions of ozone-depleting substances were the largest contributor to Eery trends, while volcanic aerosol and changes in sea surface temperature also played an important role. For all-sky conditions, Eery trends, calculated from the ERA-Interim and TOMS/OMI data over the territory of Eastern Europe, Siberia

and Northeastern Asia, were significantly larger (up to +5–8%/decade) due to a combination of decrease in ozone and cloudiness. In contrast, all-sky maximum trends in Eery, calculated from the CCM results, were only +3–4%/decade. While Eery trends for Northern Eurasia were generally positive, negative trends were observed in July over central Arctic regions due to an increase in cloudiness. Finally, changes in the ultraviolet (UV) resources (characteristics of UV radiation for beneficial (vitamin D production) or adverse (sunburn) effects on human health) were assessed. When defining a "UV optimum" condition with the best balance in Eery for human health, the observed increases in Eery led to a noticeable reduction of the area with UV optimum for skin types 1 and 2, especially in April. In contrast, in central Arctic regions, decreases in Eery in July resulted in a change from "UV excess" to "UV optimum" conditions for skin types 2 and 3. Using INM-RSHU chemistry–climate model the influence of different factors on the total ozone content and Eery in the atmosphere over northern Eurasia from 1979 to 2059 has been analyzed. The sensitivity of modeled ozone contents to different input data on sea-surface temperature (SST) has been estimated. The ozone trends may significantly differ depending on the SSTs used. The results of the model experiment, which considers variations in the anthropogenic emissions of halogen-containing substances, suggest a nonlinear Eery decrease due to the recovery of the ozone layer in the 21st century. The values of Eery for 2016–2020 are 2–5% higher than its values for1979–1983, on average, for all of northern Eurasia (with its maximum of 6% in the polar latitudes). The Eery values equalize in 2035–2039 and then gradually decrease (when compared to those for 1979–1983) by 4–6% for Asia and 6–8% for northern Europe in 2055–2059. Therefore, variations are observed in the spatial distribution of UV resources, which are most significant in spring and summer: these variations are manifested in the extension of UV-deficiency zones in the north and the reduction of UV-excess zones in the south.

In Siberia, a series of UV-B radiation measurements obtained at the TOR station of IAO for 2003–2016 has been used to study the relation between UV radiation and factors affecting it, such as the total ozone column (TOC), total cloud amount index (N_{tot}), AOT, and albedo [Belan et al., 2020, Belan et al., 2021]. It has been found that under conditions of a clear and transparent atmosphere ($N_{tot} \leq 2$, $AOT_{500} \leq 0.15$) a 1% increase in total ozone leads to an average UV-B radiation decrease of 1.45%. The average contribution of AOT to a change in the daily UV-B radiation inflow is from 4.3 to 10.9% depending on the cloud amount index. Cloudiness can reduce an increase in the UV-B radiation by an average of 0.7–28.7% depending on the cloud amount. An increment in the albedo of the underlying surface contributes to an increase in the UV-B radiation, on average, 4–8% for TOC = 300–400 DU and 9–13% for TOC = 400–500 DU for stable snow cover and the solar zenith

angle ranging from 52 to 68°. For days with fresh snow, an increase in the UV-B radiation can reach 66% at TOC = 300–400 DU.

The set of parameters measured at the Fonovaya Observatory has been extended. Now we can conduct measurements of the incoming solar radiation in the wavelength range of 0.280–2.8 μm and the radiation balance in the ranges of 0.3–2.8 and 4.5–42 μm [Belan et al., 2022a]. A new ultraviolet radiation detector based on artificial periclase nanocrystals (MgO) has been developed [Tentukov et al., 2022].

The data measured at the Fonovaya Observatory indicate that the daily radiation balance is -1.20±1.18 MJ/m^2 from November to March, when the ground surface is covered by a stable snow cover, and -8.83±4.49 MJ/m^2 from May to September, when the surface is free of snow. In the period of stable snow cover from December to March, the diurnal absorption of the solar radiation by the surface did not exceed 2 MJ/m^2, while in the summer period it ranged from 10 to 25 MJ/m^2 [Belan et al., 2022b].

In the study [Kulikov et. al., 2019], it was shown that solar radiation with a wavelength of 121.6 nm can lead to the formation of a noticeable amount of H_2O_2 inside the particles of polar mesospheric clouds. In this work, complex measurements of H_2O_2 production were performed for the first time inside thin (50 nm) ice samples of H_2O and H_2O:O_2 by vacuum ultraviolet radiation with a wavelength of 121.6 nm in wide temperature ranges (20–140 K).

References

1. Antokhin P.N., Arshinova V.G., Arshinov M.Yu., Belan B.D., Belan S.B., Golobokova L.P., Davydov D.K., Ivlev G.A., Kozlov A.V., Kozlov A.S., Otmakhov V.I., Rasskazchikova T.M., Simonenkov D.V., Tolmachev G.N. and Fofonov A.V. Change in the Air Composition upon the Transition from the Troposphere to the Stratosphere // Atmospheric and Oceanic Optics, 2021, V. 34. No. 06. P. 567–576.
2. Arshinov M.Yu.,. Arshinova V.G., Belan B.D., Davydov D.K., Ivlev G.A., Kozlov A.S., Kuibida L.V., Rasskazchikova T.M., Simonenkov D.V., Tolmachev G.N. and Fofonov A.V. Anomalous Vertical Distribution of Organic Aerosol over the South of Western Siberia in September 2018 // Atmospheric and Oceanic Optics, 2021, V. 34. No. 05. P. 495–502.
3. Belan B.D., Ancellet G., Andreeva I.S., Antokhin P.N., Arshinova V.G., Arshinov M.Y., Balin Y.S., Barsuk V.E., Belan S.B., Chernov D.G., Davydov D.K., Fofonov A.V., Ivlev G.A., Kotel'nikov S.N., Kozlov A.S., Kozlov A.V., Law K., Mikhal'chishin A.V., Moseikin I.A., Nasonov S.V., Nédélec P., Okhlopkova O.V., Ol'kin S.E., Panchenko M.V., Paris J.-D., Penner I.E., Ptashnik I.V., Rasskazchikova T.M., Reznikova I.K., Romanovskii O.A., Safatov A.S., Savkin D.E., Simonenkov D.V., Sklyadneva T.K., Tolmachev G.N., Yakovlev S.V., Zenkova P.N. Integrated airborne investigation of the air composition over the Russian sector of the Arctic // Atmos. Meas. Tech., 2022, V. 15. No. 13. P. 3941–3967 / https://doi.org/10.5194/amt-15-3941-2022.

4. Belan B.D., Ivlev G.A., Sklyadneva T.K. Studying the Relationship of Ultraviolet Radiation with Meteorological Factors and Atmospheric Turbidity: Part I. Role of Total Ozone Content, Clouds, and Aerosol Optical Depth // Atmospheric and Oceanic Optics, 2020, V. 33, No. 6, P. 638–644,2020.
5. Belan B.D., Ivlev G.A., Sklyadneva T.K. The Relationship of Ultraviolet Radiation, Meteorological Factors and Atmospheric Turbidity: Part II–Role of Surface Albedo // Atmospheric and Oceanic Optics, V. 34, No. 2, P. 129–134. DOI: 10.1134/S1024856021020020, 2021.
6. Belan B.D., Ivlev G.A., Kozlov A.V., Pestunov D.A., Sklyadneva T K., Fofonov A.V. Solar radiation measurements at the Fonovaya observatory. Part I Methodical aspects and specifications // Optika Atmosfery i Okeana. V. 35. No. 09. P. 759–765. DOI: 10.15372/AOO20220909 [in Russian], 2022a
7. Belan B.D., Ivlev G.A., Kozlov A.V., Pestunov D.A., Sklyadneva T.K., Fofonov A.V. Solar radiation measurements at the Fonovaya observatory. Part II. Measurement results of 2021 . // Optika Atmosfery i Okeana. V. 35. No. 10. P. 843–849. DOI: 10.15372/AOO20221007 [in Russian], 2022b
8. Chubarova N.E., Pastukhova A.S., Zhdanova E.Y., Volpert E.V., Smyshlyaev S.P., Galin V.Y. Effects of Ozone and Clouds on Temporal Variability of Surface UV Radiation and UV Resources over Northern Eurasia Derived from Measurements and Modeling. Atmosphere 2020, 11, 59. https://doi.org/10.3390/atmos11010059
9. Chubarova N.Y., Androsova Y.Y., Lezina Y.A. The Dynamics Of The Atmospheric Pollutants During The Covid-19 Pandemic 2020 And Their Relationship With Meteorological Conditions In Moscow. GEOGRAPHY, ENVIRONMENT, SUSTAINABILITY. 14(4):168–182. https://doi.org/10.24057/2071-9388-2021-012, 2021a
10. Chubarova N.E., Poliukhov A.A. & Volodin E.M. Improving the Calculation of the Sulfate Aerosol Evolution and Radiative Effects in the Institute of Numerical Mathematics, Russian Academy of Sciences, Climate Model. Izv. Atmos. Ocean. Phys. 57, 370–378, https://doi.org/10.1134/S0001433821040150, 2021b
11. Chubarova N.E., V.A. Rosental, E.Yu. Zhdanova, A.A. Poliukhov. New radiation complex at the Moscow State University Meteorological Observatory of the BSRN standard: methodological aspects and first measurement results. . Atmospheric and oceanic optics, 35, № 8, p. 670-67, 2022a
12. Chubarova N.E., Vogel H., Androsova E.E., Kirsanov A.A., Popovicheva O.B., Vogel B., and Rivin G.S. Columnar and surface urban aerosol in the Moscow megacity according to measurements and simulations with the COSMO-ART model, Atmos. Chem. Phys., 22, 10443–10466, https://doi.org/10.5194/acp-22-10443-2022, 2022b
13. Golobokova L.P., Khodzher T.V., Izosimova O.N., Zenkova P.N., Pochyufarov A.O., Khuriganowa O.I., Onishyuk N.A., Marinayte I.I., Polkin V.V., Radionov V.F., Sakerin S.M., Lisitzin A.P. and Shevchenko V.P. Chemical Composition of Atmospheric Aerosol in the Arctic Region and Adjoining Seas along the Routes of Marine Expeditions in 2018–2019 // Atmospheric and Oceanic Optics, 2020, V. 33. No. 05. P. 480–489.
14. Gorbarenko E.V. Radiation Climate of Moscow. Russian Meteorology and Hydrology, Allerton Press Inc. (United States), V 45, p. 478–487, 2020.

15. Gorbarenko E.V. Sunshine Variability in Moscow in 1955–2017. Russian Meteorology and Hydrology, издательство Allerton Press Inc. (United States), V. 44, № 6, p. 384–393, 2019.
16. Gorchakov G.I., Buntov D.V., Karpov A.V., Kopeikin V.M., Mirsaitov S.F., Gushchin R.A. and Datsenko O.I. The Saltating Particle Aleurite Mode in Wind–Sand Flux over a Desertified Area // Doklady Earth Sciences. 2019a. V. 488. No 1. P. 1103–1106.
17. Gorchakov G.I., Buntov D.V., Karpov A.V., Gushchin R.A., Datsenko O.I. Wind Effect on the Size Distribution of Saltating Particles // Atmospheric and Oceanic Optics. 2020a. 33(2). P.198–205.
18. Gorchakov G.I., Karpov A.V., Gushchin R.A., Datsenko O.I., Buntov D.V. Vertical profiles of the saltating particle concentration on a desertified area // Doklady Earth Sciences. 2021a. V. 496, No 2. P. 119–124.
19. Gorchakov G.I., Karpov A.V., Gushchin R.A., Datsenko O.I., Buntov D.V. Vertical Distribution of Aleurite and Sand Particles in Windsand Flux over a Desertified Area // Izvestiya, Atmospheric and Oceanic Physics, 2021b, V. 57, No. 5, P. 486–494.
20. Gorchakov G.I., Karpov A.V., Gushchin R.A., Datsenko O.I., Buntov D.V Stratification of Aleurite and Sand Particle Size Distribution in Windsand Flux over Desertified Areas // Atmospheric and Oceanic Optics. 2021c. V. 34, No. 5. P. 438–442.
21. Gorchakov G.I., Karpov A.V. Gushchin, R.A. Turbulent fluxes of the dust aerosol on the desertified area // Doklady Earth Sciences. 2020b. V. 494. P. 799–802.
22. Gorchakov G.I., Kopeikin V.M., Karpov A.V., Gushchin R.A., Datsenko O.I., Buntov D.V. Wind–Sand Flux Electrization over Desertified Areas // Doklady Earth Sciences. 2022a. V. 505, Part 1, P. 483–488.
23. Gorchakov G.I., Kopeikin V.M,. Karpov A.V., Gushchin R.A., Datsenko O.I., Buntov D.V. Dusty Plasma of a Wind-Sand Flux in Desertified Areas // Atmospheric and Oceanic Physics. 2022b. V. 58. No. 5. P. 466–475.
24. Gorchakov G.I., Datsenko O.I., Kopeikin V.M., Karpov A.V., Gushchin R.A., Gorchakova I.A., Mirsaitov S.F. Ponomareva T.Y.. Dust Haze over the North China Plain // Atmospheric and Oceanic Optics. 2022c. V. 35. No 2. P. 125–132.
25. Gorchakov G.I., Sitnov S.A., Karpov A.V., Gorchakova I.A., Gushchin R.A., Datsenko O.I. Eurasian Large-Scale Hazes in Summer 2016 // Izv. Atmos. Ocean. Phys. 2019b. V. 55, No 3. P. 261–270.
26. Gorchakov G.I., Karpov A.V., Gorchakova I.A., Gushchin R.A., and Datsenko O. I. Smog and Smoke Haze over the North China Plain in June 2007 // Atmospheric and Oceanic Optics. 2019c. Vol. 32, No. 6. P. 643–649.
27. Grebennikov V.S., D.S Zubachev, V.A. Korshunov, D.G. Sakhibgareev, I.A. Chernikhc. Observations of Stratospheric Aerosol at Rosgidromet Lidar Stations after the Eruption of the Raikoke Volcano in June 2019 // Atmospheric and Oceanic Optics. 2020. Vol. 33. No. 5. pp. 519–523.
28. Ivanov V.N., D.S. Zubachev, V.A. Korshunov, D.G. Sakhibgareev. Network lidar AK-3 for middle atmosphere sensing: design, methods of measurements, results. // Proceedings of MGO. 2020. V. 598. pp. 155–187.
29. Kabanov D.M., Sakerin S.M. and Turchinovich Yu.S. Interannual and Seasonal Variations in the Atmospheric Aerosol Optical Depth in the Region of Tomsk (1995–2018) // Atmospheric and Oceanic Optics, 2019, V. 32. No. 06. P. 663–670.

30. Kabanov D.M., Ritter C., Sakerin S.M. Interannual and seasonal variations in aerosol optical depth of the atmosphere in two regions of Spitsbergen Archipelago (2002–2018) // Atmospheric Measurement Techniques. 2020. V. 13. P. 5303–5317. DOI: 10.5194/amt-13-5303-2020
31. Karpov A.V., Gorchakov G.I., Gushchin R.A., Datsenko O.I. Vertical Turbulent Dust-Aerosol Fluxes Izvestiya, Atmospheric and Oceanic Physics, 2021. V. 57, No. 5. P. 495–503.
32. Konovalov I. B., Golovushkin N. A., Beekmann M., Panchenko M. V., and Andreae M. O. Inferring the absorption properties of organic aerosol in Siberian biomass burning plumes from remote optical observations // Atmos. Meas. Tech., 2021, V. 14, P. 6647–6673, https://doi.org/10.5194/amt-14-6647-2021
33. Korshunov V.A., D.S Zubachev. Manifestation of Solar Activity Effects in Lidar Observations of Stratospheric Aerosol // Geomagnetism and Aeronomy. 2022. Vol. 62. No. 1. pp. 67–74.
34. Korshunov V.A. Lidar observations of stratospheric aerosols at Obninck in 2012–2021: influence of volcanic eruptions and biomass burning // Fundamental and Applied Climatology. Vol. 8. No. 3. pp. 31–51, doi:10.21513/2410-8758-2022-3-31-51.
35. Korshunov V.A.. Multiple scattering in cirrus clouds and taking it into account when interpreting lidar measurements in the stratosphere // Atmospheric and Oceanic Optics, 2022. Vol. 35. No. 2. pp. 151–157.
36. Korshunov V.A., D.S. Zubachev. Characteristics of cirrus clouds from lidar measurements at Obninsk // Proceeding of MGO. 2021. V. 602. pp. 68–78.
37. Kulikov, M. Yu., Feigin, A. M., & Schrems, O., H_2O_2 photoproduction inside H_2O and H_2O:O_2 ices at 20–140K // Scientific Reports, 9, 11375, doi:10.1038/s41598-019-47915-w, https://www.nature.com/articles/s41598-019-47915-w , 2019.
38. Mikhailov E.F., Vlasenko S.S. High-humidity tandem differential mobility analyzer for accurate determination of aerosol hygroscopic growth, microstructure, and activity coefficients over a wide range of relative humidity, Atmos. Meas. Tech., 13, 2035–2056, 2020.
39. Mikhailov E.F., Pöhlker M.L., Reinmuth-Selzle K. et al., 2021: Water uptake of subpollen aerosol particles: hygroscopic growth, cloud condensation nuclei activation, and liquid–liquid phase separation // Atmos. Chem. Phys., 21, 6999–7022.
40. Panchenko M.V., Kabanov M.V., Pkhalagov Yu.A., Belan B.D., Kozlov V.S., Sakerin S.M., Kabanov D.M., Uzhegov V.N., Shchelkanov N.N., Polkin V.V., Terpugova S.A., Tolmachev G.N., Yausheva E.P., Arshinov M.Yu., Simonenkov D.V., Shmargunov V.P., Chernov D.G., Turchinovich Yu.S., Pol'kin Vas.V., Zhuravleva T.B., Nasrtdinov I.M. and Zenkova P.N. Integrated Studies of Tropospheric Aerosol at the Institute of Atmospheric Optics (Development Stages) // Atmospheric and Oceanic Optics, 2020, V. 33. No. 01. P. 27–41.
41. Panchenko M.V., Yausheva E.P., Chernov D.G., Kozlov V.S., Makarov V.I., Popova S.A., Shmargunov V.P. Submicron aerosol and Black Carbon in the troposphere of Southwestern Siberia (1997–2018) // Atmosphere, 2021. V.12. No. 3. P. 351–370. DOI: 10.3390/atmos12030351
42. Panchenko M.V., Pol'kin V.V., Pol'kin Vas.V., Kozlov V.S., Yausheva E.P. and Shmargunov V.P. Size Distribution of Dry Matter of Particles in the Surface Atmospheric Layer in the Suburban Region of Tomsk within the Empirical

Classification of Aerosol Weather Types // Atmospheric and Oceanic Optics, 2019, V. 32. No. 06. P. 655–662.
43. Panchenko M.V., Kozlov V.S., Polkin V.V., Polkin Vas.V., Terpugova S.A., Uzhegov V.N., Chernov D.G., Shmargunov V.P., Yausheva E.P., Zenkova P.N. Aerosol characteristics in the near-ground layer of the atmosphere of the city of Tomsk in different types of aerosol weather // Atmosphere. 2020. V. 11. No. 1. P. 20–39. DOI: 10.3390/atmos1101002
44. Pastukhova A.S., Chubarova N.E., Zhdanova Y.Y., Galin V.Y., Smyshlyaev S.P. The forecast of erythemal UV irradiance over the territory of Northern Eurasia according to the INM-RSHU chemical-climate model . Izvestiya, Atmospheric and Oceanic Physics, 2019, Vol. 55, No. 3, pp. 242–250. © Pleiades Publishing, Ltd., 2019.
45. Petäjä T., Duplissy E.-M., Tabakova K., Arshinov M. (IAO), Balin Y. (IAO), Belan B. (IAO), Panchenko M. (IAO). Intergrative and comprehensive Understanding on Polar Environments (iCUPE): the concept and initial results // Atmos. Chem. Phys. 2020. V. 20. No. 14. P. 8551–8592. https://doi.org/10.5194/acp-20-8551-2020
46. Poliukhov A.A., Chubarova N.Y. & Volodin E.M. Impact of Inclusion of the Indirect Effects of Sulfate Aerosol on Radiation and Cloudiness in the INMCM Model. Izv. Atmos. Ocean. Phys. 58, 486–493 (2022). https://doi.org/10.1134/S0001433822050097
47. Pol'kin V.V., Panchenko M.V. Time Variations in Submicron and Coarse Particle Concentrations in the Surface Air Layer at the Aerosol Station of Institute of Atmospheric Optics, Siberian Branch, Russian Academy of Sciences, Tomsk (2000–2020) // Atmospheric and Oceanic Optics, 2022, V. 35. No. 06. P. 661–666.
48. Pol'kin Vas. V., Pol'kin V.V., Panchenko M. V. Long-term observations of the aureole scattering phase function in the surface air layer of the suburbs of Tomsk (2010–2021) // Optika Atmosfery i Okeana. 2022. V. 35. No. 12. P. 987–992. DOI: 10.15372/AOO20221203 [in Russian].
49. Radionov V.F., Kabanov D.M., Polkin V.V., Sakerin S.M., Izosimova O.N. Aerosol characteristics over the Arctic seas of Eurasia: results of measurements in 2018 and average spatial distribution in the summer-autumn periods of 2007–2018 // Arctic and Antarctic Research, 2019, V.65. No. 04, P. 405-421 [In Russian] .
50. Radionov V.F., Sidorova O.R., Golobokova L.P., Khuriganova O.I., Khodzher T.V., Sakerin S.M., Kabanov D.M., Chernov D.G., Kozlov V.S., Panchenko M.V. – 5.2. Aerosol component of the Atmosphere in Barentsburg, P. 282–304 // Current State of Environment of the Svalbard Archipelago: Collective monograph [ed. by L.M. Savatyugin]. St. Petersburg: AARI, 2020. 304 pp.
51. Radionov V.F., Rusina E.N., Sibir E.E Long-term variability of integral and spectral transparency of the atmosphere at Mirny observatory, Antarctica, 2020, Russian Meteorology and Hydrology 45(2):74–80.
52. Safatov A.S., Andreeva I.S., Buryak G.A., Olkin S.E., Reznikova I.K., Belan B.D., Panchenko M.V., Simonenkov D.V. Long-Term Studies of Biological Components of Atmospheric Aerosol: Trends and Variability // Atmosphere. 2022. V. 13. Iss. 5. 651. 20 p. DOI:10.3390/atmos13050651
53. Sakerin S.M., Golobokova L.P., Kabanov D.M., Kalashnikova D.A., Kozlov V.S., Kruglinsky I.A., Makarov V.I., Makshtas A.P., Popova S.A., Radi-

onov V.F., Simonova G.V., Turchinovich Yu.S., Khodzher T.V., Khuriganowa O.I., Chankina O.V. and Chernov D.G. Measurements of Physicochemical Characteristics of Atmospheric Aerosol at Research Station Ice Base Cape Baranov in 2018 // Atmospheric and Oceanic Optics, 2019, V. 32. No. 05. P. 511–520.

54. Sakerin S.M., Kabanov D.M., Makarov V.I., Polkin V.V., Popova S.A., Chankina O.V., Pochufarov A.O., Radionov V.F., Rize D.D. Spatial distribution of atmospheric aerosol physicochemical characteristics in Russian sector of the Arctic Ocean // Atmosphere, 2020a, V. 11(11), 1170. https://doi.org/10.3390/atmos1111170
55. Sakerin S.M., Zenkova P.N., Kabanov D.M., Kalashnikova D.A., Lisitzin A.P., Makarov V.I., Polkin V.V., Popova S.A., Simonova G.V., Chankina O.V. and Shevchenko V.P. Results of Studying Physicochemical Characteristics of Atmospheric Aerosol in the 71st Cruise of RV Akademik Mstislav Keldysh // Atmospheric and Oceanic Optics, 2020b, V. 33. No. 05. P. 470–479.
56. Sakerin S.M., Kruglinsky I.A., Kabanov D.M., Kalashnikova D.A. , Kravchishina M.D., Makarov V.I., Novigatinsky A.N., Popova S.A., Pochufarov A.O., Simonova G.V., Turchinovich Yu.S., Darin F.A. Spatiotemporal variations in atmospheric aerosol characteristics over the Kara, Barents, Norwegian, and Greenland Seas (2018-2021 expeditions) // Atmospheric and Oceanic Optics. 2022a. V.35. No.6. P.651–660. DOI: 10.1134/S1024856022060203.
57. Sakerin S.M., Golobokova L.P., Kabanov D.M., Khuriganowa O.I., Pol'kin V.V., Radionov V.F., Sidorova O.R., Turchinovich Yu.S. Spatial distribution of aerosol characteristics over the South Atlantic and Southern Ocean, using multiyear (2004-2021) measurements in Russian Antarctic expeditions // Atmosphere, 2022b, V. 13. P. 427. https://doi.org/10.3390/atmos13030427
58. Shatunova M.V., Khlestova Y.O. & Chubarova N.E. Forecast of Microphysical and Optical Characteristics of Large-Scale Cloud Cover and Its Radiative Effect Using the COSMO Mesoscale Weather Prediction Model. Atmos Ocean Opt 33, 154–160 (2020).
59. Shuvalova J.; Chubarova N.; Shatunova M. Impact of Cloud Condensation Nuclei Reduction on Cloud Characteristics and Solar Radiation during COVID-19 Lockdown 2020 in Moscow. Atmosphere 2022, 13, 1710. https://doi.org/10.3390/atmos13101710
60. Sibir E.E., Radionov V.F., Rusina E.N. Database of hourly and daily sums of total radiation at Russian antarctic stations: analysis of changes in total radiation for the entire period of observations in Antarctica. Arctic and Antarctic Research. 2021;67(3):249-260. (In Russ.) https://doi.org/10.30758/0555-2648-2021-67-2-249-260
61. Tentyukov M.P., Lyutoev V.P., Belan B.D., Simonenkov D.V., Golovataya O.S. Ultraviolet Radiation Detector Based on Artificial Periclase Nanocrystals (MgO) // Atmospheric and Oceanic Optics, 2022, V. 35, No. 1, P. 89–96.
62. Uzhegov V.N., Kozlov V.S., Konovalov I.B., Panchenko M.V., Zenkova P.N., Polkin V.V., Romashchenko V.A., Chernov D.G., Shmargunov V.P., Yausheva E.P., "Relationships between aerosol absorption, scattering and extinction of radiation in combustion and pyrolysis smokes" //Proc. SPIE 12341, 28th International Symposium on Atmospheric and Ocean Optics: Atmospheric Physics, 123412W (7 December 2022); https://doi.org/10.1117/12.2644803

63. Vlasenko S.S., Volkova K.A., Ionov D.V. et al. Variation of Carboneceous Atmospheric Aerosol Near St. Petersburg // Izv. Atmos. Ocean. Phys. 55, 619–627 (2019). https://doi.org/10.1134/S0001433819060161
64. Volkova K.A., Anikin S.S., Mihailov E.F. et al. Seasonal and Daily Variability of Aerosol Particle Concentrations near St. Petersburg // Atmos Ocean Opt 33, 524–530 (2020). https://doi.org/10.1134/S102485602005019X
65. Volpert E.V., Chubarova N.E. Long-term Changes in Solar Radiation in Northern Eurasia during the Warm Season According to Measurements and Reconstruction Model. Russ. Meteorol. Hydrol. 46, 507–518 (2021). https://doi.org/10.3103/S1068373921080021
66. Zenkova P.N., Terpugova S.A., Pol'kin V.V., Pol'kin Vas.V., Uzhegov V.N., Kozlov V.S., Yausheva E.P. and Panchenko M.V. Development of an Empirical Model of Optical Characteristics of Aerosol in Western Siberia // Atmospheric and Oceanic Optics, 2021, V. 34. No. 04. P. 320–326.
67. Zenkova P.N., Chernov D.G., Shmargunov V.P., Panchenko M.V. and Belan B.D. Submicron Aerosol and Absorbing Substance in the Troposphere of the Russian Sector of the Arctic According to Measurements Onboard the Tu-134 Optik Aircraft Laboratory in 2020 // Atmospheric and Oceanic Optics, 2022, V. 35. No. 01. P. 43–51.
68. Zhdanova, E. Y., Chubarova, N. Y., and Lyapustin, A. I.: Assessment of urban aerosol pollution over the Moscow megacity by the MAIAC aerosol product, Atmos. Meas. Tech., 13, 877–891, https://doi.org/10.5194/amt-13-877-2020, 2020.
69. Zhuravleva T.B., Artyushina A.V., Vinogradova A.A. and Voronina Yu.V. Black Carbon in the Near-Surface Atmosphere Far Away from Emission Sources: Comparison of Measurements and MERRA-2 Reanalysis Data // Atmospheric and Oceanic Optics, 2020, V. 33. No. 06. P. 591–601.
70. Zhuravleva T.B., Nasrtdinov I.M. and Vinogradova A.A. Direct Radiative Effects of Smoke Aerosol in the Region of Tiksi Station (Russian Arctic): Preliminary Results. // Atmospheric and Oceanic Optics, 2019, V. 32. No. 03. P. 296–305.
71. Zhuravleva T.B., Nastrdinov I.M., Konovalov I.B., Golovushkin N.A., Beekmann M. Impact of the Atmospheric Photochemical Evolution of the Organic Component of Biomass Burning Aerosol on its Radiative Forcing Efficiency: a Box Model Analysis // Atmosphere. 2021. V. 12. doi:10.3390/10.3390/atmos12121555.
72. Zhuravleva T. B., Nasrtdinov I. M., Konovalov I. B., Golovushkin N. A. Radiative forcing of smoke aerosol taking into account the photochemical evolution of its organic component: influence of illumination condtions and underlying surface albedo // Optika Atmosfery i Okeana. 2022. V. 35. No. 09. P. 748–758. DOI: 10.15372/AOO20220908 [in Russian].

Remote sensing of the atmosphere

Since the 1990s, the IAO carries out lidar monitoring of the middle atmosphere to study the behavior of the aerosol component and the temperature conditions. The 2011–2021 lidar data on the optical parameters were used to estimate the variability of the background aerosol content in the stratosphere

[Marichev and Bochkovskii, 2020a, 2022a]. A steady trend to maximal filling of the lower stratosphere (10-30 km) with background aerosol in winter, low aerosol content (down to complete absence) in summer, and an intermediate value with a decrease in spring and an increase in fall was detected. In the upper stratosphere (30-50 km), the background aerosol was practically absent in the summer season. Thus, the intra-annual cyclicity in filling of the stratosphere of Western Siberia with background aerosol was demonstrated.

An optical-lidar model of the stratospheric aerosol in Western Siberia was proposed for different seasons and months [Marichev et al., 2022]. The comparison of the proposed model with the known ones revealed a discrepancy of the latter with the actual state of the stratospheric aerosol of Western Siberia. This discrepancy can lead to gross errors in the calculation of lidar signals and radiation extinction. Lidar observations of aerosol filling of the upper troposphere and stratosphere with pyrocumulative emissions of combustion aerosols from Siberian fires were carried out in Western Siberia, in Tomsk, in August 2019 [Cheremisin et al., 2022]. The results obtained expand the knowledge of sources of aerosol filling of the stratosphere and, ultimately, can be used for more reliable estimation of the climatic effect of aerosol.

The lidar study of thermal conditions in the stratosphere over Tomsk revealed every year events of winter sudden stratospheric warming (SSW). According to the experimental statistics, minor SSW events are observed more often than major ones. The SSW events differ both in the duration (from several days to a month and longer) and in the amplitude of positive deviation from the monthly mean value with a maximum up to 60 K for the major SSW events. The stratopause height for intense warming events can descend to 27 km (standard stratopause height is 50-55 km). For Western Siberia, the vertical temperature distribution is in a good agreement with the CIRA-86 model distribution for most cases in the long period from April to November [Marichev and Bochkovskii, 2020b, 2022b].

In August-October 2017, stratospheric aerosol layers of non-volcanic origin were observed at the Siberian Lidar Station of the IAO. In these layers, the maximal scattering ratio R(H) at a wavelength of 532 nm reached 5.8. The constructed back trajectories of air mass movements showed that these aerosol layers in the stratosphere over Tomsk originated from the Canadian forest fires in North America that took place in mid-August. Due to pyroconvection, the biomass burning products were raised to stratospheric heights and spread throughout the Northern Hemisphere. The results of laser sensing at two wavelengths of 355 nm and 532 nm allowed us to analyze thoroughly the dynamics of the observed anomalous aerosol layers and to obtain qualitative information on the sizes of aerosol particles forming these layers. The results of observations based on the Angström exponent suggest that its value for the background ensemble of scattering aerosol particles at altitudes of 16-

19 km is about 2.8. At the higher levels (altitudes of 23-25 km), it approaches 4 (X = 3.6–3.8). At the heights of localization of pronounced aerosol layers, its value reaches unity (X = 1) [Nevzorov et al., 2019].

In 2019–2022, scientific team of the OIAP continued to study the atmospheric composition by spectroscopic methods. Refined estimates of trends in the CO TCs in different regions of Eurasia and, including Russia, have been obtained. A slowdown in the rate of decrease in CO TCs in the background regions of Eurasia has been revealed [Rakitin et al., 2020]. The contribution of climate change to the ongoing decrease in CO TCs in Moscow has been established [Rakitin et al., 2021]. The influence of meteorological conditions on the decrease in concentrations of the main atmospheric pollutants in Moscow during the lockdown period of the COVID-19 pandemic in 2020 was studied [Skorokhod et al., 2022].

A multifunctional software-computer complex TROPOMI_tools has been developed. It provides the automatic collection, processing, and analysis of measurement data from several satellite monitoring systems (MODIS, AIRS, OMI, TROPOMI). The results of testing the TROPOMI_tools have been published in several papers [Rakitin et al., 2021; Skorokhod et al., 2022]. Measurements of the Sentinel-5P TROPOMI spectrometer with high spatial resolution of tropospheric and stratospheric content of NO_2 and CO TCs were validated against ground-based spectroscopic data of the OIAP in Moscow and Zvenigorod (Zvenigorod Scientific Station – ZSS). The characteristics of agreement between satellite and ground-based measurements were analyzed with respect to the spatial resolution, cloud conditions, seasons, observed angles, and the height of the planetary boundary layer (PBL). The obtained differences are in good agreement with the results of TROPOMI validation versus data from the international observational networks such as NDACC, MAXDOAS, and Pandonia for NO_2, NDACC and TCCON for CO.

NO_2 TCs measured by the OMI satellite instrument were validated against ground-based measurements at 10 NDACC stations for the 2004–2020 period. Linear trends of NO_2 TCs at ground-based stations, as well as seasonal and latitudinal dependence of the characteristics of comparison of OMI and NDACC measurements were estimated. For the ZSS site, characteristics of the differences between OMI and ground-based data on the tropospheric and stratospheric NO_2 columns as well as agreement between the trends in tropospheric and stratospheric columns from OMI data and ZSS measurements were estimated. For other 9 NDACC stations measuring only NO_2 TCs, the agreement between the trends obtained from OMI and ground-based data was generally much worse.

The OIAP team together with the Faculty of Physics of MSU develop the chemical transport models to validate the small-scale structures of NO_2 distribution fields detected during satellite measurements and to detect the

sources of NO_2 emissions [Mukhartova et al., 2019, 2021; Postylyakov et al., 2020a; Davydova et al., 2021]. At present, regular measurements of nitrogen dioxide content from satellites are carried out using the TROPOMI, OMI, and GOME-2 instruments. The horizontal spatial resolution achieved by them with global coverage is tens of kilometers, which is sufficient to study the stratospheric NO_2 columns. However, tropospheric anthropogenic sources of nitrogen dioxide can have significantly smaller spatial scales (emissions from industrial pipes, highways). Since 2018, by using the newest TROPOMI satellite instruments, spatial resolution of measurements of up to 3.5 x 5.5 km^2 has been achieved for pixels located strictly in the nadir viewing. In 2016–2017, the first experiments on highly detailed sounding of tropospheric NO_2 were carried out by the IAP team. Measurements of the GSA spectrometer, which is installed on the Resurs-P series satellites, were used in this experiment. Based on the survey, for the first time the algorithm for retrieval of the NO_2 content in the troposphere with a spatial resolution of about 2.4 km on a 120 m grid was developed. Measurement errors for this algorithm are typical for satellite methods and total 10^{15} cm^{-2}. The ability to identify the sources of pollution and determine their power based on Resurs-P data has been demonstrated by [Davydova et al., 2021; Mukhartova et al., 2021]. To validate the large-scale structures detected in the retrieved NO_2 distribution fields, the results were compared to the TROPOMI and OMI data [Postylyakov et al., 2019a, 2019b, 2020a]. The comparison confirmed the reliability of the results obtained.

The OIAP continues to develop and improve the ground-based method of multi-angle differential spectroscopy (DOAS) for determining the content of NO_2, H_2CO and other reactive gases in PBL. In 2016, the OIAP team participated in the CINDI-2 international campaign for comparison the instruments and methods for measuring NO_2 and other gases using the DOAS method. The CINDI-2 campaign involved 36 spectral instruments from 26 different scientific groups. Kreher et al. [2020], Wang et al. [2020] discussed the results of comparisons of retrieval methods for chemically active substances that affect ozone chemistry such as NO_2, O_4, O_3, H_2CO, HNO_2. Based on the results of the comparisons, measurement modes and parameters for processing measurements of the DOAS method were formulated and recommended.

Temporal variability of the formaldehyde (H_2CO) TCs observed at the ZSS site of the OIAP and at the IAO (Tomsk) was estimated [Bruchkovskii et al., 2019]. A statistically significant positive trend in formaldehyde TCs depending on temperature at T>5°C at both observational sites was detected. The observed positive trend is probably caused by an increase in biogenic emissions of isoprene and other non-methane VOCs with an increase in temperature, as well as by increase in areas of forest and peat fires. In the air

masses arriving at the ZSS from Moscow, there is a stable increase in formaldehyde TCs by an average of $0.4\pm0.1\times10^{16}$ cm^{-2} at temperatures above zero and by $0.8\pm0.2\times10^{16}$ cm^{-2} at temperatures below zero. Despite the significant distance from Moscow, the values observed at the ZSS are generally 10% higher than those observed in Tomsk. In Tomsk, a statistically significant increase in formaldehyde TCs with winds from the direction of the main urban development ($3.24\pm0.3\times1016$ cm^{-2}) compared to TCs observed in other wind directions ($2.63\pm0.2\times10^{16}$ cm^{-2}) was recorded only at temperatures above 25°C .

Cloudiness and aerosol have a significant effect on the possibility of trace gases (TGs) (NO_2, H_2CO, etc.) retrieval in the lower troposphere using DOAS methods. Since there is a large volume of optical observations using the DOAS method, which are not accompanied by direct measurements of their characteristics, solving the problem of determining the properties of clouds and aerosols from the spectral measurements themselves could improve the accuracy of TGs retrieval. In a series of studies [Nikitin et al., 2019, 2010; Postylyakov et al., 2020b; Chulichkov et al., 2021] consider the problems of determining the characteristics of cloudiness (lower boundary, optical depth, etc.) and aerosol (optical depth, etc.) from the characteristics of the measured scattered solar radiation (O_4 optical depth, chromaticity index, absolute intensity, etc.). Machine learning methods are used as methods for solving nonlinear problems: artificial neural networks method and method of random forest.

For many years, the Department of Atmospheric Physics and the Laboratory for Study the Ozone Layer and Upper Atmosphere of SPbU applied different ground-based methods to study various parameters of the atmosphere, including gas composition using spectral measurements in the UV, visible, IR and MW spectral regions.

The SPbU observation station in Peterhof is equipped with a spectral complex based on a Bruker IFS 125HR Fourier spectrometer. Regular measurements of the solar IR spectra since 2009 make it possible to study the temporal variations of the TCs and vertical structure of various climatically and ecologically important atmospheric TGs. Ground-based FTIR measurements, along with satellite ones, provide information spatio-temporal variability of TGs, including their long-term trends [Timofeev et al., 2020a]. The FTIR retrieval techniques are permanently being improved to achieve higher accuracy and harmonization of datasets [Polyakov et al., 2019a, 2019b, 2020a; Virolainen et al., 2020a, 2020b; Polyakov et al., 2021].

In 2019–2022, spatio-temporal variations of TCs of different TGs were studied using consistent ground-based FTIR and satellite measurements, as well as the results of numerical modeling in the vicinity of St. Petersburg [Timofeev et al., 2019; Nikitenko et al., 2021; Polyakov et al., 2020b, 2021;

Nerobelov et al., 2021a, 2021b, 2022a, 2022b, 2022c; Virolainen et al., 2021]. The SPbU observational station participated in complex experiments to validate TROPOMI satellite measurements of formaldehyde [Vigoroux et al., 2020] and methane and CO [Sha et al., 2021]. CO, HCN, and C_2H_6 FTIR measurements were used to study the air pollution from forest fires in the Arctic and mid-latitude regions of the Northern Hemisphere [Lutsch et al., 2020].

The information content of FTIR measurements with respect to the elements of the TGs vertical structure was also studied [Timofeev et al., 2021a; Virolainen et al., 2022]. New information on the elements of the vertical distribution of ozone, CO_2, and HNO_3 was obtained; FTIR measurements were compared to satellite data and the results of numerical modelling [Virolainen et al., 2022; Nikitenko et al., 2022; Timofeev et al., 2021b; Bordovskaya et al., 2022]. Vertical distribution of methane in the troposphere of Western Siberia was retrieved and analyzed [Makarova et al., 2021b].

Zenith measurements at low solar angles in the UV and VIS spectral regions using DOAS technique and OceanOptics spectrometers provide information on the NO_2 content and its emissions in the vicinity of St. Petersburg [Ionov and Poberovsky, 2020; Ionov et al., 2022a].

Research in the field of ground-based MW atmospheric sounding at St. Petersburg State University was aimed at improving the methods for interpreting measurements from the RPG-HATPRO radiometer to derive the cloud liquid water path [Biryukov and Kostov, 2020; Kostsov et al., 2019, 2020].

In 2019–2020, EMME (Emission Monitoring Mobile Experiment) campaigns were carried out using Bruker EM27/SUN instruments and mobile DOAS measurements as a part of the European VERIFY program. The program was implemented by an international team from St. Petersburg State University (Russia), Karlsruhe Institute of Technology (Germany) and the University of Bremen (Germany). During the campaigns, data were obtained on the distribution of TC of methane, CO, CO2, and NOx around the metropolis of St. Petersburg [Makarova et al., 2021a]. The measurements provided the information on the specific and integral emissions of the most important anthropogenic greenhouse gas – CO_2 in the metropolis of St. Petersburg [Makarova et al., 2021a; Ionov et al., 2021; Nerobelov et al., 2021c; Timofeev et al., 2020b, 2022]. The measurements showed a significant underestimation of anthropogenic CO_2 emissions in St. Petersburg by the inventory method. Satellite measurements (TROPOMI, OCO-2, GOSAT, IASI) of XH_2O, XCO_2, XCH_4, and XCO were validated against ground-based measurements in the vicinity of St. Petersburg and Yekaterinburg within the COCCON program [Alberti et al., 2022].

Measurements of optical and microphysical parameters of atmospheric aerosol using CIMEL equipment and local data near St. Petersburg were analyzed [Vlasenko et al., 2019; Volkova et al., 2020].

Together with the team of MGO, ozone TC variations were studied using the FTIR method, Dobson and M-124 ozonometers, including comparisons of various ground-based and satellite data [Nerobelov et al., 2022a, 2022b]. The first attempts were made to interpret the measurements of the new Russian UFOS ozonometer to derive data on ozone TCs [Ionov and Privalov, 2021].

The results of systematic (2003-2017) measurements of the TCs and the averaged mole fraction of CH_4 and CO at the Novolazarevskaya Antarctic station using a diffraction spectrometer with a resolution of 0.2 cm^{-1} are presented by RPA "Typhoon" team [Ustinov et al., 2019, 2020]. During the measurement period, the mean XCH_4 and XCO were (1663±34) ppb and (37±8) ppb respectively. Trends and characteristics of seasonal variations of CH_4 and CO were estimated, and the results of comparison with ground and satellite data were given.

The MGO team provides the operation of the Roshydromet ground-based ozonometric network. Observations at 28 stations have been conducted since 1973 (Solomatnikova et al., 2020, 2021, 2022). A separate analysis was carried out for stations in the Arctic region. Measurements of erythemal UV radiation are performed at 12 stations.

A significant role in providing ground-based ozone TC measurements is played by the calibration of measuring equipment. Binding of M-124 ozonometers to the world scale is carried out by regular calibrations against the Dobson spectrophotometer No. 108, which is a standard of the Roshydromet ozonometric network.

Roshydromet ozonometric network currently is in the re-equipment process. The software, calibration methods and calculation of ozone TCs were improved in the frame of trial operation of new UFOS spectrometers intended for complex measurements of the spectral composition of the total UV radiation and ozone TCs.

Ground-based observations at 38 European stations were analyzed to assess the response of the ozone layer over Europe to extreme ozone depletion in the Arctic in 2020. The database on ozone TCs is replenished annually, coming from the AARI Russian Antarctic stations Mirny, Novolazarevskaya and Vostok and from AARI research expedition ships. Until the early 2000s, there was a steady decrease in the ozone TCs at Antarctic stations in the Antarctic spring; currently, there is a tendency for the ozone content to return to the values observed in the period before the manifestation of the ozone hole effect [Sibir et al., 2020].

Since 1972, the MGO team participates in international programs of global background monitoring of the atmospheric composition (Program of the

Global Atmosphere Watch – GAW WMO). Currently, greenhouse gases studies are included in the obligatory program of observations at background monitoring stations, and data from Russian stations are submitted to international data centers [Ivakhov et al., 2019, Paramonova et al., 2020].

Kulikov et al. [2020] compared values of 15 convective indices obtained from radiosonde and microwave temperature and water vapor profiles simultaneously measure over Nizhny Novgorod during 5 convective seasons of 2014-2018. They found good correlation (with coefficients of ~0.7-0.85) for most indices.

The mathematical tools of the optimal estimation method for retrieval of tropospheric temperature profiles (0–10 km) from radiometric data are presented in [Belikovich et al., 2020]. It uses the parameterization based on empirical orthogonal functions which are obtained by a singular analysis of covariance matrix of the radiosonde measurement data.

Belikovich et al. [2021] analyzed the differences between ground-based observed and simulated microwave spectra of atmospheric thermal radiation within the range of 20–59 GHz obtained from more than 4 years of passive microwave and radiosonde observations over Nizhny Novgorod. In the subsequent study [Belikovich et al., 2022], it was shown that the use of a technically more complex absorption model based on the application of the Energy Corrected Sudden formalism makes it possible to minimize the systematic shift of the simulated spectra from the measured ones to 0.6 K.

The results of the development of a mobile solid-state microwave spectroradiometer that operates in the 5-mm absorption band of molecular oxygen are presented in [Shvetsov et al., 2020].

References

1. Carlos A., Tu Q., Hase F., Makarova M.V., Gribanov K., Foka St.C., Zakharov V., Blumenstock T., Buchwitz M., Diekmann C., Ertl B., Frey M.M., Imhasin H.Kh., Ionov D.V., Khosrawi F., Osipov S.I., Reuter M., Schneider M., Warneke T. Investigation of spaceborne trace gas products over St Petersburg and Yekaterinburg, Russia, by using COllaborative Column Carbon Observing Network (COCCON) observations Atmos. Meas. Tech., 15, 2199–2229, 2022 https://doi.org/10.5194/amt-15-2199-2022
2. Belikovich M.V., Kulikov M.Y., Ryskin V.G., Shvetsov A.A., Krasilnikov A.A., Skalyga N.K., Serov E.A., Feigin A.M., Application of empirical orthogonal functions parameterization in the problem of retrieval of the tropospheric thermal structure by radiometric data // Radiophysics and Quantum Electronics, V. 62, № 9, p. 591–605, https://doi.org/10.1007/s11141-020-10005-3 , 2020.
3. Belikovich M.V., Kulikov M.Yu., Makarov D.S., Skalyga N.K., Ryskin V.G., Shvetsov A.A., Krasil'nikov A.A., Dementyeva S.O., Serov E.A. and Feigin A.M. Long-term Observations of Microwave Brightness Temperatures over a Metropolitan Area: Comparison of Radiometric Data and Spectra Simulated with the use of Radiosonde Measurements // Remote Sensing, 13, 2061, 2021. https://doi.org/10.3390/rs13112061

4. Belikovich M.V., Makarov D.S., Serov E.A., Kulikov M.Y., Feigin A.M., Validation of Atmospheric Absorption Models within the 20–60 GHz Band by Simultaneous Radiosonde and Microwave Observations: The Advantage of Using ECS Formalism // Remote Sensing. 2022, 14, 6042. https://doi.org/10.3390/rs14236042
5. Biryukov E.Y., Kostsov V.S. Application of the Regression Algorithm to the Problem of Studying Horizontal Inhomogeneity of the Cloud Liquid Water Path by Ground-Based Microwave Measurements in the Angular Scanning Mode. Atmos Ocean Opt 33, 602–609 (2020). https://doi.org/10.1134/S10248 5602006007X
6. Bordovskaya Yu. I., Ya.A. Virolainen, Yu.M. Timofeyev. Comparison of ground-based and satellite methods for determining vertical ozone profiles // Sovremennye problemy distancionnogo zondirovaniya Zemli iz kosmosa. 2022, V. 19, № 2, P. 225–231
7. Bruchkouski, I., Borovski, A., Dzhola, A., Elansky N., Postylyakov O., Bazhenov O., Romanovskii O., Sadovnikov S., Kanaya Y. Observations of Integral Formaldehyde Content in the Lower Troposphere in Urban Agglomerations of Moscow and Tomsk Using the Method of Differential Optical Absorption Spectroscopy. Atmos Ocean Opt, 2019, 32, 248–256. doi:10.1134/S102485 6019030047
8. Cheremisin A.A., Marichev V.N., Bochkovskii D.A. et al. Stratospheric Aerosol of Siberian Forest Fires According to Lidar Observations in Tomsk in August 2019 // Atmos Ocean Opt 35, 57–64 (2022). https://doi.org/10.1134/S1024856022010043
9. Chulichkov A.I., Nikitin S.V., Borovski A.N., Postylyakov O.V. Computer-aided measuring system based on an artificial neural network for estimating atmospheric parameter. Proc. IEEE, 2021 International Conference on Information Technology and Nanotechnology (ITNT), 20-24 Sept. 2021, 2021, ISBN:978-1-6654-3217-7, doi:10.1109/ITNT52450.2021.9649031.
10. Davydova M.A., Elansky N.F., 6. Zakharova S.A., Postylyakov O.V. Application of a Numerical-Asymptotic Approach to the Problem of Restoring the Parameters of a Local Stationary Source of Anthropogenic Pollution. Doklady Mathematics, 2021, Vol. 103, No. 1, 26–31. doi: 10.1134/S1064562421010026
11. Ionov, D.V., Poberovskii, A.V. Variability of Nitrogen Oxides in the Atmospheric Surface Layer near Saint Petersburg // Russ. Meteorol. Hydrol. 45, 720–726 (2020). https://doi.org/10.3103/S1068373920100064
12. Ionov, D. V., Makarova, M. V., Hase, F., Foka, S. C., Kostsov, V. S., Alberti, C., Blumenstock, T., Warneke, T., and Virolainen, Y. A., 2021: The CO2 integral emission by the megacity of St Petersburg as quantified from ground-based FTIR measurements combined with dispersion modelling //Atmos. Chem. Phys., 21, 10939–10963. doi: 10.5194/acp-21-10939-2021.
13. Ionov D.V., Makarova M.V., Kostsov V.S., Фока S.F. Assessment of the NOx integral emission from the St.Petersburg megacity by means of mobile DOAS measurements combined with dispersion modelling. 2022a, Atmospheric Pollution Research., V. 13, N. 12, стр. 101598 https://doi.org/10.1016/j.apr.2022.101598
14. Ionov D.V., Privalov V.I. The Differential Spectroscopy Technique DOAS in the Problem of Determining the Total Ozone Content from Measurements of

Ground-Based UV Spectrometer UFOS // Atmos Ocean Opt 35, 1–7 (2022b). https://doi.org/10.1134/S1024856022010079

15. Ivakhov V.M., Paramonova N.N., Privalov V.I., Zinchenko A.V., Loskutova M.A., Makshtas A.P., Kustov V.Y., Laurila T., Aurela M., Asmi E. Atmospheric concentration of carbon dioxide at tiksi and cape baranov stations in 2010–2017 // Russian Meteorology and Hydrology. 2019. V. 44. № 4. P. 291–299.
16. Kostsov V.S., Kniffka A., Stenge M., Ionov D.V. 2019: Cross-comparison of cloud liquid water path derived from observations by two space-borne and one ground-based instrument in Northen Europe // Atmospheric Measurement Techniques., 12, 5927–5946. https://doi.org/10.5194/amt-12-5927-2019.
17. Kostsov V.S., Ionov D.V., Kniffka A., 2020: Detection of the cloud liquid water path horizontal inhomogeneity in a coastline area by means of ground-based microwave observations: feasibility study // Atmos. Meas. Tech., 13, 8, 4565–4587. https://doi.org/10.5194/amt-13-4565-2020.
18. Kreher, K., Van Roozendael, M., Hendrick, F., Apituley, A., Dimitropoulou, E., Frieß, U., Richter, A., Wagner, T., Lampel, J., Abuhassan, N., Ang, L., Anguas, M., Bais, A., Benavent, N., Bösch, T., Bognar, K., Borovski, A., Bruchkouski, I., Cede, A., Chan, K. L., Donner, S., Drosoglou, T., Fayt, C., Finkenzeller, H., Garcia-Nieto, D., Gielen, C., Gómez-Martín, L., Hao, N., Henzing, B., Herman, J. R., Hermans, C., Hoque, S., Irie, H., Jin, J., Johnston, P., Khayyam Butt, J., Khokhar, F., Koenig, T. K., Kuhn, J., Kumar, V., Liu, C., Ma, J., Merlaud, A., Mishra, A. K., Müller, M., Navarro-Comas, M., Ostendorf, M., Pazmino, A., Peters, E., Pinardi, G., Pinharanda, M., Piters, A., Platt, U., Postylyakov, O., Prados-Roman, C., Puentedura, O., Querel, R., Saiz-Lopez, A., Schönhardt, A., Schreier, S. F., Seyler, A., Sinha, V., Spinei, E., Strong, K., Tack, F., Tian, X., Tiefengraber, M., Tirpitz, J.-L., van Gent, J., Volkamer, R., Vrekoussis, M., Wang, S., Wang, Z., Wenig, M., Wittrock, F., Xie, P. H., Xu, J., Yela, M., Zhang, C., Zhao, X. Intercomparison of NO2, O4, O3 and HCHO slant column measurements by MAX-DOAS and zenith-sky UV–visible spectrometers during CINDI-2. Atmos. Meas. Tech., 13, 2169–2208, doi:10.5194/amt-13-2169-2020, 2020.
19. Kulikov M.Yu., M.V. Belikovich, N.K. Skalyga, M.V. Shatalina, S.O. Dementyeva, V. G. Ryskin, A.A. Shvetsov, A.A. Krasil'nikov, E.A. Serov and A.M. Feigin, Skills of Thunderstorm Prediction by Convective Indices over a Metropolitan Area: Comparison of Microwave and Radiosonde Data // Remote Sensing, 12(4), 604; https://doi.org/10.3390/rs12040604, 2020.
20. Lutsch, E., Strong, K., Jones, D. B. A., Blumenstock, T., Conway, S., Fisher, J.A., Hannigan, J. W., Hase, F., Kasai, Y., Mahieu, E., Makarova, M., Morino, I., Nagahama, T., Notholt, J., Ortega, I., Palm, M., Poberovskii, A.V., Sussmann, R., and Warneke, T., 2020: Detection and attribution of wildfire pollution in the Arctic and northern midlatitudes using a network of Fourier-transform infrared spectrometers and GEOS-Chem. Atmos. Chem. Phys., 20, 21, 12813–12851. https://doi.org/10.5194/acp-20-12813-2020.
21. Makarova, M.V., Alberti, C., Ionov, D.V., Hase, F., Foka, S.C., Blumenstock, T., Warneke, T., Virolainen, Ya.A., Kostsov, V.S., Frey, M., Poberovskii, A.V., Timofeyev, Yu.M., Paramonova, N.N., Volkova, K.A., Zaitsev, N.A., Biryukov, E.Y., Osipov, S.I., Makarov, B.K., Polyakov, A.V., Ivakhov, V.M., Imhasin, H.Kh., and Mikhailov, E.F., 2021a: Emission Monitoring Mobile Experiment

(EMME): an overview and first results of the St. Petersburg megacity campaign-2019. Atmos. Meas. Tech., 14, 1047–1073. https://doi.org/10.5194/amt-14-1047-2021a.

22. Makarova M.V., Serdyukov V.I., Arshinov M.Y. et al. The First Complex Experiment on Determining Parameters of the Vertical Distribution of Methane in the Troposphere over Western Siberia from Solar Spectra Recorded with an IFS-125M FTIR Spectrometer and In Situ Aircraft Measurements // Atmos Ocean Opt 34, 61–67 (2021b). https://doi.org/10.1134/S1024856021010073
23. Marichev V.N., Bochkovskii D.A. Lidar complex of a small station of high-altitude atmosphere sounding of IAO SB RAS . // Optika Atmosfery i Okeana. 2020a. V. 33. No. 05. P. 399–406. DOI: 10.15372/AOO20200510 [in Russian].
24. Marichev V.N., Bochkovskii D.A. Lidar studies of winter stratospheric warming over Tomsk // Proceedings of SPIE. 2020b. V. 11560. CID: 1156087. doi.org/10.1117/12.2575302
25. Marichev V.N., Bochkovskii D.A. Lidar monitoring of stratospheric aerosol over Tomsk in 2021. Proc. SPIE 12341, 28th International Symposium on Atmospheric and Ocean Optics: Atmospheric Physics, 123417A (7 December2022a); doi: 10.1117/12.2644746
26. Marichev V.N., Bochkovskii D.A. Investigations of the thermal regime of the stratosphere over Tomsk in 2021 based on lidar monitoring. Proc. SPIE12341, 28th International Symposium on Atmospheric and Ocean Optics: Atmospheric Physics, 123417B (7 December 2022b); doi: 10.1117/12.2644747
27. Marichev, V.N., Bochkovsky, D.A. & Elizarov, A.I. Optical Aerosol Model of the Western Siberian Stratosphere Based on Lidar Monitoring Results // Atmos Ocean Opt 35 (Suppl 1), S64–S69 (2022). https://doi.org/10.1134/S1024856023010104
28. Mukhartova Y.V., M.A. Davydova, N.F. Elansky, O.V. Postylyakov, S.A. Zakharova, A.N. Borovski. On application of nonlinear reaction-diffusion-advection models to simulation of transport of chemically-active impurities. Proc. SPIE, 11157, 111570X, 2019, doi:10.1117/12.2535489.
29. Mukhartova Y.V. , O.V. Postylyakov, M.A. Davydova, S.A. Zakharova. High-detailed tropospheric transport of NOx from ground sources: comparison of model data and satellite imagery. Proc. SPIE 11859, 1185906, 2021; doi:10.1117/12.2600283.
30. Nerobelov G., Timofeyev Y., Smyshlyaev S., Foka S., Mammarella I., Virolainen Y., 2021a: Validation of WRF-Chem Model and CAMS Performance in Estimating Near-Surface Atmospheric CO2 Mixing Ratio in the Area of Saint Petersburg (Russia) // Atmosphere, 12, 387. https://doi.org/10.3390/atmos12030387.
31. Nerobelov, G.M., Timofeyev, Y.M., Smyshlyaev, S.P. et al. Comparison of CAMS Data on CO2 with Measurements in Peterhof // Atmos Ocean Opt 34, 689–694 (2021b). https://doi.org/10.1134/S102485602106018X
32. Nerobelov G.M., Timofeyev Y.M. Estimates of CO_2 Emissions and Uptake by the Water Surface near St. Petersburg Megalopolis // Atmos Ocean Opt 34, 422–427 (2021c). https://doi.org/10.1134/S1024856021050158
33. Nerobelov G., Y. Timofeyev, Y. Virolainen, A. Polyakov, A. Solomatnikova, A. Poberovskii, O. Kirner, O. Al-Subari, S. Smyshlyaev and E. Rozanov Measurements and Modelling of Total Ozone Columns near St. Petersburg, Russia // Remote Sensing 2022a, V. 14, № 16 10.3390/rs14163944

34. Nerobelov G.M., Al-Subari O., Timofeyev Y.M. et al. Comparison of Ground-Based Measurement Results of Total Ozone near St. Petersburg // Izv. Atmos. Ocean. Phys. 58, 494–499 (2022b). https://doi.org/10.1134/S0001433822050073
35. Nerobelov G.M., Timofeyev Y.M., Poberovskii A.V. et al. Ground-Based Spectroscopic Measurements of the Total Ammonia Content in the Vicinity of St. Petersburg // Izv. Atmos. Ocean. Phys. 58, 560–568 (2022c). https://doi.org/10.1134/S0001433822060123
36. Nevzorov A.V., Dolgii S.I., Makeev A.P., El'nikov A.V. Results of observations of aerosol from North American forest fires in the stratosphere over Tomsk in late summer and fall of 2017 . // Optika Atmosfery i Okeana. 2019. V. 32. No. 02. P. 162–167. DOI: 10.15372/AOO20190211 [in Russian].
37. Nikitenko A.A., G.M. Nerobelov, Yu.M. Timofeev, A.V. Poberovsky, 2021: Analysis of ground-based spectroscopic measurements of CO2 in Peterhof // Sovremennye problemy distancionnogo zondirovaniya Zemli iz kosmosa, V. 18, № 6, P. 57–70.
38. Nikitenko A.A., Timofeev Y.M., Virolainen Y.A. et al. Comparison of Stratospheric CO2 Measurements by Ground- and Satellite-Based Methods. // Atmos Ocean Opt 35, 341–344 (2022). https://doi.org/10.1134/S1024856022040145
39. Nikitin S.V., A.I. Chulichkov, A.N. Borovski, O.V. Postylyakov. Estimation of cloudiness and aerosol characteristics in the atmosphere from spectral measurements of scattered solar radiation using a neural network Proc. SPIE, 11152, 111521H, 2019, doi:10.1117/12.2535490.
40. Nikitin St.V., A.I. Chulichkov, Al.N. Borovski, O.V. Postylyakov. On estimation of atmospheric scattering characteristics from spectral measurements of solar radiation using machine learning algorithms. Proc. SPIE 11531, 115310V; 2020, doi:10.1117/12.2574237.
41. Paramonova N.N., Privalov V.I., Ivakhov V.M., et al. Physical and chemical characteristics of the atmosphere // In: Obzor fonovogo sostoyaniya okruzhayuschey sredy na territorii stran SNG za 2019. Ed. Chernogaeva G.M., Moskva, 2020. P. 13-30 [in Russian].
42. Polyakov A.V., Virolainen Y.A. & Makarova M.V. Method for Inversion of the Transparency Spectra for Evaluating the Content of CCl2F2 in the Atmosphere // J Appl Spectrosc 86, 449–456 (2019a). https://doi.org/10.1007/s10812-019-00840-2
43. Polyakov A.V., Virolainen Y.A. & Makarova M.V. Technique for Inverting Transmission Spectra to Measure Freon Concentration // J Appl Spectrosc 85, 1085–1093 (2019b). https://doi.org/10.1007/s10812-019-00763-y
44. Polyakov A.V., Poberovsky A.V., Virolainen Y.A. et al. Transparency Spectra Inversion Technique for Evaluating the Atmospheric Content of Ccl3f Freon // J Appl Spectrosc 87, 92–98 (2020a). https://doi.org/10.1007/s10812-020-00968-6
45. Polyakov A., Virolainen Ya., Poberovskiy A., Makarova M. & Timofeyev Y., 2020b: Atmospheric HCFC-22 total columns near St. Petersburg: stabilization with start of a decrease // International Journal of Remote Sensing, 41, 11, 4365–4371. DOI: 10.1080/01431161.2020.1717668.
46. Polyakov A., A. Poberovsky, M. Makarova, Ya. Virolainen, Yu. Timofeyev, A. Nikulina, 2021: Measurements of CFC-11, CFC-12, and HCFC-22 total columns in the atmosphere at the St. Petersburg site in 2009-2019 // Atmos. Meas. Tech., 14, 8, 5349–5368, https://doi.org/10.5194/amt-14-5349-2021.

47. Postylyakov O.V., A.N. Borovski, N.F. Elansky, M.A. Davydova, S.A. Zakharova, A.A. Makarenkov. Comparison of space high-detailed experimental and model data on tropospheric NO_2 distribution // Proc. SPIE, 11208, 112082S, 2019a, doi:10.1117/12.2540770.
48. Postylyakov O.V., A.N. Borovski, M.A. Davydova, A.A. Makarenkov. Preliminary validation of high-detailed GSA/Resurs-P tropospheric NO2 maps with alternative satellite measurements and transport simulations // Proc. SPIE, 11152, 111520F, 2019b, doi:10.1117/12.2535487.
49. Postylyakov O.V., Al.N. Borovski, K.A Shukurov, Iu.V. Mukhartova, M.A. Davydova, A.A. Makarenkov. On validation high-detail mapping of tropospheric NO_2 using GSA/Resurs-P observations with simulated data // Proc. SPIE 11531, 1153109, 2020a, doi:10.1117/12.2574240.
50. Postylyakov O.V., A.N. Borovski, A.I. Chulichkov, S.V. Nikitin. On estimation of cloudiness characteristics and parameters of DOAS retrieval from spectral measurements using a neural network // IOP Conference Series: Earth and Environmental Science, 2020b, 489, 012031, doi:10.1088/1755-1315/489/1/012031.
51. Rakitin V.S., Skorokhod A.I., Pankratova N.V., Shtabkin Yu.A., Rakitina A.V., Wang G., Vasilieva A.V., Makarova M.V. and Wang P. Recent changes of atmospheric composition in background and urban Eurasian regions in XXI-th century // 2020 IOP Conf. Ser.: Earth Environ. Sci. 606 012048 doi:10.1088/1755-1315/606/1/012048 https://iopscience.iop.org/article/10.1088/1755-1315/606/1/012048/pdf
52. Rakitin V.S., Elansky N.F., Skorokhod A.I., Dzhola A.V., Rakitina A.V., Shilkin A.V., Kitillova N.S., Kazakov A.V. Long-term tendencies of Carbon monoxid Total content in the Moscow megapolis atmosphere // Izvestiya, Atmospheric and Oceanic Physics, 2021, V 57, № 1, 116–125. DOI: 10.1134/S0001433821010102
53. Sha M.K., B. Langerock, J.-F.L. Blavier, Th. Blumenstock, T. Borsdorff, M. Buschmann, A. Dehn, M. De Maziere, N.M. Deutscher, D.G. Feist, O.E. Garcia, D.W.T. Griffith, M. Grutter, J.W. Hannigan, F. Hase, P. Heikkinen, Ch. Hermans, L.T. Iraci, P. Jeseck, N. Jones, R. Kivi, N. Kumps, J. Landgraf, A. Lorente, E. Mahieu, M.V. Makarova, J. Mellqvist, J.-M. Metzger, I. Morino, T. Nagahama, J. Notholt, H. Ohyama, I. Ortega, M. Palm, Ch. Petri, D.F. Pollard, M. Rettinger, J. Robinson, S. Roche, C.M. Roehl, A.N. Rohling, C. Rousogenous, M. Schneider, K. Shiomi, D. Smale, W. Stremme, K. Strong, R. Sussmann, Y. Te, O. Uchino, V.A. Velazco, C. Vigouroux, M. Vrekoussis, P. Wang, Th. Warneke, T. Wizenberg, D. Wunch, S. Yamanouchi, Y. Yang, and M. Zhou, 2021: Validation of methane and carbon monoxide from Sentinel-5 Precursor using TCCON and NDACC-IRWG stations. Atmos. Meas. Tech., 14, 9, 6249–6304, https://doi.org/10.5194/amt-14-6249-2021
54. Shvetsov A.A., M.V. Belikovich, A.A. Krasilnikov, M.Yu. Kulikov, L.M. Kukin, V.G. Ryskin, O.S. Bolshakov, I.V. Lesnov, A.M. Shitov, A.M. Feigin, V.B. Khaikin, and I.V. Petrov, A 5-mm Wavelength-Range Spectroradiometer for Studying the Atmosphere and Underlying Surface // Instruments and Experimental Techniques, Vol. 63, No. 6, pp. 885–889, doi: 10.1134/S0020441220050358, 2020.
55. Sibir E.E., Radionov V.F., Rusina E.N. Results of long-term observations of total ozone in Antarctica and over the Atlantic and Southern Oceans, Russian Meteorology and Hydrology. 2020. T. 45. № 3. C. 161–168.

56. Skorokhod A.I., Rakitin V.S., and Kirillova N.S. Impact of COVID-19 Pandemic Preventing Measures and Meteorological Conditions on the Atmospheric Air Composition in Moscow in 2020 // Russian Meteorology and Hydrology, 2022, Vol. 47, No. 3, pp. 183–190 IF = 0,788 (2021) DOI: 10.3103/S106837 3922030037 https://www.ncbi.nlm.nih.gov/pmc/articles/PMC9243816
57. Solomatnikova A.A., Romashkina K.I., Volohina D.Yu. Features of the state of ozone layer over regions of Russian Federation // In: Obzor sostiyaniya I zagryzaneniya okruzhayuschey sredy v Rossiyskoy Federacii za 2019 god, Roshydromet, 2020, P. 36-39 [in Russian].
58. Solomatnikova A.A., Romashkina K.I., Volohina D.Yu. Features of the state of ozone layer over regions of Russian Federation // In: Obzor sostiyaniya I zagryzaneniya okruzhayuschey sredy v Rossiyskoy Federacii za 2020 god, Roshydromet, 2021, P. 36–39 [in Russian].
59. Solomatnikova A.A., Romashkina K.I., Zhukova M.P. Features of the state of ozone layer over regions of Russian Federation // In: Obzor sostiyaniya I zagryzaneniya okruzhayuschey sredy v Rossiyskoy Federacii za 2021 god, Roshydromet, 2022, P. 36–39 [in Russian].
60. Timofeyev, Y.M., Berezin, I.A., Virolainen, Y.A. et al. Spatial–Temporal CO2 Variations near St. Petersburg Based on Satellite and Ground-Based Measurements // Izv. Atmos. Ocean. Phys. 55, 59–64 (2019). https://doi.org/10.1134/S0001433819010109
61. Timofeev, Y.M., Polyakov, A.V., Virolainen, Y.A. et al. Estimates of Trends of Climatically Important Atmospheric Gases Near St. Petersburg // Izv. Atmos. Ocean. Phys. 56, 79–84 (2020a). https://doi.org/10.1134/S0001433820010119
62. Timofeev Yu.M., G.M. Nerobelov, Y.A. Virolainen, A.V. Poberovskii, and S.C. Foka, 2020b: Estimates of CO2 Anthropogenic Emission from the Megacity St. Petersburg // Doklady Earth Sciences, Part 1, 753–756. DOI: 10.1134/S1028334X20090184
63. Timofeev Y.M., Filippov N.N. & Poberovsky A.V. Analysis of the Information Content and Vertical Resolution of Ground-Based IR Spectroscopy for Determining the Vertical Structure of CO2 // Atmos Ocean Opt 34, 87–92 (2021a). https://doi.org/10.1134/S1024856021020093
64. Timofeyev, Y.M., Nerobelov, G.M., Poberovskii, A.V. et al. Determining Both Tropospheric and Stratospheric CO2 Contents Using a Ground-Based IR Spectroscopic Method // Izv. Atmos. Ocean. Phys. 57, 286–296 (2021b). https://doi.org/10.1134/S0001433821020110
65. Timofeyev Y.M., Nerobelov G.M. & Poberovskii A.V. Experimental Estimates of Integral Anthropogenic CO2 Emissions in the City of St. Petersburg // Izv. Atmos. Ocean. Phys. 58, 237–245 (2022). https://doi.org/10.1134/S0001433822030100
66. Ustinov V.P., Baranova E.L., Visheratin K.N., Grachev M.I., Kal'sin A.V. Carbon Monoxide Variations in the Antarctic Atmosphere from Ground-Based and Satellite Measurement Data. Izvestiya, Atmospheric and Oceanic Physics, 2019, Vol. 55, No. 9, pp. 1210–1217. DOI: 10.1134/S0001433819090536
67. Ustinov V.P., Baranova E.L., Visheratin K.N., Grachev M.I., Kal'sin A.V. Variations of total methane in the atmosphere of Antarctica.// Arctic and Antarctic Research, 2020, V. 66, N 1, p. 66–81 [in Russian].
68. Vigouroux Corinne, Bavo Langerock, Carlos Augusto Bauer Aquino, Thomas Blumenstock, Zhibin Cheng, Martine De Maziere, Isabelle De Smedt, Michel

Grutter, James W. Hannigan, Nicholas Jones, Rigel Kivi, Diego Loyola, Erik Lutsch, Emmanuel Mahieu, Maria Makarova, Jean-Marc Metzger, Isamu Morino, Isao Murata, Tomoo Nagahama, Justus Notholt, Ivan Ortega, Mathias Palm, Gaia Pinardi, Amelie Rohling, Dan Smale, Wolfgang Stremme, Kim Strong, Ralf Sussmann, Yao Te, Michel van Roozendael, Pucai Wang, and Holger Winkler, 2020: TROPOMI–Sentinel-5 Precursor formaldehyde validation using an extensive network of ground-based Fourier-transform infrared stations. Atmos. Meas. Tech., 13, 7, 3751–3767. https://doi.org/10.5194/amt-13-3751-2020.

69. Virolainen Y.A., Polyakov A.V. & Kirner O. Optimization of Procedure for Determining Chlorine Nitrate in the Atmosphere from Ground-Based Spectroscopic Measurements // J Appl Spectrosc 87, 319–325 (2020a). https://doi.org/10.1007/s10812-020-01002-5
70. Virolainen Y.A., Nikitenko A.A. & Timofeyev Y.M. Intercalibration of Satellite and Ground-Based Measurements of CO_2 Content at the NDACC St. Petersburg Station // J Appl Spectrosc 87, 888–892 (2020b). https://doi.org/10.1007/s10812-020-01085-0
71. Virolainen Y.A., Polyakov,A.V. & Timofeyev Y.M. Analysis of the Variability of Stratospheric Gases Near St. Petersburg Using Ground-Based Spectroscopic Measurements // Izv. Atmos. Ocean. Phys 57, 148–158 (2021). https://doi.org/10.1134/S0001433821010138
72. Virolainen Ya. A., Timofeev Yu. M., Poberovsky A. V., Polyakov A. V. Information content of ground-based FTIR method for atmospheric HNO3 vertical structure retrieval // Optika Atmosfery i Okeana. 2022. V. 35. No. 11. P. 906–911. DOI: 10.15372/AOO20221105 [in Russian].
73. Vlasenko S.S., Volkova K.A., Ionov D.V. et al. Variation of Carboneceous Atmospheric Aerosol Near St. Petersburg // Izv. Atmos. Ocean. Phys. 55, 619–627 (2019). https://doi.org/10.1134/S0001433819060161
74. Volkova, K.A., Anikin, S.S., Mihailov, E.F. et al. Seasonal and Daily Variability of Aerosol Particle Concentrations near St. Petersburg // Atmos Ocean Opt 33, 524–530 (2020). https://doi.org/10.1134/S102485602005019X
75. Wang, Y., Apituley, A., Bais, A., Beirle, S., Benavent, N., Borovski, A., Bruchkouski, I., Chan, K. L., Donner, S., Drosoglou, T., Finkenzeller, H., Friedrich, M. M., Frieß, U., Garcia-Nieto, D., Gómez-Martín, L., Hendrick, F., Hilboll, A., Jin, J., Johnston, P., Koenig, T. K., Kreher, K., Kumar, V., Kyuberis, A., Lampel, J., Liu, C., Liu, H., Ma, J., Polyansky, O. L., Postylyakov, O., Querel, R., Saiz-Lopez, A., Schmitt, S., Tian, X., Tirpitz, J.-L., Van Roozendael, M., Volkamer, R., Wang, Z., Xie, P., Xing, C., Xu, J., Yela, M., Zhang, C., Wagner, T. Inter-comparison of MAX-DOAS measurements of tropospheric HONO slant column densities and vertical profiles during the CINDI-2 campaign, Atmos. Meas. Tech., 13, 5087–5116, https://doi.org/10.5194/amt-13-5087-2020, 2020.
76. Zakharova S. M. Davydova, A. Borovski, K. Shukurov, Y. Mukhartova, A. Makarenkov, O. Postylyakov. Experiments on high-detailed mapping of tropospheric NO2 using GSA/Resurs-P observations: results, validation with models and measurements, estimation of emission power, Proc. SPIE 11859, 1185905, 2021; doi:10.1117/12.2600316

Satellite measurements and their results

Research on a wide range of actual problems in satellite remote sensing of the atmosphere and the Earth's surface was carried out in the following areas:

1. Satellite instruments, calibration and validation of satellite data and information products.
2. Determination of the atmosphere and surface characteristics from satellite measurements in various spectral ranges.
3. Using satellite measurement data and information products to study various processes and phenomena in the atmosphere, ocean and on land, in numerical weather prediction (NWP) and climate research.

During the reporting period, the national constellation of meteorological satellites was extended by launching new polar-orbital (LEO) and geostationary (GEO) satellites of the Meteor-M and Electro-L series. In addition, on February 28, 2022, the Arktika-M No. 1 satellite was launched into a highly elliptical Molniya-type orbit, complementing the LEO and GEO weather satellites in terms of operational providing the hydrometeorological data for the Arctic region of the Earth in a quasi-continuous mode [Asmus et al., 2021].

The first direction includes a review of studies on the control of on-board radiometric calibration of instruments of Russian operational weather satellites carried out as part of the modernization of the calibration / validation system of satellite data and products created at SRC Planeta, see [Rublev et al, 2021]. In the paper [Timofeev et al., 2019] the first Russian hyperspectral infrared (IR) sounder, namely, infrared Fourier transform spectrometer IKFS-2 performance and operation on board "Meteor-M" No. 2 spacecraft are analyzed, including the assessment of the measurements' quality (the errors of radiometric and spectral calibration) and their information content. Kozlov et al., [2022] presented new results on noise covariance matrix characterization of IKFS-2 measurements. The study of the Earth's climate changes based on the analysis of the outgoing thermal IR radiation spectra, registered by various satellite instruments requires their careful intercalibration. Kozlov et al., [2019] described the intercalibration of SI-1 Fourier spectrometers (Meteor-28 and Meteor-29 satellites, 1977 and 1979) and IKFS-2 (Meteor-M No. 2), necessary for the analysis of changes in IR spectra of the atmosphere over past 40 years. The studies [Zabolotskikh, 2021; Zabolotskikh, Balashova, 2021] described the method of external calibration of measurements of the MTVZA-GYa microwave radiometer onboard Meteor-M No. 2-2 satellite in eight imaging channels (frequency range 10.6 – 36.5 GHz) using measurements of the AMSR2 microwave radiometer (GCOM-W spacecraft, JAXA) as reference.

Several publications of SPbU team are dedicated to the validation of various satellite-based information products, as well as to the comparison of

ground-based and satellite measurements. Thus, in [Kostsov et al., 2019], comparisons of estimates were carried out of the liquid water amount in clouds (cloud liquid water path) for the Northern Europe territory retrieved from remote ground-based microwave (RPG-HATPRO spectrometer) and satellite (SEVIRI and AVHRR scanners – imager) measurements. In [Bordovskaya et al., 2022] measurements of ozone vertical profiles in the atmosphere of St. Petersburg were compared using ground-based infrared spectroscopic method and satellite-based microwave method (MLS instrument, EOS Aura satellite) for the period 2018-2020. The analysis of the total ozone content (TOC) retrieval errors from the IKFS-2 data of the Meteor-M No. 2 was performed in [Polyakov et al., 2021; Nerobelov et al., 2022].

Several works are dedicated to the results of comparing ground-based and satellite spectroscopic measurements of the atmospheric total CO_2 content (XCO_2). In the paper [Virolainen et al., 2020], a comparison of ground-based (Bruker 125HR Fourier spectrometer) and satellite (OCO spectrometer onboard OCO-2 satellite) measurements of XCO_2 near St. Petersburg was carried out. Comparisons of ground-based and satellite (ACE instrument) measurements of the XCO_2 in the troposphere and stratosphere [Nikitenko et al. 2022] showed that there is good agreement between both types of measurements. The results of comparison of the satellite (Sentinel-5P spacecraft) and ground-based (TCCON and NDACC-IRWG networks) spectroscopic measurements of CH_4 and CO content in the atmosphere are presented in [Sha et al., 2021].

The accuracy of the of temperature and relative humidity profile retrievals from IKFS-2 / Meteor-M No. 2 data was evaluated in [Filei et al., 2019] through comparison with the radiosonde data and NWP products.

The results of the research in the second direction are presented in numerous publications. Moreover, several papers are dedicated to the development of methods for obtaining various atmospheric remote sensing products using artificial neural network (ANN) or machine learning (ML) algorithms, which have been developed actively in recent years.

During the reporting period, considerable attention was paid to the traditional topic of satellite meteorology [Uspensky, 2021] – the development of methods for satellite monitoring of cloud and precipitation parameters. General technological aspects of the ML algorithms application for classification of clouds and snow cover detection from the scanner – imagers measurements on the Meteor-M, Electro-L and Himawari spacecrafts are considered in [Kramareva et al., 2019].

In the study [Volkova et al., 2021] an overview of various methods (threshold technique and MO algorithms) is presented for remote derivation of cloud cover and precipitation characteristics using multi-channel scanner-imagers data from LEO and GEO weather satellites. Moreover, the study

analyzed the results of satellite products validation obtained from the comparison with ground-based meteorological observations and independent satellite estimates. Publications on the same topic include [Andreev et al., 2019; Filei et al., 2019; Filei 2019a, 2019b, 2020a, 2020b; Filei and Marenko. 2021; Volkova et al., 2020; Chursin and Kuzhevskaya, 2020]. In [Kuchma and Shamilova, 2022] an algorithm is developed and validated for detecting potential fog from the Japanese GEO weather satellite Himawari-8 data for Far Eastern region of Russia. In the studies [Kuchma et al., 2022; Filei, 2020a, 2020b; Filei et al, 2021], new algorithms are developed for remote derivation of marine aerosol and volcanic ash parameters from measurements of scanner-imagers installed on-board LEO and GEO weather satellites.

Specialists from IAO performed a series of studies on satellite monitoring of cloud parameters. The statistical models (distribution laws, parameters) of cloud cover characteristics for 14 types of cloud formations over the territory of Western Siberia in summer were developed based on the results of cloud classification from satellite-based MODIS / EOS Terra and VIIRS / S-NPP scanner-imagers data [Astafurov et al., 2021a]. According to [Astafurov et al., 2021b], these models can be used to parameterize and to account for the influence of clouds in climate modeling on the territory of Western Siberia. An ANN algorithm is proposed in the papers [Skorokhodov et al., 2022a, 2022b] for estimating the lower boundary height of a single-layer cloudiness over the territory of Western Siberia from MODIS data; moreover, the CALIOP lidar (CALIPSO satellite) data and CPR radar (CloudSat satellite) data together with ASOS ground network measurements were used as a reference for the ANN training. Furthermore, the algorithms have been developed and tested for estimating the influence of broken cloudiness (cloud adjacency effect) on retrieved reflectance of cloudless Earth's surface areas while using satellite-based MODIS observations through gaps in a broken cloud field [Tarasenkov et al., 2021a, 2021b, 2022].

Uspensky et al. [2021] provided an overview of methods and technical devices developed in our country for the Earth’s atmosphere temperature and humidity profiles sounding from satellites. A brief description is given of existing and forthcoming atmospheric sounders as well as of satellite data processing algorithms and technologies. Filei et al. [2021] considered the application of ANN algorithms for atmospheric temperature and humidity profiles retrieval from microwave radiometer MTVZA-GYa measurements on board Meteor-M No. 2-2 satellite. Filei et al. [2022] presented the application of the ANN algorithm for the retrieval of total precipitable water in the atmosphere over water and land surfaces from the MTVZA-GYa measurements on board the Meteor-M No. 2-2 satellite. The derivation of the total atmospheric water vapor content over the cloudless ocean from MTVZA-GYa measurements using the regression technique was described in [Kostornaya et al., 2020].

Research was continued on an important part of satellite – based remote sensing of the atmosphere – the development of methods for derivation of TOCs and total content of number of small gas species of the atmosphere, including greenhouse gases. The studies [Timofeev et al., 2021; Polyakov et al., 2019] describe an ANN algorithm for TOC estimation from IKFS-2 data onboard the Meteor-M No. 2 satellite using for the ANN training the TOC estimates from the OMI spectrometer data aboard the AURA satellite. Bloshchinskiy et al. [2022] considered a retrieval of the TOC values from the MSU-GS scanner-imager data (the key payload of Electro-L No. 3 GEO satellite) using the ANN algorithm and TOC estimates from OMPS/S-NPP measurements for ANN training.

Uspensky [2022] provided an overview of the twenty-year development of methods and measuring techniques for the satellite-based derivation of the concentration of long-lived carbon-containing greenhouse gases in the atmosphere – carbon dioxide CO_2 and methane CH_4, both in Russia and abroad. The physical and mathematical foundations for data "inversion" of near-IR and IR spectrometers data are given. The information on Russian and foreign satellite system for atmospheric CO_2 and CH_4 concentrations monitoring is presented. Golomolzin et al. [2022] described the technique for the retrieval of atmospheric column-averaged dry-air mole fractions of carbon dioxide (XCO_2) from IKFS-2 data onboard Meteor-M No. 2 satellite. The method of XCO_2 estimating is a second-order regression, whose predictors are the effective spectral optical depths of the atmosphere in the infrared region of 8–14 μm. The reference XCO_2 values for the regression training were the results of contact CO_2 measurements on the tall tower at the ZOTTO international observatory (Central Siberia) and at the NOAA observatory on the Mauna Loa volcano (Hawaii) in 2015–2016. The methodology was verified by comparing the IKFS-2 based XCO_2 estimates with parallel independent estimates over Siberia from the OCO and CrIS spectrometers data on board the OCO-2 and NOAA-20 satellites (USA).

The team from OIAP performed a series of studies on remote determination of the nitrogen dioxide (NO_2) integral content in the troposphere with high spatial resolution based on measurements of the GSA spectrometer installed on the Resurs-P series Earth observation satellites. The developed technique makes it possible to obtain estimates of the desired NO_2 distribution in the troposphere with a spatial resolution of about 2.4 km on a 120 m grid. To validate large-scale structures detected in the retrieved NO_2 distribution fields and confirm their reliability, the estimates derived from GSA spectrometer data were compared in [Postylyakov et al., 2019a, 2019b, 2020] with similar estimates from TROPOMI (Sentinel-5P satellite) and OMI spectrometers (Aura satellite) data. To validate small-scale structures and to find sources of NO_2 emissions, the OIAP, together with the Faculty of Physics of

MSU, is developing chemical transport models (CTMs) of the appropriate scale [Mukhartova, et al., 2019, 2021; Davydova et al., 2021; Zakharova et al., 2021]. Using the CTM it was demonstrated the ability to detect local (point) sources of pollution and to determine their power from GSA/Resurs-P data.

In the Laboratory of Climate and Environmental Physics of the INSM UFU, the methods were developed for remote derivation the CH_4 and the HDO/H_2O ratio vertical profiles [Zadvornykh, et al., 2019, 2021] in the Earth's atmosphere from TANSO-FTS spectrometer (GOSAT-2 satellite) measurements of the thermal and near-infrared ranges. For the first time, the vertical profile of the relative content of the isotopologues HDO/H_2O (δD) in atmospheric water vapor was evaluated. Moreover, it is shown that the simultaneous use of the outgoing atmospheric radiation spectra in the thermal and near IR ranges gives a higher correlation of satellite-based δD estimates with ground-based measurements at FTIR stations of the international TCCON network [Zadvornykh, et al., 2022]. Gribanov et al. [2022] investigated the possibility of determining the $^{13}CO_2/^{12}CO_2$ relative content in the atmosphere from the IASI-type hyperspectral IR sounder data. Experiments with synthetic measurements of the IASI-NG spectrometer demonstrate that the vertical profiles of the $^{13}CO_2$ concentration and the $^{13}CO_2/^{12}CO_2$ relative content in the atmosphere are adequately retrieved in the troposphere for an altitude range of 2–11 km.

In the IAO an algorithm has been developed for retrieving the reflection coefficients of the Earth's surface, taking into account the influence of radiation polarization [Tarasenkov et al., 2020]. To estimate the error of the algorithm, the measurements were used in MODIS five channels over test points in the center of coniferous forests for the summer period of the year. A comparison of the results of algorithms used with or without polarization, the NASA MOD09 algorithm as well as the algorithm without atmospheric correction, shows that the average values of the new estimates (considering the influence of polarization) are closer to the reference values than those obtained using the NASA MOD09 algorithm.

Research & Production Association «Typhoon» performed studies of the high-altitude jet stream characteristics and wind fields in the upper troposphere using measurements of the SEVIRI scanner-imager onboard the European GEO Meteorological Satellites Meteosat – 8, -9,-10, as well as their relationship with climatic parameters and large-scale atmospheric phenomena [Nerushev et al., 2019, 2020a]. Nerushev et al. [2021a] developed a statistical model for the temporal variability of the high-altitude jet streams characteristics in the Northern hemisphere, determined from SEVIRI measurements, the predictors of which are the temperature characteristics of the troposphere, the area of the Arctic Sea ice and the indices of large-scale processes. Nerushev et al. [2021b] considered the relationship of anomalies of the average month-

ly surface air temperature at meteorological stations in Europe and the European territory of Russia with the characteristics of high-altitude jet streams. In [Nerushev, Ivangorodsky, 2019; Nerushev et al., 2020b, 2022] a method was proposed for determining turbulence zones in the upper troposphere from SEVIRI measurements and a statistical model of the temporal variability of the areas of turbulence zones was developed.

From a large number of publications on various applications of satellite remote sensing results (referred above to the third direction), we will focus on those that relate to monitoring of natural hazards and anthropogenic greenhouse gas emissions, as well as NWP and climate research.

Asmus et al. [2019] presented methods and examples of the use of SRC "Planeta" satellite-based information products for monitoring natural hazards on the territory of Russia, including floods, fire conditions, tropical cyclone releases, environmental pollution, volcanic activity, etc. Girina et al. [2019] described the developed information system "Remote monitoring of the activity of volcanoes of Kamchatka and the Kuriles", with the help of which the operational and long-term archives of Earth remote sensing data are prepared. The results of satellite monitoring of the Bezymianny and Klyuchevskoy volcanoes eruptions using this information system are given in [Girina et al., 2020, 2021]. Volkova, et al. [2020] described the use of the SEVIRI / Meteosat measurements for the diagnosis of dangerous weather phenomena. In the study [Chursin, et al., 2020], the ANN algorithm was used to identify the probable thunderstorm development zones from satellite data. Frolova et al. [2022] presented the first results of mesoscale cyclones monitoring in the Arctic region forming of a map of their recurrence from the MSU-GS scanner – imager measurements onboard the Arktika-M No. 1 satellite.

In the studies [Timofeev et al., 2019a, Timofeev et al., 2019b Timofeev et al., 2020a, Timofeev et al., 2020b, Nikitenko et al., 2020] the examples of using estimates of the total CO_2 content in the atmosphere from OCO-2 satellite data for analysis of spatiotemporal variations and evaluation of anthropogenic emissions in various cities of the Russian Federation are presented.

In relation to the information support of NWP, Tsyrulnikov et al. [2019, 2021] described the global data assimilation system of the Hydrometcenter of Russia based on a three-dimensional variational approach and present the results of assimilation in this system of microwave and infrared atmospheric sounder observations from Meteor-M series satellites. Technique and results of adaptive correction of atmospheric sounding and imaging channels of the microwave imager – sounder MTVZA-GYa / Meteor-M are described. Assimilation of infrared sounder IFKS-2 observations, that includes a new scheme for selection of the most informative channels, is presented. Numerical experiments show that short-range forecasts almost equally benefit from assimilation of IKFS-2 and IASI data.

As for climate research, Uspensky [2022] discussed the use of IKFS-2 / Meteor-M measurements for remote derivation of the atmospheric parameters related to so – called essential climate variables (ECV) of the atmosphere, whose monitoring is necessary to characterize the climate system and its changes. The ECVs include the concentrations of the main atmosphere greenhouse gases (water vapor, carbon dioxide, methane, and ozone), characteristics of clouds and aerosols, as well as vertical temperature profiles, etc. The ability of forming multiyear homogeneous series containing IKFS-2 measurements and satellite-based estimates of the aforementioned atmospheric ECVs is analyzed. Astafurov et al. [2021] discussed the multiyear variability of cloud fields' structure and their characteristics over some zones of Western Siberia in the summer of the 2001–2019 period is investigated, based on the results of cloud classification form MODIS and VIIRS scanner – imager measurements. Pokrovsky [2019] presented the results of the analysis of the climatic series of global and regional clouds for 1983-2009, obtained within the framework of the ISCCP international satellite project. The results of the analysis show that global and regional cloud cover show a decrease of 2–6%. Based on ground-based observations and remote sensing data for the atmosphere, ocean and cryosphere, slow climatic fluctuations in the temperature of the waters within surface oceanic layer and for ocean depths up to 700 m in the northern hemisphere are identified and investigated as a response to the corresponding modulations of solar activity [Pokrovsky et al., 2020, 2022].

An assumption of chemical equilibrium condition for nighttime ozone is widely used to retrieve the spatiotemporal distributions of nighttime O, H, and some other characteristics at 80–100 km from satellite data. In the study [Kulikov et al., 2019], the criterion for validity of this assumption developed in [Kulikov et al., 2018] is applied to Sounding of the Atmosphere using Broadband Emission Radiometry (SABER) data (temperature, ozone, and volume emission rate at 2 μm due to OH* transitions (9–7) and (8–6)) to define the boundary of this equilibrium in 2003–2005. It was shown that the retrieval of mesopause characteristics below this boundary can lead to significant (up to 5–8 times) errors.

In the study [Kulikov and Belikovich, 2020], the new source of $O(^1D)$ in the mesopause region due to the process $OH(v\geq5) + O(^3P) \rightarrow OH(0\leq v'\leq v-5) + O(^1D)$ is applied to SABER data to estimate the nighttime $O(^1D)$ distributions for the years 2003–2005. It was found that nighttime concentrations of $O(^1D)$ are comparable with daytime concentrations of this component and, in principle, can impact noticeably the chemistry and thermal balance of the mesopause region.

Kulikov et al. [2021] proposed the criteria for detecting the 2-day photochemical oscillations caused by the nonlinear response of mesospheric chem-

istry to diurnal variations of solar radiation. Their application to the SABER database allowed us to obtain the first experimental evidence that this phenomenon exists in the real mesopause.

Kulikov et al. [2022a, 2022b] analyzed the retrieval quality of the daytime distributions of O, H, OH, HO_2 and chemical heating rate at 77-100 km from the long-term (2003–2015) SABER database using the improved photochemical equilibrium condition for daytime ozone and revised model of excited OH with constants corresponding to published data. It was found that these improvements of the retrieval procedure led to significant (up to 200%) changes in daytime distributions of mentioned characteristics.

References

1. Andreev A.I., Shamilova Y.A. & Kholodov E.I. Using Convolutional Neural Networks for Cloud Detection from Meteor-M No. 2 MSU-MR Data. // Russ. Meteorol. Hydrol. 44, 459–466 (2019). https://doi.org/10.3103/S1068373919070045
2. Asmus V.V., Ioffe G.M., Kramareva L.S. et al. Satellite Monitoring of Natural Hazards on the Territory of Russia. // Russ. Meteorol. Hydrol. 44, 719–728 (2019). https://doi.org/10.3103/S1068373919110013
3. Asmus, V.V., Milekhin, O.E., Kramareva, L.S. et al. Arktika-M: The World's First Highly Elliptical Orbit Hydrometeorological Space System // Russ. Meteorol. Hydrol. 2021б 46, 805–816 (2021). https://doi.org/10.3103/S1068373921120013
4. Astafurov A.V., Skorokhodov A.V. Using the results of cloud classification based on satellite data for solving climatological and meteorological problems // Russian Meteorology and Hydrology. 2021b. V. 46(12). pp. 839–848.
5. Astafurov A.V., Skorokhodov A.V., Kuryanovich K.V. Summer statistical models of cloud parameters over Western Siberia according to MODIS data // Russian Meteorology and Hydrology. 2021a. V. 46(11). pp. 735–746.
6. Bloshchinskiy V.D, Kuchma M.O., Kukharsky A.V. Determination of the total ozone content in atmospheric column according to the data of Electro-l no. 3 spacecraft using neural networks // Issledovanie Zemli iz Kosmosa. 2022. № 4. P. 79–85. DOI: 10.31857/S0205961422040029. [in Russian].
7. Bordovskaya Yu.I., Virolainen Ya.A., Timofeyev Yu.M. Comparison of ground-based and satellite methods for determining vertical ozone profiles // Sovremennye problemy distantsionnogo zondirovaniya Zemli iz kosmosa, 2022, Vol. 19, No. 2, pp. 225–231 DOI: 10.21046/2070-7401-2022-19-2-225-231 [in Russian]
8. Chursin V.V., Kuzhevskaia I. V. Neural network detection of potential thunderstorm zones from remote sensing data // Geosfernye Issledovaniya. 2022. № 3. C. 162–171. DOI: 10.17223/25421379/24/11. [in Russian].
9. Davydova M.A., Elansky N.F., Zakharova S.A., Postylyakov O.V. Application of a Numerical-Asymptotic Approach to the Problem of Restoring the Parameters of a Local Stationary Source of Anthropogenic Pollution. Doklady Mathematics, 2021, Vol. 103, No. 1, 26–31. doi: 10.1134/S1064562421010026.
10. Filei A.A., Davidenko A.N., Kiseleva Y.V. et al. Validation of Results of Atmospheric Temperature and Humidity Sounding with a Fourier Infrared Spec-

trometer onboard the Meteor-M No. 2 Satellite // Russ. Meteorol. Hydrol. 44, 216–221 (2019). https://doi.org/10.3103/S1068373919030087
11. Filei A. A. Retrieval of the cloud optical depth and particle effective radii from MSU-MR daytime measurements // Optika Atmosfery i Okeana. 2019a. V. 32. No. 08. P. 650–656. DOI: 10.15372/AOO20190807 [in Russian].
12. Filei A.A. Determination of cloud phase using MSU-MR measurements onboard Meteor-M N 2 // Optika Atmosfery i Okeana. 2019b. V. 32. No. 05. P. 376–380. DOI: 10.15372/AOO20190506 [in Russian].
13. Filei A. A. Retrieval of the cloud top height from using Meteor-M No. 2-2 MSU-MR measurements // Optika Atmosfery i Okeana. 2020a. V. 33. No. 12. P. 918–925. DOI: 10.15372/AOO20201203 [in Russian].
14. Filei A.A. Development of optical parameters of volcanic cloud models for remote sensing of Earth from space . // Optika Atmosfery i Okeana. 2020b. V. 33. No. 02. P. 127–134. DOI: 10.15372/AOO20200207 [in Russian].
15. Filei A.A., Marenco F. Retrieval of Volcanic Ash Parameters from Satellite Data. // Russ. Meteorol. Hydrol. 2021,46, 269–279. https://doi.org/10.3103/S1068373921040087.
16. Filei A.A., Andreev A.I., and Uspensky A.B. Using Artificial Neural Networks for Retrieval of Temperature-humidity State of the Atmosphere According to the Meteor-M No. 2 MTVZA-GYa Satellite Microwave Radiometer // Issledovanie Zemli iz Kosmosa, No. 6 (2021) [in Russian].
17. Filei A.A., Andreev A.I., Kuchm, M.O. et al. Retrieval of Total Precipitable Water from Meteor-M No. 2-2 MTVZA-GYa Data Using a Neural Network Algorithm. // Russ. Meteorol. Hydrol. 47, 272–280 (2022). https://doi.org/10.3103/S1068373922040033.
18. Frolova E.A., Nesterov E.S., Salagina A.A. Using Arktika-M No. 1 satellite MSU-GS data for monitoring and analyzing mesoscale cyclones in the Arctic region // Sovremennye problemy distantsionnogo zondirovaniya Zemli iz kosmosa. 2022. Vol. 19. № 4,pp. 293–305. DOI: 10.21046/2070-7401-2022-19-4-293-305.
19. Girina O.A., Loupian E.A., Melnikov D.V. et al. Creation and development of the information system “Remote Monitoring of Kamchatka and Kuril Islands Volcanic Activity // Sovremennye problemy distantsionnogo zondirovaniya Zemli iz kosmosa. 2019. T. 16. № 3. pp. 249–265.
20. Girina O.A., Melnikov D.V., Manevich A.G. et al. Analysis of the events of the explosive eruption of Bezymianny volcano on October 21, 2020, based on satellite data // Sovremennye problemy distantsionnogo zondirovaniya Zemli iz kosmosa. 2020. T. 17. № 5. C. 297–303. DOI: 10.21046/2070-7401-2020-17-5-297-303.
21. Girina O.A., Loupian E.A., Manevich A.G. et al. Remote observations of the 2019–2020 explosive-effusive eruption of Klyuchevskoy volcano // Sovremennye problemy distantsionnogo zondirovaniya Zemli iz kosmosa, 2021. T. 18. № 1. C. 81–91. DOI: 10.21046/2070-7401-2021-18-1-81-91.
22. Golomolzin, V.V., Rublev, A.N., Kiseleva, Y.V. et al. Retrieval of Total Column Carbon Dioxide over Russia from Meteor-M No. 2 Satellite Data. // Russ. Meteorol. Hydrol. 47, 304–314 (2022). https://doi.org/10.3103/S1068373922040069.
23. Kostsov V.S., Kniffka A., Stenge M., Ionov D.V. Cross-comparison of cloud liquid water path derived from observations by two space-borne and one ground-

based instrument in Northern Europe // Atmospheric Measurement Techniques. 2019. 12, 5927–5946. https://doi.org/10.5194/amt-12-5927-2019.
24. Kozlov, D.A., Kozlov, I.A., Uspensky, A.B. et al. Characterization of the Noise Covariance Matrix of the IKFS-2 Infrared Fourier Transform Spectrometer Measurements // Izv. Atmos. Ocean. Phys. 58, 2022. pp. 1160–1172.
25. https://doi.org/10.1134/S0001433822090110.
26. Kozlov D.A., Zavelevich F.S., Timofeev Yu. M. et al. Intercalibration of SI-1 and IKFS-2 spaceborne infrared Fourier transform spectrometers // Sovremennye problemy distantsionnogo zondirovaniya Zemli iz kosmosa, 2019, Vol. 16, No. 6, pp. 72–80. DOI: 10.21046/2070-7401-2019-16-6-72-80 [in Russian].
27. Kostornaya A.A., Rublev A.N., Golomolzin V.V. The determination of the total atmospheric water vapor content over the oceans using the MTVZA-GY microwave radiometer measurements. // Computational Technologies. 2020. 25(4) pp. 83–98. DOI:10.25743/ICT.2020.25.4.008. [in Russian].
28. Kramareva, L.S., Andreev, A.I., Bloshchinskiy et al. The use of neural networks in hydrometeorology problems // Computational Technologies. 2019. Vol. 24, No. 6. P. 50–59. (In Russ.) DOI: 10.25743/ICT.2019.24.6.007.
29. Kuchma M.O., Shamilova J.A. Near-real-time detection of potential fog by Himawari-8 geostationary satellite data // Gidrometeorologicheskie Issledovaniya i Prognosy. 2022. №3 (385). C. 113-126. DOI: 10.37162/2618-9631-2022-3-113–126. [in Russian].
30. Kuchma M.O., Kholodov E.I., Amel'chenko Y.A. Two-channel algorithm for determining the aerosol optical thickness above the sea surface using the MSU-MR instrument of the METEOR-M no. 2 satellite // Issledovanie Zemli iz Kosmosa. 2022. № 2. C. 88–94. DOI: 10.31857/S0205961422020051. [in Russian].
31. Kulikov M.Yu., Nechaev A.A., Belikovich M.V., Vorobeva E.V., Grygalashvyly M., Sonnemann G.R., & Feigin A.M.: Boundary of nighttime ozone chemical equilibrium in the mesopause region from SABER data: Implications for derivation of atomic oxygen and atomic hydrogen // Geophysical Research Letters, 46 (2), 997–1004, doi:10.1029/2018GL080364, https://agupubs.onlinelibrary.wiley.com/doi/abs/10.1029/2018GL080364, 2019.
32. Kulikov M.Yu. and Belikovich M.V.: Nighttime O(1D) distributions in the mesopause region derived from SABER data // Ann. Geophys., 38, 815–822, https://doi.org/10.5194/angeo-38-815-2020 , 2020.
33. Kulikov M.Y., Belikovich M. V., Feigin A.M. The 2-day photochemical oscillations in the mesopause region: the first experimental evidence? // Geophysical Research Letters. – V. 48. e2021GL092795, 2021. https://doi.org/10.1029/2021GL092795.
34. Kulikov M.Yu., M.V. Belikovich, M. Grygalashvyly, G.R. Sonnemann, and A.M. Feigin, Retrieving daytime distributions of O, H, OH, HO2, and chemical heating rate in the mesopause region from satellite observations of ozone and OH* volume emission: The evaluation of the importance of the reaction $H+O_3$ ->O2+OH in the ozone balance // Advances in Space Research, 2022, 69(9), 3362–3373. https://doi.org/10.1016/j.asr.2022.02.011
35. Kulikov M.Y., Belikovich M.V., Grygalashvyly M., G.R. Sonnemann, and A.M. Feigin. The revised method for retrieving daytime distributions of atomic oxygen and odd-hydrogens in the mesopause region from satellite observations // Earth Planets Space, 2022, 74, 44. https://doi.org/10.1186/s40623-022-01603-8

36. Mukhartova Y.V., Davydova M.A., Elansky N.F. et al. On application of non-linear reaction-diffusion-advection models to simulation of transport of chemically – active impurities. // Proc. SPIE, 11157, 111570X, 2019, doi:10.1117/12.2535489.
37. Mukhartova Y.V., Postylyakov O.V., Davydova M.A. et al. High-detailed tropospheric transport of NOx from ground sources: comparison of model data and satellite imagery. Proc. SPIE 11859, 1185906, 2021; doi:10.1117/12.2600283.
38. Nerobelov G., Timofeyev Y., Virolainen Y. et al. Measurements and Modelling of Total Ozone Columns near St. Petersburg, Russia // Remote Sens. 2022, Vol. 14, Issue 16. 10.3390/rs14163944
39. Nerushev A.F., Visheratin K.N., and Ivangorodsky R.V. Dynamics of High-Altitude Jet Streams from Satellite Measurements and Their Relationship with Climatic Parameters and Large-Scale Atmospheric Phenomena // Izvestiya, Atmospheric and Oceanic Physics, 2019, Vol. 55, No. 9, pp. 1198–1209. DOI: 10.1134/S0001433819090329.
40. Nerushev A.F., Ivangorodsky R.V. Determination of turbulence zones in the upper troposphere based on satellite measurements // Sovremennye problemy distantsionnogo zondirovaniya Zemli iz kosmosa, 2019, Vol. 16, No. 1, pp. 205–215. DOI: 10.21046/2070-7401-2019-16-1-205-215.
41. Nerushev. A.F., Visheratin K.N. and Ivangorodsky R.V. Characteristics of the upper troposphere wind field according to the satellite measurements and their connection with climatic parameters // IOP Conference Series: Earth and Environmental Science, 2020a.Volume 606, 012041. Doi: 10.1088/1755-1315/606/1/012041.
42. Nerushev A.F., Visheratin K.N., Ivangorodsky R.V. Turbulence in the upper troposphere according to long-term satellite measurements and its relationship with climatic parameters // Sovremennye problemy distantsionnogo zondirovaniya Zemli iz kosmosa, 2020b, Vol. 17, No. 6, pp. 82–86. DOI: 10.21046/2070-7401-2020-17-6-82-86.
43. Nerushev, A.F., Visheratin, K.N. & Ivangorodsky, R.V. Statistical Model of the Time Variability of the Characteristics of High-Altitude Jet Currents in the Northern Hemisphere Based on Satellite Measurements. // Izv. Atmos. Ocean. Phys. 2021a. 57, pp. 354–364. https://doi.org/10.1134/S0001433821040198.
44. Nerushev A.F., Visheratin K.N., L.K. Kulizhnikova, Ivangorodsky R.V. The relationship of surface air temperature anomalies and the characteristics of high-altitude jet streams // Sovremennye problemy distantsionnogo zondirovaniya Zemli iz kosmosa, 2021b, Vol. 18, No. 1, pp. 199–209. DOI: 10.21046/2070-7401-2021-18-1-199-209.
45. Nerushev A.F., Visheratin K.N. and Ivangorodsky R.V. Satellite-derived estimations of the clear-air turbulence in the upper troposphere // IOP Conf. Series: Earth and Environmental Science. 1040 (2022) 012025. DOI:10.1088/1755-1315/1040/1/012025.
46. Nikitenko A.A., Timofeev Yu.M., Virolainen Ya. A. et al. Comparison of CO_2 measurements in stratosphere by ground-based and satellite methods // Atmospheric and Oceanic Optics, 2022, No3, 191–194.
47. Nikitenko A.A., Timofeev Yu. M., Berezin I.A. et al. The Analysis of OCO-2 Satellite Measurements of CO2 in the Vicinity of Russian Cities // Atmospheric and Oceanic Optics, 2020, V. 33. No. 06. pp. 650–655.

48. Pokrovsky O.M., Cloud changes in the period of global warming: The results of the international satellite project. // Izv., Atmos. Ocean. Phys., 2019, vol. 55, no. 9, pp. 1189–1197.
49. Pokrovsky O. M. and Pokrovsky I. O. Identification of a Fundamental Climatic Oscillations Using Wavelet Analysis of the Combined Data of Ground and Satellite Observations // Issledovanie Zemli iz Kosmosa. 2020. № 6. c. 59–72. [in Russian].
50. Pokrovsky O.M. and Pokrovsky I.O. Coherence of fluctuations of the components of the global climate system with slow fluctuations of solar activity according to ground and satellite observations // Issledovanie Zemli iz Kosmosa. 2022, № 3, p. 1–14.
51. Polyakov A.,. Virolainen Ya., Nerobelov G., et al. Total ozone measurements using IKFS-2 spectrometer aboard Meteor M N2 satellite in 2019–2020 // Intern. Journ. of Remote Sensing, 2021, 42:22, 8709-8733, DOI: 10.1080/01431161.2021.1985741.
52. Polyakov A.V., Timofeyev Y.M., Virolainen Y.A. et al. Atmospheric ozone monitoring with Russian spectrometer IKFS-2 // Zhurnal Prikladnoii Spektroskopii. 2019;86(4):597-601. [in Russian].
53. Postylyakov O.V., Borovski A.N., Elansky N.F. et al. Comparison of space high-detailed experimental and model data on tropospheric NO2 distribution. Proc. SPIE, 11208, 112082S, 2019a, doi:10.1117/12.2540770.
54. Postylyakov O.V., Borovski A.N., Davydova M.A. et al. Preliminary validation of high-detailed GSA/Resurs-P tropospheric NO2 maps wi th alternative satellite measurements and transport simulations. // Proc. SPIE, 11152, 111520F, 2019b, doi:10.1117/12.2535487.
55. Postylyakov O.V., Borovski A.N., Shukurov K.A. et al. On validation high-detail mapping of tropospheric NO2 using GSA/Resurs-P observations with simulated data. // Proc. SPIE 11531, 1153109, 2020, doi:10.1117/12.2574240.
56. Rublev A.N., Kozlov D.A. et al. Monitoring of the Essential Climate Variables of the Atmosphere from Satellite-based Infrared Sounder IKFS-2. // Russ. Meteorol. Hydrol. 47, 819–828 (2022). https://doi.org/10.3103/S1068373922110012.
57. Rublev A., Kiseleva Ju., Uspensky A. et al. On-orbit calibration of Russian satellite instruments: New issues // GSICS Quarterly Spring Issue 2021. – 2021. – Vol. 15. – No. 1. – P. 4–6. DOI: 10.25923/m6pq-w122.
58. Sha M.K., Langerock B., Blavier J.-F.L. et al. Validation of methane and carbon monoxide from Sentinel-5 Precursor using TCCON and NDACC-IRWG stations // Atmos. Meas. Tech., 2021:14, 9, 6249–6304, https://doi.org/10.5194/amt-14-6249-2021
59. Skorokhodov A.V., Kuryanovich K.V. Using CloudSat CPR to improve the efficiency of the neural network approach to retrieving the cloud base height in Aqua MODIS satellite images // Sovremennye problemy distantsionnogo zondirovaniya Zemli iz kosmosa. 2022b. V. 19. No. 5. P. 63–75.
60. Skorokhodov A.V., Kuryanovich K.V. Using CALIOP data for estimating the cloud base heights in MODIS satellite images // Sovremennye problemy distantsionnogo zondirovaniya Zemli iz kosmosa. 2022a. V. 19. No. 2. pp. 43–56 [in Russian].
61. Tarasenkov M.V., Zimovaya A.V., Belov V.V. and Engel M.V. Retrieval of Reflection Coefficients of the Earth's Surface from MODIS Satellite Measure-

ments Considering Radiation Polarization // Atmospheric and Oceanic Optics, 2020, V. 33. No. 02. P. 179–187. https://doi.org/10.1134/S1024856020020128.
62. Tarasenkov M.V., Zonov M.N., Engel' M.V. et al. Estimation of the broken cloud effect on retrieving reflectance of cloudless earth surface regions from MODIS imagery //Russian Meteorology and Hydrology. 2021a. V. 46. No. 11. P. 747–754.
63. Tarasenkov M.V., Zonov M.N., Belov V.V. et al. Passive Satellite Sensing of the Earth's Surface through Breaks in Cloud Fields // Atmospheric and Oceanic Optics, 2021b, V. 34, No. 6, P. 695–703.
64. Tarasenkov M.V., Engel M.V., Zonov M.N. et al. Assessing the cloud adjacency effect on retrieval of the ground surface reflectance from MODIS satellite data for the Baikal area // Atmosphere. 2022, V. 13, No. 12. 2054. 16 p. https://doi.org/10.3390/atmos13122054.
65. Timofeyev Y.M., Uspensky A.B. and Zavelevich et al. Hyperspectral Infrared Atmospheric Sounder IKFS-2 on "Meteor-M" No. 2 – four F.S. years in orbit // Journal of Quantitative Spectroscopy & Radiative Transfer, Nov. 2019, 106579. http://doi.org/10.1016/j.jqrst.2019.106579.
66. Timofeev, Y.M., Nerobelov, G.M., Polyakov, A.V. et al. Satellite Monitoring of the Ozonosphere // Russ. Meteorol. Hydrol. 2021. 46, pp. 849–855. https://doi.org/10.3103/S1068373921120062.
67. Timofeyev Y.M., Berezin I.A., Virolainen Y.A. et al. Spatial–Temporal CO2 Variations near St. Petersburg Based on Satellite and Ground-Based Measurements // Izv. Atmos. Ocean. Phys. 55, 59–64 (2019). https://doi.org/10.1134/S0001433819010109.
68. Timofeyev Y.M., Berezin I.A., Virolainen Y.A. et al.. Analysis of mesoscale variability of carbon dioxide in the vicinity of Moscow megacity based on satellite data // Sovremennye problemy distantsionnogo zondirovaniya Zemli iz kosmosa, 2019. 16, 4, 263–270. DOI: 10.21046/2070-7401-2019-16-4-263-270.
69. Timofeev Yu.M., Berezin I.A., Virolainen Ya. A. et al. Estimates of Anthropogenic CO2 Emissions for Moscow and St. Petersburg Based on OCO-2 Satellite Measurements // Atmospheric and Oceanic Optics, 2020, V. 33. No. 06. pp. 656–660.
70. Timofeev Y.M., Polyakov A.V., Virolainen Y.A. et al. First Satellite Measurements of Carbon Dioxide in the Earth's Atmosphere (From the SI-1 Spectrometer Aboard the Meteor Satellite in 1979). Izv. Atmos. Ocean. Phys. 56, 401–404 (2020). https://doi.org/10.1134/S000143382004009X
71. Tsyrulnikov M.D., Svirenko P.I., Gayfulin D.R. et al. Development of the Operational Data Assimilation System of the Hydrometcenter of Russia // Gidrometeorologicheskie Issledovaniya i Prognose, No. 4 (2019) [in Russian].
72. Tsyrulnikov M.D., Gayfulin D.R., Svirenko P.I. et al. Assimilation of Observations from Meteorological Satellites in the Hydrometcenter of Russia. // Russ. Meteorol. Hydrol. 46, 856–865 (2021). https://doi.org/10.3103/S1068373921120074.
73. Uspensky A.B. 60th anniversary of satellite meteorology // Meteorologiya i Gidrologiya, 2021,12, pp. 5–10. [in Russian].
74. Uspensky A.B., Timofeev Y.M., Kozlov D.A. et al. Development of Methods and Instruments for Remote Temperature and Humidity Sensing of the Earth's Atmosphere // Russ. Meteorol. Hydrol. 2021, 46, pp. 821–829. https://doi.org/10.3103/S1068373921120037.

75. Uspensky A.B. Satellite Measurements of Greenhouse Gas Distribution in the Atmosphere // Fundamental and Applied Climatology, 2022, V. 8, No. 1, pp. 122–144. DOI: 10.21513/2410-8758-2022-1-15-49. [in Russian].
76. Virolainen Y.A., Nikitenko A.A., Timofeyev Yu.M. Intercalibration of satellite and ground-based measurements of CO_2 mean mole fractions at the NDACC site St. Petersburg // Zhurnal Prikladnoii Spektroskopii. 2020. 87(5):816-820. (In Russian).
77. Volkova E.V., Andreev A.I. & Kostornaya A.A. Cloud Cover and Precipitation Monitoring Based on Data from Polar Orbiting and Geostationary Satellites. Russ. Meteorol. Hydrol. 46, 830–838 (2021). https://doi.org/10.3103/S106837 3921120049.
78. Volkova E.V., Kostornaya A.A., Amikishieva R.A. Determination of cloud cover parameters using automatic satellite data processing systems // Geographical bulletin, 2020, № 3, pp. 124–134, DOI: 10.17072/2079-7877-2020-3-124-134. [in Russian].
79. Volkova E.V., Kukharsky A.V. The automated technology for retrieving cloud cover properties, precipitation and weather hazards based on SEVIRI/Meteosat (MSG) data for the European part of Russia // Gidrometeorologicheskie Issledovaniya i Prognosy, 2020, № 4 (378), p. 43–62. doi 10.37162/2618-9631-2020-4-43-62. [in Russian].
80. Zabolotskikh E.V. External Calibration of MTVZA-GYa Microwave Radiometer Measurements in Scanner Channels. Part 1. The Modeling // Russ. Meteorol. Hydrol. 2021, Vol. 46, No. 10, pp. 689–696.
81. Zabolotskikh E.V., Balashova E.A. External Calibration of MTVZA-GYa Microwave Radiometer Measurements in Scanner Channels. Part 2. The Experiment // Russ. Meteorol. Hydrol. 2021, Vol. 46, No. 11, pp. 755–761.
82. Zakharova S., Davydova M., Borovski A. et al. Experiments on high-detailed mapping of tropospheric NO_2 using GSA/Resurs-P observations: results, validation with models and measurements, estimation of emission power // Proc. SPIE 11859, 1185905, 2021; doi:10.1117/12.2600316.
83. Zadvornykh I.V., Gribanov K.G., Zakharov V.I. et al. Methane Vertical Profile Retrieval from the Thermal and Near-Infrared Atmospheric Spectra. // Atmos Ocean Opt, 2019, 32(2), 152–157. https://doi.org/10.1134/S1024856019020179.
84. Zadvornykh I.V., Gribanov K.G., Denisova N.Yu. et al. Method for Retrieval of the HDO/H2O Ratio Vertical Profile in the Atmosphere from Satellite Spectra Simultaneously Measured in Thermal and Near-IR Ranges // Atmospheric and Oceanic Optics, 2021, V. 34. No. 02. pp. 81–86.
85. Zadvornykh I.V., Gribanov K.G., Zakharov V.I., Imasu R. Retrieval of HDO relative content in atmosphere from simultaneous GOSAT-2 measurements in the thermal and near-IR . // Optika Atmosfery i Okeana. 2022. V. 35. No. 12. P. 999–1003. DOI: 10.15372/AOO20221205 [in Russian].

Научное издание

НАЦИОНАЛЬНЫЙ ОТЧЕТ РОССИИ
ПО МЕТЕОРОЛОГИИ И АТМОСФЕРНЫМ НАУКАМ
В 2019–2022 гг.

XXXVIII Генеральная Ассамблея
Международного союза геодезии и геофизики
Берлин, Германия, 11–20 июля 2023 г.

На английском языке

Редакторы:
И.И. Мохов, А.А. Криволуцкий

Подготовка оригинал-макета:
Издательство «МАКС Пресс»
Главный редактор: *Е.М. Бугачева*
Компьютерная верстка: *Н.С. Двыдова*
Обложка: *А.В. Кононова*

Подписано в печать 07.07.2023 г.
Формат 60x90 1/16. Усл. печ. л. 27,5.
Тираж 100 экз. Заказ 102.

Издательство ООО “МАКС Пресс”
Лицензия ИД N 00510 от 01.12.99 г.

119992, ГСП-2, Москва, Ленинские горы,
МГУ им. М.В. Ломоносова, 2-й учебный корпус, 527 к.
Тел. 8(495)939-3890/91. Тел./Факс 8(495)939-3891.

Отпечатано в полном соответствии с качеством
предоставленных материалов в ООО «Фотоэксперт»
109316, г. Москва, Волгоградский проспект, д. 42,
корп. 5, эт. 1, пом. I, ком. 6.3-23Н